

GOLD-BEARING QUARTZ-BRECCIA ZONES  
IN ARCHEAN METASEDIMENTS OF THE GORDON LAKE REGION,  
NORTHWEST TERRITORIES, CANADA

by

Timothy Robert Stokes



Submitted in partial fulfilment  
of the requirements for the degree of

Doctor of Philosophy

at

Dalhousie University

Halifax, Nova Scotia, Canada

May 1991

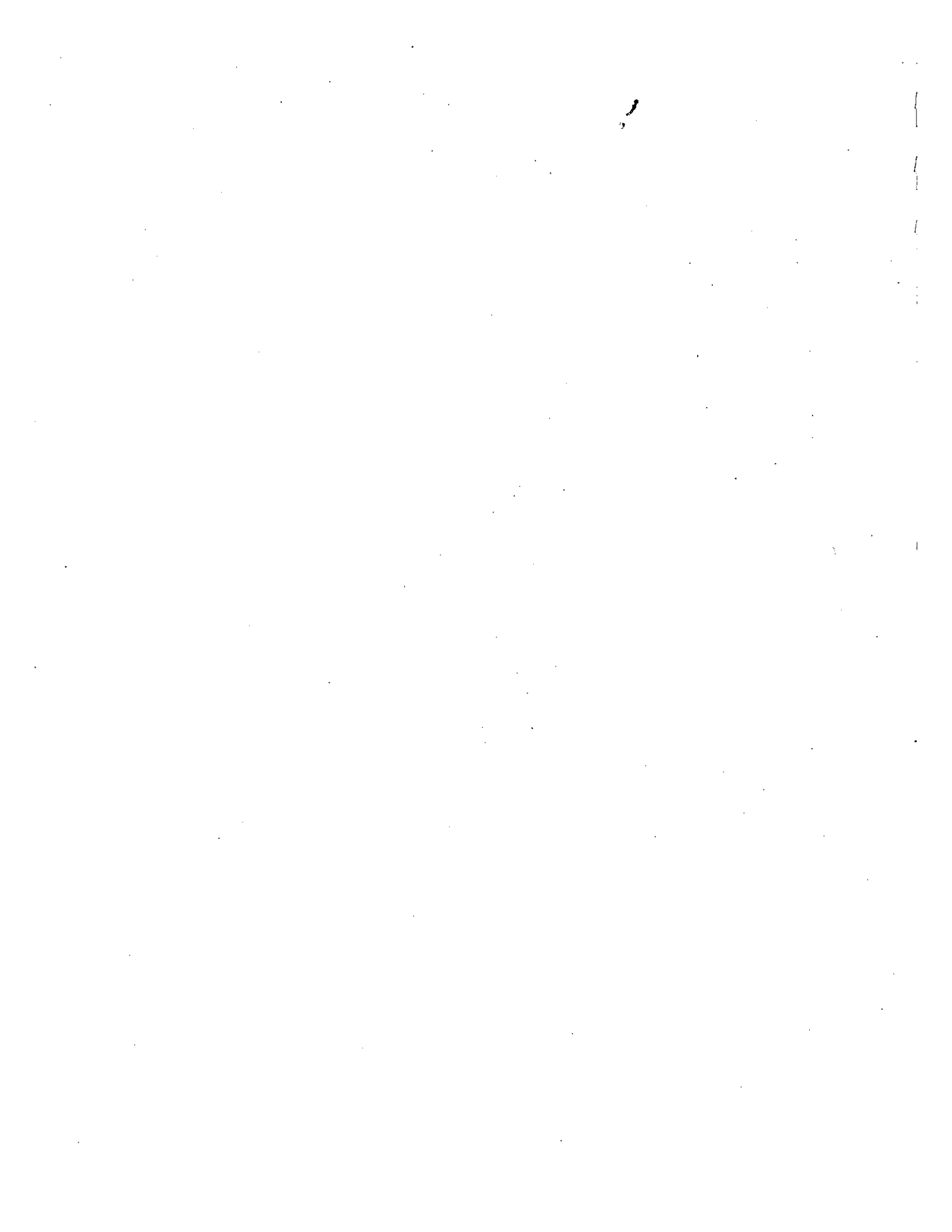
GOLD-BEARING QUARTZ-BRECCIA ZONES  
IN ARCHEAN METASEDIMENTS OF THE GORDON LAKE REGION,  
NORTHWEST TERRITORIES, CANADA

by

Timothy Robert Stokes



Submitted in partial fulfilment  
of the requirements for the degree of  
Doctor of Philosophy  
at  
Dalhousie University  
Halifax, Nova Scotia, Canada  
May 1991



DALHOUSIE UNIVERSITY

FACULTY OF GRADUATE STUDIES

The undersigned hereby certify that they have read and recommend to the Faculty of Graduate Studies for acceptance a thesis entitled "Gold-bearing Quartz-breccia Zones in Archean Metasediments of the Gordon Lake Region, Northwest Territories, Canada"

by Timothy Robert Stokes

in partial fulfillment of the requirements for the degree of Doctor of Philosophy.

(C)

Dated April 16, 1991

External Examiner

[Signature]

Research Supervisor

[Signature]

Examining Committee

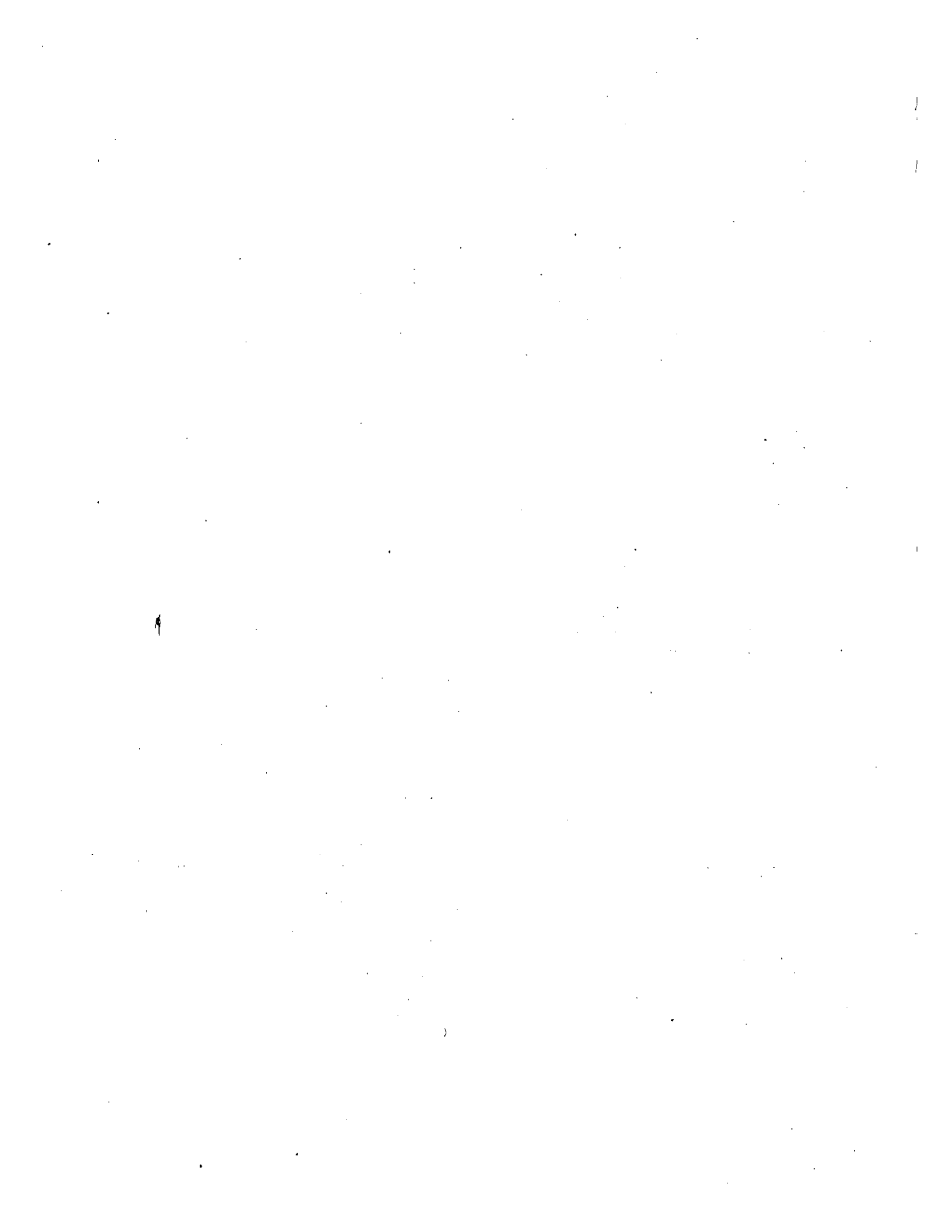
[Signature]

[Signature]

[Signature]

\_\_\_\_\_

\_\_\_\_\_



DALHOUSIE UNIVERSITY

Date \_\_\_\_\_

Author Timothy Robert Stokes

Title GOLD-BEARING QUARTZ-BRECCIA ZONES IN ARCHEAN  
METASEDIMENTS OF THE GORDON LAKE REGION,  
NORTHWEST TERRITORIES, CANADA

Department or School: Geology

Degree: Ph.D. Convocation: October Year: 1990

Permission is herewith granted to Dalhousie University to circulate and to have copied for non-commercial purposes, at its discretion, the above title upon the request of individuals or institutions.

\_\_\_\_\_  
Signature of Author

THE AUTHOR RESERVES OTHER PUBLICATION RIGHTS, AND NEITHER THE THESIS NOR EXTENSIVE EXTRACTS FROM IT MAY BE PRINTED OR OTHERWISE REPRODUCED WITHOUT THE AUTHOR'S WRITTEN PERMISSION.

THE AUTHOR ATTESTS THAT PERMISSION HAS BEEN OBTAINED FOR THE USE OF ANY COPYRIGHTED MATERIAL APPEARING IN THIS THESIS (OTHER THAN BRIEF EXCERPTS REQUIRING ONLY PROPER ACKNOWLEDGEMENTS IN SCHOLARLY WRITING) AND THAT SUCH USE IS CLEARLY ACKNOWLEDGED.



## TABLE OF CONTENTS

List of Figures.....	xii
List of Tables.....	xxi
Abstract.....	xxviii
Acknowledgements.....	xxiv
<u>CHAPTER 1</u> - INTRODUCTION.....	1
1.1 General Statement.....	1
1.2 Aims and Objectives of Thesis.....	3
1.3 Thesis Approach.....	4
1.4 Model Philosophy and Exploration Criteria.....	4
<u>CHAPTER 2</u> - METATURBIDITE-HOSTED GOLD DEPOSITS WITH PARTICULAR REFERENCE TO THE SLAVE PROVINCE.....	6
2.1 Definition and Character.....	6
2.2 Metallogenic Distribution.....	7
2.3 Gold Occurrences within the Slave Province.....	9
2.4 Previous Studies on Gold Mineralization within the Yellowknife Basin.....	10
2.5 Proposed Genetic Models for the Formation of Metaturbidite-Hosted Gold Deposits.....	12
<u>CHAPTER 3</u> - GEOLOGY OF THE SLAVE PROVINCE.....	15
3.1 Introduction.....	15
3.2 Granite-Gneiss Basement.....	17
3.3 Supracrustal Sequences.....	17
3.4 The Yellowknife Volcanic Belt.....	19
3.5 Late Granitoids.....	21
3.6 Metallogeny of the Slave Province.....	21



3.7 Proposed Tectonic Models for the Slave Province.....22

CHAPTER 4 - GEOLOGY OF THE YELLOWKNIFE BASIN AND  
METATURBIDITES OF THE BURWASH FORMATION:  
PREVIOUS STUDIES.....30

4.1 Introduction.....30

4.2 Lithology and Petrography.....31

4.3 Metamorphism.....32

4.4 Structure.....34

    4.4.1 Early ( $D_0$ ) Deformation .....34

    4.4.2  $D_1$  Deformation.....35

    4.4.3  $D_2$  Deformation.....35

    4.4.4  $D_3$  Structures.....38

    4.4.5 "Refold" Structures.....40

    4.4.6 Summary of Fyson's Structural Model.....40

CHAPTER 5 - GEOLOGY OF THE SOUTHERN END OF GORDON LAKE...42

5.1 Regional Setting.....42

5.2 Lithology.....44

    5.2.1 Graywackes.....49

    5.2.2 Siltstones.....49

    5.2.3 Interpretation of Regional Lithology.....50

5.3 Metamorphism.....50

    5.3.1 Metamorphic Mineral Assemblages.....50

    5.3.2 Interpretation of Metamorphic Mineral  
    Assemblages.....55

5.4 Structural Geology .....59

    5.4.1 Fold Types, Morphology, and Distribution....59

5.4.1.1	F <sub>1</sub> and Earlier (F <sub>0</sub> ) Folds.....	59
5.4.1.2	F <sub>3</sub> Folds.....	61
5.4.1.3	Regional Refold.....	64
5.4.2	Cleavages and Quartz Inclusion Fabrics.....	64
5.4.2.1	Quartz Inclusion Trails in Biotite Porphyroblasts.....	68
5.4.2.2	Strain and Microstructure of D <sub>3</sub> Cleavages.....	72
5.4.2.3	Strain and Microstructure of D <sub>4</sub> Cleavages.....	76
5.4.3	Lineations.....	81
5.4.4	Other Structures.....	81
5.5	Strain Analysis of the Vertical Stretching Lination at Gordon Lake.....	82
5.5.1	Fry Analysis.....	82
5.5.2	Interpretation of Stretching Lination Data.....	84
5.6	Strain Analysis of Deformed Quartz Veins.....	86
5.7	Structural Evolution of the Gordon Lake Refold.....	88
5.7.1	Formation of the Vertical Isoclinal Folds...88	
5.7.2	Refold Formation.....	89
5.8	Tectonic Models.....	94
5.9	Summary.....	97
<u>CHAPTER 6 - QUARTZ VEINS AND QUARTZ-BRECCIAS OF THE GORDON LAKE REGION: CLASSIFICATION AND MODELS FOR THEIR EMPLACEMENT.....</u>		99
6.1	Quartz Vein Morphology and Distribution.....	100
6.1.1	Type 1 - Bedding-parallel Veins.....	100
6.1.2	Type 2 - D <sub>3</sub> -Deformed, Echelon Veins, and Networks.....	100

6.1.3	Type 3 - $S_{3S}$ -parallel Veins.....	105
6.1.4	Type 4 - Boudinaged 'East Limb' Veins.....	106
6.1.5	Type 5 - Sub-horizontal Veins.....	107
6.1.6	Type 6 - $S_4$ -parallel Veins.....	107
6.1.7	Type 7 - Rotated 'Z' Veins.....	108
6.1.8	Other Vein Types.....	108
6.2	Quartz-Breccia Morphology and Distribution.....	109
6.2.1	Breccia Type I - Sub-parallel to $F_1$ Fold Axial Traces.....	109
6.2.2	Breccia Type II - Sub-parallel to $F_3$ Fold Axial Traces.....	112
6.2.3	Breccia Type III - Strata-bound and Silt- stone-hosted.....	112
6.2.4	Breccia Type IV - Graywacke-Hosted.....	115
6.2.5	Breccia Type V - East Limb Breccias.....	116
6.3	Quartz Veins and Quartz-Breccias: Formation Mechanisms and Time of Emplacement.....	116
6.3.1	Mechanisms and Time of Quartz Vein Emplacement.....	118
6.3.2	Quartz Microstructure and Vein Deformation.....	121
6.3.3	Mechanisms and Timing of Quartz-Breccia Emplacement.....	122
6.4	Models for the Formation of the Strata-bound, Siltstone-hosted Type III Quartz-Breccias.....	123
6.5	Summary of Quartz Vein and Quartz-Breccia Formation.....	125
 <b>CHAPTER 7 - THE KIDNEY POND ZONE 1 AND OTHER QUARTZ- BRECCIA OCCURRENCES OF THE KNIGHT BAY PROPERTY.....</b>		
7.1	Introduction and Previous Work.....	128

7.2	Structural and Lithological Setting of Kidney Pond Quartz-Breccia Zones.....	130
7.3	Stratigraphic Section across Kidney Pond Quartz-Breccia Zones 1 and 2.....	139
7.4	Matrix, Sulphide, and Gold Mineralogy of the Kidney Pond Zone 1 Quartz-Breccia.....	139
7.5	Time of Formation for the Kidney Pond Zone 1 Quartz-Breccia.....	150
7.6	Arsenopyrite Geothermometry.....	152
7.7	Summary.....	154

**CHAPTER 8 - A FLUID INCLUSION STUDY OF QUARTZ-BRECCIAS AND VEINS OF THE GORDON LAKE REGION.....** 155

8.1	Introduction and Purpose.....	155
8.2	Previous Fluid Inclusion Studies of Similar Gold-Quartz Vein Systems, with Particular Reference to those of the Yellowknife Basin.....	156
8.3	Approach.....	162
8.4	Fluid Inclusion Petrography.....	164
	8.4.1 Quartz Microstructure <sup>and</sup> Inclusion Morphology.....	164
	8.4.2 Classification of Fluid Inclusion Types....	167
8.5	Thermometric Analysis and Results.....	172
8.6	Volatile Analysis Using a Heated Crushing and Gas Chromatography Technique.....	175
8.7	Interpretation of Thermometric and Volatile Data...177	
	8.7.1 Estimates of Salinity.....	179
	8.7.2 Estimates of Fluid Composition.....	180
	8.7.3 Estimates of Pressure and Temperature of Trapping.....	183
8.8	Evolution of a Saline Fluid in the Gordon Lake Region and its Possible Role in Gold Mineralization.....	183

9.9 Summary of Fluid Inclusion Study.....188

CHAPTER 9 - GEOCHEMISTRY OF HOST LITHOLOGIES, QUARTZ- BRECCIAS AND VEINS OF THE GORDON LAKE REGION.....190

9.1 Introduction and Purpose.....190

9.2 Previous Geochemical Studies of Metaturbidite-Hosted Gold Deposits and Provenance of Metaturbidites with Particular Reference to the Yellowknife Basin.....191

9.3 Sample Collection, Preparation, and Analysis.....194 X

9.4 Results and Precision/Accuracy Analysis.....196

9.5 Comparison of Major, Trace, Gold, and Volatile Analyses between Breccias, Veins, and Host Lithologies.....197

9.6 Gold-Sulphide Associations.....206

9.7 Geochemical Indications of Tectonic Setting and Provenance of the Gordon Lake Metaturbidites.....207

9.8 Summary of Geochemical Study.....213

CHAPTER 10 - Ar<sup>40</sup>Ar/<sup>39</sup>Ar GEOCHRONOLOGICAL STUDY OF THERMAL AND TEMPORAL EVENTS IN THE GORDON LAKE REGION.....214

10.1 Purpose and Aims of Study.....214

10.2 Previous Geochronological Studies.....214

10.3 Sample Descriptions.....220

10.4 Sample Preparation and Analysis.....224

10.5 Spectra and Average Plateau Ages.....224

10.6 Microprobe Analysis of Biotites and Hornblende....227

10.7 Interpretation of Plateau Ages and Spectra.....227

10.8 A Thermochronological Model for Metamorphism and Quartz-Brecciation.....233

10.9 Summary of <sup>40</sup>Ar/<sup>39</sup>Ar Dating Study.....234

<u>CHAPTER 11</u>	- TOWARDS A CONSTRAINED GENETIC MODEL FOR THE CONCENTRATION OF GOLD-BEARING QUARTZ- BRECCIAS IN THE GORDON LAKE REGION.....	235
11.1	Introduction.....	235
11.2	Applicability of Previously Suggested Genetic Models.....	235
11.2.1	Genesis Related to Granites.....	235
11.2.2	Syngenetic and Syngenetic-Epigenetic Models.....	237
11.2.3	Genesis by Lateral Secretion and Meta- morphic Fluids.....	237
11.3	Source of Metamorphic Fluids and Gold.....	238
11.4	Mechanisms of Fluid Transport and Migration.....	240
11.5	Regional Focussing of Fluids.....	241
11.6	Structural, Lithological, and Fluid Pressure Constraints on the formation of Type III and IV Gold-Bearing Quartz-Breccia Zones.....	242
11.6.1	Structural Constraints.....	244
11.7.1	Lithological Constraints.....	244
11.7.3	Fluid Pressure Constraints.....	245
11.7	Physico-chemical Constraints on Fluid Trapping and Gold/Sulphide Concentration at Gordon Lake.....	246
11.8	Post-ore Modifaction and Preservation.....	248
11.9	Summary of Geentic Model.....	249
<u>CHAPTER 12</u>	- CONCLUSIONS.....	250
<u>CHAPTER 13</u>	- RECOMMENDATIONS FOR FURTHER RESEARCH.....	253
<u>CHAPTER 14</u>	- EXPLORATION CRITERIA AND APPROACH.....	255
APPENDIX A5	- Metaturbidite Petrography; Cleavage Morph- ology and Microstructure; Fry Analysis and Quartz vein Strain Data.....	257

APPENDIX A6 -	Quartz Vein Microstructure.....	305
APPENDIX A7 -	Kidney Pond Geological Cross-sections; Arsenopyrite Compositional Data.....	308
APPENDIX A8 -	Fluid Inclusion Morphology, Thermometric Data, and Bulk Volatile Analysis.....	328
APPENDIX A9 -	Geochemical Data; Sample Locations; Precision/Accuracy Analysis; Isogon Calc- culations; Sulphide Compositional Data...	344
APPENDIX A10 -	$^{40}\text{Ar}/^{39}\text{Ar}$ Step Heating Data; Biotite and Hornblende Compositional Data.....	394
RESUME.....		407
REFERENCES.....		412

## LIST OF FIGURES

Figure 1.1	Location of Gordon Lake within the North-west Territories.....2
Figure 2.1	Gold occurrences in the Yellowknife Basin...11
Figure 3.1	Geology of the Slave Province.....16
Figure 3.2	Geology of the Yellowknife Basin.....18
Figure 3.3	Stratigraphic column for the Yellowknife Supergroup.....20
Figure 3.4	Gold metallogeny of the Slave Province.....23
Figure 3.4	Rifting model for the evolution of the Yellowknife Basin (Henderson, 1985).....25
Figure 3.5	Division of the Slave Province into four structural domains (Kusky, 1989).....26
Figure 3.6	Accretion of the Slave Province (Kusky, 1989).....27
Figure 3.7	Tectonic evolution of the Slave Province by subduction along reactivated rifts (Fyson and Helmstaedt, 1988).....29
Figure 4.1	$D_0$ , $D_1$ , and re-fold structures of the Yellowknife Basin (Fyson, 1984b).....36
Figure 4.2	$D_2$ , $D_3$ and re-fold hinges of the Yellowknife Basin (Fyson, 1984b).....37
Figure 4.3	Sketch of $S_2/S_3$ fabric relationships (Fyson, 1984b).....39
Figure 5.1	Aerial photograph mosaic of the south end of Gordon Lake.....45
Figure 5.2	Structural and lithologic map of the south end of Gordon Lake.....46
Figure 5.3	Photographs of mesoscale structures.....47/48
Figure 5.4	Metamorphic map of the south end of Gordon Lake.....52
Figure 5.5	Photographs of metamorphic biotites and aggregates.....53/54



Figure 5.6	Distribution of syn-D <sub>3</sub> , multi-mineralic aggregates within the Gordon Lake region.....	56
Figure 5.7	Metamorphic mineral assemblages and structural events within the Gordon Lake region.....	58
Figure 5.8	Facing directions of F <sub>1</sub> fold closures across the Gordon Lake re-fold.....	62
Figure 5.9	Map of F <sub>1</sub> folds at Kidney Pond and comparison to a fault-propagation fold.....	63
Figure 5.10	Bedding, cleavage, and lineation data from the Gordon Lake re-fold.....	65/66/67
Figure 5.11	Sketch of cleavage relationships around the Gordon Lake re-fold.....	69
Figure 5.12	Quartz inclusion trails in biotite porphyroblasts from the west shore of Gordon Lake.....	70
Figure 5.13	Quartz inclusion trails in biotite porphyroblasts from the east shore of Gordon Lake.....	71
Figure 5.14	Block sketch of D <sub>3</sub> cleavage in graywacke with vertical stretch lineation.....	73
Figure 5.15	Photomicrographs of YZ, XZ, and XY sections of coarse- to medium-grained graywackes from the east and west limbs of the Gordon Lake re-fold.....	74/75
Figure 5.16	Photomicrographs of D <sub>4</sub> crenulation structures.....	77/78
Figure 5.17	Distribution and orientation of S <sub>4E</sub> crenulation.....	80
Figure 5.18	YZ and XZ strain ellipse axes of six samples across the Gordon Lake re-fold.....	83
Figure 5.19	Flinn Plot of strain fields for six samples across the Gordon Lake re-fold.....	85
Figure 5.20	Possible models for the time of formation of the Gordon Lake re-fold.....	92
Figure 6.1	The seven principal vein types of the Gordon Lake region.....	102

Figure 6.2	Photographs of quartz veins types.....	103/104
Figure 6.3	Sketches of quartz-breccia Types I, II, III, IV, and V.....	111
Figure 6.4	Photographs of quartz-breccia types....	113/114
Figure 6.5	Vein frequency versus time of emplacement.....	117
Figure 6.6	Schematic Mohr's circles illustrating vein formation and fracturing parallel $S_3s$ .....	120
Figure 6.7	Schematic diagram illustrating formation of the Type III quartz-breccias by repeated echelon fracturing.....	124
Figure 6.8	Schematic diagram showing the formation of Type III quartz-breccias as "dilatational jogs".....	126
Figure 7.1	Location of Kidney Pond quartz-breccias and other quartz-breccias within the Knight Bay claim block.....	129
Figure 7.2	Structural and general lithological location of the Kidney Pond quartz-breccia zones.....	131
Figure 7.3	Detailed structural and lithologic map of outcrop to the north of Kidney Pond Zone 1 quartz-breccia.....	132
Figure 7.4	Underground geological map of the Kidney Pond Zone 1 quartz-breccia.....	134
Figure 7.5	Lithological map of Kidney Pond Zone 1 as interpreted from drill hole data of Caelles (1984).....	135
Figure 7.6	Sub-surface maps of Zone 1 quartz-breccia at Kidney Pond as interpreted by Caelles (1984) and as interpreted by writer.....	136
Figure 7.7	Compilation geological map of Wooferine, Chane, T-11/T-2, and T-15 quartz-breccia zones of the Lynx area.....	138
Figure 7.8	Stratigraphic section and facies associations across Kidney Pond Zone 1 and 2 quartz-breccias.....	140

Figure 7.9	Depth of stratigraphic section across Kidney Pond Zone 1 and 2 quartz-breccias versus plots of average bed thickness, bed thickness variation, average grain size, and grain size variation.....	141
Figure 7.10	Paragenetic relationships between breccia matrix, sulphides, and gold deposition.....	142
Figure 7.11	Representative core samples displaying breccia mineralogy and fabric relation- ships.....	143
Figure 7.12	Microphotographs of quartz-breccia alter- ation mineralogy and gold.....	146/147
Figure 7.13	Polish thin section sketches of mineral- ized breccia samples from the Kidney Pond Zone 1.....	149
Figure 7.14	Pseudosecondary T-X plot of Kretschmar and Scott (1976) displaying arsenopyrite compositions as atomic percent arsenic versus temperature.....	153
Figure 8.1	Photomicrographs of quartz microstructure and fluid inclusion morphology from Gordon Lake veins and breccias.....	165/166
Figure 8.2	Sketches of fluid inclusion morphology and quartz microstructure.....	168
Figure 8.3	Photomicrographs of fluid inclusion types within Gordon Lake veins and breccias..	169/170
Figure 8.4	Frequency histograms for $T_h$ , $T_m(\text{ice/hy-}$ $\text{ha})$ , $T_e$ , and $T_m(\text{halite})$ for veins and breccias of the Gordon Lake region.....	173
Figure 8.5	Estimation of mole % of $\text{CH}_4$ from the final melting temperature of $\text{CO}_2(\text{S})$ and homogenization temperature of $\text{CO}_2(\text{L})$ and $\text{CO}_2(\text{V})$ from Heyen et al. (1982).....	176
Figure 8.6	Ternary $\text{NaCl-CaCl}_2\text{-H}_2\text{O}$ plots with approx- imate fields of breccia and vein salinity..	181
Figure 8.7	Homogenization temperature versus salin- ity plot for breccia and vein samples.....	182
Figure 8.8	Estimation of pressure correction from	

	phase diagram for water (25 wt.% NaCl) and arsenopyrite geothermometer.....	184
Figure 8.9	Comparison of homogenization temperature and salinity fields of this fluid inclu- sion study with others of the Yellowknife region.....	185
Figure 9.1	Log concentration plots of arsenic versus gold for graywackes, siltstones, quartz veins, and breccias.....	198
Figure 9.2	Plots of SiO <sub>2</sub> versus Na <sub>2</sub> O, CaO, K <sub>2</sub> O, Al <sub>2</sub> O <sub>3</sub> , TiO <sub>2</sub> , and MnO for graywackes and siltstone types.....	199
Figure 9.3	Plots of SiO <sub>2</sub> versus MgO, Fe <sub>2</sub> O <sub>3</sub> , P <sub>2</sub> O <sub>5</sub> , C, and, log S for graywackes and silt- stone types.....	200
Figure 9.4	Plots of SiO <sub>2</sub> versus log Au, log As, log Sb, Pb, Zn, and Cu for graywackes and siltstone types.....	201
Figure 9.5	Plots of SiO <sub>2</sub> versus Zr, Nb, Y, Ga, Cr, and V for graywackes and siltstone types.....	202
Figure 9.6	Plots of SiO <sub>2</sub> versus Ba, Ni, Sr, and Rb for graywackes and siltstone types.....	203
Figure 9.7	Isochon plot of sulphide-rich black silt- stones (adjacent to the quartz-breccia zones) versus dark grey/black siltstones (distal from the quartz-breccia zone).....	205
Figure 9.8	Major element data from graywackes of the Burwash Formation plotted on tectonic discrimination diagrams of Bhatia (1983)...	208
Figure 9.9	Trace element data from Gordon Lake gray- wackes and siltstones plotted on tectonic discrimination diagrams of Bhatia and Crook (1986).....	210
Figure 9.10	Trace element from other Archean cratons plotted on tectonic discrimination dia- grams (Bhatia and Crook, 1986, Figure 10)..	211
Figure 9.11	AFM diagrams from Jenner et al. (1981) and for Gordon Lake graywackes and silt- stones, Cameron River metavolcanics and	

	the Spud Lake granites.....	212
Figure 10.1	Some recent U-Pb zircon ages for the Slave Province and Yellowknife Basin.....	217
Figure 10.2	Location of U-Pb zircon ages within the Slave Province.....	218
Figure 10.3	Location of U-Pb zircon ages within the Yellowknife Basin.....	219
Figure 10.4	Locations and $^{40}\text{Ar}/^{39}\text{Ar}$ spectra for muscovite, hornblende, and biotite samples.....	221
Figure 10.5	Photomicrographs of dating samples displaying fabric and textural relationships.....	222/223
Figure 10.6	Photomicrographs of the separated material used for $^{40}\text{Ar}/^{39}\text{Ar}$ dating.....	225/226
Figure 10.7	Phlogopite-biotite diagram with the compositions of the quartz-breccia and metamorphic biotites.....	228
Figure 10.8	Plot of activation energy versus mole percent annite (Harrison et al. 1985).....	229
Figure 10.9	Geological events within the Yellowknife Basin and $^{40}\text{Ar}/^{39}\text{Ar}$ dates from Gordon Lake.....	231
Figure 11.1	Post-metamorphic ( $D_4$ ) deformation of the east limb of the Gordon Lake refold with accompanying fluid focussing and development of gold-bearing quartz-breccia zones..	243
Figure A5.1	Fry plot data for YZ section of graywacke sample 22/6/4.....	262
Figure A5.2	Fry plot data for XZ section of graywacke sample 22/6/4.....	263
Figure A5.3	Fry plot data for XY section of graywacke sample 22/6/4.....	264
Figure A5.4	Fry plot data for YZ section of siltstone sample 86-115.....	265
Figure A5.5	Fry plot data for XZ section of siltstone sample 86-115.....	266

Figure A5.6	Fry plot data for XY section of siltstone sample 86-115.....	267
Figure A5.7	Fry plot data for YZ section of graywacke sample 87-66.....	268
Figure A5.8	Fry plot data for XZ section of graywacke sample 87-66.....	269
Figure A5.9	Fry plot data for XY section of graywacke sample 87-66.....	270
Figure A5.10	Fry plot data for YZ section of graywacke sample 87-51.....	271
Figure A5.11	Fry plot data for XZ section of graywacke sample 87-51.....	272
Figure A5.12	Fry plot data for XY section of graywacke sample 87-51.....	273
Figure A5.13	Fry plot data for YZ section of graywacke sample 87-34b.....	274
Figure A5.14	Fry plot data for XZ section of graywacke sample 87-34b.....	275
Figure A5.15	Fry plot data for XY section of graywacke sample 87-34b.....	276
Figure A5.16	Fry plot data for YZ section of siltstone sample 86-78.....	277
Figure A5.17	Fry plot data for XZ section of siltstone sample 86-78.....	278
Figure A5.18	Fry plot data for XY section of siltstone sample 86-78.....	279
Figure A5.19	Field tracing of D <sub>4</sub> crenulated quartz from outcrop at location S6.....	280
Figure A5.20	Field tracing of D <sub>4</sub> crenulated quartz from outcrop at location S3.....	281
Figure A5.21	Field tracing of D <sub>4</sub> crenulated quartz from outcrop at location S2.....	282
Figure A5.22	Field tracing of D <sub>4</sub> crenulated quartz from outcrop at location S5.....	283

Figure A5.23	Location of D <sub>4</sub> crenulated quartz veins....	284
Figure A7.1	Geological cross-section across Kidney Pond Zone 1 from A1 - A1'.....	309
Figure A7.2	Geological cross-section across Kidney Pond Zone 1 from A -A'.....	310
Figure A7.3	Geological cross-section across Kidney Pond Zone 1 from B - B'.....	311
Figure A7.4	Geological cross-section across Kidney Pond Zone 1 from C -C'.....	312
Figure A7.5	Geological cross-section across Kidney Pond Zone 1 from D - D'.....	313
Figure A7.6	Geological cross-section across Kidney Pond Zone 1 from E - E'.....	314
Figure A7.7	Geological cross-section across Kidney Pond Zone 1 from F - F'.....	315
Figure A7.8	Geological cross-section across Kidney Pond Zone 1 from G - G'.....	316
Figure A7.9	Geological cross-section across Kidney Pond Zone 1 from H - H'.....	317
Figure A7.10	Geological cross-section across Kidney Pond Zone 1 from I'.....	318
Figure A7.11	Geological cross-section across Kidney Pond Zone 1 from J - J'.....	319
Figure A7.12	Geological cross-section across Kidney Pond Zone 1 from K - K'.....	320
Figure A7.13	Graph of At.% arsenic for the fine and coarse arsenopyrite from the Kidney Pond Zone 1 quartz-breccia.....	321
Figure A9.1	Geochemical sample location map of Gordon Lake for lithology types.....	345
Figure A9.2	Geochemical sample location map of Kidney Pond area for lithology types.....	346
Figure A9.3	Geochemical sample location map of Kidney Pond Zone 1 for lithology types....	347
Figure A9.4	Geochemical sample location for Cameron	

	River Volcanic Belt.....	348
Figure A9.5	Geochemical sample location map of Gordon Lake for quartz veins and breccias.....	349
Figure A9.6	Geochemical sample location map of Kidney Pond area for quartz veins.....	350
Figure A9.7	Geochemical sample location map of Kidney Pond Zone 1 for quartz-breccias....	351
Figure A9.8	Gold precision analysis from duplicates...	352
Figure A9.9	Inter-laboratory comparison of some trace elements.....	353





## LIST OF TABLES

Table 2.1	Grades and tonnages for gold deposits within the Slave Province and other Archean terranes.....8
Table 5.1	Structural nomenclature used in this thesis compared to that of Fyson.....43
Table 5.2	D <sub>3</sub> and D <sub>4</sub> cleavage nomenclature for the west and east limbs of the Gordon Lake refold.....60
Table 5.3	Possible models for the time of formation of the Gordon Lake refold.....93
Table 5.4	Deformation styles within metasedimentary supracrustal rocks and previously proposed tectonic models for the Slave Province.....96
Table 6.1	Quartz vein types and visual estimates of relative proportions.....101
Table 6.2	Quartz-breccia types and visual estimates of relative proportions.....110
Table 7.1	Constraints on the time of formation for the Type III strata-bound siltstone-hosted quartz-breccias.....151
Table 8.1	Some typical fluid inclusion data from other metaturbidite-hosted gold deposits...157
Table 8.2	Previously recognized fluid inclusion types within quartz veins hosted in metaturbidite of the Yellowknife Basin.....160
Table 8.3	Quartz veins and quartz-breccias selected for thermometric analysis.....163
Table 8.4	Bulk crushing/gas chromatography volatile analyses of fluid inclusions.....178
Table 9.1	Geochemical techniques and number of samples analyzed.....195
Table 10.1	Descriptions and locations of <sup>40</sup> Ar/ <sup>39</sup> Ar dating samples from the Gordon Lake.....215
Table A5.1	Petrographic and modal analysis of typical graywackes from the west limb of the Gordon Lake refold.....285

Table A5.2	Petrographic and modal analysis of typical siltstones from the west limb of the Gordon Lake refold.....	286
Table A5.3	Petrographic and modal analysis of typical graywackes from the east limb of the Gordon Lake refold.....	287
Table A5.4	Petrographic and modal analysis of typical siltstones from the east limb of the Gordon Lake refold.....	288
Table A5.5	D <sub>3</sub> cleavage morphology and microstructure in graywackes from the west limb of the Gordon Lake Refold.....	289
Table A5.6	D <sub>3</sub> cleavage morphology and microstructure in siltstones from the west limb of the Gordon Lake refold.....	290
Table A5.7	D <sub>3</sub> cleavage morphology and microstructure in graywackes from the east limb of the Gordon Lake refold.....	291
Table A5.8	D <sub>3</sub> cleavage morphology and microstructure in siltstones from the east limb of the Gordon Lake refold.....	292
Table A5.9	Crenulation cleavage (S <sub>4</sub> ) microstructure from the west limb of the Gordon Lake refold.....	293
Table A5.10	Crenulation cleavage (S <sub>4E</sub> ) microstructure from the centre and east limb of the Gordon Lake refold.....	294
Table A5.11	Petrographic analysis of metamorphic aggregates from siltstones of the south Gordon Lake region.....	295
Table A5.12	Petrography of quartz inclusions within biotite porphyroblasts from the west limb and Centre of the Gordon Lake refold.....	296
Table A5.13	Petrography of quartz inclusions within biotite porphyroblasts from the east limb of the Gordon Lake refold.....	297
Table A5.14	Petrography and microstructure of graywackes and siltstones analyzed by Fry technique.....	298

Table A5.15	Measured ellipse ratios from Fry analyzes and calculation of k value.....	299
Table A5.16	Measured ellipse ratios from Fry analyzes and calculation of k value.....	300
Table A5.17	Summary of measured and uncorrected ellipse data.....	301
Table A5.18	Summary of corrected ellipse data after applying matrix method of Shimamoto and Ikeda (1976).....	302
Table A5.19	Calculation of $D_4$ shear strains from deformed $S_{3S}$ -parallel veins.....	303
Table A5.20	Extensional and shortening data from deformed quartz veins.....	304
Table A6.1	Quartz microstructure of typical Bedding-parallel (Type 1), $D_3$ -deformed (Type 2), and Syn- $D_3$ veins.....	306
Table A6.2	Quartz microstructure of typical $S_{3S}$ -parallel (Type 3) and East Limb (Type 4) veins.....	307
Table A7.1	Gold Occurrences of the Knight Bay Property.....	322
Table A7.2	Compositions of fine needle-shaped arsenopyrite from the Kidney Pond Zone 1 quartz-breccia.....	323
Table A7.3	Compositions of fine needle-shaped arsenopyrite from the Kidney Pond Zone 1 quartz-breccia.....	324
Table A7.4	Compositions of coarse pyramidal arsenopyrite from the Kidney Pond Zone 1 quartz-breccia.....	325
Table A7.5	Summary of arsenopyrite compositional data and sample descriptions.....	326
Table A8.1	Fluid inclusion nomenclature used in this study, adapted from Roedder (1984).....	331
Table A8.2	Quartz microstructure and fluid inclusion morphology of veins from Gordon Lake.....	332

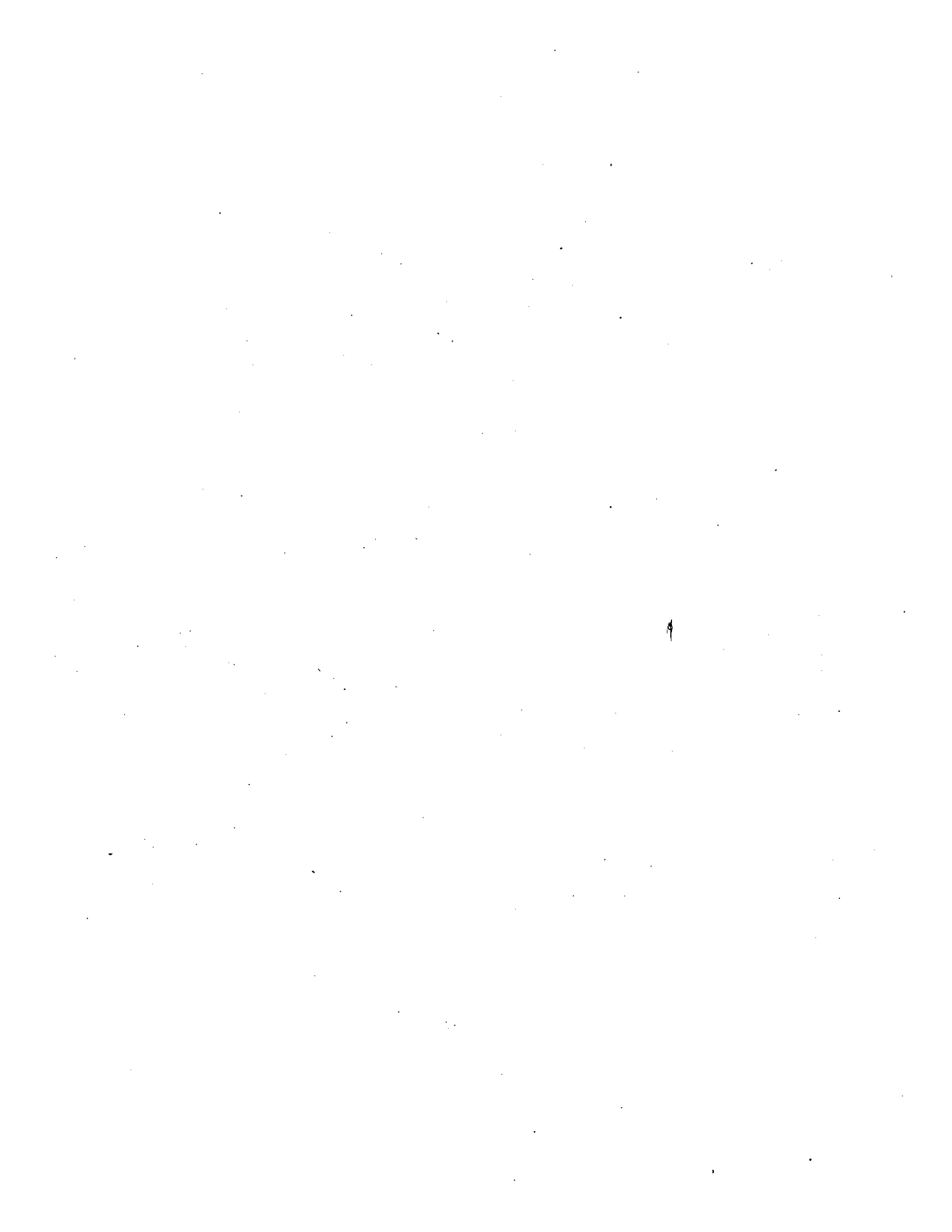
Table A8.3	Quartz microstructure and fluid inclusion morphology of Gordon Lake quartz-breccias..	333
Table A8.4	Fluid inclusion abundance and types in quartz veins from Gordon Lake.....	334
Table A8.5	Fluid inclusion abundance and types in quartz-breccias from Gordon Lake.....	335
Table A8.6	Fluid inclusion thermometric data for quartz-breccias.....	336
Table A8.7	Fluid inclusion thermometric data for quartz-breccias.....	337
Table A8.8	Fluid inclusion thermometric data for quartz-breccias.....	338
Table A8.9	Fluid inclusion thermometric data for quartz veins.....	339
Table A8.10	Fluid inclusion thermometric data for quartz veins.....	340
Table A8.11	Fluid inclusion thermometric data for quartz veins.....	341
Table A8.12	Temperature of homogenization and salinity data for quartz-breccias.....	342
Table A8.13	Temperature of homogenization and salinity data for quartz veins.....	343
Table A9.1	Duplicates: X.R.F. major and trace element data.....	354
Table A9.2	Standards: X.R.F. major and trace element data.....	355
Table A9.3	Graywackes: X.R.F. major and trace element data.....	356
Table A9.4	Light grey siltstones: X.R.F. major and trace element data.....	357
Table A9.5	Dark grey to black siltstones: X.R.F. major and trace element data.....	358
Table A9.6	Sulphide-rich black siltstones: X.R.F. major and trace element data.....	359
Table A9.7	Interbedded siltstones: X.R.F. major and	

	trace element data.....	360
Table A9.8	Bedding parallel, pre-D <sub>3</sub> and syn-D <sub>3</sub> quartz veins: X.R.F. major and trace element data.....	361
Table A9.9	S <sub>4</sub> -parallel, Rotated 'Z', and East Limb quartz veins: X.R.F. major and trace element data.....	362
Table A9.10	Quartz-breccias from the Lynx area and south Gordon Lake: X.R.F. major and trace element data.....	363
Table A9.11	Type III quartz-breccias from Kidney Pond Zone 1: X.R.F. major and trace element data.....	364
Table A9.12	Mafic dyke, Cameron River volcanics and Spud Lake granites: X.R.F. major and trace element data.....	365
Table A9.13	Duplicates: Neutron Activation trace element and gold data.....	366
Table A9.14	Standards: Neutron Activation trace element and gold data.....	367
Table A9.15	Graywackes: Neutron Activation trace element and gold data.....	368
Table A9.16	Light grey siltstones: Neutron Activation trace element and gold data.....	369
Table A9.17	Dark grey to black siltstones: Neutron Activation trace element and gold data.....	370
Table A9.18	Sulphide-rich black siltstones: Neutron Activation trace element and gold data.....	371
Table A9.19	Interbedded siltstones: Neutron Activation trace element and gold data.....	372
Table A9.20	Bedding parallel, pre-D <sub>3</sub> and syn-D <sub>3</sub> quartz veins: Neutron Activation trace element and gold data.....	373
Table A9.21	S <sub>4</sub> -parallel, Rotated 'Z', and East Limb quartz veins: Neutron Activation trace element and gold data.....	374
Table A9.22	Quartz-breccias from the Lynx area and	

	south Gordon Lake: Neutron Activation trace element and gold data.....	375
Table A9.23	Type III quartz-breccias from Kidney Pond Zone 1: Neutron Activation trace element and gold data.....	376
Table A9.24	Mafic dyke, Cameron River volcanics and Spud Lake granites: Neutron Activation trace element and gold data.....	377
Table A9.25	X.R.F major and trace element precision analysis.....	378
Table A9.26	X.R.F major and trace element precision analysis.....	379
Table A9.27	X.R.F major and trace element precision analysis.....	380
Table A9.28	X.R.F major and trace element precision analysis and breccia homogeneity test.....	381
Table A9.29	X.R.F major and trace element precision analysis of standards.....	382
Table A9.30	Neutron Activation gold and trace element precision analysis.....	383
Table A9.31	Neutron Activation gold and trace element precision analysis.....	384
Table A9.32	Neutron Activation gold and trace element precision analysis.....	385
Table A9.33	Neutron Activation gold and trace element precision analysis.....	386
Table A9.34	Neutron Activation gold and trace element precision analysis.....	387
Table A9.35	X.R.F. major and trace element accuracy analysis.....	388
Table A9.36	Neutron activation gold and trace element accuracy analysis.....	389
Table A9.37	Gold analysis of heavy/light separates from quarta breccias and veins.....	390
Table A9.38	Isochon data for X.R.F. major and trace elements.....	391

Table A9.39	Isochon data for Neutron Activation gold and trace elements.....	392
Table A9.40	Compositions of pyrrhotite, pyrite, and chalcopyrite from the Kidney Pond Zone 1 quartz-breccia.....	393
Table A10.1	Summary of step-heating data and calculation of average plateau age and error for hornblende (TS12-6-4).....	399
Table A10.2	Summary of step-heating data and calculation of average plateau age and error for muscovite (TS22-6-8).....	400
Table A10.3	Summary of step-heating data and calculation of average plateau age and error for quartz-breccia biotite (TS83-04).....	401
Table A10.4	Summary of step-heating data and calculation of average plateau age and error for metamorphic biotite (TS86-94).....	402
Table A10.5	Summary of step-heating data and calculation of average plateau age and error for metamorphic biotite (TS86-84).....	403
Table A10.6	Major oxide data for hornblende (TS12-6-4).....	404
Table A10.7	Major oxide data for quartz-breccia biotite (TS83-04) .....	405
Table A10.8	Major oxide data for uncrenulated metamorphic biotite (TS86-94) and crenulated metamorphic biotite (TS86-84).....	406





## ABSTRACT

Strata-bound, gold-bearing quartz-breccia zones at Gordon Lake, near Yellowknife, N.W.T., occur within carbon-rich siltstone beds of the Archean Burwash Formation, and are located within the hinge domain of a subvertical regional refold. Structural analysis indicates that although some quartz veining developed before peak metamorphism and formation of a regional cleavage ( $S_3$ ), more significant quartz veining, brecciation, and gold mineralization occurred later (late- $D_3$  to syn- $D_4$ ), concurrent with formation of a crenulation cleavage ( $S_4$ ) and counter-clockwise rotation of the east limb of the refold. Microfractures within the quartz-breccias have abundant fluid inclusions of high salinity (~ 25 wt% NaCl-CaCl<sub>2</sub>) and hydrocarbon concentration (e.g., CH<sub>4</sub> and C<sub>2</sub>H<sub>2</sub>). Gold in the quartz breccias occurs with arsenopyrite, pyrite, and pyrrhotite, and was probably emplaced at ca. 450 ± 40°C and a depth of 7-12 km. Hydrothermal alteration enriched the siltstone host in Au, As, Sb, (Br), S, K, Ca, and Na. The high C and low SiO<sub>2</sub> content of the host siltstone is probably a primary feature of the metasediments rather than a product of alteration. <sup>40</sup>Ar/<sup>39</sup>Ar dating of a metamorphic hornblende and a muscovite from a post-metamorphic pluton constrain the time of ( $D_3$ ) peak metamorphism to ca. 2600 Ma. A plateau age of 2573 ± 9 Ma for a biotite from the largest quartz-breccia zone gives a minimum age for mineralization, consistent with the late metamorphic timing of the brecciation event. The data are compatible with a genetic model that derives the gold and the fluids from the arc-related volcanoclastic metaturbidite pile, transports the gold as chloride complexes in a moderately saline (and oxidized?) fluid, and deposits the gold, quartz, and sulphides in hydraulically-induced brittle fractures within the reducing carbon-rich siltstones.



## ACKNOWLEDGEMENTS

I am indebted to numerous people who have assisted me throughout my time at Dalhousie, and who, if I miss by name, are nevertheless much appreciated<sup>for</sup> their help. In particular I must thank my supervisor Marcos Zentilli for his continuous support and enthusiasm for my project, especially in the later stages when both funding and moral support was needed the most. In addition, I am indebted to Nick Culshaw for field visits to Gordon Lake, his energetic and stimulating approach to unraveling the structures of region, and for his critical reviews of numerous drafts of Chapters 5, 6, and 7. I would like to thank Becky Jamison for her interest in my study and for her assistance in editing the first drafts of my thesis. I would also like to thank Peter Reynolds and his lab for "opening my eyes" to the world and problems of Ar-Ar dating. I would also like to thank Gordon Brown for his preparation of thin, polished, and fluid inclusion sections and for always helping in anyway possible.

Outside of Dalhousie I would like to thank Brendan Murphy of St Francis Xavier University for reading the thesis in its very early stages, (even though it almost gave him some grey hairs) and for his never doubting belief that I would finish sometime. In addition, I would like to thank Dan Kontak from the Nova Scotia Department of Mines and Energy for his advice in the fluid inclusion study, for reading sections of the thesis, and for always keeping me on my "academic toes".

This study would not have been possible without both funding from three Mineral Development Agreements (1987-88, 1988-89, and 1989-90) with the Government of the Northwest Territories and logistical support from the Geology Division of the Northwest Territories. In Yellowknife, I am indebted to Bill Padgham, John Brophy, and Bill Fyson

who always showed great interest in my study and visited me at various stages in the field. I am also greatly indebted to Giant Bay Resources, Burnaby, B.C., who knowingly or not, have contributed greatly to this study by allowing me access to their property, field camp, and boating equipment. Juan Caelles must be especially thanked for initiating this study in 1986 by providing a summer mapping project, which eventually developed into this thesis.

Without doubt the greatest debt I owe during this thesis is to my wife Joanne, who has supported me endlessly throughout the last five years, and without whom this study would have never been completed.

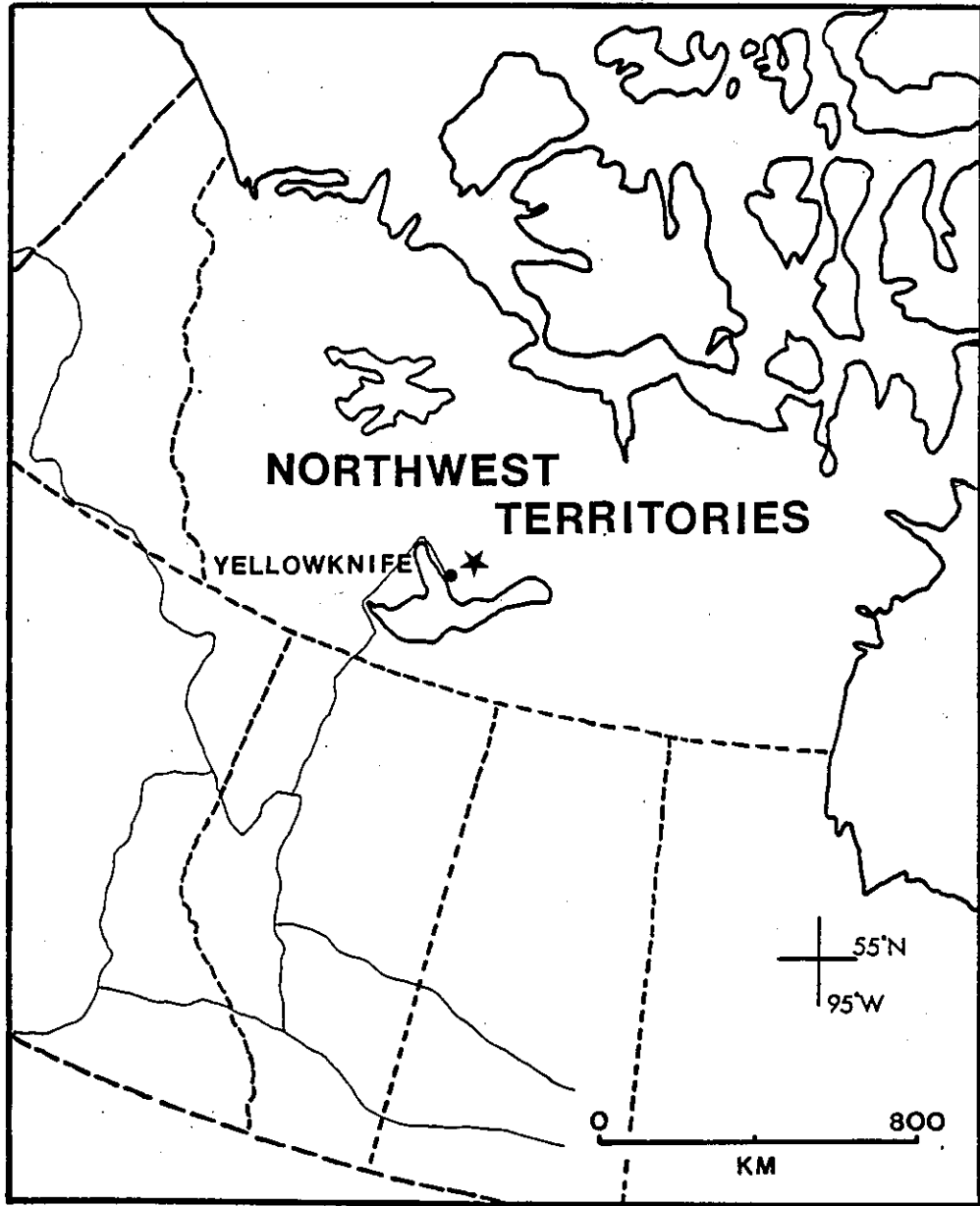
CHAPTER 1  
INTRODUCTION

1.1 GENERAL STATEMENT

Gold exploration and mineral deposit research within Archean greenstone terranes has primarily focussed on shear zones hosted within mafic-dominated metavolcanic belts (e.g., the Abitibi Volcanic Belt; Hodgson and Hamilton, 1989; Robert et al. 1989). Adjacent metasedimentary rocks within greenstone belts have generally been given less attention as exploration targets, except where iron formation sequences occur (e.g., Foster and Wilson, 1984; Groves et al. 1988). The Slave Province of north-western Canada is a typical example of an Archean terrane where exploration and mining for gold have concentrated on the mafic metavolcanic belts (e.g., the Yellowknife Volcanic Belt), with a more recent emphasis on iron formation-rich metasedimentary rocks (e.g., Conwoyto Lake region, Lhotka and Nesbitt, 1989). However, numerous gold-quartz vein occurrences also exist within the vast regions of metaturbidites that are devoid of iron formation (e.g., the Yellowknife Basin). Most of these gold occurrences have been ignored as potential targets for large economic gold deposits, as they are characterized by single veins or vein systems that are of small tonnage and erratic gold grade. Consequently these vein systems have received only minor attention in past geological studies and their controls and genesis are poorly constrained. Thus, leaving exploration geologists few criteria to work with other than locating quartz zones with anomalous gold values. This thesis attempts to demonstrate that the gold-quartz vein systems within the metaturbidites may, if better understood, provide excellent exploration targets.

The region studied in this thesis is located at the southern end of Gordon Lake (Figure 1.1), where a variant

Figure 1.1 Location of Gordon Lake field area (star) within the Northwest Territories.



of metaturbidite-hosted gold deposit was discovered (ca. 1983, Padgham, 1986), in an area of known gold-quartz vein concentration (Henderson, 1985). This new deposit type, originally classified as gold bearing "quartz-stockworks" (Padgham, 1984, 1986), was later termed "zones (or bodies) of quartz veining and brecciation" (Caelles 1984, 1985, 1987a, 1987b; Burston and Caelles, 1986). It is from this term that the phrase "quartz-breccia zone" is derived (and subsequently used throughout this thesis), as it better describes the geometrical relationship between the quartz and host material (Chapters 6 and 7). At present, these quartz-breccia zones are only known to occur in the Gordon Lake region of the Yellowknife Basin. The fundamental advantages of exploring and mining for these gold-bearing quartz-breccia zones (compared to single and multiple vein systems) are their potential for larger tonnages, greater mineable widths, and more homogeneous gold distribution. An additional consideration is that, as the quartz-breccia zones are confined to a specific region they are more readily adaptable for economic mineral extraction (i.e., by a series of small mines and one centralized mill).

## 1.2 AIMS AND OBJECTIVES OF THESIS

The primary aims of this thesis are to determine the geological controls of the gold bearing quartz-breccia zones and to explain their apparent concentration at the southern end of Gordon Lake. This thesis includes: 1) a detailed study of the structural, lithological, and temporal controls of the quartz-brecciation; 2) mapping of regional structures to investigate their relationship to the quartz-breccia zones; and 3) an examination of the possible physico-chemical conditions during brecciation and gold deposition. From this work it is possible to provide constraints for a regional genetic model for the evolution of the quartz-breccias. Finally, practical exploration



criteria are suggested that might assist in the location of similar deposits within the Yellowknife Basin, and in other metasedimentary terranes worldwide.

In an attempt to place these gold deposits into a regional context, this thesis also addresses other geological problems including: 1) the structural development of a critical 'refold' region within the Yellowknife Basin; 2) the mechanisms of vein formation and their relationship to structural and metamorphic processes; 3) the timing of metamorphism, mineralization, volcanism, and granite emplacement; and 4) the overall structural evolution of the Gordon Lake region in terms of previous tectonic models suggested for the Slave Province.

### 1.3 THESIS APPROACH

Field mapping for this thesis was carried out in the summers of 1986, 1987, 1988. During this time approximately 600 samples were collected for structural, mineralogical, and lithochemical studies. This project was planned as a field-oriented study, and it is primarily from this that the model for the formation the quartz-breccia zones is developed (Chapters 5, 6, and 7). Laboratory techniques such as fluid inclusions, geochemistry, and  $^{40}\text{Ar}/^{39}\text{Ar}$  dating were used to further test and constrain this model (Chapters 8, 9, and 10 respectively).

### 1.4 MODEL PHILOSOPHY AND EXPLORATION CRITERIA

The principal purpose of any ore deposit model is that it should successfully predict, using exploration criteria, where other similar deposits may be located. These exploration criteria are defined as specific geological features that show a spatial and temporal relationship to mineralization (Hodgson and Troop, 1988); with the type of criteria depending on the scale of the search (i.e., from regional reconnaissance to prospects

within a mining camp). The criteria determined can be developed from either genetic or empirical models (Ohle and Bates 1981; Hodgson and Troop 1988). Genetic models require the documentation of known deposits and camp geology, the interpretation of geological data into a working model, and the use of this model to predict other occurrences. The empirical approach includes the documentation of features and characteristics of all known deposits in a region, statistical correlation and evaluation of these data, and finally a rating of the most favourable features to define exploration criteria. Both approaches have distinct advantages and disadvantages. The genetic models use all available data but the result is influenced by the smaller number of occurrences studied. On the other hand, empirical models use a broad and quantified data base, but much of the data are left unused. In this thesis, the quartz-breccia zones at Gordon Lake were investigated using a genetic model approach, as only limited data is available on gold-vein occurrences within the region and as the quartz-breccias are a new variant of metaturbidite-hosted gold deposit.

## CHAPTER 2

### METATURBIDITE-HOSTED GOLD DEPOSITS WITH PARTICULAR REFERENCE TO THE SLAVE PROVINCE

#### 2.1 DEFINITION AND CHARACTER

Metaturbidite-hosted gold deposits (MHGD) are defined as economic, extractable zones of gold mineralization within quartz vein systems that are hosted by sedimentary sequences (including shales, siltstones, sandstones, and graywackes) of marine origin (Boyle, 1986). These sequences have commonly undergone complex deformation, metamorphism, and intrusion. Differences in the host sequences include the presence or absence of interbedded volcanic rocks, black sulphide-rich shales, carbonates, and iron formation.

The gold-quartz systems hosted by metaturbidites can occur in a variety of vein styles - single veins, echelon vein swarms, stockworks, or localized breccia pods. Typically, these vein systems occur parallel to bedding, crosscut bedding, develop in the hinge regions of folds (saddle-reefs) and along faults/ductile shear zones, or follow earlier formed anisotropies (e.g., cleavages). The style of vein system depends on the type and timing of structural and metamorphic events, in addition to the host lithology and stratigraphy.

Vein systems in MHGD are mineralogically simple, with the main gangue mineral being quartz of various types (e.g., glassy, white, grey, black, massive, and fibrous). Other non-metallic gangue minerals include carbonates, feldspars, micas, and chlorites, whereas metallic minerals include arsenopyrite, pyrite, pyrrhotite, and more rarely galena, chalcopyrite, sphalerite, and gold (Boyle, 1986). Wall rock alteration is generally minimal and the effects extend only 1-5 m from the quartz vein systems. Wall rock alteration types include, in order of decreasing

abundance, silicification, chloritization, sericitization, and carbonatization (Boyle, 1986).

## 2.2 METALLOGENIC DISTRIBUTION

MHGD are distributed worldwide and range in age from Archean to Tertiary. Abundant MHGD occur within the Cambrian-Ordovician flysch, including the Meguma Group, Nova Scotia (Graves and Zentilli, 1982; Henderson, 1983; Smith et al. 1985; Mawer, 1987; Kontak et al. 1990), the Ballarat Slate Belt, N.S.W., Australia (Glasson and Keays, 1978; Sandiford and Keays, 1986), the Northern Belt of the Southern Uplands, Great Britain (Steed and Morris, 1986), and the Carolina Slate Belt (Bell, 1986; Hardy, 1989). Younger MHGD include those hosted in the volcanic-rich Cretaceous Valdez Group, Alaska (Goldfarb et al. 1986; Read and Meinert, 1986) and the Carboniferous-Jurassic Otago schist of New Zealand (Henley et al. 1976; Paterson, 1986).

Within Archean greenstone terranes MHGD occur in a variety of environments. Deposits associated with iron formation are found in the Brazilian Shield (Gair, 1962), Western Australia (Groves et al. 1988), South Dakota, U.S.A. (Sawkins and Rye, 1974), Zimbabwe (Foster and Wilson 1984; Foster et al. 1986), and the Slave Province (Gibbins, 1981; Lhotka and Nesbitt, 1989). Examples of deposits in Archean metasedimentary rocks lacking iron formation include the Timiskaming Group of the Superior Province (Hodgson and MacGeehan, 1982; Kerrich and Watson, 1984), and the Burwash Formation in the Yellowknife Basin (Padgham, 1986). One important variant of Archean gold deposits hosted in metasedimentary rocks is found at Hemlo, north of Lake Superior (Patterson, 1984; Burk et al. 1986; Kuhns et al. 1986). Though not a true lode MHGD, because most of the gold is disseminated within the metasedimentary and volcanic sequences, it is significant due to its size (Table 2.1).

Table 2.1 Grades and tonnages for gold deposits within the Slave Province and other Archean terranes.

Deposit/ Location	Type/Host Rock	Size/Reserves (1000 tonnes)	Average Grade (g/t)	
SLAVE PROVINCE				
Giant Mine, Yellowknife	shear zones in metavolcanics	2,665	8.8	1
Nerco-Con Yellowknife	shear zones in metavolcanics	2,765	10.2	1
Ptarmigan, Yellowknife	quartz veins in metaturbidites	250	11.0	1
Lupin, Contwoyto	banded iron formation	3,572	10.8	1
Kidney Pond Gordon Lake	quartz-breccia in metaturbidites	127	11.0	2
Camlaren Gordon Lake	quartz-veins in metaturbidites	59	17.1	3
Thompson- Ludmark	quartz-veins in metaturbidites	121	18.0	3
-----				
OTHER				
Sigma Mine Abitibi	shear zones/veins in metavolcanics	5,000	4.7	4
Hemlo Deposits	disseminated in metasediments/ metavolcanics	76,000	8.2	5
Golden Mile Kalgoorlie	shear zones/veins in metavolcanics	(1200 tonnes of gold, produced as of 1987) 6		

- 1 Ellis (1989)  
 2 Burston and Caelles (1986)  
 3 Padgham (1984)  
 4 Robert et al. (1989)  
 5 Nisbet (1989)  
 6 Boulter et al. (1987)

### 2.3 GOLD OCCURRENCES WITHIN THE SLAVE PROVINCE

Gold mining and exploration within the Slave Province of the Northwest Territories have proceeded almost continuously since the early 1930's. The first gold was mined in the region in 1935 from the Rich property, a small MHGD on the east shore of Yellowknife Bay. In 1936 gold was found within altered mafic volcanic rocks at Yellowknife, and by 1938 the Con Mine was in production, and still is today, together with the Giant Mine. Until the early 1980's the major gold producers within the Slave were Archean volcanic-hosted lode gold deposits (AVHLGD). However, the iron formation-hosted gold deposits found at Contwoyto and Cullaton Lakes (e.g. the Lupin Mine, Kerswill et al. 1983; Kerswill, 1984, 1986) are now the most important producers in the N.W.T. The Lupin Mine accounted for 55% (or 6050 kg) of the gold produced in the N.W.T. in 1988 (Ellis, 1988).

Padgham (1984) classified gold deposits within the N.W.T. into six categories that include:

- 1) shear zones in volcanic rocks
- 2) quartz veins along sedimentary-volcanic rocks contacts
- 3) quartz veins in metaturbidites (lacking iron formation)
- 4) quartz veins in iron formation
- 5) paleo-placers
- 6) Quaternary placers

The MHGD (categories 3 and 4) account for 273 out of the 560 gold showings and deposits within the Slave Province (Padgham, 1986). Of these 11 occur in shear zones, 94 in iron formation and 168 as "epigenetic" gold-quartz veins in metaturbidites lacking iron formation (Padgham, 1984). This thesis is primarily concerned with the latter group. Padgham (1986) classified these "epigenetic" gold-quartz vein systems into three types:

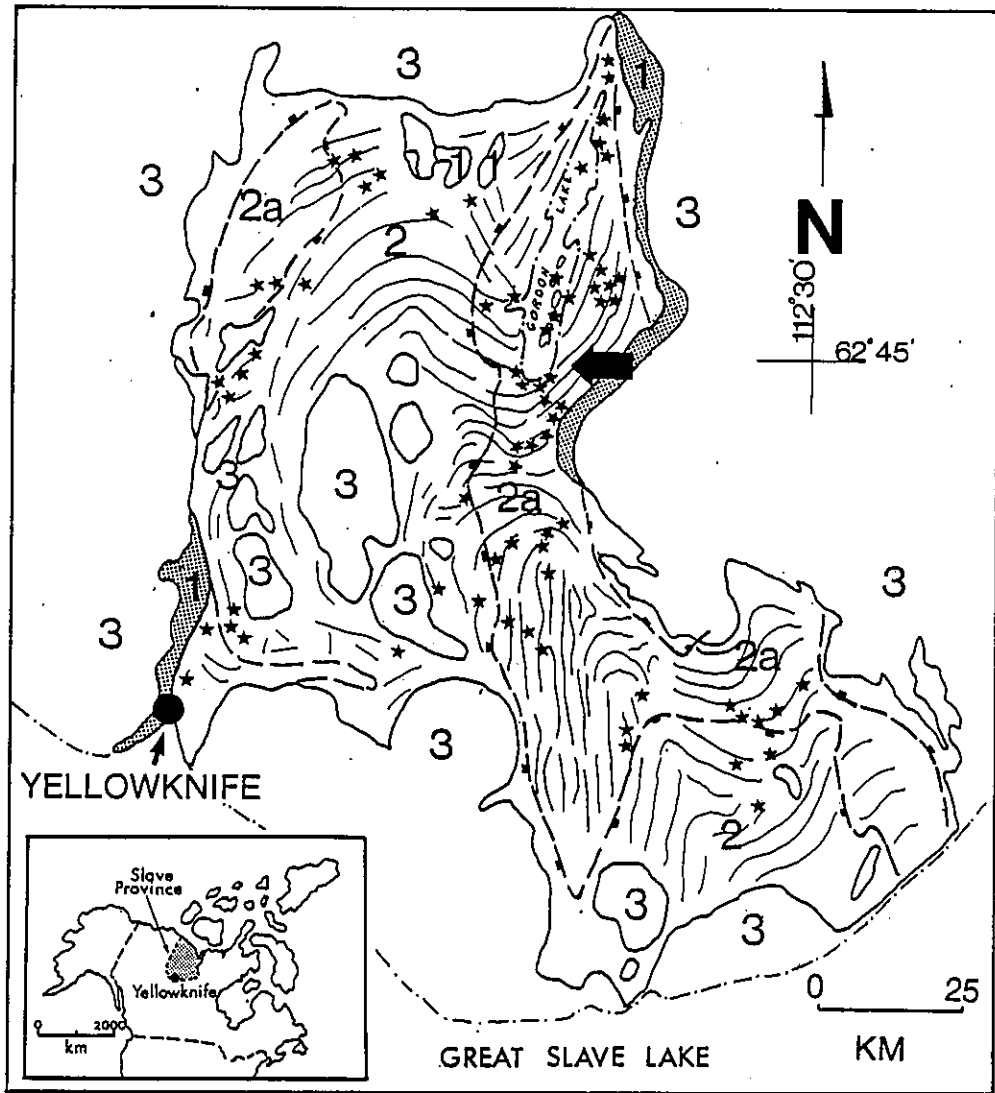
- 1) vein deposits (<1 million tonnes) proximal to sedimentary-volcanic rocks contacts; e.g., the Salmita, Tundra, and Discovery Mines (Tremblay, 1952; Wiwchar, 1957; Ransom and Robb, 1986).
- 2) narrow, erratically mineralized veins in distal metaturbidites, such as the Ptarmigan Mine (Boyle, 1961, 1979; Brophy, 1987b), Camlaren Mine (Wiwchar, 1957), Thompson-Lundmark Mine (Lord, 1951).
- 3) quartz stockworks in distal turbidites, such as the Giant Bay property on Gordon Lake (Caelles, 1984, 1985; Burston and Caelles, 1986; Chapter 7).

Approximately 80% of the 168 gold-quartz vein systems in metaturbidites (lacking iron formation) occur within the Yellowknife Basin (Figure 2.1; Padgham, 1986). Tables with typical grades and tonnages for these vein systems are found in Padgham (1984, 1986). Compared to Archean lode deposits these gold-quartz vein systems are usually smaller in tonnage, but can be richer in grade (Table 2.1).

#### 2.4 PREVIOUS STUDIES ON GOLD MINERALIZATION WITHIN THE YELLOWKNIFE BASIN

Research on gold mineralization within the Yellowknife Basin has concentrated on the origin and structure of the AVHLGD found at Yellowknife (e.g., Boyle, 1961; Henderson and Brown, 1966; Kerrich and Allison, 1978; Kerrich, 1981; Henderson, 1981, 1985; Helmstaedt and Padgham, 1986a, 1986b; and references within). Most authors agree that the shear zones formed as thrusts associated with lateral shortening during emplacement of a nearby granitoid complex. Stable isotope and geochemical studies (Boyle, 1961, 1979; Kerrich, 1981; Kerrich and Fyfe, 1988) indicate that mineralizing fluids were probably

Figure 2.1 Geology and structure of the Yellowknife Basin, with the location of Gordon Lake and the distribution of gold-quartz vein occurrences (adapted from Padgham, 1986 and Fyson, 1984b).



- |    |                            |                                |
|----|----------------------------|--------------------------------|
| 1  | Metavolcanic rocks         |                                |
| 2a | Greenschist metaturbidites | ~                              |
| 2  | Amphibolite metaturbidites | 2<br>~<br>2a                   |
| 3  | Granitoids                 | * Gold-quartz vein occurrences |



derived by metamorphic devolatilization and were focussed into the evolving shear systems. However, Helmstaedt and Padgham (1986b) contended that the close spatial association of felsic porphyries with the gold-bearing shear zones indicates that gold was deposited from hydrothermal systems related to the early felsic phases of the granitoid complex.

Geological studies (other than detailed mapping) of MHGD of the Yellowknife Basin are limited in number. However, they do include the geochemical, fluid inclusion, and stable isotope investigations of Boyle (1961, 1979), Ramsay (1973), English (1981), Brophy (1987a), and Swatton (1987). These studies are discussed in Chapters 8, 9, and 11.

## 2.5 PROPOSED GENETIC MODELS FOR THE FORMATION OF METATURBIDITE-HOSTED GOLD DEPOSITS

Genetic models for the formation of MHGD have been debated for over a century (Boyle, 1986, 1987). However, the development of any genetic model for the formation of the gold bearing quartz-breccias at Gordon Lake must take into consideration four fundamental parameters: 1) the source of mineralizing fluids; 2) the physical and chemical mechanisms of fluid migration and transport of ore components; 3) the trapping, concentration, and precipitation of vein constituents; and 4) post-ore modification and preservation. The characteristics of most of these processes are still hotly debated. Some of the possible options for each of the four parameters are listed below:

### 1. POSSIBLE SOURCES OF MINERALIZING FLUID

- (i) Magmatic: Colvine et al. (1984), Newton et al. (1980), Cameron (1988), Burrows et al. (1986), Spooner et al. (1988).

(ii) Metamorphic: Kerrich and Fyfe (1987), Read and Meinert (1986), Glasson and Keays (1978), Paterson (1986).

(iii) Exhalative: Haynes (1986), Hutchinson and Burlington (1984).

#### 2a. PHYSICAL TRANSPORT OF GOLD-BEARING FLUIDS

(i) Lateral Secretion: Boyle (1961).

(ii) Single-Pass Flow: Yardley (1987).

(iii) Multi-Pass Flow: Etheridge (1983)

(iv) Hydraulic Fracturing: Phillips (1972, 1986).

(v) Shear Zone Focussing: Kerrich and Fyfe (1987); Boulter et al. (1987).

(vi) Migration and Trapping between Permeable and Impermeable Layers: Mawer (1987).

(vii) Migration along Cleavage Planes: Glasson and Keays (1978).

#### 2b. CHEMICAL TRANSPORT OF GOLD IN HYDROTHERMAL FLUIDS

(i) Thio-Sulphide Complexes: Romberger (1988); Seward (1973, 1982)

(ii) Chloro-Complexes: Henley (1973)

(iii) Thio-Arsenide Complexes: Grigoryeva and Sukeva (1981).

#### 3. GOLD TRAPPING, CONCENTRATION, AND PRECIPITATION

(i) Change in Thermal Gradient from high to lower temperatures: (Groves et al. 1987)

(ii) Rapid Decompression and/or change in fluid pressure conditions during hydraulic fracturing: (Kennedy, 1950; Gretener, 1981; Sibson, 1987)

(iii) Immiscibility with the exsolution of a CO<sub>2</sub> vapour phase: (Bowers and Helgeson, 1983; Pichavant et al., 1983)

(iv) Changes in pH and Oxygen fugacity: (Romberger,

1988)

(v) Wall rock Interaction: (Kerrick et al. 1977;  
Bottrell et al. 1988)

4. POST-ORE MODIFICATION AND PRESERVATION

(i) Time of Emplacement: Pre-, syn- or post-regional  
and/or contact metamorphism.

(ii) Remobilization: e.g., Infiltration of meteoric  
waters.

(iii) Uplift and Erosion Rates

(iv) Glacial Effects

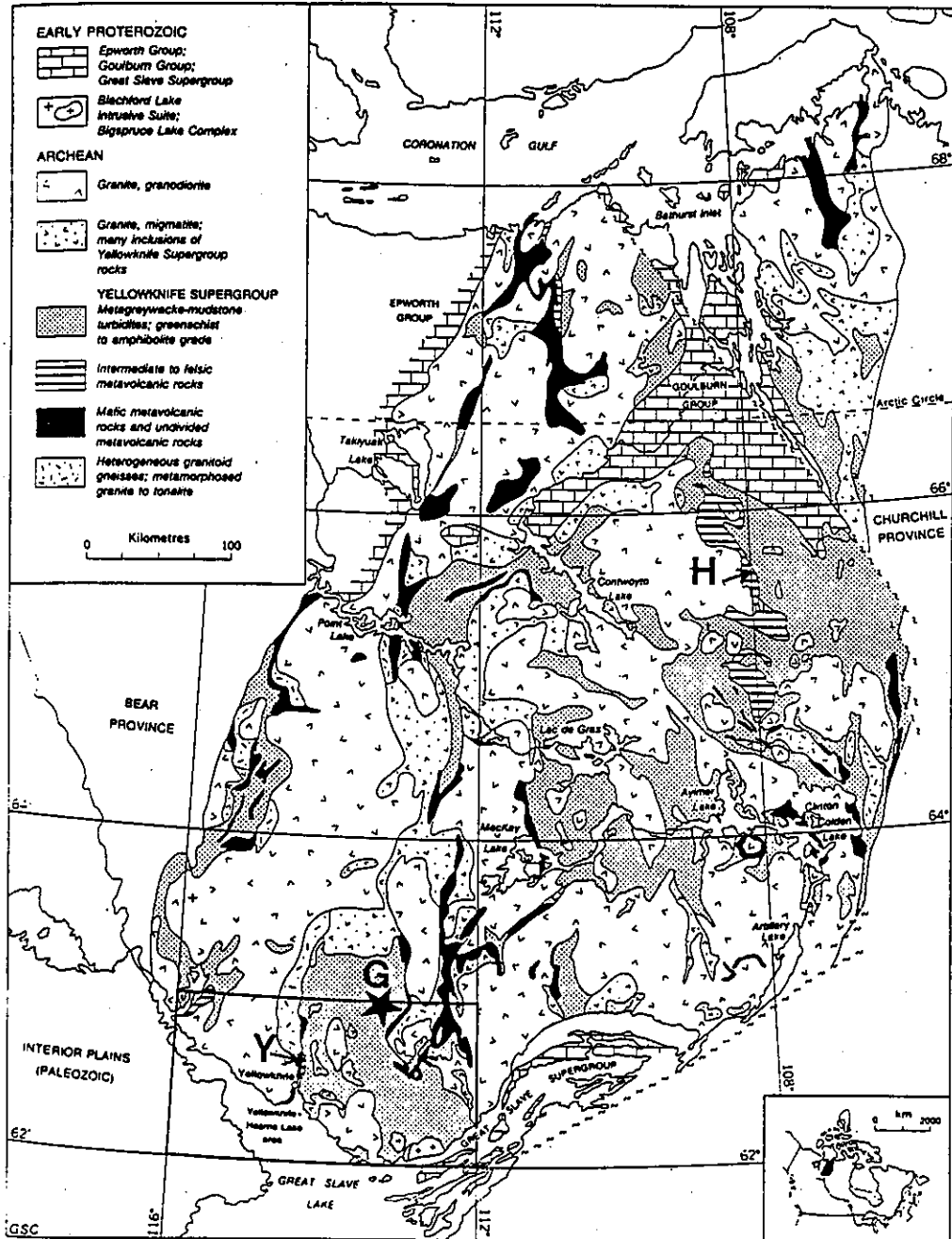
CHAPTER 3  
GEOLOGY OF THE SLAVE PROVINCE

3.1 INTRODUCTION

The Slave Structural Province, located in the north-western part of the Canadian Shield, is an Archean granite-greenstone craton that covers an area of approximately 200,000 km<sup>2</sup> (Figure 3.1). The Slave Province has been an essentially stable craton for 2500 Ma, with the exception of minor Proterozoic deformation and mafic dyke intrusion (Henderson, 1985). The Slave Province is unconformably overlain to the west by Proterozoic rocks of the Bear Province (Hoffman, 1980) and to the east is separated from the Proterozoic Churchill Province by the Thelon suture (Thompson and Henderson, 1983). Surface outcrop of Slave Province comprises: 5% granite-gneiss basement (2800-3500 Ma), 50% supracrustal metavolcanic and metasedimentary rocks of the Yellowknife Supergroup (2600-2700 Ma), and 45% younger granitoid complexes (2500-2600 Ma). The basement rocks are overlain by the supracrustal rocks that form oval domains of metasedimentary rock, bounded by linear metavolcanic belts. The basement and supracrustal rocks are both intruded by the younger granitoids.

The Slave Province differs from most other Archean terranes in that it has relatively young greenstone belts (2600-2700 Ma), lacks komatiitic flows within the mafic volcanic sequences, and has greater surface exposure of metasedimentary rocks compared to metavolcanic rocks (5:1) within the greenstone belts. This greater proportion of metasedimentary rocks has been attributed to a shallow erosion level (McGlynn and Henderson, 1970) and/or deposition of sediments on a thick sialic plate that was less susceptible to subduction during tectonic movement (Padgham, 1987).

Figure 3.1 Geology of the Slave Province, taken from Henderson (1985, Figure 1), with the location of Gordon Lake (G), the Yellowknife Volcanic Belt (Y), and the Hackett River Volcanic Belt (H).



### 3.2 GRANITE-GNEISS BASEMENT

The basement rocks include complex assemblages of tonalitic and trondhjemitic material, with localized zones of orthogneiss, migmatitic gneiss, and granodiorite (Padgham, 1985). The best mapped areas of basement include Point Lake, part of the Anton Complex (Figure 3.2; Easton, 1985), and the Sleepy Dragon Complex (Davidson, 1972; Baragar and McGlynn, 1976; Henderson, 1985). Typical U-Pb zircon dates from these gneisses give an age of  $3155 \pm 3$  Ma at Point Lake (Krogh and Gibbins, 1978) and  $2819 +40/-31$  Ma for the Sleepy Dragon Terrane (Henderson et al. 1987; Chapter 10).

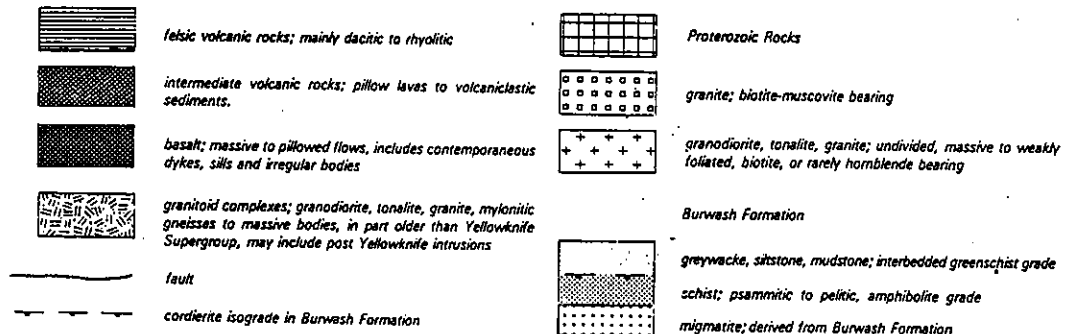
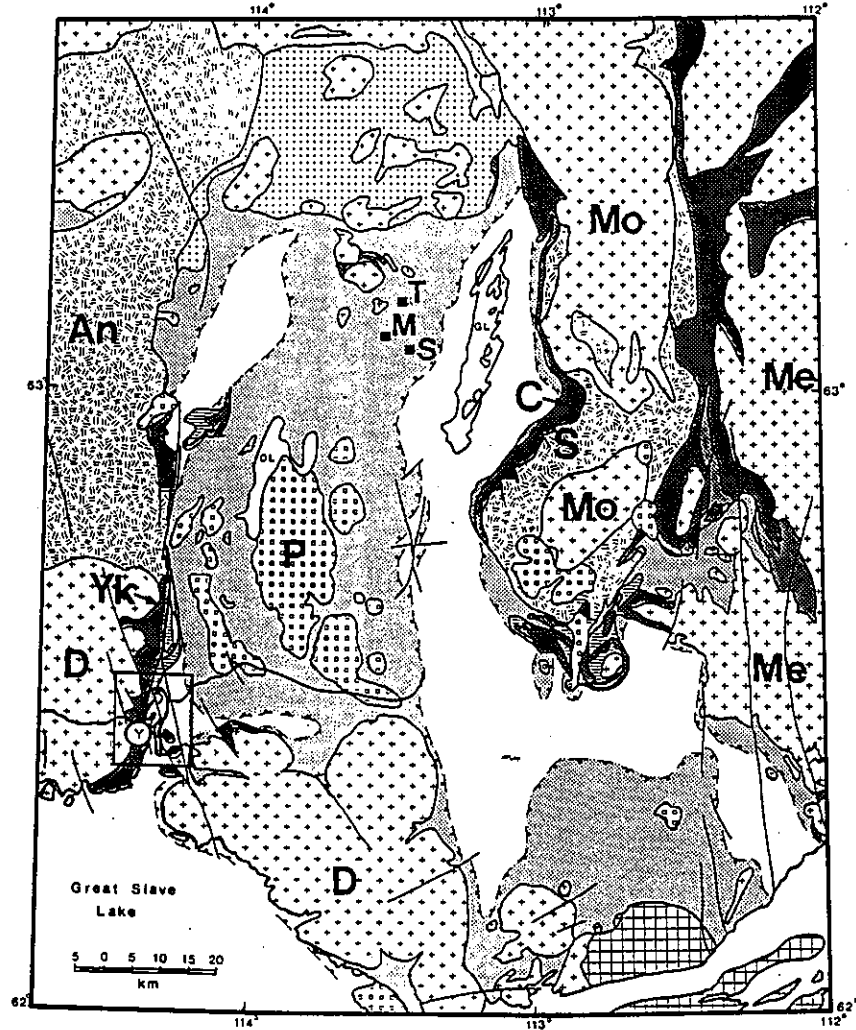
### 3.3 SUPRACRUSTAL SEQUENCES

The supracrustal sequences that make up the Yellowknife Supergroup are composed of approximately 15-20% volcanic rocks, which form nineteen rectilinear belts along the margins of the larger metasedimentary (predominantly metaturbidite) domains<sup>1</sup>, of which the Yellowknife Basin is the best known. The metavolcanic belts occur as two distinct types (Padgham, 1985) - the Yellowknife type (a thick tholeiitic basalt base capped by thinner layers of felsic material), and the Hackett River type (thick felsic flows covered by a thin sequence of basalts). The Yellowknife type is most abundant in the west and southern parts of the Slave, where the Yellowknife Volcanic Belt is the type section (Figure 3.1). The Hackett River type, dominant in the north-eastern part of the Slave Province (Figure 3.1), is characterized by pyroclastic rocks and flows of rhyolitic to basaltic composition (Lambert, 1978; Padgham, 1985).

---

<sup>1</sup>. The term "metasedimentary domain" of Fyson (1984, 1987) is preferred over "sedimentary basins" of Henderson (1981, 1985), as the latter has misleading genetic connotations. However, for the sake of simplicity, the commonly applied term "Yellowknife Basin" is used here to describe a geographical, rather than a geological region of the Slave Province.

Figure 3.2 Detailed geology of the Yellowknife Basin taken from Henderson (1987, Figure 1-1). Basement rocks: Anton Complex (An) and Sleepy Dragon Complex (S). Volcanic rocks: Yellowknife Volcanic Belt (Yk) and Cameron River Volcanic Belt (C). Late granitoids: Defeat Plutonic Suite (D), Meander Lake Plutonic Suite (Me), Prosperous Granite suite (P), and Morose Granite Suite (Mo). The Awry and Stagg Plutonic Suites are located 30-40 Km west of Yellowknife. Minor late granites west of Gordon Lake include: Mac Lake (M), Spud Lake (S), and Thistlewaite Lake (T).



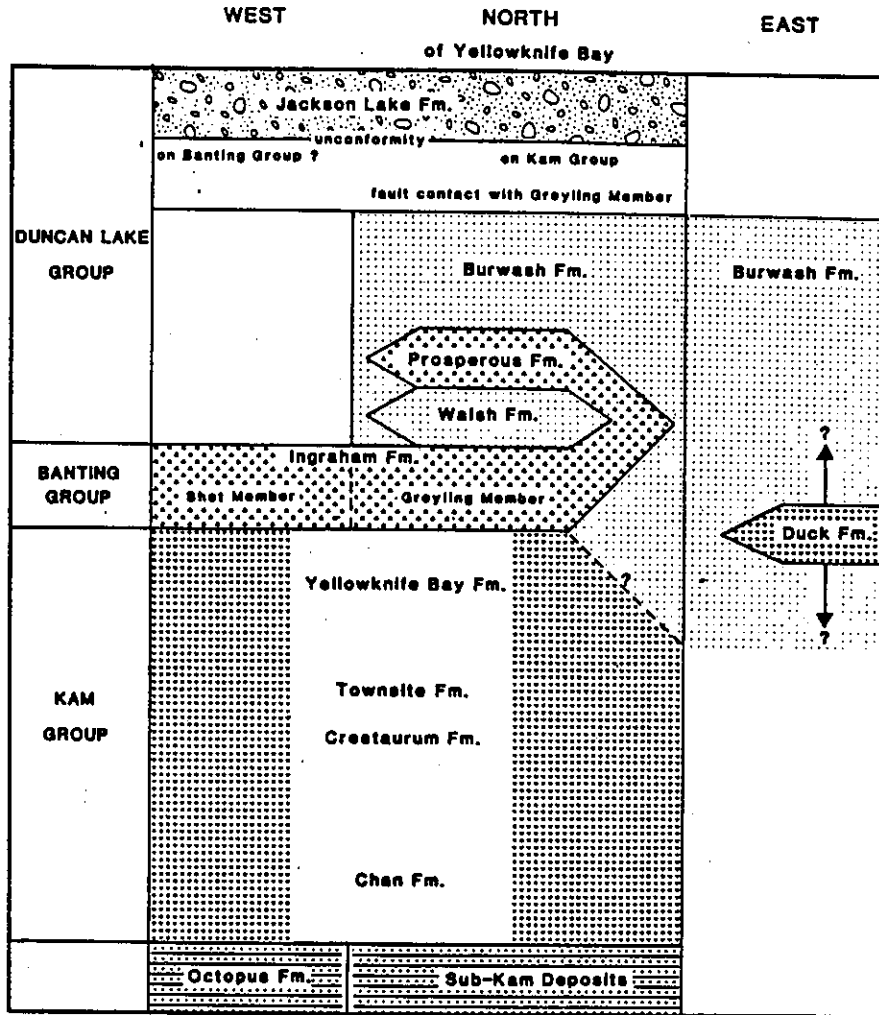
Most of the metasedimentary rocks of the Yellowknife Supergroup are monotonous graywacke-siltstone turbidite sequences, indicative of submarine fan deposition (Henderson, 1985). However, some of these turbidite sequences contain iron formation; i.e., the Contwoyto Formation of the Point Lake - Contwoyto Lake region (Bostock, 1980). The metaturbidites have primarily been studied in the Yellowknife region (Henderson, 1972, 1975, 1987), but also in other parts of the Slave Province (Padgham, 1985; Bostock, 1980; Henderson and Easton, 1977). The metaturbidites in general overlie and interfinger with the volcanic rocks, but in some cases these contacts are faulted (Henderson, 1985). Along some of these contacts, stratigraphically equivalent, coarser conglomerate and sandstone sediments of fluvial origin occur (Henderson, 1981, 1985). However, recent work by Helmstaedt and Padgham (1986a) indicate that some of these coarse metasedimentary rocks, such as the Jackson Lake Formation, are probably younger than the metaturbidites.

#### 3.4 THE YELLOWKNIFE VOLCANIC BELT

The Yellowknife Volcanic Belt, on the western edge of the Yellowknife Basin (Figure 3.2), is one of the best studied regions in the N.W.T. and has played an important role in the development the Yellowknife Supergroup stratigraphy and tectonic models for the Slave Province. Rocks of the Yellowknife Volcanic Belt interfinger with and are in part overlain by the metaturbidites of the Burwash Formation. The stratigraphic relationships across the Yellowknife Volcanic Belt are summarized in Figure 3.3 (Helmstaedt and Padgham, 1986a). The lower part of the belt is comprised of the Kam Group; a 10 km-thick sequence of mafic volcanic rocks with a gabbro-dyked base that grades upwards into massive and pillowed basaltic flows. The Kam Group is overlain by the Banting Group; a 1-2 km-



Figure 3.3 Stratigraphic Column of the Yellowknife Supergroup from Padgham and Helmstaedt (1986a, Figure 4). The light stipple represents metasediments of Burwash and Walsh Formations, the light stipple with boulder symbols conglomerates of the Jackson Lake Formation, and heavy stipple metavolcanics of the Banting and Kam Groups.



thick sequence of calc-alkaline volcanic rocks, including ash flow tuffs and pillow breccias.

### 3.5 LATE GRANITOIDS

Both the basement and supracrustal rocks are intruded by various (2500-2600 Ma) granitoid rocks including: 1) sub-volcanic stocks, dykes, and sills associated with mafic to felsic volcanism; 2) syntectonic to late tectonic, mesozonal tonalite-granodiorite batholiths; and 3) late tectonic granodiorite-granite-leucogranite-pegmatite dykes, stocks and batholiths (Meintzer and Wise, 1987; Ayres and Cerny, 1982). Six of the best studied late granite suites (Henderson, 1985; Atkinson 1987, 1989) border or occur within the Yellowknife Basin (Figure 3.2). These include: i) the Defeat Plutonic Suite ( $2620 \pm 8$  Ma and  $2618 +7/-20$  Ma, U-Pb zircon age, Henderson et al. 1987); ii) the Stagg Plutonic Suite ( $2581 +29/-24$  Ma, U-Pb zircon age, Henderson et al. 1987); iii) the Meander Lake Plutonic Suite; iv) the Awry Plutonic Suite (2550-2630 Ma, U-Pb zircon age, Henderson et al. 1987); v) the Prosperous Granite Suite ( $2525 \pm 25$  Ma, Rb-Sr, Green et al. 1968), and vi) the Morose Granite Suite.

### 3.6 METALLOGENY OF THE SLAVE PROVINCE

Historically, most of the gold production from the Slave Province has come from shear zones within the mafic volcanic rocks (85%), and to a lesser extent sedimentary-volcanic contact deposits (10%), while the iron formation deposits have yielded 4%, and the gold-quartz veins in metaturbidites (lacking iron formation), 1% (Padgham and Brophy, 1984). Gold mineralization also occurs in the Anialik tonalite/trondjemite terrane near the Coronation Gulf (Abrahams and Spooner, 1988), and within shear zones of other late granitoids (Padgham and Brophy, 1984; Atkinson, 1987).

Padgham (1986), in an attempt to integrate gold deposit types and their genetic associations, divided the Slave Province into four metallogenic zones (Figure 3.4). He suggested that three controlling factors account for this apparent zonation: 1) timing, whereby the formation of a gold deposit depended on the availability of mineralizing fluids and entrapment structures during a single (Pan-Slave) gold event which accompanied widespread metamorphism and/or melting; 2) structure, where the occurrence of gold mineralization events depended on the structural and metamorphic maturity of a particular supracrustal domain; and 3) erosion, whereby a hierarchy of gold deposits is present, related to the depth of formation in the crust and varying erosion levels.

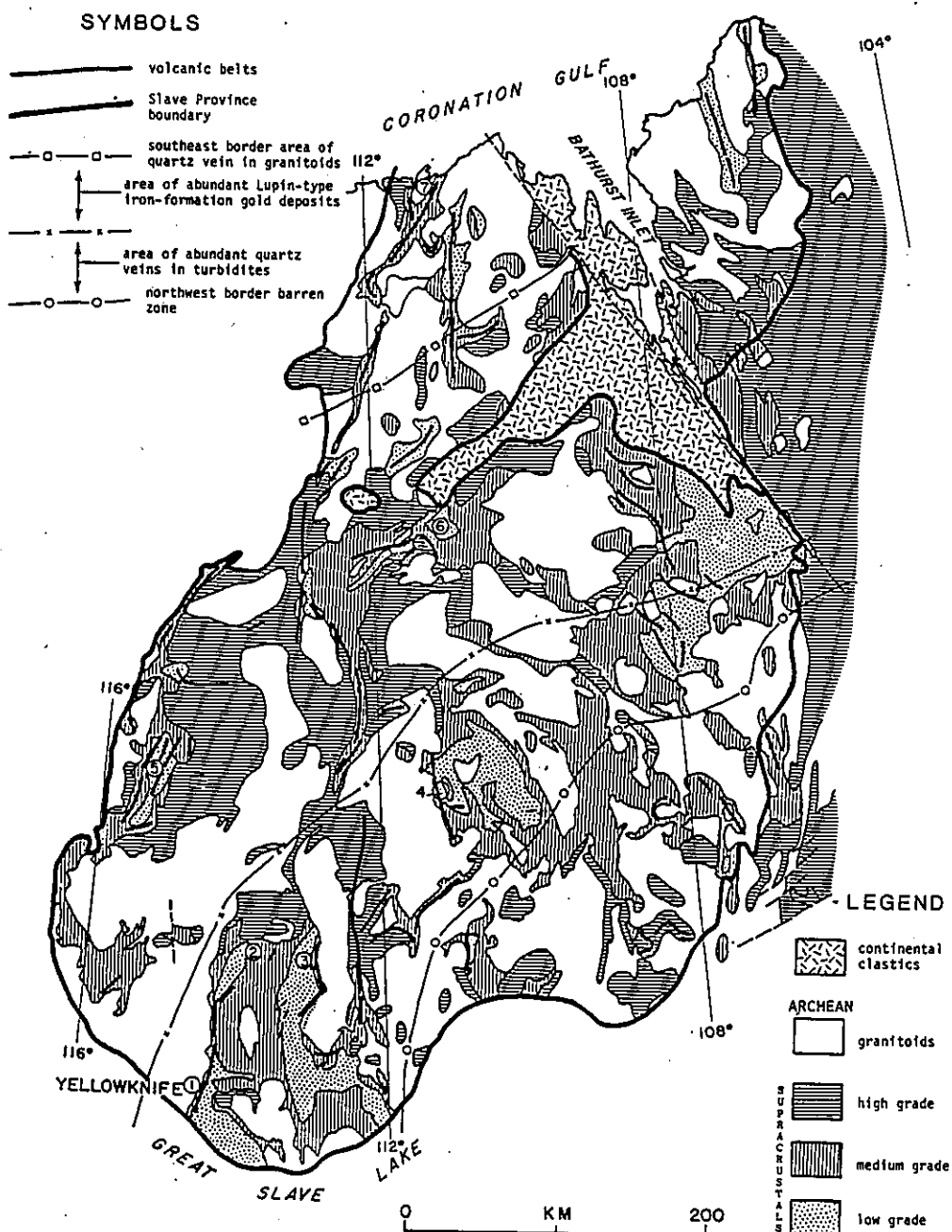
Other important mineral occurrences include volcanogenic massive sulphide deposits (Bubar and Heslop, 1985) found in the Hackett Lake felsic volcanic rocks (with a notable lack of gold and copper, but higher silver, zinc, and lead values as compared to most other Archean massive sulphide deposits) and pegmatites associated with late plutons (rich in Li, Be, Sn, W and Ta; Padgham, 1985).

### 3.7 PROPOSED TECTONIC MODELS FOR THE SLAVE PROVINCE

Various tectonic settings, suggested for the Slave Province, have important implications for the types of gold deposits, their genesis and metallogenic distribution (e.g., Boyle, 1979; Mitchel and Garson, 1981). The tectonic models proposed for the Slave Province include:

- 1) Folinsbee et al. (1968) suggested that the development of the Yellowknife Volcanic Belt was similar in setting and time span to that of the Miocene island arc system of Japan.

Figure 3.4 Division of the Slave Province into four metallogenic zones based on distribution of gold deposit type taken from Padgham (1986, Figure 1). Major gold occurrences include: 1) Con and Giant Mines, 2) Discovery Mine, 3) Camlaren Mine, 4) Salmida and Tundra Mines, 5) Indin gold district, 6) Lupin Mine, and 7) Arcadia district.



2) McGlynn and Henderson (1970), J.B. Henderson (1981, 1985), and Easton (1985) indicated that a continental (or intracratonic) rifting model (Figure 3.5) was more likely. In this model one or more basins were formed by normal/listric faulting of a thick sialic basement, followed by extrusion of mafic and felsic flows with concurrent deposition of turbiditic sediments.

3) Hoffman (1986) suggested that the rifting model was inconsistent with the stratigraphy of most continental rift environments (where volcanic piles overlie the sediments). He indicated that a rift model could not readily account for the later granitoids and the prevalence of compressional over extensional structures, and gives no explanation for the unconformities (possible thrusts) found along the contacts between basement and supracrustal rocks. He proposed that an arc-trench progradation model better explained the development of the granite-greenstone terranes.

4) Kusky (1986, 1988, 1989, 1990) described the tectonic framework of the Slave Province in terms of a simplified collision-subduction model. He subdivided the Slave Province into four basic north-south trending terranes (Figure 3.6); the Anton (an older Archean microcontinent), the Sleepy Dragon (an accreted micro-continent or nappe sliver), the Contwoyto (a westerly verging and thrusting fore-arc accretionary complex), and the Hackett River (an island arc). He hypothesised that the tectonic evolution of the Slave involved the formation of an easterly dipping subduction zone (Figure 3.7). King (1989) agreed with the general concepts of the model, but commented on the unclear and possibly premature classification of the four terranes, and the lack of consistent structural evidence for a

Figure 3.5 Extensional rifting model for the tectonic evolution of the Yellowknife Basin from Henderson (1985, Figure 42).

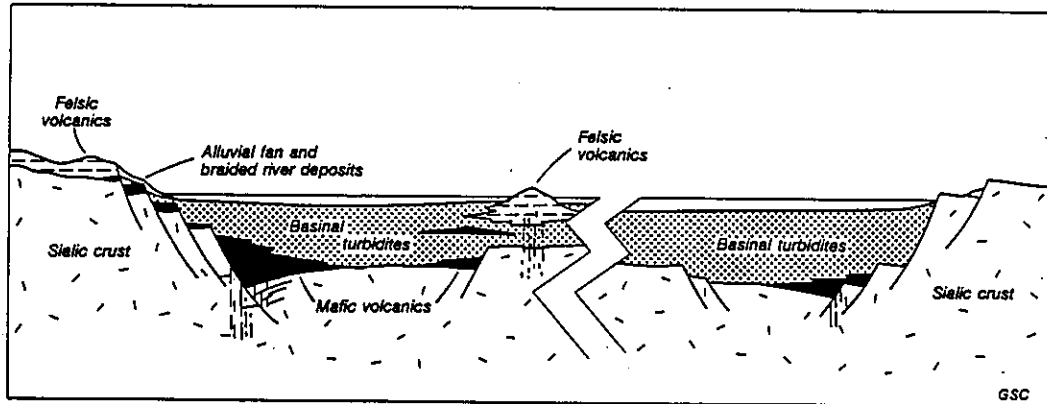


Figure 3.6 Division of the Slave Province into four structural domains (Anaton Terrane, Sleepy Dragon Terrane (SDT), Contwoyto Terrane, and Hackett River Volcanic Arc) from Kusky (1988, Figure 2).

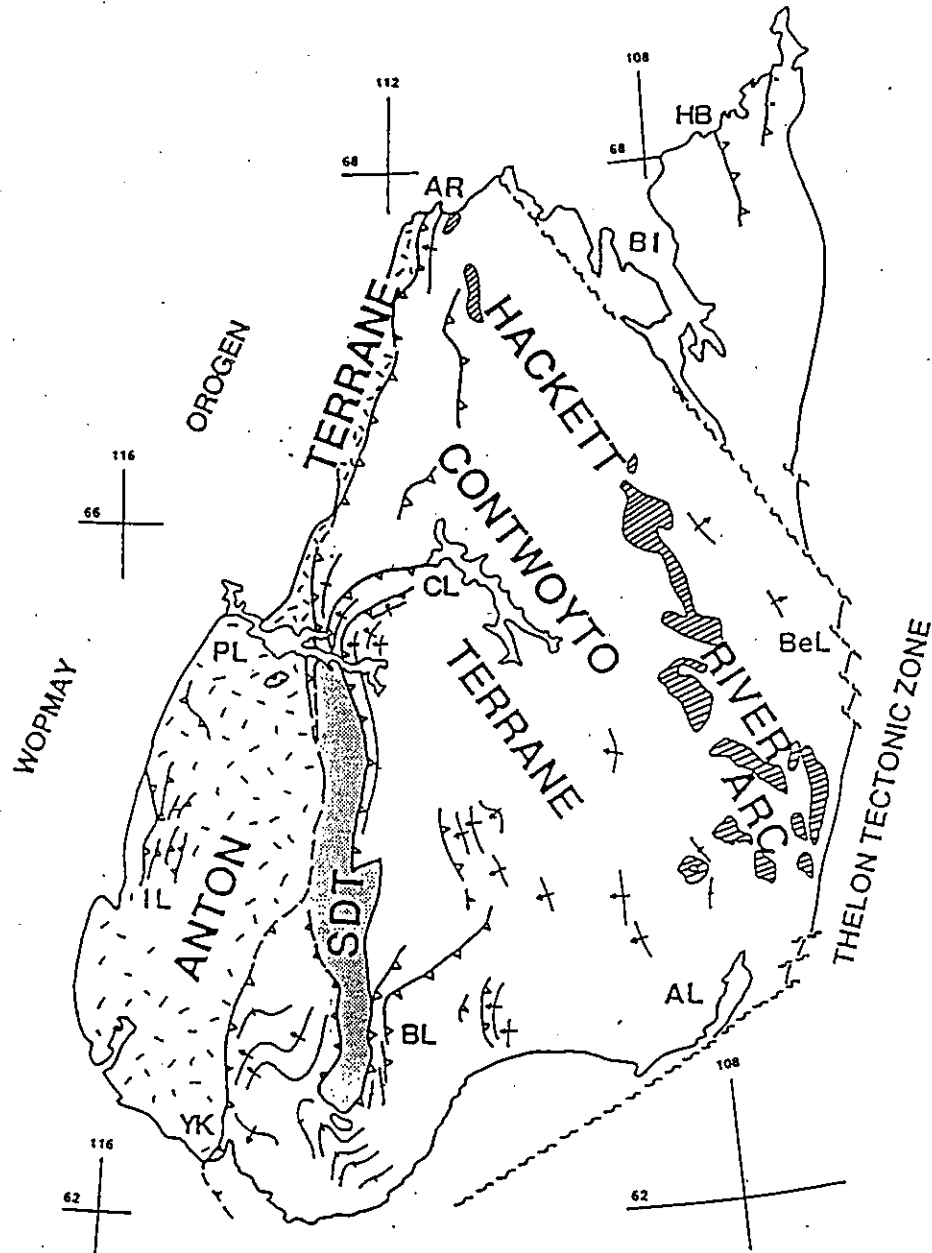
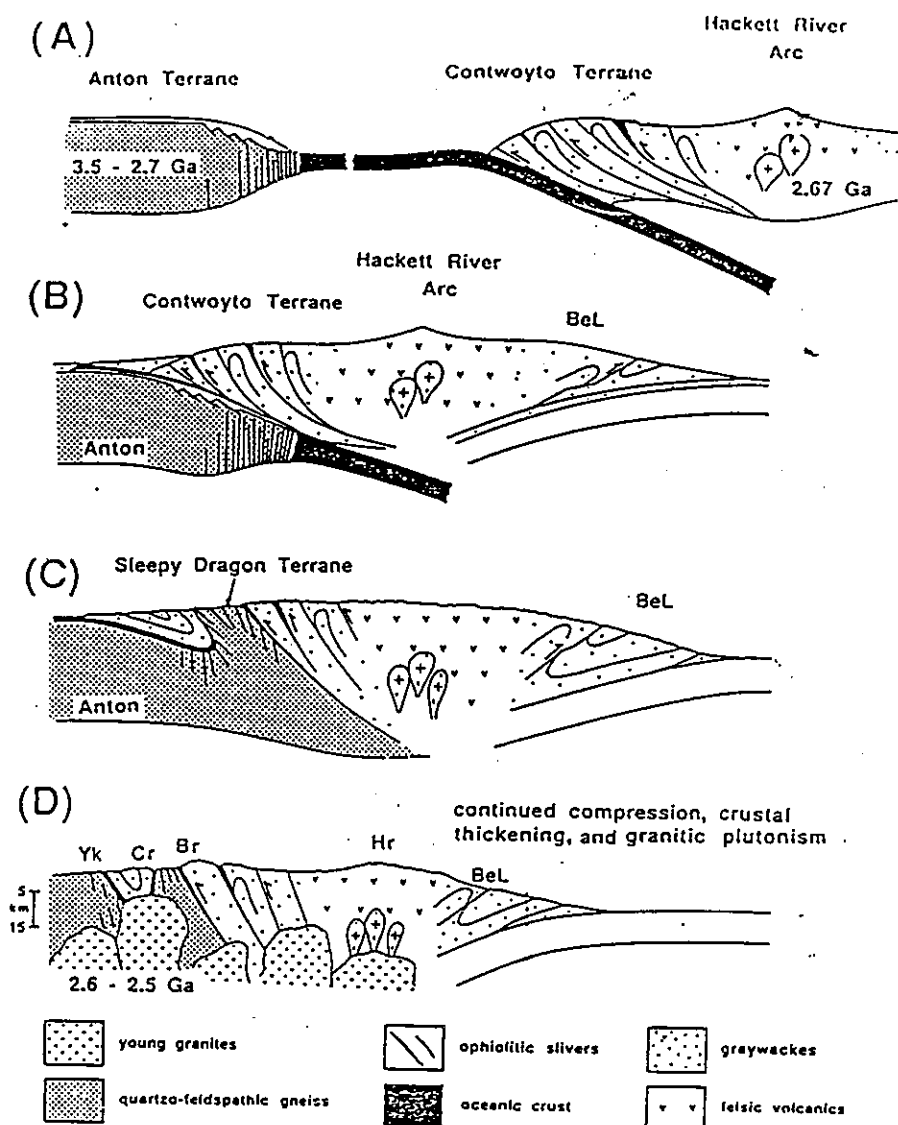


Figure 3.7 Model depicting the accretion of the Slave Province, taken from Kusky (1988, Figure 3). BeL - Beechy Lake domain; Yk - Yellowknife; Cr - Cameron River; Br - Beaulieu River; Hr - Hackett River.





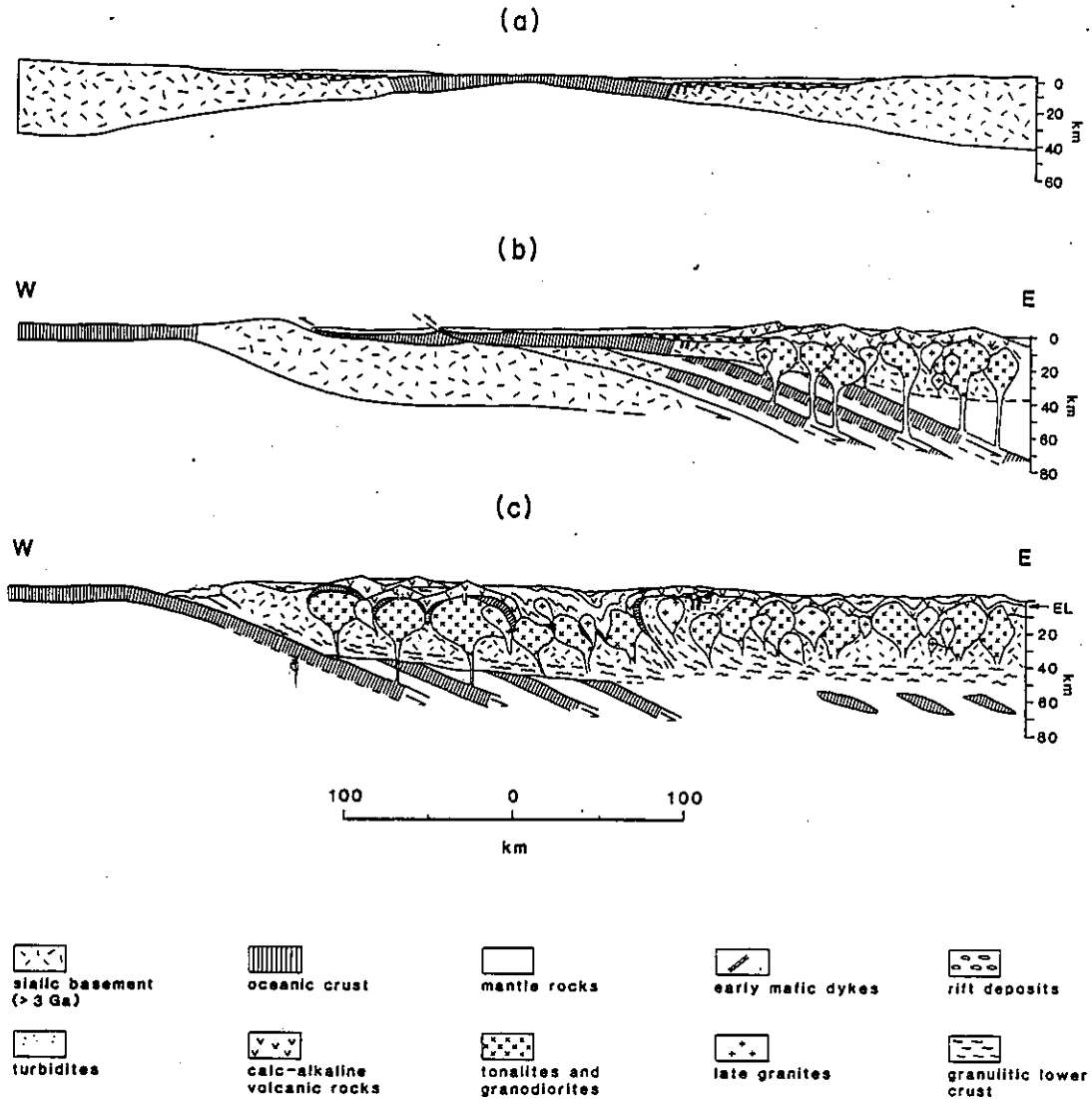
westerly verging accretionary wedge and basement/supracrustal thrusts.

5) Padgham and Helmstaedt (1986a) examined the Lower Kam Group of the Yellowknife Volcanic Belt and interpreted the dyke systems as part of an oceanic ophiolite sequence rather than a product of intracontinental rifting. They suggested that the Yellowknife volcanic rocks were the result of sea floor spreading in a marginal basin setting, similar to the Mesozoic Rocas Verdes ophiolites in southern Chile (Tarney et al. 1976; Helmstaedt et al. 1986).

6) Fyson and Helmstaedt (1988) and Fyson (1990) also indicated that a simple rift model did not satisfactorily explain the tectonic development of the Slave Province. They proposed the formation of an easterly-dipping subduction zone and tectonic underplating along reactivated, earlier rift fractures (Figure 3.8). Later granitoids were then emplaced along some of these crustal fractures, resulting in complex deformation patterns within the overlying metasedimentary and volcanic rocks.

In summary, no single model is widely accepted for the tectonic development of the Slave Province. However, any successful model must explain and take into account: i) the exact nature of the basement-supracrustal contacts (i.e., whether these are thrusts or deformed unconformities; Fyson, 1990); ii) the high proportion of metasedimentary to metavolcanic rocks; iii) the shape and character of the volcanic belts; iv) the contrasting structures within the metasedimentary and metavolcanic rocks; and v) the evidence for westerly vergence in the supracrustal metasedimentary rocks and possible thrusts (King, 1989).

Figure 3.8 Model for the tectonic evolution of the Slave Province by subduction along reactivated rift faults, taken from Fyson and Helmstaedt (1988, Figure 7).



## CHAPTER 4

### GEOLOGY OF THE YELLOWKNIFE BASIN AND METATURBIDITES OF THE BURWASH FORMATION: PREVIOUS STUDIES

#### 4.1 INTRODUCTION

The Yellowknife Basin is the southern most metasedimentary region of the Slave Province and covers an area of approximately 120 x 180 km. The Basin mainly consists of metaturbidites of the Burwash Formation, which are bordered to the southwest by the Yellowknife Volcanic Belt and to the northeast by the Cameron River Volcanic Belt (Figure 3.2). The metaturbidites are predominantly monotonous sequences of graywackes, siltstones, and mudstones<sup>2</sup>. Coarser metasedimentary rocks, such as conglomerates and sandstones, are found along the metaturbidite/metavolcanic contacts, which display some evidence of later disruption and faulting (Drury, 1977). The metaturbidites are also intruded by a series of later granodiorites and potassic granites - the Prosperous Granite Suite, the Defeat Plutonic Suite, and the Meander Lake Plutonic Suite (Henderson, 1985).

Correlation of the Burwash Formation stratigraphy across the Yellowknife Basin is difficult, as the region was deformed by at least four structural events (Fyson, 1982) and no good marker beds are present (Henderson, 1975). However, Henderson (1970, 1975), from a stratigraphic section measured near Yellowknife, assigned a total thickness of 5 km to the Burwash Formation. Gravity data from the Yellowknife Bay area (Gibb and Thomas, 1980) indicated that the metasedimentary rocks are typically 1-3 km thick, with a maximum of up to 7 km. Further gravity

---

<sup>2</sup> The graywackes, siltstones and mudstones discussed in this thesis are all metamorphosed to a least lower greenschist facies, but since their primary characteristics are still clearly evident these lithological names are commonly used instead of metagraywacke, metasiltstone, slate, respectively.

(McGrath et al., 1983) and seismic work (Clee et al., 1975) indicated that the volcanic belt does not extend beneath the metaturbidites, but that the latter are most probably underlain by basement granitoid gneiss and/or late granitoids.

Regional variations of graywacke- and siltstone-dominated sequences are not well defined. However, there are areas, such as between Duncan Lake and Prosperous Lake (Henderson, 1985) and the centre of Gordon Lake (Henderson and Jolliffe, 1939), that are dominated by black, carbon-rich siltstone and mudstone sequences.

#### 4.2 LITHOLOGY AND PETROGRAPHY

The metaturbidites of the Burwash Formation (extensively studied by Henderson, 1970, 1972, 1975, 1981, 1985, 1987), characteristically form striped outcrop surfaces, of steeply-dipping and alternating graywacke and siltstone beds. The striping is due to the variation in colour - the coarser graywackes weather light grey, whereas the finer siltstones are dark grey to black. Some sequences display graded bedding similar to the turbidite flow units of Bouma (1962). However, complete Bouma sequences are the exception rather than the rule, with usually only the A and E units present (Henderson, 1975). Primary post-depositional features are usually well preserved along bedding contacts and include flames, lode casts, rip-up clasts, ball and pillow structures, and sandstone dykes (Henderson, 1975). Along with graded bedding these structures provide good indicators of younging direction, and are of considerable importance for mapping.

Distributed within the turbidites, especially close to the volcanic belts, are metre-thick sequences of tuffaceous material (Henderson, 1985) with typically white to yellow felsic laminae alternating with black mudstone.

These sequences probably represent changes from felsic volcanic activity to depositional quiescence (Henderson, 1985), but also imply high biological activity. Carbonate concretions and layers found within graywacke beds, probably represent metamorphosed carbonate zones within the sediment (Henderson, 1975). Since these are deep-sea sediments, these carbonates most likely represent diagenetic oxidation of carbon within the sediments (M. Zentilli, personal communication, 1991)

Detailed petrographic studies on graywackes of the Burwash Formation were carried out by Henderson (1975, 1981). He showed that the graywackes are typically composed of a fine-grained matrix (40%), quartz clasts (25%), rock fragments (20%), and feldspar clasts (15%); and that most of the material was derived from both volcanic and granitic sources. From the rock fragments he concluded that most of the detritus was felsic volcanic in origin, with lesser contributions from granitic and mafic volcanic sources. However, remarkably little is said about the origin of the matrix material (Chapter 9).

#### 4.3 METAMORPHISM

Previous studies of metamorphism within the Yellowknife Basin have concentrated on the Burwash Formation, a unit with a relatively uniform bulk composition and therefore the most obvious candidate for the determination of metamorphic reactions (e.g., Kamineni, 1973; Ramsay, 1973; Ramsay and Kamineni, 1977; Thompson, 1978; Kamineni et al. 1979; Henderson 1985).

Typically, amphibolite facies and greenschist facies metasedimentary rocks are distinguished by the presence or absence of cordierite, which defines a mappable isograd (Henderson, 1943). Amphibolite facies assemblages within the metaturbidites include quartz, biotite, plagioclase, cordierite, andalusite, garnet, amphibole, staurolite, and

sillimanite, whereas greenschist facies assemblages include chlorite, biotite, quartz, plagioclase, muscovite, and epidote (Henderson, 1985).

The amphibolite facies rocks are confined to the western and south-eastern margins of the Yellowknife Basin and surround the late granites (Figure 3.2). Biotite-rich assemblages predominate in greenschist facies regions, but some regions devoid of biotite do occur, such as along the centre of Gordon Lake and north of Yellowknife Bay (Henderson, 1943).

There is considerable debate within the Yellowknife Basin as to the exact origin, P/T conditions, and timing of metamorphism. This is in part due to the different emplacement ages of the later granites and the complex overprinting of metamorphic assemblages. Folinsbee (1942) and Henderson (1943) suggested that because the granites occurred within the higher grade regions they must have provided the heat source for metamorphism. However, this suggestion is not compatible with the great widths of the metamorphic aureoles. Davidson (1967) proposed that granites (in the Benjamin Lake area) were produced at depth by the same thermal conditions that caused the metamorphism, and were intruded after the host rocks were already metamorphosed. This idea was supported by Ramsay and Kamineni (1977) who identified four metamorphic stages related to a single progressive heating event, and proposed that metamorphism was related to the development and decay of a low pressure/high temperature thermal dome. Thompson (1989a, 1989b) proposed a P-T-t model for the thinning and thickening of a 35 km-thick sialic crust (representing the Slave craton) that could account for low pressure metamorphism without relying solely on heat from granites. His model involved three stages: i) crustal thinning (to half the original thickness) and an increased thermal gradient suitable for a low pressure and  $<500^{\circ}\text{C}$

metamorphism (ca. 2660 Ma); ii) thickening (to two or three times the original thickness) that, with partial melting at depth, increased the thermal gradient to peak metamorphic conditions (ca. 2600 Ma), and was accompanied by the later intrusion of granites (ca. 2550-2600 Ma); and iii) an exhumation phase with slow cooling, uplift, and erosion.

#### 4.4 STRUCTURE

Most of the early structural mapping in the Slave Province concentrated on the Yellowknife region, in particular the Yellowknife Volcanic Belt and the Burwash Formation (Henderson 1941a, 1941b, 1943; Jolliffe 1942, 1946; Fortier 1946, 1947; Boyle 1961; Henderson and Brown 1966). Later contributors to mapping of the Yellowknife Volcanic Belt included Helmstaedt et al. (1979, 1980, 1981) and Helmstaedt and Padgham (1986a, 1986b; references therein). Recent structural studies in the Burwash Formation include those of Fyson (1975, 1980, 1981, 1982, 1984a, 1984b, 1987a and 1987b), Drury (1977), and Henderson (1985). The following sections, based primarily on Fyson's work, provide a summary of the structures within the metaturbidites of the Yellowknife Basin and includes his interpretation of these data.

##### 4.4.1 Early (D<sub>0</sub>) Deformation

Fyson (1982) termed the earliest structural event D<sub>0</sub>, and attributed it to initial tilting of both the metavolcanic rocks and the metaturbidites, resulting in the overall sub-vertical attitude of the supracrustal sequences. Evidence for D<sub>0</sub> includes a 5-10 km-wide, asymmetric synclinal structure, which has a 25 km north-south trending axial trace parallel to the Yellowknife Volcanic Belt - Burwash Formation contact (Fyson, 1982). The easterly facing, sub-vertical Yellowknife Volcanic Belt form one limb of the syncline, while the other limb is made

of steeply dipping, westerly facing metaturbidites. Other  $D_0$  fold axes occur where later  $F_1$  folds form "structural fold fronts" (Fyson, 1981). These are defined by the opposing  $F_1$  fold facing directions and were mapped by Fyson (1984b) throughout the Yellowknife Basin (Figure 4.1). No cleavage was found associated with  $D_0$  folding.

#### 4.4.2 $D_1$ Deformation

Fold structures that dominate the structural pattern in outcrop and are clearly visible in aerial photographs are assigned to  $D_1$ . The  $F_1$  folds are typically curvilinear and isoclinal, with moderately to steeply plunging fold axes and axial surfaces (Figure 4.1), and generally verge in a westerly direction (Fyson, 1981). The plunge of these fold axes is in part correlated with the metamorphic grade of the metaturbidites - the higher the grade the shallower the plunge (Fyson and Helmstaedt, 1988). Two types of  $F_1$  folding are apparent based on the orientation of fold axial traces (Fyson, 1982) -  $F_{1A}$  trend north-south, and  $F_{1B}$  trend east-west. However, some folds with axial trace orientations between  $F_{1A}$  and  $F_{1B}$  are difficult to ascribe to one group or another. The relationship of  $F_1$  folds to the later plutons is complex, because some folds curve around granodiorite plutons, and others are cut by the more potassic granites (Fyson, 1982).  $S_1$  cleavages are rarely found, except in higher grade metaturbidites near pluton margins, and are in most cases obliterated by  $S_2$  and the more pervasive  $S_3$  (Fyson, 1984b).

#### 4.4.3 $D_2$ Deformation

$D_2$  structures, which are rare, include sub-vertical, minor  $F_2$  folds and  $S_2$  cleavage (defined by fine-grained muscovite, chlorite, and quartz), that are identified by their east-west orientation (Figure 4.2; Fyson, 1982). However, these structures are frequently masked and



Figure 4.1  $F_0$ ,  $F_1$ , and re-fold structures of the Yellowknife Basin, taken from Fyson (1984b, Figure 2). Location of re-fold structures: G - Gordon Lake; R - Ross Lake; Cl - Cleft Lake; Ca - Cambell Lake; P - Prestige Lake; and W - Wagenitz Lake.

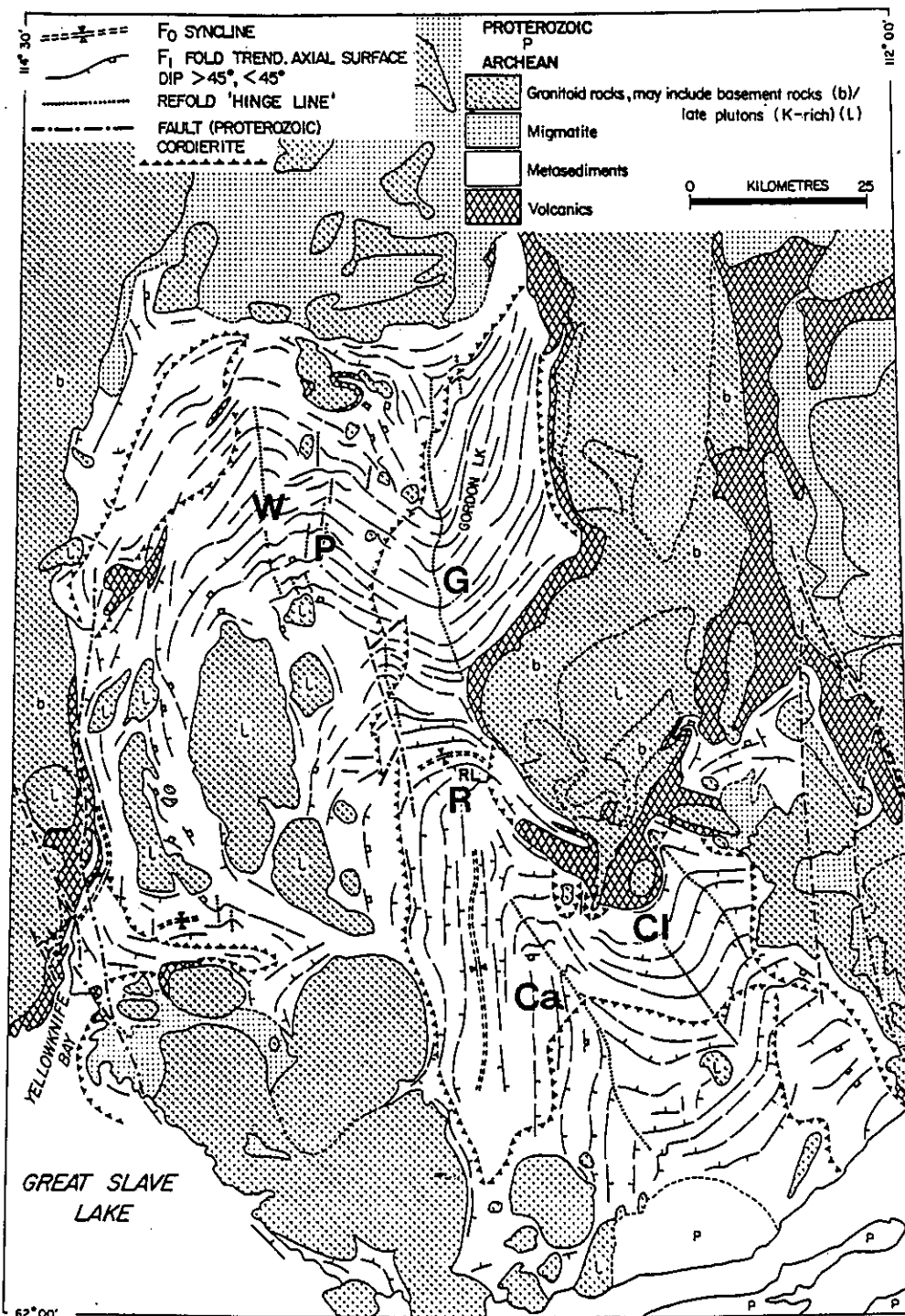


Figure 4.2  $S_2$  and  $S_3$  fabrics and refold hinges of the Yellowknife Basin taken from Fyson (1984b, Figure 3). Rocks type patterns similar to Figure 4.1.

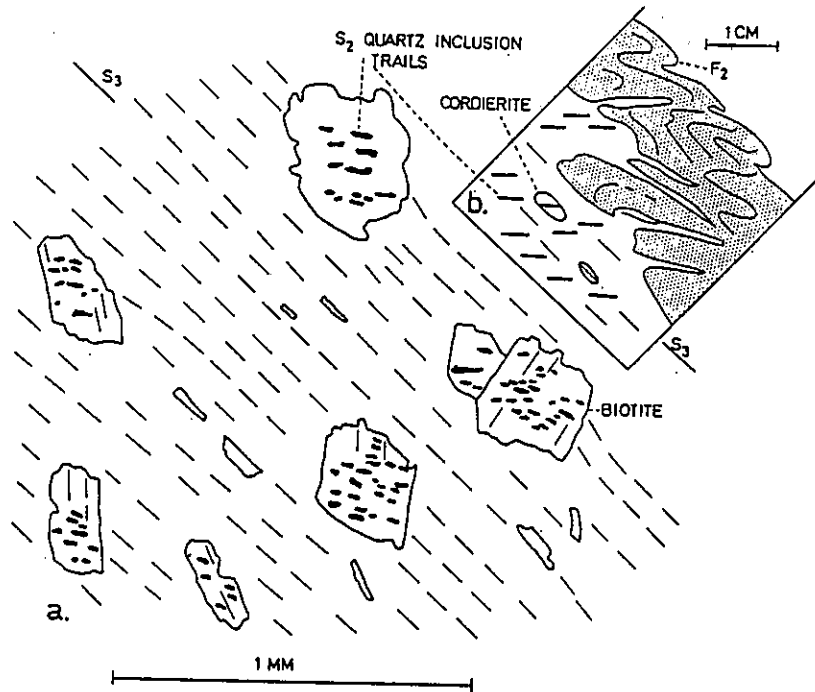


overprinted by  $D_3$ . Therefore, evidence of  $S_2$  is more commonly preserved as east-west trending quartz inclusions within biotite porphyroblasts, which are associated with the development of  $S_3$ . The quartz inclusion fabric is readily apparent in thin section (Fyson, 1975, Fig. 4; Fyson 1980, Fig. 4 and 5) and is found throughout the Yellowknife Basin (Figure 4.3). Some flattening of primary sedimentary structures, such as flames, is also assigned to  $D_2$  (Fyson, 1984b).

#### 4.4.4 $D_3$ Structures

$D_3$  is recorded as a north-south-trending pervasive cleavage ( $S_3$ ) that predominates throughout the Yellowknife region (Figure 4.2). The character of  $S_3$  depends on lithology, metamorphic grade, and the degree of preservation of earlier cleavages (Fyson, 1984b).  $S_3$  is steeply dipping, transects  $F_1$  folds, crenulates and overprints  $S_2$  fabrics, and re-orientes primary structures (such as micro-concretions and sand dykes). Minor, mesoscale  $F_3$  folds, parallel to  $S_3$ , are also found on the limbs of  $F_1$  and  $F_2$  folds. Fyson (1984a, 1984b) recognized two types of  $S_3$  fabric based on their relative strike orientation -  $S_{3A}$  strikes northwest to southeast, whereas  $S_{3B}$  strikes north-northeast to south-southwest. The meeting of these two cleavage sets forms "cleavage fronts" (Fyson, 1984a), such as at Gordon Lake, where it appears that  $S_{3A}$  is crenulated to form  $S_{3B}$ . Within these cleavage front regions a "herring-bone" cleavage pattern occurs in alternating fine and coarse siltstone sequences. Here the original  $S_{3A}$  cleavage is preserved in the coarse-grained metasedimentary rocks and the new crenulation cleavage ( $S_{3B}$ ) forms in the fine-grained metasedimentary rocks.

Figure 4.3 Sketch of  $S_2/S_3$  fabric relationships, taken from Fyson (1984b, Figure 7). (a)  $S_2$  quartz inclusion trails in biotite porphyroblasts oblique to  $S_3$  fabric. (b)  $S_2$  inclusion trails in siltstone (white) oriented sub-parallel to axial traces of  $F_2$  folds in quartzite bed (shaded).



#### 4.4.5 "Refold" Structures

Major features of the Yellowknife Basin, visible in aerial photographs, are "cross folds" (Henderson, 1943; Fortier 1946) or "refolds" (Fyson, 1984a). The refolds mainly close north-south, occur within predominantly greenschist facies metaturbidites, and are the result of folding of  $F_1$  folds (Figure 4.1). The hinge axes of the refolds are sub-vertical, while their hinge traces can extend for up to 50 km, such as at Gordon lake. Other refold hinge traces are found at Ross Lake, Cleft Lake, Prestige Lake, Wagenitz Lake, and Cambell Lake (Figure 4.1). The north-south hinge traces of the refolds are sub-parallel to  $S_3$  and some of the later, elongated granite plutons (Fyson, 1984a). The age of refold formation clearly post-dates  $D_1$ . However, the constraints on the upper age of refold formation are less clear. Henderson (1943), Fortier (1947) and Drury (1977) suggested that the refolds developed during the formation of the pervasive north-south cleavage ( $S_3$ ). Fyson contended that, since the east-west quartz inclusion fabric ( $S_2$ ) is traceable across the refold, the refolds must have developed between  $D_1$  and  $D_2$  (Fyson, 1984b). This thesis demonstrates that refold formation at Gordon Lake is a much later event in the structural history of the region (Chapter 5).

#### 4.4.6 Summary of Fyson's Structural Model

Fyson (1982) stated that the fold and cleavage structures found within the Burwash Formation of the Yellowknife region probably represent a progressive deformation with no major discontinuities. In addition Fyson (1984b) stated that even though many structures appear parallel (e.g., refold hinge lines,  $S_3$ ,  $F_0$  fold axes, and metavolcanic/metasedimentary contacts) this does not necessarily imply synchronous development. The differing orientations of  $F_{1A}/F_{1B}$  folds and  $S_2/S_3$  cleavages

confirm this and indicate successive increments of the bulk strain were imposed in more than one direction (Fyson, 1984b).

Fyson (1982, 1990) and Fyson and Helmstaedt (1988) proposed a model for the structural development of the Yellowknife Basin, involving regional extension (listric faulting) and volcanism along deep crustal fractures during development of a rifted continental margin. Subsequent closure of the basin was associated with easterly underthrusting (possibly along reactivated crustal fractures) and diapiric emplacement of granite plutons. Fyson (1982) suggested that  $D_0$  and  $D_1$  structures formed during early compression and diapirism associated with granodiorites, whereas  $D_2$  and  $D_3$  accompanied later compression and diapirism associated with potassic granites. Fyson (1984a, 1984b) also proposed a model for refold formation that post-dated  $D_1$  and pre-dated  $D_2$ , whereby differential (strike-slip?) movement along the deep crustal fractures was transmitted into the overlying, more ductile metasedimentary rocks and formed the refold patterns.

## CHAPTER 5

### GEOLOGY OF THE SOUTHERN END OF GORDON LAKE

This chapter details the results of mapping carried out by the writer at the southern end of Gordon Lake during the summers of 1986-1989 (Maps 1, 2, and 3 in back pocket of thesis). Many of the structures present at Gordon Lake are similar to those recognized by Fyson (1982, 1984b) during regional studies within the Yellowknife Basin (Section 4.3). Fyson's nomenclature has therefore been retained with some modification (Table 5.1). Based on the analysis of field, petrofabric, and strain data a model was developed for the structural history of the Gordon Lake region (Section 5.6). This structural model, in addition to data from quartz-veins and breccias, is used in Chapter 6 to explain the concentration of gold-bearing quartz-breccia zones at the southern end of Gordon Lake.

#### 5.1 REGIONAL SETTING

Gordon Lake has a northerly trend, is approximately 40 km long, and has an average width of 4 km. The lake has a ragged indented shoreline with hundreds of islands ranging from a few square metres to kilometres (e.g., Zenith Island) in size. The best outcrops occur on wave-washed shorelines, whereas most inland outcrops are covered by lichens.

The Gordon Lake region is underlain by greenschist-facies metaturbidites of the Burwash Formation, with amphibolite-facies metaturbidites occurring 3-6 km to the west and 4-15 km to the east (Figure 3.2). The Cameron River Volcanic Belt borders the amphibolite-facies metaturbidites to the east. The main plutons of the Prosperous Granitic Suite occur within amphibolite-facies metaturbidites 20-30 km southwest of Gordon Lake (Figure 3.2). However, minor plutons of the Prosperous Granitic

Table 5.1 Structural nomenclature used in this thesis compared to that of Fyson.

Structure	Fyson <sup>1</sup>	Fyson <sup>2</sup>	This Thesis
Kilometre scale folds defined isoclinal fold fronts	F <sub>1</sub>	F <sub>0</sub>	Not found at Gordon Lake
Isoclinal Folds visible in aerial photographs and mappable by top reversals	F <sub>2</sub>	F <sub>1A</sub> F <sub>1B</sub>	F <sub>1</sub>
East-west trending minor folds and quartz inclusions trails in biotite porphyroblasts	S <sub>2</sub>	S <sub>2</sub> F <sub>2</sub>	No F <sub>2</sub> folds found at Gordon Lake. Quartz inclusion trails syn-S <sub>3</sub>
Regional, pervasive northwest striking cleavage and minor folds.	S <sub>3</sub>	S <sub>3A</sub>	S <sub>3s</sub> S <sub>3g</sub>
Northeast striking and/or crenulation cleavage	-	S <sub>3B</sub>	S <sub>4</sub> S <sub>4E</sub> S <sub>3Es</sub> S <sub>3Eg</sub>

Fyson<sup>1</sup> - see Fyson 1975 and 1980 references

Fyson<sup>2</sup> - see Fyson 1981, 1982, 1984a, 1984b, 1987, 1990 and Fyson and Helmstaedt 1988



Suite at Mac Lake, Thistlethwaite Lake, and Spud Lake are 5-10 km to the west of Gordon Lake (Figure 3.2; Henderson, 1941a, 1941b). (Mapping of the Spud Lake granite indicated that the pluton crosscuts both the ( $F_1$ ) isoclinal folds and the regional ( $D_3$ ), north- to northwest-striking cleavage.) North-northwest and east-northeast striking diabase dykes and faults of Early Proterozoic age also crosscut the Gordon Lake region (Henderson, 1985).

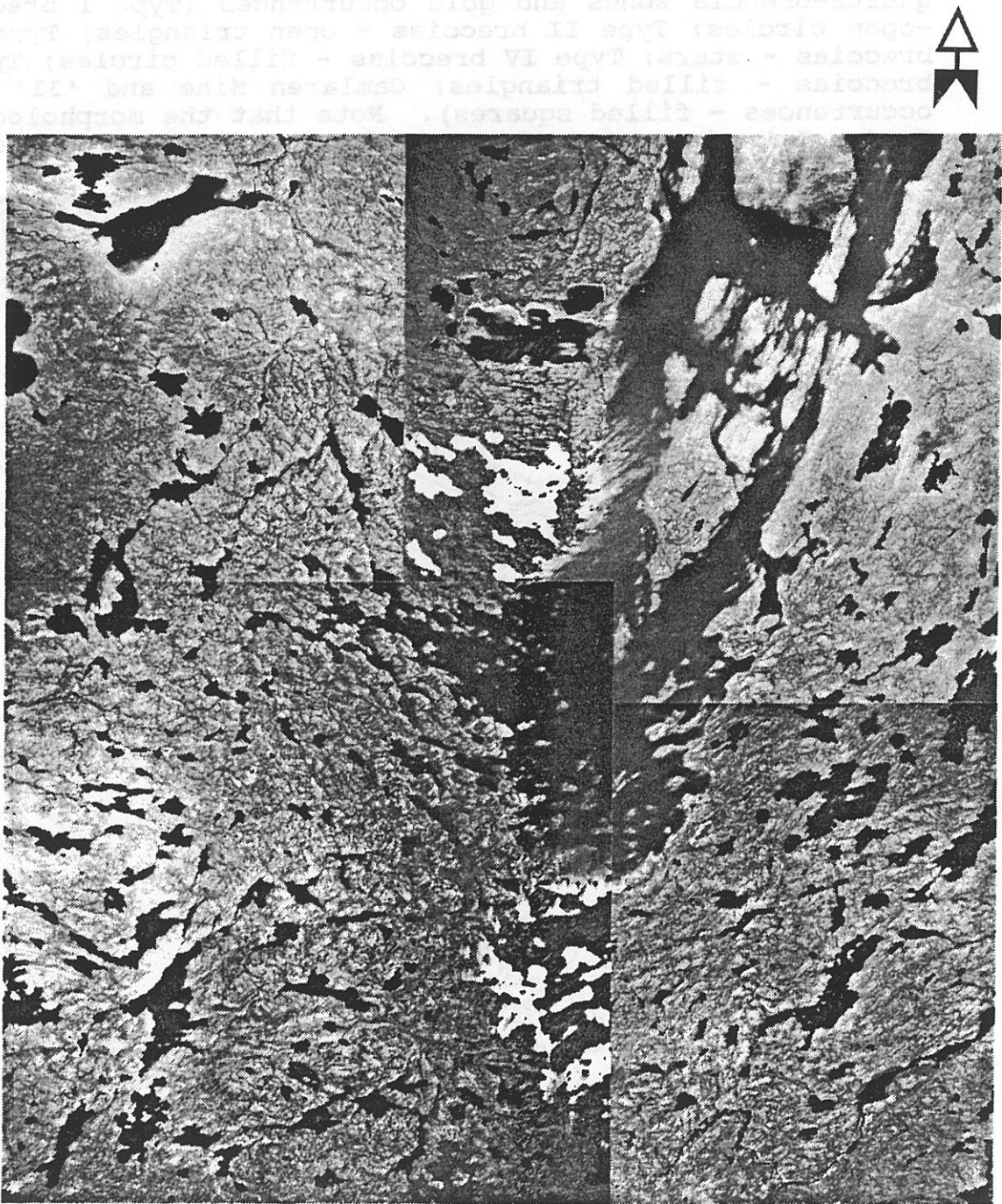
Previous mapping at Gordon Lake (Henderson 1941a, 1941b) and other topical studies (Henderson and Jolliffe, 1939; Henderson, 1943; Fortier, 1946; Fyson 1975, 1984a, 1984b; Henderson, 1985) have delineated a regional, kilometre-scale re-fold structure (Figure 5.1). This structure has attracted considerable attention as a possible control on the concentration of gold-quartz vein occurrences (Henderson and Jolliffe, 1939; Henderson 1985) and as a "cleavage front", where two cleavage sets meet (Fyson, 1984a, 1984b).

## 5.2 LITHOLOGY

The central part of Gordon Lake is underlain by siltstone-dominated metaturbidites (with >30% siltstones) that are surrounded to the south, east, and west by graywacke-dominated metaturbidites (with <30% siltstones, Figure 5.2). Sequences (0.1-1.0 m wide) of alternating fine and coarse siltstone beds (Figure 5.3a) occur along the south-western shore of Gordon Lake, and are associated with the transition from graywacke-dominated to siltstone-dominated metaturbidites. The main quartz-breccia zones at Kidney Pond lie within this lithological transition (Chapter 7).

The metaturbidites were divided, for the purposes of measuring a stratigraphic section across the Kidney Pond quartz-breccia Zones 1 and 2 (Section 7.3) and litho-chemical analysis (Chapter 9), into:

Figure 5.1 Aerial photograph mosaic of the southern end of Gordon Lake.

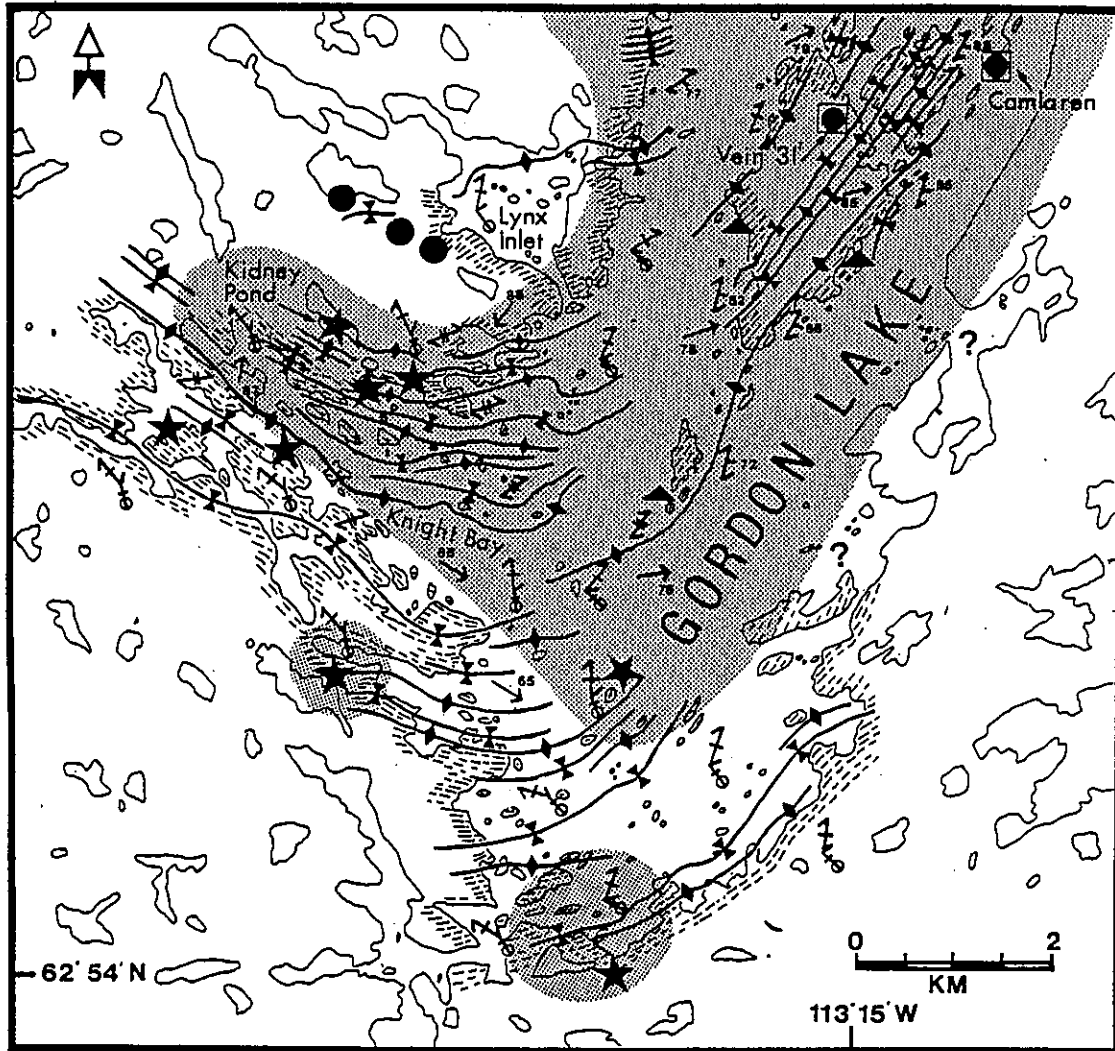


5 KM

Graywacke dominated  
(30% effect area)

1. Limestone  
2. Crinoidal cleavage  
3. Graywacke cleavage  
4. Limestone cleavage  
5. Axial trace

Figure 5.2 Simplified structural and lithologic map of the south end of Gordon Lake, with the location of major quartz-breccia zones and gold occurrences (Type I breccias - open circles; Type II breccias - open triangles; Type III breccias - stars; Type IV breccias - filled circles; Type V breccias - filled triangles; Camlaren Mine and '31' vein occurrences - filled squares). Note that the morphology of Gordon Lake in part outlines both the refold structure and siltstone-dominated region.




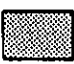

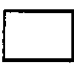


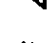
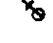
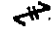
- |  |   |
|--|---|
|  Bedding                              |  Siltstone dominated (>30% siltstones) |
|  F <sub>1</sub> Anticline axial trace |  Graywacke dominated (<30% siltstones) |
|  F <sub>1</sub> Syncline axial trace  |   |
|  S <sub>3</sub> Siltstone cleavage    |   |
|  S <sub>3</sub> Graywacke cleavage    |   |
|  S <sub>4</sub> Crenulation cleavage  |   |
|  L <sub>3</sub> Lineation             |   |

Figure 5.3 Photographs of mesoscale structures in outcrop:

a) Alternating fine and coarse siltstone beds; south-west shoreline of Gordon Lake.

b) Flame structures along bedding contacts oriented sub-parallel to  $S_{3S}$ .

c) Minor  $F_3$  folds in finely bedded siltstones. Note, pen parallel to  $S_{3S}$  and offset of bedding along  $S_{3S}$ -parallel (Type 3) veins.

d)  $S_{3S}/S_4$  'herring bone' cleavage pattern within central region of re-fold. Pen is oriented sub-parallel to  $S_{3S}$  in coarse siltstone bed.

e) A sub-vertical  $F_1$  fold hinge transected by the north-west striking,  $D_3$  cleavage (1) with a folded bedding-parallel (Type 1) vein (2).

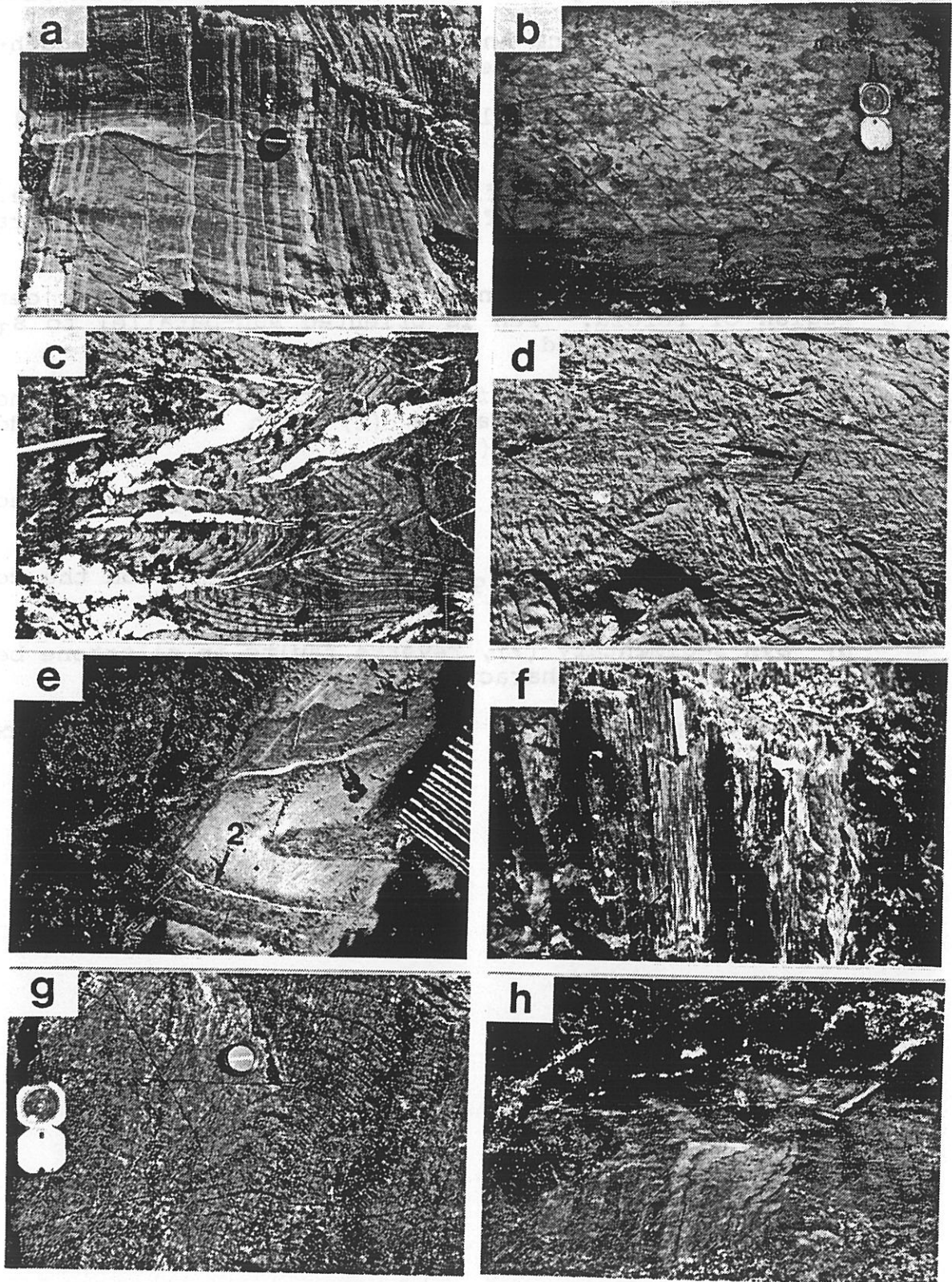
f) Steeply plunging  $L_3$  bedding/cleavage intersection lineation in siltstone.

g)  $D_4$  kink bands of  $S_{3g}$  in graywacke beds from the centre of the re-fold.

h) Syn-sedimentary (?), reverse faults in siltstone beds. Note strata-bound character of deformation.

(All photographs viewed in shallow dipping outcrop, except for 5.3f that is viewed in steeply dipping outcrop)

Figure 5.3



- i) medium- to coarse-grained graywackes
- ii) fine-grained graywackes
- iii) coarse-grained siltstones
- iv) fine-grained siltstones (to mudstones)

#### 5.2.1 Graywackes

At Gordon Lake the graywacke beds are typically 0.1-2 m thick, light to dark tan in weathered outcrop, and light to medium grey on freshly broken surfaces. However, some graywackes in the Lynx Inlet area (Figure 5.2) are dark grey to black in hand specimens. Typically, graywacke beds display a thick graded division (Bouma A) and a thinner pelitic division (Bouma E). In medium- to coarse-grained graywackes, clasts range in size from 0.2-0.4 mm, are poorly sorted and sub-angular. In the fine-grained graywackes, clasts have an average size of 0.08-0.2 mm, and are also poorly sorted and sub-angular. Typically, graywackes consist of 25-35% quartz ( $\pm$  minor plagioclase) clasts that are surrounded by a metamorphically recrystallized matrix of fine-grained quartz, chlorite, biotite, and opaque material (Table A5.1 and A5.3).

#### 5.2.2 Siltstones

Siltstone beds vary from thin laminae to about half a metre thick. The coarse siltstones weather to a light grey, whereas the fine siltstones are usually dark grey to black. Typically, the coarse siltstones consist of 20-55% clasts, ranging in size from 0.02-0.04 mm (Table A5.2 and A5.4). The clasts are predominantly quartz and are surrounded by a metamorphically recrystallized matrix composed of fine muscovite, chlorite, biotite, and opaque material. The fine siltstones have a similar matrix, but have 30-40% clasts ranging in size from 0.005-0.01 mm. The black colour of the fine siltstones is due to the presence of greater amounts of opaque (carbonaceous) material.

### 5.2.3 Interpretation of Regional Lithology

The graywacke-dominated regions at Gordon Lake are similar to other parts of the Yellowknife Basin and represent areas of mid- to outer-fan turbidite deposition (Henderson, 1975, 1987). However, regions dominated by siltstones suggest a transition to a more distal, pelagic environment. On the south-western shore of Gordon Lake the alternating coarse and fine siltstone beds reflect bottom-current winnowing processes (Pickering et al. 1987; F. Hein, personal communication, 1989) and a change in depositional conditions, from high energy graywackes to lower energy siltstones. The black siltstone sequences probably indicate a more restricted, anoxic environment, whereas the darker graywacke sequences might represent turbidite flows that occasionally invaded these anoxic environments and mixed with the finer black sediments.

## 5.3 METAMORPHISM

The metamorphic mineral assemblages and their relationship to structural fabrics were examined at Gordon Lake in order to constrain the time of peak-metamorphism and delimit metamorphic facies within the region. These data provide a framework for the structural interpretation, estimates of P-T conditions, and a base for the  $^{40}\text{Ar}/^{39}\text{Ar}$  dating (Chapter 10).

### 5.3.1 Metamorphic Mineral Assemblages

The Gordon Lake metaturbidites contain variable amounts of quartz, plagioclase, muscovite, chlorite, biotite, cordierite, tourmaline, epidote, and opaque minerals (possibly magnetite, pyrite, ilmenite, and carbonaceous material). Three mineral assemblages were recognized in the Gordon Lake region:

- i) chlorite-quartz-muscovite-plagioclase  
(lower greenschist facies)

ii) biotite-chlorite-quartz-muscovite-plagioclase  
(upper greenschist facies)

iii) cordierite-biotite-chlorite-quartz-muscovite  
-plagioclase (lower amphibolite facies)

The difference between assemblages i) and ii), not defined in outcrop, was recognized in thin section and plotted on Figure 5.4. Cordierite, visible in hand specimen and outcrop, occurs outside of the region mapped and was only examined at exposures adjacent to the Spud Lake pluton.

Within the siltstones fine-grained (5-20  $\mu\text{m}$ ) muscovite and chlorite are oriented parallel to  $S_{3S}$ , and form the limbs of  $D_4$  microfolds (Section 5.4.2). In the graywackes fine-grained chlorite and muscovite surround quartz clasts and have a weak preferred orientation along  $S_{3G}$ . Various morphologies of biotite are found within both graywackes and siltstones. In graywackes, biotite porphyroblasts commonly have an embayed texture, minor quartz inclusions, and a weak preferred orientation along  $S_{3G}$ . Within siltstones, five distinct biotite morphologies were recognized: a) large (50-800  $\mu\text{m}$ ) porphyroblasts, oriented parallel to  $S_{3S}$ , deflect  $S_{3S}$ -forming minerals, have planar arrays of quartz inclusions, and develop quartz/chlorite pressure shadows (Figure 5.5a and 5.5b); b) rare, smaller (50-200  $\mu\text{m}$ ) porphyroblasts are sub-parallel to  $S_{3S}$ , in part cross-cut  $S_{3S}$ -forming minerals, and are without quartz inclusions or well developed pressure shadows (Figure 5.5c); c)  $D_4$  folded porphyroblasts with and without quartz inclusions (Figure 5.5d); d) fine-grained biotite (<20  $\mu\text{m}$ ) along  $S_{3S}$  and  $S_4$  cleavage seams (Gray, 1978); and e) close to areas of lower amphibolite facies, coarse (0.5-2.0 mm) porphyroblasts with and without inclusions that are commonly elongated sub-parallel  $S_{3S}$  (Figure 5.5e). Coarse ( $\approx$  1 cm) cordierite porphyroblasts, found in the metaturbidites adjacent to the Spud Lake



Figure 5.4 Metamorphic map of the south end of Gordon Lake. Regions of biotite-present and biotite-absent assemblages determined from thin section, with cordierite-present assemblages taken from Henderson (1941a, 1941b).

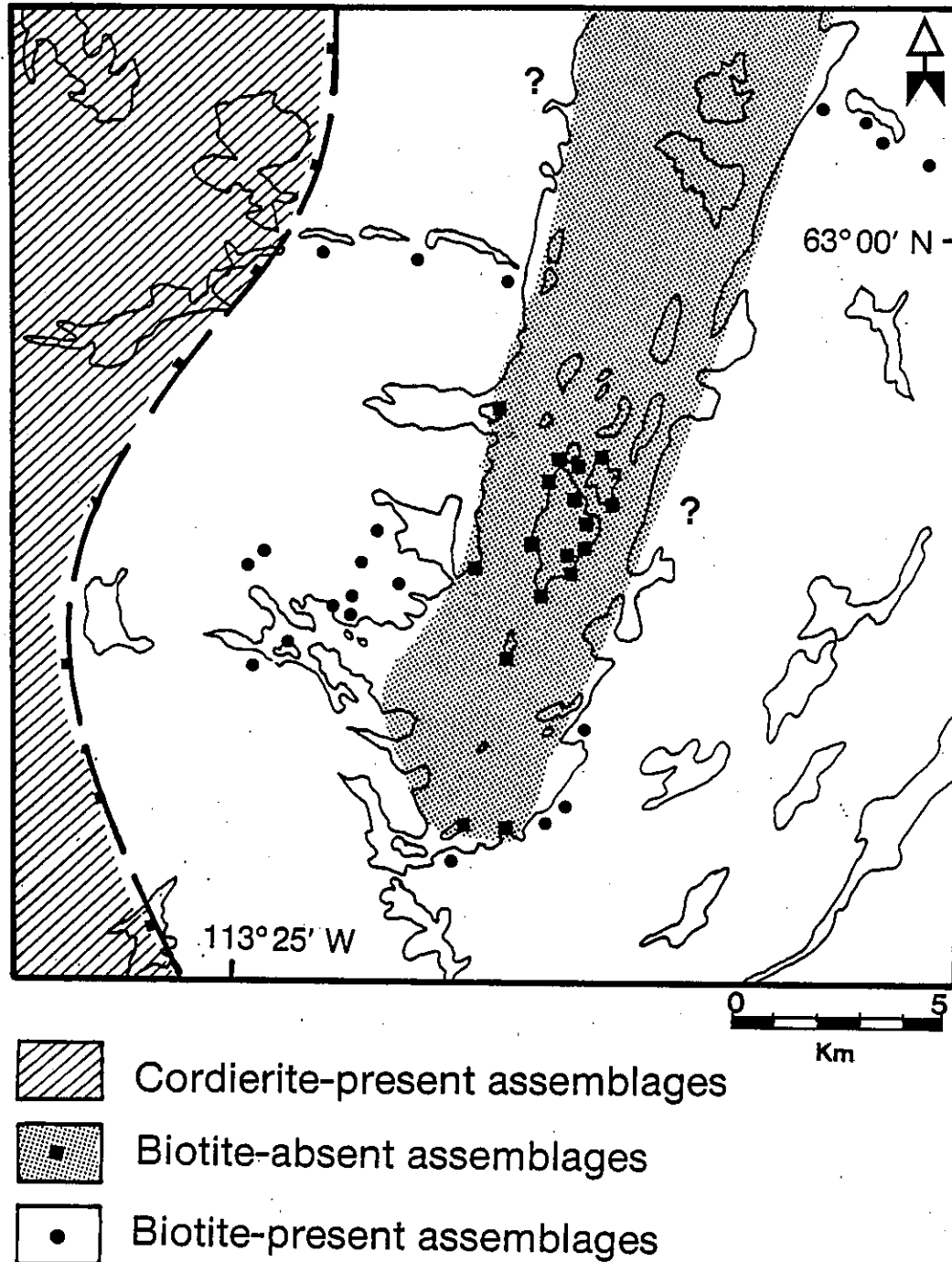
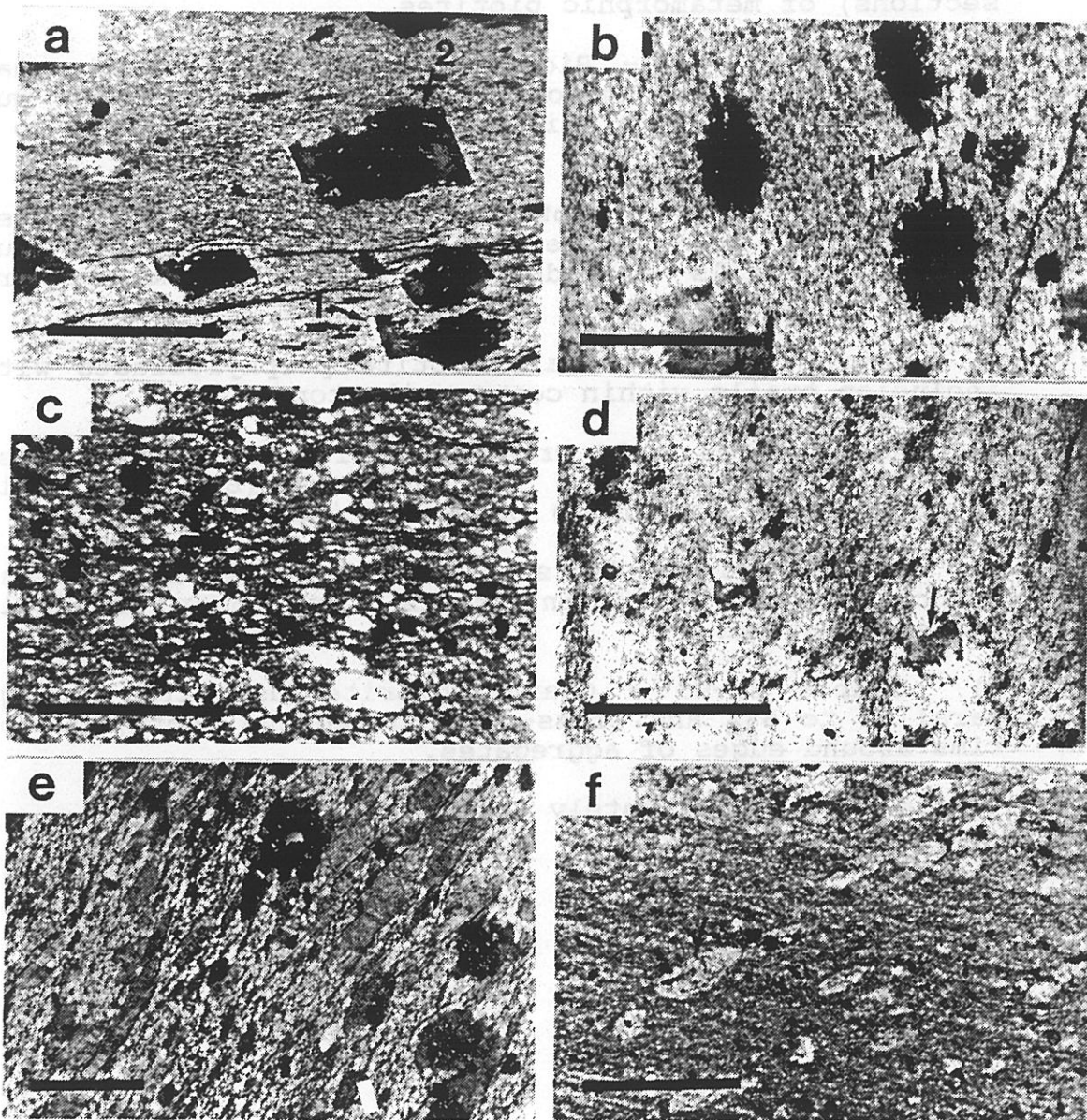


Figure 5.5 Photomicrographs (taken from horizontal or YZ sections) of metamorphic biotites.

- a) Sample 86-94 - Biotite porphyroblasts with quartz-chlorite pressure shadows (1). Note, internal quartz inclusion trails with slight curvature and parallel to  $S_{3s}$  (2).
- b) Sample 86-83 - Biotite porphyroblasts with pressure shadows (1) sub-parallel  $S_{3s}$ . Note, internal quartz inclusion trails and deflection of  $S_{3s}$  matrix around porphyroblasts.
- c) Sample 86-115 - Small biotite porphyroblasts without inclusion trails within coarse siltstone.
- d) Sample 86-84 -  $D_4$  crenulated biotites. Note, pressure shadows sub-parallel to old cleavage ( $S_{3s}$ ) and folding (with possible rotation?) of quartz inclusion trails.
- e) Sample 23/6/1 - Coarse biotite porphyroblasts with and without quartz inclusion trails from lower amphibolite-grade siltstone.
- f) Sample 87-95 - Quartz-chlorite-muscovite aggregates parallel to  $S_{3s}$  and cross-cutting bedding. Note, muscovite rims around edges of aggregates.

(Scale bars approximately 0.4 mm)

Figure 5.5



granite, have a poikiloblastic texture and commonly overprint earlier biotites oriented sub-parallel to  $S_{3S}$ .

Multi-mineralic aggregates are common in black and grey siltstones and are found throughout the region (Figure 5.6 and Table A5.11). These aggregates vary in size from 0.1-1.5 mm, are oriented sub-parallel to  $S_{3S}$  or  $S_{3Es}$  (Figure 5.5f) and have assemblages which include:

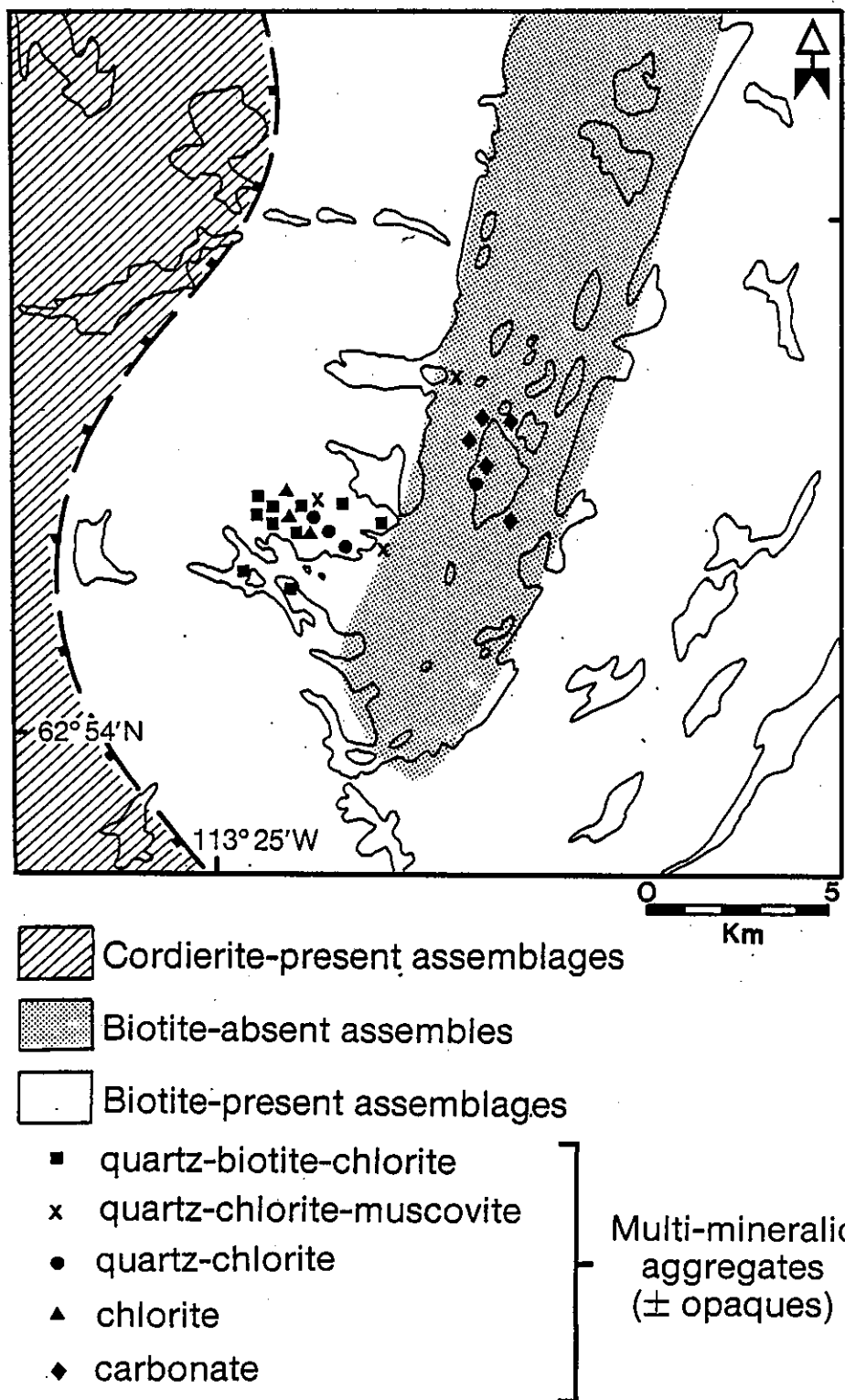
- i) quartz-chlorite-biotite ( $\pm$  opaque minerals)
- ii) quartz-chlorite-muscovite ( $\pm$  opaque minerals)
- iii) quartz-chlorite ( $\pm$  opaque minerals)
- iv) chlorite ( $\pm$  opaque minerals)
- v) carbonate ( $\pm$  quartz and opaque minerals)

Type iv) and some Type i) aggregates occur in the siltstone sequences that host the quartz-breccias (Figure 7.11a and 7.11b). The carbonate aggregates (Type v), confined to the east limb of the refold, commonly have opaque material oriented perpendicular to  $S_{3Es}$  (Figure 5.12e). Some aggregates display mineral zonation with biotite or muscovite rims and chlorite-quartz centres (Figure 5.5f), while others have biotite centres and quartz-chlorite rims (Figure 7.11b).

### 5.3.2 Interpretation of Metamorphic Assemblages

In general the types of metamorphic assemblages agree with those described by previous workers in the Yellowknife Basin (Ramsay and Kamineni, 1977; Thompson, 1978; Kamineni et al. 1979; Swatton, 1987). At Gordon Lake the distribution of metamorphic mineral assemblages (Figure 5.4) indicates a biotite-free area in the centre of the lake, that in part coincides with the siltstone-dominated lithology (Section 5.2). The simplest explanation for this region is that it did not reach the higher P-T conditions of the surrounding areas. However, other possibilities include unsuitable bulk rock composition for the

Figure 5.6 Distribution of syn-D<sub>3</sub>, multi-mineralic aggregates found in thin section within the Gordon Lake region.

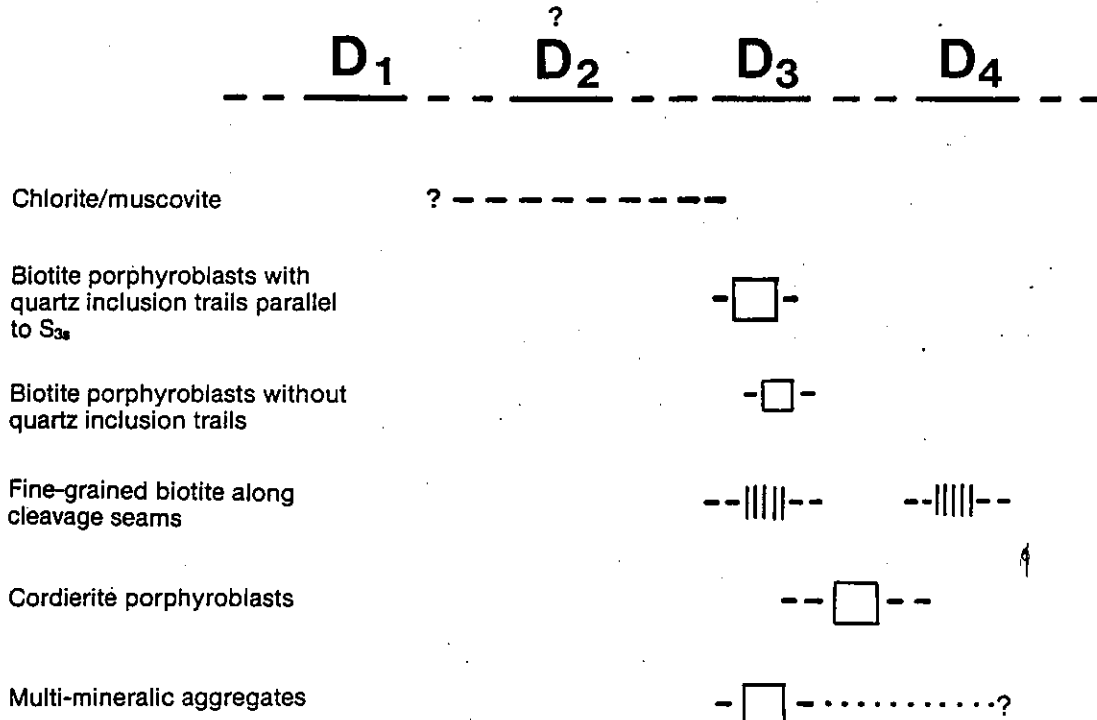


development of biotite, and/or biotite removal by later deformation and associated retrogression. Preliminary inspection of major oxide data for siltstones of biotite-absent and biotite-present regions (Tables A9.4 and A9.5) does not support bulk compositional variations.

The relationships between mineral growth and structural events (Figure 5.7 and Section 5.4) is as follows: 1) muscovite and chlorite, oriented along  $D_3$  cleavages, developed during  $D_3$  or earlier; 2) biotite porphyroblasts, that are parallel to  $S_3s$  with pressure shadows, formed during  $D_3$ ; and 3) cordierite, that occurs close to granitic plutons and overprints biotite, probably developed after  $D_3$  (Figure 5.7). Post-peak-metamorphic deformation ( $D_4$ ) is recorded by folding of biotite porphyroblasts in crenulated siltstone beds. Most of the multi-mineralic aggregates, that are oriented parallel to  $S_{3s}$  and  $S_3E_s$ , developed during prograde  $D_3$  conditions with some, such as Types i), ii), and iii) undergoing later ( $D_4$ ?) retrogression. The precursor to some aggregates was probably biotite, but for others it is less clear.

P-T conditions are difficult to estimate from the mineral assemblages present as none are suitable for thermobarometry. However, the presence of both biotite and cordierite places some broad constraints on the conditions of peak  $D_3$  metamorphism. Biotite can initially form over a wide range of pressures (1-7 kbars) and temperatures (350-450°C; Yardley, 1989, Figure 3.11). However, cordierite forms at temperatures of greater than 500°C and pressures of less than 4 kbars (Winkler, 1974, Figure 14-1; Yardley, 1989, Figure 3.11). These low pressure/high temperature conditions are not dissimilar to those suggested by Ramsay and Kamineni (1977), in which an early phase of metamorphism developed at 3.0-4.5 kbars and at temperatures of less than 500°C (syn- $D_3$ ?), followed by a later phase

Figure 5.7 Metamorphic mineral assemblages and structural events within the Gordon Lake region. (Squares - the main period of porphyroblast growth; solid vertical lines - mineral growth along cleavage seams; dashed horizontal lines - limits of mineral growth; and dotted horizontal lines - possible retrogression)



(post-D<sub>3</sub>?) at 2.5-3.5 kbars and temperatures of at least 300°C, and up to 700°C adjacent to plutons.

#### 5.4 STRUCTURAL GEOLOGY

The structures found at Gordon Lake and described in the rest of this thesis include: major (F<sub>1</sub>) isoclinal folds, quartz inclusion trails in biotite porphyroblasts, a regional (km scale) re-fold, minor (F<sub>3</sub>) folds, northwest striking cleavages (S<sub>3s</sub> and S<sub>3g</sub>) on the re-fold's west limb, north-northeast striking cleavages (S<sub>3Es</sub> and S<sub>3Eg</sub><sup>3</sup>) on the re-fold's east limb, and crenulation cleavages (S<sub>4</sub> and S<sub>4E</sub>). The structural nomenclature used in this thesis is similar to that of Fyson (1982, 1984b), except that cleavages S<sub>4</sub> and S<sub>3E</sub> are used in preference to S<sub>3b</sub> (Table 5.1). In addition, siltstone and graywacke cleavages are designated by subscripts 's' and 'g', respectively (Table 5.2).

##### 5.4.1 Fold Types, Morphology and Distribution

At Gordon Lake there are three phases of folding including: vertical F<sub>1</sub> isoclinal folds (20-400 m wavelength) that are folded to form the kilometre-scale Gordon Lake "re-fold" (Figures 5.1 and 5.2), and F<sub>3</sub> folds (1-4 m wavelength), superimposed on the limbs of F<sub>1</sub> folds. No F<sub>2</sub> folds, with easterly striking axial traces (Fyson, 1980, 1982) were recognized.

##### 5.4.1.1 F<sub>1</sub> and Earlier (F<sub>0</sub>) Folds

The early or F<sub>1</sub> folds are clearly visible on aerial photographs and have distinct curvilinear strike lines that define the regional re-fold structure at Gordon Lake. The strike lines are defined by bedding and, as the folds have an isoclinal geometry, F<sub>1</sub> axial traces. The limbs of F<sub>1</sub>

<sup>3</sup>. The designation '3E' for the morphologically distinct, northeast-trending graywacke and siltstone cleavages of the re-fold's east limb is used to distinguish it from the northwest-trending cleavages of the re-fold's west limb.



Table 5.2 D<sub>3</sub> and D<sub>4</sub> cleavage nomenclature for the west and east limbs of the Gordon Lake refold.

<u>West Limb</u>		
	Siltstones	Graywackes
D <sub>3</sub> cleavages	S <sub>3s</sub>	S <sub>3g</sub>
D <sub>4</sub> crenulation cleavage	S <sub>4</sub>	-
<u>East Limb</u>		
	Siltstones	Graywackes
D <sub>3</sub> cleavages	S <sub>3Es</sub>	S <sub>3Eg</sub>
D <sub>4</sub> crenulation cleavage	S <sub>4E</sub>	-

folds are steeply dipping and consequently the fold axes have vertical to sub-vertical plunges.  $F_1$  fold axial traces are recognised by fold closures, or more commonly, by changes in facing directions determined from primary structures like graded bedding, and load and flame features. The axial traces of  $F_1$  folds are mappable for up to 5 km and usually spaced 10-200 m apart (Map 1). These folds are consistently transected by  $D_3$  cleavages (Figure 5.3e). No cleavage was found associated with  $F_1$  in outcrop or thin section.

Within the map region, seven  $F_1$  fold hinges were located in outcrop and nine interpreted from bedding and facing orientations (Figure 5.8). On the west limb of the refold the  $F_1$  hinges face to the west-northwest, while on the east limb they face to the southwest. All fold facing directions indicate that the presence of an earlier ( $D_0$ ) anticline/syncline is unlikely in this region.

The best mapped  $F_1$  anticline and syncline occur near the Kidney Pond quartz-breccia zones (Figure 5.9a). The anticline has a well defined west-southwest facing hinge and a west-southwest striking axial trace. The north limb of the  $F_1$  fold is at least 200 m thick, while the south limb is 20-30 m thick. The southern limb also forms the northern limb of a syncline. West of the exposed  $F_1$  anticline hinge, the axial trace appears to die out, as does the associated syncline, but to the east both are mappable for 400-450 m. One interpretation of the Kidney fold geometry is that they developed as fault-propagation folds (Figure 5.9b) within an accretionary prism. These folds were subsequently tilted and deformed by vertical stretching and/or flattening during  $D_3$ .

#### 5.4.1.2 $F_3$ Folds

Metre scale  $F_3$  folds with an axial planar  $D_3$  cleavage are found throughout the region.  $F_3$  folds are vertical and

Figure 5.8 Facing directions of  $F_1$  fold closures across the Gordon Lake refold determined during this study.

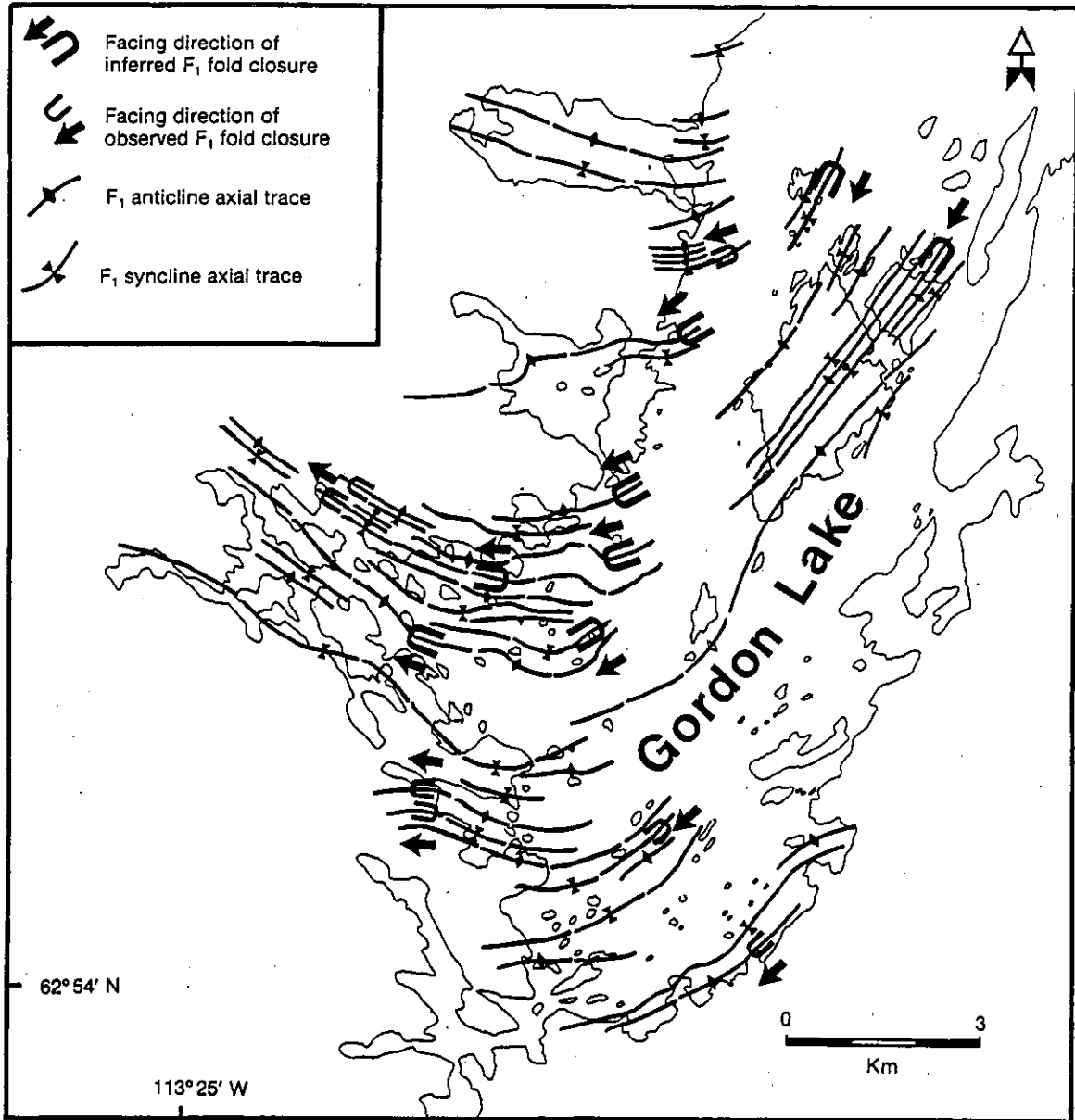
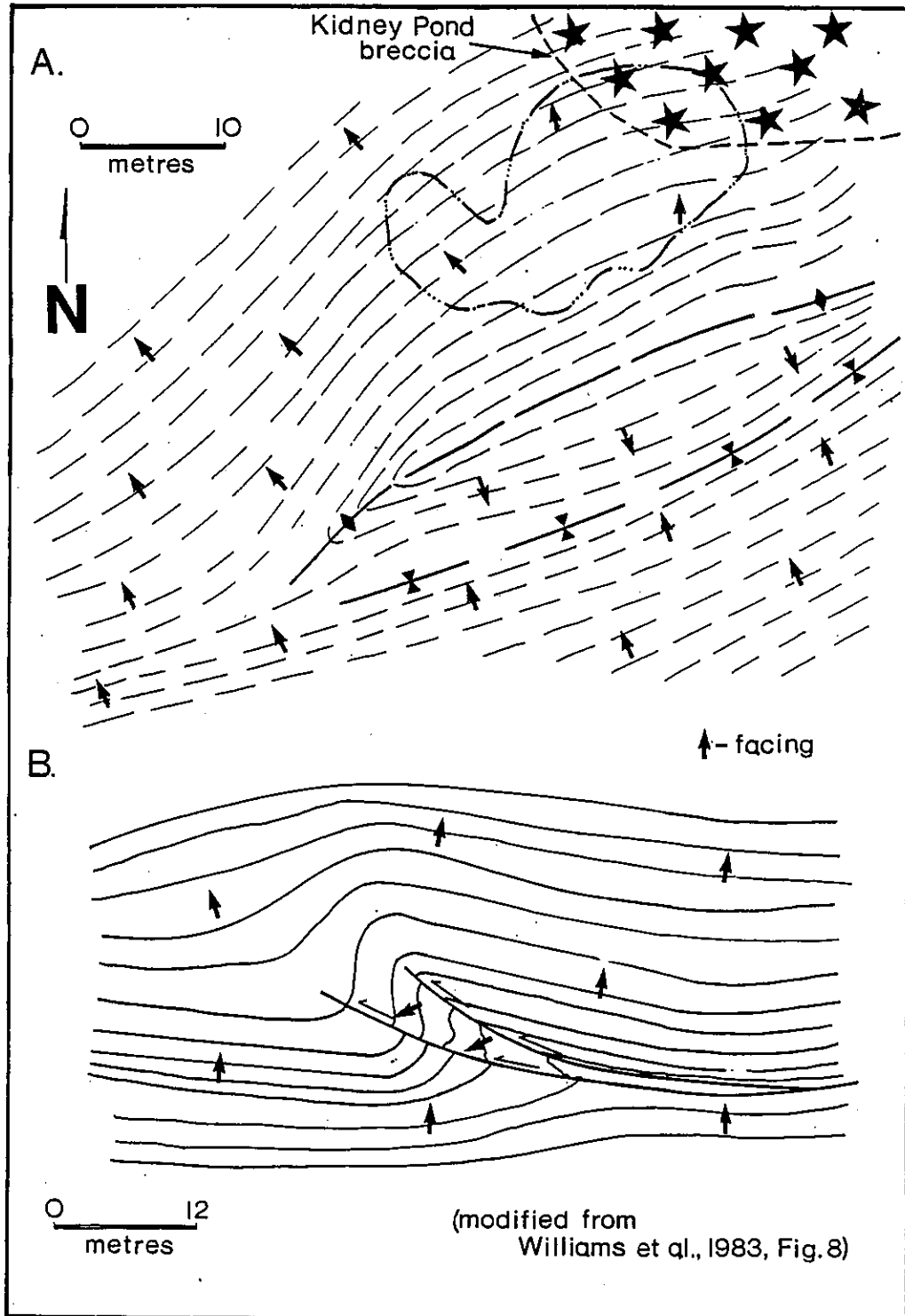


Figure 5.9 A - Map of Kidney Pond  $F_1$  fold structures with bedding strike (dashed lines) and facing directions (arrows). B - Formation of an  $F_1$  fold by fault-propagation folding, modified from Williams and Chapman (1983).



have close to tight interlimb angles (Figures 5.3c). Commonly these folds have minor fractures sub-parallel to their axial plane, which are quartz-filled (Chapter 6). Larger scale (100's of metres)  $F_3$  folds may also be present, as in the Lynx Inlet area (Figure 5.2). In this case  $S_{3g}$  is axial planar, whereas  $S_{3s}$  is convergent to the southeast (Map 1).

#### 5.4.1.3 Regional Refold

The regional refold which deforms early vertical  $F_1$  folds is a kilometre-scale open fold with an asymmetric profile. The refold has a sub-vertical plunge and an interlimb angle of 70-90° with the west limb striking north-northwest and the east limb north-northeast.

#### 5.4.2 Cleavages and Quartz Inclusion Fabrics

Cleavage orientations of both graywackes and siltstones across the southern end of Gordon Lake are shown on Map 1.  $S_{3s}$ ,  $S_{3g}$ ,  $S_{3Es}$ , and  $S_{3Eg}$  cleavages (Table 5.2) are steeply dipping, clearly transect all  $F_1$  folds, and re-orient primary sedimentary structures (e.g., mud clasts and flames, Figure 5.3b). On the refold's west limb  $S_{3s}$  strikes to the northwest (Plot 2, Figure 5.10), while on the east limb  $S_{3Es}$  strikes to the north-northeast (Plot 14, Figure 5.10) and is within 10-30° of bedding. In outcrops of fine-grained siltstone on the west limb and in the central part of the refold  $S_{3s}$  is crenulated to form a new cleavage ( $S_4$ ). This crenulation cleavage forms, with  $S_{3s}$  in coarser siltstones and  $S_{3g}$  in graywackes, a distinctive "herring-bone" cleavage pattern (Figure 5.3d; Fyson 1984a).  $S_4$  is consistently oriented counter-clockwise<sup>4</sup> from bedding; but does vary in strike sympathetically with the strike of bedding, from the west limb to the central part

---

<sup>4</sup>. Rotational sense is always given looking down the plunge of the refold.

Figure 5.10a and 5.10b Bedding, cleavage and lineation data from the Gordon Lake refold. Line A on map of Gordon Lake represents the eastern limit of  $S_{3S}$  and  $S_4$ , Line B the western limit of  $S_{3ES}$ , Line C the western limit of  $S_4$ , and Line D separates north-east striking from north-west striking  $D_3$  graywacke cleavages. The central domain is a complex region of cleavages, where  $S_{3S}$ ,  $S_{3ES}$  and  $S_4$  are commonly indistinguishable. All structural data plotted on equal-area lower-hemisphere projections.

West Limb Domain: 1) Bedding contoured at 0.5, 4.6, 8.7, 12.8, 17.0 and 21.1% / 1% unit area; 2)  $S_{3S}$  contoured at 0.0, 7.2, 14.3, 21.5, 28.6 and 35.8% / 1% unit area; 3)  $S_4$  contoured at 2.0, 10.0, 18.0, 26.0, 34.0 and 42.0% / 1% unit area; 4)  $S_{3g}$  contoured at 1.4, 9.1, 16.9, 24.7, 32.4 and 40.2% / 1% unit area; and 5)  $L_3$  contoured at 6.0, 16.0, 26.0, 36.0, 56.0 and 76.0% / 1% unit area.

Central Domain: 6) Bedding contoured at 0.6, 3.5, 6.5, 9.4, 12.3 and 15.3% / 1% unit area; 7)  $S_{3S} + S_{3ES} + S_4$  contoured at 0.7, 2.2, 3.8, 5.3, 6.8 and 8.4% / 1% unit area; 8)  $S_{3g} + S_{3Eg}$  contoured at 1.4, 7.6, 13.8, 20.0, 26.2 and 32.4% / 1% unit area; and 9)  $L_3 + L_{3E}$  contoured at 7.0, 16.0, 25.0 and 52.0 / 1% unit area.

East Limb Domain: 10) Bedding contoured at 0.6, 5.0, 9.5, 13.9, 18.4 and 22.4% / 1% unit area; 11)  $S_{3ES}$  contoured at 0.7, 5.3, 9.8, 14.4, 18.9 and 23.5% / 1% unit area; 12)  $S_{3g} + S_{3Eg}$  contoured at 2.2, 6.3, 10.4, 14.4, 18.5 and 22.6% / 1% unit area; and 13)  $L_{3E}$  contoured at 3.0, 13.0, 23.0, 33.0, 53.0 and 73.0% / 1% unit area.

Total map area: 14) All bedding data contoured at 0.2, 2.0, 3.8, 5.7, 7.5 and 9.3% / 1% unit area; 15) all  $D_3$  siltstone cleavage data contoured at 0.2, 2.8, 5.5, 8.1, 10.7 and 13.4% / 1% unit area; 16) all  $D_3$  graywacke cleavage data contoured at 0.6, 5.1, 9.6, 14.2, 18.8 and 23.3% / 1% unit area.

Figure 5.10a

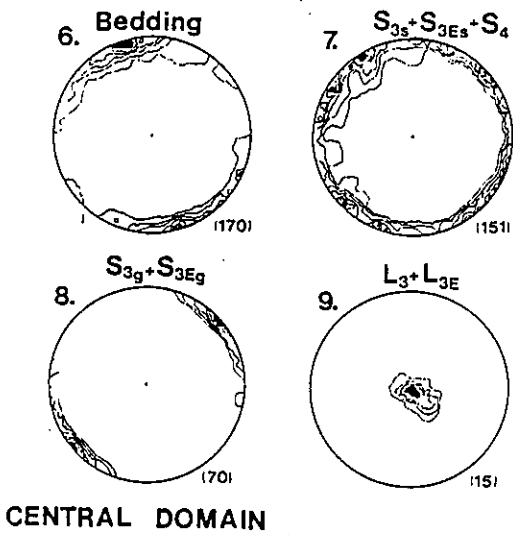
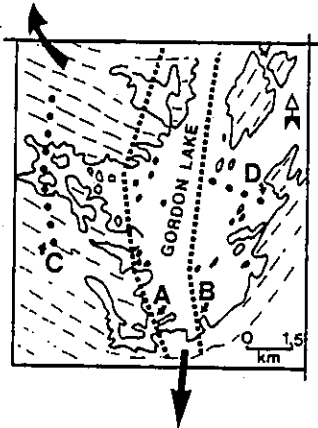
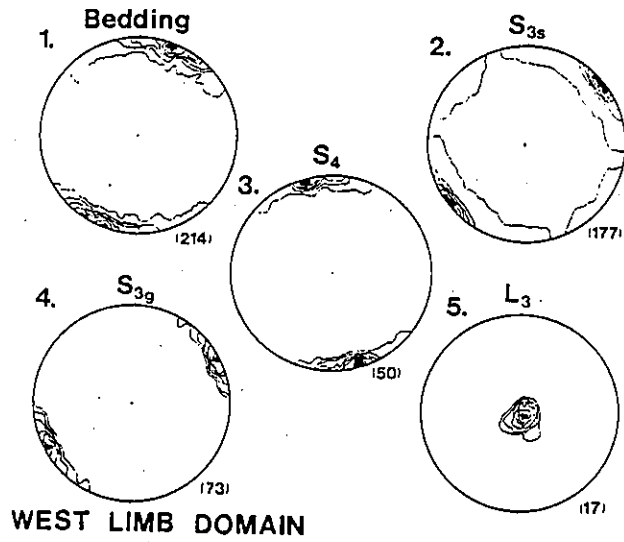
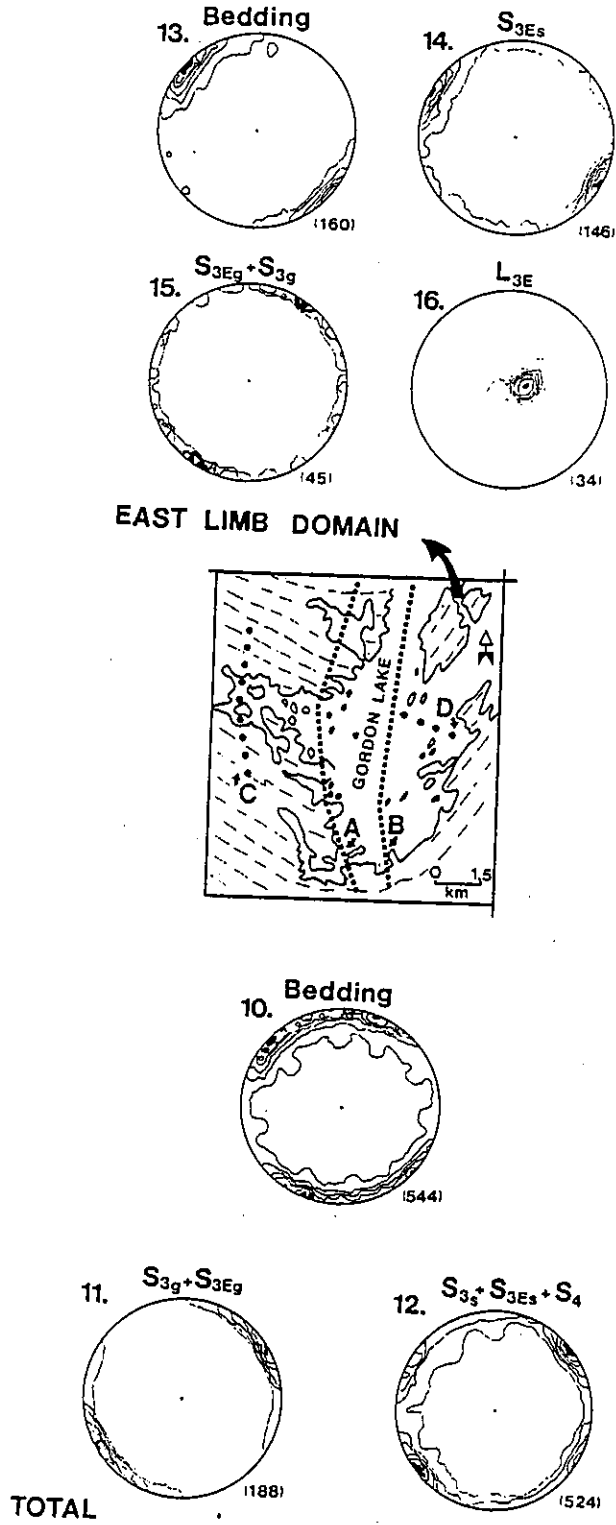


Figure 5.10b





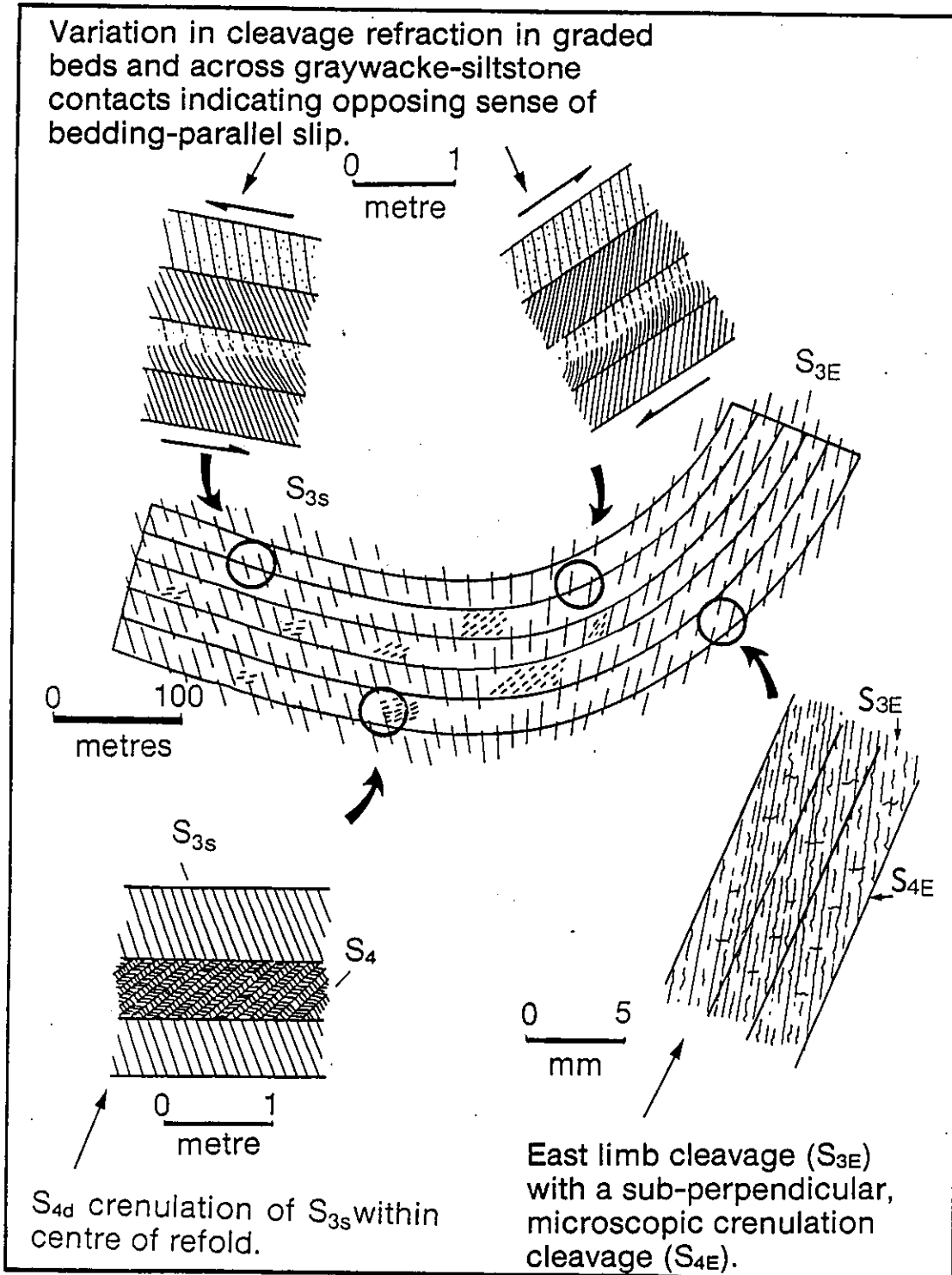
of the refold (Figure 5.11, Map 1).  $D_3$  graywacke cleavage consistently strikes north-northwest on the west limb of the refold (Plot 4, Figure 5.10) and forms a refracting cleavage with  $S_{3S}$  in graded beds, indicating a sinistral sense of bedding-parallel slip. In the central region of the refold this  $D_3$  cleavage refraction, though less clear, is the reverse (Figure 5.11). On the east limb  $D_3$  graywacke cleavage strikes both north-northeast and north-west (Plot 15, Figure 5.10). The north-northeast striking graywacke cleavage ( $S_{3Eg}$ ) is restricted to the northern part of Zenith Island, while the north-westerly striking graywacke cleavage ( $S_{3g}$ ) occurs along the southeast shoreline of Gordon Lake and appears to transect the east limb of the refold (Map 1). The changes in strike of  $S_{3g}$  and  $S_{3Eg}$  across the refold are probably the result of later ( $D_4$ ) rotation of the graywacke beds.

#### 5.4.2.1 Quartz Inclusion Trails in Biotite Porphyroblasts

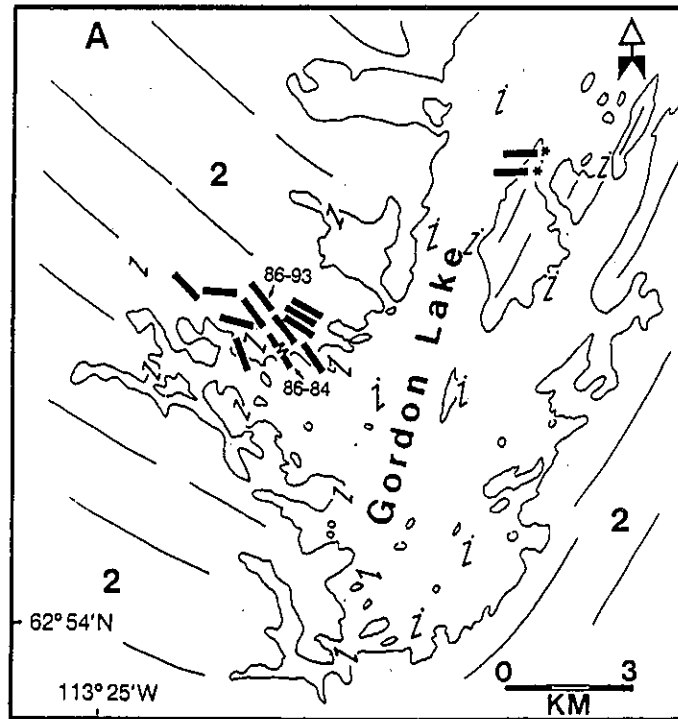
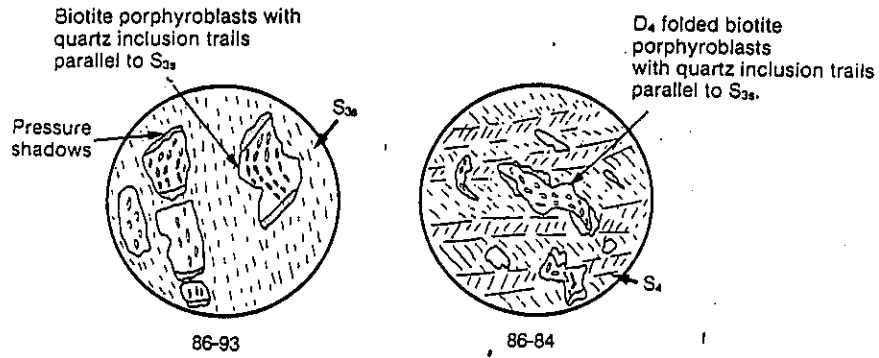
Biotite porphyroblasts in oriented siltstone samples, from the east and west shore of south Gordon Lake, commonly display planar arrays of quartz inclusion trails. On the west limb of the refold the inclusion trails strike north-west, are sub-parallel to  $S_{3S}$ , and occur both parallel to and perpendicular to the basal cleavages of the biotite porphyroblasts (Figure 5.12 and Table A5.12). Commonly these inclusion trails display minor curvature that is continuous with the external  $S_{3S}$  fabric, and indicates minor adjustments of  $S_{3S}$  orientation during non-coaxial ( $D_3$ ) strain.

On the eastern shore of Gordon Lake, of the few samples taken, one sample (29/6/7) has easterly striking quartz inclusion trails with an enveloping cleavage ( $S_{3Es}$ ) that strikes north-south and crenulates an earlier cleavage ( $S_{3S}$ ?), that is sub-parallel to the inclusion trails (Figure 5.13 and Table A5.13). This east-west geometry

Figure 5.11 Sketch of  $S_{3s}$ ,  $S_{3Es}$ ,  $S_4$ , and  $S_{4e}$  cleavage relationships around the Gordon Lake reflow.

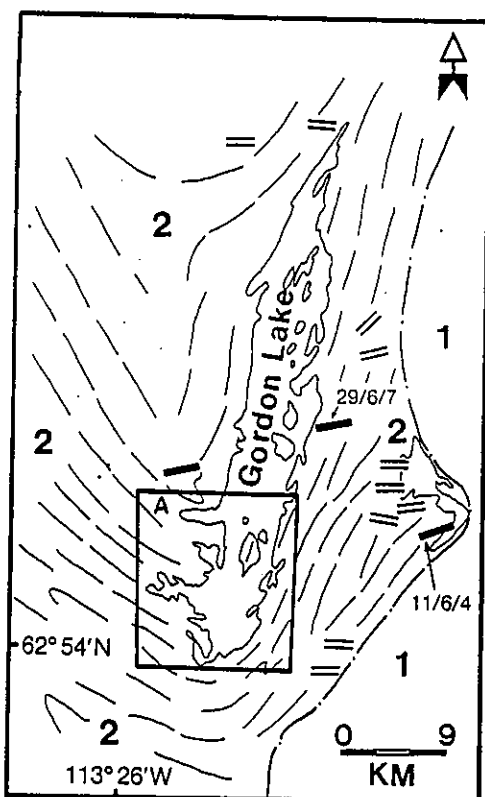
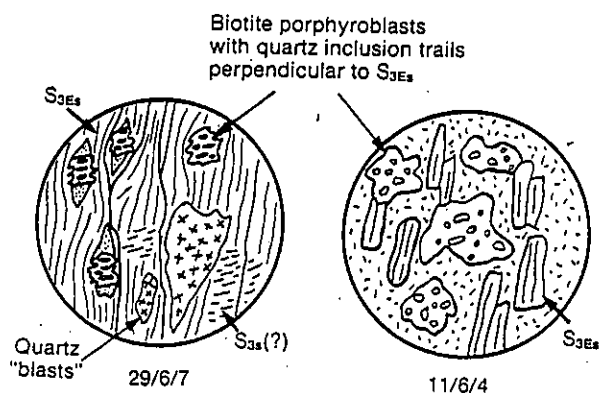


**Figure 5.12** Distribution and orientation of quartz inclusion trails within biotite porphyroblasts on the west shore of Gordon Lake (area A located on Figure 5.13).



- 2** Metaturbidites
- Quartz inclusion trails in biotite porphyroblasts
- Opaque mineral trails in carbonate aggregates
- $S_{3s}$
- $S_{3Es}$
- Bedding strike lines
- $D_4$  folded biotite porphyroblasts with quartz inclusion trails parallel to  $S_{3s}$ .

**Figure 5.13** Distribution and orientation of quartz inclusion trails within biotite porphyroblasts on the east shore of Gordon Lake, with inset of area A on Figure 5.12.



- 1 Metavolcanic rocks
- 2 Metaturbidites
- Quartz-inclusion trails in biotite porphyroblasts (this thesis)
- == Quartz-inclusion trails in biotite porphyroblasts (Fyson 1975, 1990)
- /// Bedding strike lines

compares well with data from the refold's east limb collected by Fyson (1990, Figure 3).

#### 5.4.2.2 Strain and Microstructure of D<sub>3</sub> Cleavages

The D<sub>3</sub> graywacke cleavage (S<sub>3G</sub> and S<sub>3EG</sub>) displays distinct differences in strain characteristics between YZ, XZ, and XY sections (Figure 5.14 and 5.15). In all cases the D<sub>3</sub> graywacke cleavage is typified by a vertical stretch parallel to the L<sub>3</sub> lineation (Section 5.4.3). In the YZ section the D<sub>3</sub> graywacke cleavage displays weak preferred orientation and truncation of clasts, traces of pressure shadows around clasts, and some alignment of metamorphic minerals (see Table A5.5 and A5.7). However, in XZ sections most clasts are truncated, have a preferred elongation defining the vertical stretch, and well developed pressure shadows. In addition, most metamorphic minerals are aligned and well developed discontinuous, cleavage seams of biotite/iron oxide are present. Typically, S<sub>3EG</sub> differs from S<sub>3G</sub> (Figure 5.15) in that the former lacks biotite, is carbonate-rich, displays a greater preferred orientation and elongation of clasts, and has more aligned metamorphic minerals and well developed cleavage seams.

The D<sub>3</sub> siltstone cleavage, like the D<sub>3</sub> graywacke cleavage, exhibits a strong vertical stretch, displayed by the preferential alignment of metamorphic minerals, opaque minerals, and multi-mineralic aggregates. S<sub>3S</sub> is typically composed of quartz, muscovite, chlorite, biotite, and opaque minerals and is characterized by spaced (continuous and zonal) cleavage seams, and oriented quartz clasts and metamorphic minerals (Table A5.6). In comparison, S<sub>3ES</sub> is composed of fine muscovite, chlorite, quartz, carbonate, and minor opaque material (Table A5.8), and has only poorly developed cleavage seams; probably due to the absence of biotite and/or iron oxide. In YZ sections a faint,

Figure 5.14 Block sketch of  $D_3$  cleavage in graywacke with vertical stretch lineation.  $YZ$ ,  $XZ$ , and  $XY$  planes are perpendicular to cleavage and lineation, perpendicular to cleavage and parallel to lineation, and parallel both cleavage and lineation, respectively.

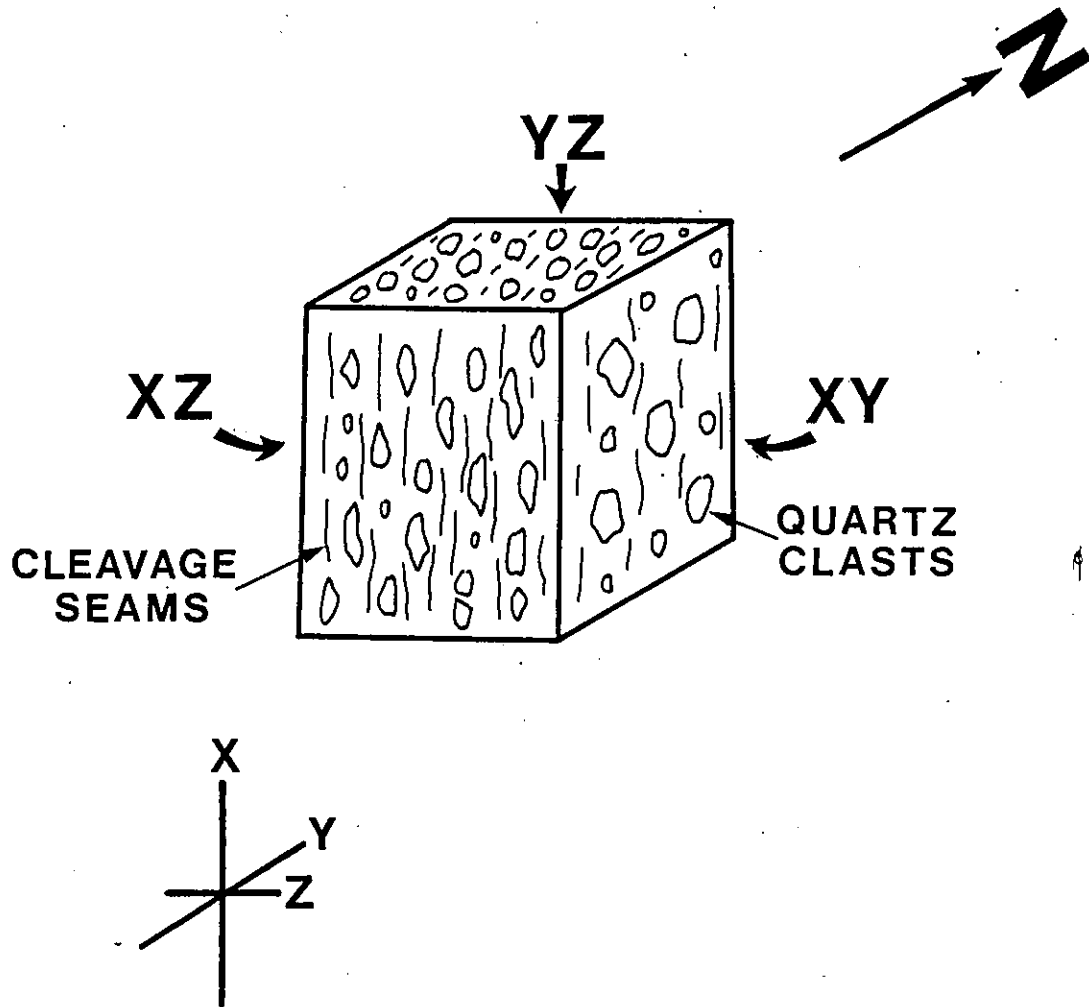
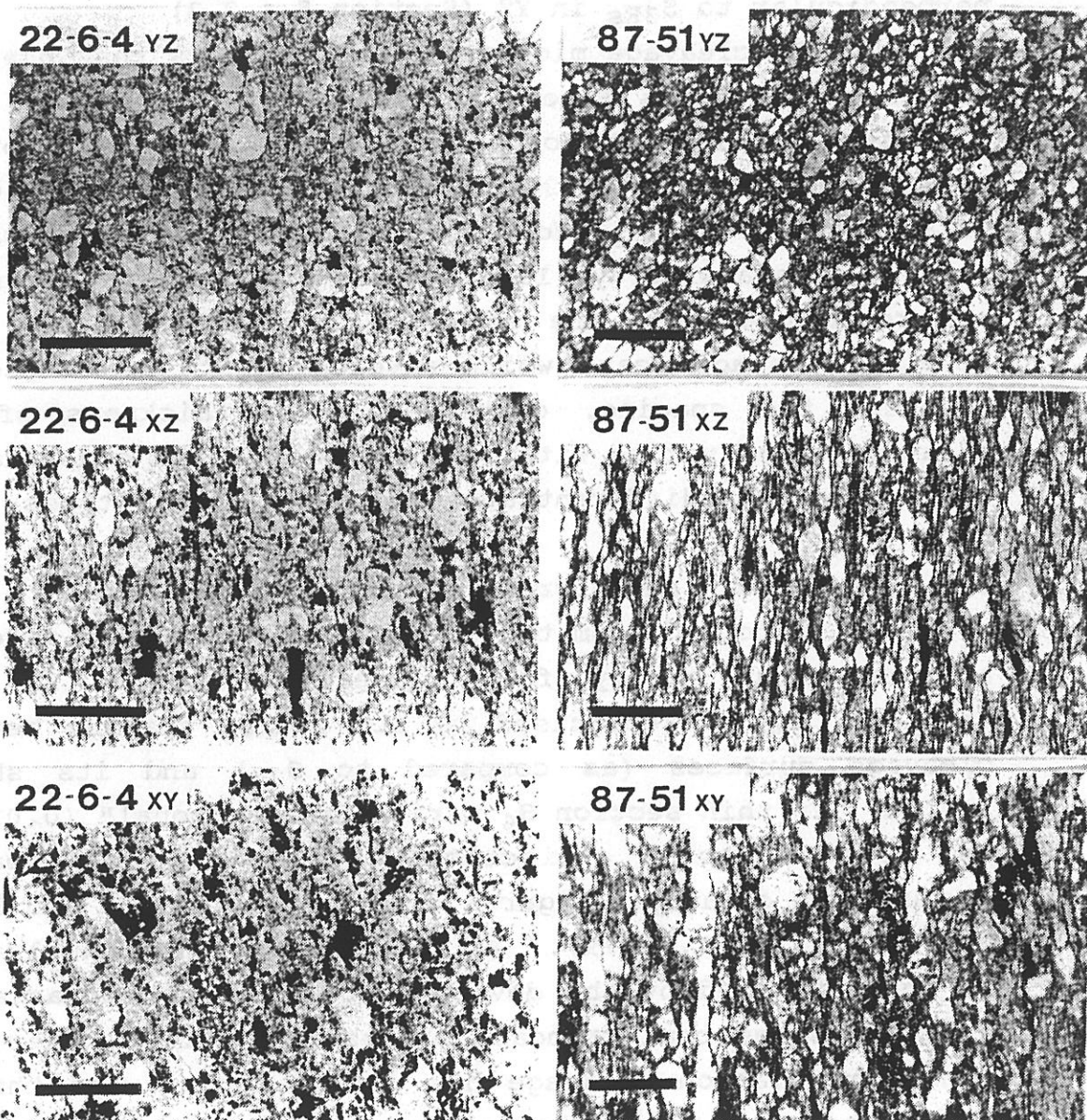


Figure 5.15 Photomicrographs of YZ, XZ, and XY sections of medium- to coarse-grained graywackes, 2/6/4 and 87-51, from the west and east limbs of the refold, respectively. Note, the greater elongation of clasts in XZ and XY sections of 87-51 as compared to 22/6/4.

(Scale bars approximately 0.5 mm)

Figure 5.15



crystallites were found in all zones with average size also greater than 0.05  $\mu$ m or with less than 50% chlorite. The mineralogy is composed of chlorite, quartz, and opaque minerals. In some zones, chlorite and quartz crystals are found in scattered microfractures, whereas quartz crystals are found in the microfractures, and the chlorite crystals are found in the microfractures. The chlorite crystals are generally oriented along cleavage planes. The chlorite crystals are generally oriented along cleavage planes.



discontinuous crenulation fabric ( $S_{4E}$ ) occurs sub-perpendicular to  $S_{3Es}$  in YZ (Section 5.4.2.3)

The  $D_3$  cleavage microstructure suggests that pressure solution mechanisms (i.e., Durney 1972; Gray, 1978) were important in cleavage formation; with  $S_{3s}$  and  $S_{3Es}$  forming a "slaty" cleavage in the siltstones (Powell, 1974; Gray, 1978) and  $S_{3g}$  and  $S_{3Eg}$  forming a morphologically equivalent "rough" cleavage (Gray, 1978) in the graywackes. The slaty and rough cleavages are essentially similar in that they develop cleavage seams which envelop clasts or fragments. However, the spacing, continuity, and thickness of the cleavage seams varies with rock grain-size and clast/matrix ratio, and thus differentiates the two cleavage types.

#### 5.4.2.3 Strain and Microstructure of $D_4$ Cleavages

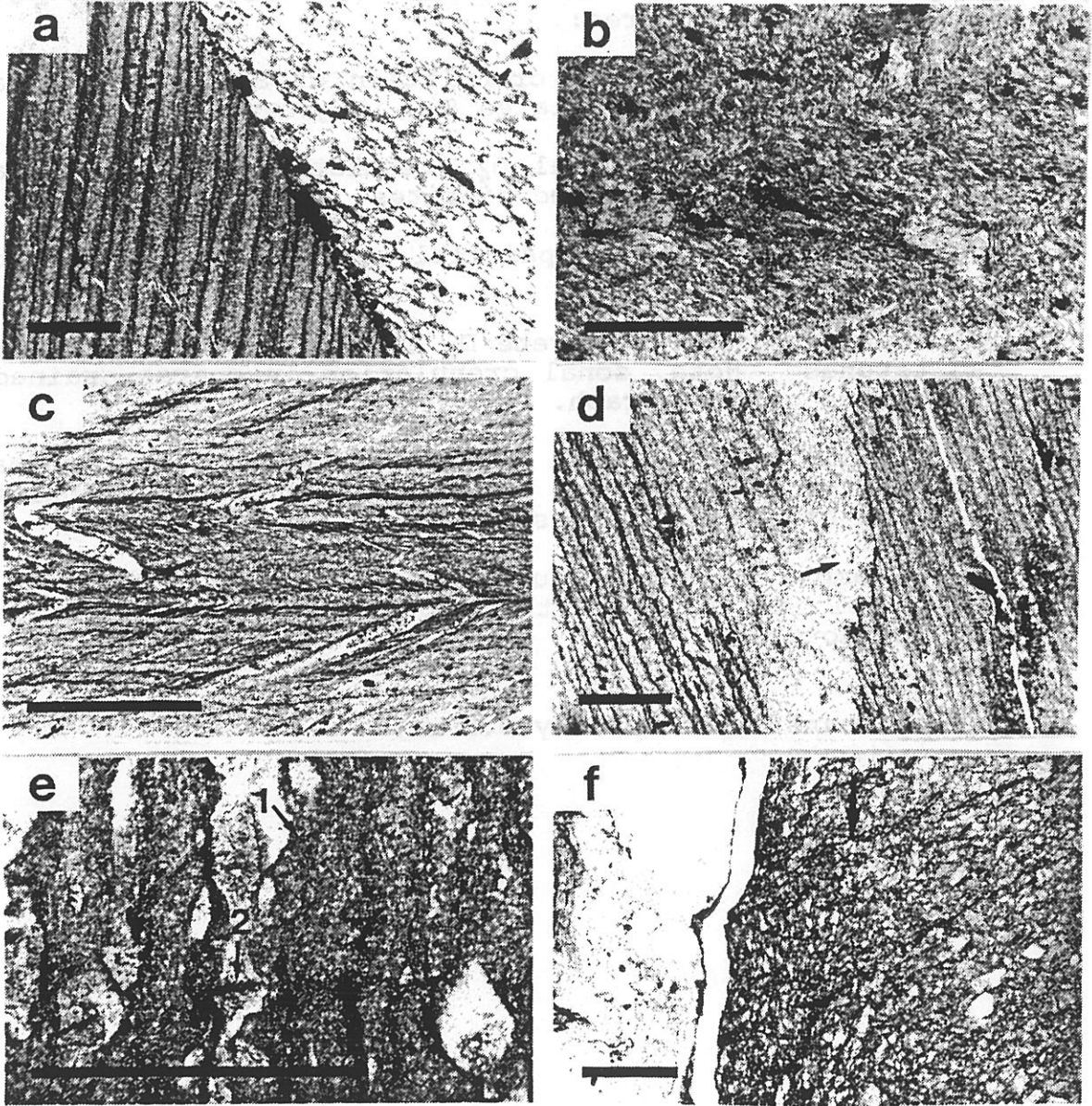
$S_4$  is formed from the crenulation of  $S_{3s}$  and develops a steep, but rarely found lineation ( $L_4$ ). In hand specimen,  $S_4$  is recognised by its coarse spacing between cleavage surfaces (as compared to  $S_{3s}$ ) and its sheeny lustre. In thin section  $S_4$  varies from a "zonal" (0.03-0.1 mm spaced) to a "discrete" (0.01-0.03 mm spaced) crenulation cleavage (Figures 5.16a, 5.16b, 5.16d and Table A5.9; Gray, 1977, 1979). (A discrete crenulation cleavage is characterized by the development of sharp boundaries or cleavage seams that truncate the earlier fabric, whereas a zonal crenulation cleavage has diffuse boundaries through which the earlier fabric can be traced; Gray, 1978.) No crenulations were found in siltstones with average clast size greater than 0.05 mm or with less than 50% matrix material.  $S_4$  mineralogy is composed of fine muscovite, chlorite, and opaque material oriented along the limbs of microfolds, whereas quartz grains are found concentrated in the microfold hinges, and fine grained biotite and/or iron oxides along cleavage seams. Biotite porphyroblasts that occur in crenulated siltstones are generally folded by  $D_4$

Figure 5.16 Photomicrographs (in YZ section) of  $D_4$  crenulation structures:

- a) Sample 86-250 -  $S_4$  crenulation of  $S_{3s}$  in fine grained siltstone, with uncrenulated  $S_{3g}$  in graywacke.
- b) Sample 86-84 - Zonal  $D_4$  crenulation in a fine grained siltstone, with  $D_4$  folded biotites.
- c) Sample 86-250 -  $S_3$ -parallel veins folded and truncated by  $S_4$ .
- d) Sample 86-99 - Discrete  $D_4$  crenulations in fine-grained siltstones. Note, zonal crenulation in coarse-grained bed in centre of photograph.
- e) Sample 87-147 - Fine grained siltstone with carbonate aggregates sub-parallel to  $S_{3Es}$ . Note,  $S_{4E}$  crenulations (1) and opaque material sub-parallel to  $S_{4E}$  (2).
- f) Sample 87-13 - Boudinaged 'neck' of (Type 4) vein parallel to  $S_{3Es}$  with cross-cutting (extensional?) microfractures.

(Scale bars approximately 0.5 mm)

Figure 5.16

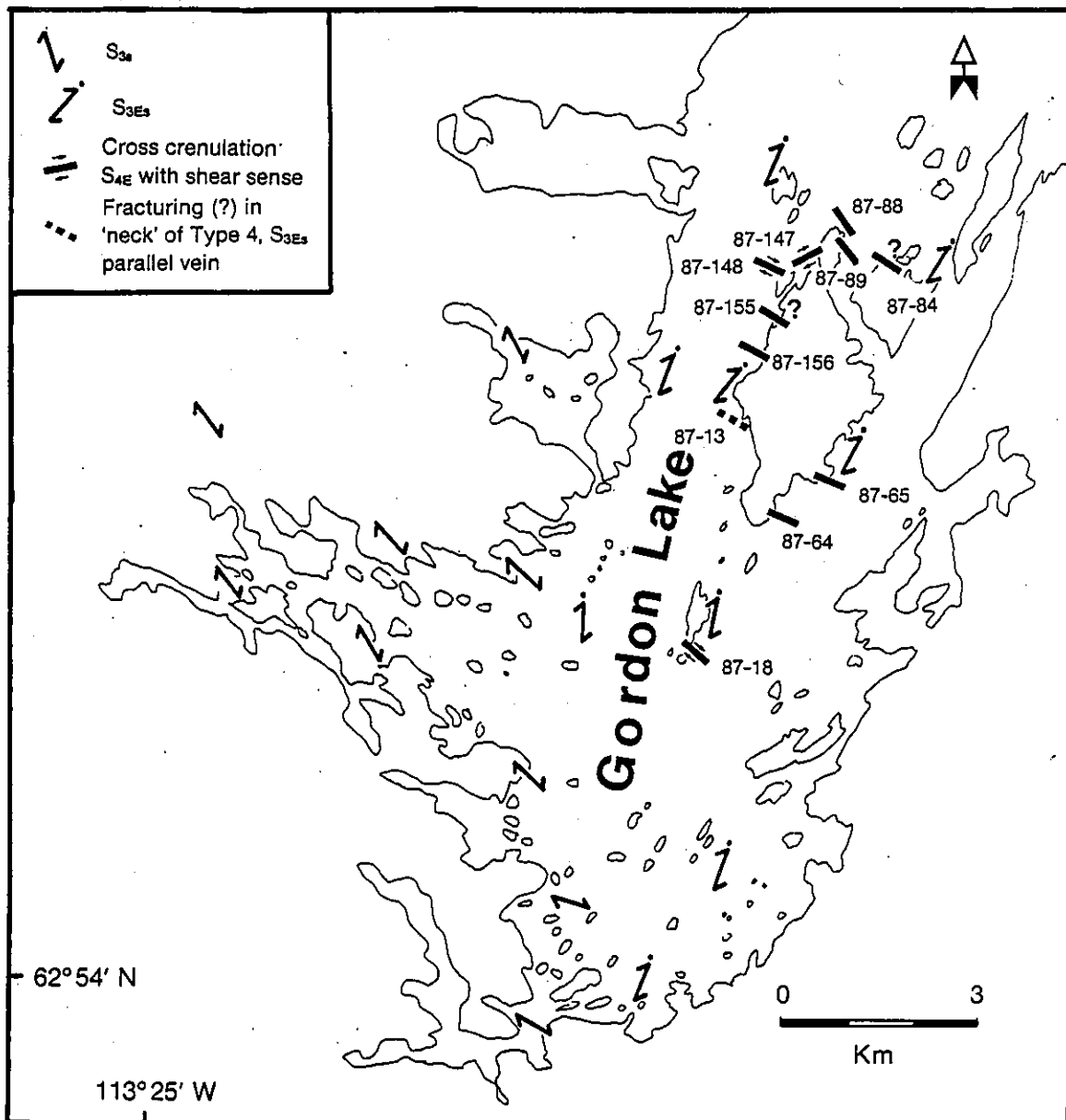


(Figure 5.16b), but where cleavage seams are well developed there is commonly a lack of biotite porphyroblasts. The folding of biotite porphyroblasts suggests that the crenulation cleavage event ( $D_4$ ) is post-peak or late metamorphic in age. However, the lack of biotite porphyroblasts across the refold precludes complete confirmation of this. Quartz veinlets (parallel to  $S_{3S}$ ) in crenulated siltstones are both folded and in some places truncated (Figures 5.16c), indicating that pressure solution is an important deformation mechanism responsible for  $S_4$  formation.

The crenulation cleavage event ( $D_4$ ) within the fine-grained siltstones is characterized by folded quartz veins and microfolds of  $S_{3S}$  and is the result of shortening of this earlier fabric; which lies in the contractional field of the  $D_4$  strain ellipse. The steep plunges of the crenulation axes, seen in orientated thin sections, indicate that  $D_4$  is sub-horizontal. This sub-horizontal deformation probably include a combination of both pure and simple shear, but based on: i) the confinement of  $S_4$  to the central region of the refold, ii) the consistent strike of  $S_4$  with respect to bedding around the refold, and iii) the offset and rotation of  $S_{3S}$ -parallel veins along bedding in the refold centre (Section 5.5.2) it is apparent that a major component of  $D_4$  is simple shear. This ( $D_4$ ) simple shear component could have developed during bedding-parallel and flexural slip associated with counter-clockwise rotation of the refold's east limb.

On the refold's east limb a poorly developed crenulation cleavage ( $S_{4E}$ ) occurs sub-perpendicular to  $S_{3ES}$  (Figure 5.17 and Table A5.10).  $S_{4E}$  generally strikes northeast, and in some cases displays a dextral sense of offset. Commonly carbonate aggregates, elongated parallel  $S_{3ES}$ , act as a loci for  $S_{4E}$  (Figure 5.16e). In some cases, the 'neck' regions of boudinaged East Limb veins (that are

Figure 5.17 Distribution and orientation of  $S_{4E}$  crenulation found in thin section sub-perpendicular to  $S_{3Es}$ .



sub-parallel to  $S_{3ES}$ , Section 6.1.4) display possible microfractures with similar orientations to  $S_{4E}$  (Figures 5.16f). Explanations for the sub-perpendicular orientation of  $S_{4E}$  to the main  $S_{3E}$  cleavage and its sub-parallelism to the microfractures are unclear. On the one hand the fine  $S_{4E}$  crenulation cleavage implies a sub-horizontal contractional event post-dating  $S_{3ES}$ . Whereas, on the other hand, the boudinaged character of the East Limb veins and the fine microfractures in the vein necks suggest a phase of sub-horizontal extension in a similar orientation. The most likely explanation for these post- $D_3$  structures is that they developed during different stages of  $D_4$  counter-clockwise rotation of the refold's east limb; possibly with an early contractional phase sub-perpendicular to  $S_{3E}$  and then a later sub-horizontal extension or flattening sub-parallel to  $S_{3E}$ .

#### 5.4.3 Lineations

$L_3$  is defined in the field by the intersection of  $S_{3S}$  and  $S_{3G}$  with bedding (Figure 5.3f), while  $L_{3E}$  is the intersection of  $S_{3ES}$  and  $S_{3EG}$  with bedding.  $L_3$  and  $L_{3E}$  are also parallel to a stretch lineation (generally found in thin section) that is defined by elongated quartz clasts, lithic clasts, multi-mineralic aggregates and a preferred alignment of metamorphic minerals (Section 5.5). On the west limb of the refold  $L_3$  is vertical (Plot 5, Figure 5.10), whereas on the east limb  $L_{3E}$  has a steep easterly plunge (Plot 16, Figure 5.10). This steep easterly plunge is in part explained by the shallower ( $75-85^\circ$ ) bedding dips found on the east limb.

#### 5.4.4 Other Structures

Rare, strata-bound intrafolial folds and reverse faults (Figure 5.3g) are found in the Kidney Pond region (Map 1) and are transected by  $S_{3S}$  and  $S_{3G}$ . These

structures formed pre-D<sub>3</sub>, and might represent syn-sedimentary slumping and faulting.

Rare kink bands (Figure 5.3h) in coarse siltstones and graywackes occur in the central region of the refold. These kink bands fold S<sub>3g</sub>, have vertical axial traces, and probably represent D<sub>4</sub> deformation of the more competent graywackes.

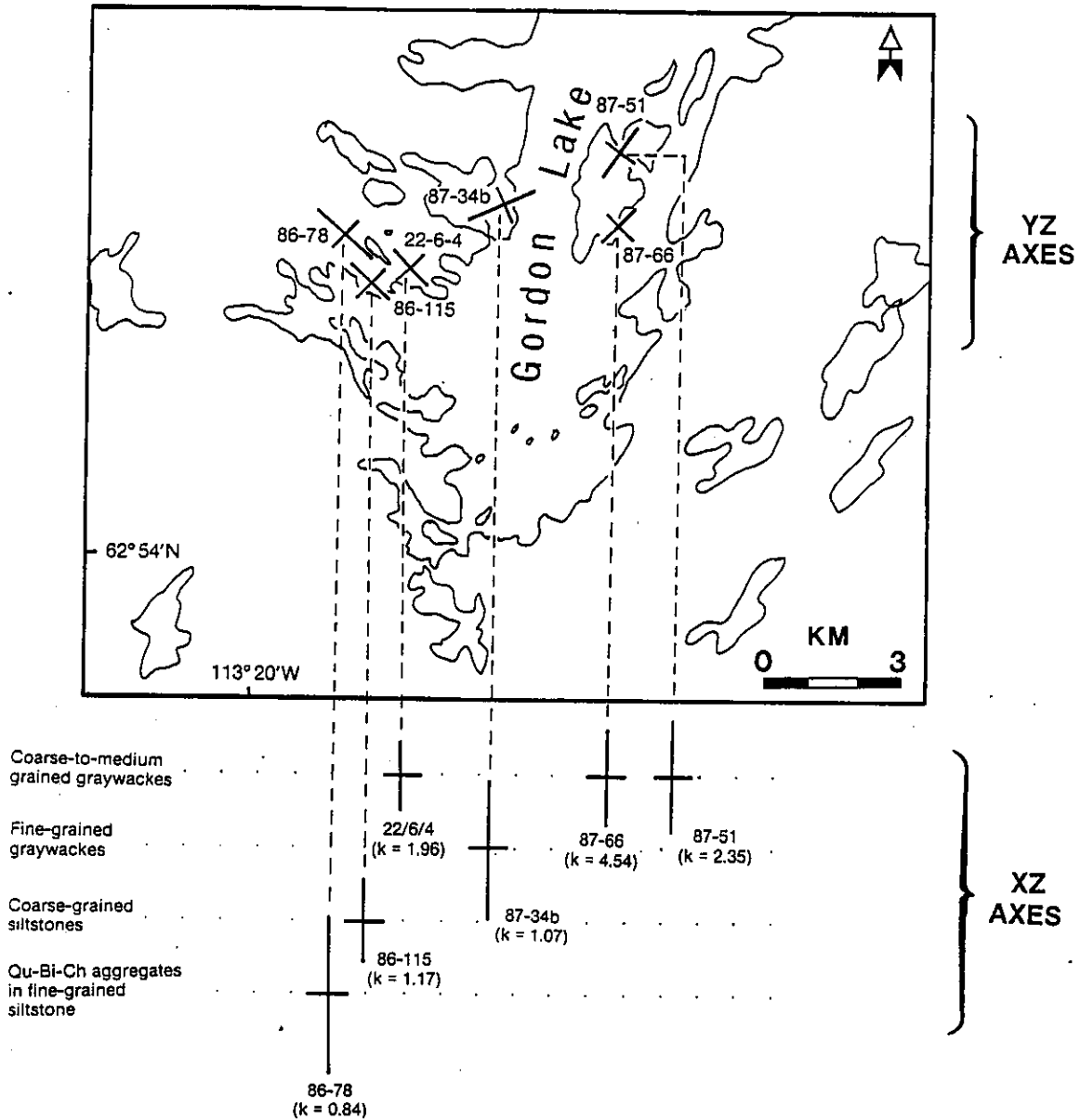
#### 5.5 STRAIN ANALYSIS OF VERTICAL STRETCHING LINEATION AT GORDON LAKE

It is apparent from the inspection of oriented thin sections that the principal stretching direction of the finite strain ellipsoid associated with the D<sub>3</sub> cleavage (defined by elongated quartz clasts and multi-mineralic aggregates, and aligned metamorphic minerals), lies parallel to the macroscopic D<sub>3</sub> cleavage/bedding lineation. This stretching lineation, not noted in the earlier studies of Fyson (1975, 1984a, 1984b), is common in other parts of the Slave (e.g., James, 1989, 1990; Fyson 1990) and other Archean terranes (e.g., Hudleston, 1976; Hudleston et al. 1988). The Fry technique (Fry, 1979; Appendix A5.1) was used to evaluate the shape of the stretching lineation's finite strain ellipsoid by utilizing quartz clasts and metamorphic aggregates from graywackes and siltstones, respectively. The Fry technique is better suited than the Rf/Phi analysis for the strain analysis of graywacke clasts as it measures the relative motion of deforming clasts in a ductile matrix, rather than clast deformation alone. Errors in the Fry technique and the effects of pressure solution are discussed in Appendix A5.3.

##### 5.5.1 Fry Analysis

Six samples were selected from across the Gordon Lake refold to obtain 3-D strain data (Table A5.14 and Figure 5.18). The six samples included three coarse- to medium-

Figure 5.18 YZ and XZ strain ellipse axes for six samples from across the Gordon Lake re-fold, using manual Fry data (Table A5.18).





grained graywackes (87-51, 87-66, and 22/6/4), a fine-grained graywacke (87-34b), a coarse-grained siltstone (86-115), and a fine-grained siltstone with multi-mineralic aggregates (86-78). Thin sections were taken along the YZ, XZ, and XY sections of each sample and ellipse ratios ( $R_{yz}$ ,  $R_{xz}$ ,  $R_{xy}$ ) obtained using a manual Fry analysis and three computerized Fry analyzes (Figures A5.1 - A5.18 and Tables A5.15 to A5.17). Two of the three measured ellipse ratios ( $R_{yz}$  and  $R_{xy}$ ) were then used to evaluate the shape of the finite strain ellipsoid in a Flinn graph (Flinn, 1962; Ramsay and Huber, 1983). From this graph a k-value is obtained where:

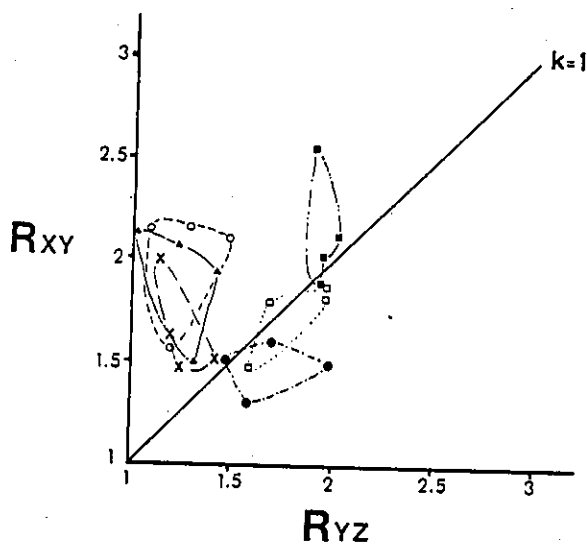
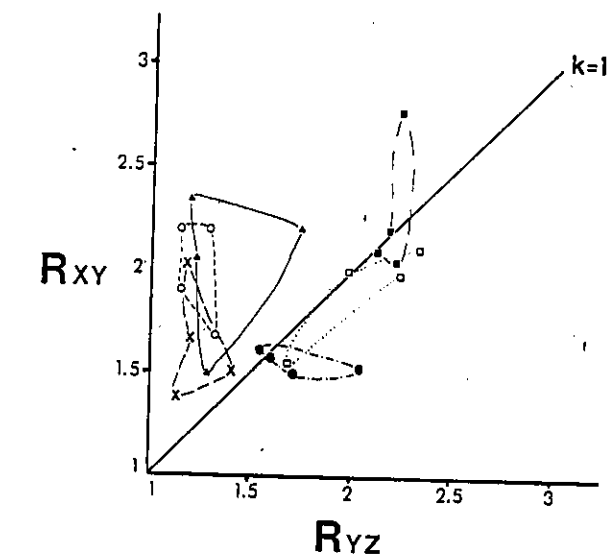
$$k = (R_{xy} - 1)/(R_{yz} - 1)$$

If  $k > 1$  the ellipsoid is prolate, and if  $k < 1$  the ellipsoid is oblate. A Flinn graph (Figure 5.19a), using the four  $R_{yz}$  and  $R_{xy}$  ratios for each sample, defined the apparent ellipsoid fields of the six samples. In an attempt to "smooth" the ellipse data and make  $R_{yz}$ ,  $R_{xz}$ , and  $R_{xy}$  ratios inter-dependent, a best-fit ellipsoid was calculated for each sample, adapting a technique from Shimamoto and Ikeda (1976). From the axes of the best fit ellipsoids new "corrected" ellipse ratios were obtained (Table A5.18) and plotted onto a second Flinn graph (Figure 5.19b). From this second graph it is apparent that the fields, though similar to the first graph, are smaller and probably more representative of the ellipsoid shape.

### 5.5.2 Interpretation of Stretching Lineation Data

From the strain fields of the Flinn graphs it is evident that the finite strain ellipsoids of the coarse- to medium-grained graywackes (87-51 and 87-66) from the east limb of the refold are prolate with  $k \approx 5$ . The finite strain ellipsoid from the coarse- to medium-grained graywacke (22-6-4) from the west limb is also prolate, but has a lower k value ( $\approx 3$ ). The coarse siltstone (86-115)

Figure 5.19 Flinn Plot of strain fields for six samples across the Gordon lake refold using uncorrected (a) and corrected (b) ellipse data.



Coarse- to medium-grained graywackes { x 22-6-4 (W)  
o 87-51 (E)  
▲ 87-66 (E)

Fine-grained graywacke { □ 87-34b (C)

Coarse grained siltstone { ● 86-115 (W)

Qz-Bi-Ch aggregates in fine-grained siltstone { ■ 86-78 (W)

and fine-grained graywacke (87-34b) plot close to the plane strain region (with  $k \approx 0.8-1.0$ ). The multi-mineralic aggregates from the fine siltstones (86-78) plot close to the plane strain region, but have one data point in the prolate region.

This small data base of six samples confirms that the principal direction of extension is vertical in the Gordon Lake region (Figure 5.18). There is some suggestion that the finer-grained rocks produce a more plane strain ellipsoid as compared to the prolate ellipsoid of the coarser-grained rocks. This variation in ellipsoid shape is probably due to differences in clast size, matrix/clast ratios and deformation mechanisms (i.e., pressure solution). However, the more prolate shape of the finite strain ellipsoids of the graywackes from the east limb (87-51, 87-66), as compared to the west limb graywacke (22/6/4), is possibly a function of increased vertical extension within the east limb region of the refold.

In comparison to finite strain ellipsoid data obtained from folded and thrustured slate belts, which have predominantly oblate strain ellipsoid shape (Pfiffner and Ramsay, 1982, Figure A1), the strain data for the Gordon Lake metasedimentary rocks are significantly different. Indeed, the finite strain ellipsoid data are more compatible with prolate strains obtained by Brun et al. (1981) from cover rocks between three or more inflating gneissic domes, and agree with strains modelled by Dixon and Summers (1983) for subsiding, inter-diapiric synclines.

#### 5.6 STRAIN ANALYSIS OF DEFORMED QUARTZ VEINS

Deformed quartz veins within siltstone beds of the Gordon Lake region can provide important information about the  $D_3$  and  $D_4$  strain history. However, the interpretation of strain data obtained from veins is based on the assumptions: i) that vein deformation represents regional

strain characteristics and not just local inhomogeneous strain; ii) that veins act as competent planar sheets surrounded by an incompetent host material, with folding implying shortening and boudinage elongation; and iii) that the time of vein emplacement is known relative to the deformation (Talbot, 1970; Ramsay and Huber, 1983).

At Gordon Lake estimates of  $D_4$  and  $D_3$  strain were obtained from three types of deformed quartz veins including: a)  $D_4$ -crenulated,  $S_3$ -parallel veins from the central part of the refold; b)  $D_4$ -boudinaged veins from the east limb, and c) a  $D_3$ -deformed, bedding-parallel vein. Four  $D_4$ -crenulated veins were traced from outcrops in the central region of the Gordon Lake refold, and measurements of bedding,  $S_{3S}$  and  $S_4$  were obtained at each location (Figures A5.19 to A5.23). Estimates of  $D_4$  shortening and shear strain were then calculated from the four vein overlays using formulae of Ramsay (1967, p. 52, 1983) and De Paor (1987), and by an orthographic net technique of De Paor (1983, 1986). The shear strains ( $0.87 - 1.77\gamma$ ) obtained from these two methods (Table A5.19) are consistent with the presence of a component of sub-horizontal, ( $D_4$ ) bedding-parallel shear within the fine siltstones. These values are equivalent to shear strains obtained for flexural slip folding of the refold (Ramsay 1967, Figure 7-57), in which the east and west limbs were originally parallel and striking  $110^\circ$ .

Strain data obtained from three  $D_4$ -boudinaged east limb veins (Table A5.20) indicate extensions of approximately +0.44 to +0.66. While data from a  $D_3$ -deformed bedding parallel vein indicates an extension of 0.21. This data provides some constraints on the magnitudes of  $D_3$  and  $D_4$  strains.

## 5.7 STRUCTURAL EVOLUTION OF THE GORDON LAKE REFOLD

Any structural model developed for the Gordon Lake region must consider the following factors: i) how did the early  $F_1$  isoclinal folds form; ii) what mechanisms are responsible for the steepening of these folds; iii) why is there a vertical stretching lineation; and iv) how and when did the refold form?.

### 5.7.1 Formation of the Vertical Isoclinal Folds

The deformational history of the  $F_1$  isoclinal folds at Gordon Lake is difficult to establish as their early geometry is obscured by later structural events. However, they are characterised by: i) steep fold axes, ii) long sinuous limbs (Map 1), iii) the presence of fault-propagation folds (e.g., Figure 5.9), iv) evidence for soft sediment deformation (Section 5.4.4), v) the lack of an earlier folding phase (Section 5.1.1.1), and vi) the absence of an  $S_1$  cleavage.

Steeply plunging folds in metasedimentary rocks are common to many parts of the Slave Province (e.g., Contwoyto Lake region; King et al. 1988, Relf, 1989) and to other Archean terranes, such as the Quetico Belt (Kehlenbeck, 1986; Borradaile et al. 1988; Devaney and Williams, 1989) and the adjoining Vermillion District (Hudleston, 1976; Bauer, 1986; Hudleston, 1988). Within the Yellowknife Basin various mechanisms have been suggested for the formation of the steeply plunging isoclinal folds. Drury (1977) suggested that the isoclinal folds were formed by gravitational sliding of unconsolidated sediments during diapiric emplacement of granites. Fyson (1977, 1982) disputed this, and indicated that an early phase of large wavelength folding (developed during basinal subsidence) was probably overprinted by a second phase of tighter folding during regional convergence, with diapirism playing only a minor role in fold formation. Kusky (1989, 1990),

based on evidence of subduction-related thrusting along the volcanic/basement rock contacts, suggested that these folds formed during deformation of an accretionary prism.

In consideration of the mechanisms above and the characteristics of the  $F_1$  fold geometry it is suggested that these early folds probably developed within an accretionary prism during tectonic convergence. An accretionary prism environment would explain the variety of deformational structures as the sediments lithified; e.g., from soft-sediment to fault-propagation folds (Knipe and Needham, 1984). Typically, thrust surfaces would be narrow, cryptic, and only recognizable by repeated stratigraphy.

Steeping of these early fold axes could be accommodated by shortening of the prism (i.e., convergence), diapiric subsidence of the metasedimentary rocks, or more likely a combination of both mechanisms. Shortening of the metasedimentary prism in the later stages of accretion would probably coincide with a change in sediment rheology and deformation style (Knipe and Needham, 1986). The  $F_1$  fold axes might be bodily rotated into steeper attitudes as fault-bounded 'packages' (e.g., Hibbard and Karig, 1987; Agar, 1988) and/or (if the  $F_1$  axes are tilted) deformed/rotated by pure shear. Diapiric emplacement of plutons into the accretionary prism could cause subsidence of the folded sediments, further steepening of  $F_1$  fold axes, and development of a vertical stretching lineation (e.g., Brun et al. 1981; Dixon and Summer, 1983).

#### 5.7.2 Refold Formation

At some stage in the structural history of the Gordon Lake region the vertical  $F_1$  isoclinal folds were folded to form a regional, steeply plunging refold structure (Section 5.4.1.3). The timing of the refold formation must take

into account the following observations (listed in approximate order of decreasing importance):

i) A crenulation cleavage ( $S_4$ ) that is confined to the central region of the refold, forms a herring-bone cleavage pattern with the earlier siltstone and graywacke cleavages ( $S_{3S}$  and  $S_{3G}$ ), and is consistently counter-clockwise from bedding, probably developed during bedding-parallel slip associated with counter-clockwise rotation of the refold's east limb (Section 5.4.2.3). Estimates of  $D_4$  bedding-parallel shear strains ( $0.88-1.77 \gamma$ ) were obtained from crenulated,  $S_{3S}$ -parallel veins. These shear strains are appropriate for rotation of the refold's east limb by a bedding-parallel slip mechanism (Section 5.6).

ii) The graywacke cleavage ( $S_{3G}$ ) transects the refold's east limb in the southeast of Gordon Lake, and in addition varies in strike from west-northwest on the east limb to northwest on the west limb. In the Zenith Island region the graywacke cleavage ( $S_{3EG}$ ) strikes north-easterly (Map 1, Section 5.4.2). The differences in strike of  $S_{3G}$  and  $S_{3EG}$  across the refold are probably the result of graywacke bed rotation during  $D_4$ .

iii) On the east limb of the refold abundant boudinaged veins occur sub-parallel to the north-northeast-striking siltstone cleavage ( $S_{3ES}$ ), which itself has a faint sub-perpendicular crenulation cleavage ( $S_{4E}$ ). These east limb structures suggest  $D_4$  contraction and extension along  $S_{3ES}$  (Section 5.4.2.1), at some stage of refold formation.

iv) Quartz inclusion trails in biotite porphyroblasts on the refold's west limb strike northwest and sub-parallel to  $S_{3S}$ , whereas those on the east limb strike east-west and

possibly represent the remnants of rotated and crenulated  $S_{3S}$  fabric (Section 5.3).

v) The finite strain ellipsoid in the medium- to coarse-grained graywackes is prolate and has a sub-vertical direction of maximum extension. In addition, the strain ellipsoid shape appears more prolate on the refold's east limb as compared to the west limb (Section 5.5), suggesting that the east limb has undergone an additional increment of ( $D_4$ ?) strain.

vi) Changes in  $D_3$  cleavage refraction across the refold, with a sinistral sense of bedding-parallel slip on the west limb and a dextral sense in the central region (Figure 5.11), indicate possible refolding prior to  $D_4$ .

No observation precisely constrains the time of refold formation. Of six possible chronologies for the time of refold formation three (2, 3 and 4; Figure 5.20) are rejected as they do not explain the  $D_4$ -related structures. The remaining three include: i) Chronology 1 - with initiation of refold formation pre- $D_3$  and  $D_3$  and  $D_4$  cleavages overprinting an already part-folded structure; ii) Chronology 5 - where  $D_3$  cleavage formation was coeval with refolding, and that as the refold hinge tightened during  $D_4$  the east limb was preferentially rotated in a counter-clockwise direction; and iii) Chronology 6 - where  $D_3$  was imposed on a steeply dipping, west-northwest-striking homocline of  $F_1$  folded metaturbidites, and during  $D_4$  the eastern part of this homocline was preferentially rotated to form a north-northeast striking limb.

Relative limb movement during closure of the refold further sub-divides these three chronologies (Table 5.3). In Chronologies 1 and 5 the west and east limbs could move during  $D_3$  and  $D_4$  (1a/5a), or alternatively both limbs could



Figure 5.20 Possible chronologies (solid lines) for the time of formation of the Gordon Lake refold (\* - unlikely models as they do not include the D<sub>4</sub> crenulation event).

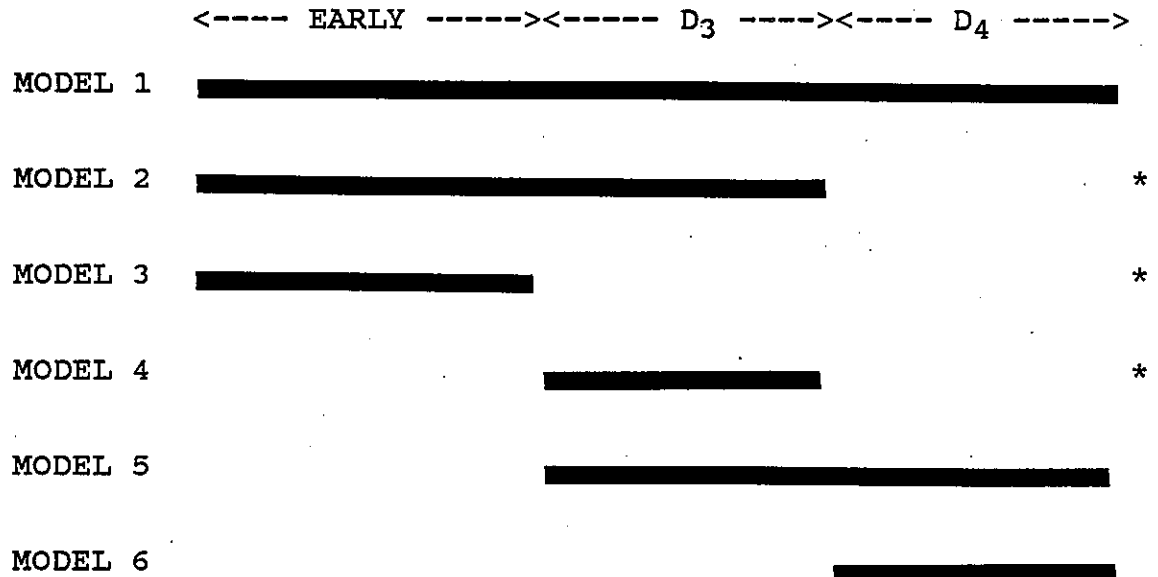


Table 5.3 Five end-member chronologies and deformational histories for re-fold formation. Structural observations/data, listed in order of decreasing reliability, support (Y) or detract (N) from each deformational history. Sub-chronology A indicates that the west and east limbs could move during  $D_3$  and  $D_4$ , whereas in sub-chronology B both limbs could move during  $D_3$ , but only the east limb moves during  $D_4$ .

STRUCTURAL OBSERVATION	CHRONOLOGY 1		CHRONOLOGY 5		CHRONOLOGY 6
	Refold Formation pre- $D_3$ to $D_4$		Refold Formation syn- $D_3$ and $D_4$		Refold Formation syn- $D_4$
	1A	1B	5A	5B	
$S_4/S_3$ herring-bone pattern in refold centre	Y <sup>1</sup>	Y <sup>1</sup>	Y <sup>1</sup>	Y <sup>1</sup>	Y
Transection of east limb $S_{3g}$	Y	Y	N <sup>2</sup>	N <sup>2</sup>	Y
Variations in strike of $S_{3g}$ across refold	N	Y	N	Y	Y <sup>3</sup>
$D_4$ shear strain of 0.88-1.77 $\gamma$ for flexural-slip folding of refold	Y <sup>1</sup>	Y	Y <sup>1</sup>	Y	Y
$D_4$ deformation of East limb and horizontal veins	N	Y	N	Y	Y
$D_4$ deformation of $S_{3s}$ -parallel veins in refold centre	Y <sup>1</sup>	Y	Y <sup>1</sup>	Y	Y
$S_3$ refraction across refold	Y	Y	Y	Y	N
Strike of quartz inclusion trails on west and east limbs	N	Y	N	Y	Y
Vertical stretch lineation ( $D_3$ ) greater on east limb (if true?)	N	Y	N	Y	Y

- 1 Only with refold hinge migration.
- 2 Under certain deformational conditions cleavages can transect folds of the same age.
- 3 Change in  $D_3$  graywacke strike of Chronology 6 >> than both Chronology 1 and 5.

move during  $D_3$  with only the east limb moves during  $D_4$  (1b/5b). In both Chronologies 1 and 5 refold closure could probably develop by similar deformation mechanisms, which would include major components of buckling and flexural slip. In comparison to the Chronologies 1 and 5, Chronology 6 implies that  $D_4$  was accountable for all deformation of the east limb. In this case, the west limb is fixed during complete formation of the refold and the type of deformation resembles a shear zone; whereby the west limb is undeformed during  $D_4$  and the east limb lies within a region of shearing.

From structural observations (Table 5.3) it is not possible to uniquely determine which chronology/deformational history is the most likely. However, this study demonstrates that refold formation is primarily a  $D_3/D_4$  event, not a pre- $D_3$  event (e.g., Fyson 1984a, 1984b), and that at some stage during refold closure the west limb was fixed relative to the east limb. The distinction between three chronologies, though unclear, is important in terms of folding mechanisms for the refold. Refolding during  $D_3/D_4$  infers a major component of buckling, and refolding during  $D_4$  alone suggests a major component of shearing.

## 5.8 TECTONIC MODELS

The lithological, metamorphic, and structural study completed at Gordon Lake places constraints on any tectonic models proposed for the Yellowknife Basin. The points to be considered include: i) deposition of metaturbidites in a volcanic-rich tectonic setting (i.e., an island arc, Chapter 9); ii) the formation of accretionary-type folds (with sub-horizontal fold axes and a tight fold geometry) during early ( $D_1$ ) deformation; iii) the steeping of the early  $F_1$  fold axes; iv) the development of a syn-metamorphic ( $D_3$ ), steeply dipping cleavage with a vertical stretching lineation; and v) the late metamorphic ( $D_4$ )

development of sub-horizontal, dextral bedding-parallel slip in the refold centre by preferential deformation of the refold's east limb.

Three previously proposed tectonic settings for the Slave Province are outlined in Table 5.4. At Gordon Lake the metaturbidites were probably deposited in a volcanic arc setting (Chapter 9; Hoffman, 1986).  $F_1$  folding developed during progradation and accretion of these turbidites (e.g., Kusky, 1990), rather than as gravity sliding away from rising pluton (Drury, 1977). The axes of these folds were probably steepened during the latter stages of accretion; possibly similar to processes found in the other accretionary complexes, e.g. the Shimanto Belt, Southwest Japan (Hibbard and Karig, 1987; Agar, 1988).

At some stage of arc accretion magmatic activity was initiated and low pressure/high temperature metamorphic conditions were developed. These metamorphic conditions, atypical of present-day accretionary prisms, may have developed by: i) movement of the prism from a fore-arc to back-arc position with migration/out-stepping of the subduction zone (Fyson and Helmstaedt, 1988; Percival and Williams, 1989); ii) heating during plutonism and uplift associated with crustal thickening (Thompson, 1989a, 1989b) and/or subduction reversal (Kusky, 1989, 1990); and iii) horizontal migration of fluids and melts up a shallow-dipping subduction zone (e.g., Sisson and Hollister, 1988). The intrusion of granitic rocks into the already folded and metamorphosing metaturbidite pile may have resulted in the diapiric subsidence of the folded metaturbidites and the further steepening of fold axes (e.g., Dixon and Summers, 1983), the development of the steeply dipping north to north-westerly striking  $D_3$  cleavage, and a vertical stretching lineation.

Late-metamorphic deformation ( $D_4$ ) at Gordon lake is associated with rotation of the refold's east limb. It is

**Table 5.4** Deformation styles within metasedimentary supracrustal rocks and previously proposed tectonic models for the Slave Province.

---

CONTINENTAL RIFTING MODEL - McGlynn and Henderson, 1970; Henderson, 1985; Drury, 1977.

i) Deposition of metasediments during rifting of sialic basement. ii) Isoclinal fold formation during sliding of metasediments away from diapiric uprise of basement and early granites (i.e., Defeat Plutonic Suite). iii) Further deformation of metasediments and formation of re-fold patterns by intrusion of late granites (i.e., Prosperous Granitic Suite). iv) Minor later regional compression responsible for development of pervasive, steeply dipping, northerly striking cleavage.

---

RIFTING THEN CONVERGENCE (ACTIVE CONTINENTAL MARGIN) - Fyson 1977, 1982, 1984a, 1984b; Fyson and Helmstaedt 1988

i) Deposition of metasediments in the later stages of volcanic activity. ii) Possible formation of regional  $F_0$  folds by intrusion of early granodiorites. iii) Development of westerly verging isoclinal ( $F_1$ ) folds during regional compression associated with easterly directed underthrusting. iv) Formation of re-fold pattern by transcurrent movement redirected along earlier extensional fractures. v) Westward shift of subduction and emplacement of late granites, possibly controlled by fractures. vi) Sets of regional and local cleavages formed by continued compression and re-direction of stresses along early fractures.

---

ACCRETIONARY PRISM / ISLAND ARC MODEL - Hoffman, 1986, 1990; Kusky, 1989, 1990.

i) Metasediments composed of trench turbidites and mid- to outer-fan deposits. ii) Accretionary progradation of fore-arc and development of westerly verging, isoclinal folds and/or thrusts during easterly subduction. iii) Formation of later folds by regional shortening and constriction by emplacement of arc plutons. iv) Intrusion of late granites related to crustal thickening and local development of prolate strains.

---

unclear whether this deformation is the result of regional shortening, a sub-horizontal shear or a combination of both (i.e., transpression). The transition in deformational style, from coaxial shortening to sub-horizontal/transcurrent movement is typical of other Archean metasedimentary belts (e.g., Quetico Belt; Hudleston et al. 1988), and is common to large accretionary prisms with tapering subduction zones (e.g., Alaska; Dewey, 1980).

### 5.9 SUMMARY

The south end of Gordon Lake is underlain by a siltstone-dominated lithology that is surrounded to the west, east, and south by a graywacke-dominated lithology. These metaturbidites attained lower greenschist to upper greenschist facies metamorphism, with peak metamorphism (syn-D<sub>3</sub>) associated with biotite porphyroblast growth. The regional structure is dominated by a south closing, kilometre-scale sub-vertical refold of earlier (F<sub>1</sub>) isoclinal folds. This refold is transected by a pervasive, steeply dipping D<sub>3</sub> cleavage, that is characterized by a distinct vertical stretch lineation. In the central region of the refold, S<sub>3S</sub> is crenulated to form a new cleavage (S<sub>4</sub>). S<sub>4</sub> was probably formed during D<sub>4</sub> bedding-parallel slip that accompanied counter-clockwise rotation of the refold's east limb. D<sub>4</sub>-crenulated quartz veins give shear strain values that are compatible with flexural-slip folding of the refold's east limb. Refolding may have spanned both D<sub>3</sub> and D<sub>4</sub>, or have been restricted to D<sub>4</sub>. The tectonic history of the region is compatible with subduction-related models whereby: 1) F<sub>1</sub> folds developed in an accretionary prism; 2) later shortening of the accretionary prism and the diapiric emplacement of granites resulted in the steeping of F<sub>1</sub> fold axes and formation of a vertical stretching lineation; and 3) D<sub>4</sub> rotation of the

refold's east limb was the result of continued convergence and/or transcurrent movement.

## CHAPTER 6

### QUARTZ VEINS AND QUARTZ-BRECCIAS OF THE GORDON LAKE REGION: CLASSIFICATION AND MODELS FOR THEIR EMPLACEMENT

This chapter describes the quartz vein and quartz-breccia morphologies found within the Gordon Lake region, and classifies them into twelve principal vein and breccia types - based on their different structural setting, host lithology, mineralogy, microstructure, and gold association. From this classification scheme a temporal framework for the emplacement of quartz veins is developed, as well as a model for the concentration of gold-bearing quartz-breccia zones within the hinge region of the Gordon Lake refold. In addition, this classification provides an insight into the relationships between vein types and the bulk strain of the region. Future studies might be able to utilize this quartz vein framework to develop a more detailed understanding of the deformational history of the region (e.g., Talbot, 1970). Previous classification schemes for quartz veins within the metaturbidites of the Burwash Formation include those of Fyson (1987a) and Swatton (1987) for the Yellowknife and Bullmoose Lake regions, respectively.

At the southern end of Gordon Lake a series of previously undocumented quartz-breccia zones occur and are characterized by the presence of host rock fragments/clasts distributed throughout an abundant quartz matrix. Veins have fewer rock fragments, which, where present, are generally confined to the vein/wall rock contacts. Commonly, the veins vary in width from a few millimetres to a maximum of 1.5 m, whereas the quartz-breccia zones vary from 10 cm to 10 m in width. At Gordon Lake the quartz veins and quartz-breccias make up approximately 1-2% of outcrop, with the quartz-breccias making up at least a third of this.



## 6.1. QUARTZ VEIN MORPHOLOGY AND DISTRIBUTION

Seven principal types of quartz veins were recognised at Gordon Lake (Table 6.1 and Figure 6.1). No one vein type was more favourable for visible gold, but sulphides occur most frequently in the  $S_{3S}$ -parallel (Type 3), boudinaged East Limb (Type 4), and Rotated 'Z' (Type 7) veins.

### 6.1.1 Type 1 - Bedding-parallel Veins

These veins occur parallel to bedding surfaces in coarse- and fine-grained siltstones, and are commonly made up of alternating quartz layers and siltstone selvages (<2-10 mm wide). They vary from 0.5-10 cm wide and are traceable along strike for up to 10 m or more. Typically, the quartz layers and siltstone selvages are not continuous, and are only 10-20 cm long. All the bedding-parallel veins are folded by  $D_3$  (Figure 6.2a), locally deformed by  $D_4$ , and less commonly folded around  $F_1$  fold hinges (Figure 5.3e). Quartz in these veins is generally white and has a sugary texture in hand specimen. In thin section the quartz generally occurs as fine (100-200  $\mu\text{m}$ ), equant, and sub-polygonal grains with no undulatory extinction. Other secondary minerals include chlorite, biotite, muscovite, and opaque material (Tables A6.1). Overall, these veins have a similar morphology to the "crack-seal" veins of Ramsay (1980) and veins found in the Meguma metaturbidites of Nova Scotia (Graves and Zentilli, 1982; Mawer, 1985; Smith et al. 1985).

### 6.1.2 Type 2 - $D_3$ -Deformed, Echelon Veins and Networks

These veins which are all deformed by  $D_3$ , occur throughout the mapped region, and are commonly confined to graywacke beds. They vary in morphology from veinlets (mm to cm in width) to interconnecting vein systems and massive metre scale "blebs" or lenses. Typically, the veinlets are

Table 6.1 Quartz vein types and visual estimate of relative proportions.

Vein Type	Morphological Description	Structural Timing	Proportion (%)
1 -	Bedding-parallel veins	Pre-D <sub>1</sub>	5%
2 -	D <sub>3</sub> -deformed, graywacke-hosted echelon and reticulate veins	Pre-D <sub>3</sub>	20%
3 -	Siltstone-hosted, S <sub>3S</sub> -parallel veins	Syn-D <sub>3</sub>	25%
4 -	Stretched/boudinaged East Limb veins	D <sub>3</sub> /D <sub>4</sub>	20%
5 -	Sub-horizontal veins	Syn-D <sub>3</sub>	10%
6 -	S <sub>4</sub> -parallel veins	Syn-D <sub>4</sub>	5%
7 -	Rotated 'Z' veins.	D <sub>3</sub> /D <sub>4</sub>	10%
8 -	Others	-	5%

Figure 6.1 The seven principal vein types of the Gordon Lake region. Sketch of horizontal (Type 5) veins includes three  $S_{3S}$ -parallel (Type 3) veins, while sketch of  $S_4$ -parallel (Type 6) veins includes four Type 3 veins deformed by  $D_4$ . The  $S_4$ -parallel (Type 6) and Rotated 'Z' (Type 7) veins are confined to central region of the refold (bounded by dashed lines A and B), while the East Limb (Type 4) veins occur only to the east of line B.

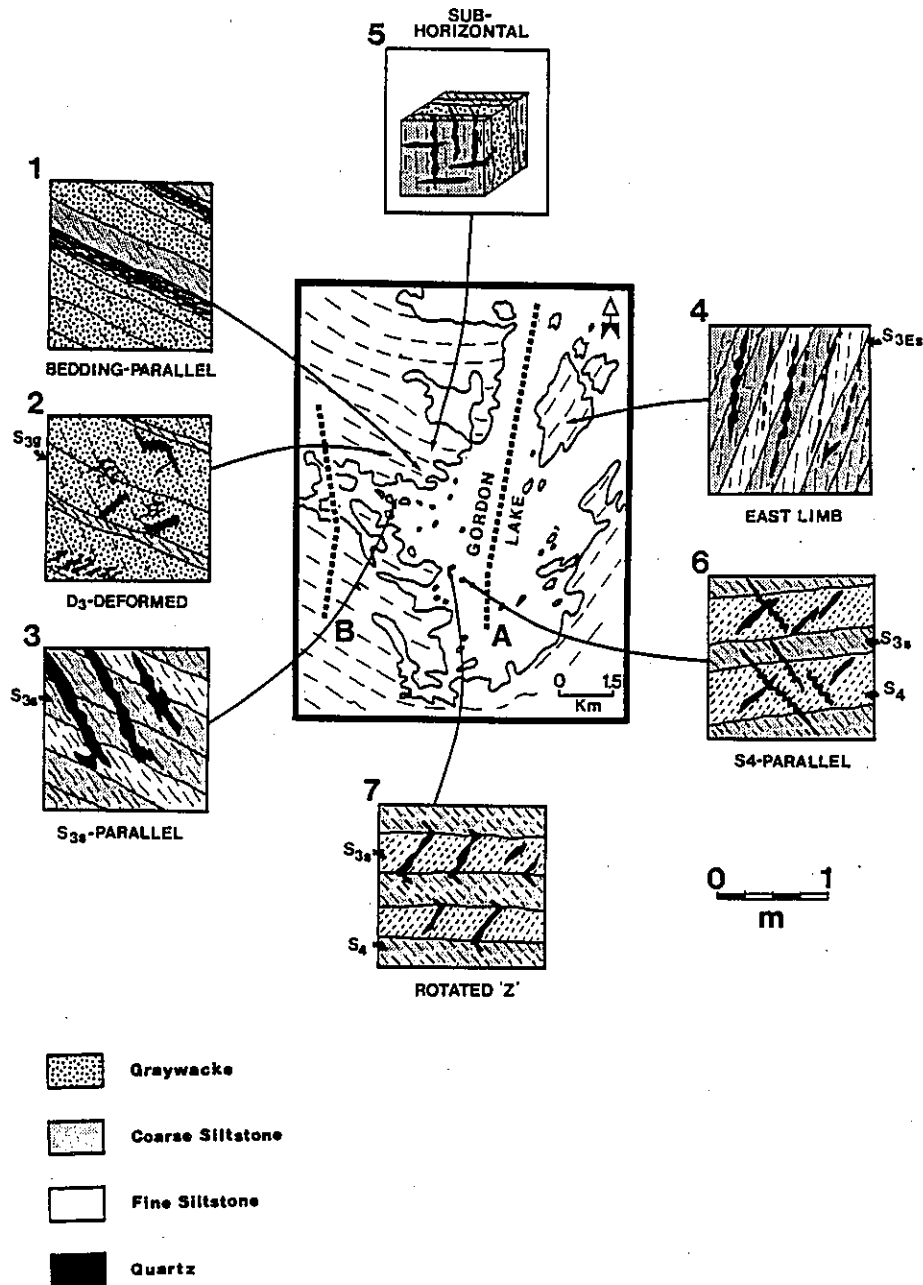
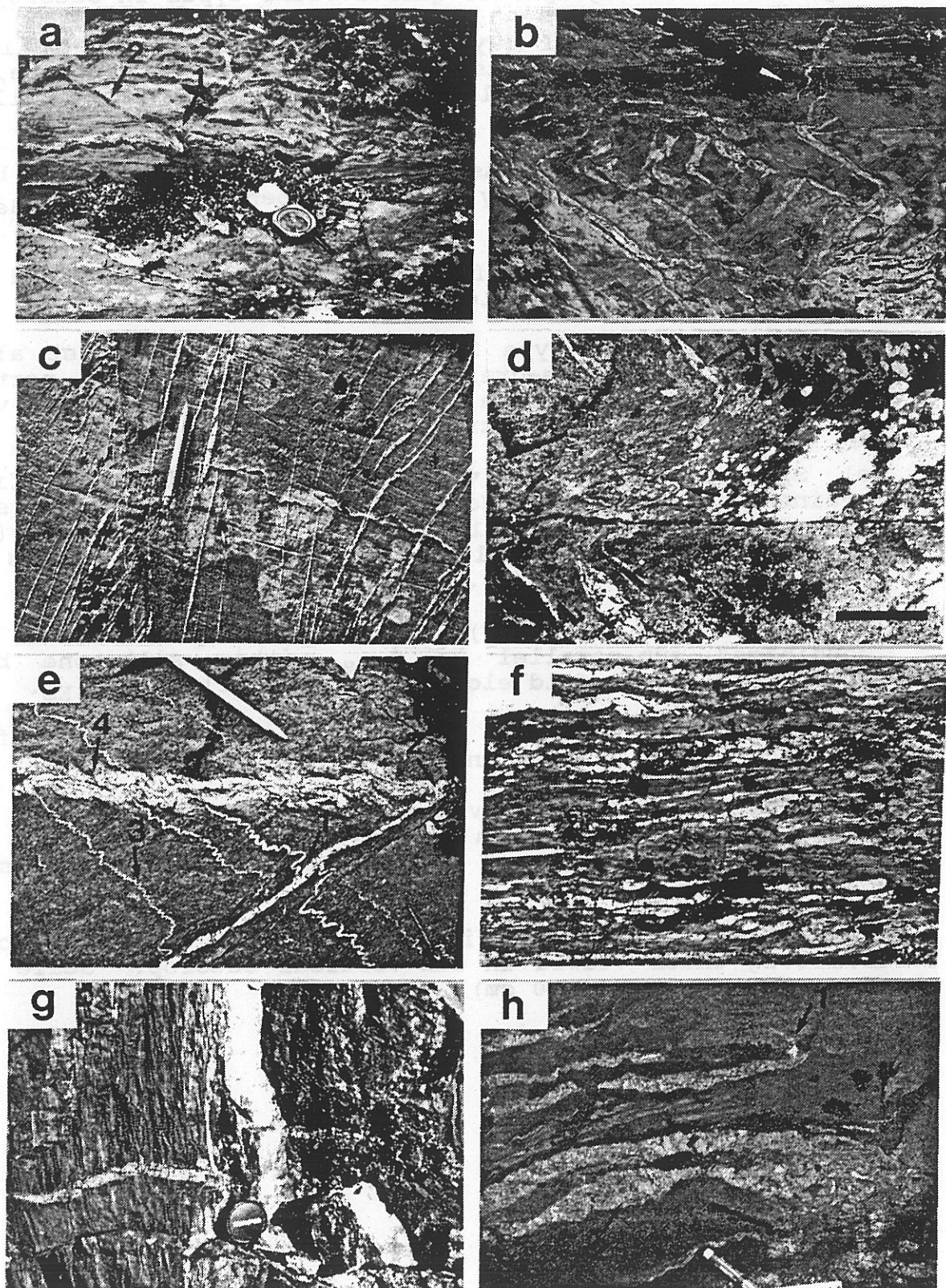


Figure 6.2 Photographs of quartz veins types in outcrop:

- a) Bedding-parallel (Type 1) vein deformed by  $D_3$  in a siltstone bed along siltstone/graywacke contact. Note,  $F_3$  folds in bedding parallel veins (1) and minor  $S_{3S}$ -parallel veins (2).
- b) Pre- $D_3$  echelon veins (Type 2) in graywacke bed both folded and re-oriented by  $D_3$ . Note, pen parallel to  $S_{3S}$  in siltstone bed.
- c) Reticulate network of Pre- $D_3$  (Type 2) veins folded and reoriented by  $S_{3g}$  (parallel to pen).
- d)  $S_{3S}$ -parallel (Type 3) veins folded and offset along bedding by  $D_4$  in fine-grained siltstone bed. Note, north-west orientation of Type 3 vein (1) and  $F_4$  folds in vein parallel to north-east striking  $S_4$  (2).
- e)  $S_4$ -parallel (Type 6) vein with minor boudinage in fine-grained siltstone bed. Note, cross-cutting relationship with  $S_{3S}$ -parallel vein (1) and bedding parallel vein (2),  $D_4$  folding of  $S_{3S}$ -parallel vein (3), and  $D_3$  folds of bedding parallel vein (4).
- f) East limb (Type 4) veins intensely stretched and boudinaged sub-parallel to  $S_{3ES}$  within siltstone bed. Note, quartz vein fold elongated sub-parallel to  $S_{3ES}$ .
- g) Horizontal (Type 5) veins from west limb of re-fold cross-cutting  $L_3$  lineation and  $S_{3S}$ -parallel vein.
- h) Rotated 'Z' (Type 7) veins from centre of re-fold. Note, unrotated vein tips in graywacke sub-parallel to  $S_{3g}$  (1) and central body of vein within siltstone bed sub-parallel to  $S_4$  (2).

(All photographs viewed in sub-horizontal outcrop except for 6.2g which viewed in sub-vertical outcrop. Scale bar for 6.2d represents 20 cm).

Figure 6.2



intensely folded, rotated and boudinaged by  $S_{3g}$ , whereas larger veins or blebs are less deformed. Commonly the smaller veins form echelon and sigmoidal arrays (Figure 6.2b). However, no relationships were recognized between the orientation of echelon arrays and limbs of  $F_1$  folds. In other places, these veins occur as  $D_3$ -deformed reticulate networks with either one fracture direction predominating or two fracture directions forming a conjugate set (with typical 'T' and 'X' vein junctions, Figure 6.2c). In most cases the wall rock and vein contacts are sharp with no evidence of alteration. Mineralogically the  $D_3$ -deformed veins consist of 70-80% white quartz, 10-20% chlorite, 5% K-feldspar, plus minor biotite and opaque material. The quartz microstructure of these veins is similar to that of the bedding-parallel veins and is comprised of fine (100-300  $\mu\text{m}$ ), equant, and sub-polygonal grains with minor to no undulatory extinction. The consistent folding and rotation of these veins by  $S_{3g}$  and their lack of association with  $F_1$  folds indicate that they were probably emplaced pre- $D_3$  (before any  $D_3$  cleavage formation), but post- $D_1$ .

#### 6.1.3. Type 3 - $S_{3s}$ -parallel Veins

The Type 3 veins, hosted predominantly within siltstone beds, are characterized by their parallelism to  $S_{3s}$ . These veins are typically 10-30 cm wide, 4-5 m long, display minor boudinage, and are 'wrapped' by the  $S_{3s}$  cleavage. Locally,  $S_{3s}$ -parallel veins are found parallel to  $F_3$  fold axial traces (Figure 5.3c), are associated with minor displacements parallel to  $S_{3s}$ , and crosscut or abut bedding-parallel veins (Figure 6.2a and 6.2e). Elongate siltstone fragments, fractured parallel to  $S_{3s}$ , are also found along the vein/wall rock contacts. Rarely,  $S_{3s}$ -parallel veins have small, unfolded, perpendicular arms that distinctly cut  $S_{3s}$ . In sub-vertical outcrop, Type 3

veins are distinguished from the  $D_3$ -deformed (Type 2) veins by their steeper dip, parallelism to  $S_{3S}$ , and lack of folding. Commonly in the central region of the refold Type 3 veins are crenulated and folded by  $S_4$ , and in some cases offset along bedding (Figure 6.2d).

The  $S_{3S}$ -parallel veins have a more varied mineralogy than the  $D_3$ -deformed (Type 2) and Bedding-parallel (Type 1) veins, with 50-80% light to dark grey quartz, 10-30% K-feldspar, 5-15% chlorite and biotite, plus minor sulphides (trace to 5%). Vein/wall-rock contacts are commonly coated with biotite and chlorite, whereas the host siltstone locally displays chlorite and biotite alteration zones a few centimetres wide. Type 3 veins have a coarser quartz microstructure than the Bedding-parallel and  $D_3$ -deformed veins with irregular coarse grains (0.5-3.0 mm) that exhibit undulatory extinction and are commonly bordered by recrystallized zones of fine new grains and sub-grains. The consistent parallelism of the Type 3 veins to  $S_{3S}$ , their rare perpendicular arms, and minor boudinage indicate that they were emplaced in the late stages of  $D_3$ .

#### 6.1.4. Type 4 - Boudinaged 'East Limb' Veins.

Type 4 veins are restricted to outcrops of the refold's eastern limb and are most abundant in the Zenith Island region (Figure 6.1). These veins, generally hosted by siltstones, lie parallel to the principal north-northeast trending east limb cleavage ( $S_{3ES}$ ), are sub-parallel (within 0-20°) to bedding, and commonly exhibit pitting on weathered surfaces due to the dissolution of carbonate. Typically, they are 1-20 cm wide, 1-10 m long, and display intense stretching with isolated boudins; in both horizontal and sub-vertical surfaces. In some places minor folds in the quartz veins appear stretched along  $S_{3ES}$  (Figure 6.2f). It is unclear as to whether these folds are deformed ( $D_3$ ?) folds or folds developed during ( $D_4$ )

deformation of the refold's east limb. Rarely, Type 4 veins are associated with small undeformed veins (with quartz crystal growth perpendicular to the fracture surface) found at high angles to  $S_{3Es}$  and boudinaged bedding-parallel veins. Type 4 veins display a distinct bimodal quartz microstructure with zones (up to 60-80%) of fine sub-grains and recrystallized grains (20-50  $\mu\text{m}$ ) surrounding coarse (relict?) grains (0.2-1.0 mm). Most of the fine sub-grains and recrystallized grains are concentrated in the boudinaged "necks" of these veins. Mineralogically, Type 4 veins are comprised of 80-90% grey quartz, 10-20% carbonate, with minor biotite, chlorite, and opaque material. From their boudinaged morphology and parallelism to  $S_{3Es}$ , the Type 4 veins probably represent ( $D_4?$ ) extension and deformation of earlier  $S_{3S}$ -parallel (Type 3) veins (plus possibly both Bedding-parallel and  $D_3$ -deformed veins), with some minor syn-deformational vein formation perpendicular to  $S_{3Es}$ .

#### 6.1.5 Type 5 - Sub-horizontal Veins

Sub-horizontal or gently dipping veins occur throughout the region. They cut the steep stretching ( $L_3$ ) lineation, and in some cases cross cut  $S_{3S}$ -parallel veins (Figure 6.2g). The Type 5 veins vary in thickness from 1-5 cm and are up to 1-5  $\text{m}^2$  in areal extent. Typically, these veins have a similar mineralogy and microstructure to the  $S_{3S}$ -parallel (Type 3) veins. On the west limb of the refold the veins are generally planar, whereas on the east limb they are more folded. The sub-horizontal veins were emplaced in the latter stages of  $D_3$ , while those on the east limb probably underwent later ( $D_4?$ ) buckling.

#### 6.1.6 Type 6 - $S_4$ -parallel Veins

The northeast to east-northeast striking,  $S_4$ -parallel veins are hosted by siltstones and concentrated



within the central portion of the refold. Typically, they are 0.5-5 cm wide, 1-3 m long, and cross cut both the  $S_{3S}$ -parallel (Type 3) and Bedding-parallel (Type 1) veins (Figure 6.2e). Mineralogically, they are similar to  $S_{3S}$ -parallel (Type 3) veins, but with greater amounts of K-feldspar around the vein rims. The Type 6 veins have a similar quartz microstructure to  $S_{3S}$ -parallel (Type 3) veins with coarse grains (1-3 mm) displaying undulatory extinction, while sub-grains and new recrystallized grains are concentrated along the boundaries of the coarse grains. The orientation of Type 6 veins, their cross cutting relationships, and apparent concentration in the crenulated, central region of the refold indicate that they were probably emplaced syn- $D_4$ .

#### 6.1.7 Type 7 - Rotated 'Z' Veins

'Z'-shaped echelon veins occur in sequences of alternating coarse and fine siltstone and are confined to the central region of the refold. The tips of the veins lie sub-parallel to  $S_{3S}$  in coarse siltstones, whereas the middle portions of the veins within finer siltstones are sub-parallel to  $S_4$  and at an angle of 20-50° to their respective tips (Figure 6.2h). East of the central region the angle between the tips and middle portions of the veins becomes more acute and they are almost indistinguishable from the East Limb (Type 4) veins. These quartz veins have a similar mineralogy and microstructure to  $S_{3S}$ -parallel (Type 3) veins. The morphology of the Type 7 veins suggest that they were initially parallel to  $S_{3S}$  (i.e., Type 3 veins) and were subsequently deformed by ( $D_4$ ) dextral bedding-parallel slip during the formation of  $S_4$ .

#### 6.1.8 Other Vein Types

Rare, saddle reef-type veins (e.g., Sandiford and Keays, 1986) occur in the hinge regions of  $F_1$  folds and

vary in width from centimetre to metre scale (e.g., the Camlaren Mine; Henderson and Jolliffe, 1943, Figure 1). Commonly, the saddle reef veins are asymmetric, whereby a greater proportion of the vein material is preferentially located along one limb of the fold. Fine quartz-filled joints occur as conjugate fracture sets in graywacke beds and are commonly associated with metacarbonate concretions. These joints do not propagate into the adjacent siltstone beds and are unaffected by  $D_3$  and  $D_4$ . Their origin and time of emplacement is unclear. Massive, white-grey quartz veins occur within the nearby muscovite-rich Spud Lake pluton, and are typically 1-2 m in length and 10-30 cm wide.

## 6.2 QUARTZ-BRECCIA MORPHOLOGY AND DISTRIBUTION

The quartz-breccias found at Gordon Lake are morphologically distinct from the veins and are characterized by: i) 'jig-saw' fitting clasts distributed throughout a matrix of both grey/white quartz and feldspar, ii) minor clast alteration and rotation, and iii) matrix/clast ratios of approximately 3:1. The breccia types vary in their dimensions, structural setting, distribution, and host lithology, and are divisible into five types (Table 6.2 and Figure 6.3). Of the five types the most favourable for sulphide and gold mineralization are the siltstone-hosted (Types III) and the graywacke-hosted (Type IV) quartz-breccias.

### 6.2.1 Breccia Type I - Sub-parallel $F_1$ Fold Axial Traces

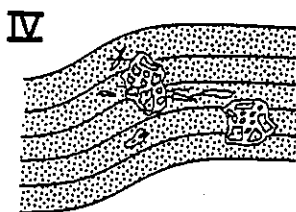
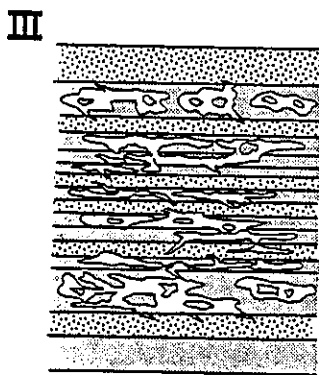
Type I breccia zones are confined to the axial surfaces of  $F_1$  folds and occur in at least two locations within the mapped region. Similar quartz systems related to axial surfaces of isoclinal folds were reported by Swatton (1987) and Brophy (1986) in other parts of the Yellowknife Basin. Typically, at Gordon Lake these breccia

Table 6.2 Breccia types and visual estimate of relative proportions.

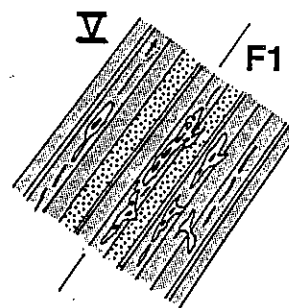
Breccia Type	Description	Proportion of breccias found at Gordon Lake
I	Sub-parallel to $F_1$ fold axial traces.	15%
II	Sub-parallel to $F_3$ fold axial traces.	5%
III	Stratabound siltstone-hosted.	40%
IV	Graywacke-hosted breccias.	30%
V	Boudinaged East Limb breccias.	10%

Figure 6.3 Diagrammatic sketches of quartz-breccia Types I, II, III, IV, and V and their distribution. Types III and IV are confined to the west limb of refold, Type V to east limb, whereas types I and II are regionally distributed throughout the Yellowknife Basin. (Scale only approximate)

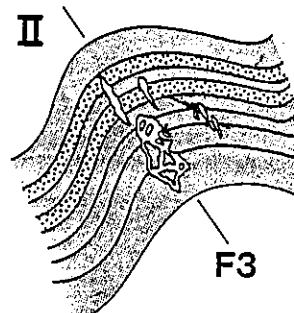
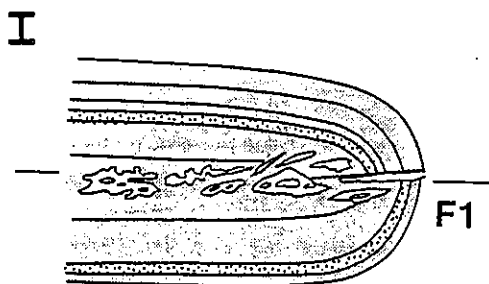
WEST LIMB






EAST LIMB



REGIONAL



-  Graywacke
-  Siltstone
-  Quartz

0 metres 5

zones are 0.1-3 m wide and associated with (0.5-1 m) bedding offsets (Figure 6.4a) along the  $F_1$  axial surfaces. Typically, they occur as sporadic 'pinch and swell' zones along the  $F_1$  axial surfaces, but are nevertheless traceable for up to 10's of metres. Side veins along these breccia zones are commonly folded and deformed by  $D_3$  (Figure 6.4a). A Type I breccia zone exposed near Kidney Pond occurs in a siltstone-dominated sequence, is traceable for 50-100 m and consists of predominantly white quartz and 10-20% chlorite. The Type I breccias were probably emplaced during or after  $D_1$  folding, but before  $D_3$ .

#### 6.2.2 Breccia Type II - Sub-parallel $F_3$ Fold Axial Traces.

Type II breccias are confined to  $F_3$  fold axial surfaces and were found in at least four locations within the mapped region. They are narrower and shorter than Type I breccias, and typically occur as brecciated zones associated with echelon veins and offsets along  $F_3$  axial surfaces (Figure 6.4b). This breccia type probably formed syn- $D_3$  during  $F_3$  fold hinge formation.

#### 6.2.3 Breccia Type III - Strata-bound and Siltstone Hosted

The Type III breccias, typified by the 'Kidney Pond Zone 1' (described in Chapter 7), were found in eight localities within the map area (Figure 5.2) and are confined to the west and central portions of the refold. These breccias form strata-bound zones within siltstone-dominated sequences (commonly black and carbon-rich) and are situated away from  $F_1$  fold axial traces and hinges. The largest stratabound breccia zone is found at Kidney Pond (Chapter 7). However, most of this zone lies beneath a swamp and it is only delineated from drill-hole data, minor trenching, and an underground incline (presently flooded). The best surface exposure of a strata-bound breccia occurs in a sequence of alternating black

Figure 6.4 Photographs of quartz-breccia types in outcrop:

a) Type I, quartz-breccia sub-parallel to axial trace of  $F_1$  anticline. Note, offsets along hinge (1) and vein offshoots deformed by  $D_3$  (2).

b) Type II, quartz-breccia sub-parallel to  $F_3$  axial trace. Note, offsets of bedding in fold hinge (1) and massive breccia zone (2).

c) Type V, East Limb breccia. Note, elongated clasts sub-parallel  $S_{3Es}$ .

d) Type VI, irregular graywacke-hosted breccia. Note, "jig-saw" character of breccia fragments

e) Early (?) stage of Type III, strata-bound quartz-breccia formation. Note, rotation of echelon veins hosted in black siltstone sub-parallel to  $S_4$  (1) and unrotated vein tips sub-parallel to  $S_{3g}$  (and pen, 2) in graywacke bed.

f) Later (?) stage of Type III strata-bound quartz-breccia formation with rotated echelon veins in black siltstone and initiation of wall rock brecciation.

g) Final (?) stage of Type III strata-bound quartz-breccia formation. Note, complete brecciation of black siltstone unit, and angular character of fragments with feldspar rims.

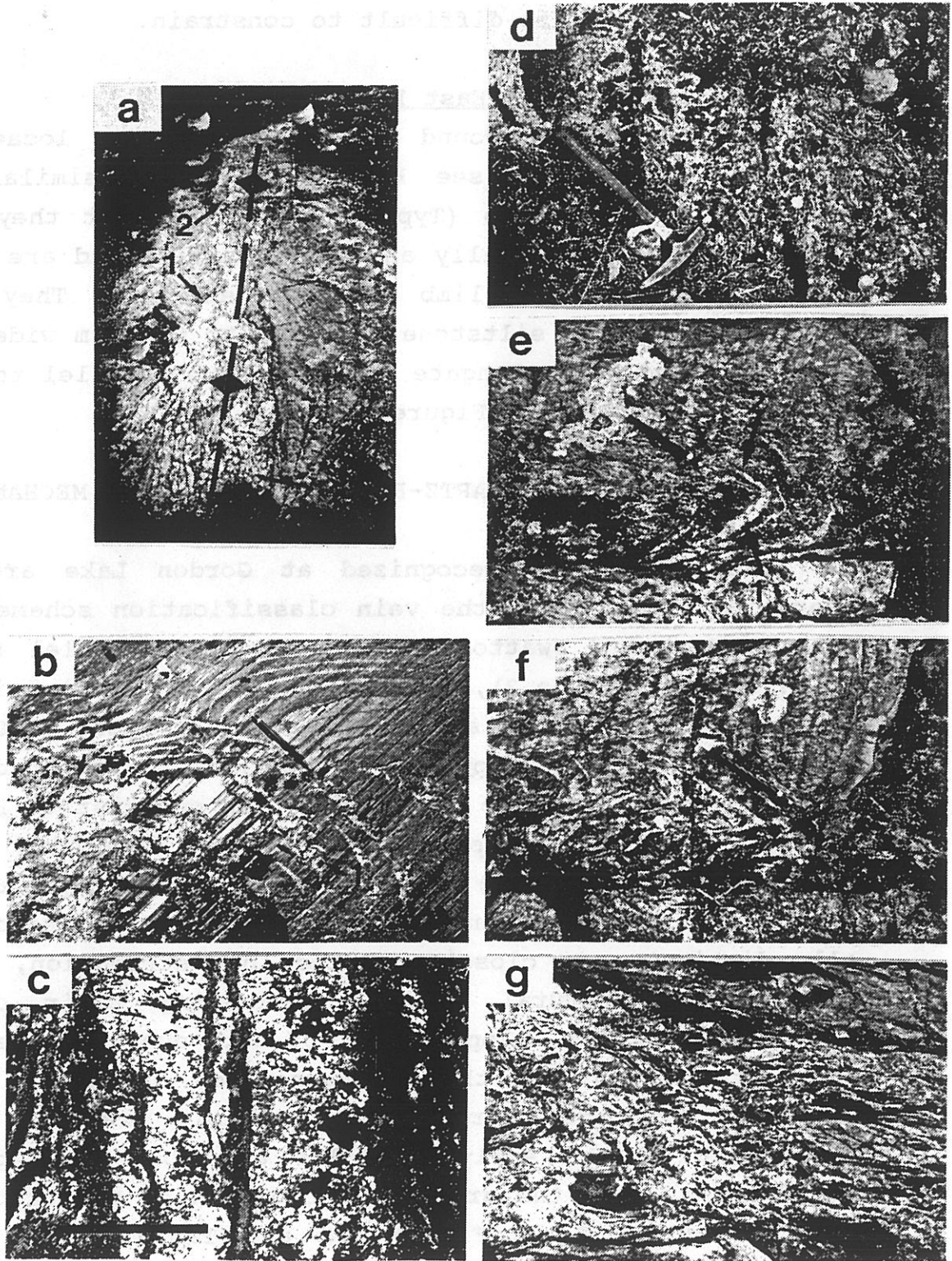
(All photographs viewed in sub-horizontal outcrop. Scale bar for 6.4c is approximately 20 cm.)

siltstones, coarse siltstones, and graywackes on the south shore of an inlet to the south of Knight Bay. Here, a strata-bound, siltstone-hosted quartz-breccia is exposed, which has a strike length of 75-100 m and varies in width from 0.5-3 m. The quartz-fracture filling morphologies within this zone include: i) individual veins rotated sub-parallel to  $S_4$  (Figure 6.4e), ii) rotated veins with brecciation and isolation of wall rock clasts (Figure 6.4f), and iii) some siltstone beds which are totally brecciated (Figures 6.4g). The strata-bound quartz-breccia zone is not confined to a single siltstone bed, but in effect 'steps-over' from one siltstone bed to another along the strike of the zone, partly fracturing intervening graywacke beds. (This characteristic is also seen from mapping of the Kidney Pond Zone 1 quartz-breccia, Figure 7.5.) The siltstone fragments are commonly elongate, angular, fractured sub-parallel to  $S_{3S}$  (Chapter 7), and show little evidence of rotation or alteration. The matrix material is composed of grey quartz, feldspar, biotite, chlorite, and sulphides. The strata-bound character of these breccias, the consistent association of breccias with  $S_4$  crenulated siltstone beds, the  $D_4$  rotation of individual veinlets, and the fracturing of clasts suggest that the Type III breccias probably formed in the latter of stages of  $D_3$  and during  $D_4$ .

#### 6.2.4 Breccia Type IV - Graywacke Hosted Breccias

Type IV breccias occur as irregular pods or lenses within graywacke-dominated lithologies (Figure 6.4d) and, like the strata-bound (Type III) breccias, are apparently confined to the central portion of the refold. The largest zones occur to the west of the Lynx inlet and are 1-5m wide, 10-30 m long, and of limited depth (Chapter 7). The breccias, though mineralogical similar to Type III, are not strata-bound or constrained by any obvious feature other

Figure 6.4





than minor flexures in bedding. The time of emplacement of this quartz-breccia is difficult to constrain.

#### 6.2.5 Breccia Type V - East Limb Breccias

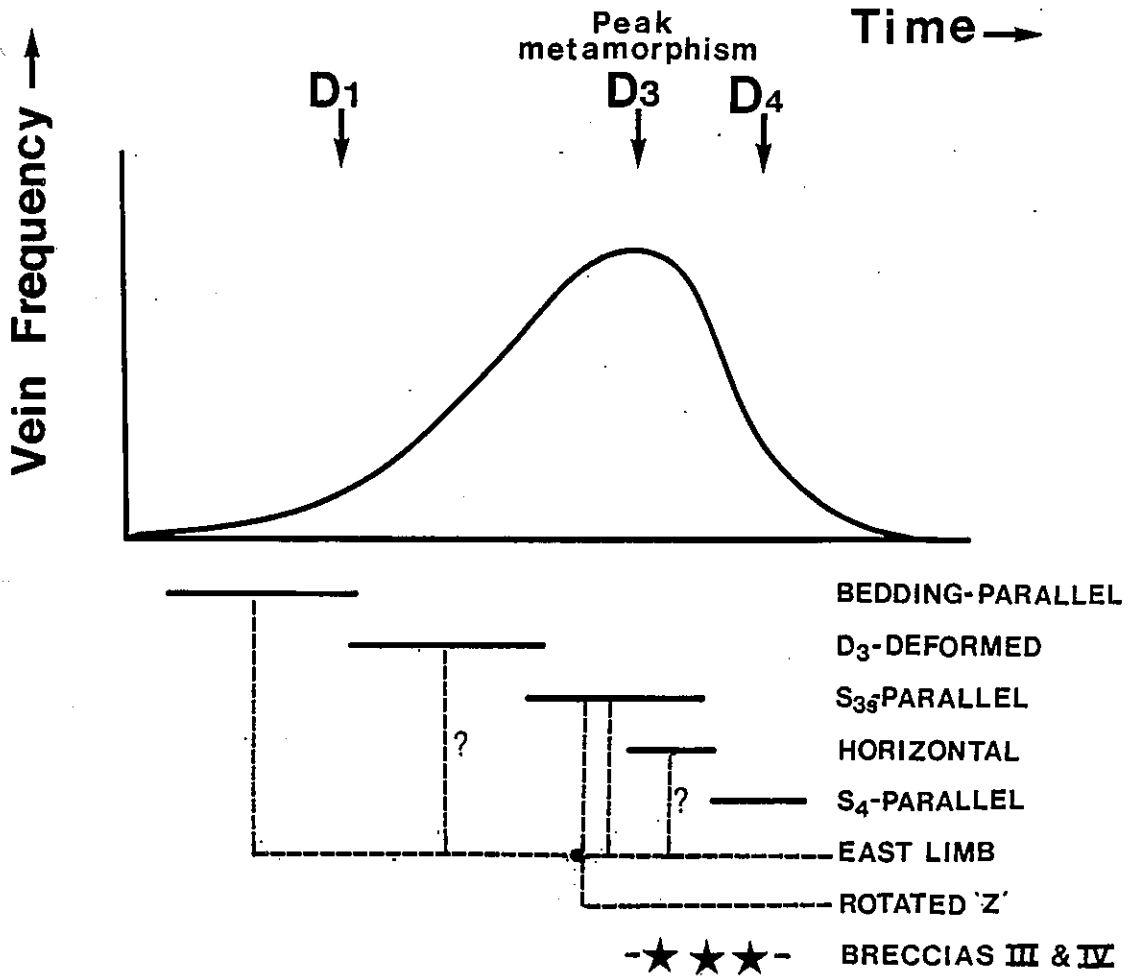
These breccias, found in at least three locations within the map area (see Figure 5.2), are similar in morphology to East Limb (Type 4) veins in that they are boudinaged (both vertically and horizontally) and are sub-parallel to the east limb ( $S_{3ES}$ ) cleavage. They are strata-bound within siltstone beds, up to 0.5-2 m wide, 1-10 m long, and have elongate fragments sub-parallel to the vein/wall rock contact (Figure 6.4c).

### 6.3 QUARTZ VEINS AND QUARTZ-BRECCIAS: FORMATION MECHANISMS AND TIME OF EMPLACEMENT.

The vein types recognized at Gordon Lake are in general agreement with the vein classification schemes of Fyson (1987a) and Swatton (1987). Bedding-parallel (Type 1),  $D_3$ -deformed (Type 2), and  $S_{3S}$ -parallel (Type 3) veins are comparable to A, B, and C vein types of Fyson (1987a), except that Type 2 appears predominantly confined to graywackes and Type 3 to siltstones. In contrast to Fyson (1987a) other vein types were recognized, including sub-horizontal veins (Type 5) and  $S_4$ -parallel veins (Type 6).

Quartz veins and quartz-breccias, though morphologically distinct, are closely related in distribution, host rocks, and structural timing, indicating their close genetic association. Emplacement of both quartz veins and quartz-breccias within the metaturbidites of Gordon Lake spanned a prolonged period that probably pre-dated the development of the early  $F_1$  folds and post-dated peak-metamorphism, with the greatest proportion of quartz being emplaced during  $D_3$  (Figure 6.5 and Table 6.1). Age relationships for the vein types were determined from structural and cross-cutting relationships, whereby the

Figure 6.5 Schematic diagram of vein frequency (or proportion of vein type, Table 6.1) versus time of emplacement. Solid lines indicate time of vein formation. Dashed lines represent genetic associations between vein types; where i) East Limb veins are (D<sub>4</sub>) deformed equivalents of S<sub>3S</sub>-parallel, bedding-parallel, and possibly Pre-D<sub>3</sub> and horizontal veins, and ii) Rotated 'Z' veins are (D<sub>4</sub>) deformed S<sub>3S</sub>-parallel veins.



bedding-parallel (Type 1) veins are cut by the  $S_{3S}$ -parallel (Type 3) and  $S_4$ -parallel (Type 6) veins, and the  $S_{3S}$ -parallel (Type 3) veins are cut by the shallow-dipping (Type 5) veins. Cross-cutting relationships between the  $D_3$ -deformed (Type 2) and  $S_{3S}$ -parallel veins are less clear, probably because the former is hosted predominantly in graywackes and the latter in siltstones.

#### 6.3.1 Mechanisms and Timing of Quartz Vein Emplacement

The time of emplacement of the early bedding-parallel veins is constrained by their folding around  $F_1$  fold hinges and their consistent deformation by  $D_3$ . The bedding-parallel veins, with their characteristic crack-seal morphology, formed along siltstone bedding surfaces, and are similar to those found in other metaturbidite terranes (e.g. the Meguma, Nova Scotia). Mechanisms for the formation of bedding-parallel veins include regional compression with fluid overpressuring and hydrofracturing (Graves and Zentill, 1982) and shearing along detachment surfaces within an accretionary wedge (Fitches et al., 1986; Roering and Smit, 1986). Both mechanisms require the veins to have developed while the sediments were sub-horizontal. This is not inconsistent with the observations at Gordon Lake, whereby the bedding-parallel veins developed pre- or syn- $D_1$  in a deforming metasedimentary pile - possible as an accretionary wedge.

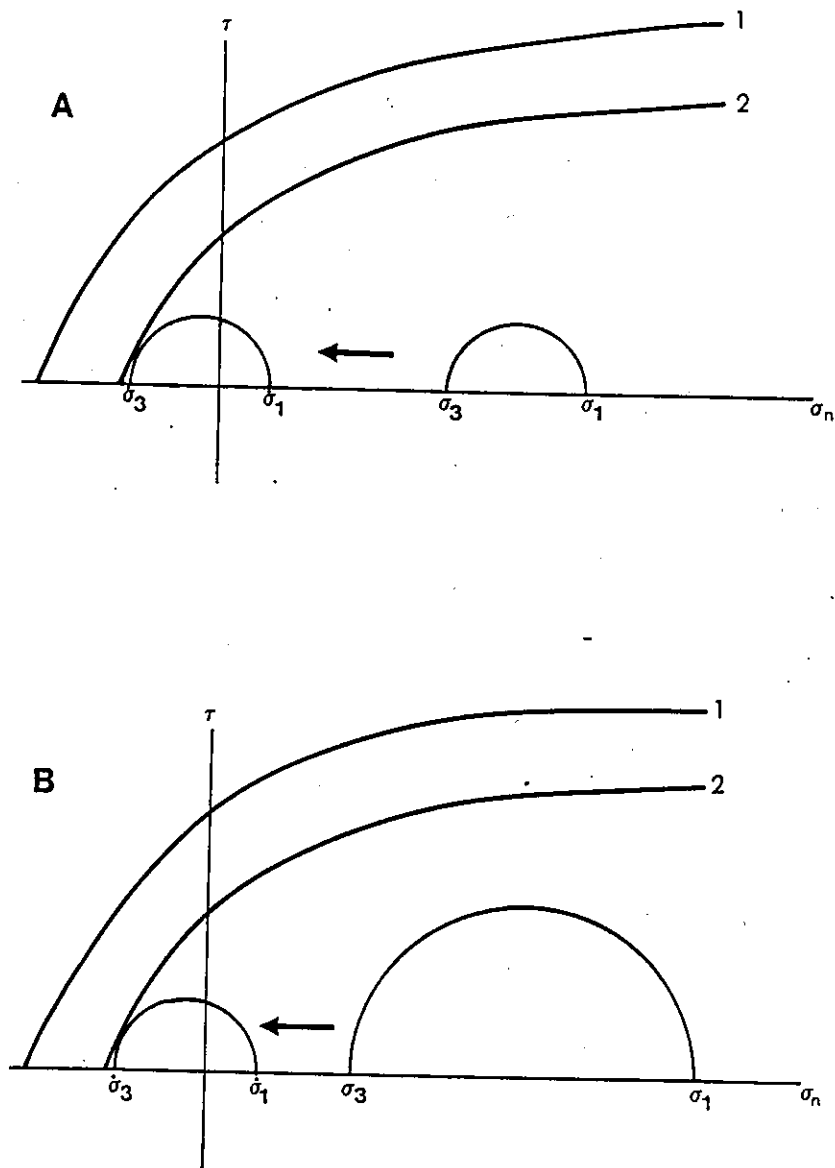
The Type 2 echelon veins and networks hosted in graywackes are consistently folded and rotated by  $D_3$ , suggesting pre- $D_3$  emplacement. Any mechanism for their formation must explain their general preference for a graywacke host and their tendency to form both networks and echelon vein systems. The lack of fracturing within siltstones, during Type 2 vein formation in the graywackes, is possibly explained by: i) the ability of the pore fluids to migrate from the siltstones, and therefore reduce fluid

pressures, and ii) the more ductile character of the siltstones (e.g., Beach, 1975, 1977). Most Type 2 veins probably formed as tensile and conjugate shear fractures during (post-D<sub>1</sub> to pre-D<sub>3</sub>) regional shortening.

Most quartz veins were emplaced during (D<sub>3</sub>) peak-metamorphic conditions (Table 6.1). This is probably a result of the greater amounts of metamorphic fluids available and the more suitable fracturing conditions. In D<sub>3</sub>, fluid pressures probably increased preferentially within the siltstones due to a permeability decrease in the adjacent metamorphically recrystallized graywackes and a reduction of the siltstone 'rock volume' during S<sub>3S</sub> development. Fracturing and vein formation might have occurred parallel to S<sub>3S</sub> if the localized fluid pressure exceeded the tensile strength of the cleaved rock and the imposed deformational stresses (e.g., Kerrich and Allison, 1978). This is apparent from a schematic Mohr's circle, where extension parallel to the cleavage is favoured by: i) an envelope of failure at lower shear stresses; ii) high fluid pressures, which would decrease the effective pressure and consequently move the Mohr's circle towards the failure envelop; and iii) low deviatoric stresses at the time of high fluid pressures (Figure 6.6). It is envisaged that formation of the S<sub>3S</sub>-parallel (Type 3) veins occurred as a cyclic (or pulsing) process whereby: 1) the S<sub>3S</sub> cleavage developed in the siltstones; 2) fluid pressures increased within the siltstones and overcame the deformational stresses and tensile strength of the S<sub>3S</sub>-cleaved rock, resulting in fracturing and quartz precipitation parallel to S<sub>3S</sub>; 3) fluid pressures decreased instantaneously with fracturing and S<sub>3S</sub> formation continued with minor vein boudinage; and 4) fluid pressures increased and the cycle repeated itself.

Sub-horizontal (Type 5) veins developed perpendicular to the vertical stretching lineation during the late stages

Figure 6.6 Schematic Mohr's circles illustrating vein formation and fracturing parallel a cleavage (e.g.,  $S_{3S}$ ). Effective normal stresses plotted on x axis and shear stresses on y axis. Failure envelope 1 is for an isotropic rock and envelope 2 is for the same rock with a well developed cleavage/anisotropy. Extensional veining parallel the cleavage is favoured by conditions of either increasing fluid pressure alone (i.e., reducing the effective pressure, A) or by both increasing the fluid pressure and lowering the deviatoric stress (B).



of  $D_3$ , as evident from their lack of  $D_3$  folding (on the refold's west limb) and the common cross cutting relationships with  $S_{3S}$ -parallel (Type 3) veins. The sub-horizontal veins probably formed as a brittle response due to the  $D_3$  vertical stretching, under conditions of high fluid pressures.

$D_4$  deformation of veins is confined to both the central and eastern areas of the refold.  $D_4$ , associated with rotation of the refold's east limb and dextral bedding-parallel slip in the refold centre (Section 5.6), resulted in deformation of earlier veins and included:

i) the rotation of some  $S_{3S}$ -parallel veins (Type 3) to form 'Z'-shaped veins (Type 7) in the refold centre; ii) the folding of sub-horizontal (Type 5) veins on the east limb of the refold; and iii) the rotation, stretching and boudinaging of predominantly  $S_{3S}$ -parallel veins (Type 3), and to a lesser extent bedding-parallel (Type 1) and  $D_3$ -deformed (Type 2) veins, to form the intensely boudinaged (Type 4) veins on the refold's east limb. The  $S_4$ -parallel veins (Type 5) probably formed during  $D_4$  by a similar mechanism to the  $S_{3S}$ -parallel veins.

### 6.3.2 Quartz Microstructure and Vein Deformation

The quartz microstructure of the seven quartz vein types gives some indication as to their deformational history. Two principal types of microstructural texture were recognized including, fine (0.05-0.3mm) sub-polygonal grains of the bedding-parallel and  $D_3$ -deformed veins (e.g., Figure 8.1a and Table A6.1) and coarse (0.5-3.0 mm) grains with minor to moderate grain boundary recrystallization of the  $S_{3S}$ -parallel, sub-horizontal, and  $S_4$ -parallel veins (e.g., Figure 8.1c and Table A6.2). A possible sub-type of this latter group includes the bimodal distribution of coarse grains and fine recrystallized grains and sub-grains of the East Limb (Type 4) veins (e.g., Figure 8.1b and

Table A6.2). The quartz microstructure of the pre-D<sub>3</sub> (Types 1 and 2) veins indicates an almost annealed or equilibrated texture, and is probably a result of thermal energy added during D<sub>3</sub> peak-metamorphism. On the other hand, the coarse-grained microstructure of the syn-D<sub>3</sub> and syn-D<sub>4</sub> veins indicates varied amounts of dynamic recrystallization and deformation during D<sub>3</sub>/D<sub>4</sub>. The bimodal-type microstructure of the East Limb veins possibly indicates a more extended phase of dynamic recrystallization, and supports the hypothesis that the East Limb (Type 4) veins were originally S<sub>3S</sub>-parallel veins, that underwent intensive post-D<sub>3</sub> deformation during D<sub>4</sub> rotation of the refold's east limb (Section 6.3.1).

### 6.3.3 Mechanisms and Timing of Quartz-Breccia Emplacement

The Type I and II quartz-breccias confined to the axial surfaces of F<sub>1</sub> and F<sub>3</sub> folds, respectively, were probably formed during closure of the folds. The syn-D<sub>1</sub> to pre-D<sub>3</sub> time of emplacement for Type I breccias is constrained by the age of the fold and later D<sub>3</sub> deformation of breccia offshoots, while the Type II breccias probably formed syn-D<sub>3</sub>. Precise mechanisms to explain the formation and geometry of the Type I and II breccias are unclear, but D<sub>1</sub> and D<sub>3</sub> folding of the metaturbidites probably localized dilations and fluid overpressures in the hinge regions of these folds, creating zones of fracturing.

The siltstone-hosted Type III and graywacke-hosted Type IV quartz-breccias are distinct from breccia Type I and II in that they are not confined to the hinge regions or axial surfaces of F<sub>1</sub> or F<sub>3</sub> folds, and are concentrated in the hinge region of the Gordon Lake refold. As the Type III breccias are strata-bound, occur only in black siltstone beds with an S<sub>4</sub> cleavage, and have clasts that are typically fractured sub-parallel to S<sub>3S</sub> they were probably emplaced during late D<sub>3</sub> and syn-D<sub>4</sub>. (This time of

Type III quartz-breccia formation is further constrained in Section 7.5.). It is hypothesised that, as both  $S_4$  and the stratabound (Type III) quartz-breccias developed preferentially in the black siltstones and are confined to the central part of the refold, they probably formed during the same deformation,  $D_4$ . A major component of this deformation is bedding-parallel slip, developed during counter-clockwise rotation of the refold's east limb.

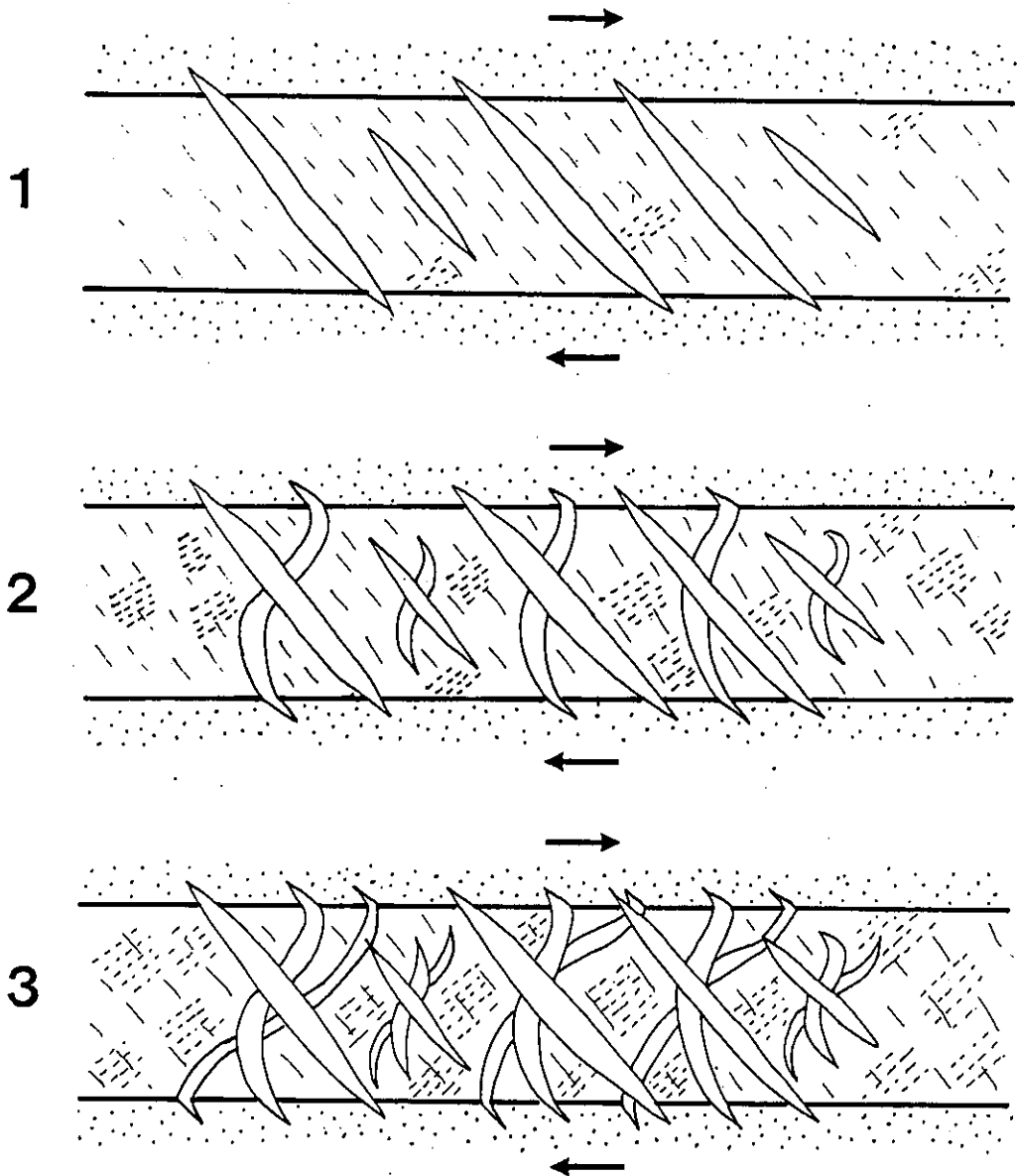
The time of emplacement of the Type IV breccias is not well constrained. However, based on their similar distribution and mineralogy to the Type III breccia they probably formed at the same time, and were most likely the result of dilations developed during late  $D_3$ /syn- $D_4$  buckling of graywacke sequences. The strata-bound and boudinaged morphology of Type V breccias suggest that they were probably Type III breccias formed in the early stages of  $D_4$  and subsequently stretched and boudinaged during rotation of the refold's east limb.

#### 6.4 MODELS FOR THE FORMATION OF THE STRATA-BOUND SILTSTONE-HOSTED TYPE III QUARTZ-BRECCIA ZONES

Two possible end-member models are suggested for the formation of the Type III quartz-breccia; i) the siltstone beds became localized zones of shearing within which progressive and repeated echelon veining occurred (e.g., Ramsay and Huber, 1983, Figure 2.11), and/or ii) shearing along the bedding contacts on either side of siltstone units localized dilational jogs (e.g., Sibson, 1986, 1990). In the first model bedding-parallel slip concentrated in the least competent sequence (such as fine grained, carbon-rich siltstone beds) induced echelon fractures sub-parallel to  $S_{3S}$  in the black siltstone beds (Step 1, Figure 6.7). These earlier veins were then progressively rotated and overprinted by new echelon veins (Steps 2, Figure 6.7). Repetition of this process eventually developed zones of



Figure 6.7 Simplified sketch illustrating the formation of the siltstone-hosted strata-bound (Type III) quartz-breccias by repeated echelon fracturing. (1) Formation of first set of echelon veins parallel  $S_{3S}$  (long dashes) in fine-grained siltstone bed during initiation of  $D_4$  dextral bedding-parallel slip, with minor  $S_4$  development (short dashes). Siltstone bed bounded by coarse-grained units (i.e. graywackes, stippled) (2) Rotation of first set of echelon veins and emplacement of second set of cross cutting echelon veins. (3) Rotation of first and second set of echelon veins, emplacement of third echelon vein set, isolation of wall rock and brecciation, and further development of  $S_4$ . (Siltstone beds are approximately one metre in width.)

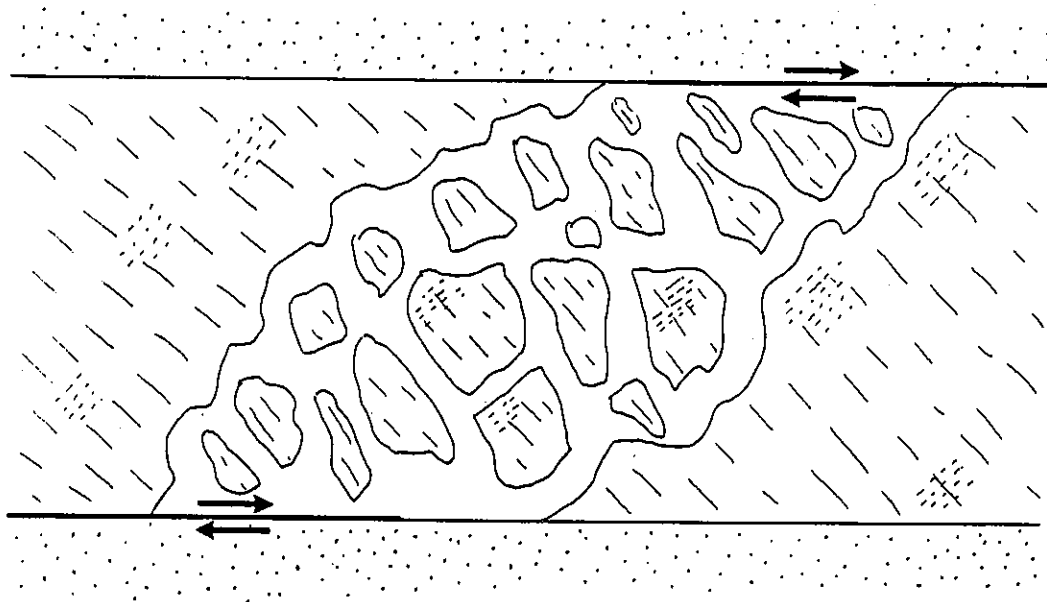


strata-bound brecciation (Step 3, Figure 6.7). Evidence to support this model includes the rotation of individual veins sub-parallel to  $S_4$  and unrotated vein tips in the adjacent, undeformed beds (Figure 6.4f and 6.4g). In the second model it is suggested that bedding-parallel slip was concentrated along the bedding contacts between beds of high competency contrast (i.e., alternating black siltstones and graywackes). Transfer of shear across the siltstone beds (from one zone of bedding-parallel slip to another) localized regions of extension or dilation (Figure 6.8). Evidence that supports this second model includes the large amount of matrix material present, the lack (in some cases) of vein overprinting, the presence of highly sheared carbon-rich material along the breccia/wall rock contact (Section 7.2).

#### 6.5 SUMMARY OF QUARTZ VEIN AND QUARTZ-BRECCIA FORMATION

Quartz vein and quartz-breccia formation in the Gordon Lake region extend from pre- $D_1$  to syn- $D_4$ , with the bulk of the quartz being emplaced syn- to post-peak metamorphism ( $D_3$ ). Bedding-parallel veins (Type 1) were emplaced pre- or syn- $D_1$  by some type of hydrofracturing and/or bedding-parallel shear mechanism. Echelon veins and networks (Type 2) were emplaced post- $D_1$  (but pre- $D_3$ ) during regional shortening, and resulted in extensional and conjugate fracturing of graywacke beds. Type I, quartz-breccia zones were probably emplaced along the axial surfaces of  $F_1$  folds syn- to post- $D_1$  (but pre- $D_3$ ). During peak-metamorphism ( $D_3$ ) Type 3 veins were emplaced sub-parallel to  $S_3$  and Type II breccias developed along the axial traces of  $F_3$  folds. In the later stages of  $D_3$  sub-horizontal veins (Type 5) were emplaced and cross-cut the vertical stretching lineation. During  $D_4$  rotation of the refold's east limb, bedding-parallel slip in the refold centre deformed earlier veins (principally Type 3) and

Figure 6.8 Simplified sketch showing the formation of the siltstone-hosted strata-bound (Type III) quartz-breccias as a "dilatational jog" within a siltstone bed bounded by offset dextral, bedding-parallel shear surfaces along bedding contacts with coarse-grained units (i.e., graywacke, stippled). Long dashes represent  $S_{3S}$  and short dashes  $S_4$  within the fine-grained siltstone bed. (Siltstone bed is approximately one metre in width.)



developed boudinaged East Limb (Type 4) and 'Z'-shaped (Type 7) veins. Veins also developed parallel to  $S_4$  (Type 6) in the refold centre. In the latter stages of  $D_3$  and during  $D_4$ , bedding-parallel slip within black siltstone beds developed zones of dilation, forming the Type III strata-bound quartz-breccias. Some of these were boudinaged by rotation of the refold's east limb (Type V). In graywacke-dominated areas late  $D_3$ /syn- $D_4$  deformation (of predominately buckling?) developed small, irregular quartz-breccia pods (Type IV).

## CHAPTER 7

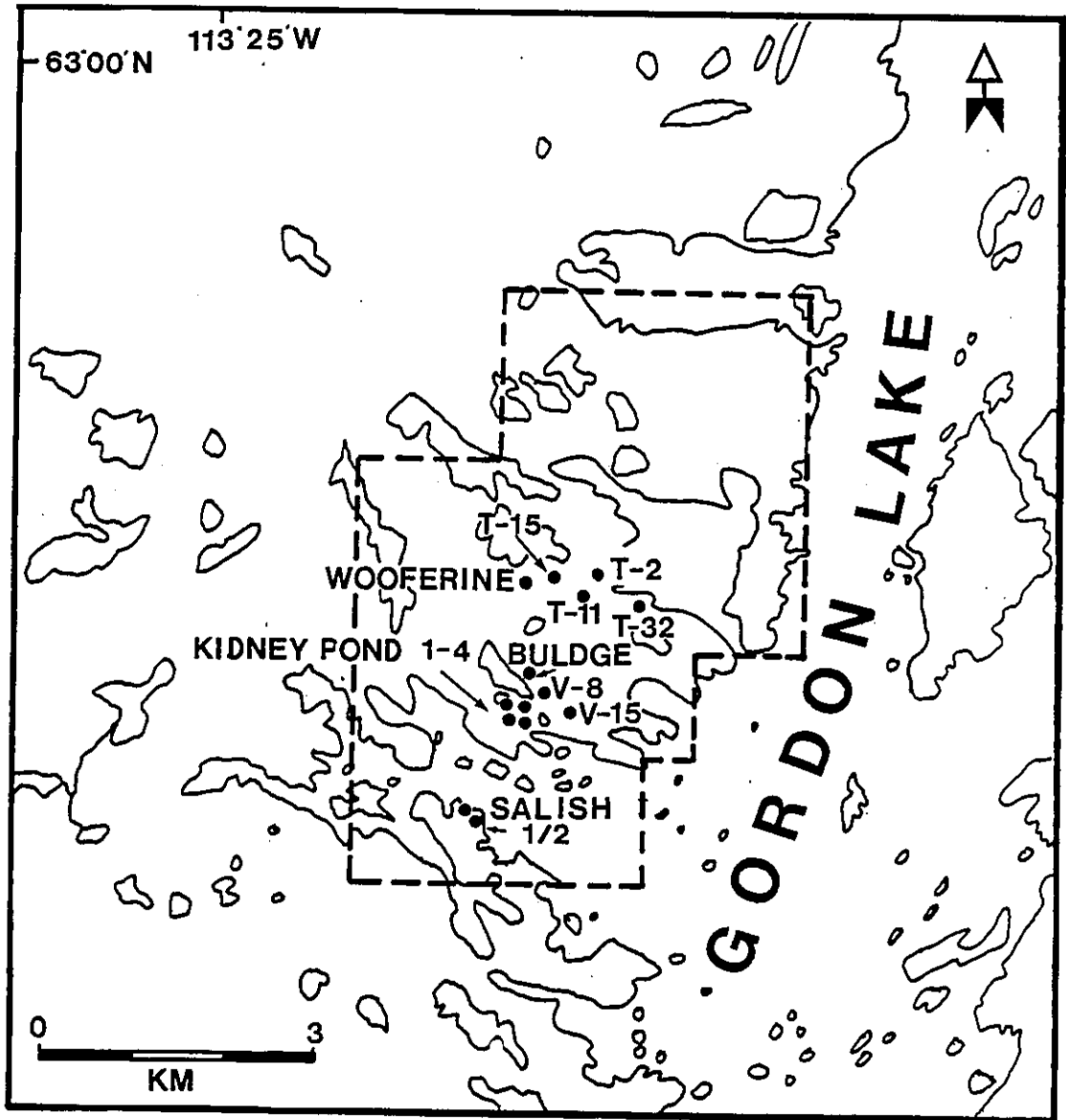
### THE KIDNEY POND ZONE 1 AND OTHER QUARTZ-BRECCIA OCCURRENCES OF THE KNIGHT BAY PROPERTY

In this chapter the structure, host lithology and mineralogy of the gold-bearing quartz-breccia occurrences, located at Knight Bay on the south-western edge of Gordon Lake (Figure 5.2), are described from detailed surface and underground mapping completed during this study. From these descriptions a better understanding of the morphology and timing of formation for the stratabound (Type III) quartz-breccias is obtained, as well as a paragenetic framework for the deposition of breccia matrix material, sulphides, and gold. In addition, the composition of arsenopyrite in the quartz-breccia host-rock was determined, so that geothermometric data might be obtained for the sulphide assemblages within the breccia zones.

#### 7.1 INTRODUCTION AND PREVIOUS WORK

The gold-bearing quartz-breccias at Knight Bay are located within the central portion of the Gordon Lake refold and include the siltstone-hosted stratabound breccias (Type III), the graywacke-hosted breccias (Type IV) and the East Limb breccias (Type V). Most of these breccias occur within the 'The Knight Bay' property that covers 15 claim blocks (2894 km<sup>2</sup>) and is solely owned by Giant Bay Resources Ltd., Vancouver, B.C., as of November 1987 (Caelles, 1987a, 1987b). The most favorably gold mineralized quartz-breccia body, the Kidney Pond Zone 1, is located on the north shore of Knight Bay (Figure 7.1). The other mineralized quartz-breccia zones include Kidney Pond Zones 2, 3, and 4, the Salish Zones 1 and 2, V-15, V-8, T-32, T-2, T-11, T-15 and the Wooferine (Figure 7.1 and Table A7.1).

Figure 7.1 Location of the Kidney Pond quartz-breccias and other quartz-breccias within Knight Bay claim block of Giant Bay Resources Ltd., Burnaby, B.C.; adapted from Caelles (1984, 1985).



The Knight Bay region has a long history of exploration, with the first known drilling and trenching done by the Borealis Syndicate in 1938 (Thompson, 1938) and later diamond drilling (790 m) in 1944 by Lynx Yellowknife Mines (Knutsen, 1984a, 1984b). The most extensive work was carried out by Giant Bay Resources Ltd. from 1983 to 1987 and includes 12,140 m of surface drilling, 500 m of percussion drilling, a 490 m decline (with 300 m of drifting and 240 m of raising), and 820 m of underground diamond drilling (Caelles, 1984, 1985, 1987a, 1987b; Burston and Caelles, 1986). Most of this work was confined to the exploration of the Kidney Pond Zone 1. Caelles (1984, 1985) described the general mineralogy of the Kidney Pond Zone 1 quartz-breccia and suggested a genetic model (Chapter 11). However, he did not attempt to relate the breccia morphology and sulphide mineralization to a structural framework.

## 7.2 STRUCTURAL AND LITHOLOGICAL SETTING OF THE KIDNEY POND QUARTZ-BRECCIA ZONES

Within the Kidney Pond area there are four major quartz-breccia zones, Zones 1, 2, 3, and 4 (Figure 7.2). The Kidney Pond Zone 1 quartz-breccia is located on the north limb of a vertically plunging, west-northwest-trending  $F_1$  anticline. Zone 1 has poor surface exposure and lies almost entirely below the Kidney Pond swamp. Drilling and an access ramp have exposed the breccia zone and defined its strata-bound character and dimensions (260 m strike length, 5-30 m wide, and a depth of at least 180 m; Caelles, 1984). Total reserves for Zone 1 are 175,000 tonnes at 16g/t (using a cut-off grade of 3 g/t and with assays cut to 96g/t; Burston and Caelles, 1986).

Surface mapping to the north of Zone 1 (Figure 7.3) has indicated that graywacke and siltstone sequences are traceable for at least 200m, whereas individual beds can

Figure 7.2 Structural and lithological location of the Kidney Pond quartz-breccia Zones 1, 2, 3 and 4. A-A', B-B' and C-C' locate the stratigraphic section across Zones 1 and 2 (Figure 7.8). Light stipple represents dark grey to black siltstone sequences.

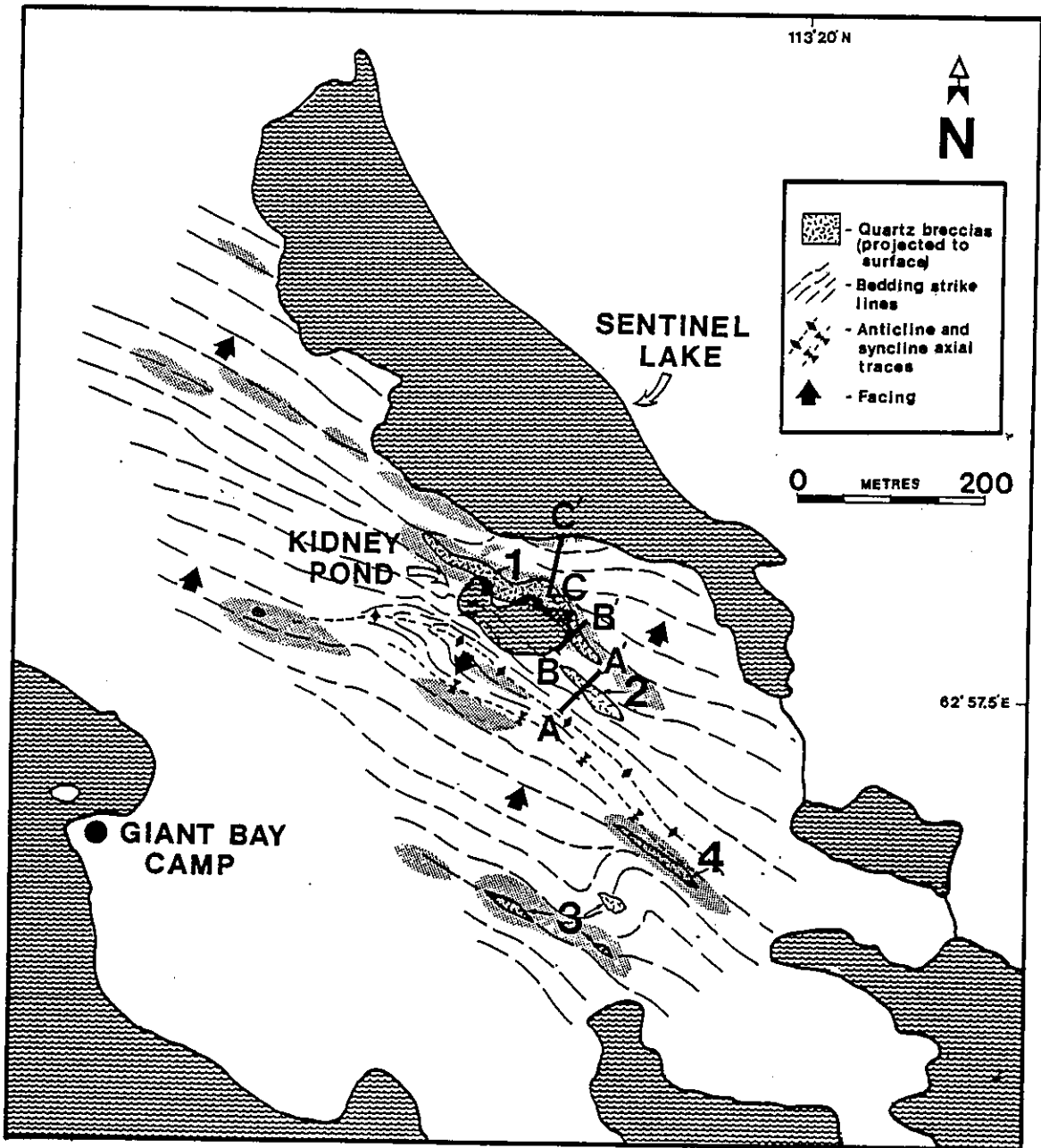
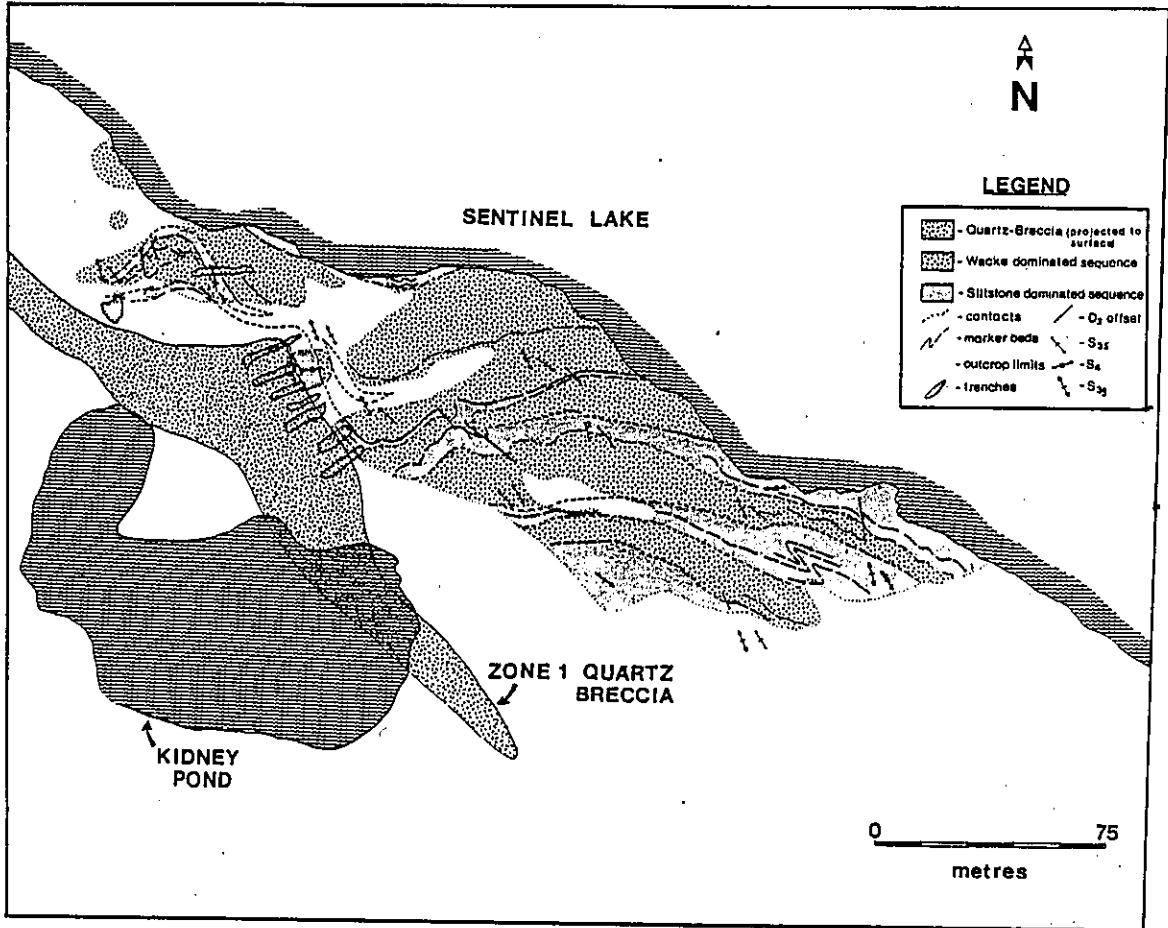




Figure 7.3 Detailed structural and lithologic map of outcrop north of Kidney Pond Zone 1 quartz-breccia. Sub-surface outline of quartz-breccia taken from Caelles (1984, 1985).



only be followed for tens of metres. This is in part due to thinning and thickening of individual beds, which typically include up to 30-40 cm reductions in bed width over 1 m strike lengths. Generally, graywacke-dominated sequences have low amplitude, gentle to open folds, that bound siltstone-dominated sequences which are tightly folded and faulted (Figure 7.3). This difference in structural style indicates that the graywackes probably deformed predominantly by buckling, whereas deformation in the siltstones was associated with major component of bedding-parallel slip.

Mapping of Zone 1 underground exposure (Figure 7.4) and surface trenches to the north of Zone 1 confirm the general strata-bound character of the breccia within the black siltstones and the presence of carbonaceous shear surfaces parallel to the breccia/wall rock contacts. Cross-sections (Figures A7.1 to A7.12) and a lithologic map (Figure 7.5) were constructed from the 1983 and 1984 diamond drill data reported by Caelles (1984). Caelles (1984, 1985) suggested that the Kidney Pond Zone 1 quartz-breccia is confined to single folded, thinning and thickening, sequence of black siltstones (Figure 7.6a). A re-interpretation of these data using the new lithological map and cross-sections indicates that the sequences of graywackes, grey siltstones and black siltstones ( $\pm$  quartz-brecciation) are more or less linear and are relatively continuous along the strike of Zone 1. All the quartz-breccia drill-hole intersections (of both low and high gold grade) are confined principally to two black siltstone sequences (Figure 7.6b). Within these two black siltstone sequences the quartz-breccias occur as an interconnected three-dimensional array of sub-parallel lenses, with 'step overs' from one black siltstone sequence to the other, linked by minor veining in the intervening graywacke beds. The explanation for this 'step over'

Figure 7.4 Underground geological map of the south-east end of the Kidney Pond Zone 1 quartz-breccia at approximately 60 m below surface. K.P. - Kidney Pond outline projected from surface.

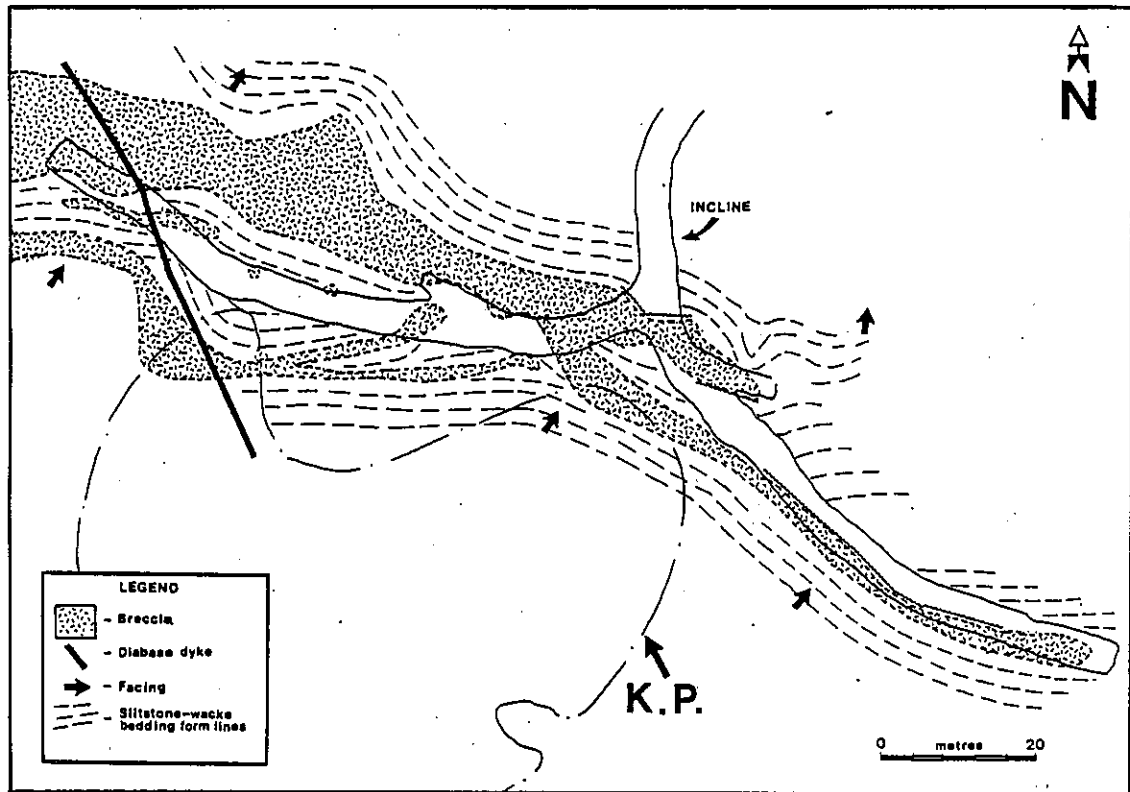
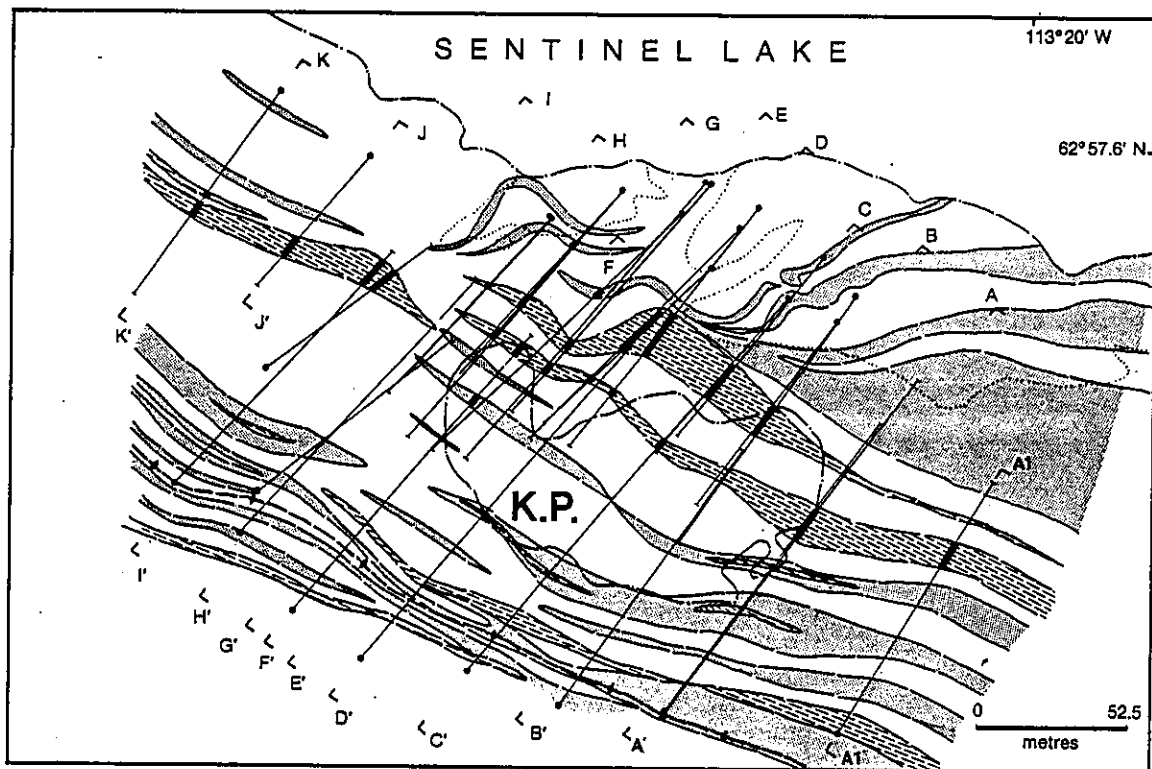


Figure 7.5 Lithological map of Kidney Pond Zone 1 interpreted from drill hole of Caelles (1984; Figures A7.1-A7.12) and projected to surface.





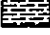


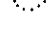

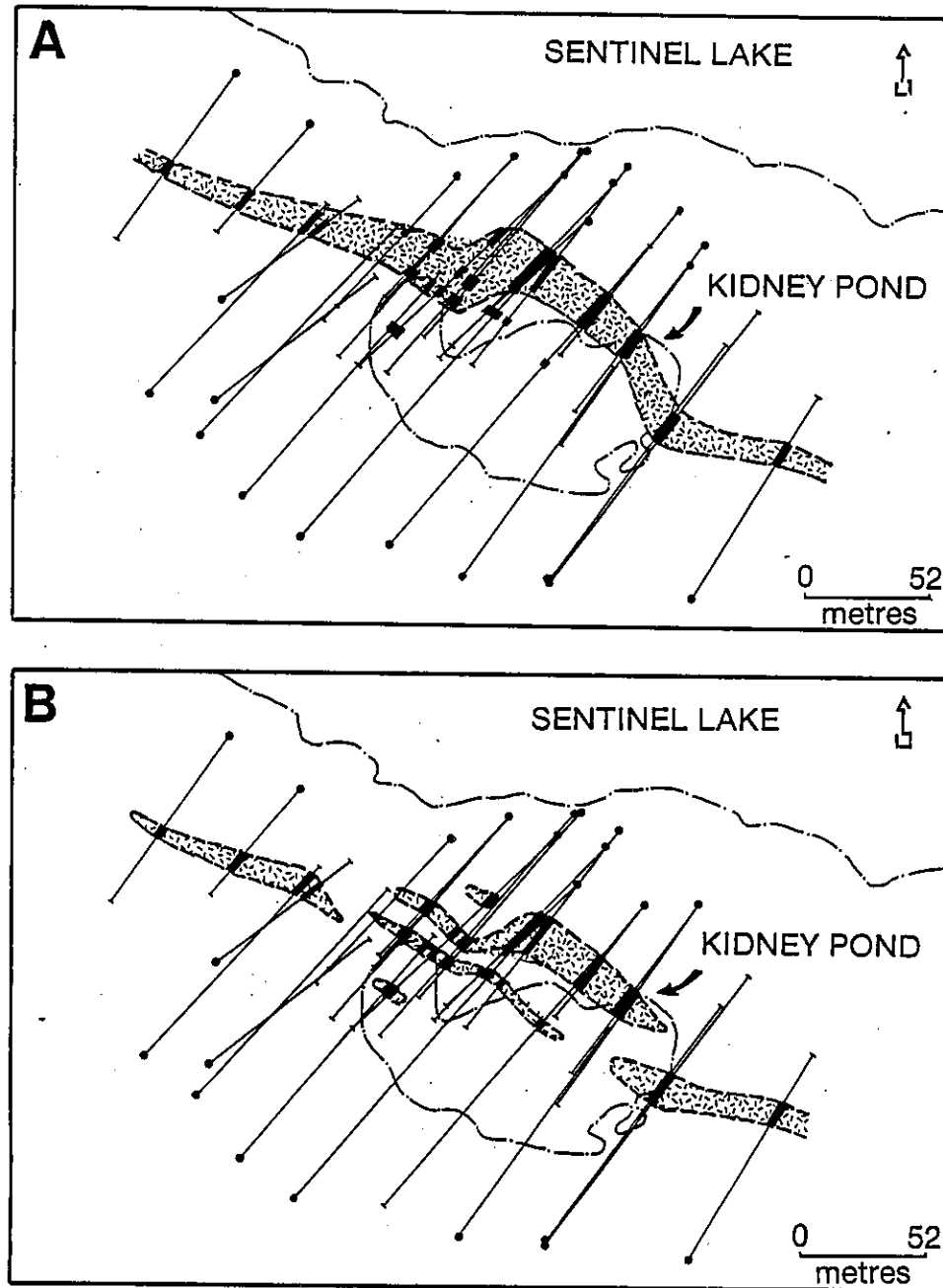


-  Graywacke beds
-  Grey siltstone beds
-  Black siltstone beds
-  F<sub>1</sub> anticline axial trace
-  Diamond drill hole with gold-bearing quartz-breccia intersections (solid black)
-  Surface outcrop
-  Location of south-east facing cross-section

Figure 7.6 Sub-surface maps of Kidney Pond Zone 1 quartz-breccia. A - as interpreted by Caelles (1984) and B - as interpreted by writer from projecting drill hole data of Caelles (1984) to surface.



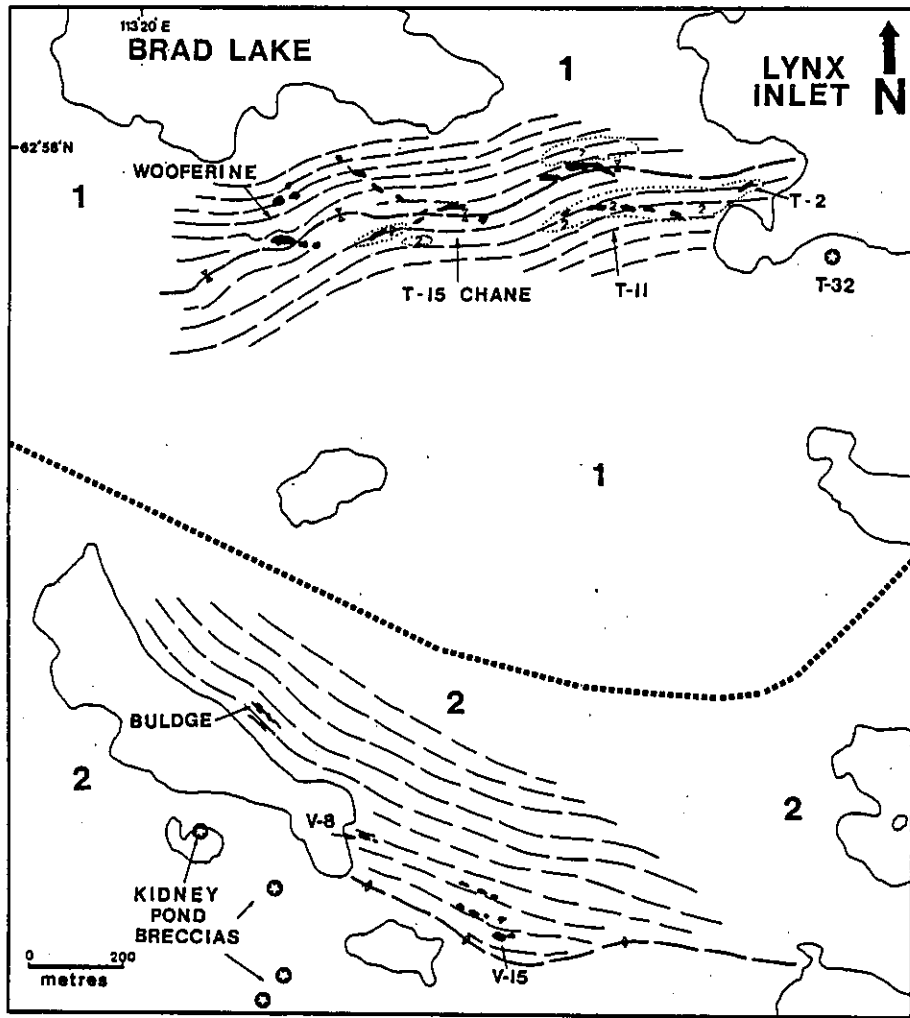
-  Quartz-breccia hosted in black siltstone
-  Diamond drill hole with gold-bearing quartz-breccia intersections (solid black)

effect is unclear, but it is possibly a function of lateral changes in siltstone lithology along strike (i.e., from a fine black siltstone to a coarser grey siltstone).

Zone 2, located to the south-east of Zone 1, extends intermittently for 300 m strike length, has a maximum width of 5 m, and is hosted predominantly in grey-black siltstones. Zone 2 is traceable in outcrop for at least 60 m, occurs as 'pinch and swell' zones of veining, and has typical gold intersections of 16g/tonne gold over 2.3 m and 26g/ton gold over 5.8 m (Table A7.1). Zone 3 comprises three small breccia showings that are possibly connected at depth (Caelles, 1985). Two showings are strata-bound bodies hosted in siltstones, whereas the third cross-cuts a minor flex and is hosted in a more graywacke-dominated lithology. Zone 4 has a strike length of approximately 90 m and is, like Zone 1, located below a swamp. Diamond drilling of this zone indicated that it is strata-bound within black siltstones, is similar in mineralogy and breccia morphology to Zone 1, but has no significant gold mineralization (Caelles, 1984).

Most of the gold bearing, Type IV quartz-breccia zones to the north (T-2, T-15, T-32, Chane, and Wooferine) are hosted in grey to black graywacke-dominated sequences, but a few (T-11 and T-22) occur within siltstones. Typically these breccia zones are discordant to bedding and occur where there are minor folds or flexures in bedding (Figure 7.7). The age of these folds or flexures is unclear, but the north-south trend of their axial traces suggests that are possibly  $D_3$  or  $D_4$  in age. In addition, a noticeable increase in carbonaceous material and arsenopyrite occurs within graywacke and siltstone beds adjacent to these breccia zones.

Figure 7.7 Compilation geological map of Wooferyne, Chane, T-11/T-2 and T-15 quartz-breccia zones of the Lynx area from Caelles (1984, 1985).



- 1 Graywacke dominated lithology (>30% graywackes)
- 2 Siltstone dominated lithology (<30% graywackes)
- Bedding strike lines and quartz-breccias (solid black)
- F<sub>1</sub> anticline/syncline axial traces
- Approximate lithological contacts

### 7.3 STRATIGRAPHIC SECTION ACROSS THE KIDNEY POND QUARTZ-BRECCIA ZONES 1 AND 2

Since a correlation was recognized between the strata-bound quartz-breccia zones and the siltstone-dominated sequences, a detailed (1m = 2 cm) stratigraphic section was completed, using both surface exposure and drill core, across the Zone 1 and 2 breccias (Figure 7.8). Using this stratigraphic section and plot of average bed thickness, average grain size, bed thickness variation, and grain size variation four distinct facies associations were recognized. These included: 1 - thick-bedded graywacke sequences; 2 - thick- to medium-bedded sequences of alternating graywackes and siltstones; 3 - medium- to thin-bedded sequences of alternating graywackes and siltstones; and 4 - thin-bedded to laminated sequences of siltstones. Typically, quartz-breccia Zones 1 and 2 occur within the siltstone-rich sequences (facies association 4) and close to the contacts between facies associations 3 and 4. Graywacke-rich sequences (facies association 1) occur within 10 m of the breccia zones, whereas thin graywacke beds are commonly interspersed within the breccia siltstone host. The distribution, thickness, and competency contrast between the graywacke and siltstone beds probably played an important role in localizing the zones of quartz-brecciation (Section 11.6.2).

### 7.4 MATRIX, SULPHIDE, AND GOLD MINERALOGY OF THE KIDNEY POND ZONE 1 QUARTZ-BRECCIA

From the relationships between the breccia matrix, sulphides, and gold of the Kidney Pond Zone 1 a paragenetic sequence of quartz-breccia mineralogy was developed (Figure 7.10). In drill core, two distinct phases of brecciation were recognized (e.g., CD20-10.0, Figure 7.11). An early (mm-cm scale) breccia phase is distinguished by equidimensional fragments of black siltstone set in a



Figure 7.8 Stratigraphic section measured across Kidney Pond Zone 1 and 2 quartz breccias. Interpreted facies associations are defined by: 1 - thick- to very thick-bedded graywackes with <10% siltstones; 2 - alternating thick- to medium-bedded, graywackes and siltstones, with a graywacke/siltstone ratio of approximately 60/40; 3- alternating thin- to medium-bedded graywackes and siltstones, with a graywacke/ siltstone ratio of 40/60; 4- thin- to medium-bedded siltstones with <10% graywackes. Stars locate zones of quartz-brecciation. (Scale in metres.)

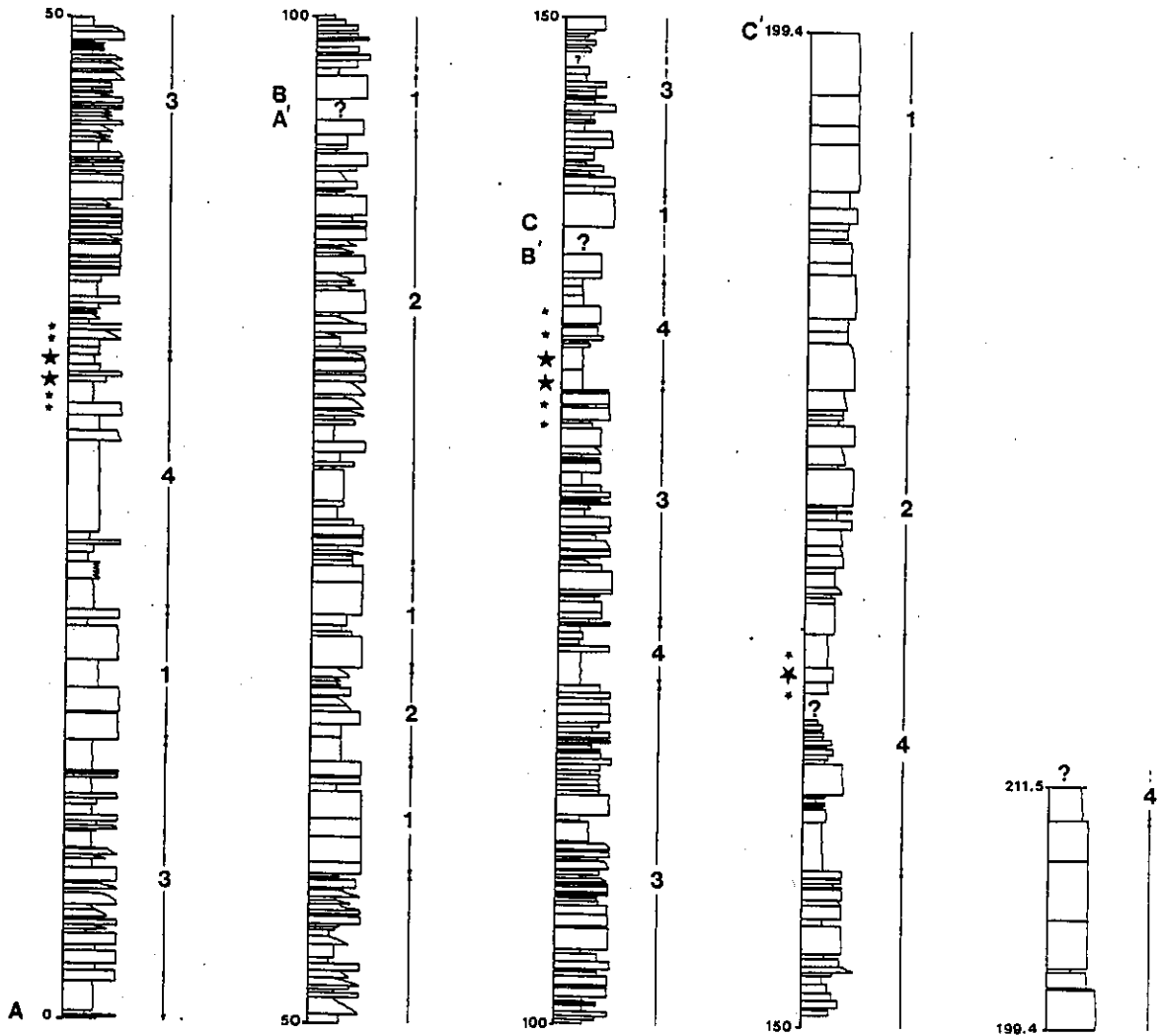


Figure 7.9 Depth of stratigraphic section across Kidney Pond Zone 1 and 2 quartz breccias versus plots of average bed thickness, bed thickness variation, average grain size, and grain size variation.

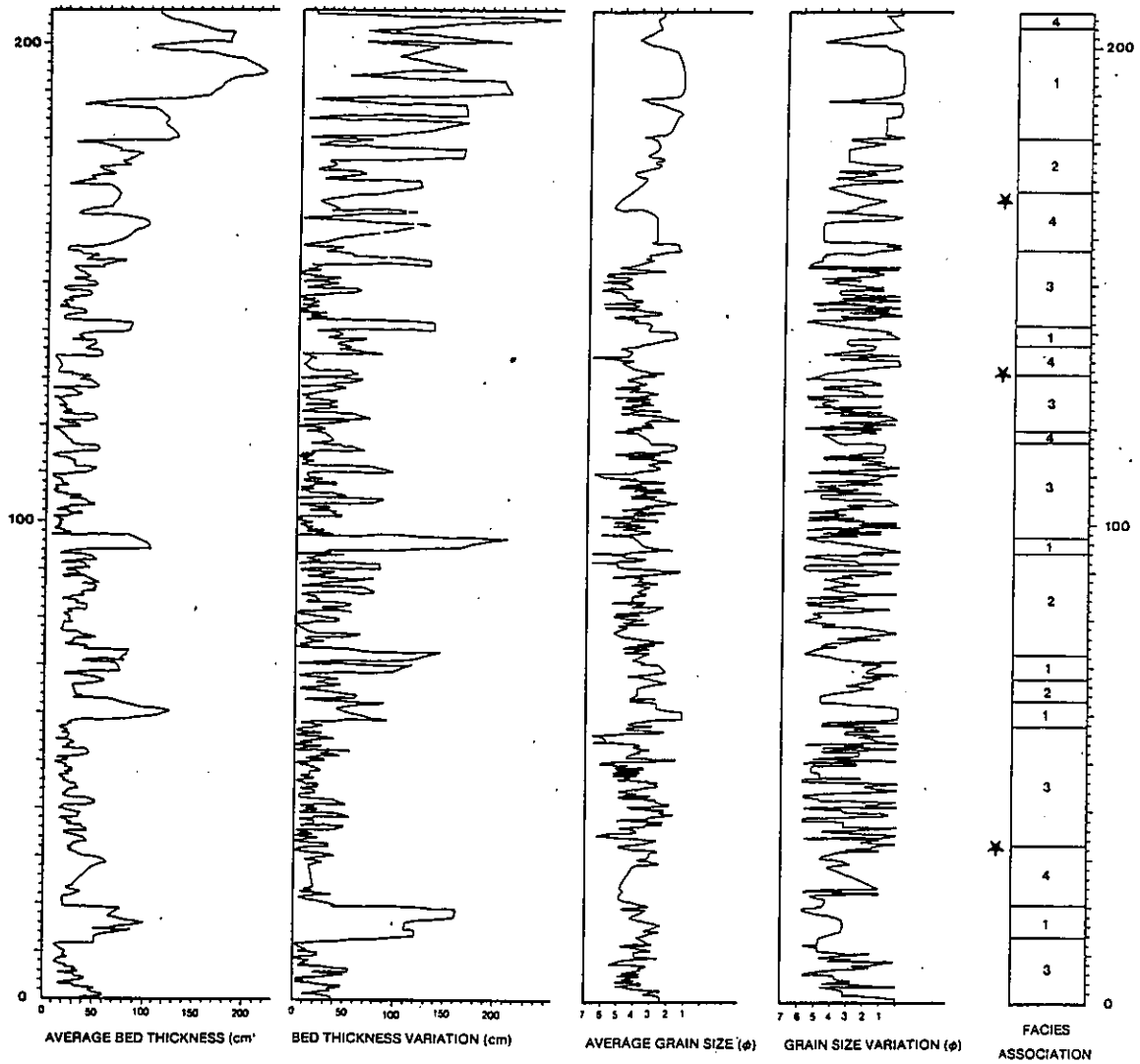


Figure 7.10 Paragenetic relationships between breccia matrix, sulphide, and gold deposition.

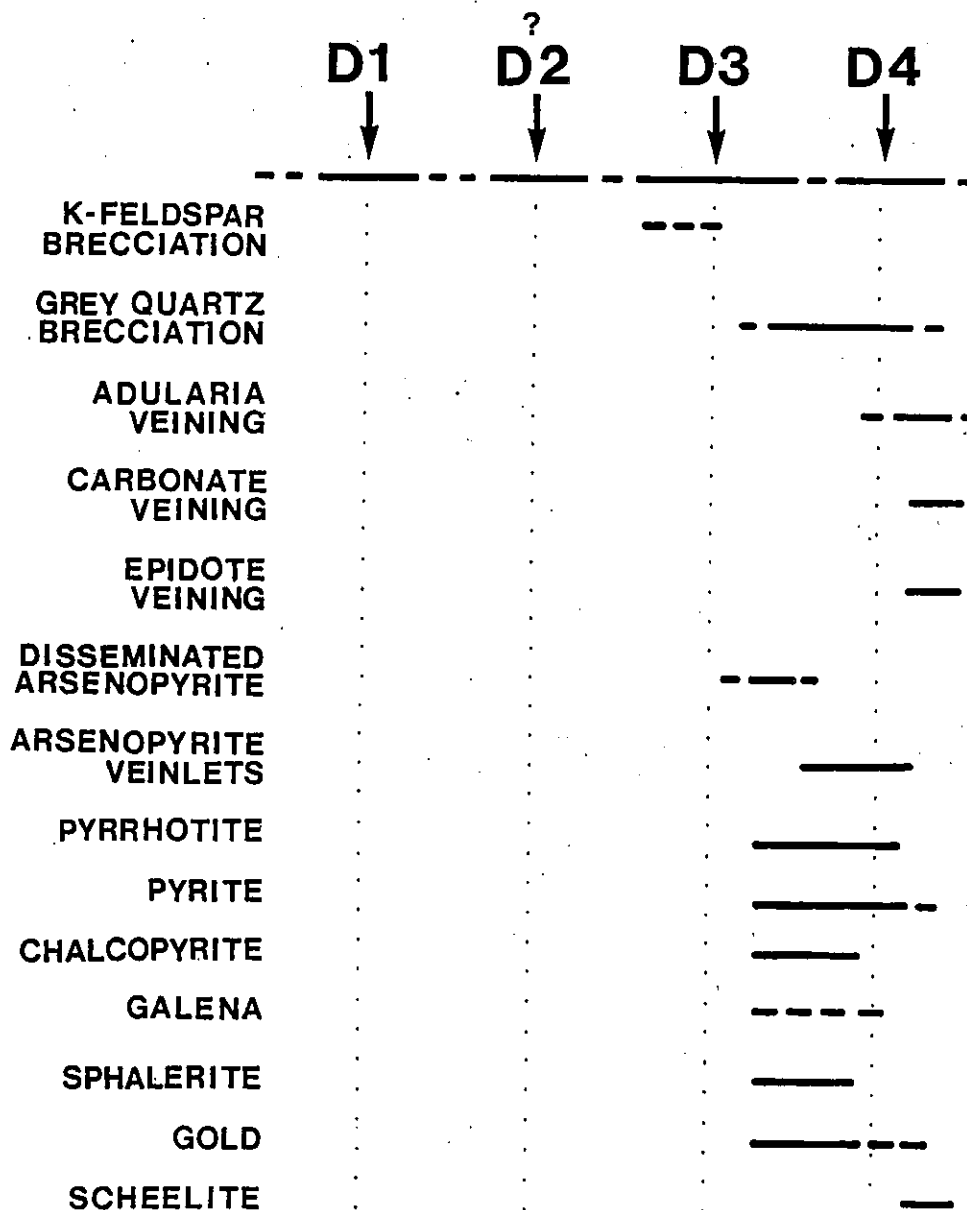
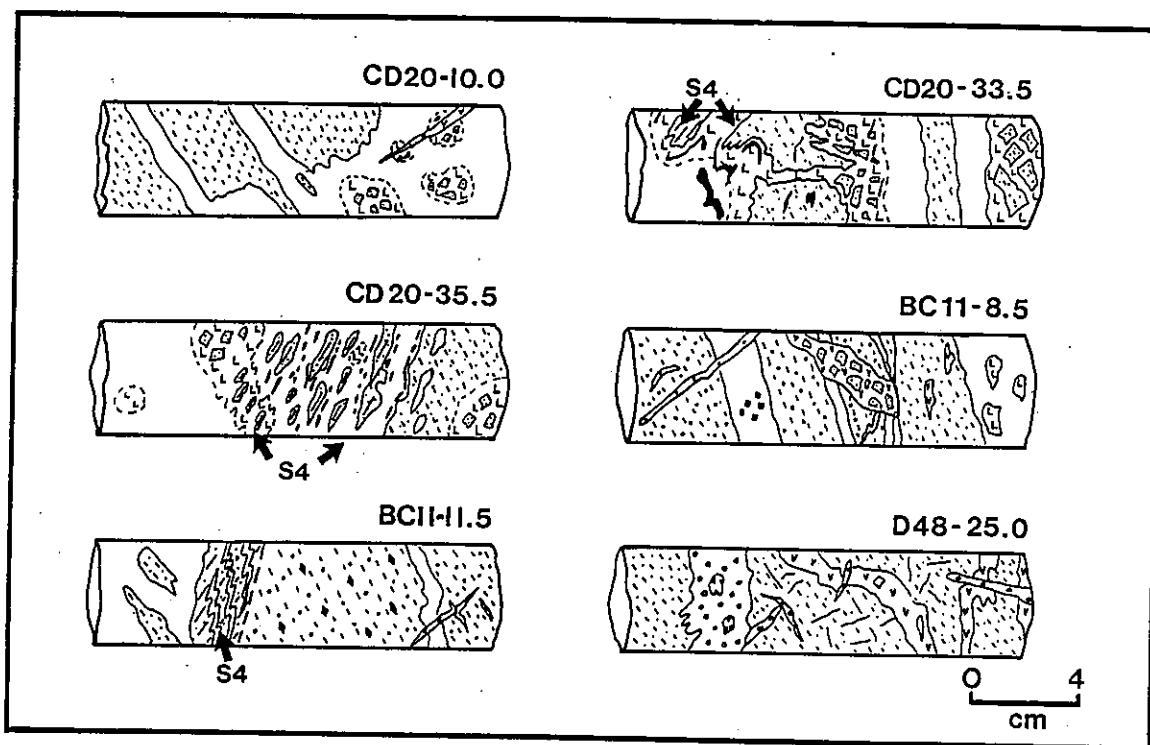

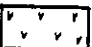
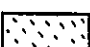
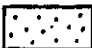

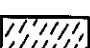
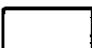
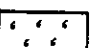
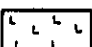
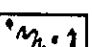


Figure 7.11 Representative drill core from the Kidney Pond Zone 1 breccia displaying breccia mineralogy and fabric relationships.



	Fine Siltstone		Adularia		S3 cleavage
	Coarse Siltstone		Carbonate		S4 cleavage
	Grey Quartz		Epidote		
	K-Feldspar		Sulphides		

matrix of white K-feldspar ( $\pm$  minor plagioclase) and coarse biotite. This early breccia phase is surrounded by a later (cm-dm scale) breccia phase, characterized by grey quartz and elongate wall rock fragments fractured sub-parallel to  $S_{3S}$ . The grey quartz accounts for 75-85% of the breccia matrix and appears closely associated with the sulphide and gold mineralization. Approximately 30% of the black siltstone within and adjacent to quartz-breccia is deformed and crenulated by  $D_4$ , as is 10-20% of the K-feldspar-rich breccia, the grey quartz breccia and associated sulphides (e.g., CD20-33.5, Figure 7.11).

Examination of the grey quartz in thin section indicates that it is composed of 60-70% quartz with abundant solid inclusions and 30-40% quartz free of inclusions (Figure 8.1c). Typically, both quartz types have coarse quartz grains (0.2-1.5 mm) displaying undulatory extinction that are bounded by thin zones of fine (10-50  $\mu\text{m}$ ) recrystallized grains and sub-grains. Fine (50-100  $\mu\text{m}$ ) grains and sub-grains occur where the quartz is deformed by  $D_4$ , with some grains and sub-grains elongated sub-parallel to  $S_4$ . The solid inclusions within the dominant quartz type are black, amorphous, up to 5-20  $\mu\text{m}$  in size and make up 3-10% of the quartz grains. The irregular shape of the solid inclusions and their non-reflective character suggest that they are probably carbonaceous in origin. (Analysis of similar solid inclusions from grey quartz veins of the Con and Giant Mines at Yellowknife, indicated that they were "primarily due to disseminated carbon and graphite"; Boyle, 1953). The two quartz types when examined by cathodoluminescence, neither produced luminescence nor were distinguishable from each other (L. Jansa, personal communication, 1990).

Alteration of the host rock within and adjacent to the quartz-breccias varied. Siltstone fragments within the early (K-feldspar-rich) breccia phase display sharp edges,

and do not appear altered in hand specimen. However, in thin section the fragments are silicified, sericitized, and partly assimilated into the matrix (Figure 7.12e). The larger, elongate siltstone fragments, within the grey quartz, are typically silicified and altered by secondary biotite and chlorite (Figure 7.12c). The secondary biotite, is commonly coarse (up to 5 mm in size), forms radial textures, possibly cross cuts metamorphic biotite, and is free of inclusions (Figures 7.12d and 10.4a).

Chlorite ( $\pm$  opaque material) and quartz-biotite-chlorite ( $\pm$  opaque material) multi-mineralic aggregates commonly occur within the black siltstones beds adjacent to the Kidney Pond quartz-breccia zones. These aggregates are ovoid in shape, range in size from 0.2-1 mm, are oriented sub-parallel to  $S_{3S}$  with distinct pressure shadows, stretched along  $L_3$ , and in some cases crenulated by  $S_4$  (Figures 7.12a and 7.12b). Within the quartz-biotite-chlorite aggregates, ragged biotite is commonly surrounded by quartz and chlorite. Chlorite aggregates also occur within the host siltstones adjacent to the V-15 zone. Both types of aggregates probably developed as an alteration response to the emplacement of the quartz-breccias. (Similar aggregates were recognized around gold deposits within the metaturbidites of the Meguma Terrane, Nova Scotia; S. Douma, personal communication, 1990). Possible explanations for their development include: i) their formation as syn- $D_3$  mineral growths, ii) the replacement of syngenetic pyrite grains during  $D_3$  (Burston and Caelles, 1986), or iii) the replacement of  $D_3$  biotite (or possibly cordierite) porphyroblasts in the late phases of  $D_3$  or syn- $D_4$ .

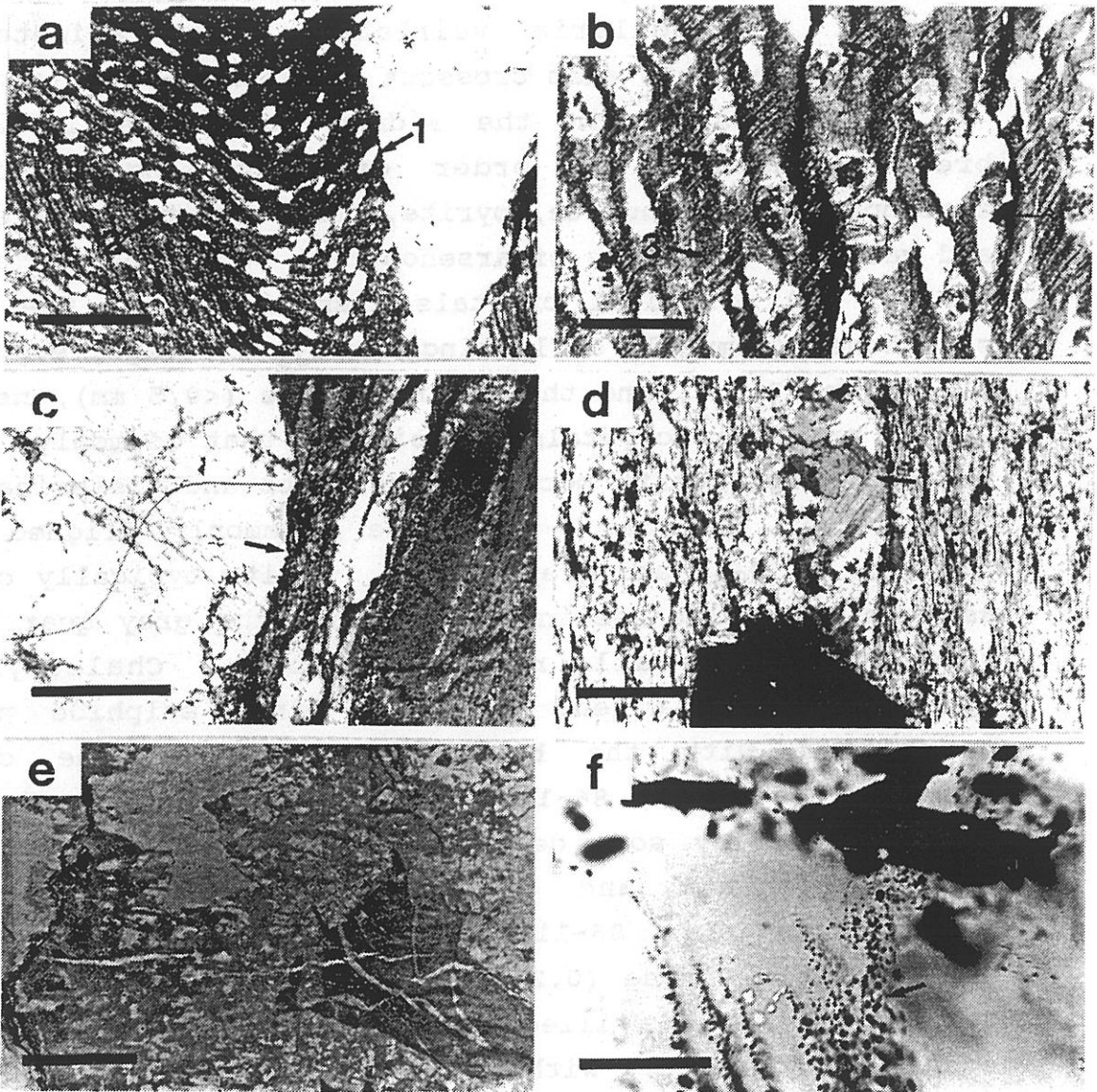
Late veinlets of pink adularia crosscut both phases of brecciation. Most adularia veinlets are deformed by  $D_4$ , but in one sample an adularia veinlet had siltstone inclusions, which were both crenulated and rotated;

Figure 7.12 Microphotographs of quartz-breccia alteration mineralogy and gold.

- a) Chlorite aggregates in black siltstone bed within the Kidney Pond Zone 1 quartz-breccia. Note elongation of aggregates sub-parallel to  $S_3$  (1) and folding by  $S_4$  (2).
- b) Quartz-biotite-chlorite aggregates in black siltstone adjacent to the Kidney Pond Zone 1 quartz-breccia. Note the ragged biotites in centre of the aggregates (1), pressure shadows around the aggregates (2), and the development of  $S_4$  (3).
- c) Biotitized and chloritized siltstone associated with grey quartz phase of brecciation. Note fracturing sub-parallel to  $S_{3s}$ .
- d) Secondary biotites, associated with breccia mineralization, in  $D_3$  pressure shadow around coarse arsenopyrite crystal. Note stellate texture of the secondary biotite, its lack of internal inclusions, and its possible cross cutting relationship with metamorphic biotites.
- e) Silicified and sericitized black siltstone fragment associated with early phase of K-feldspar-rich brecciation.
- f) Fine gold grains along healed microfractures within grey quartz. Large gold grain in upper part of photograph.

(All microphotographs viewed in YZ section, except 7.11 f where orientation is unknown. (Scale bars for 7.11a, &.11b, 7.11c, 7.11d, and 7.11e approximately 1 mm, while scale bar for 7.11f is approximately 50  $\mu$ m.)

Figure 7.12



contacts between myofibrils and the sarcolemma host, and  
is found in the close association with the sarcolemma  
sarcomere and myofibrils (e.g., 10-15), where they  
are within intramembranous myofibrils zones of 10-15  
myofibrils (e.g., 10-15), and they form the  
myofibrils (Figure 7.12). The intramembranous  
myofibrils form the sarcolemma and are  
the sarcolemma and myofibrils.

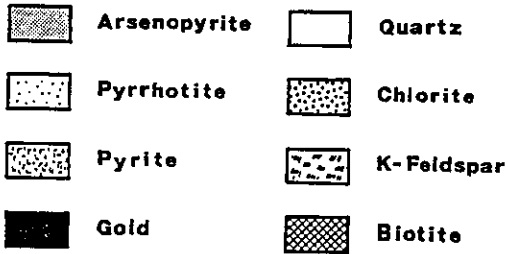
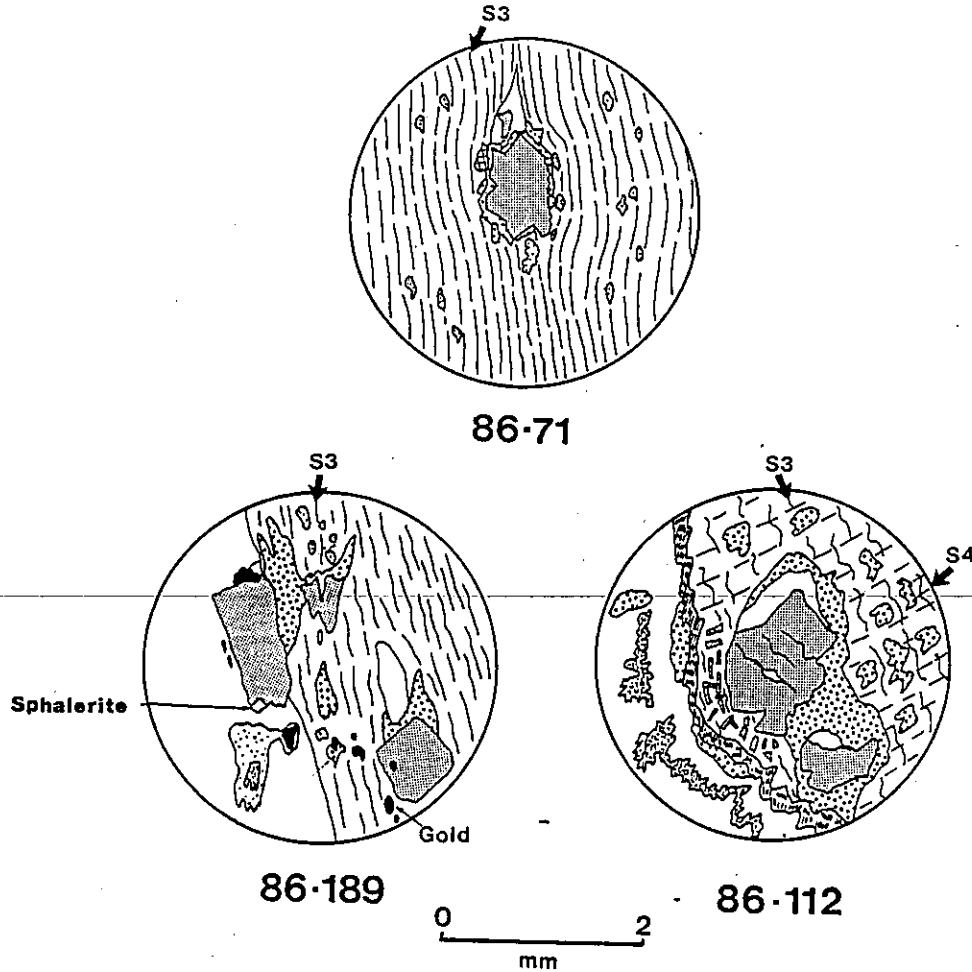


indicating this veinlet was emplaced post-S<sub>4</sub>. Rare calcite-filled fractures with minor associated scheelite crosscut the adularia veinlets. Rare epidote and tourmaline veinlets also crosscut the quartz-breccia zones.

Sulphides within the Kidney Pond Zone 1 quartz-breccia include, in order of decreasing abundance, arsenopyrite, pyrrhotite, pyrite, chalcopyrite, sphalerite, and galena. Two types of arsenopyrite occur, one as coarse (0.25-2 mm) pyramidal crystals disseminated in the black siltstones (commonly deflecting the S<sub>3S</sub> cleavage, e.g., 86-71, Figure 7.13), and the other as fine (<0.5 mm), needle-shaped prismatic crystals in veinlets that commonly crosscut S<sub>3S</sub>. Pyrrhotite occurs as veinlets and disseminations both within the black siltstone (commonly aligned subparallel to S<sub>3S</sub>) and grey quartz. Pyrite typically occurs as veinlets and disseminations within the grey quartz and along breccia/wall rock contacts. Chalcopyrite, sphalerite, and galena occur as minor sulphide phases associated with the both pyrrhotite and the coarse arsenopyrite (e.g., 86-189, Figure 7.13). The sulphides commonly display some deformation by D<sub>4</sub>, with folding of pyrite veinlets and possible brittle fracturing of arsenopyrite (e.g., 86-112, Figure 7.13).

Visible coarse (0.2-1 mm) gold was reported in 14 of 39 diamond holes drilled on Zone 1 (Caelles, 1984) and occurs predominantly within the grey quartz and along the contacts between grey quartz and the siltstone host. Gold is found: i) in close association with the coarse arsenopyrite and pyrrhotite (e.g., 86-189, Figure 7.13); ii) within intensely recrystallized zones of fine-grained quartz (e.g., Figure 8.1d), and iii) along healed microfractures (Figure 7.12f). Preliminary microprobe analysis indicates that the gold is approximately 85 wt% pure with 15 wt% silver (R. McKay, personal communication, 1989).

Figure 7.13 Reflected light sketches of mineralized breccia samples from the Kidney Pond Zone 1, showing gold, sulphide and fabric relationships. Note, i) the deflection of  $S_3$  around the coarse pyramidal arsenopyrite (86-71); ii)  $D_4$  folding of pyrite and possible fracturing of an arsenopyrite crystal (86-112); and iii) gold occurring in pressure shadows around the syn- $D_3$  pyramidal arsenopyrite in association with pyrrhotite and sphalerite (86-189).



#### 7.5 TIME OF FORMATION FOR THE KIDNEY POND ZONE 1 QUARTZ-BRECCIA.

Generally, the coarse-grained quartz microstructure of Kidney Pond quartz-breccia is similar to that of the syn-D<sub>3</sub> and syn-D<sub>4</sub> veins (Section 6.3.2), and is consistent with the quartz-breccia being emplaced syn- to post-D<sub>3</sub>, and in some localities (where fine grains sub-grains are elongated sub-parallel to S<sub>4</sub>) undergoing deformation by D<sub>4</sub>. Mineralogical/fabric associations within the quartz-breccia zones display both D<sub>3</sub> and D<sub>4</sub> characteristics. The D<sub>3</sub> associations include: i) coarse arsenopyrite crystals, hosted in rocks adjacent to the quartz-breccias, that deflect S<sub>3</sub>; ii) syn-D<sub>3</sub> multi-mineralic aggregates of chlorite and quartz-biotite-chlorite adjacent to the breccia zones; and iii) the early K-feldspar-rich phase of brecciation (Table 7.1). However, most mineralogical/fabric associations are related to D<sub>4</sub> and include: i) the consistent D<sub>4</sub> crenulation of quartz-breccia zones and their host rocks; ii) the late grey quartz phase of brecciation with fragments fractured parallel to S<sub>3S</sub>; iii) D<sub>4</sub> folding and deformation of sulphides; iv) veinlets of fine needle-shaped arsenopyrite cross-cutting S<sub>3S</sub>; and v) a secondary biotite phase that appears to cross-cut metamorphic biotite (Table 7.1).

The consistent spatial association between the quartz-breccias and D<sub>4</sub> fabrics indicates that D<sub>4</sub> is the principal deformational event controlling their formation. However, the actual time of quartz-brecciation probably spans an interval from late D<sub>3</sub> to syn-D<sub>4</sub>. This time span possibly represents either: i) a diachronous event, whereby the D<sub>4</sub> deformation gradually overprinted D<sub>3</sub>, or ii) a distinct time interval, whereby a syn- to late-D<sub>3</sub> alteration/thermal halo developed around the quartz-breccia localities before the main (syn-D<sub>4</sub>) phase of fracturing. This halo might explain the syn-D<sub>3</sub> formation of the coarse

Table 7.1 Constraints on the timing of formation for the Type III, strata-bound siltstone-hosted quartz-breccias.

	<Pre-D <sub>3</sub> >	<early-D <sub>3</sub> -late>	<--D <sub>4</sub> -->
Confinement of Type III breccias to D <sub>4</sub> crenulated siltstones			█
D <sub>4</sub> folding of S <sub>3s</sub> -parallel veins			█
Early brecciation phase with equant siltstone fragments and no S <sub>3s</sub>	? █ ?		
Late brecciation phase with elongate siltstone fragments fractured parallel to S <sub>3s</sub>		█	
D <sub>4</sub> crenulation of breccia and host-rock			█
Quartz microstructure with coarse grains and recrystallized new grains and sub-grains along boundaries.	? █ ?		
Quartz microstructure with fine grains and sub-grains elongated parallel to S <sub>4</sub>			█ ?
Syn-D <sub>3</sub> chlorite and quartz-biotite-chlorite aggregates		█	
Coarse secondary (breccia) biotite possibly overprinting syn-D <sub>3</sub> metamorphic biotite porphyroblasts		? █ ?	
Syn-D <sub>3</sub> coarse pyramidal arsenopyrite deflecting S <sub>3s</sub>		█	
Fine needle-shaped arsenopyrite in veinlets that cross-cut S <sub>3s</sub>			█
D <sub>4</sub> folding of pyrite veinlets			█

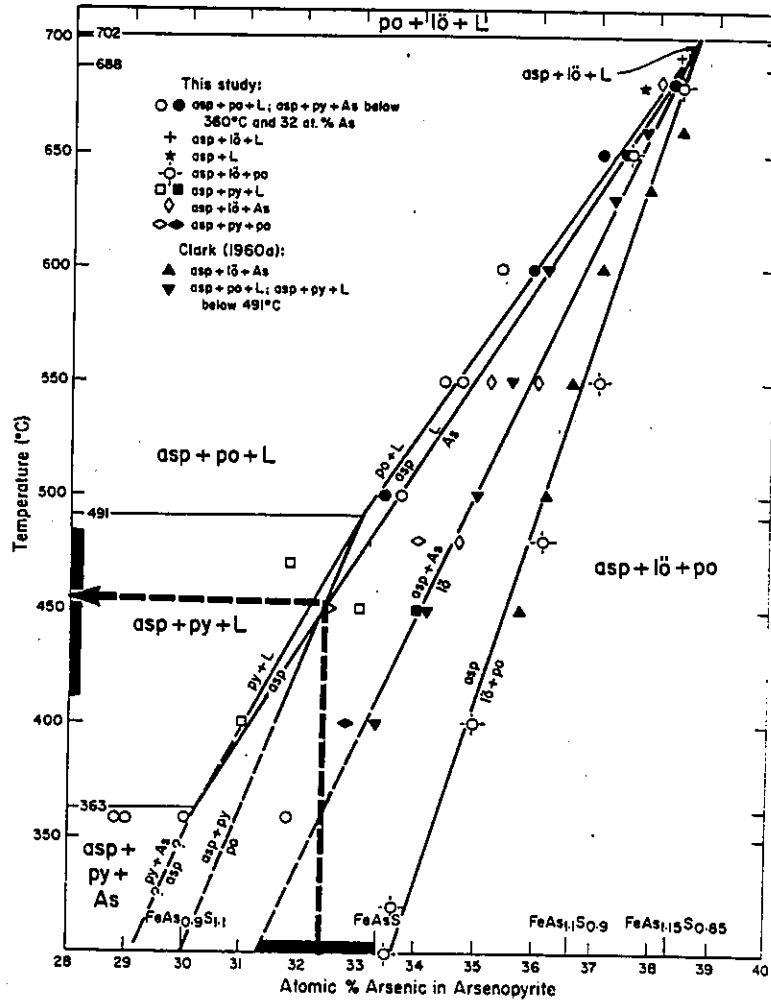
arsenopyrite and multi-mineralic aggregates within host siltstones (Table 7.1).

The exact time of gold emplacement within the quartz-breccias is unclear. It is likely that some gold was introduced into the breccia zone at some stage of  $D_3$ , as evident from the association between gold and the coarse arsenopyrite (Section 6.4). However, gold is also found associated with ( $D_4$ ?) recrystallised zones of grey quartz and along secondary healed microfractures, indicating either a later stage of gold introduction, or remobilization of earlier gold.

#### 7.6 ARSENOPYRITE GEOTHERMOMETRY

Forty-two arsenopyrite compositions were collected from five siltstone wallrock and quartz-breccia samples from the Kidney Pond Zone 1 (Tables A7.2-A7.4). Pyrite and pyrrhotite were found in all samples (indicating the apparent equilibrium between arsenopyrite, pyrrhotite and pyrite), as well as minor sphalerite and chalcopyrite. The needle-shaped arsenopyrite gave a range of 31.87-33.48 At.% arsenic, with a mean of 32.71 At.% arsenic. On the other hand, the coarse pyramidal arsenopyrite gave a wider (and slightly lower) range of 29.74-32.48 At.% arsenic, with a mean of 31.37 At.% arsenic (Figure A9.10). It is unclear from this pilot study whether the difference in mean At.% arsenic between the fine and coarse arsenopyrite is significant. From both sets of data a combined mean of 32.37 At.% arsenic was obtained, and used to determine the temperature of formation of the arsenopyrite from pseudosecondary temperature versus At.% arsenic plot (Figure 7.14; Kretschmar and Scott, 1976). A temperature of  $455 \pm 40$  °C was estimated using the arsenopyrite-pyrite-pyrrhotite assemblage line (which has an additional error of  $\pm 0.4$  to  $\pm 0.5$  At.% or  $\pm 25$  °C; Kretschmar, 1973). A root

Figure 7.14 Pseudosecondary T-X plot of Kreschmar and Scott (1976) displaying arsenopyrite compositions as atomic percent arsenic versus temperature. (Solid bars indicate range and uncertainty of estimate.)



mean square addition was used to calculate the analytical and theoretical errors.

#### 7.7 SUMMARY

The Kidney Pond quartz-breccia Zone 1 is strata-bound and hosted within medium- to thin-bedded black siltstone sequences, with rare interbedded graywackes. The sub-surface morphology of Zone 1 indicates that the quartz-breccias, confined to two black siltstone sequences, occurred as an interconnected, three dimensional array of sub-parallel lenses, with 'step overs', from one black siltstone sequence to the other.

The quartz-breccia event probably started during D<sub>3</sub> with the development of disseminated coarse arsenopyrite and multi-mineralic aggregates within the siltstone host, possibly the result of a pre-fracturing alteration/thermal event. Early microfracturing and brecciation was associated with precipitation of K-feldspar. In the latter stages of D<sub>3</sub> and early-D<sub>4</sub> a pervasive phase of grey quartz-brecciation occurred with fracturing sub-parallel to S<sub>3S</sub> and localized zones of crenulation. Late adularia, epidote and carbonate veinlets cross-cut the breccia zones with only minor deformation by D<sub>4</sub>. Most of the sulphides and gold were probably deposited with the grey quartz, syn-D<sub>3</sub> to early D<sub>4</sub>, as evident from arsenopyrite crystals with D<sub>3</sub> pressure shadows and D<sub>4</sub> folds in pyrite veinlets. Alteration mineralogy around and within the quartz-breccia zones include secondary biotite and chlorite, with some silicification and sericitization of the siltstone wall rock. Coarse- and fine-grained arsenopyrite from wall rock and the quartz-breccia indicate a formation temperature of 455 ± 40 °C for the sulphide assemblages.

## CHAPTER 8

### A FLUID INCLUSION STUDY OF QUARTZ-BRECCIAS AND VEINS OF THE GORDON LAKE REGION

#### 8.1 INTRODUCTION AND PURPOSE

The purpose of this fluid inclusion study was to: i) provide some constraints on the physico-chemical conditions of gold deposition and quartz-breccia formation at Gordon Lake; ii) determine the types of fluid inclusions present and their relative compositions; and iii) assist in the development of a model for the evolution, transport, and trapping of gold mineralizing fluids within the Gordon Lake refold.

A further aim of this study was to investigate the relationship between carbon compounds and gold within the quartz-breccias. This relationship is evident from: i) the field mapping of strata-bound quartz-breccia zones that are consistently hosted within black carbon-rich siltstone sequences (Chapters 6 and 7); ii) the geochemical analysis of siltstone beds proximal and adjacent to the quartz-breccia zones (Chapter 9); and iii) the dark grey colour of quartz within the breccias (Chapter 7). All these factors suggest that carbon and gold are linked genetically, and that C-H volatiles might be preserved within the fluid inclusions of these quartz-breccias.

During this study the types, compositions, and homogenization temperatures of fluid inclusions within a granite-hosted quartz vein were also examined. These data might provide some insight as to whether granite-related fluids played a role in the formation of metaturbidite-hosted quartz veins and breccias.

Good summaries of fluid inclusion theory, techniques, and applications are provided by Hollister and Crawford (1981), Roedder (1984), and Shepherd et al. (1985). Most



of the fluid inclusion methodology and nomenclature (Table A8.1) used in this study are taken from Roedder (1984).

## 8.2 PREVIOUS FLUID INCLUSION STUDIES OF SIMILAR GOLD-QUARTZ VEIN SYSTEMS WITH PARTICULAR REFERENCE TO THOSE OF THE YELLOWKNIFE BASIN

Fluid inclusion studies have played a significant role in the investigation of fluid systems within many types of gold deposits and in particular AVHLGD (e.g., Guha et al., 1983; Smith et al., 1984; Wood et al., 1986; Phillips and Groves, 1987; Ho, 1987; Robert and Kelly, 1987; Walsh et al., 1988). Summaries of fluid inclusion data on AVHLGD (Colvine et al., 1984; Roberts, 1987) indicate that: i) fluid inclusion homogenization temperatures (Th) range from 200-400°C; ii) fluid salinities are low (>2 to <4 wt % NaCl equivalent); and iii) fluid inclusions are H<sub>2</sub>O/CO<sub>2</sub>-bearing.

Fluid inclusion studies within MHGD are predominantly confined to Phanerozoic metasedimentary terranes. These studies include: i) the Cambrian-Ordovician Meguma gold deposits of Nova Scotia (e.g., Kontak et al. 1988; Kontak and Smith 1989); ii) the Carboniferous-Jurassic gold lodes from the Otago schist, New Zealand (e.g., Paterson, 1986; McKeag and Craw, 1989; McKeag et al., 1989); iii) the auriferous vein systems in the Ordovician graywackes at Clontibret, Ireland (Steed and Morris, 1986); iv) auriferous veins hosted in the Cambrian metasediments of the Dolgellau Gold Belt, North Wales (Bottrell et al., 1988); and v) the lode-gold mineralization in the Cretaceous Valdez Group of Alaska (e.g., Reid and Meinert, 1986; Goldfarb et al. 1986, 1989).

Fluid inclusions within MHGD, as compared to AVHLGD, are commonly small (<20µm, Roedder, 1984) and have a greater range in homogenization temperatures (90-380°C) and fluid salinities (2-19 wt % NaCl, Table 8.1). Volatiles

Table 8.1 Typical fluid inclusion data from other meta-turbidite-hosted gold deposits.

Gold District	Ht °C	Salinity wt % NaCl	Volatiles (mole %)	Author
Meguma Terrane, Nova Scotia.	230-380	<4 - 6 (m)	85% H <sub>2</sub> O, 14-15% CO <sub>2</sub> 1-2% CH <sub>4</sub>	Kontak et al. (1988)
Dolgellau Belt, North Wales	140-324	0 - 19 (r)	H <sub>2</sub> O, CO <sub>2</sub> , N <sub>2</sub> , CH <sub>4</sub> .	Bottrell et al. (1988)
Dolaucothi Gold Mines, South Wales	110-390	3 - 18 (r)	H <sub>2</sub> O, CO <sub>2</sub> ?	Annels & Roberts (1989)
Otago Schist, New Zealand	238-278	1 - 10 (r) 6 - 7 (m)	H <sub>2</sub> O, CO <sub>2</sub>	Paterson (1986)
Seward Penin- sula, Alaska	90-390	3 - 7 (m)	H <sub>2</sub> O, CO <sub>2</sub> CH <sub>4</sub>	Goldfarb et al. (1986)
Clontibret, Ireland	240-300	2 - 4 (m)	H <sub>2</sub> O, CO <sub>2</sub>	Steed et al. (1986)

(r - range; m - median)

are common to both deposit types, but  $\text{CH}_4$  and  $\text{N}_2$  are more abundant within MHGD; especially when they are hosted in carbon-rich metasediments (Bottrell et al. 1988).

Secondary inclusions are abundant in both MHGD and AVHLGD, the result of their syn-tectonic mode of quartz-vein emplacement. In many cases repeated sub-grain development and recrystallization have removed primary inclusions, leaving secondary inclusions around new grain boundaries (Kerrich 1976; Wilkins and Barkas, 1978) and along healed microfractures. However, these secondary inclusions may still be associated with gold-bearing fluids, as gold is commonly late in many vein systems (Roedder, 1984; Robert and Kelly, 1987). In addition, the secondary inclusions may provide details about the fluid conditions during metamorphism, whereby the earliest sets of secondary inclusions are related to peak metamorphism and successive later sets are related to retrograde events (Crawford and Hollister, 1986).

Fluid inclusion studies of gold-quartz vein occurrences within the Archean Slave Province include those on quartz veins within shear zones of the Yellowknife Volcanic Belt (Boyle, 1954; Kerrich, 1979; Relf, 1987; Kerrich and Fyfe, 1987, 1988) and on gold-quartz veins within the metaturbidites of the Yellowknife Basin (Ramsay, 1973; English, 1981; Swatton, 1987).

Boyle (1954) used decrepitation temperatures in an attempt to map the source and transport direction of gold-bearing fluids within the Giant-Campbell and Negus-Rycon shear zones. In this experiment he was not totally successful, but he did find that gold occurred preferentially in "microcrystalline" (recrystallized) quartz and was associated with secondary inclusion microfractures. Kerrich (1979) and Kerrich and Fyfe (1987, 1988), reported  $T_h$  of 340-360°C, salinities of <2 wt % (NaCl equivalent), and ubiquitous  $\text{CO}_2$  for primary

inclusions from quartz veins within the Con Mine. They also observed halite daughter minerals in aqueous inclusions of late-stage barren veins. These, they suggested, were the result of either: i) an incursion of hypersaline formational brines into fracture systems, or ii) immiscibility of the vein-forming fluid in which the solutes preferentially partitioned into an aqueous phase, leaving a vapour phase of low salinity. Relf (1987), as part of an alteration study of felsic volcanic-hosted shear zones, south of Yellowknife, found that quartz was dominated by secondary fluid inclusions along healed microfractures. From these inclusions she obtained salinities of approximately 20-30 wt % NaCl equivalent, a range in Th of 100-200°C, and low eutectic temperatures (Te) of -50 to -60 °C (indicating the presence of CaCl<sub>2</sub> and/or MgCl<sub>2</sub> in addition to NaCl). She suggested that this saline fluid was in part meteoric, entering the shear zones during the waning stages of regional greenschist metamorphism.

Ramsay (1973), in addition to his metamorphic study on the metaturbidites of the Burwash Formation, completed a comprehensive petrographic classification of inclusion types (Table 8.2) and a Th study of 40 quartz vein samples (20 mineralized and 20 unmineralized) from a region between Yellowknife Bay and Prosperous Lake. From 204 inclusions he obtained Th of 115-165°C for secondary inclusions and 210-270°C (with a maximum of 335°C) for primary inclusions. From the presence of halite he inferred that the secondary inclusions were probably more saline (approximately 30 wt % NaCl equivalent) than the primary inclusions. He recognized little difference in fluid inclusion types, Th, CO<sub>2</sub> content, and salinity between the mineralized or unmineralized veins. However, he did notice that fluid inclusions from the gold mineralized veins were generally smaller and vapour dominated.

**Table 8.2** Previously recognized fluid inclusion types within quartz veins hosted in metaturbidites of the Yellowknife Basin.

---

Types of fluid inclusions recognised by Ramsay (1973):

- i) liquid-rich, two-phase (15-25% vapour) primary and secondary inclusions
- ii) liquid-rich, three-phase (with halite/sylvite daughter minerals), secondary inclusions
- iii) two-phase, vapour-rich primary inclusions
- iv) vapour-filled primary and secondary inclusions
- vi) CO<sub>2</sub>-bearing primary and secondary inclusions
- v) liquid-filled secondary inclusions

Types of fluid inclusions recognized by English (1981):

- 1) liquid-rich (5-15% vapour) two phase secondary inclusions ( $\pm$  a small halite daughter mineral)
  - 2) liquid-rich (10-30% vapour) three phase H<sub>2</sub>O-CO<sub>2</sub> ( $\pm$ CH<sub>4</sub>) primary inclusions
  - 3) liquid-dominated multiphase secondary inclusions ( $\pm$  halite, sylvite and calcite)
  - 4) vapour-rich primary and secondary inclusions dominated by CO<sub>2</sub> ( $\pm$ CH<sub>4</sub>)
  - 5) CO<sub>2</sub>-bearing negative primary inclusions
-

English (1981) completed a fluid inclusion and oxygen isotope study on nine gold occurrences within the Yellowknife Basin. Using 60 samples he took 200 freezing and 500 heating measurements, and concluded that two fluids were present: a primary fluid of low salinity (5 wt % NaCl equivalent) with Th of 200-330°C, and a secondary fluid of higher salinity (10-30 wt % NaCl equivalent) and lower Th of 100-220°C. He confirmed the presence of CO<sub>2</sub> by the use of a microscopic crushing stage, but was unable to observe any clathrate formation during freezing. He suggested that gold was deposited during the introduction of the primary fluid and was possibly remobilized by the later secondary fluid.

From eight veins in the Bullmoose mine, Swatton (1987) indicated that approximately 80% of the fluid inclusions were secondary, two-phase, and liquid-dominated, and that rarer primary inclusions were vapour-dominated and occasionally contained CO<sub>2</sub>. From 60 heating measurements he indicated a primary low salinity fluid (3 wt % NaCl equivalent) with an average Th of 280°C, and secondary saline fluid (8-10 wt % NaCl equivalent) with an average Th of 200°C. Again, like English (1981) he noted the apparent lack of visible CO<sub>2</sub>, but suggested that CO<sub>2</sub> and CH<sub>4</sub> were dissolved in the aqueous phase and thus recorded a higher apparent salinity. He speculated that the primary and secondary fluids were the result of either "a single metamorphic fluid of constant composition which interacted with a Ca, Na and Cl rich source at lower temperatures" or "several metamorphic fluids of similar compositions which cooled at different rates".

In summary, the three fluid inclusion studies within metaturbidite-hosted quartz vein occurrences of the Yellowknife Basin recorded similar inclusion types and comparable Th data. However, with respect to these studies, the writer is particularly concerned with: i) the

criteria by which primary inclusions were distinguished from secondary inclusions (and thus the possible recognition of two separate fluids); ii) the lack of attention given to the structural time of vein emplacement and its effect on inclusion morphology and microstructure; iii) the statistical validity of the Th data collected by Swatton (1987) and English (1981) - i.e., an average of 4-6 measurements per sample); and iv) the absence of freezing and salinity data from Ramsay (1973) and Swatton (1987).

### 8.3 APPROACH

For this study twenty-five quartz vein and breccia samples were prepared as doubly-polished thin sections of approximately 50-60 $\mu$ m thickness. After petrographic examination twelve samples, with significant fluid inclusion populations, were selected for thermometric and direct volatile analysis; including six quartz-breccias, five metaturbidite-hosted veins, and one granite-hosted vein from the Spud Lake pluton (Table 8.3). The five metaturbidite-hosted veins were emplaced syn-D1 to syn-D4, whereas the granite-hosted vein was emplaced at least post-D3 (the age of the Spud Lake pluton, Chapter 4).

For each sample, thermometric measurements were obtained using a USGS-type, gas-flow heating/freezing stage (from Fluid Inc., Denver, Colorado) in the Fluid Inclusion Laboratory at Dalhousie University. Approximately 40-50 heating/freezing measurements were taken from the two samples with the most abundant inclusions (86-63 and 22/6/10). For the other ten samples, with smaller and less abundant inclusions, 5-20 measurements were taken from each to verify heating and freezing data. Finally, small chips from the twelve samples were cleaned and sent to the Fluid Inclusion Laboratory at University of Toronto for volatile analysis by a heated crushing stage and gas chromatography technique (Sections 8.6 and A8.1).

Table 8.3 Quartz vein and quartz-breccia from the Gordon Lake region selected for thermometric analysis.

Sample number	Sample location	Host rock	Gold (ppb)
22/6/10	Granite-hosted vein (Spud Lake)	-	NA
87-13	Boudinaged vein (Zenith Island)	S	<2
87-124	Syn-D <sub>4</sub> vein (Knight Bay)	S	4
87-130	Bedding-parallel vein (Knight Bay)	S	210
86-88	Pre-D <sub>3</sub> vein (near Kidney Pond)	W	<5
86-124	Pre-D <sub>3</sub> vein (near Kidney Pond)	W	NA
86-59	Breccia from Kidney Pond Zone 1	BS	87
86-63	Breccia from Kidney Pond Zone 1	BS	222
86-76	Breccia from Kidney Pond Zone 1	BS	267
86-77	Breccia from Kidney Pond Zone 1	BS	7
86-168	Breccia from Lynx Inlet area	W	542
86-189	Breccia from Kidney Pond Zone 1	BS	VG

Host rock types: S - grey siltstone,; BS - black siltstone; W - graywacke.

Gold analysis: NA - not available; VG - visible gold.



#### 8.4 FLUID INCLUSION PETROGRAPHY

Careful petrography was completed on the twelve samples (Tables A8.2 and A8.3) to determine: a) the quartz microstructure (i.e., variations in quartz grain size and the degree of recrystallization); b) the inclusion morphology (i.e., whether distributed in isolated arrays, healed microfractures or along grain boundaries); and c) the inclusion types (their phase ratios and relative abundance).

##### 8.4.1 Quartz Microstructure and Inclusion Morphology

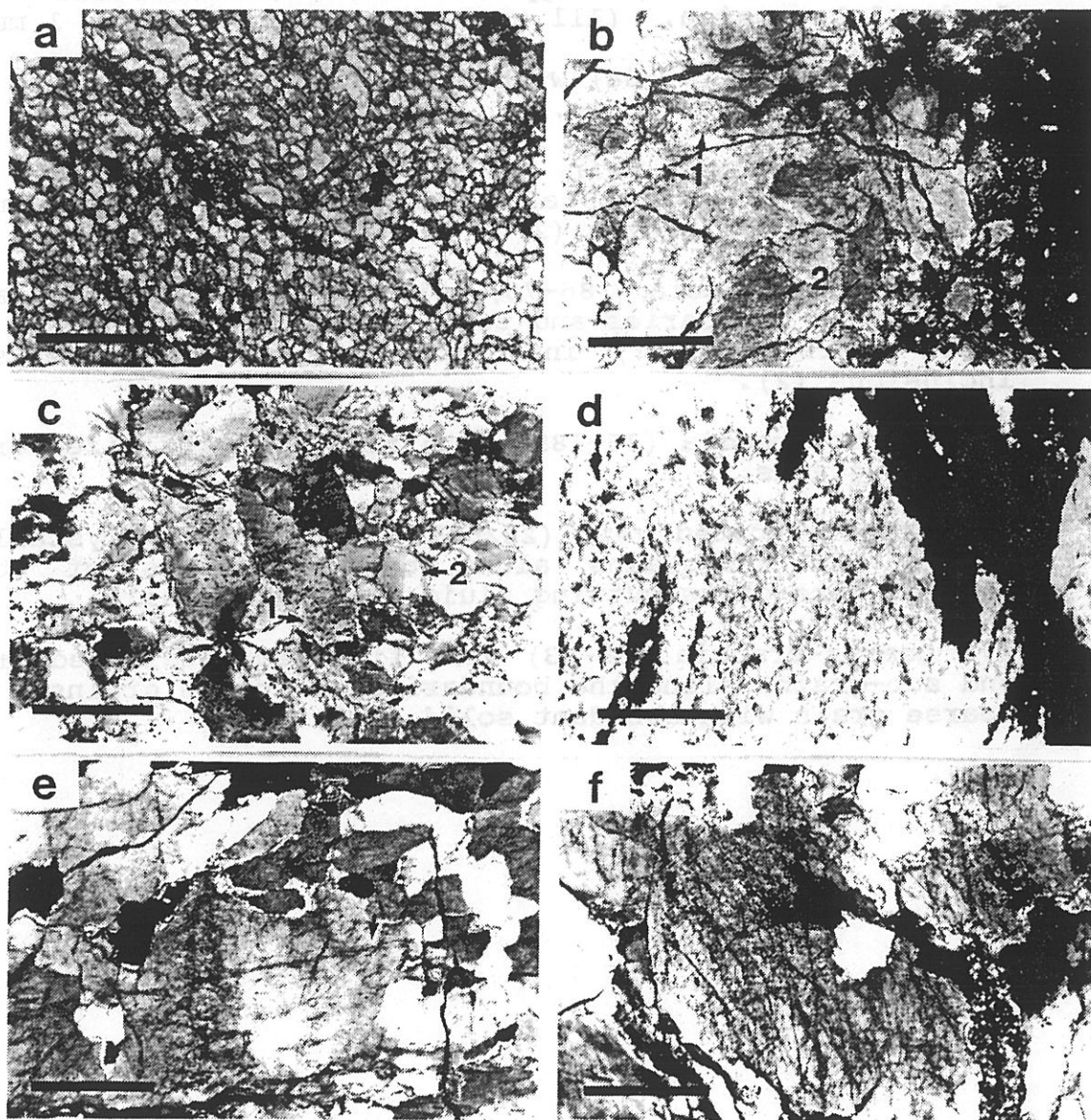
All twelve samples indicated varying degrees of recrystallization (Tables A8.2 and A8.3, Chapter 6). The early D3-deformed and bedding-parallel veins (86-88, 86-124 and 87-130) have an equant, sub-polygonal, fine-grained microstructure (Figure 8.1a), suggesting static recrystallization and recovery (i.e., annealing, Section 6.3.2). The east limb vein (87-13) is composed of 60-70% fine sub-grains and recrystallized grains (10-20 $\mu$ m) surrounding relicts of older coarse (0.25-0.5 mm) grains (Figure 8.1b). Four of the quartz-breccia samples (86-63, 86-76, 86-59 and 86-77) were characterised by coarse (0.25-2.0 mm) grains surrounded by fine (20-50  $\mu$ m) grains and sub-grains (e.g., Figures 8.1f and 8.1c). Two of the quartz-breccia samples (86-168 and 86-189) display intense recrystallization (e.g., Figure 8.1d) with fine grains and sub-grains (50-300 $\mu$ m), some with a preferred elongation sub-parallel to  $S_4$ . The  $S_4$ -parallel vein (87-124) has a microstructure similar to the quartz-breccias. The structurally late granite-hosted vein (22-6-10) is the least deformed. It has coarse (2-3 mm) grains, minor undulatory extinction, and some fine (20-50  $\mu$ m) grains and sub-grains concentrated along the boundaries of the coarse grains (Figure 8.1e).

All inclusions in the twelve samples appear secondary in origin based on the criteria of Roedder (1984, p.43-45)

Figure 8.1 Photomicrographs of quartz microstructure and fluid inclusion morphology from veins and breccias of the Gordon Lake region. (All scale bars approximately 1 mm.)

- a) Pre-D<sub>3</sub> vein (86-88) with fine-grained, equant, and sub-polygonal microstructure.
- b) East Limb vein (87-13) with zones of fine recrystallized grains and sub-grains (1), surrounding coarse (relict?) grains (2).
- c) Quartz-breccia (86-76) with fine recrystallization along grain boundaries and two types of quartz grains; with solid (carbonaceous?) inclusions (1), and without solid inclusions (2).
- d) Quartz-breccia (86-189) with fine recrystallized grains and sub-grains.
- e) Granite-hosted vein (22/6/10) with fine recrystallized grains and sub-grains along the boundaries of coarse grains. Note cross-cutting fluid inclusion trails.
- f) Quartz-breccia (86-63) with fine recrystallized grains and sub-grains along the boundaries of coarse grains. Note coarse grain with abundant solid inclusions.

Figure 8.1



and Bodnar et al. (1985). Most of these secondary fluid inclusions occur along healed microfractures (Figure 8.2a and 8.2d). However, in sample 86-88 a significant secondary inclusion population occurs along the grain boundaries (Figure 8.2b). Sample 87-13 is distinct from the others in that isolated inclusions (most with inconsistent phase ratios) predominate within the coarse relict grains, and few to no healed microfractures are present (Figure 8.2c).

#### 8.4.2 Classification of Fluid Inclusion Types

Seven types of secondary fluid inclusions were recognized based on the differing proportions and characteristics of vapour (V), liquid (L) and solid (S) phases. The abundance of each inclusion type (relative to other inclusions in the same sample) was estimated visually (Table A8.4 and A8.5). The inclusion types recognized at room temperature include the following:

Type I - Two-phase, aqueous inclusions with 5-10% vapour, and a sharp V/L contact (Figure 8.3a). These inclusions are found principally along healed microfractures, but also occur along recrystallized grain boundaries.

Type II - Three-phase inclusions with L-H<sub>2</sub>O, V-H<sub>2</sub>O and V-CO<sub>2</sub> phases. Typically the vapour phases are difficult to distinguish, form a broad dark rim around the V/L contact, and make 10-20% of the inclusion (Figure 8.3b). These inclusions predominantly occur along healed microfractures.

Type III - Two-phase, vapour-dominated inclusions. These inclusions have >50% vapour, commonly occur along secondary healed microfractures, and in some cases are almost indistinguishable from Type VII inclusions.

Figure 8.2 Sketches of fluid inclusion morphology and quartz microstructure. A) Pre-D<sub>3</sub> vein (86-88) with fine sub-polygonal grains, Type V inclusions along grain boundaries, and Type I and II/VII along microfractures cross-cutting grain boundaries. B) East limb vein (87-13) with coarse (relict?) grains surrounded by fine-grained recrystallized zones. Isolated and arrays of Type I and Type II inclusions, but no microfractures. C) Bedding parallel vein (87-130) with fine sub-polygonal quartz grains and Type I inclusions along microfractures that cross-cut grain boundaries. D) Quartz-breccia (86-63) with fine recrystallized grains and sub-grains plus along boundaries of coarse grains. Type I, II, and IV inclusions along intersecting microfractures. (All scale bars  $\approx$  0.25 mm.)

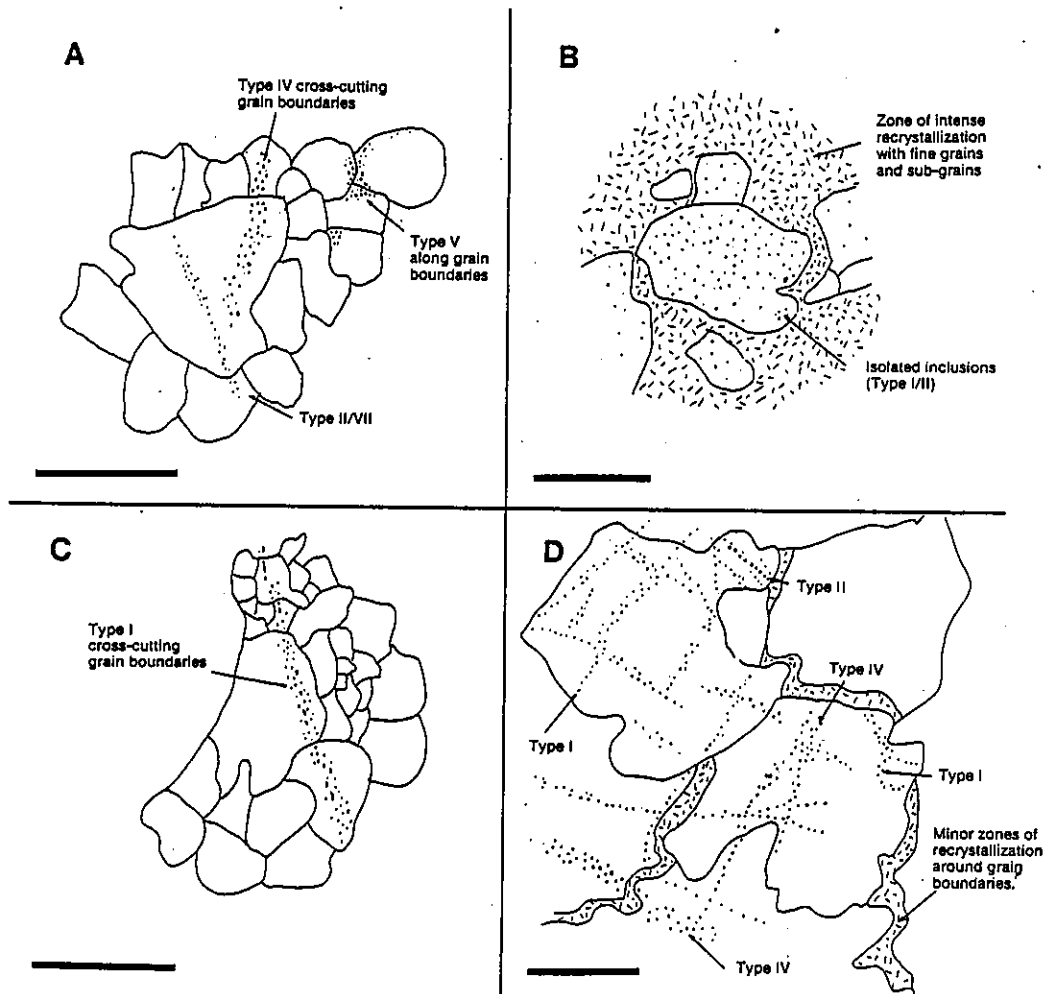
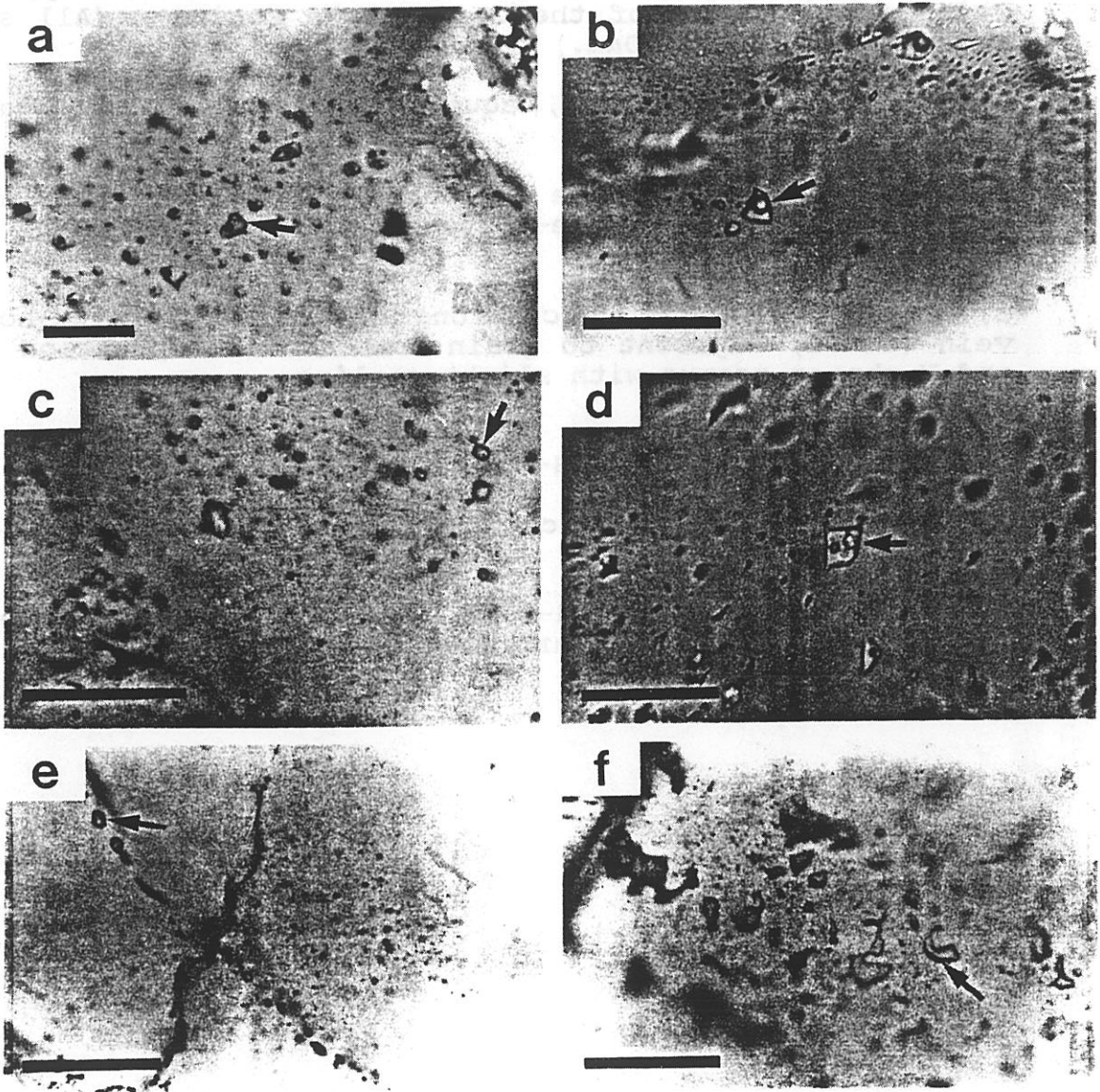


Figure 8.3 Photomicrographs of fluid inclusion types in veins and breccias of the Gordon Lake region. (All scale bars approximately  $50\mu\text{m}$ .)

- a) Type I - Two-phase, aqueous inclusions from quartz-breccia (86-63).
- b) Type II - Three-phase inclusion with L-H<sub>2</sub>O, V-H<sub>2</sub>O and V-CO<sub>2</sub> phases from granite-hosted vein (22/6/10). Note dark vapour bubble rim.
- c) Type V, CO<sub>2</sub>-rich inclusions from metaturbidite-hosted vein (86-88) adjacent to grain boundaries. Separation of L and V phases occurs with slight cooling.
- d) Type IV - Three (or multi-) phase, aqueous inclusions including L-H<sub>2</sub>O, V-H<sub>2</sub>O, S-NaCl and possible S-KCl.
- e) Type VII, vapour-rich inclusions along healed microfracture (86-88).
- f) Type VI, liquid-rich inclusions along healed microfracture from metaturbidite-hosted vein (86-88).

Figure 8.3



Type IV - Three- (or multi-) phase, aqueous inclusions including L-H<sub>2</sub>O, V-H<sub>2</sub>O, S-NaCl, and possible S-KCl phases (Figure 8.3d). These inclusions only occur along healed microfractures, and have solid daughter phases that are mainly cubic (halite).

Type V - Single-phase, CO<sub>2</sub>-rich inclusions. These rare inclusions are small, and are principally found along the boundaries of recrystallized grains (eg., 86-88, Figure 8.3c). They are detected by the separation of L-CO<sub>2</sub> and V-CO<sub>2</sub> phases on cooling.

Type VI - Liquid-rich, aqueous inclusions. These inclusions are commonly found along numerous secondary planes, exhibiting necked and irregular forms (Figure 8.3f).

Type VII - Vapour-rich, aqueous inclusions. These inclusions commonly occur along healed microfractures (Figure 8.3e)

Fluid inclusion Types I and IV are the most abundant, are found in almost every sample along healed microfractures, and are readily available for thermometric analysis. No petrographic evidence was found for H<sub>2</sub>O-CO<sub>2</sub> immiscibility (e.g., Types I, II and V occurring along the same healed microfracture; Crawford and Hollister, 1986) or for cross-cutting relationships between types of fluid inclusion microfractures. No significant differences in inclusion morphology or types were recognized between the six quartz-breccia and five metaturbidite-hosted quartz vein samples. However, fluid and solid inclusions were generally more abundant in the quartz-breccias, whereas numerous fluid inclusions were also found in the granite-hosted vein.



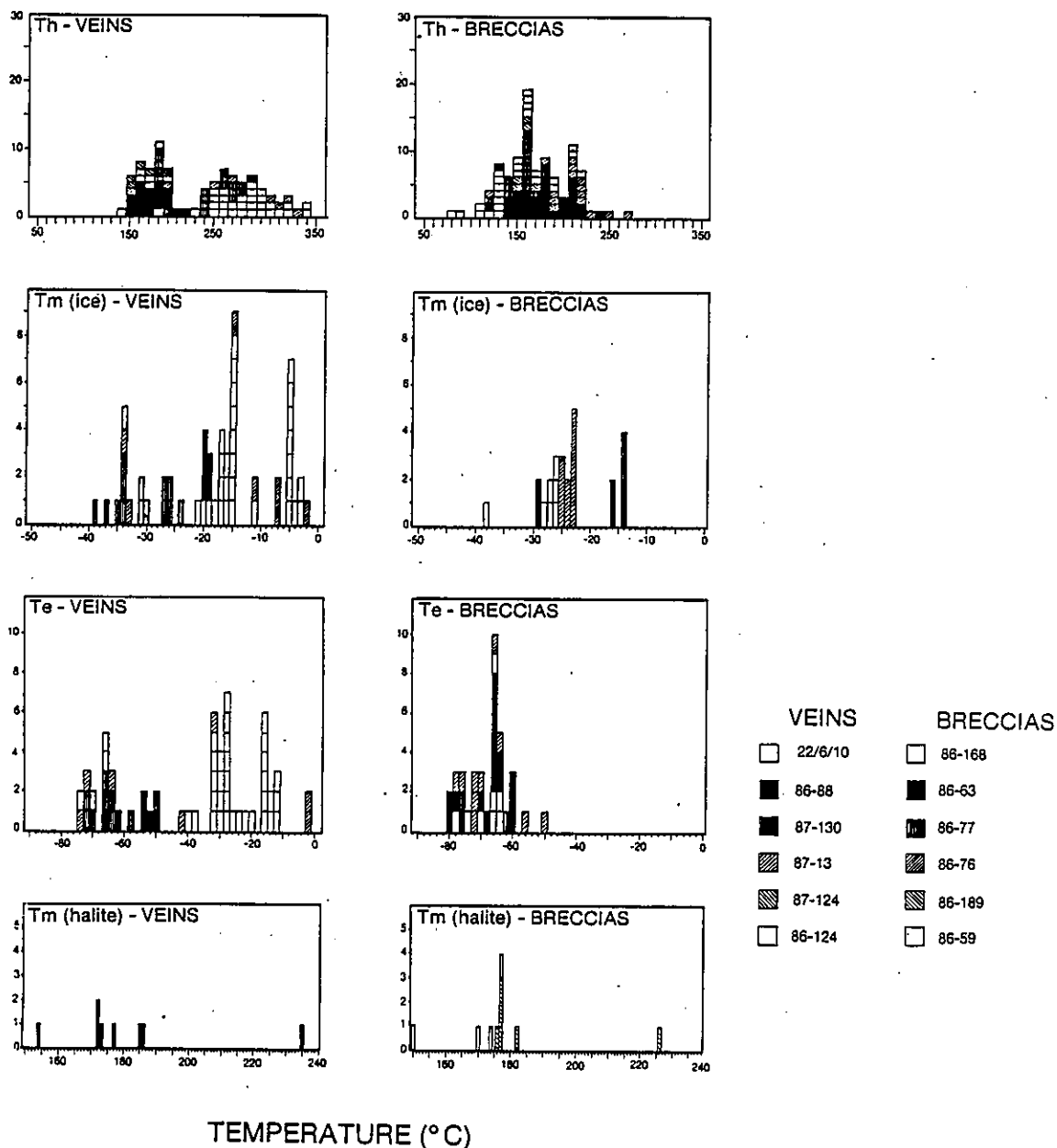
## 8.5 THERMOMETRIC ANALYSIS AND RESULTS

Thermometric analysis of fluid inclusions is a non-destructive technique for measuring temperatures of homogenization and estimating fluid compositions. The heating/freezing stage used was calibrated to  $\pm 0.1^\circ\text{C}$  using  $-56.6^\circ\text{C}$ ,  $0^\circ\text{C}$ , and  $374^\circ\text{C}$  synthetic standards of pure  $\text{CO}_2$ , pure  $\text{H}_2\text{O}$ , and a  $\text{NaCl-H}_2\text{O}$  mixture, respectively. Heating and freezing rates varied, but were kept at approximately  $1^\circ\text{C}$  per minute for both melting point and homogenization determinations. Measurement of melting temperatures were reproducible to within  $\pm 0.5^\circ\text{C}$  for most inclusions. Homogenization temperatures were reproducible to within  $\pm 0.5^\circ\text{C}$  for large inclusions. However, for smaller inclusions (3-10 $\mu\text{m}$ ) the error was greater, up to  $\pm 3^\circ\text{C}$ . As it was not possible to distinguish between hydrohalite and ice during freezing runs, the type of final melting temperature, either  $T_m(\text{ice})$  or  $T_m(\text{hy-ha})$ , depended on whether halite was absent or present in the inclusion.

Frequency histograms of  $T_h$ ,  $T_e$ ,  $T_m(\text{ice/hy-ha})$ , and temperature of halite dissolution,  $T_m(\text{halite})$ , were constructed (Figure 8.4) from the results of approximately 200 heating and 200 freezing runs on Type I, II, and IV inclusions (Tables A8-6 to A8-9). Homogenization temperatures for the breccia samples range from  $80-270^\circ\text{C}$  with a peak at approximately  $160^\circ\text{C}$ , while  $T_h$  for the metaturbidite-hosted veins range from  $140-330^\circ\text{C}$  with a peak at  $160-180^\circ\text{C}$ . The few temperatures of halite dissolution that were measured ranged from  $148-235^\circ\text{C}$  for the metaturbidite-hosted veins and  $140-226^\circ\text{C}$  for the breccias, with concentrations at  $172-181^\circ\text{C}$  and  $170-182^\circ\text{C}$ , respectively. In all samples temperatures of halite dissolution were greater than vapour-bubble homogenization temperatures.

The freezing characteristics of the vein and breccia samples were hampered by unsuccessful attempts to:

Figure 8.4 Frequency histograms of Th, Tm(ice/hy-ha), Te and Tm(halite) for twelve quartz vein and breccia samples of the Gordon Lake region.



TEMPERATURE (°C)

i) recognize phase changes within some of the smaller inclusions, and ii) freeze many of the inclusions, even at temperatures of  $-150^{\circ}\text{C}$  or lower. Nevertheless, eutectic temperatures ( $T_e$ ) for the breccias ranged from  $-50$  to  $-80^{\circ}\text{C}$  with a peak at  $-66^{\circ}\text{C}$ , and for the metaturbidite-hosted veins ranged from  $-2^{\circ}$  to  $-74^{\circ}\text{C}$  with a peak at  $-66^{\circ}\text{C}$ . Final ice/hydrohalite melting temperatures for the breccias ranged from  $-14^{\circ}$  to  $-38^{\circ}\text{C}$  with a peak at  $-23^{\circ}$  to  $-29^{\circ}\text{C}$ , while for the meta-turbidite-hosted veins they ranged from  $-2$  to  $-39^{\circ}\text{C}$  with peaks at  $-34^{\circ}\text{C}$ , and  $-20^{\circ}\text{C}$ .

Of particular interest are the similar, but varied  $T_h$  ( $154$ - $325^{\circ}\text{C}$ ),  $T_m(\text{ice})$  ( $-33.5^{\circ}\text{C}$  to  $7.4^{\circ}\text{C}$ ), and  $T_e$  ( $-73.4$  to  $-2.2^{\circ}\text{C}$ ) data obtained from isolated inclusions within the East Limb vein (87-13). These data, along with the vein's recrystallized microstructure and deformational history (Chapter 6), suggest that the saline secondary fluid was probably emplaced along microfractures (syn- $D_3$ ), but was later redistributed into isolated inclusions or arrays during  $D_4$ .

The granite-hosted vein gave quite distinct  $T_h$ ,  $T_m(\text{ice})$  and  $T_e$  values compared to the metaturbidite-hosted veins and breccias.  $T_h$  values ranged from  $140$ - $330^{\circ}\text{C}$  with a peak at  $260$ - $290^{\circ}\text{C}$ ,  $T_e$  values ranged from  $-11^{\circ}\text{C}$  to  $-73^{\circ}\text{C}$  with peaks at  $-30^{\circ}\text{C}$  and  $-14^{\circ}\text{C}$ , and  $T_m(\text{ice})$  values ranged from  $-3^{\circ}$  to  $-34^{\circ}\text{C}$  with a peaks at  $15^{\circ}\text{C}$  and  $5^{\circ}\text{C}$ .

In summary, the  $T_h$ ,  $T_e$ , and  $T_m(\text{ice/hy-ha})$  data from the quartz-breccias are similar to those of the five metaturbidite-hosted veins, except that  $T_e$  and  $T_m(\text{ice/hy-ha})$  values for the veins are slightly lower. The  $T_h$ ,  $T_m(\text{ice})$ , and  $T_e$  data of the granite-hosted quartz vein (22/6/10) are distinctly higher than both the quartz-breccias and metaturbidite-hosted veins. Estimation of  $\text{CO}_2$  concentrations within the Type II,  $\text{H}_2\text{O}-\text{CO}_2$  inclusions were hindered by both the absence of clathrate formation during freezing runs, and the lack of well defined phases to

calculate molar volumes (e.g., Burruss, 1981). These factors indicate that CO<sub>2</sub> concentrations are probably <1-4 mole % (C. Bray, 1990, personal communication; D. Kontak, 1990, personal communication).

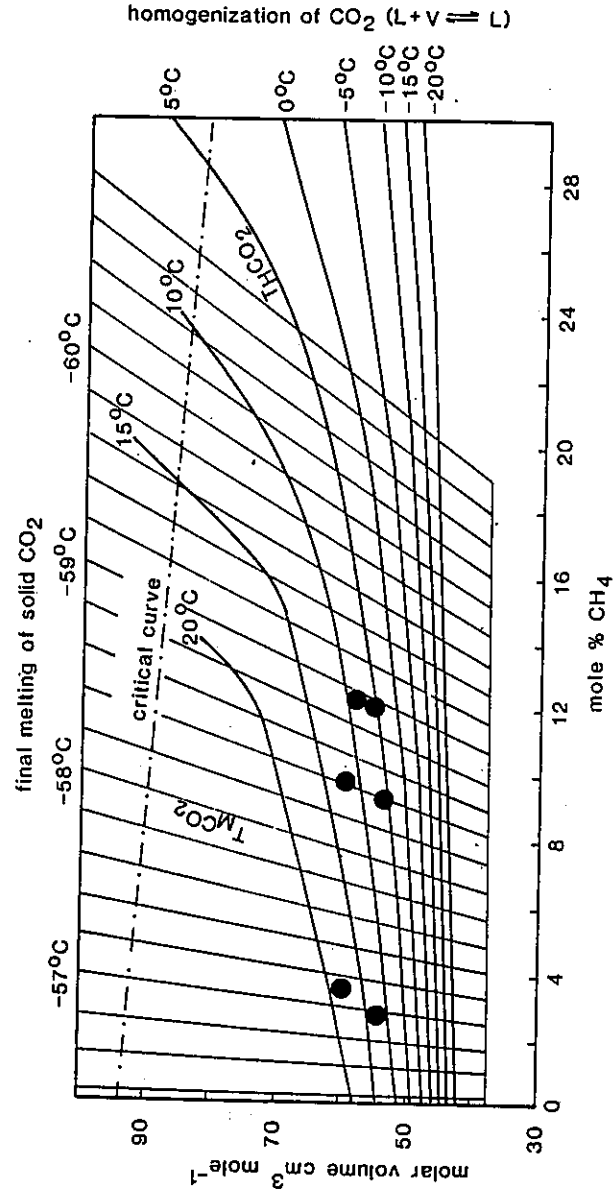
Freezing runs on Type V, CO<sub>2</sub>-rich inclusions (from sample 86-88) displayed a decreased CO<sub>2</sub> triple point (-56.6°C) and a wide temperature interval for the melting of solid CO<sub>2</sub> (Table A8.10), indicating the presence of CH<sub>4</sub>. Data from the final melting temperature of solid CO<sub>2</sub> and homogenization temperature of the CO<sub>2</sub> liquid and vapour phases indicated a concentration of 4-12 mole % CH<sub>4</sub> for these inclusions (Figure 8.5).

#### 8.6 VOLATILE ANALYSIS USING A HEATED CRUSHING STAGE AND GAS CHROMATOGRAPHY TECHNIQUE

Fluid inclusion thermometry is a useful technique for determining fluid compositions and homogenization temperatures. However, it is unable to quantify the more complex volatile species that occur in fluid inclusions such as N<sub>2</sub>, CO, CH<sub>4</sub>, C<sub>2</sub>H<sub>6</sub>, C<sub>3</sub>H<sub>8</sub>, and other C-H compounds. Generally it is preferable to determine the exact composition of individual inclusions or populations within a sample. This can be achieved by using techniques such as laser Raman microprobe spectroscopy (Pasteris et al., 1988). However, the amounts of complex hydrocarbon volatiles sought are probably in the order of ppm and below the detection limits (approximately 1 mole %; E. Spooner, personal communication, 1989) of laser Raman spectroscopy. An alternative technique that is capable of measuring low concentrations of volatiles is to use a heated crushing stage and gas chromatography technique (Section A8.1). This technique produces an aggregate or bulk volatile analysis for all inclusions present in the sample.

From the twelve samples prepared, four of the purest (with the least extraneous material) were analyzed

Figure 8.5 Estimation of mole % of CH<sub>4</sub> from the final melting temperature of CO<sub>2</sub>(S) and homogenization temperature of CO<sub>2</sub>(L) and CO<sub>2</sub>(V) from Heyen et al. (1982). Six measurements taken from the CO<sub>2</sub>-rich inclusions of sample 86-88 (Table A8.10).



(C. Bray, 1989, personal communication). These four samples included two quartz-breccias (86-63 and 86-77), a metaturbidite-hosted vein (87-13) and the granite-hosted vein (22/6/10). From the volatile data (Table 8.4) it is apparent that H<sub>2</sub>O, CO<sub>2</sub> and CH<sub>4</sub> are the major fluid components. The low CO<sub>2</sub> values obtained for the four samples possibly explain the general lack of CO<sub>2</sub>-rich (Type V) and H<sub>2</sub>O-CO<sub>2</sub> (Type II) inclusions (Tables A8.4 and A8.5). High CH<sub>4</sub> concentrations occur in the breccia samples (86-63, 86-76) and the metaturbidite-hosted vein (87-13), and show some correlation with the concentration of other C-H complexes.

#### 8.7 INTERPRETATION OF THERMOMETRIC AND VOLATILE DATA

From this fluid inclusion study it is possible to provide some P/T/X constraints on the trapping conditions of the secondary fluid, quartz-brecciation, and possibly gold mineralization. However, certain assumptions must be taken into consideration, including: i) the time of emplacement of secondary fluid along the healed microfractures; ii) the P/T conditions of metamorphism and brecciation; and iii) the relationship between gold deposition and the secondary fluid.

From petrographic data it is apparent that most of the secondary fluid inclusions occur along healed microfractures. A syn-D<sub>3</sub> time of formation for the microfractures is partly constrained by the fact that only a few secondary microfractures cross cut the fine sub-polygonal quartz grains of the early bedding-parallel and D<sub>3</sub>-deformed veins (e.g., 86-88, 87-130, and 86-124), whereas abundant microfractures occur within the syn-D<sub>3</sub> veins/breccias. An upper time limit for the emplacement of the secondary inclusions along microfractures is provided by the isolated inclusion morphology, varied thermometric data, and D<sub>4</sub>-deformed quartz microstructure of the East

Table 8.4 Crushing-gas chromatography volatile analyzes  
(all data in mole %, unless indicated otherwise).

	86-77	22/6/10	86-63	87-13
N <sub>2</sub>	0.537	0.036	0.073	0.102
O <sub>2</sub>	0.000	0.000	0.000	0.000
Ar	0.000	0.000	0.000	0.000
CO	0.000	0.000	0.000	0.000
CH <sub>4</sub>	1.369	0.211	1.184	5.630
CO <sub>2</sub>	0.142	0.916	1.912	0.500
H <sub>2</sub> O	97.911	98.824	96.744	93.617
C <sub>2</sub> H <sub>4</sub>	7 ppm	2 ppm	3 ppm	7 ppm
C <sub>2</sub> H <sub>6</sub>	0.020	58 ppm	0.042	0.089
C <sub>2</sub> H <sub>2</sub>	1 ppm	1 ppm	992 ppm	1 ppm
COS	25 ppm	14 ppm	15 ppm	36 ppm
C <sub>3</sub> H <sub>6</sub>	27 ppb	4 ppb	7 ppb	15 ppb
C <sub>3</sub> H <sub>8</sub>	0.017	62 ppm	0.043	0.055
C <sub>4</sub> H <sub>8</sub>	0.000	0.000	0.000	0.000
C <sub>4</sub> H <sub>10</sub>	0.000	0.000	0.000	0.000

87-77 - Grey-black quartz from the Kidney Pond Zone 1 quartz-breccia.

22/6/10 - White-grey quartz from vein hosted in Spud Lake granite.

86-63 - Grey quartz from the Kidney Pond Zone 1 quartz-breccia.

87-13 - White-grey quartz from a boudnaged East Limb vein.

Limb veins (e.g., 87-13); indicating a microstructural redistribution of the fluid from microfractures into isolated arrays during D<sub>4</sub>. Thus, the time of emplacement of this secondary fluid is probably syn-D<sub>3</sub> to early D<sub>4</sub> (i.e., syn- to late metamorphic).

The relationship between gold deposition and this secondary fluid is more difficult to determine. Petrography suggests that gold deposition is probably syn-D<sub>3</sub> to early D<sub>4</sub> (Section 7.4 and 7.5), with some gold grains occurring along healed microfractures (Figure 7.11f). Therefore, it is reasonable to conclude that the secondary fluid was probably associated with gold deposition. However, it is unclear as to whether this fluid: i) transported gold to the site of deposition, ii) is a product of the gold mineralizing process, or iii) was involved in the later remobilization of gold.

#### 8.7.1 Estimates of Salinity

The presence of halite daughter minerals and the consistently low eutectic temperatures of all the samples (except 22/6/10) indicate that the dissolved salts are probably dominated by NaCl and CaCl<sub>2</sub> (Crawford, 1981). Eutectic temperatures below -65°C indicate the presence of other salts such as LiCl<sub>2</sub> (Roedder, 1984) or MgCl<sub>2</sub> (Taylor et al. 1983). Four methods were applied to determine the wt % salt (Tables A8.11 and A8.12) and include: i) the calculation of equivalent wt % NaCl from the dissolution of halite equation from Sterner et al. (1987); 2) the calculation of equivalent wt % NaCl from the final ice melting temperature equation of Roedder (p.233, 1984); iii) the estimation of wt % CaCl<sub>2</sub> from the CaCl<sub>2</sub>-H<sub>2</sub>O phase diagram (Crawford, 1981); and iv) the estimation of wt % NaCl-CaCl<sub>2</sub> combined from the ternary NaCl-CaCl<sub>2</sub>-H<sub>2</sub>O plot (Vanko et al. 1988; Williams-Jones, 1990). The ternary plot probably gives the most reasonable salinity data as



both NaCl and CaCl<sub>2</sub> are considered (Figure 8.6). The salinities were calculated for individual inclusions with T<sub>m</sub>(ice/hy-ha) and Th data, and plotted as fields on Th versus salinity diagram (Figure 8.7). From this diagram at least two (and possibly three) distinct secondary fluids are apparent. The breccias and the metaturbidite-hosted veins have overlapping Th-salinity fields; with the veins having a slightly larger field. Both fields indicate a low temperature, but very saline (NaCl-CaCl<sub>2</sub>) fluid. Two higher temperature, less saline, and more NaCl-rich fluid fields are associated with the granite-hosted vein.

#### 8.7.2 Estimates of Fluid Compositions

Petrographic and thermometric data suggest that CO<sub>2</sub> concentrations are low (<1-4 mole %) within the secondary inclusions of the metaturbidite-hosted breccias and veins. This is confirmed by the bulk crushing analyses of 86-76, 86-63 and 87-13. Most of this CO<sub>2</sub> is probably accounted for by the abundance of Type II, H<sub>2</sub>O-CO<sub>2</sub> inclusions in the three samples. However, these three samples display much greater concentrations of CH<sub>4</sub> (up to 5.6 mole) than was expected from the petrography and thermometry. The high CH<sub>4</sub> concentrations and CH<sub>4</sub>/CO<sub>2</sub> ratios (0.6-11.3) of the metaturbidite-hosted vein/breccia samples, might be accounted for by: i) high methane concentrations in the Type II, H<sub>2</sub>O-CO<sub>2</sub> inclusions or Type V, CO<sub>2</sub>-rich inclusions; ii) a previously unrecognized CH<sub>4</sub>-rich inclusion set; or iii) dissolved methane in the aqueous inclusions (Collins, 1979). The granite-hosted vein (22/6/10) has the lowest CH<sub>4</sub>/CO<sub>2</sub> ratio (0.2) of the four samples. In this case the CO<sub>2</sub> and CH<sub>4</sub> are probably accounted for by the abundance of H<sub>2</sub>O-CO<sub>2</sub> (Type II) inclusions.

Figure 8.6 Ternary NaCl-CaCl<sub>2</sub>-H<sub>2</sub>O plots, adapted from Vanko et al. (1989) and Williams-Jones (1990), with approximate salinity compositions (shaded areas) for the six quartz-breccias (A) and five metaturbidite-hosted quartz-veins (B). (Contours in °C)

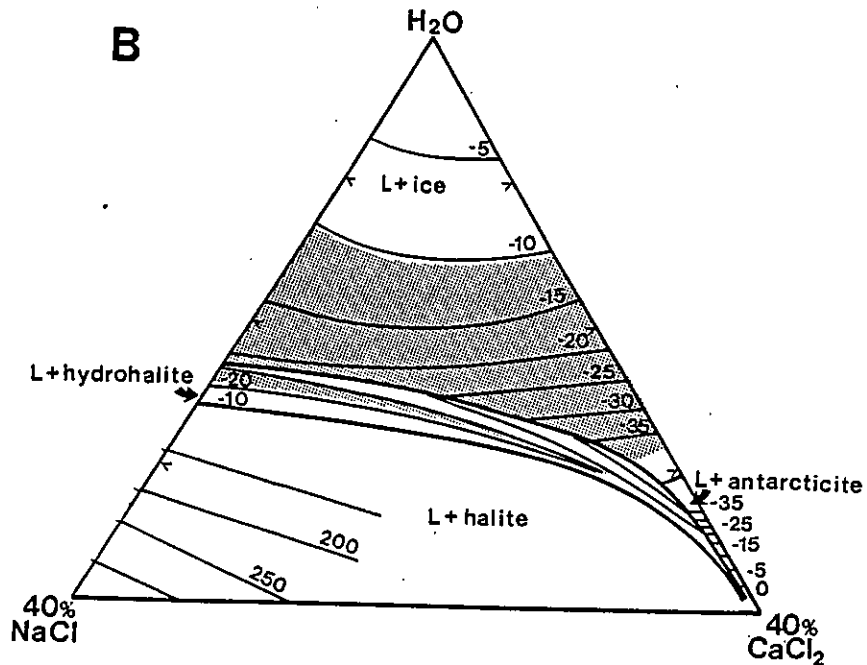
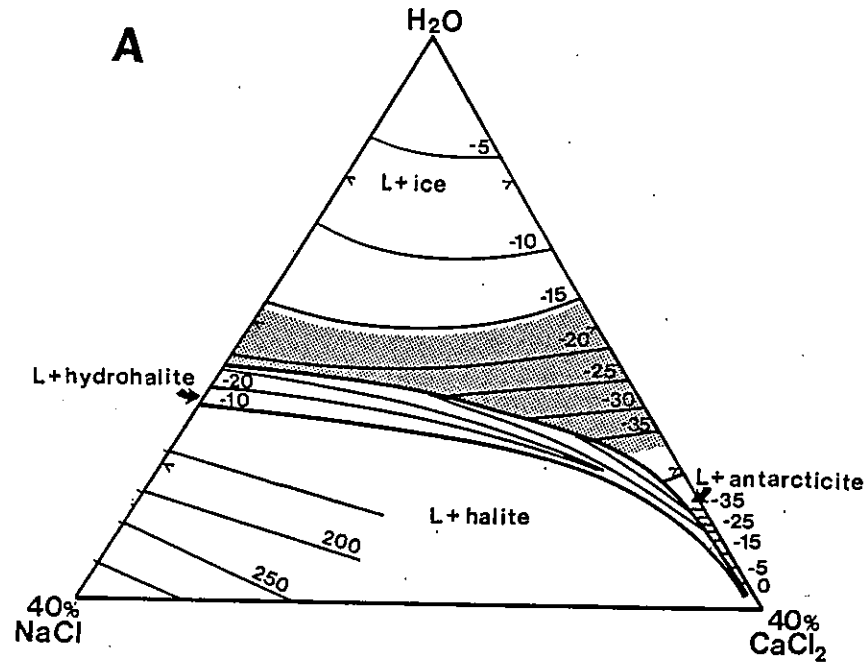
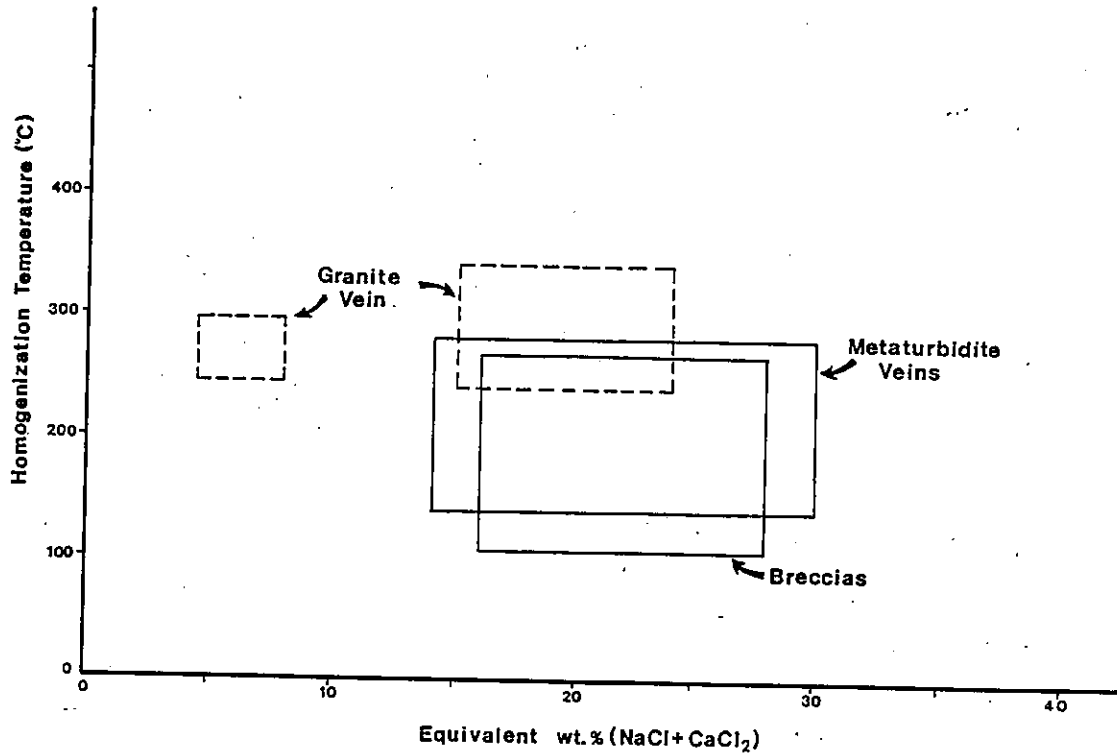


Figure 8.7 Homogenization temperature versus salinity for the six quartz-breccias, the five metaturbidite-hosted quartz veins and the granite-hosted quartz vein of the Gordon Lake region.



### 8.7.3 Estimates of Pressure and Temperature of Trapping

Various methods are used in fluid inclusion studies to estimate the pressure of fluid trapping (Roedder and Bodnar, 1980; Shepherd et al. 1985). In this case, the P/T trapping conditions of the secondary fluid within the quartz-breccia were estimated using an isochore and an independent geothermometer; assuming a  $T_h$  of  $170 \pm 34^\circ\text{C}$  (one sigma standard deviation) and a salinity of 25 wt % NaCl equivalent for the fluid. Arsenopyrite geothermometry indicated a temperature of at least  $455 \pm 40^\circ\text{C}$  for the sulphide assemblages in the quartz-breccia (Section 7.5). With this independent temperature measurement and a NaCl-H<sub>2</sub>O phase diagram for 25 wt % NaCl equivalent (Roedder and Bodnar, 1980) a pressure of entrapment for the secondary fluid of 2.0 to 3.5 kbars was estimated (Figure 8.8). This trapping pressure agrees with the range of pressures suggested by the metamorphic assemblages (Section 5.5.2). In addition, a trapping pressure of 2.0 to 3.5 kbars is within the brittle-ductile regime (a depth of 10-15 km) required for tectonic breccia formation (Sibson, 1990).

## 8.8 EVOLUTION OF A SALINE FLUID IN THE GORDON LAKE REGION AND ITS POSSIBLE ROLE IN GOLD MINERALIZATION

It is apparent from petrographic observations (Section 8.4) that all quartz veins and breccias at Gordon Lake are dominated by secondary aqueous inclusions ( $\pm$  halite) that occur primarily along healed microfractures. In general, these secondary inclusions are more saline and CaCl<sub>2</sub>-rich (Figure 8.9) compared to those found by Ramsay (1973), English (1981), or Swatton (1987). However, they are similar in salinity and composition to secondary inclusions studied by Relf (1987). Therefore, it is reasonable to suggest that a high salinity fluid occurred within all quartz veins and shear zones of the Yellowknife Basin during some stage of metamorphism. However, at

Figure 8.8 The trapping pressure for the secondary fluid and quartz-breccia was estimated using the phase diagram for water assuming a salinity of 25 wt.% NaCl (Roedder and Bodnar, 1980). A mean  $T_h$  of  $170 \pm 34^\circ\text{C}$  was calculated from the quartz-breccia samples and a temperature of entrapment ( $T_t$ ) for the sulphides of  $455 \pm 40^\circ\text{C}$  was obtained from arsenopyrite geothermometry. The trapping pressure estimate ( $P_t$ ) was obtained from where these two fields intersected.

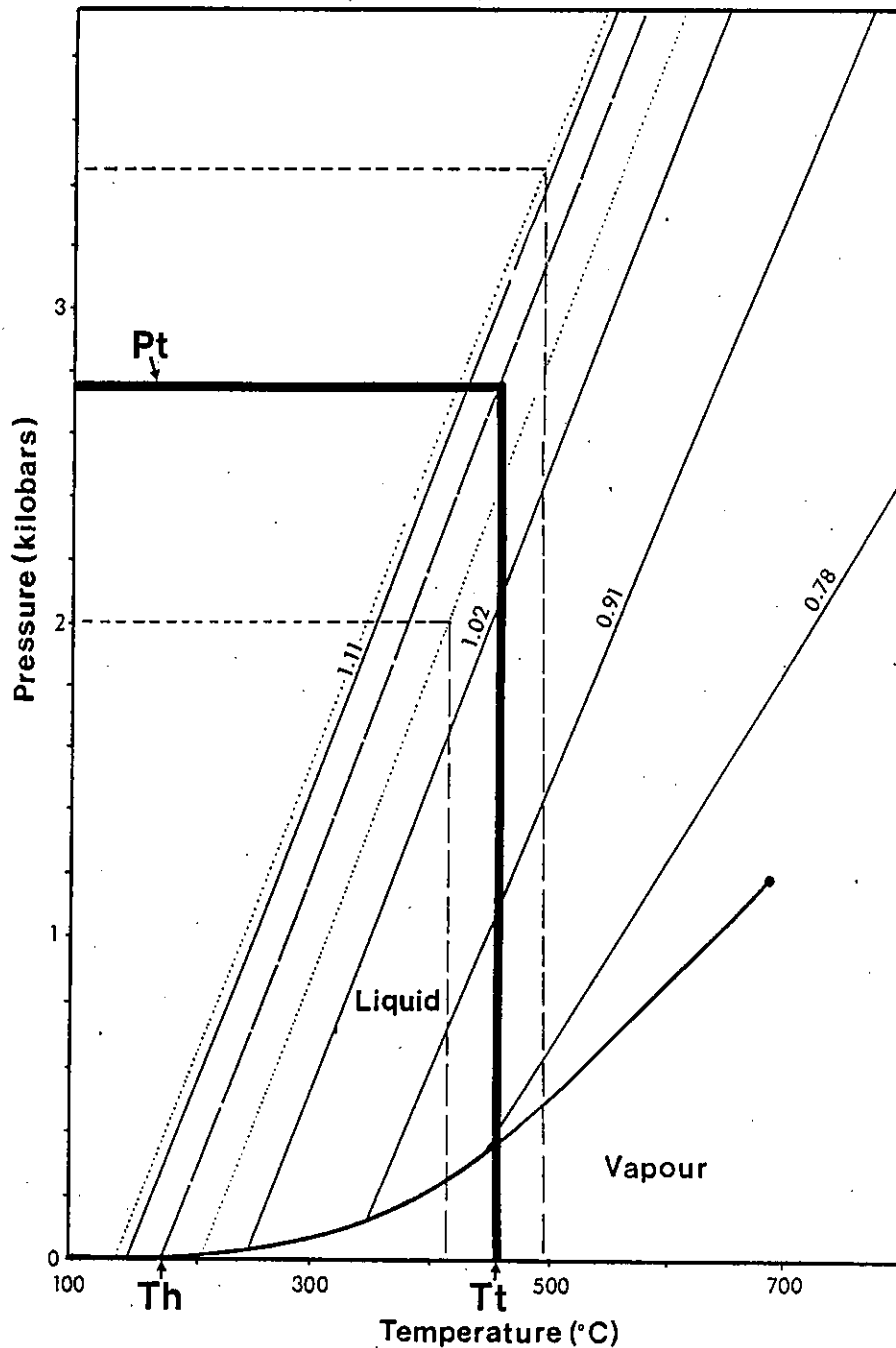
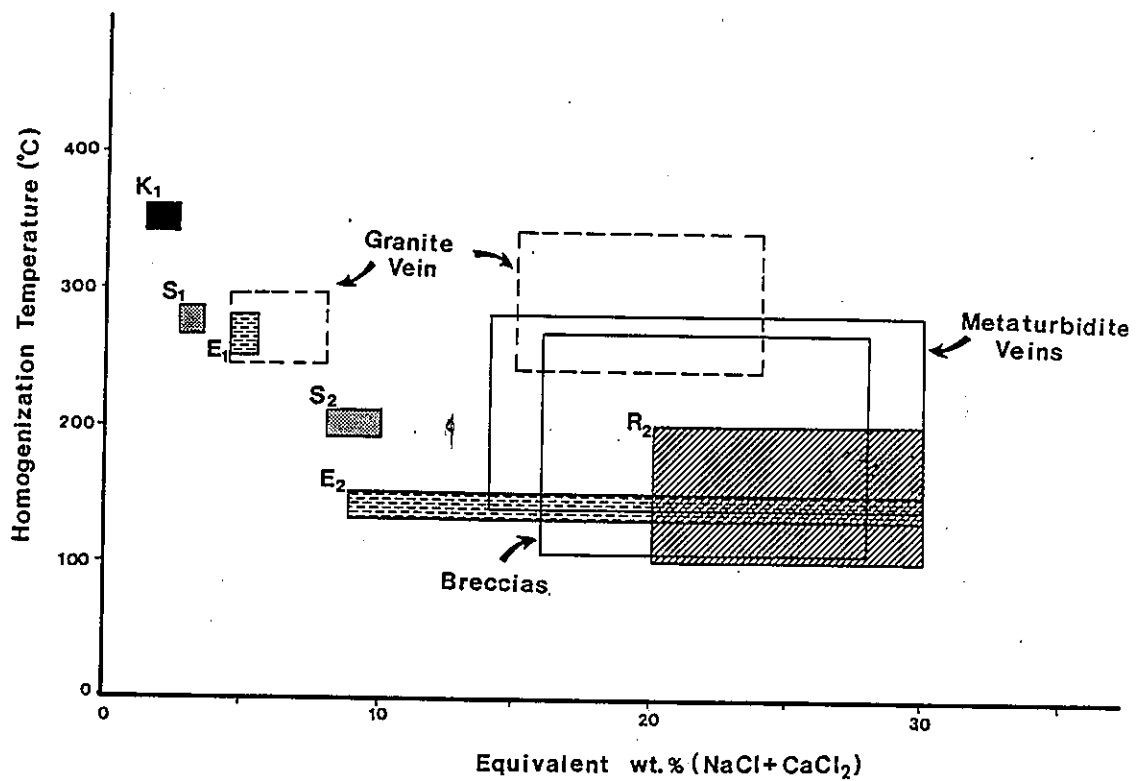


Figure 8.9 Comparison of homogenization temperature and salinity fields of this fluid inclusion study with others of the Yellowknife region.  $K_1$  - primary inclusions of Kerrich and Fyfe (1987);  $S_1$  - primary inclusions of Swatton (1987);  $S_2$  - secondary inclusions of Swatton (1987);  $E_1$  - primary inclusions of English (1980);  $E_2$  - secondary inclusions of English (1980);  $R_2$  - secondary inclusions of Relf (1989).



Gordon Lake it is less clear as to: i) whether the saline fluid is distinct from an earlier vein-forming fluid, ii) why the  $\text{CH}_4$  is enriched compared to  $\text{CO}_2$  within the saline fluid, iii) what is the relationship between the saline fluid and gold mineralization, and iv) what is the origin of the saline fluid?

The lack of primary inclusions and predominance of secondary inclusions along healed microfractures within the quartz of Gordon Lake contrasts with the findings of other fluid inclusion workers (English, 1981; Swatton, 1987; Ramsay, 1973). All these studies found "primary inclusions" based on their isolated character, larger size, and higher Th. However, recent fluid inclusion studies (Bodnar et al. 1985, Crawford and Hollister, 1986) indicate that the isolated character and size of inclusions are not sufficient criteria to define their primary origin. The lack of well defined primary inclusions at Gordon Lake is typical of other syn-tectonically formed vein systems that are dominated by secondary inclusions along healed microfractures (i.e., the Sigma Mine, Robert and Kelly, 1987; the Annapurna Himal region, Nepal, Craw, 1990).

The high  $\text{CH}_4/\text{CO}_2$  ratios (0.6-11.3) found within the inclusion fluids by bulk volatile analysis are difficult to evaluate based on the lack of other comparable studies. Lower  $\text{CH}_4/\text{CO}_2$  ratios (0.09-0.24) were obtained from a bulk volatile analysis of quartz material from the Beaver Dam gold deposit within the Meguma metaturbidite terrane (Kontak et al. 1988; D. Kontak, 1990, personal communication) and the Juneau Gold Belt (Goldfarb et al. 1990). Both studies accounted for the greater amount of  $\text{CO}_2$  by the abundance of  $\text{H}_2\text{O}-\text{CO}_2$  inclusions. High  $\text{CH}_4/\text{CO}_2$  ratios (2.58-15.45), comparable to those from this study, were obtained by bulk volatile data from fluid inclusions of the Dolgellau gold belt, North Wales (Bottrell et al., 1988). In this case it was suggested that the high  $\text{CH}_4/\text{CO}_2$  ratios

were probably the result of increased interaction between the vein-forming fluid and a carbon-rich wallrock.

The deposition of gold within Archean and meta-turbidite terranes is typically associated with a low salinity (>2 to <4 wt % NaCl), CO<sub>2</sub>-rich fluid (Roedder, 1982; Colvine et al. 1984; Boyle, 1986; Roberts, 1987). This type of fluid was not found in the fluid inclusion study at Gordon Lake. However, the saline CH<sub>4</sub>-rich fluid found in quartz veins and breccias of Gordon Lake may have been either a product of gold deposition and/or responsible for later gold remobilization. The interaction between a less saline, gold-bearing fluid and the carbon-rich rock might have deposited gold, produced methane and increased the salinity of the residual fluid; found as secondary inclusions along healed microfractures (e.g., Bottrell et al. 1988). Additionally the saline fluid might have acted as a fluid "carrier" by remobilizing and re-concentrating earlier formed gold (Guha and Kanwar, 1987).

Mechanisms for generating a high salinity (25 wt % NaCl-CaCl<sub>2</sub> combined) fluid within the Gordon Lake region include one or more of the following: 1) an influx of a saline fluid, derived from devolatilization reactions and the tectonic expulsion of and remaining connate waters during peak-metamorphism (e.g., Oliver, 1987; Craw, 1990); 2) the formation of a saline fluid during retrograde metamorphism (Crawford et al. 1979); 3) the reaction of less saline aqueous metamorphic fluids with carbon-rich rocks to produce CH<sub>4</sub> and a more saline residual fluid (Bottrell et al. 1988); 4) the immiscible separation of a low salinity, metamorphic H<sub>2</sub>O-CO<sub>2</sub> fluid (with the fractionation of salt into the aqueous phase; Bowers and Helgeson, 1983); or 5) the formation of brines associated with the emplacement of granite bodies (e.g., Williams-Jones et al, 1989; Wilson et al. 1980). Of the five mechanisms the last one is the least likely, as there are



no direct spatial or alteration relationships between granites and the metaturbidite-hosted veins/breccias. In addition, inclusion data (from sample 22/6/10) indicate that quartz veins associated with the late Spud Lake granite have higher Th, lower salinities, and lack  $\text{CaCl}_2$ . The lack of petrographic evidence for  $\text{CO}_2$  and  $\text{H}_2\text{O}$  unmixing probably discounts fluid immiscibility. The third mechanism does not explain the regional distribution of this saline fluid, but it might explain the high salinities of fluid inclusions found locally within regions dominated by carbon-rich rocks (i.e., Gordon Lake). Petrographic evidence for retrograde metamorphism is not abundant, but some is present (e.g., mineral changes within the multi-mineralic aggregates). The first mechanism, which invokes a metamorphic fluid derived from prograde reactions, is probably the most appropriate for the generation and distribution of a saline fluid that might be found regionally in both the metaturbidites and metavolcanic sequences.

#### 8.9 SUMMARY OF FLUID INCLUSION STUDY

Petrography of eleven quartz vein and breccia samples hosted within metaturbidites of the Gordon Lake region indicates that all of the fluid inclusions are secondary in origin and most are related to healed microfractures. The microstructure and timing of these veins suggest that this secondary fluid is syn- to late metamorphic in age and is probably associated with some late stage deposition and/or remobilization of gold. Seven types of fluid inclusions were recognized, of these the most abundant were two-phase aqueous (Type I) and three-phase aqueous (L- $\text{H}_2\text{O}$ , V- $\text{H}_2\text{O}$  and S- $\text{NaCl}$ ; Type IV). Thermometric data for these inclusions indicate homogenization temperatures of 140-330°C and high salinities of 25-30 wt % ( $\text{NaCl}$ - $\text{CaCl}_2$  combined). A bulk volatile analysis of fluid inclusions indicates high

concentrations of  $\text{CH}_4$  (up to 5.6 mole %) and high  $\text{CH}_4/\text{CO}_2$  ratios (0.6-11.3). The predominance of  $\text{CH}_4$  over  $\text{CO}_2$  is possibly the result of interaction between the vein forming fluid and carbon-rich rock.

Fluid trapping pressures of 2.0-3.5 kbars were estimated for the secondary fluid, using a fluid isochore and an arsenopyrite geothermometer. These pressures are within the range of P/T conditions for metamorphism and brittle-ductile breccia formation. Mechanisms to generate this saline fluid are unclear, but it is suggested that the fluid was generated by devolatilization reactions and the tectonic expulsion of any remaining connate waters during metamorphism. The salinity of these fluids was possibly increased during localized reactions with carbon-rich rocks and/or retrograde metamorphic reactions.

## CHAPTER 9

### GEOCHEMISTRY OF HOST LITHOLOGIES, QUARTZ BRECCIAS AND VEINS OF THE GORDON LAKE REGION

#### 9.1 INTRODUCTION AND PURPOSE

A pilot geochemical study was completed in the Gordon Lake region and included investigations into: i) the distribution of major elements, trace elements, and gold within quartz-breccias, quartz veins, siltstones, and graywackes; and ii) the tectonic environment and provenance of the metaturbidites.

The first part of this study attempted to answer specific questions, accessory to the proposed structural-lithological model for quartz-breccia formation (Chapters 6 and 7). Are the breccias significantly enriched in gold compared to other vein types? How is the gold distributed within the quartz-breccia? Are the black siltstones preferentially enriched in gold, trace elements, and volatiles compared to the other siltstones and graywackes? Are there any halos of major or trace element enrichment or depletion around the brecciation zones? Is there any geochemical association between carbon in the black siltstones and the breccia mineralization? In addition it is important, for the economic recovery of gold from these quartz-breccias, to better understand the association between gold and sulphides. Especially to ascertain whether gold occurs as "free gold", as sub-microscopic particles incorporated within the sulphides, or as "invisible" (solid solution) gold within sulphides (Springer, 1983). Indications that sub-microscopic and "invisible" gold might be present at Gordon Lake included: i) the close association between arsenopyrite and gold (Brophy, 1987a); ii) the difficulties in distinguishing quartz-breccia material with low and high gold grades (Caelles, 1985); and iii) evidence from recent literature

for the common occurrence of "invisible" gold in many gold deposits (e.g., Cabri et al. 1989; Cathelineau et al. 1990; Cook and Chryssoulis, 1990).

In the second part of the geochemical study, major and trace element lithochemistry was used to differentiate the possible tectonic environments and/or provenance of the metaturbidites. Turbidites deposited in an oceanic island arc, continental arc, or active continental margin setting are probably more favorable for primary gold accumulation compared to those from passive continental margins (Boyle, 1979). In addition, gold within mafic volcanic debris may be more readily available for leaching compared to siliceous volcanic material (Keays, 1984).

#### 9.2. PREVIOUS GEOCHEMICAL STUDIES OF METATURBIDITE-HOSTED GOLD DEPOSITS AND THE PROVENANCE OF METATURBIDITES, WITH PARTICULAR REFERENCE TO THE YELLOWKNIFE BASIN

Elements most frequently associated with MHGD include Au, Ag, Mg, Ca, Zn, Cu, Cd, Zn, B, Pb, As, Sb, S, W, Mn, and Fe, and to a lesser extent Hg, In, Tl, Bi, Se, Te, Mo, F, Co, and Ni (Boyle, 1986). In most cases, alteration around these deposits is limited, but where present it is characterized by silica, pyrite, and arsenopyrite; and to a lesser extent by chlorite, sericite, and carbonate (Boyle, 1986). Most geochemical studies of metaturbidite-hosted gold districts are confined to the Phanerozoic. Examples include the Au-W lode systems of the Otago Schist, New Zealand (Paterson and Rankin, 1979; Paterson, 1986), the Ordovician Au-rich lodes at Clontibret, Ireland (Steed and Morris, 1986), and the Au-quartz veins of the Cambrian-Ordovician Meguma Terrane, Nova Scotia (Clifford et al. 1983; Crocket et al. 1983; Smith, 1984; Crocket et al. 1986; Kontak and Smith, 1987)

Within the Yellowknife Basin geochemical investig-

ations have focussed on the lithochemistry of the gold-bearing shear zones of the Yellowknife Volcanic Belt (Boyle, 1961, 1979; Kerrich and Fyfe 1987, 1988). Boyle (1961) concluded that metamorphic fluids were introduced into shear zones and interacted with the mafic volcanic wall rocks, producing a pervasive carbonate-sericite-pyrite-arsenopyrite alteration. This alteration was accompanied by the addition of  $H_2O$ ,  $CO_2$ , S, K, As, Ag, Sb, and Au and the loss of  $SiO_2$ , Ca, Na, Fe, Mg, and Mn. Kerrich and Fyfe (1987) emphasized the selective chemistry of these shear zone fluids (whereby Au, As, B, Sb, W, and Pd are extremely enriched compared to the transition and base metals), and noted that hydrothermal alteration around the shear zones was characterized by hydrolysis of the Fe-, Mg-, Ca-, and Mn-silicates to carbonates, the introduction of K and  $CO_2$ , and the loss of Na.

Boyle (1961 and 1979) carried out a study on the gold-quartz vein occurrences within the amphibolite grade Burwash metaturbidites at the Ptarmigan mine and Burwash Prospect (10 km north-east and 1 km east of Yellowknife, respectively). He concluded that vein alteration halos were poorly defined and limited in width (<1 metre), but that minor sericite bleaching, tourmaline, and carbonate were present. Major element analyses across these veins systems indicated slight decreases in  $SiO_2$  and  $Na_2O$  in the wall rock adjacent to the veins, with minor to significant increases in  $Al_2O_3$ , total Fe, CaO, MgO,  $K_2O$ ,  $H_2O$ ,  $TiO_2$ ,  $P_2O_5$ ,  $CO_2$ , and S. Marked increases in trace elements such as Cs, Cu, Ag, B, Ga, Sc, As, V, Te, Co, Ni, Zn, Cd, Sn, Pb, and W were found near to the veins. Boyle (1961) attributed the more pervasive and greater widths of the alteration around metavolcanic-hosted veins, compared to those hosted within metasediments, to a difference in vein genesis. He suggested that the quartz within the metavolcanic rocks was derived locally, and that alteration

was due to the interaction of volatiles with the wall rock. In contrast, quartz in the metasediment-hosted veins originated from the lateral and vertical secretions of silica into structurally prepared sites.

Brophy (1987a) initiated a preliminary geochemical study (using gold, major, and trace element analyses) of auriferous quartz veins and their host metasediments within the Yellowknife Basin. He was able to discriminate between background and anomalous Au and As values in siltstones and graywackes, both distal and proximal to gold-quartz veining systems. He also found that a wider (>2 m) geochemical halo existed around the Kidney Pond Zone 1 quartz-breccia, compared to other gold-quartz vein occurrences within the Yellowknife Basin.

Major element chemistry, in addition to detailed petrography, has been used by many workers to investigate the source of Archean turbidite detritus (e.g., Condie, 1981). Within the Yellowknife Basin, Henderson (1975, 1985, 1987) suggested that the metaturbidites of the Burwash Formation were probably derived from sialic material, since the average composition of the graywackes is similar to granodiorite. He also noted that the abundant quartz and feldspar clasts were probably granitic and felsic volcanic in origin. Jenner et al. (1981) pointed out that the detrital source of graywackes could not be determined from clast petrography alone, as graywackes consist of up to 15-75% matrix material (Pettijohn, 1975) and many of the original sedimentary clasts are destroyed by post-depositional processes (e.g., Whetten and Hawkins, 1970; Graves, 1989). Jenner et al. (1981) used major and trace element data, with an assumed sample composition of 85% graywackes and 15% mudstones (typical of a Burwash Formation stratigraphic section) to model possible detrital sources. From these models he concluded that the Burwash Formation was probably derived

from a mixed provenance of 55% felsic volcanic, 20% mafic-intermediate volcanic, 25% granitic rocks (of which 5-10% of the latter were of basement origin). Jenner et al. (1981) also concluded that their geochemical data were more compatible with tectonic models in which no extensive sialic basement was present and where mafic volcanic sequences erupted onto an oceanic floor (e.g., Folinsee et al. 1968; Green and Baadsgaard, 1971), rather than the rifting of a sialic basement (Henderson, 1981, 1985).

### 9.3 SAMPLE COLLECTION, PREPARATION AND ANALYSIS

Seventy-two samples were selected from around the Kidney Pond Zone 1 and the south Gordon Lake region (Figures A9.1 to A9.7) and analyzed for gold, major and trace elements (Table 9.1). These samples included: i) mineralized quartz-breccias, ii) various quartz vein types, iii) black sulphide-rich siltstones adjacent to the breccia zones, iv) siltstones and graywackes proximal and distal to the breccia zones, v) mafic and felsic volcanic rocks from the Cameron River Volcanic Belt, and vi) granitic rocks from the Spud Lake pluton. All samples were rubbed with abrasive paper to remove saw marks, washed and brushed with water, crushed using a steel lined jaw crusher, and finally powdered using tungsten carbide ring grinders. No sieving was done or required on powders sent for gold and Neutron Activation analysis (N.A.). However, some of the samples sent for X-Ray Florescence analysis (X.R.F.) required sieving with plastic nets for pelletization. For both the X.R.F. and N.A. analyses 10% duplicates were submitted, as well as two Geological Survey of Canada standards (JB-1 and JG-1, Abbey, 1983).

Ten quartz-breccia and vein samples were selected for heavy mineral separation and gold analysis. Each sample was divided into heavy and light separates (in the Mineral Processing laboratories of Technical University of Nova

Table 9.1 Geochemical techniques and number of samples analyzed.

Number of samples	Elements analyzed	Analytical technique	Laboratory Location
72	major and trace	X-ray Fluorescence	St Mary's University, Halifax, Nova Scotia.
72	gold and trace	Neutron Activation	Bondar Clegg Ltd., Toronto, Ontario.
20	volatiles (CO <sub>2</sub> , C, and S)	LECO-IR detector and LECO-gasometric	Chemex Labs Ltd., Vancouver, British Columbia.
20	gold in heavy and light separates.	Combined fire assay and Neutron Activation	Bondar Clegg Ltd., Toronto, Ontario.



Scotia, Halifax) by a heavy liquid medium and then cleaned ultrasonically in a bath of acetone and distilled water. The twenty separates were then analyzed for gold by a combined fire assay and N.A. technique.

#### 9.4 RESULTS AND PRECISION/ACCURACY ANALYSIS

Data for the geochemical analyses are tabulated in Tables A9-1 to A9-24. A precision analysis of both the X.R.F. and N.A. data was completed using nine duplicates (Tables A9-25 to A9-34). For  $\text{SiO}_2$ ,  $\text{Al}_2\text{O}_3$ ,  $\text{K}_2\text{O}$ ,  $\text{TiO}_2$ , and  $\text{MnO}$  the precision analysis indicated less than 2% deviation, whereas for  $\text{Fe}_2\text{O}_3$ ,  $\text{P}_2\text{O}_3$ ,  $\text{MgO}$ ,  $\text{CaO}$ , and  $\text{Na}_2\text{O}$  the analysis indicated 5-15% deviation. For the X.R.F. trace element data only Cu gave large percentage deviations that could not be attributed to low limits of detection. The precision for most elements analyzed by N.A. was generally less than 10% deviation, but some elements (e.g., Ba, Ni, Cr, and Au) consistently gave ranges of 10-70% deviation. However, a log concentration plot of the duplicate gold analyses (Figure A9.8) produced a reasonably linear correlation, considering the problems with gold sampling and nugget effects (Boyle, 1979). The precision for the volatile analyses of both carbon and sulphur ranged from 0-13% deviation.

Overall accuracy of the data was gauged by the two external standards that were submitted in duplicate (Tables A10.35 and A10.36). For the X.R.F major element analyses the percentage deviation of the standards are the greatest for  $\text{Fe}_2\text{O}_3$  (70-80%) and  $\text{P}_2\text{O}_3$  (13-40%). Accuracy analysis of the trace element N.A. and X.R.F data produced greater percentage deviations, but most are probably accounted for by the low limits of detection.

Inter-laboratory trace element comparison between the St Mary's X.R.F. and Bondar-Clegg's N.A. data using Ba, Cr, Ni, Rb, Ni, Zn, and Zr (Figure A9.9) displayed reasonable

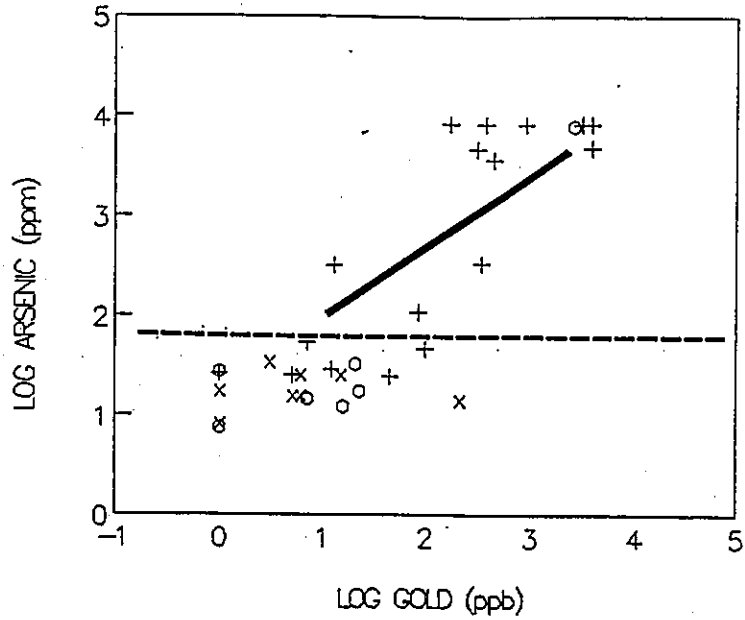
linear correlations between Ba, Cr, Ni, and Rb. The less distinct correlations between Zr and Zn are probably due to the lower detection limits of the X.R.F. technique, or to the distribution of these elements in discrete accessory minerals.

#### 9.5 COMPARISON OF MAJOR, TRACE, GOLD, AND VOLATILE ANALYSES BETWEEN BRECCIAS, VEINS, AND HOST ROCKS

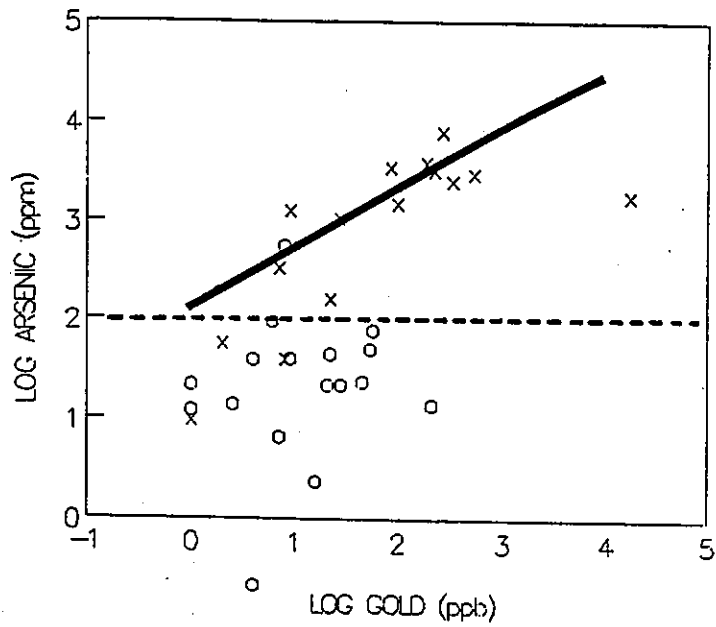
Comparison of the gold and trace element data between the quartz-breccias and quartz veins (Tables A9-20 to A9-23) yields some significant findings. Au, As, Sb, and Br are relatively enriched within the breccias, whereas transition metals (e.g., Cu, Zn, and Ni) occur in similar concentrations in both veins and breccias. The Au and As association was examined in log concentration plots for both the quartz veins and quartz-breccias, and the siltstones and graywackes (Figure 9.1A and 9.1B). In Figure 9.1B, the Au and As concentrations are greater within the breccias, and an approximate linear correlation occurs between As and Au, when As values are higher than 100 ppm. For the siltstones and graywackes (Figure 9.1A) a similar linear correlation exists. However, the flattened portion of this plot, at high As and Au concentrations, is probably a result of the upper detection limits of As by the N.A. technique.

Plots of major, trace, and volatile elements versus  $\text{SiO}_2$  were constructed to compare the geochemistry of graywackes, light-grey siltstones, dark-grey/black siltstones, interbedded siltstones, and sulphide-rich black siltstones (Figures 9.2 to 9.6).  $\text{SiO}_2$  concentration varied from 70 wt% in the graywackes to 45 wt% in the sulphide-rich black siltstones. Linear trends of  $\text{TiO}_2$ ,  $\text{Al}_2\text{O}_3$ , and  $\text{K}_2\text{O}$  were apparent from coarse- to fine-grained meta-sediments, with less distinct trends for  $\text{Fe}_2\text{O}_3$  and  $\text{CaO}$ , and no apparent trends for  $\text{Na}_2\text{O}$ ,  $\text{P}_2\text{O}_5$ ,  $\text{MgO}$  and  $\text{MnO}$ . Trace

Figure 9.1 Log concentration plots of arsenic versus gold for: A - dark grey/ black siltstones (x), light grey siltstones (+), and graywackes (o); and B - quartz veins (o) and breccias (x) with approximate linear trends.



**A**



**B**

Figure 9.2 Plots of  $\text{SiO}_2$  versus  $\text{Na}_2\text{O}$ ,  $\text{CaO}$ ,  $\text{K}_2\text{O}$ ,  $\text{Al}_2\text{O}_3$ ,  $\text{TiO}_2$ , and  $\text{MnO}$  for graywackes (o), grey siltstones (x), interbedded siltstones (+), dark grey to black siltstones (\*), and sulphide-rich black siltstones (#). (All data reported in wt.%.)

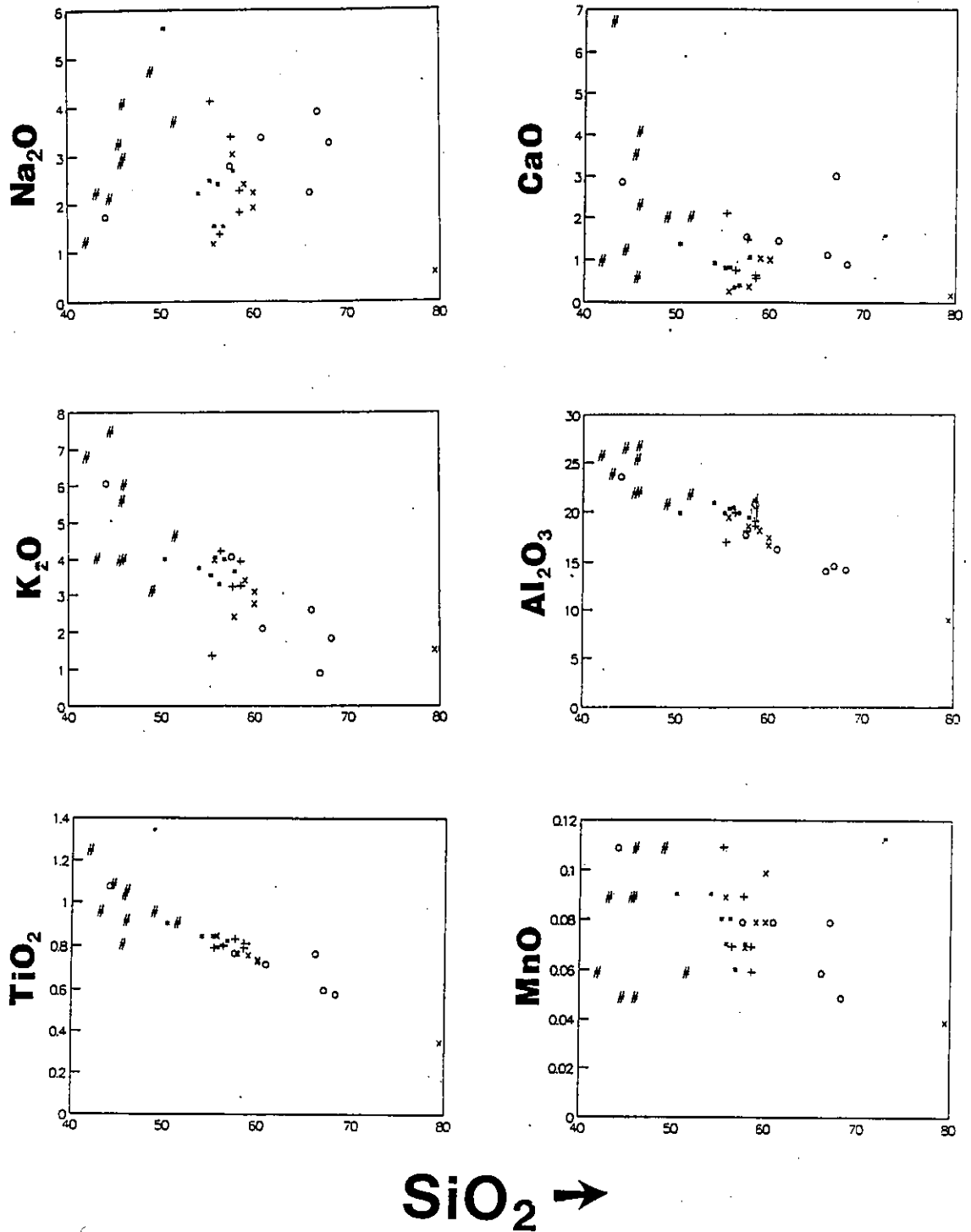


Figure 9.3 Plots of  $\text{SiO}_2$  versus  $\text{MgO}$ ,  $\text{Fe}_2\text{O}_3$ ,  $\text{P}_2\text{O}_5$ , C, and  $\log S$  for graywackes (o), grey siltstones (x), interbedded siltstones (+), dark grey/black siltstones (\*), and sulphide-rich black siltstones (#). (All data reported in wt.%.)

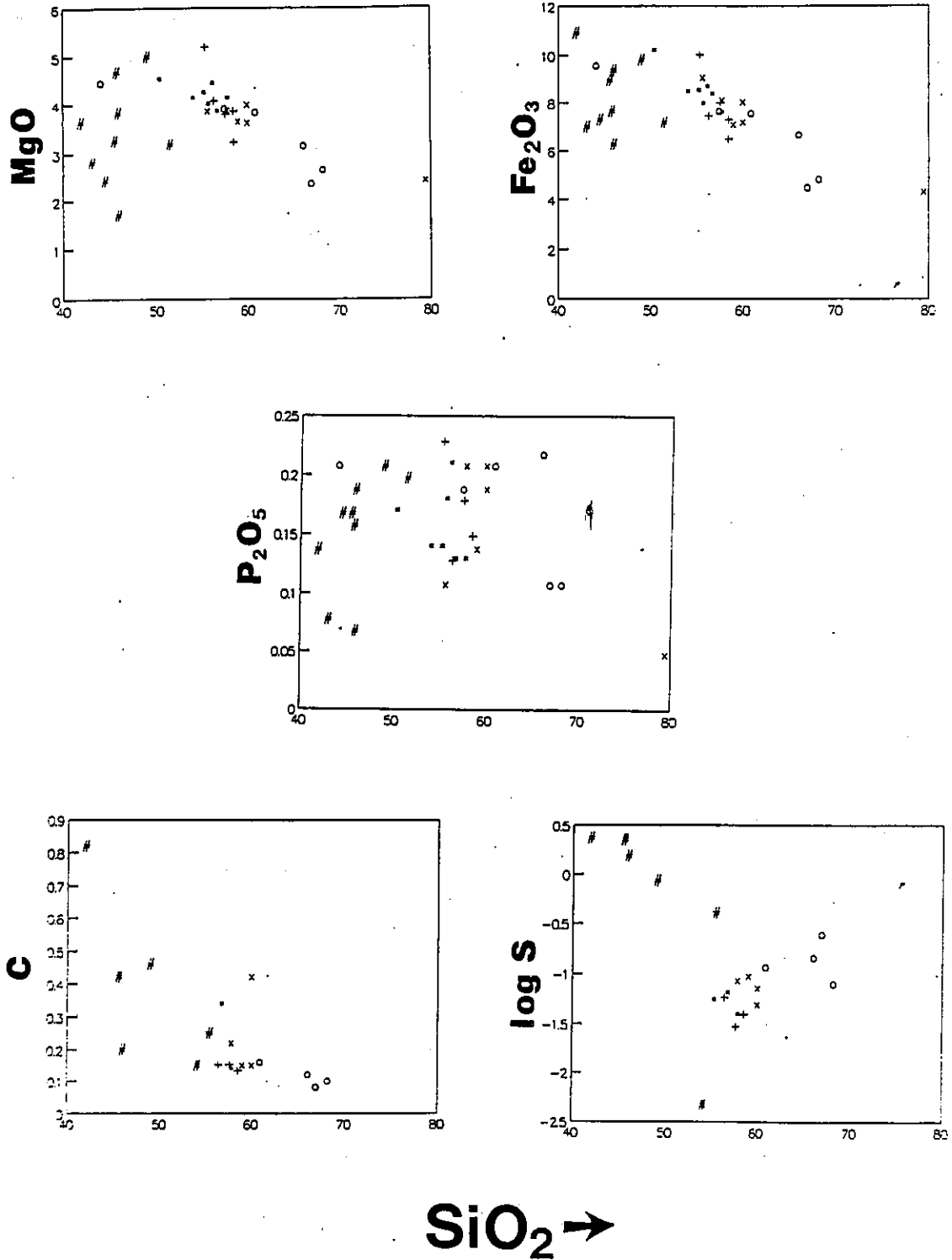
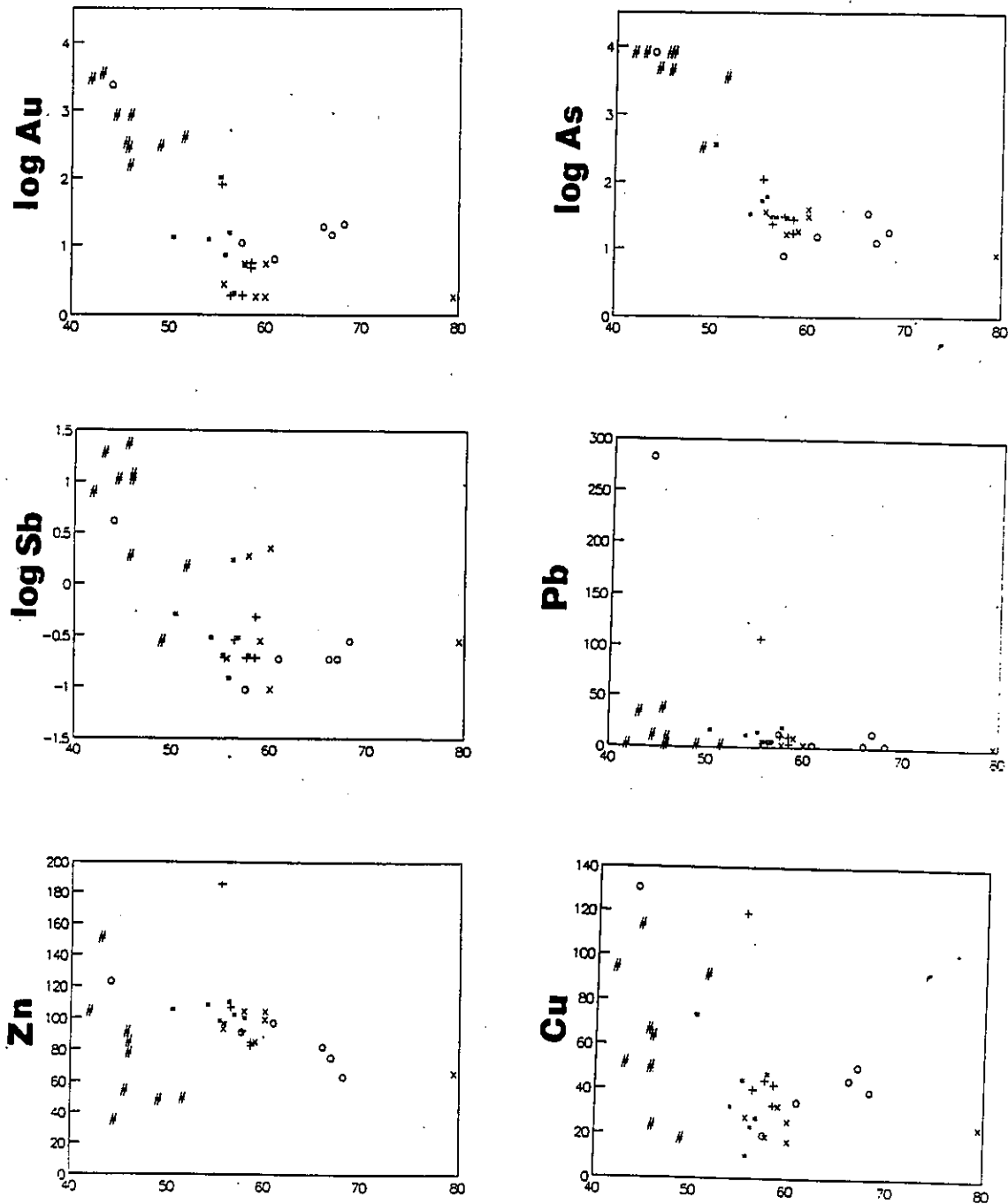


Figure 9.4 Plots of  $\text{SiO}_2$  versus  $\log \text{Au}$ ,  $\log \text{As}$ ,  $\log \text{Sb}$ ,  $\text{Pb}$ ,  $\text{Zn}$ , and  $\text{Cu}$  for graywackes (o), grey siltstones (x), interbedded siltstones (+), dark grey/black siltstones (\*), and sulphide-rich black siltstones (#). ( $\text{SiO}_2$  reported in wt.%, Au in ppb, and As, Sb, Zn, and Cu in ppm.)



$\text{SiO}_2 \rightarrow$

Figure 9.5 Plots of  $\text{SiO}_2$  versus Zr, Nb, Y, Ga, Cr, and V for graywackes (o), grey siltstones (x), interbedded siltstones (+), dark grey/black siltstones (\*), and sulphide-rich black siltstones (#). ( $\text{SiO}_2$  reported in wt.% and Zr, Nb, Y, Ga, Cr, and V in ppm.)

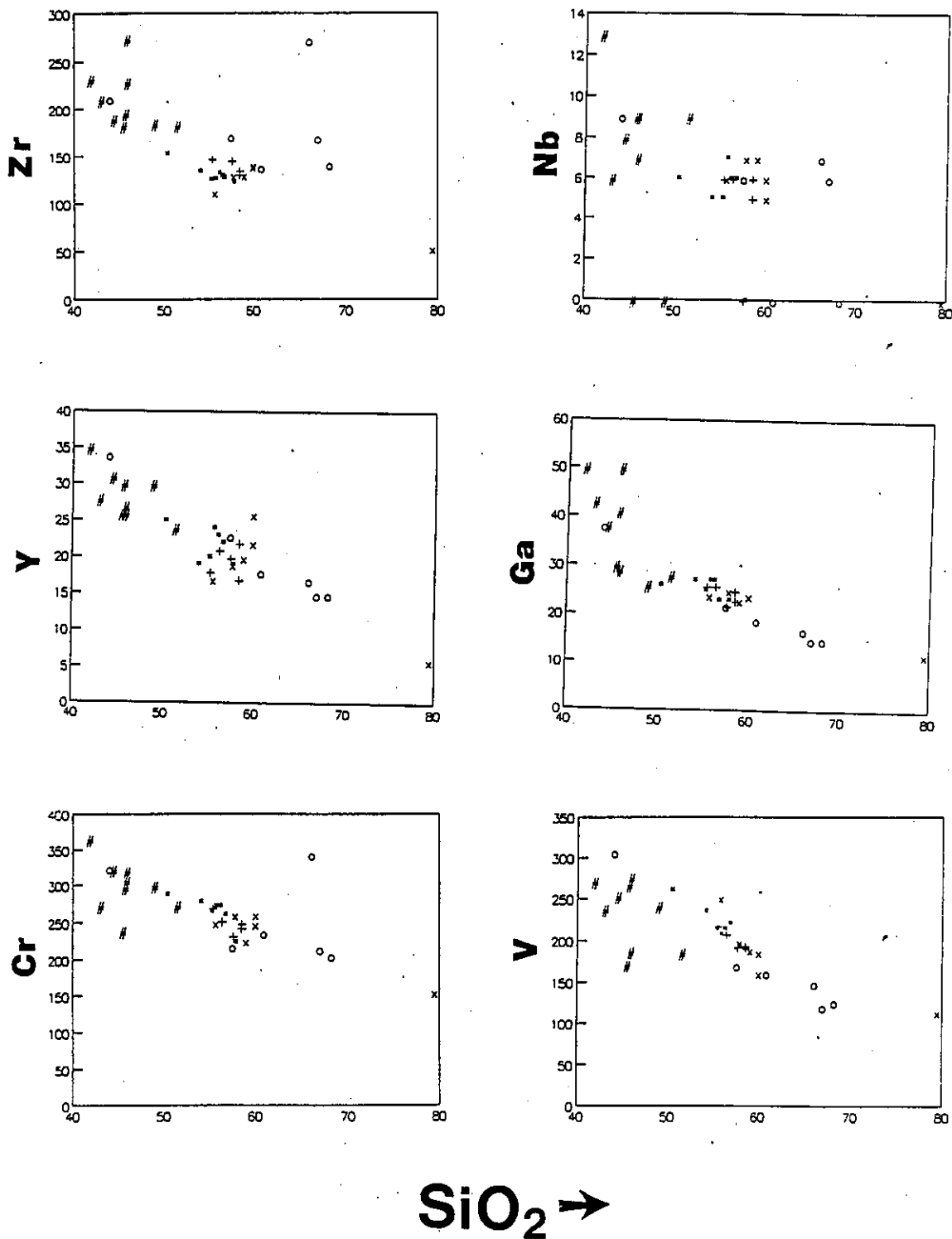
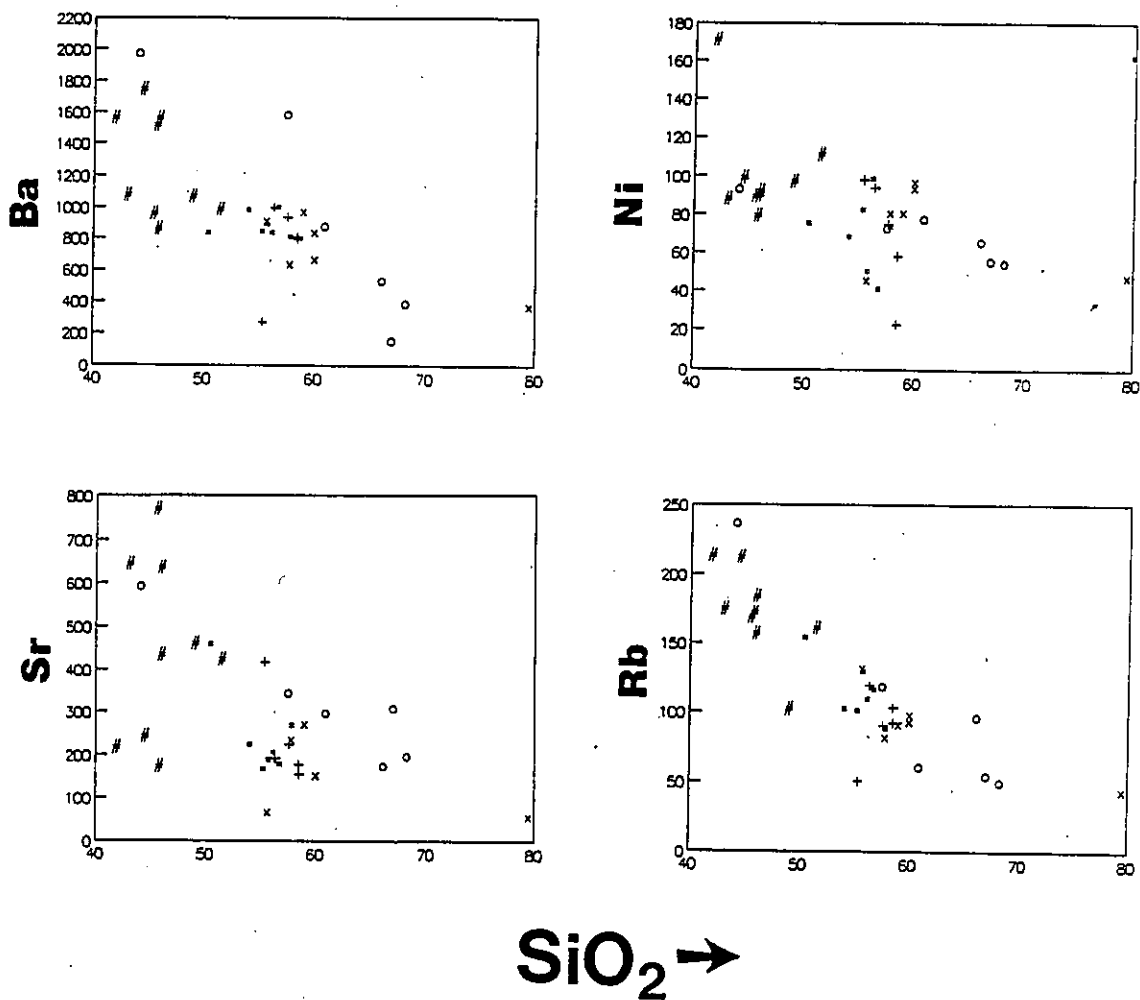


Figure 9.6 Plots of  $\text{SiO}_2$  versus Ba, Ni, Sr, and Rb for graywackes (o), grey siltstones (x), interbedded siltstones (+), dark grey/black siltstones (\*), and sulphide-rich black siltstones (#). ( $\text{SiO}_2$  reported in wt.% and Ba, Ni, Sr, and Rb in ppm.)

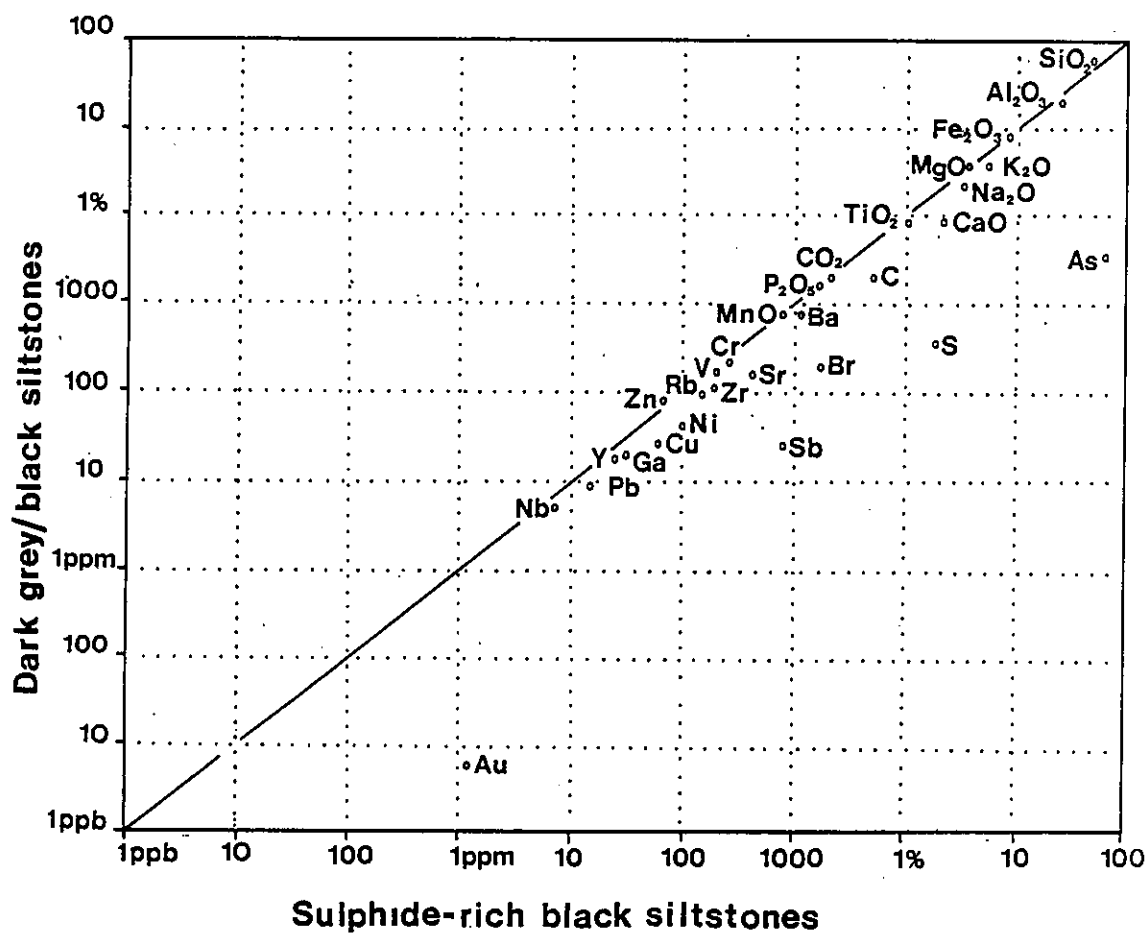




elements Cr, Ga, Y, V, Ba, Rb, and Zr display linear trends from coarse-to fine-grained metasediments, whereas Au, As, and Sb show exponential-type trends, and Sr, Nb, Pb, Ni, Cu, and Zn minor to no apparent trends. Carbon and sulphur contents are also higher within the sulphide-rich black siltstones. Most of the trends (e.g., decreasing  $\text{SiO}_2$  and increasing  $\text{Fe}_2\text{O}_3$  and  $\text{Al}_2\text{O}_3$  from coarse- to fine-grained metasediments) are due to the different bulk composition of the lithology types. However, some of elemental trends, in particular the Au, As, Sb, and S enrichments in the black siltstones (Figures 9.3 and 9.4), are related to alteration and mineralization. In general, these findings are comparable with geochemical data of Boyle (1961, 1979) and Brophy (1987a) for quartz veins within the Burwash Formation. However, it is apparent, from some of the sulphide-rich black siltstones (i.e., 27-6-3) taken 10-15 m from the Kidney Pond Zone 1, that the geochemical haloes around the quartz-breccias are significantly wider than other quartz-veins systems.

An isochron plot (Figure 9.7; Tables A9.38 and A9.39) for the sulphide-rich black siltstones (adjacent to the quartz-breccias) and dark grey/black siltstones (distal to the quartz breccias) was used to differentiate between the relative enrichments and depletions of major, trace, and volatile data. From a first approximation it is apparent that: i) Au, As, Sb, S, and Br are enriched by at least one order of magnitude in the sulphide-rich black siltstones; ii) Pb, Cu, Ni, Sr, C, CaO,  $\text{Na}_2\text{O}$ , and  $\text{K}_2\text{O}$  are also enriched; and iii)  $\text{SiO}_2$  is the only major element that is slightly depleted. Au, Sb, Br, As, and S are clearly related to the mineralizing process as are, to a lesser extent, Pb, Cu, and Ni. The  $\text{K}_2\text{O}$ , CaO, and  $\text{Na}_2\text{O}$  enrichment could be due to alteration minerals (e.g., K-feldspar, biotite, and carbonate), but might also be an artifact of the silica depletion. Three possible explanations for the

Figure 9.7 Isochon plot of eight sulphide-rich black siltstones, adjacent to the quartz-breccia zones, versus six dark grey/black siltstones, distal from the quartz-breccia zone (Tables A9.38 and A9.39).



low silica and high carbon contents in the sulphide-rich black siltstones, compared to the dark grey/black siltstones, include: i) that the sulphide-rich black siltstones are a distinct rock type with a low silica content, ii) the silica has been removed from these rocks thereby increasing carbon (e.g., Wilson and Rutledge, 1987), or iii) an enrichment of the black siltstone by other elements (e.g., volatiles), which has reduced the relative silica content. These explanations imply that either the host siltstone to the quartz-breccia is a specific lithology type or it is the product of an alteration process. Both these factors have important implications for exploration of similar quartz-breccia zones and deserve more study. Of the two explanations the first one is probably the most likely and is the simplest.

#### 9.6 GOLD-SULPHIDE ASSOCIATIONS

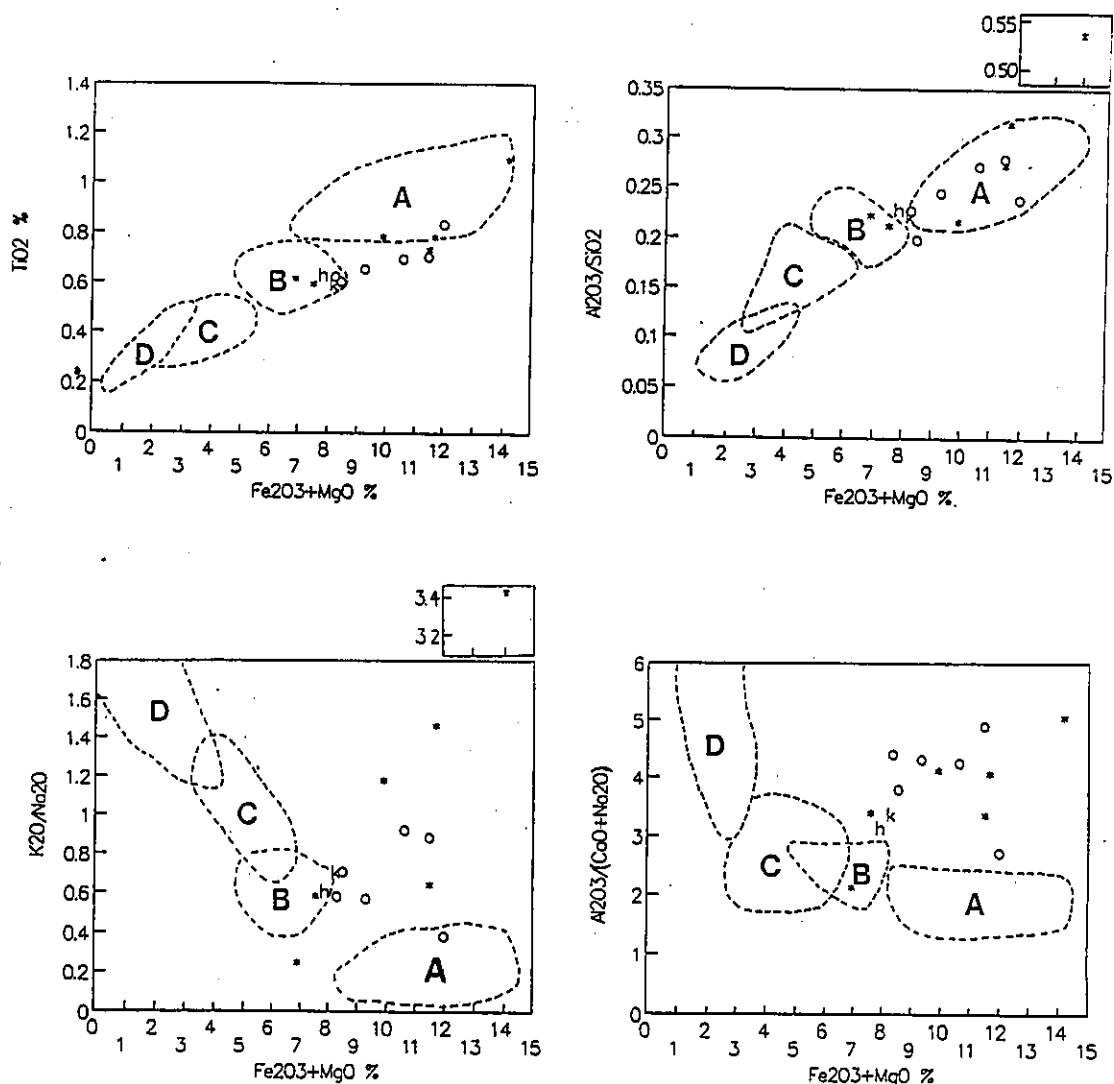
Gold within the sulphides of the Gordon Lake quartz-breccias can possibly occur as: i) free gold within and adjacent to the sulphides, ii) submicroscopic gold particles within sulphides, iii) "invisible" or solid solution gold within the sulphide structure, or iv) a combination of one or more of the above. Petrographic examination of polished thin sections indicates that free gold occurs adjacent to and within the coarse pyramidal arsenopyrite (Figure 7.12). Gold analysis of heavy mineral separates from five quartz-breccias and five veins, and petrographic examination of polished grain mounts (Table A9-37) indicates that: i) no visible free gold was present, ii) arsenopyrite and pyrite are the most abundant sulphides, and iii) higher gold values generally occur with greater proportions of arsenopyrite. Preliminary microprobe analysis of arsenopyrite, pyrite and pyrrhotite (Tables A7.2 - A7.4 and A9.40) did not detect concentrations of gold >200 ppm (the detection limit for gold by

the microprobe; B. McKay, personal communication, 1990). Typically, pyrite gave low arsenic contents (0 to 0.15 At.%) suggesting that, as pyrite has less than 0.5 At.% arsenic, it is not a good candidate for sub-microscopic or "invisible" gold (Cook and Chryssoulis, 1990). From the two types of arsenopyrite found at Kidney Pond, the coarse pyramidal and fine needle-shaped (Section 7.3), it is suggested that the finer is the most likely candidate for solid solution or "invisible" gold - as this crystallographic structure is more favourable the incorporation of gold (Cook and Chryssoulis, 1990; Wu et al. 1990).

#### 9.7 GEOCHEMICAL INDICATIONS OF TECTONIC SETTING AND PROVENANCE OF THE GORDON LAKE METATURBIDITES

The major element data obtained from six graywacke samples, along with graywacke data from Jenner et al. (1981), Henderson (1985), and Ramsay and Kamineni (1977), were plotted on four tectonic/provenance discrimination diagrams of Bhatia (1983). The fields of these diagrams (Figure 9.8) were determined from Paleozoic graywacke suites of known tectonic setting. Most the data within the  $TiO_2$  and the  $Al_2O_3/SiO_2$  plots are close to, or fall within, the continental arc or oceanic island arc fields. However, most of the data in the  $K_2O/Na_2O$  and  $Al_2O_3/(CaO+Na_2O)$  plots are scattered above the continental arc and oceanic island arc fields. The explanation for this is unclear, but extensive chemical weathering of feldspars prior to turbidite deposition can causes apparent losses in  $Na_2O$  and  $CaO$  (Sawyer, 1986). Other errors in using the major element discrimination fields of Bhatia (1983) include: 1) problems in directly comparing Phanerozoic tectonic settings with those of the Archean; ii) the chemical differences found between Phanerozoic and Archean graywacke compositions (whereby the latter have greater amounts of Fe, Mg, Ca, and transition metals; Condie,

Figure 9.8 Gordon Lake graywacke data (\*) and other graywacke data from the Burwash Formation plotted on tectonic discrimination plots of Bhatia (1983). Tectonic fields represent: A - oceanic island arc, B - continental arc, C - active continental margin, and D - passive continental margin. Other data includes: graywacke-siltstone composites from Jenner et al. 1981 (o); average of three graywacke composite samples from Henderson, 1985 (h); average of five graywackes from Ramsay and Kamineni 1977 (k).



1981), and iii) alteration effects of mineralization on graywackes, which might cause distinct major element variations (e.g.,  $K_2O$ ,  $Na_2O$ ,  $CaO$  and  $SiO_2$  in sample WO-121.5).

Two ternary diagrams of the La-Th-Sc and Th-Sc-Zr/10 (with fields defined from Paleozoic metaturbides of known tectonic setting; Bhatia and Crook, 1986) were used to plot, the less mobile, trace element data from six graywacke and six siltstone samples (Figure 9.9). These data produced good groupings close to, and within the fields of oceanic or continental arc settings. These data are comparable to Archean graywacke data from Australia, South Africa, and Greenland used by Bhatia and Crook (Figure 9.10, 1986).

Major element data from graywacke, siltstone, granite and volcanic rocks were plotted on an AFM plot similar to that of Jenner et al. (1981). Comparison of these two plots (Figures 9.11A and 9.11B) indicates that the Spud Lake granite (22-6-8 and 22-6-10) is more  $K_2O+Na_2O$ -rich compared to the average granites of the region. The Cameron Volcanic Belt (12-6-3 and 12-6-4) is similar in composition to mafic to intermediate volcanic rocks of the Yellowknife region, but slightly more Fe-rich. The felsic volcanic rock from the Cameron River Volcanic Belt appears closer to average values of the Yellowknife felsic volcanic rocks. The graywackes and siltstones plot between the mafic and felsic volcanic rocks.

From the major and trace element discrimination diagrams of Bhatia (1983) and Bhatia and Crook (1986), and comparison of AFM data with Jenner et al. (1981) it is apparent that the dominant source of detrital material for the graywackes and siltstones of the Gordon Lake region is volcanic, such as might be expected in a continental arc or oceanic island arc setting. The lack of visible mafic clasts within the graywackes suggests that most of them

Figure 9.9 Gordon Lake graywacke (filled circle) and siltstone (open circle) trace element data plotted on tectonic ternary discrimination figure of Bhatia and Crook (1986). Fields defined from Paleozoic metaturbidites of known tectonic setting (with A - oceanic island arc, B - continental arc, C - active continental margin, and D - passive continental margin).

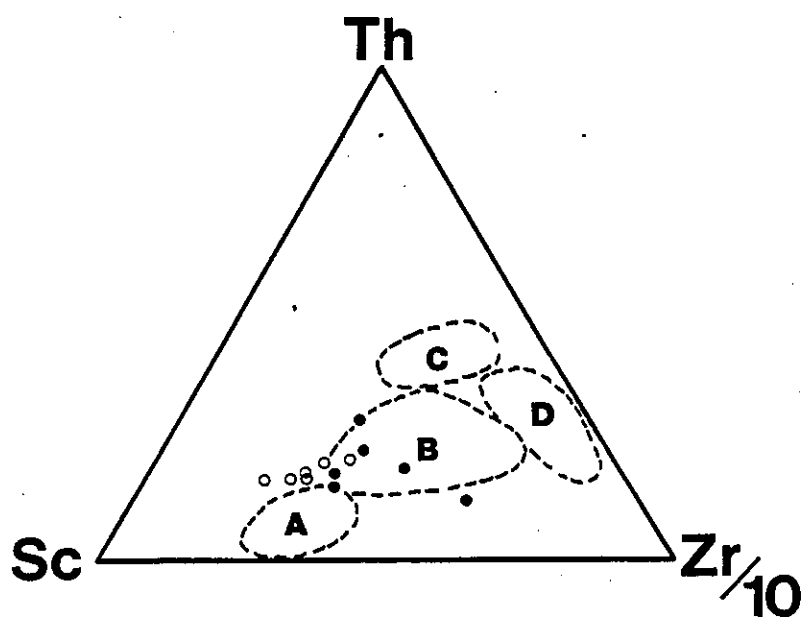
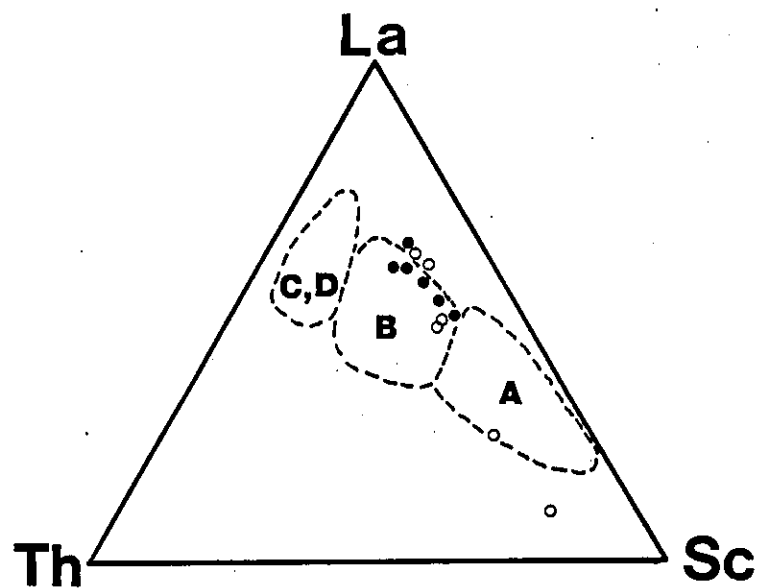


Figure 9.10 Trace element tectonic discrimination plots from Figure 10, Bhatia and Crook (1986). Tectonic fields derived from Phanerozoic data: A - oceanic island arc; B - continental arc; C - active continental margin; D - passive continental margin. Archean data taken from McLennan et al. (1984, 1983a, 1983b): Pilbara, Australia (triangles); Yilgarn, Australia (crosses); South Africa (stars); and West Greenland (boxes).

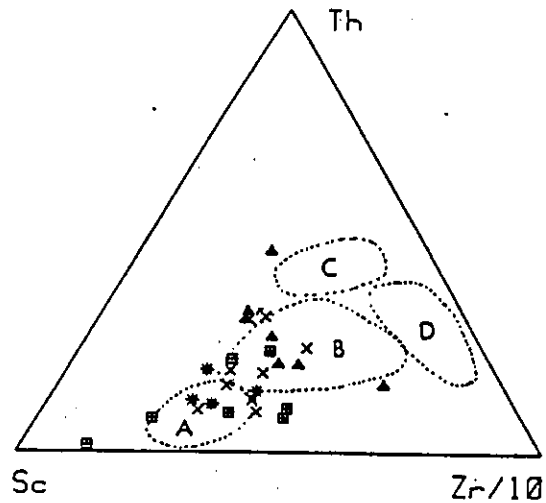
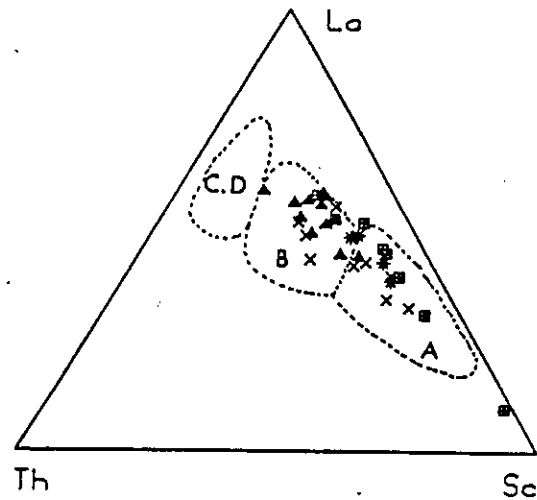
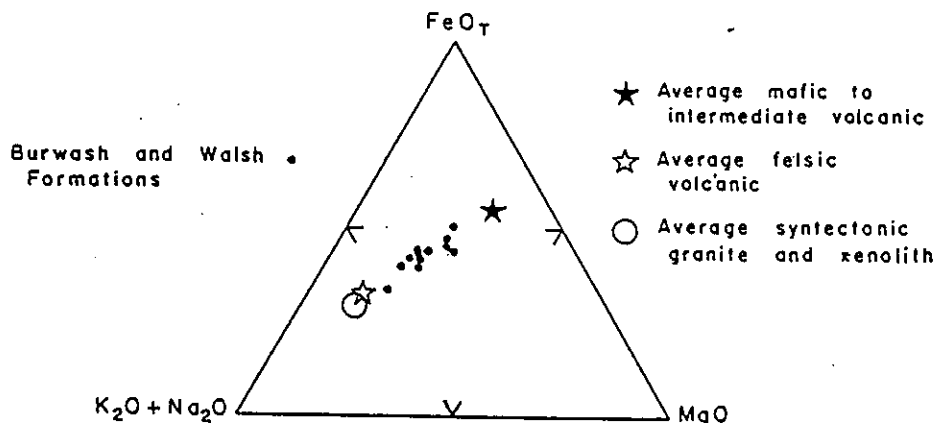


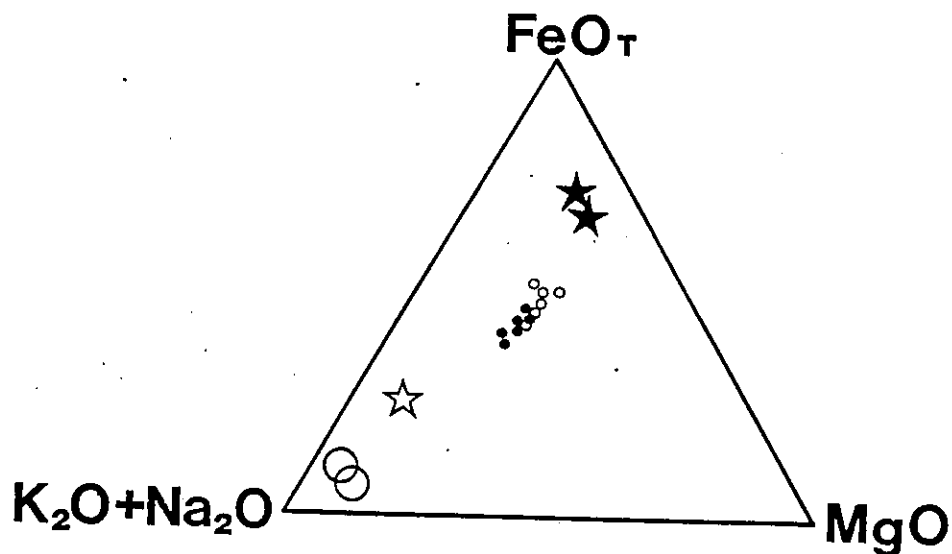


Figure 9.11 A - AFM diagram taken from Figure 5 of Jenner et al. (1981). B - AFM diagram using data from Gordon Lake graywackes (filled circles) and siltstones (small open circles), Cameron River mafic and intermediate volcanic (filled stars), Cameron River felsic, porphyry volcanic (open star), and Spud Lake granite pluton (large open circles).

**A**



**B**



broke down during weathering, diagenesis, and metamorphism to form the fine-grained matrix. This fine-grained matrix might have provide an important source material from which gold was leached.

#### 9.8 SUMMARY OF GEOCHEMICAL STUDY

Au, As, Sb, Br, and Te are significantly enriched within the quartz-breccias, compared to the other vein types. Log Au/log As concentration plots of both the breccia/veins and graywackes/siltstones give approximate linear correlations, for As values higher than 100 ppm. Major, trace, and volatile element data of the sulphide-rich black siltstones (adjacent to the quartz-breccia zones), compared to dark grey/black siltstones (distal to the quartz-breccias), show significant enrichments of Au, As, Sb, S, and Br, lesser enrichments in Pb, Cu, Ni, Sr, C, CaO, Na<sub>2</sub>O, and K<sub>2</sub>O, and a slight depletion in SiO<sub>2</sub>. Most of the trace elements and the CaO, Na<sub>2</sub>O, and K<sub>2</sub>O enrichments are due to alteration associated with the quartz-breccia. The low silica and high carbon contents indicate that the sulphide-rich black siltstones are probably a specific lithological type, rather than a product of the breccia alteration process. Free gold is found in the quartz-breccias within or adjacent to arsenopyrite. Arsenopyrite is the most common sulphide associated with gold, and analyses indicate that gold might also occur as sub-microscopic or "invisible" gold. Major and trace element discrimination plots indicate that the metaturbidites of the Gordon Lake were probably deposited in a volcanic-rich tectonic setting, such as a continental arc or oceanic island arc environment.

## CHAPTER 10

### $^{40}\text{Ar}/^{39}\text{Ar}$ DATING OF THERMAL AND TEMPORAL EVENTS IN THE GORDON LAKE REGION

#### 10.1 PURPOSE AND AIMS OF STUDY

No previous detailed  $^{40}\text{Ar}/^{39}\text{Ar}$  dating studies have been completed within the Yellowknife Basin or Slave Province, as it has been generally considered that the timing of geological events are hampered by thermal resetting episodes (e.g., Easton, 1984). Most of the recent geochronological data within the Yellowknife Basin are from U-Pb zircon ages of plutonic and volcanic rocks (Section 10.2). However,  $^{40}\text{Ar}/^{39}\text{Ar}$  data can provide constraints on the timing of thermal episodes, such as metamorphism and mineralization. In this study  $^{40}\text{Ar}/^{39}\text{Ar}$  spectra were obtained for five samples from the South Gordon Lake region; three biotites, a muscovite, and a hornblende (Table 10.1). An introduction to the  $^{40}\text{Ar}/^{39}\text{Ar}$  technique used, with related calculations and errors, is included in the Appendix (Section A10.1).

The aims of this  $^{40}\text{Ar}/^{39}\text{Ar}$  study were to: i) provide temporal constraints on the age of quartz-breccia mineralization and metamorphism at Gordon Lake; ii) obtain thermochronometric data that might constrain thermal events for the region and be compared to thermal models suggested for the Slave Province (i.e., Thompson, 1989a, 1989b); and iii) produce a precise set of data that is internally consistent and comparable to other geochronological studies within the Yellowknife Basin.

#### 10.2 PREVIOUS GEOCHRONOLOGICAL STUDIES

Most of the past geochronological studies in the Slave Province have concentrated on the basement, volcanic, granitic, and dyke rocks within the Yellowknife Basin.

Table 10.1 Descriptions and locations of  $^{40}\text{Ar}/^{39}\text{Ar}$  dating samples from the Gordon Lake region.

Sample number	Sample Description	Location
TS83-04	Biotite-rich (10-15%) white feldspar/grey quartz breccia	Underground from Kidney Pond Zone 1
TS22/6/8	White muscovite-rich granite	Spud Lake Pluton
TS86-84	Grey-black siltstone with visible metamorphic biotites	Proximal to Kidney Pond Zone 1
TS86-84	Grey siltstone with crenulated metamorphic biotites	Proximal to Kidney Pond Zone 1
TS12/6/4	Amphibole (hornblende) from mafic volcanic unit	Cameron River Volcanic Belt

A good summary of U-Pb, Pb-Pb, K-Ar, and Rb-Sr geochronological data within the Yellowknife region is provided by Easton (1984). From this compilation he recognized a clustering of K-Ar and Rb-Sr ages around 2500-2575 Ma, with K-Ar and Rb-Sr ages generally 100 million years younger than corresponding U-Pb zircon ages for the same unit. He also concluded that the U-Pb and Pb-Pb ages approximate the ages of volcanism and plutonism, whereas the K-Ar and Rb-Sr isotopic systems were totally or partially reset by later thermal events.

Recent U-Pb zircon dates of Henderson et al. (1987) and van Breemen et al. (1987) have provided constraints on the time of volcanism and plutonism within the Yellowknife Basin and other parts of the Slave Province (Figures 10.1 to 10.3). U-Pb dates for the basement vary from 2819 +30/-41 Ma for parts of the Sleepy Dragon Complex (Henderson et al. 1987) to 3964 ± 3 Ma for a tonalitic gneiss in the west of the Slave (Bowring et al. 1989). Volcanism within the Yellowknife Volcanic Belt spanned a period of at least 50 million years (ranging from 2660-2710 Ma; Henderson et al. 1987; Isachsen and Bowring 1989) and was synchronous with deposition of the Burwash Formation. This relationship is also supported by Pb/Pb ages (2685 Ma and 2700 Ma) from two detrital zircons of the Burwash Formation (Thorpe, 1971) and U-Pb dating of zircons from a metaturbidite of the Point Lake region (with ages of 2700 Ma and >2900 Ma for two groups of detrital zircons; Scharer and Allegre, 1982).

Plutonism within the Yellowknife Basin was synchronous with, and postdated both volcanism and sedimentation. van Breemen (1989) distinguished two separable plutonic events within the Slave Province; an older one at 2650-2685 Ma and a younger one at 2580-2625 Ma. The two suites of plutonic rocks are also characterised by a change in composition from early tonalites and megacrystic granodiorites, to later two mica

Figure 10.1 Some recent U-Pb zircon ages for the Slave Province and Yellowknife Basin. Adapted from Thompson, (1989, Figure 2).

- 1 - 8 from Henderson et al. (1987)
- ▲ 1 - 6 from van Breemen et al. (1987)
- 1 - 6 from Isachsen and Bowring (1989)
- ☆ 1 from Bowring et al (1988)
- ★ 1 from Bowring et al. (1989)
- 1 from Nikic et al. (1980)

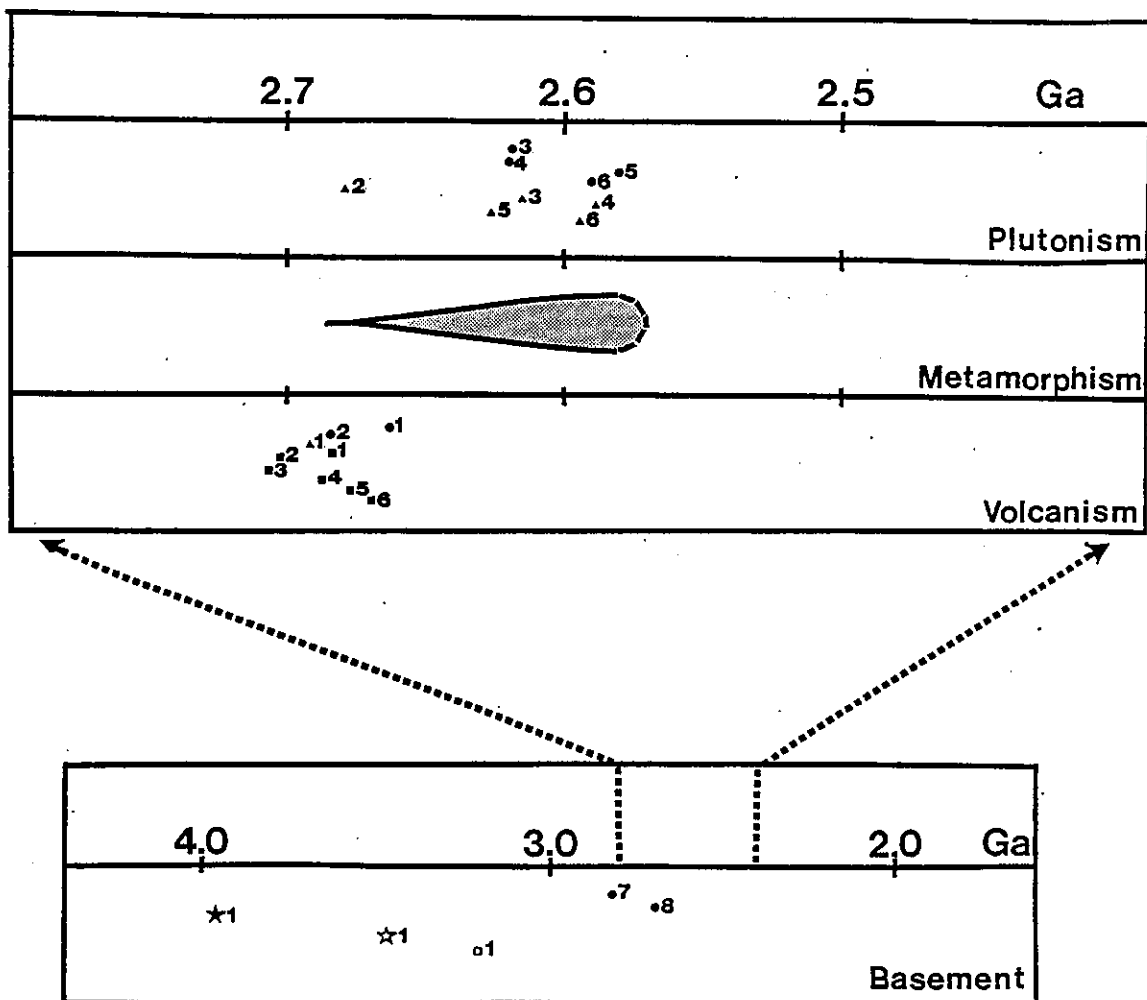


Figure 10.2 Location of U-Pb age dates in Figure 10.1. Map of the Slave Province adapted from Thompson (1989a).

- 1 - 8 from Henderson et al. (1987)
- ▲ 1 - 6 from van Breemen et al. (1987)
- 1 - 6 from Isachsen and Bowring (1989)
- ★ 1 from Bowring et al (1988)
- ★ 1 from Bowring et al. (1989)
- 1 from Nikic et al. (1980)

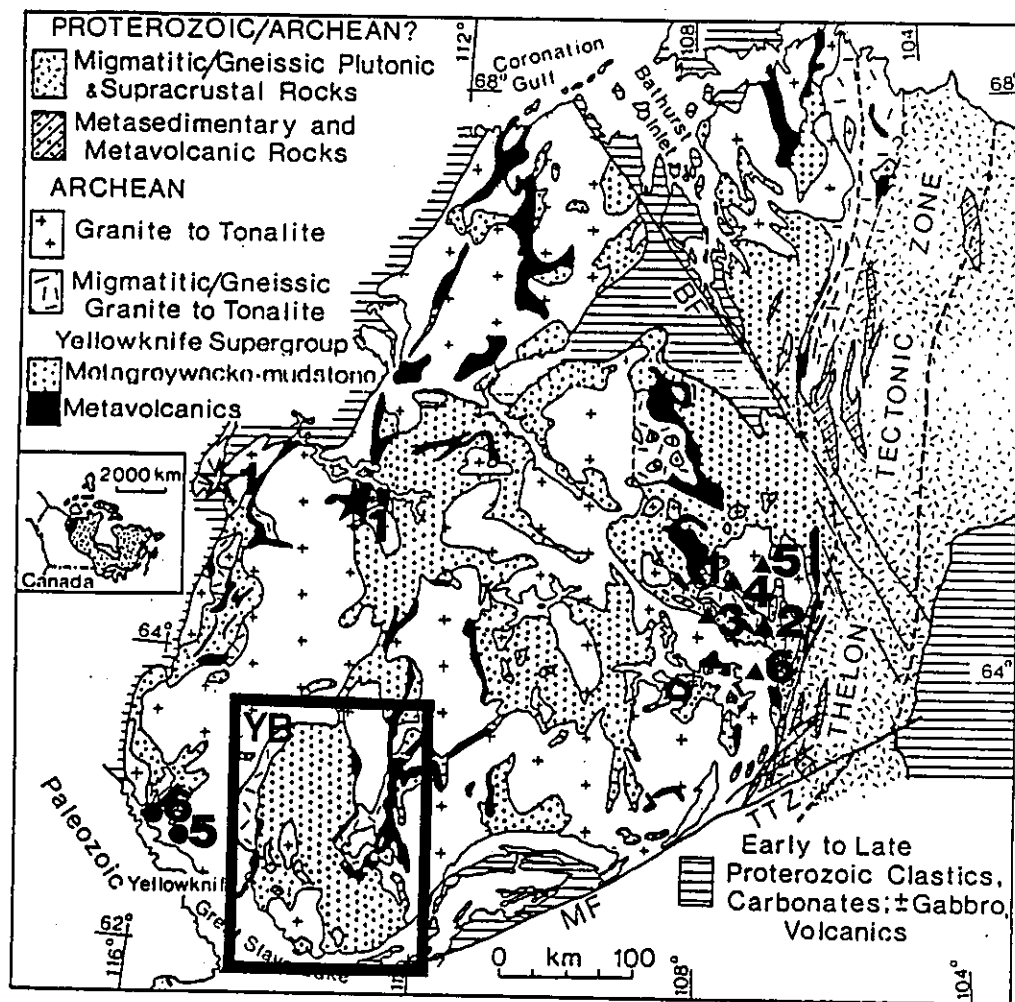
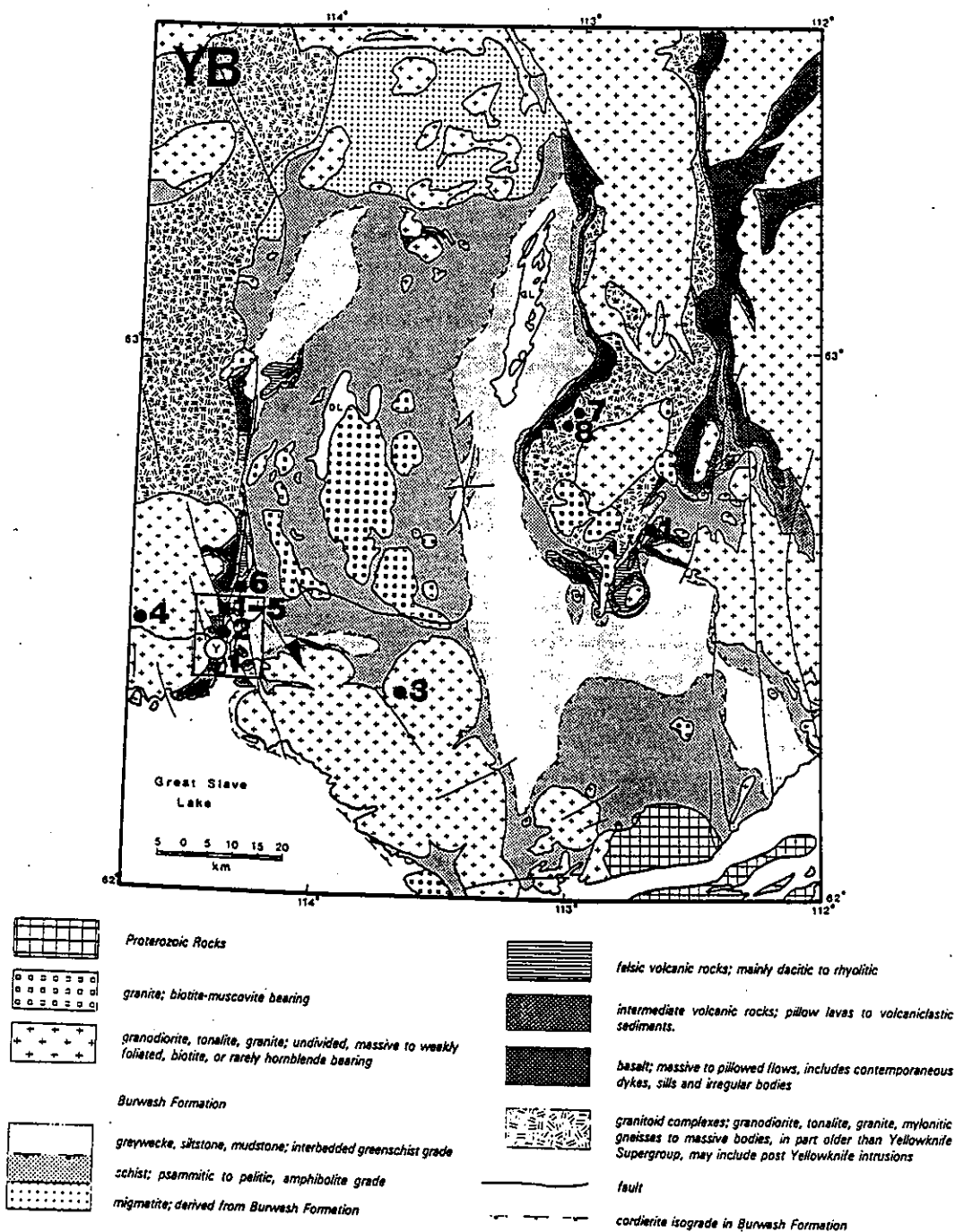


Figure 10.3 Location of U-Pb dates in Figure 10.1. Map of the Yellowknife Basin adapted from Henderson (1987).

- 1 - 8 from Henderson et al. (1987)
- ▲ 1 - 6 from van Breemen et al. (1987)
- 1 - 6 from Isachsen and Bowring (1989)
- ☆ 1 from Bowring et al (1988)
- ★ 1 from Bowring et al. (1989)
- 1 from Nikic et al. (1980)





granites and monzogranites. Thompson (1989a, 1989b) correlates these times of plutonism with regional peak metamorphic conditions at approximately 2600 Ma.

The only  $^{40}\text{Ar}/^{39}\text{Ar}$  dating within the region includes preliminary work on muscovites from gold-quartz veins of the Yellowknife Volcanic Belt (Webb and Kerrich, 1986). These muscovites gave ages of 2400 Ma and 2000 Ma, and were interpreted as the time of vein emplacement and a later thermal disturbance, respectively.

### 10.3 SAMPLE DESCRIPTIONS

All five  $^{40}\text{Ar}/^{39}\text{Ar}$  samples come from the Gordon Lake region (Figures 10.4 and 10.5). The hornblende sample (TS12-6-4) was taken from a mafic unit within the Cameron Volcanic Belt and was chosen because of hornblende's high blocking temperature (close to that of peak metamorphic conditions for the region). The muscovite sample (TS22-6-8), taken from the Spud Lake granite, was selected because it provides a lower age limit for metamorphism (as the granite was emplaced post- $D_3$ ; Section 5.1) and a minimum age of late pluton emplacement. The three biotite samples (TS83-04, TS86-94 and TS86-94) were chosen from a 1-km<sup>2</sup> area around the Kidney Pond, so that constraints might be placed on the cooling conditions of metamorphism and mineralization. The mineralization-related biotite (TS83-84) was taken from within the gold-bearing, Kidney Pond Zone 1 quartz-breccia. TS86-94 and TS86-84 are representative metamorphic (syn- $D_3$ ) biotites; but they differ in that TS86-84 was taken from a fine-grained siltstone that underwent post-metamorphic ( $D_4$ ) crenulation, whereas TS86-94 was taken from a fine-grained siltstone with no crenulation.

**Figure 10.4** Locations and  $^{40}\text{Ar}/^{39}\text{Ar}$  spectra of Gordon Lake muscovite, hornblende, and biotite samples. Rock types include: 1) Cameron River Volcanic Belt; 2) greenschist-facies metaturbidites of the Burwash Formation; 2a) amphibolite-facies metaturbidites of the Burwash Formation; 3) early and late granitic plutons; and 4) Sleepy Dragon Basement Complex.

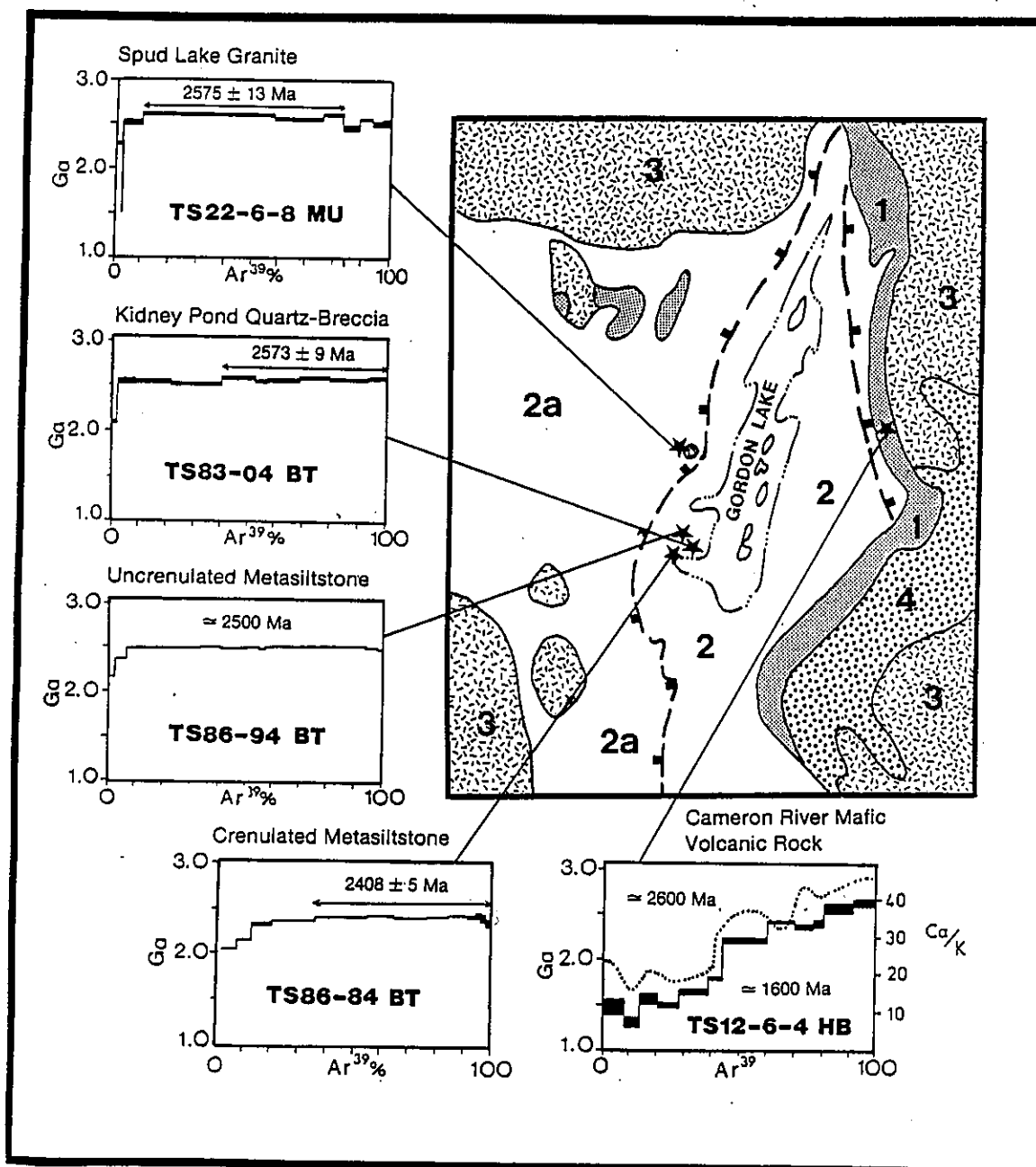


Figure 10.5 Photomicrographs of dating samples displaying fabric and textural relationships. (Scale bars  $\approx$  1 mm.)

A) The hornblende (TS12-6-4) is dark green, recrystallized with relict grains (up to 0.5-1 mm in size), and of probable metamorphic origin.

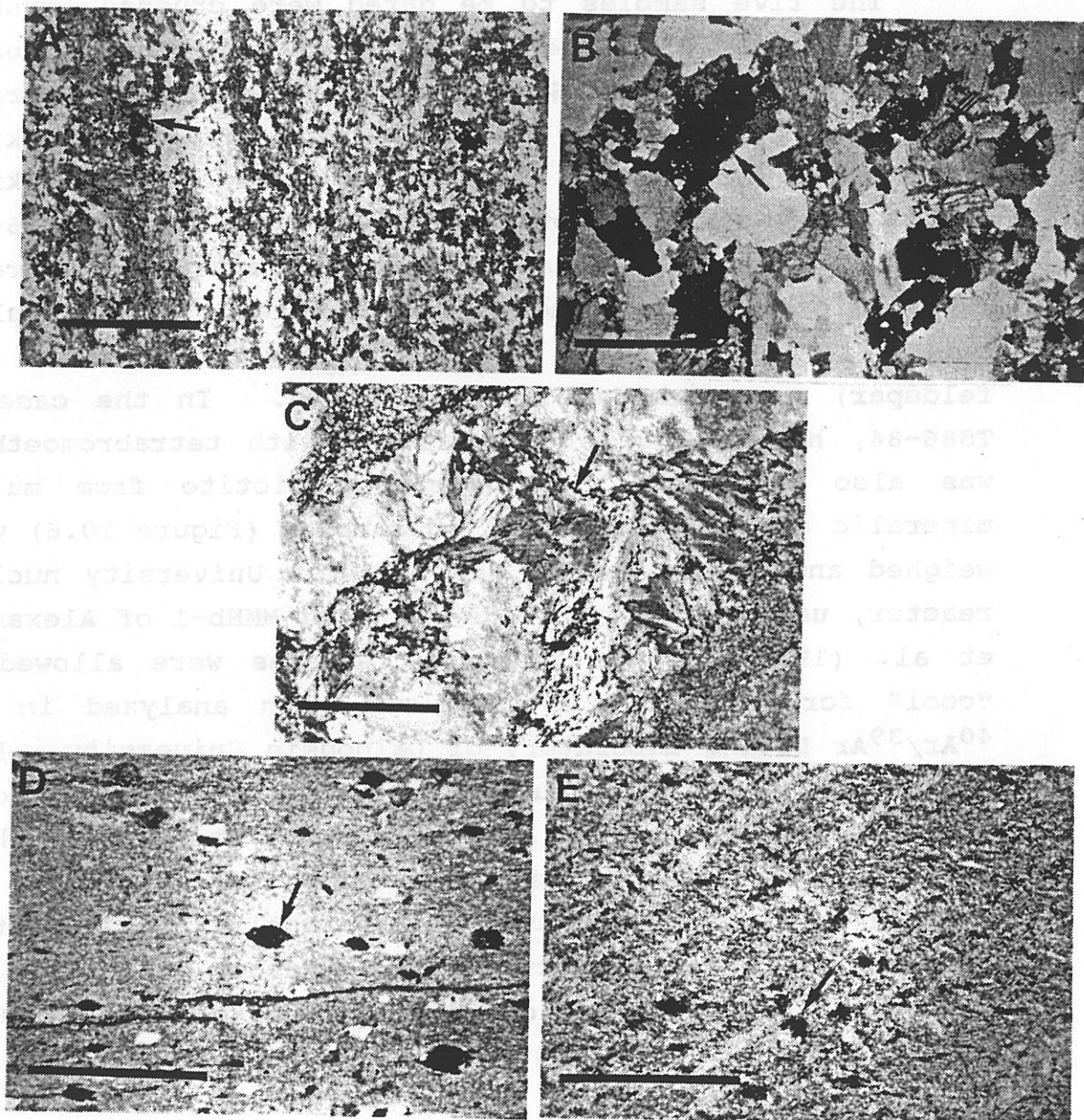
B) The muscovite (TS22-6-8) is coarse-grained (0.5-3 mm), occurs along with quartz and plagioclase, and makes up to 10% of the granite.

C) The quartz-breccia biotite (TS83-04) is purple-brown, coarse-grained (1-5 mm), and occurs as stellate masses with the K-feldspar and grey quartz (Section 7.3).

D) The uncrenulated, metamorphic biotite (TS86-94) is dark brown, 0.5-1 mm in size, deflects the  $S_{3S}$  fabric, has ( $D_3$ ) quartz-chlorite pressure shadows, and quartz inclusion trails sub-parallel to  $S_{3S}$  (Section 5.3.1)

E) The crenulated biotite (TS86-84) is finer (0.24-0.5 mm) grained than TS86-94, deflects the  $S_{3S}$  fabric, has ( $D_3$ ) quartz-chlorite pressure shadows, quartz inclusion trails sub-parallel to  $S_{3S}$ , and is folded and deformed by  $D_4$  (Section 5.3.1).

Figure 10.5



10.5. STRUCTURE AND AVERAGE PLATEAU AGES  
 The hornblende (TS17-2-4) spectrum displayed a sharp age gradient with two broad steps (at approximately 1600 and 760 Ma) that coincide with variations in Ca/K ratio (Figure 10.4 and Table A10.1). All the ages displayed relatively undisturbed spectra (Figure 10.4 and Table A10.2) from which a low plateau age was possible to calculate. The low plateau ages (LPA) and errors

#### 10.4 SAMPLE PREPARATION AND ANALYSIS

The five samples to be dated were crushed, ground, sized, and washed in the conventional manner. The coarse mica in samples TS22-6-8 and TS83-64 was easily separated from other minerals by paper panning and hand-picking, whereas the hornblende required only minor handpicking. The two fine-grained biotite samples (TS86-84 and TS86-94) were first concentrated as a magnetic fraction by a Frantz isodynamic separator, and then impurities (such as multi-mineralic grains of biotite, quartz, chlorite, and feldspar) were removed by handpicking. In the case of TS86-84, heavy liquid concentration with tetrabromoethane was also successful in separating biotite from multi-mineralic grains. The purified samples (Figure 10.6) were weighed and irradiated at the McMaster University nuclear reactor, using the hornblende standard MMHb-1 of Alexander et al. (1978). The irradiated samples were allowed to "cool" for at least a month and then analyzed in the  $^{40}\text{Ar}/^{39}\text{Ar}$  Dating Laboratory of Dalhousie University. Each sample was placed in a quartz-tube system, connected to an MS-10 mass spectrometer, and heated in a step-wise fashion by a Lindberg furnace. Each increment of extracted gas was cleaned by a titanium getter and charcoal finger, and then measured by the mass spectrometer. Further details of the analytical procedure are outlined in Muecke et al. (1988), and Reynolds et al. (1987).

#### 10.5 SPECTRA AND AVERAGE PLATEAU AGES

The hornblende (TS12-6-4) spectrum displayed a steep age gradient with two broad steps (at approximately 1600Ma and 2600 Ma) that coincide with variations in Ca/K ratio (Figure 10.4 and Table A10.1). All the micas displayed relatively undisturbed spectra (Figure 10.4 and Tables A10.2 - A10.5) from which it was possible to calculate, in three cases, average plateau ages (APA) and errors

Figure 10.6 Photomicrographs of the separated material used for  $^{40}\text{Ar}/^{39}\text{Ar}$  dating. Note the purity of mica samples 83-04, 86-94 and 22-6-8 as compared to the more multi-mineralic biotite in 86-84. (Scale bars = 1 mm.)

A) Sample TS12-6-4 includes 95% hornblende with 5% multi-mineralic grains of hornblende and quartz.

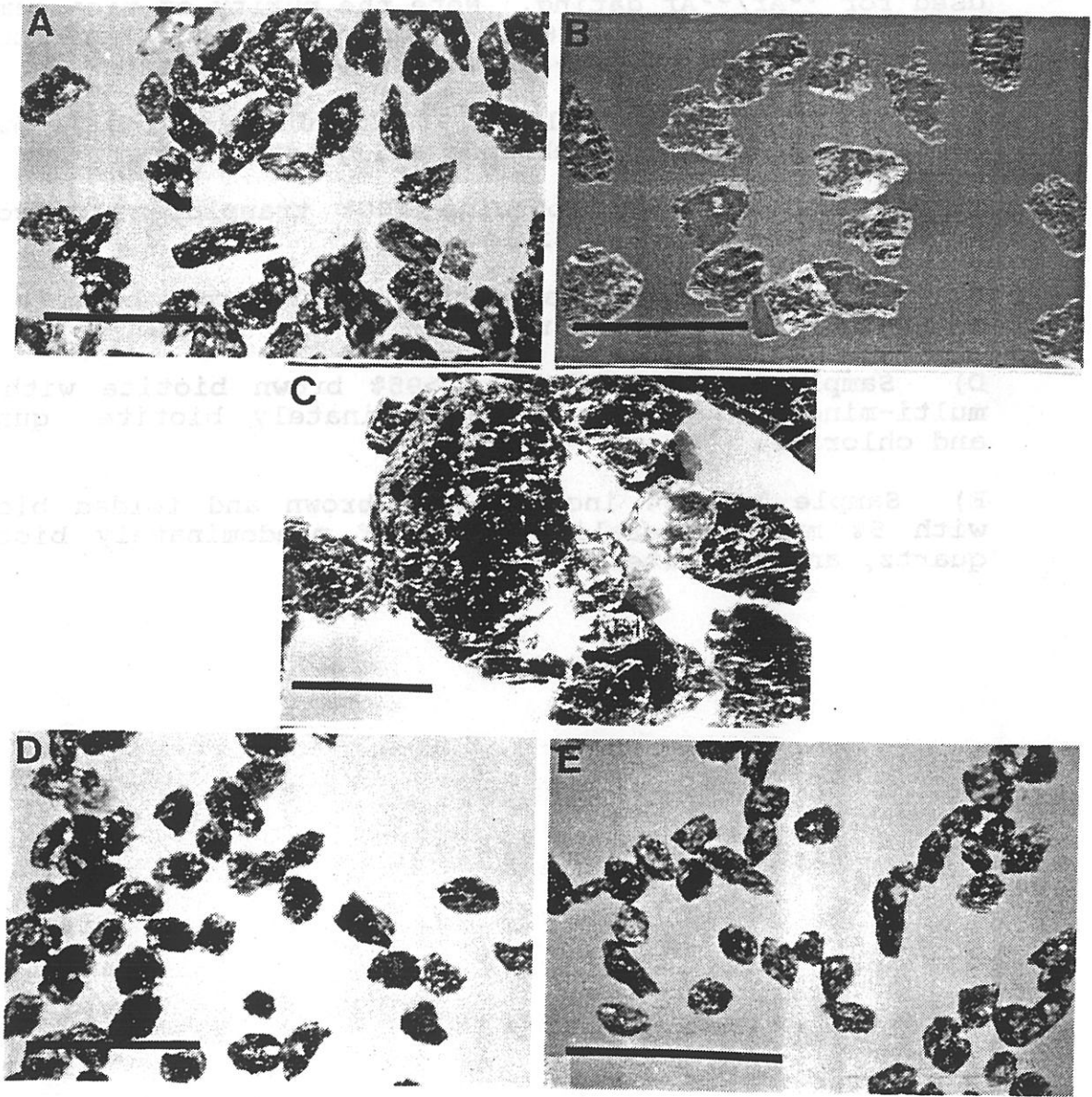
B) Sample TS22-6-8 contains 100% translucent muscovite with no other grains visible.

C) Sample TS83-04 contains 100% purple-brown biotite with no visible signs of alteration.

D) Sample TS86-94 includes >95% brown biotite with <5% multi-mineralic grains of predominately biotite, quartz, and chlorite.

E) Sample TS86-84 includes 95% brown and folded biotite with 5% multi-mineralic grains of predominately biotite, quartz, and chlorite.

Figure 10.6



(Appendix A10.2). The breccia biotite (TS83-04), Spud Lake muscovite (TS22/6/8), and crenulated metamorphic biotite (TS86-84) produced average plateau ages of  $2573 \pm 9$  Ma,  $2575 \pm 13$  Ma, and  $2408 \pm 5$  Ma, respectively. The uncrenulated metamorphic biotite (TS86-94) failed the criteria required to define an average plateau, with only 48-49% of the  $^{39}\text{Ar}$  released forming a contiguous gas fraction. However, the spectrum still represents a closure age for the uncrenulated metamorphic biotite at approximately 2500 Ma.

#### 10.6 MICROPROBE ANALYSIS OF BIOTITES AND HORNBLENDE

Data for major oxides were obtained from polished grain mounts of the three biotites and hornblende samples. The biotite data (Figure 10.7 and Table A10.7) indicate that the metamorphic biotites (TS86-94 and TS86-84) are distinct in composition from the breccia biotite (TS83-04), with a higher  $\text{Fe}/(\text{Fe}+\text{Mg})$  ratio and more  $\text{Al}_{\text{IV}}$  substituted for  $\text{SiO}_2$ . The  $\text{Fe}/(\text{Fe}+\text{Mg})$  ratio can be used to estimate the activation energy of argon within the biotite structure using data of Harrison et al. (1985), whereby the activation energy of argon decreases with increasing  $\text{Fe}/(\text{Fe}+\text{Mg})$ . In this case, the metamorphic biotites are less argon retentive than the breccia biotite, and will therefore release argon more easily during the step-heating procedure (Figure 10.8).

Preliminary data from the hornblende sample (TS12-6-4) indicates that it is a calcic-ferro-hornblende (Table A10.6). Only one type of hornblende is apparent in sample TS12-6-4, even though there is some suggestion from the Ca/K spectra (Figure 10.4) that two are present.

#### 10.7 INTERPRETATION OF PLATEAU AGES AND SPECTRA

The steep age gradient of the hornblende spectrum (TS12-6, Figure 10.4) indicates that at least one thermal



Figure 10.7 Phlogopite-biotite diagram with the compositions of the quartz-breccia biotite (TS83-04, open circles), the uncrenulated metamorphic biotite (TS86-94, filled squares), and the crenulated metamorphic biotite (TS86-84, open squares).

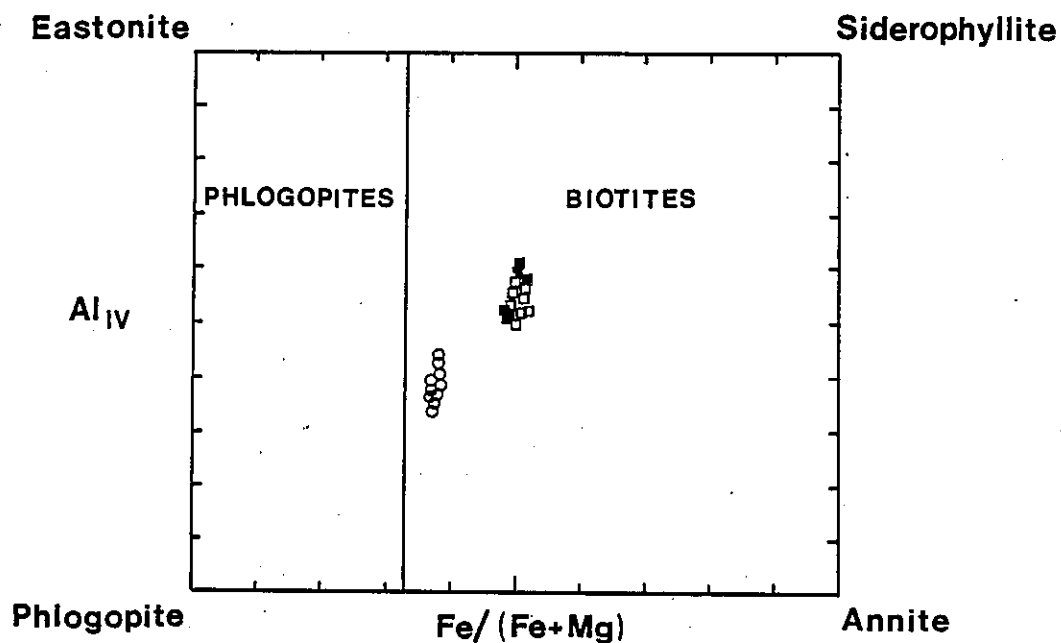
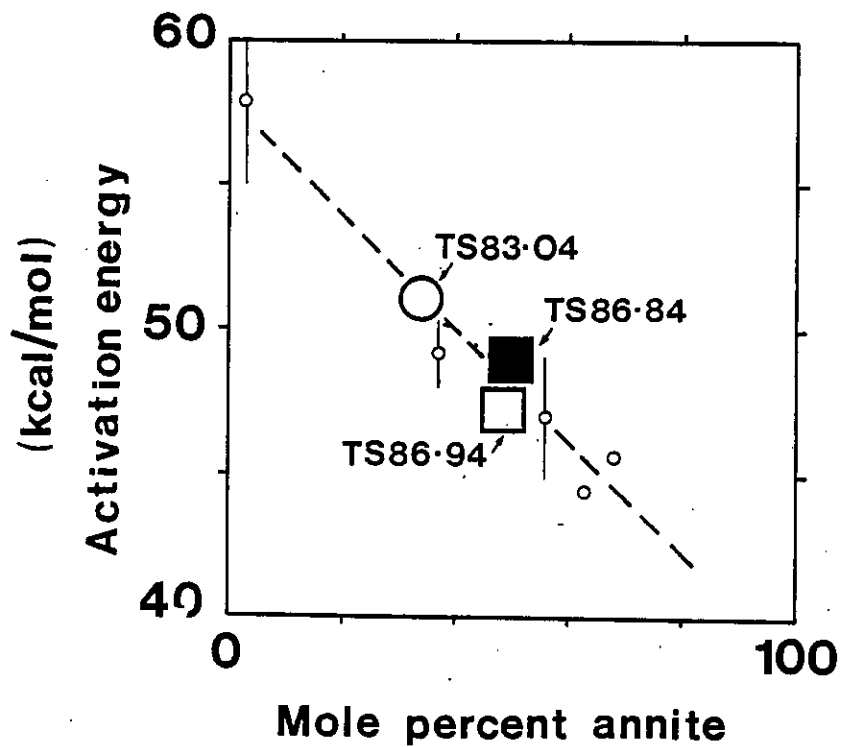


Figure 10.8 Plot of activation energy versus mole percent annite defined from data of Harrison et al. (1985; small open circles), with the linear relationship between activation energy and Fe/(Fe+Mg) composition (dashed line), and the average compositions of the quartz-breccia biotite (84-03) and metamorphic biotites (86-94 and 86-84).

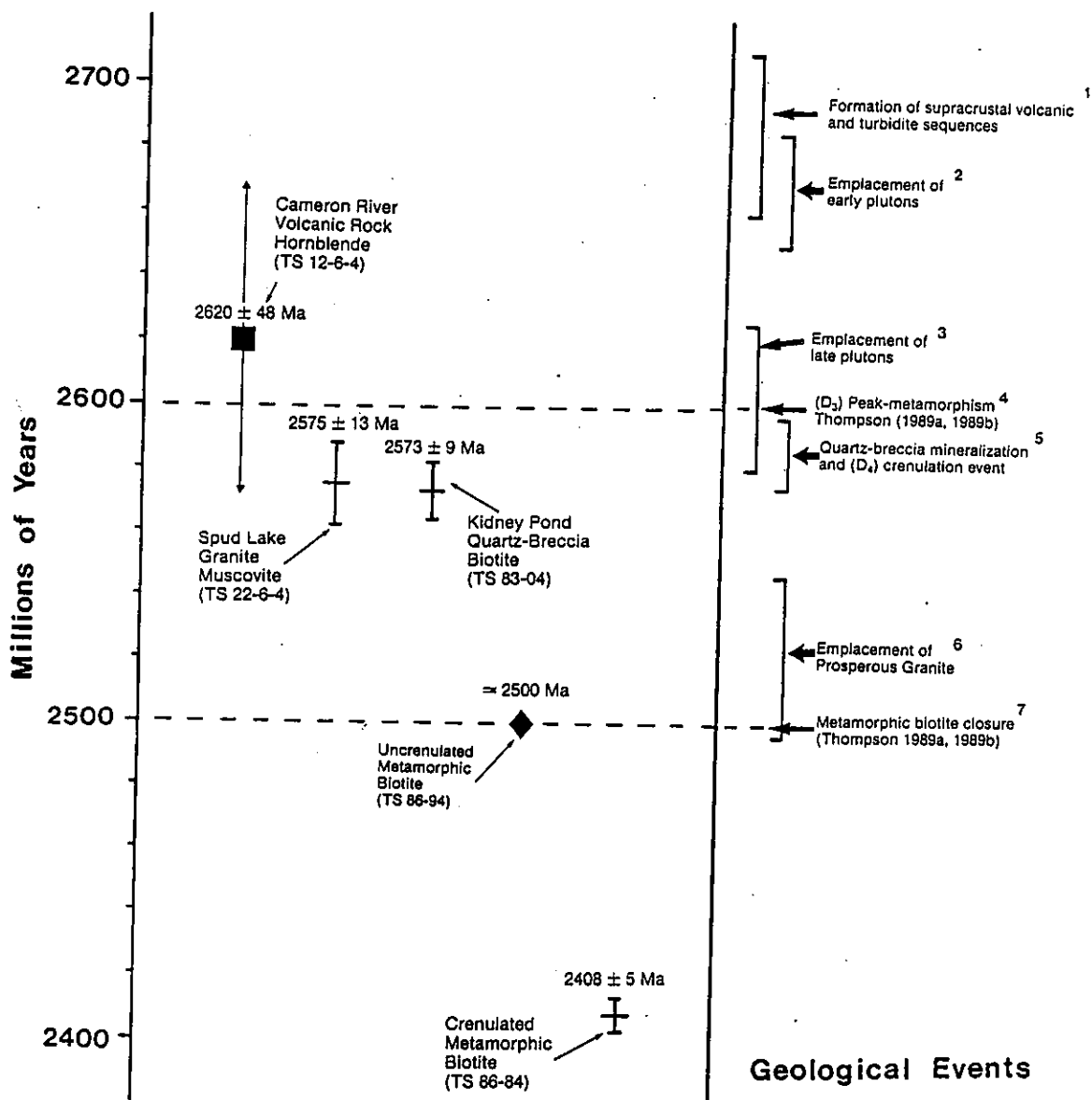


event overprinted the metamorphic hornblende. This event obviously post-dates the formation of the Cameron Volcanic Belt; which is similar in age to the Yellowknife Volcanic Belt dated at between 2660-2710 Ma (Figure 10.9; Henderson et al. 1987; Isachsen and Bowring, 1989). The hornblende spectrum displays two broad steps that coincide with distinct variations in Ca/K ratios. These two steps are either due to argon degassing of two hornblende generations or are the result of a series of thermal events. Petrographic and preliminary microprobe data do not provide evidence for two types of hornblende, so the latter explanation is preferred. The last heating-step age of the hornblende spectrum at  $2620 \pm 48$  Ma represents an approximate age for the formation of the metamorphic hornblende. This correlates well with the age of regional peak metamorphism (c.a. 2600 Ma) determined from metamorphic modelling of the Slave Province (Thompson, 1989a, 1989b). The broad step at approximately 1600 Ma is also possibly the result of a later overprinting thermal event; such as the emplacement of the Mackenzie dyke swarms during the Early to Mid Proterozoic (c.a. 1600-2000 Ma; Easton, 1984; Henderson, 1985) or detachment faulting (H. Helmstaedt, 1991, personal communication).

The average plateau age of  $2575 \pm 13$  Ma for the muscovite from the Spud Lake Pluton (TS22/6/8) represents the time at which the mineral cooled below its blocking temperature of  $350 \pm 50^\circ\text{C}$  (Jäger, 1979). This closure age is close to the time of the pluton emplacement, and is similar to a Rb-Sr whole rock age obtained for the Prosperous Granite Suite ( $2521 \pm 25$  Ma, Green et al. 1968). Since the Spud Lake granite cuts the syn-metamorphic D3 cleavage the plateau age also provides a lower constraint on the time of regional peak-metamorphism.

The spectra for the three biotite samples are more difficult to interpret as there are no comparable data from

Figure 10.9 Geological events within the Yellowknife basin and  $^{40}\text{Ar}/^{39}\text{Ar}$  dates from Gordon Lake. Sources of data for geological events include: 1) U-Pb zircon ages of Henderson et al. (1987) and Isachsen and Bowring (1989); 2) U-Pb zircon ages from van Breemen (1989); 3) U-Pb zircon ages from van Breemen (1989); 4) time of regional peak-metamorphism from thermal modelling of Thompson (1989a, 1989b); 5) time of quartz-breccia and crenulation event from structural relationships; 6) Rb-Sr whole rock age from Green et al. (1968); and 7) K-Ar closure age of metamorphic biotite from thermal modelling of Thompson (1989a, 1989b). (The horizontal lines with error bars represent  $^{40}\text{Ar}/^{39}\text{Ar}$  average plateau ages, the diamond an approximate closure age of the uncrenulated metamorphic biotite and the square the last heating-step age of the hornblende.)



the metaturbidites. Any interpretation of these spectra must take into consideration: i) the variation in grain size and purity between samples; ii) the difference in composition between the metamorphic and breccia biotites; iii) the lack of separation between individual closure events (where the range of three spectra is 160-170 million years; i.e., only 6-7 % of their total age); iv) the close proximity between sample locations.

The spectrum of uncrenulated metamorphic biotite (TS86-94) does not define an average plateau age, but indicates a closure age at approximately 2500 Ma. This closure age probably records post-metamorphic cooling of the metaturbidite pile below  $300 \pm 50^\circ\text{C}$ , and agrees with a K-Ar cooling age for biotite predicted from metamorphic modelling of the Slave Province (Thompson, 1989a, 1989b).

The younger age of  $2408 \pm 5$  Ma for the crenulated metamorphic biotite (TS86-84) could possibly be explained by: i) a 200 million year deformational event post-dating biotite closure, ii) a loss of radiogenic  $^{40}\text{Ar}$  during crenulation (e.g., Kligfield et al. 1986), or iii) the effect of the greater amount of impurities within this sample. The first explanation is difficult to reconcile with the structural history of the region. The other two explanations are more likely, as both would lower the argon retentivity of and develop a "leaky" biotite from which argon could more easily escape.

The average plateau age of  $2573 \pm 9$  Ma for the Kidney Pond quartz-breccia biotite (TS83-04) places a lower constraint on the time of mineralization and supports the structural hypothesis (Chapter 6) that breccia formation occurred just after peak-metamorphism. However, it is unclear why the age of the quartz-breccia biotite (TS83-04) is so significantly older than the metamorphic biotites (TS86-94 and TS86-84). Possible explanations for the discrepancy in plateau ages include: i) variation in

biotite grain size and sample quality; ii) differences in composition and diffusion characteristics between the breccia biotite and the metamorphic biotites (Section 10.6); iii) less argon equilibration between breccia biotite and its host compared to the metamorphic biotite and its host rock; and iv) the association of brecciation with a K-rich hydrothermal fluid and a zone of excess  $^{40}\text{Ar}$  (e.g., Rama et al. 1965). These possibilities cannot be discriminated without further work.

#### 10.8 A THERMOCHRONOLOGIC MODEL FOR METAMORPHISM AND QUARTZ-BRECCIATION

The geochronological data obtained in this study are by no means conclusive, but provide some constraints on the time of metamorphism and quartz-breccia mineralization. It is suggested that the Gordon Lake region reached ( $D_3$ ) peak metamorphic conditions at approximately 2600 Ma. This time is constrained by the last heating-step age of the hornblende ( $2620 \pm 48$  Ma) and by the post-metamorphic emplacement of the Spud Lake granite ( $2575 \pm 13$  Ma). Following peak metamorphism, as the metaturbidite pile cooled, a structurally focussed hydrothermal system developed within the centre of the refold during ( $D_4$ ) rotation of the refold's east limb. The time of the structural focussing and quartz-brecciation event is uncertain, but it did pre-date the  $2573 \pm 9$  Ma closure age of the breccia biotite (TS83-04). The cooling metaturbidite pile was also intruded (possibly slightly post-dating brecciation?) by the Spud Lake pluton at  $2575 \pm 13$  Ma. Finally, at approximately 2500 Ma the metaturbidite pile cooled below the closure temperature ( $300 \pm 50^\circ\text{C}$ ) of the metamorphic biotite (TS86-94).

10.9 SUMMARY OF  $^{40}\text{Ar}/^{39}\text{Ar}$  DATING STUDY

Five samples (three biotites, a hornblende, and a muscovite) were analyzed by the  $^{40}\text{Ar}/^{39}\text{Ar}$  dating technique, in order to provide temporal constraints on metamorphism and quartz-breccia mineralization within the Gordon Lake region. The last heating-step age of  $2620 \pm 48$  Ma for a metamorphic hornblende from the Cameron River Volcanic Belt supports a 2600 Ma age proposed for peak metamorphism within the Slave Province (Thompson 1989a, 1989b). A muscovite plateau age of  $2573 \pm 13$  Ma for the post-metamorphic Spud Lake pluton places a lower constraint on the 2600 Ma age and provides an approximate age for late granite emplacement. A plateau age of  $2573 \pm 9$  Ma for a biotite from the Kidney Pond quartz-breccia zone gives a minimum age for mineralization, and is consistent with the hypothesis that brecciation is a late metamorphic event. The spectrum of an uncrenulated metamorphic biotite indicates a closure age, for cooling of the metaturbidite pile below  $300 \pm 50^\circ\text{C}$ , of approximately 2500 Ma. A crenulated metamorphic biotite gives a plateau age of  $2408 \pm 5$  Ma. This age is interpreted not to represent a specific event, but is rather the result of argon loss/leakage during crenulation.

## CHAPTER 11

### TOWARDS A GENETIC MODEL FOR THE CONCENTRATION OF GOLD BEARING QUARTZ-BRECCIA ZONES AT GORDON LAKE

#### 11.1 INTRODUCTION

In Chapters 6 and 7 a structural/lithological model was developed to explain the occurrence of gold-bearing quartz-breccia zones in the central region of the Gordon Lake refold. In Chapters 8, 9, and 10 specific aspects of this model were investigated by a combination of fluid inclusion, geochemical, and  $^{40}\text{Ar}/^{39}\text{Ar}$  dating techniques. The aims of these studies were to provide constraints on: i) the P/T conditions and composition of the mineralizing fluid; ii) the geochemistry of the quartz-breccia zones and their host lithologies; and iii) the timing of peak-metamorphism and quartz-brecciation. The purpose of this chapter is to integrate the field and laboratory data into a comprehensive genetic model for the formation of gold-bearing quartz-breccia zones.

#### 11.2 APPLICABILITY OF PREVIOUSLY SUGGESTED GENETIC MODELS

The controversy over the origin of MHGD within the Yellowknife Basin and elsewhere has a long history (Boyle, 1979). However, at least three end-member models have been suggested: i) an epigenetic model with mineralizing fluids derived from granites (e.g., Newhouse, 1936; Lindgren, 1933); ii) a syngenetic exhalative association (e.g., Haynes, 1986); and iii) an epigenetic model with mineralizing fluids derived from metamorphic devolatilization (e.g., Boyle, 1961; Henley et al., 1976; Graves and Zentilli, 1982).

##### 11.2.1 Genesis Related to Granites

Within the Yellowknife Basin earlier workers (Henderson and Jolliffe, 1939; Coleman, 1957; McConnell,



1964; Chary, 1971) proposed that the quartz veins within the Burwash metaturbidites were derived from a magmatic source associated with emplacement of the granites; whereby mineralized fluids migrated from the granites into structurally prepared openings. Henderson and Jolliffe (1939) noted variations in vein mineralogy with the differing metamorphic grade of the metaturbidites (from quartz-feldspar-tourmaline veins in amphibolite-facies rocks to quartz-carbonate in the greenschist-facies rocks). They concluded that since the granites were responsible for the regional metamorphic pattern, then they were also responsible for the varied vein mineralogy. This interpretation concurred with other prevailing hypotheses of the time (e.g., Lindgren, 1933; Newhouse, 1936).

At Gordon Lake the effects of granite intrusions are not obvious. The nearest outcrop of granite to Kidney Pond quartz-breccia zone is located approximately 15 km to the north at Spud Lake. However, a granitic substratum (of late intrusives and/or basement) probably occurs at 5-10 km depth as suggested by McGrath et al. (1983). Thompson (1978, 1989a, 1989b) and Henderson (1985) indicated that regional metamorphism of the Burwash Formation was the result of "thermal doming" associated with granite intrusion at depth. However, the exact contribution of magmatic or metamorphic fluids to the formation of gold deposits in the Yellowknife Basin is unclear, as indicated from the stable isotope studies of Swatton (1987), Kerrich and Fyfe (1987), and Kerrich and Fyfe (1988). At Gordon Lake there is little direct evidence of a magmatic fluid associated with the formation of the quartz-breccias, which: i) have a simple "metamorphic" mineralogy (i.e., quartz, K-feldspar, biotite, chlorite, arsenopyrite, pyrrhotite and pyrite; Section 7.3); ii) lack anomalous granophile elements (e.g., Sn, Mo, Be, B, Li, and F; Chapter 9); and iii) occur within the greenschist facies of

the Burwash Formation (Figure 2.1). However, it is suggested that the granites may have played an important role in heating and consequently, metamorphically dewatering the fluid-rich sedimentary pile, rather than directly contributing significant amounts of magmatic fluid.

#### 11.2.2 Syngenetic and Syngenetic-Epigenetic Models

Syngenetic models for MHGD require the deposition of gold, sulphides, and quartz in an exhalative environment (Haynes, 1986). This model is more readily applied to gold deposits hosted by iron formation (Kerswill, 1986; Fripp, 1976). At Gordon Lake, the difficulty with this model is that the timing of gold/quartz emplacement is neither syn-sedimentary nor pre-metamorphic. A modified syngenetic-epigenetic model was suggested by Caelles (1984, 1985) for the gold-bearing, quartz-breccia zones at Kidney Pond. He hypothesised that: i) the black siltstones were crystal tuffs formed in a restricted basin; ii) gold was introduced coevally or just after sedimentation; and iii) the quartz was derived from remobilized siliceous beds and emplaced into fracture zones during deformation of the auriferous black siltstones. His hypothesis was based on the strata-bound character of the breccia bodies within black siltstone beds and the common occurrence of gold and sulphides with carbonaceous material. This hypothesis appears inconsistent with the results of the present study. It is more likely that the quartz material was generated away from the region of brecciation, and was transported with gold to the site of mineralization/dilation in the latter stages of metamorphism. Thus one source for the mineralizing fluids is invoked, rather than two.

#### 11.2.3 Genesis by Lateral Secretion and Metamorphic Fluids

Folinsbee (1942) hypothesised that gold deposits in

the Yellowknife region were related to metamorphic rather than granitic fluids. Later, Boyle (1961) developed a lateral fluid secretion model for the formation of gold-quartz occurrences of the Yellowknife region. This model involved the migration of metamorphic fluids into both shear zones within the Yellowknife Volcanic Belt and dilatant zones within the deformed metasediments of the Burwash Formation (Boyle 1961, Figure 29). As these hot metamorphic fluids migrated into dilational openings, CO<sub>2</sub>, S, Au, and chalcophile elements were mobilized and transported to the site of mineralization by diffusional processes (i.e. while the fluids were relatively stationary). This latter aspect of the model was later abandoned.

The metamorphogenic model, for other gold-quartz vein occurrences within the Burwash Formation, was further advanced by studies of Ramsay (1973), English (1981), and Swatton (1987). They suggested that: i) gold was transported as a bisulphide complex; ii) the mineralized fluids were focussed into dilational openings; iii) gold was precipitated due to a combination of temperature reduction and sulphidation.

Mineralogical, structural, metamorphic, and temporal data from this study support a similar hypothesis for the metamorphic generation, transport, and regional focussing of the gold-bearing fluids (Sections 11.3, 11.4 and 11.5). The concepts of fluid trapping and mechanisms of breccia formation are considered (Sections 11.6) along with the physico-chemical constraints on gold deposition (Section 11.7).

### 11.3 SOURCE OF METAMORPHIC FLUIDS (AND GOLD)

It is emphasised by many workers (e.g., Norris and Henley, 1976; Walther and Orville, 1982; Yardley, 1983) that sufficient fluids are present within a metasedimentary

pile to supply and develop significant quartz vein systems. Fluids available for quartz vein formation can be derived from both simple dewatering associated with compaction (i.e., the expulsion of intergranular water) and by metamorphic devolatilization (i.e., water released by mineral reactions and during cleavage formation; Fyfe et al. 1978; Etheridge et al. 1983).

The P/T conditions for metamorphic fluid generation at Gordon Lake are not well constrained by the mineral assemblages. However, the formation of biotite and cordierite at low pressures (2-5 kbars) and relatively high temperatures (500-700°C) is adequate to generate silica-rich fluids (Norris and Henley, 1976). Secondary fluid inclusions from quartz veins and breccias at Gordon Lake indicate a metamorphic fluid with a high salinity (25-30 wt % NaCl-CaCl<sub>2</sub> combined), high CH<sub>4</sub>/CO<sub>2</sub> ratios, a trapping temperature of 455 ± 40°C, and a trapping pressure of 2.0-3.5 kbars (Chapters 7 and 8). The origin of this saline fluid is unclear, but the most likely sources include: i) metamorphic devolatilization reactions and the tectonic expulsion of connate waters (e.g., Craw, 1990); ii) retrograde activity involving the hydration of minerals and the release of Na<sup>+</sup>, K<sup>+</sup>, and Ca<sup>2+</sup> (Crawford et al. 1979); or iii) an increase in the salinity of the fluid during fluid interaction with carbon-rich host rocks (e.g., Bottrell et al. 1988).

Important considerations for the evolution of a gold-bearing metamorphic fluid are: i) the stage at which gold is incorporated into the fluid, ii) the source of gold, and iii) how it is transported. Romberger (1984, 1986) concluded that no one rock type is a preferred source for gold, but rather the availability or greater mobility of gold in certain rock types is of more importance. However, there is a slight enrichment of gold in Archean ultramafic and mafic rocks, which has been attributed by some (Keays

and Scott, 1976; Keays 1984) to indicate a favourable source for gold.

At Gordon Lake the metaturbidites of the Burwash Formation pile provide the most likely source for gold because: i) the metaturbidites were deposited in a volcanic-rich tectonic setting that probably included a considerable component of mafic volcanic debris (Chapter 9); ii) gold is less tightly held within the metaturbidites due to the breakdown of detrital material by erosional, diagenetic, and metamorphic processes; and iii) the intrinsic pre- and syn-metamorphic permeability of a metaturbidite pile is high, and readily available for leaching of gold by metamorphic fluids.

#### 11.4 MECHANISMS OF FLUID TRANSPORT AND MIGRATION

The rate and quantity of metamorphic fluid released and transported within a metaturbidite pile depends upon the conditions of temperature, pressure, and rock permeability and porosity (Fyfe et al. 1978). Studies of rock permeability and porosity suggest that intergranular flow only accounts for a small proportion of the total fluid flow, and that most fluids travel along microfractures or larger scale fractures, such as veins (Walther and Orville, 1982; Yardley, 1986). Mechanisms and directions of fluid flow in low pressure\high temperature metasedimentary piles are controversial. Etheridge et al. (1983) indicated that large scale convective flow is likely under low P/high T metamorphic conditions, if an impermeable cap is present. This hypothesis was rejected by Wood and Walther (1986), who stated that the lack of a fluid potential gradient precluded convection, but favoured single-pass flow. However, leaching of gold from a metamorphic pile is probably more efficient in a convective system (Groves et al., 1987).

Pre-metamorphic deformation ( $D_0$ ,  $D_1$  and  $D_2$ ) of the

metaturbidites in the Gordon Lake region included extensive dewatering, with the expulsion of large volumes of intergranular pore fluids. These fluids were probably responsible for the formation of the pre-metamorphic bedding parallel (Type 1) and graywacke-hosted (Type 2) veins (Section 6.1). During (D<sub>3</sub>) peak-metamorphism (ca. 2600 Ma; Chapter 10) additional fluids were generated during devolatilization reactions and cleavage formation. These fluid probably accounted for the greater proportion of syn-D<sub>3</sub> veins (Types 3, 4, 5 and 7) and the formation of the gold-bearing quartz-breccia zones (Types III and IV).

#### 11.5 REGIONAL FOCUSING OF FLUIDS

A fundamental mechanism required for any anomalous region of veining or hydrothermal mineralization is fluid focussing (e.g., Etheridge et al. 1983, Fyfe and Kerrich, 1984). Focussing is a process whereby fluids are channelled preferentially into regions of dilation, and/or along zones of high permeability. Mechanisms of structural focussing are widely suggested for the formation of quartz-vein systems in shear zones (e.g., Boulter et al. 1987; Groves et al. 1987) by processes such as seismic and episodic pumping (Sibson et al. 1975, 1988). A less widely recognized, but equally important mechanism of structural focussing is related to dilatant zones in fold hinges; whereby the size of dilatant zones is dependent on the: i) competency contrasts between lithologies, ii) thicknesses and ratios of competent to incompetent beds, iii) availability of fluid, and iv) amount of imposed strain (e.g., Ramsay, 1967, 1974; Ramsay and Huber, 1987). Fluid focussing is also constrained by variations in lithology, which can control the rate of fluid production and rock permeability (e.g., Kreulen, 1980; Etheridge et al. 1983).

At Gordon Lake the principal mechanism for fluid focussing is the closure of the refold hinge. This closure

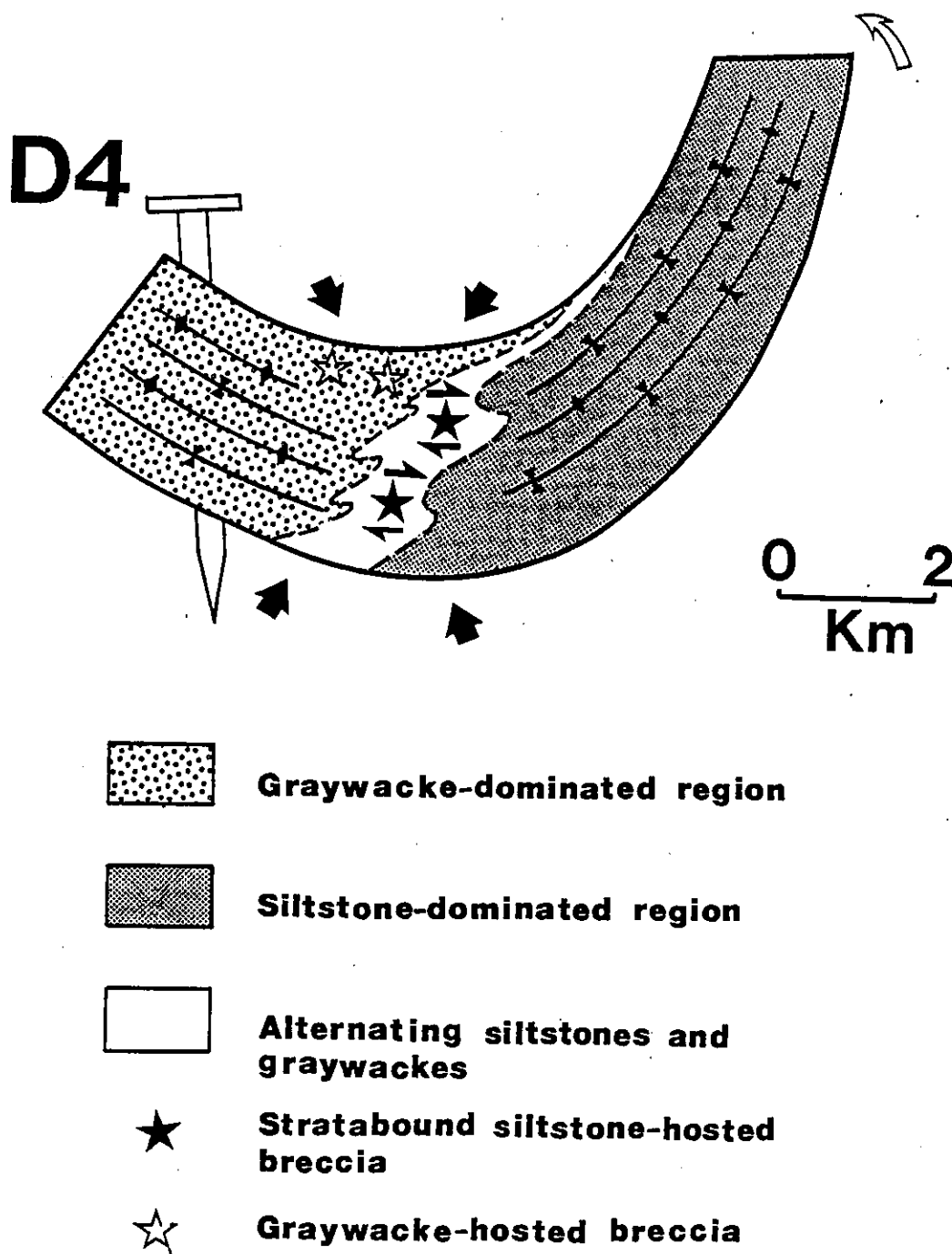
either developed during both D<sub>3</sub> and D<sub>4</sub> (forming a buckle-type fold, Figure 11.1), or during D<sub>4</sub> alone (in a type of shear zone, Section 5.6.2). In both cases dilations would develop and induce the focussing of fluids. Larger and more numerous dilations might occur if the refold underwent hinge migration, as a greater number of apparent hinge zones would have developed on the same fold. Other factors that might contribute to increased fluid flow in the refold centre include: i) the siltstone-dominated region (Section 5.2), which might act as a favourable lithological channel or locus for fluids (e.g., Kreulen, 1980); and ii) the vertical stretch, which if preferentially extenuated in the hinge region (Section 5.5), might provide a zone of high strain and an associated pressure gradient (e.g., Boulter et al. 1987).

These focussed fluids were responsible for the regional concentration of the Type III and Type IV quartz-breccias within the central part of the refold. However, further structural, lithological, and fluid pressure played important roles in the controlling the size, morphology, and mineralogy of the individual quartz-breccia zones.

#### 11.6 STRUCTURAL, LITHOLOGICAL AND FLUID PRESSURE CONSTRAINTS ON THE FORMATION OF TYPE III AND TYPE IV GOLD-BEARING QUARTZ-BRECCIA ZONES.

Field evidence indicates that the Type III and Type IV quartz-breccias are the result of syn-tectonic brecciation. This syn-tectonic or "implosion" type (Sibson, 1986) of brecciation is characterized by angular wall-rock fragments (with little to no evidence of clast rotation) that are surrounded by a quartz and K-feldspar matrix (Chapters 6 and 7). Similar breccias are found in the shear zones of AMVHGD where dilational zones occur at fault asperities or jogs (e.g., Melling et al. 1986; Sibson et al. 1988; Sibson, 1990). No transgressive faults or

Figure 11.1 Post-metamorphic ( $D_4$ ) deformation of the east limb of the Gordon Lake refold with accompanying fluid focussing and development of gold-bearing quartz-breccia zones in the centre of the refold. Type III, strata-bound quartz-breccias are located within alternating graywacke and siltstone sequences and formed by ( $D_4$ ) bedding-parallel slip mechanisms, whereas Type IV quartz-breccia probably formed by ( $D_4$ ) buckling of graywacke-dominated sequences.





shear systems are spatially associated with the Type III and IV quartz-breccias at Gordon Lake, hence alternative mechanisms are required for their formation.

#### 11.6.1 Structural Constraints

The Type III siltstone-hosted breccias typically occur on the limbs of F1 folds (Section 6.2.3), and are strata-bound within (D<sub>4</sub>) crenulated, black siltstone beds (Section 7.2). The two end-member mechanisms hypothesised for their formation include: i) localized shearing within siltstone beds and repeated echelon vein emplacement, and ii) differential shearing along contacts of siltstone beds resulting in localized zones of dilation (i.e., analogous to step-over faults; Sibson, 1990). In both cases, shearing was the result of dextral, bedding-parallel slip developed during post-metamorphic (D<sub>4</sub>) counter-clockwise rotation of the refold's east limb (Sections 5.5 and 6.4). The Type IV quartz-breccias confined to graywacke-dominated sequences are smaller, more irregular in morphology than the Type III quartz-breccias (Section 6.2.4), and have no apparent structural control (other than occurring along minor flexures in bedding). The exact mechanisms for their formation are unclear, but they possibly formed in regions of D<sub>4</sub> buckling and fracturing of graywacke beds.

#### 11.6.2 Lithological Constraints

Lithology plays an important role in determining and localizing strain during deformation (e.g., Melling et al. 1988). At Gordon Lake it is speculated that the distribution of the post-metamorphic (D<sub>4</sub>) strain varied between regional lithology types with: i) minor buckling, brittle fracture, and little to no bedding-parallel slip in graywacke-dominated sequences; ii) flexural flow and bedding-parallel slip in siltstone-dominated sequences; and

iii) the greatest bedding-parallel slip occurring in regions of alternating graywackes and siltstones (i.e., along the south-western shore of Gordon Lake). These latter regions of concentrated bedding-parallel slip probably became localized zones of high-strain and were consequently the most favourable sites to develop the strata-bound, siltstone-hosted (Type III) quartz-breccias.

### 11.6.3 Fluid Pressure Constraints

Fluid pressure and hydraulic fracturing play important and fundamental roles in the development of breccias (Phillips, 1972, 1986). Fluid pressure ( $P_f$ ) is the pressure that a fluid, present in pore spaces, exerts on grain boundaries in an opposite sense to the surrounding lithostatic pressure ( $P_l$ ). If the resultant effective pressure ( $P_e$ ) is negative (where  $P_e = P_l - P_f$ ) hydrofracturing will occur (Rubey and Hubbert, 1959; Fyfe et al. 1978; Yardley, 1989).

Regionally high fluid pressures are common to many metamorphosing metasedimentary and metavolcanic terranes (e.g., Norris and Henley, 1976). Typically, these high regional fluid pressures occur in the later stages of metamorphism and are associated with uplift and unloading of a metasedimentary/metavolcanic pile (Henley et al. 1976). At Gordon Lake it is suggested that regional high fluid pressures, developed in the latter stages of  $D_3$  peak metamorphism and were coeval with  $D_4$  counter-clockwise rotation of the refold's east limb and the development of structurally controlled dilations/traps. This dilational event probably occurred slightly below the brittle-ductile transition with temperatures of  $450 \pm 40^\circ\text{C}$  and pressures of 2.0-3.5 kbars (Spencer, 1969; Figure 5.26). Localized high fluid pressures might also have developed within the hinge region of the refold itself, where the rate of refold closure exceeded the rate at which fluids escaped. These

high fluid pressures coupled with the presence of structural traps developed zones of hydrofracturing and brecciation, where the morphology of breccia zone (i.e., Type III or IV) depended on how the host rock was deformed.

#### 11.7 PHYSICO-CHEMICAL CONSTRAINTS ON FLUID TRAPPING AND GOLD/SULPHIDE CONCENTRATION AT GORDON LAKE

The structural, lithological, and fluid pressure constraints for the formation and concentration quartz-breccia zones, described in the previous section, give no indication as to the physico-chemical conditions during mineralization. Even though pressure and temperature are important variables that control the deposition of quartz (e.g., Kennedy, 1950; Boyle 1979), other variables, such as oxygen fugacity ( $f_{O_2}$ ), sulphur fugacity ( $f_{S_2}$ ), and pH, also play important roles in the precipitation of sulphides and gold (Seward, 1984). Transport of gold from its source to site of deposition requires mobilization of the metal as complexing-ligands in an aqueous medium. The most likely ligands for the transport of gold are bisulphides (Seward, 1984), chlorides (Henley, 1973), and to a lesser extent thioarsenides (Grigoryeva and Sukeva, 1981). Typically, at fluid temperatures of 300°C, gold is more readily complexed with chloride species in acidic and oxidizing solutions and with bisulphide complexes in reduced, and near neutral conditions.

From the mineralogical assemblages, fluid inclusion, and geochemical data in this study it is possible to provide some constraints on the type of depositional conditions that might have prevailed during the formation of the Gordon Lake quartz-breccias. It is unlikely that temperature alone was the principal control in the precipitation of gold and sulphides, as the mineralizing fluids, at temperatures of  $455 \pm 40$  °C (from arsenopyrite geothermometry; Section 7.5), were emplaced into

metaturbidites in the late stages of regional metamorphism. However, rapidly decreasing pressures during dilation and brecciation might not only have caused "rapid dumping" of quartz (Kennedy, 1950), but may also have enhanced fluid immiscibility processes by assisting in the separation of volatiles phases (e.g., Bowers and Helgeson, 1983) and subsequently depositing gold (e.g., Robert and Kelly, 1987; Walsh et al. 1988). However, fluid inclusion petrography does not provide any good evidence to support the presence of fluid immiscibility (Section 8.4).

Two hypotheses are considered for the deposition of gold and sulphides at Gordon Lake; both depend on the original oxidation state of the metamorphic fluid. If the metamorphic fluid was reduced, gold may have been carried in as a bisulphide ligand, requiring oxidation and/or sulphidation at the site of deposition to destabilize the complex and precipitate gold. Wall-rock alteration around the mineralized shear zones of the Yellowknife Volcanic Belt indicate reduced iron ratios and support this model (Kerrick et al. 1977). A different hypothesis involves oxidized metamorphic fluids (Kubilius and Ferry, 1989) carrying gold as chloride complexes, which are reduced at the site of deposition. The most likely mechanism for this reduction would be the interaction between the oxidised fluids and the carbon-rich wallrock (e.g., McKeag et al. 1989, Bottrell et al. 1988). The interaction between carbon and the metamorphic fluid would produce high amounts of  $\text{CH}_4$  and other C-H volatiles, increase the salinity of the residual fluid, and deposit gold as a result of destabilization of the chloride complex. This latter hypothesis is attractive as it better explains the control exerted by carbon-rich sediments on gold concentration and precipitation. Nevertheless it remains speculative.

### 11.8 POST-ORE MODIFICATION AND PRESERVATION

An important factor not always considered in ore deposit modelling is the modification and preservation of mineralization after its formation. Firstly, if an orebody is emplaced early in the deformational/metamorphic history of a region it is more likely to be redistributed by later structural events. In the case of the gold-bearing quartz-breccias at Gordon Lake, no major remobilization of the mineralized zones has occurred, as they were formed in the later stages of metamorphism and cratonization of the Slave Province. However, it is possible that the vertical stretching lineation, observable in mesoscopic and microscopic structures, can be extended to the scale of the breccia bodies; which were probably vertically elongated to some extent. The absence of obviously primary fluid inclusions in gangue minerals suggests that some deformation and fluid interaction post-dated mineralization, supporting the hypothesis that there was some remobilization of gold (Section 8.7 and 8.8).

Erosion seems to have removed several kilometres of crust (7-12 km?) soon after the intrusion of the granites. The author is unaware of any extrusive equivalents of the Proterozoic dykes that cross the Gordon Lake area, and therefore one can assume that erosion continued to the Paleozoic, when the Pine Point Paleozoic sedimentary platform and adjacent basins developed. The Proterozoic dyke swarms do not seem to have affected the gold deposits in any way.

A major factor controlling the uncovering of these mineralized zones is glaciation. Quaternary glaciation for the region was generally from the north-east to south-west (Henderson, 1985), with striations at Gordon Lake trending 050-085°. This glacial erosion in part explains the long linear character of Gordon Lake, which was probably preferentially gouged as it is underlain by a softer

siltstone-dominated region. In addition, glaciation might explain why the strata-bound siltstone-hosted quartz-breccias occur beneath low lying areas (i.e., swamps), where ice gouging was preferential directed along the weaker linear sequences of fine-grained siltstone.

#### 11.9 SUMMARY OF GENETIC MODEL

A preferred genetic model is proposed to explain the occurrence of gold-bearing quartz-breccia zones at Gordon Lake. Oxidized, syn- to post-metamorphic fluids leached gold from the metaturbidite pile to form gold-chloride complexes. These fluids were focussed (at ca. >2573 to <2600 Ma) into the central domain of a regional refold during anti-clockwise rotation of the refold's east limb and closure of the refold hinge. The rotation of the refold's east limb induced (dominantly dextral) bedding-parallel slip in regional overpressured fluids within the refold centre. Sequences of alternating black (carbon rich) siltstones and graywackes localized bedding-parallel slip and created strata-bound zones of hydraulic fracturing and brecciation within the siltstone beds (Type III, quartz-breccias). Other smaller, irregular quartz-breccias developed in graywacke sequences (Type IV), due to localized high fluid pressures and minor flexures in bedding. Decompression during the brecciation probably led to deposition of the grey quartz, while the gold-chloride complexes were destabilized during chemical interaction between the metamorphic fluid and the carbon-rich siltstone.

CHAPTER 12  
CONCLUSIONS

Geological data from the Gordon Lake region has led to the following conclusions concerning the development of a regional refold and the genetic origin of gold-bearing quartz-breccia zones concentrated within the centre of this structure.

1. Gordon Lake is located within greenschist-facies metaturbidites of the Burwash Formation. The regional structure is dominated by a south closing, km scale, sub-vertical refold of earlier ( $F_1$ ) isoclinal folds.

2. The refold is transected by a pervasive, steeply dipping  $D_3$  cleavage, that is associated with peak metamorphism and a vertical stretching lineation. In the central region of the refold  $D_3$  siltstone cleavages are crenulated to form a new cleavage ( $S_4$ ).  $S_4$  developed during  $D_4$  bedding-parallel slip that accompanied counter-clockwise rotation of the refold's east limb. The refolding event may have spanned both  $D_3$  and  $D_4$ , or have been restricted to  $D_4$ .

3. The tectonic history of the region is compatible with subduction-related models for the Slave Province whereby: i) the  $F_1$  folds developed in an accretionary prism; ii) the  $F_1$  fold axes were steepened during later ( $D_3$ ) shortening of the accretionary prism and/or with the diapiric emplacement of granitic bodies; and iii)  $D_4$  rotation of the refold's east limb was the result of continued convergence and/or transcurrent movement.

4. Two distinct types of gold-bearing quartz-breccias occur within the centre of the refold; strata-bound,

siltstone-hosted and irregular graywacke-hosted. The Kidney Pond Zone 1 is the largest siltstone-hosted quartz-breccia with a 260 m strike-length, a width of 5-30 m, a depth of at least 180 m, and reserves of 175,000 tonnes at 16g/t. The graywacke-hosted quartz-breccias have smaller dimensions with no apparent structural control other than minor flexures in bedding.

5. The strata-bound quartz-breccias are typically hosted in black carbon-rich siltstones and are spatially associated with  $S_4$ .  $D_3/D_4$  fabric and mineralogical relationships indicate that these breccias formed in the latter stages of  $D_3$  and syn- $D_4$ . Since, both  $S_4$  and the stratabound (Type III) quartz-breccias developed preferentially in the black siltstones and are confined to the central part of the refold, they probably formed during the same deformational mechanism ( $D_4$ ); such as bedding-parallel slip which developed during counter-clockwise rotation of the refold's east limb. The smaller, graywacke-hosted quartz-breccias were probably the result of minor ( $D_4$ ) buckling of graywacke beds.

6. Arsenopyrite from the siltstone-hosted quartz-breccia and adjacent wall-rock indicate a formation temperature of  $455 \pm 40$  °C for the sulphide assemblages.

7. The quartz-breccias are dominated by saline (25-30 wt% NaCl-CaCl<sub>2</sub> combined) secondary fluid inclusions along healed microfractures, that are syn- to late metamorphic in origin, have homogenization temperatures of 140-330°C, and are probably associated with some gold deposition and/or remobilization. Bulk volatile analysis of these fluid inclusions indicates high concentrations of CH<sub>4</sub> and high CH<sub>4</sub>/CO<sub>2</sub> ratios (0.6-11.3). Fluid trapping pressures of 2.0-3.5 kbars were estimated for the secondary fluid, using



a fluid isochore and the arsenopyrite geothermometer.

8. Au, As, Sb, Br, and S are significantly enriched within sulphide-rich black siltstones adjacent the quartz-breccias, with lesser enrichments of CaO, Na<sub>2</sub>O, K<sub>2</sub>O, and C, and a slight depletion in SiO<sub>2</sub>. The low silica and high carbon contents of the sulphide-rich black siltstones, compared to other siltstones more distal to the quartz-breccias, indicates that either this lithology is a distinct siltstone unit or that it is a product an alteration process related to quartz-breccia emplacement.

9. <sup>40</sup>Ar/<sup>39</sup>Ar dating of a metamorphic hornblende and a muscovite from a post-metamorphic pluton constrain the time of (D<sub>3</sub>) peak metamorphism in the Gordon Lake region to approximately 2600 Ma. A plateau age of 2573 ± 9 Ma for a biotite from the Kidney Pond quartz-breccia zone gives a minimum age for mineralization, and is consistent with the structural relationships that indicate a late metamorphic brecciation event.

10. The mineralizing fluids were probably derived from metamorphic devolatilization reactions and dewatering of the metaturbidite pile. Most of the gold was probably leached from the mafic volcanic material within the metaturbidites. A preferred mechanism for the gold and sulphide deposition involves oxidized metamorphic fluids that transported gold as chloride complexes. The oxidized fluids were then reduced at the site of deposition by chemical interaction with carbon-rich siltstones wall-rock, producing CH<sub>4</sub> and destabilizing the chloride complexes, depositing gold,

CHAPTER 13  
RECOMMENDATIONS FOR FURTHER RESEARCH

Continued geological research in the Gordon Lake region and elsewhere within the Yellowknife Basin might include:

1. Additional structural-lithological mapping of the Gordon Lake refold to collect more: i) graywacke cleavage data from the refold's east limb; ii) orientation data from quartz inclusion trails within biotite porphyroblasts both to the east and west of the refold; iii) strain data from graywacke clasts, lithic clasts, and deformed quartz veins; iv) data on the style of  $F_1$  folding and early deformational (accretionary?) structures; and v) data from quartz-breccia zones to further constrain their regional distribution and timing.
  
2. Testing the Gordon Lake refold model at other refold sites within the Yellowknife Basin (i.e. Ross Lake and Cleft Lake), and examining these regions for similar cleavage relationships and quartz vein/breccia types.
  
3. Continued  $^{40}\text{Ar}/^{39}\text{Ar}$  dating to improve geochronological controls on the time of brecciation and metamorphism. Possible material for dating might include: a) K-feldspar from the quartz-breccias, which in conjunction with the biotite age might provide a cooling rate and a better constrained time for quartz-breccia emplacement; and b) metamorphic muscovites from siltstone beds, which compared to the biotite data, might provide a cooling rate for the metaturbidite pile and better constrain the time of peak-metamorphism.

4. Commence a comprehensive fluid inclusion study of varied (but structurally well constrained) quartz material from within the Yellowknife Basin (e.g., veins from granites, volcanic shear zones, and other vein systems within the metaturbides). The emphasis of this study might be to investigate the origin and volatile composition of the commonly found saline fluid, and to further constrain (by fluid inclusion petrography and quartz microstructure) the time of this fluid event.

5. Continued investigation into the geochemistry and genetic relationships between the carbon-rich sediments, grey quartz, gold, and sulphides by: i) additional bulk fluid inclusion geochemistry; ii) direct analysis of the black (carbon) particles within the grey quartz; iii) carbon isotope analysis of carbonate from siltstones, graywackes, and quartz-breccia material; and iv) sulphur isotope analysis of sulphide material from the quartz-breccias.

6. Continued investigation into the possible association between sub-microscopic and "invisible" gold within arsenopyrite; e.g. ion-probe analysis.

## CHAPTER 14

### EXPLORATION CRITERIA AND APPROACH

Listed below are exploration criteria, some more obvious than others, that are suggested principally for the location of similar gold-quartz vein/breccia occurrences within the Yellowknife Basin and Slave Province. These criteria might also be applied to other Archean or Phanerozoic metasedimentary terranes. Regional scale criteria [with suggested exploration approach in square brackets] include:

1. The location of a regional concentration of past or present gold producers.

[Literature research and/or government compilations]

2. The location of a regional structure, such as a refold or shear system, which displays evidence of a late (post-metamorphic) deformation and/or complexity (i.e. a crenulation cleavage).

[Geological maps, aerial photographs, and landsat imagery]

3. The location of a region dominated by metasilstone sequences (commonly characterised by weathered-out lows; i.e., swamps or lakes), as opposed to metagraywacke-dominated sequences.

[Topographic, geological and geophysical maps, aerial photographs, and landsat imagery]

4. The location of a region with abundant quartz veining, preferably where many veins are offset and rotated along bedding surfaces, indicating evidence of intense bedding-parallel slip.

[Field mapping]

At a mine camp scale exploration criteria might include:

1. The recognition of black carbon-rich metasiltstone sequences within the metasiltstone-dominated lithology, preferably where associated with sulphide (e.g., pyrrhotite) concentrations.

[Airborne geophysical maps, detailed magnetic/electromagnetic surveys]

2. The presence of arsenopyrite in wall-rock adjacent to vein systems and within veins themselves and the use of As and Sb as geochemical pathfinders for gold.

[Field mapping, lithochemistry]

~~X [Field mapping and geochemistry]~~

3. The recognition of grey to black quartz within black metasiltstone sequences.

[Field mapping]

4. The presences small (1-2 mm) multi-mineralic aggregates around vein systems indicating areas of wall rock alteration and/or a thermal halo related to mineralization.

[Field mapping]

APPENDIX A5: METATURBIDITE PETROGRAPHY

CLEAVAGE MORPHOLOGY AND  
MICROSTRUCTURE

FRY ANALYSIS AND QUARTZ  
VEIN STRAIN DATA

### A5.1 THE FRY TECHNIQUE

The Fry plot (Fry, 1979) is a relatively simple technique suitable for the strain analysis of objects set in a matrix of similar composition, (i.e., quartz clasts in a quartz-rich matrix of a graywacke). The technique is based on the principle that an anticlustered distribution of points (in this case the centriods of graywacke clasts) varies during deformation and strain forming an equally non-uniform distribution. The technique involves the measurement of clast centres relative to each other, whereby the distances between centres increase in the direction of extension and decrease in the direction of compression. The resulting plot has a central void, ringed by a clustering of points, defining the shape of the strain ellipse.

### A5.2 SAMPLE PREPARATION, FRY PLOT CONSTRUCTION AND RESULTS

For each sample three enlarged (11x17"), reverse negative photographs were made of each section (YZ, XZ and XY) and the clasts traced onto a clear overlays. Fry plots were constructed both manually (Ramsay and Huber, 1983) and by computer, using part of the INSTRAIN program of Erslev (1988). The INSTRAIN program can construct Fry plots three ways: i) a simple centre to centre Fry plot, ii) a five point Fry plot, and iii) a five point "normalized" Fry plot. The first plot measures distances between the centre points of quartz clasts, whereas in the other two the centroid of each clast is calculated from five points measured around each clast and then the distances measured. For the third plot, in addition to the determination of a centroid the centres are normalized; the centre to centre distance between two clasts is divided by the sum of their average radii. This procedure eliminates inherent variations due to clast size and sorting, and therefore reduces the effects of anticlustering (Erslev, 1988). For

construction of the manual Fry plots 40 to 105 clasts were used, for the computerized centre to centre analysis 400 to 500 clasts, and for the five point analysis 200 to 250 clasts. Best fit ellipses were drawn in the central voids of the Fry diagrams (Figures A5.1 to A5.18), and the ellipse long and short axes were measured, along with the orientation of the long axis (Phi angle; Tables A5.15-A5.17).

No one method gave consistently higher or lower ellipse ratios. However, the coarse to medium-grained graywackes (22-6-4, 87-51 and 87-66) produced better defined ellipses than the coarse-grained siltstone (86-115) and fine-grained graywacke (87-34b). This is probably due to variations in clast size, the matrix\clast ratio, and the fact that clasts in fine-grained metasediments appear more clustered. A common feature to most of the Fry plots were vacancy fields on the edges of the centre voids. These were probably a result of clast anticlustering as they are less apparent in the normalized Fry plots.

### A5.3 ERRORS IN THE FRY ANALYSIS

Both geological and analytical errors were considered in the evaluation of the strain data. Geological errors are introduced by assuming: i) that there is no volume loss, due to processes such as (open) pressure solution during deformation of the graywacke; ii) that no major clast breakdown or clast-clast interference has occurred, iii) that clasts have not undergone any recrystallization; and iv) that metamorphic mineral growth has not interfered or changed strain characteristic of the graywacke. It is likely that one or more of these processes were active during the deformational and metamorphic history of the graywacke. However, the effects of the last three are probably minimal compared to that of the first, pressure solution. This problem was addressed by Onasch (1986), who



indicated that Fry plots will only give correct data "where deformation is constant volume and the dissolution surfaces are more closely spaced than marker centres", or where some estimation of volume loss is known. In our case, it is also possible that some volume loss has occurred as evident from syn-deformational vein formation.

The principal analytical errors include: i) mistakes in digitizing clast centres and five points around clasts, ii) the measurement of the strain ellipse shape from the Fry plots. To gauge the accuracy of the Fry analysis sample 22-6-4 was sent to the University of Colorado for independent analysis. Construction of ellipses from these Fry plots gave values of:  $YZ = 1.40$ ;  $XZ = 1.91$ ; and  $XY = 1.77$  (W. Babcock, personal communication, 1989). These are in reasonable agreement when compared to the ellipse values obtained in this study (Table A5.16). To determine the precision of the Fry plot analysis repeat ellipse measurements were done on samples 87-66 and 87-51. Both ellipse ratios from the repeat analyses were within 10% of originally measured ratios.

#### A5.4 CALCULATION OF D<sub>4</sub> SHEAR STRAINS FROM DEFORMED VEINS

Crenulated quartz veins were traced from four outcrops so that estimates of D<sub>4</sub>-shear strain parallel to bedding could be calculated. Of the four veins three displayed dextral shear (S<sub>2</sub>, S<sub>3</sub> and S<sub>5</sub>) and one (S<sub>6</sub>) sinistral shear (Figures A5.19 - A5.23). In all four cases it was assumed that the quartz veins acted as independent markers of strain and that their emplacement predated D<sub>4</sub>. In addition the crenulated bed (usually a finer-grained siltstone) was treated as a zone of shear deformation. Two methods were employed to estimate shear strains. The first applied the simple shear equation derived by De Paor (1987) from work Ramsay and Huber (1983) and Ramsay (1967). Whereby shear strain is expressed as:

$$\gamma = \cot \theta' - \cot \theta$$

with  $\gamma$  = shear strain

$\theta$  = angle of line before deformation

$\theta'$  = angle of line after deformation

The equation assumes no volume loss within the zone of shearing. The second method adapted was the orthographic technique of De Paor (1986, Figure 13) which estimated minimum and maximum values of shear strain and dilation from a marker which traverses a shear zone. The results from both methods are tabulated in Table A5.19.

Figure A5.1 Fry plots obtained from INSTRAIN program (A, B, and C), and manually (D) for YZ section of coarse- to medium-grained graywacke sample 22/6/4. A - Five point centre to centre Fry plot; B - Five point centre to centre Normalized Fry plot; C - Centre to centre Fry plot; D - Manually constructed centre to centre Fry plot.

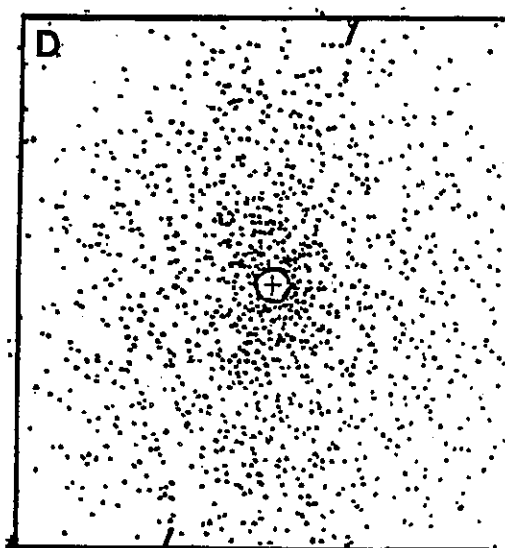
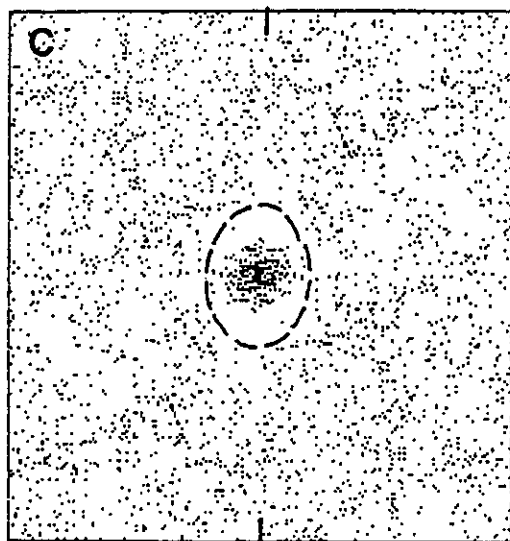
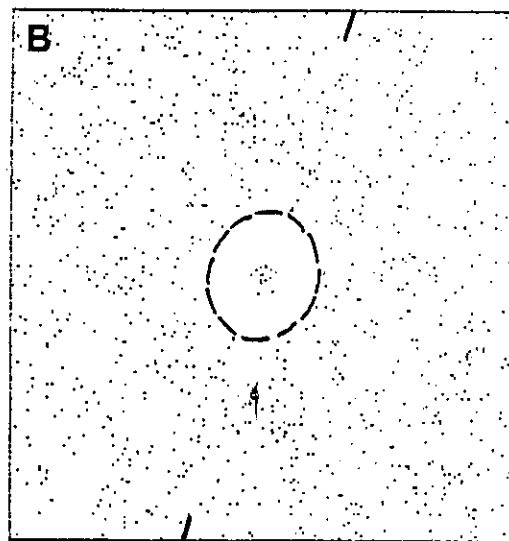
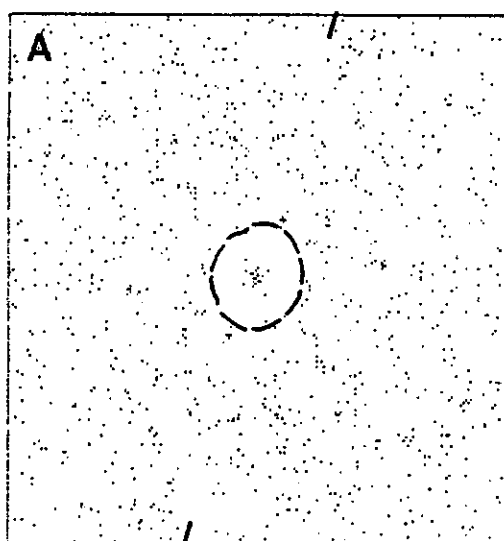


Figure A5.2 Fry plots obtained from INSTRAIN program (A, B, and C), and manually (D) for XZ section of coarse- to medium-grained graywacke sample 22/6/4. A - Five point centre to centre Fry plot; B - Five point centre to centre Normalized Fry plot; C - Centre to centre Fry plot; D - Manually constructed centre to centre Fry plot.

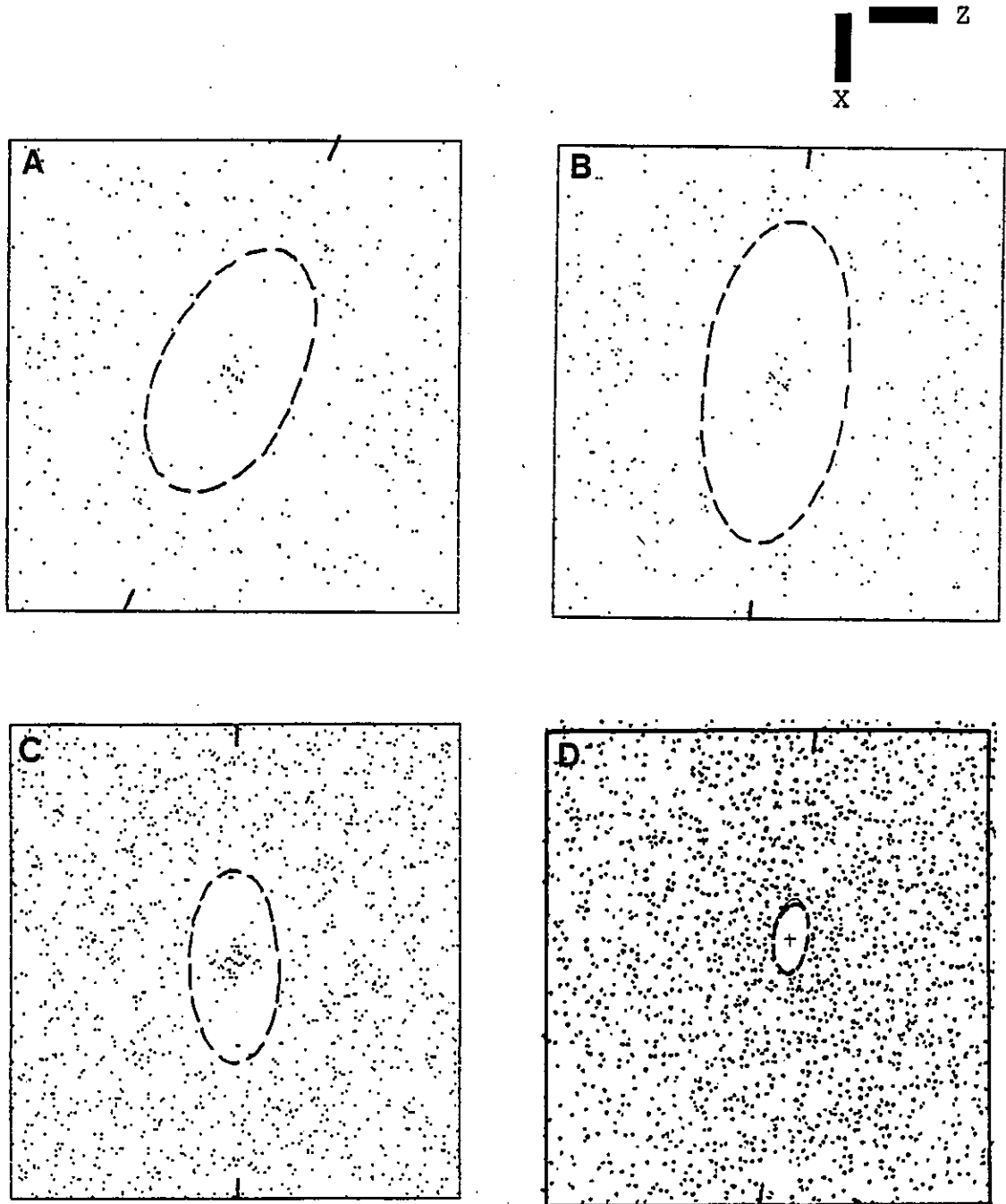


Figure A5.3 Fry plots obtained from INSTRAIN program (A, B, and C), and manually (D) for XY section of coarse- to medium-grained graywacke sample 22/6/4. A - Five point centre to centre Fry plot; B - Five point centre to centre Normalized Fry plot; C - Centre to centre Fry plot; D - Manually constructed centre to centre Fry plot.

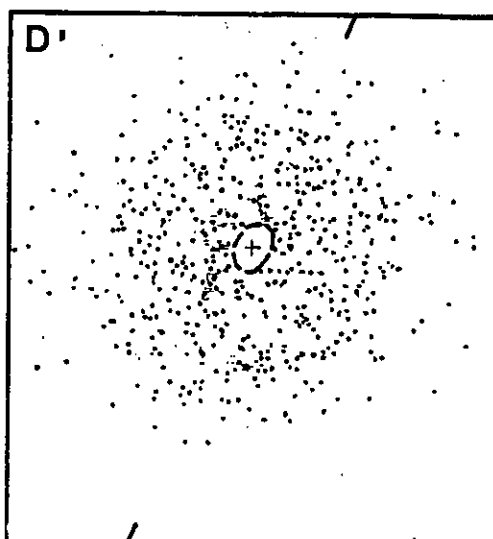
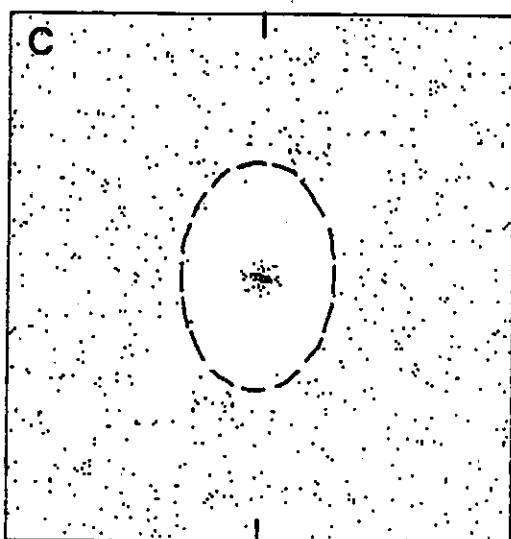
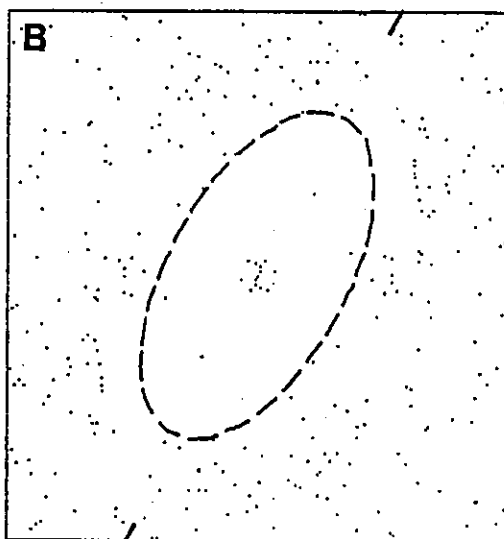
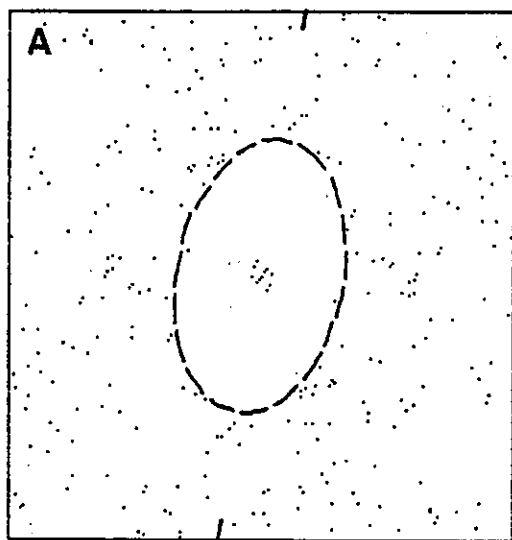


Figure A5.4 Fry plots obtained from INSTRAIN program (A, B, and C), and manually (D) for YZ section of coarse-grained siltstone sample 86-115. A - Five point centre to centre Fry plot; B - Five point centre to centre Normalized Fry plot; C - Centre to centre Fry plot; D - Manually constructed centre to centre Fry plot.

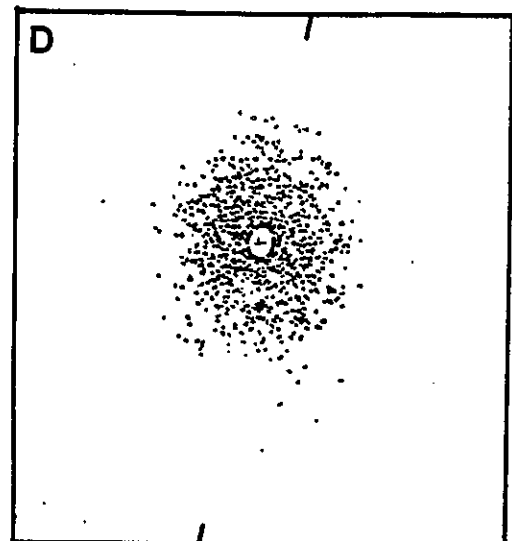
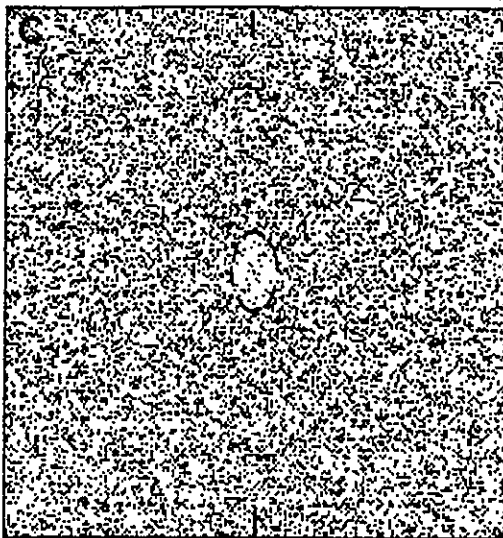
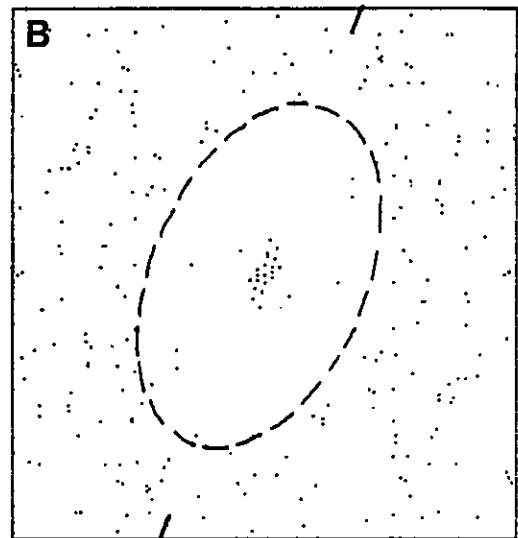
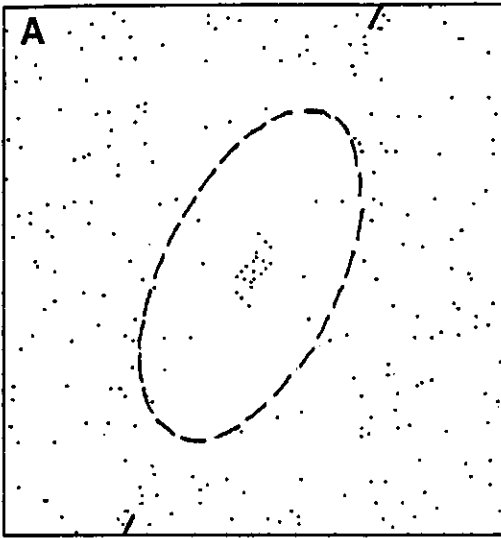


Figure A5.5 Fry plots obtained from INSTRAIN program (A, B, and C), and manually (D) for XZ section of coarse-grained siltstone sample 86-115. A - Five point centre to centre Fry plot; B - Five point centre to centre Normalized Fry plot; C - Centre to centre Fry plot; D - Manually constructed centre to centre Fry plot.

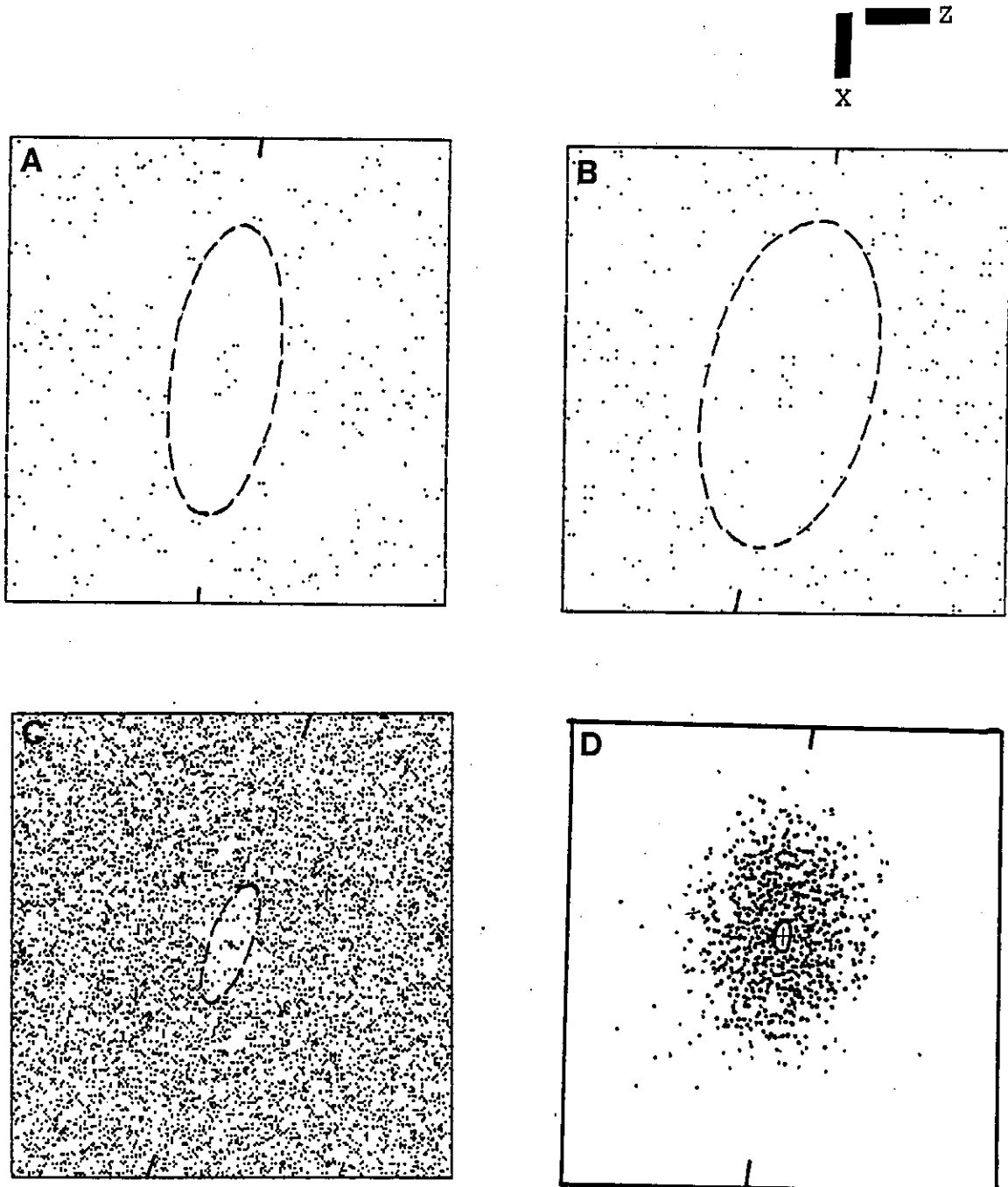


Figure A5.6 Fry plots obtained from INSTRAIN program (A, B, and C), and manually (D) for XY section of coarse-grained siltstone sample 86-115. A - Five point centre to centre Fry plot; B - Five point centre to centre Normalized Fry plot; C - Centre to centre Fry plot; D - Manually constructed centre to centre Fry plot.

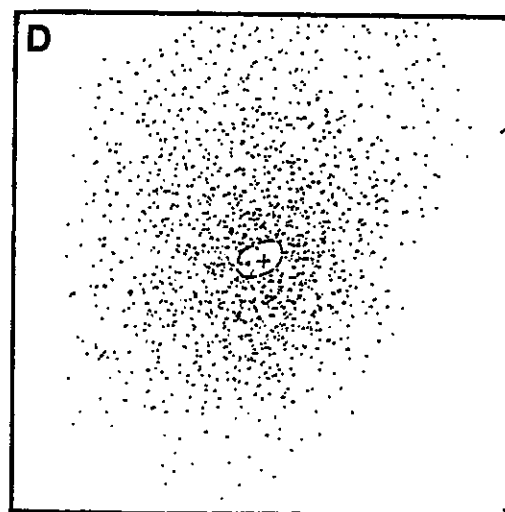
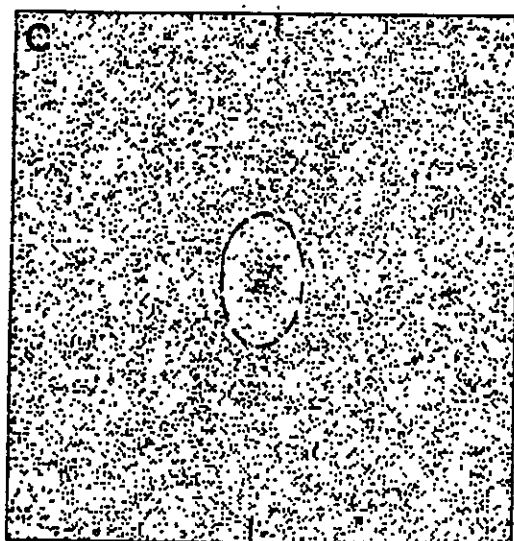
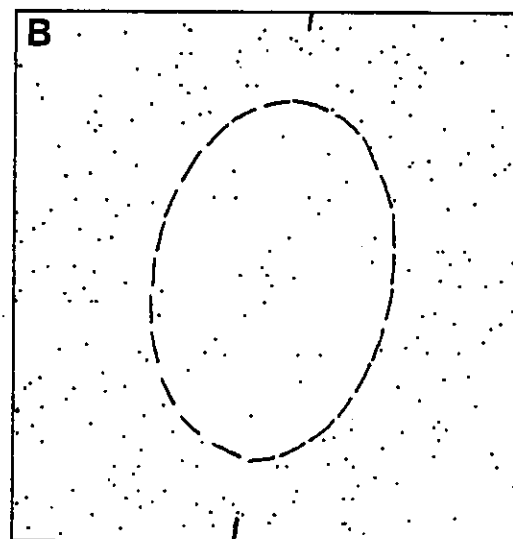
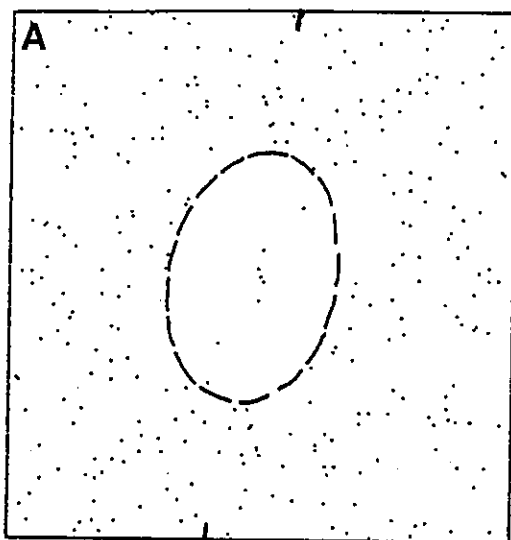




Figure A5.7 Fry plots obtained from INSTRAIN program (A, B, and C), and manually (D) for YZ section of coarse to medium-grained graywacke sample 87-66. A - Five point centre to centre Fry plot; B - Five point centre to centre Normalized Fry plot; C - Centre to centre Fry plot; D - Manually constructed centre to centre Fry plot.

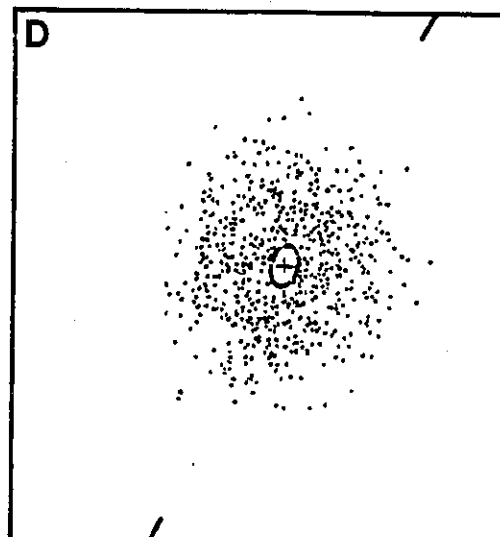
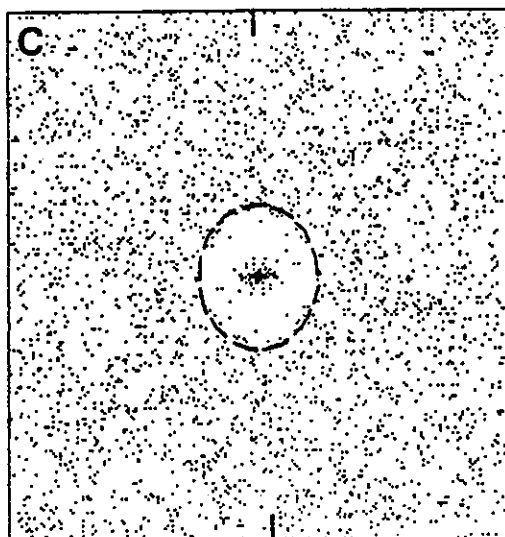
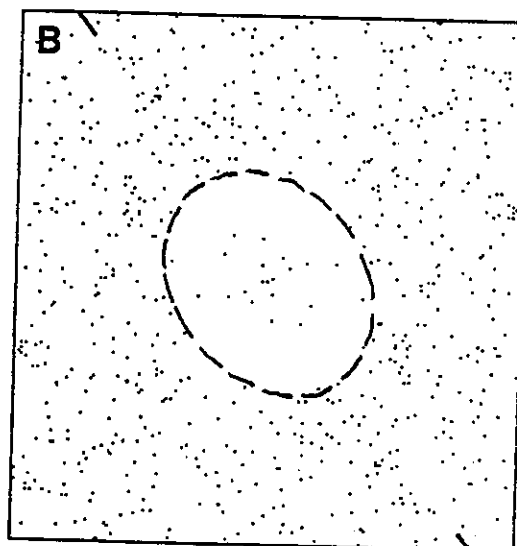
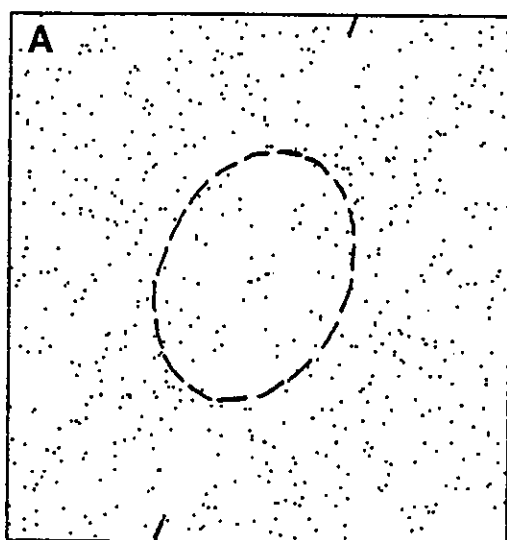


Figure A5.8 Fry plots obtained from INSTRAIN program (A, B, and C), and manually (D) for XZ section of coarse- to medium-grained graywacke sample 87-66. A - Five point centre to centre Fry plot; B -Five point centre to centre Normalized Fry plot; C - Centre to centre Fry plot; D- Manually constructed centre to centre Fry plot.

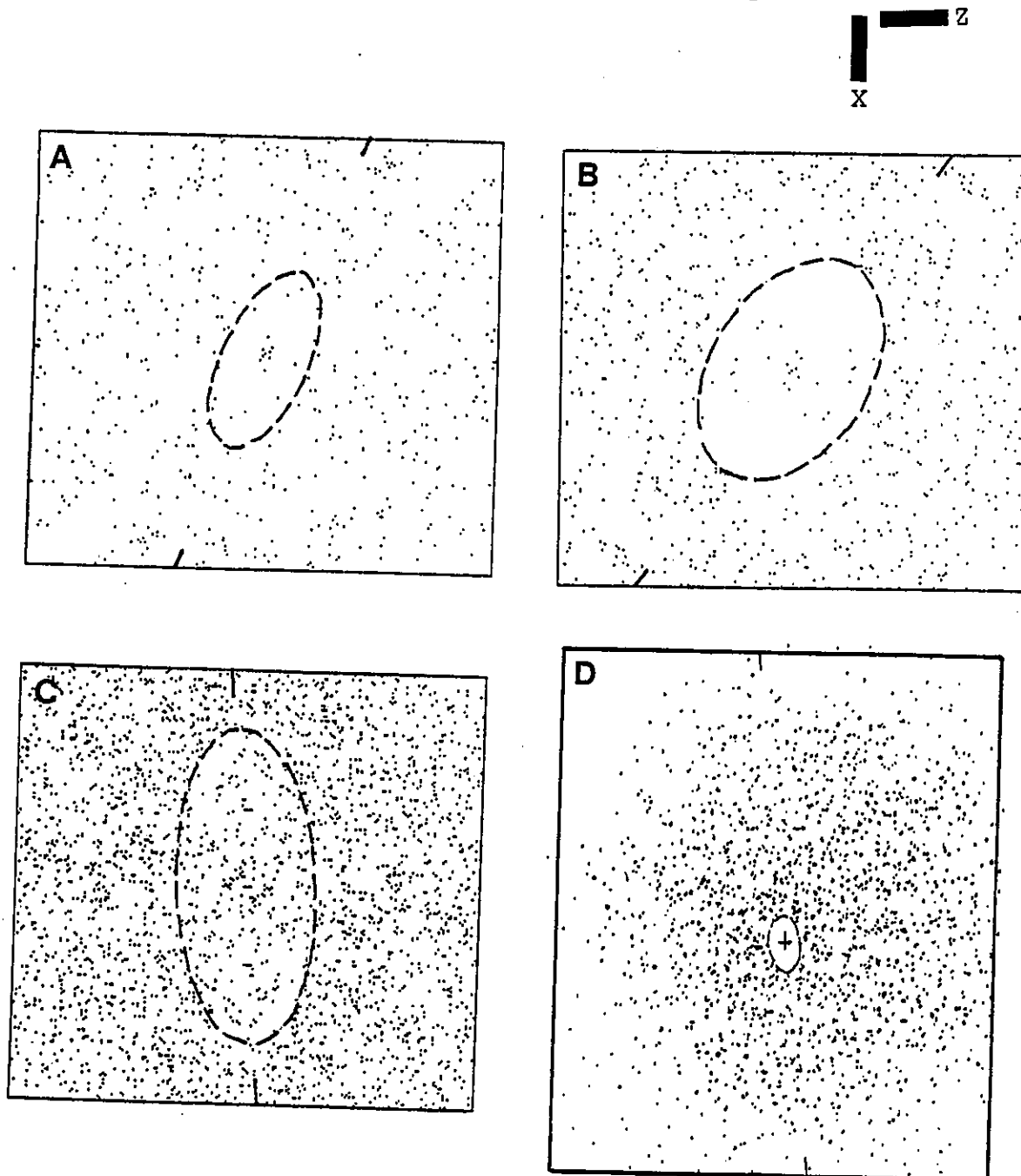


Figure A5.9 Fry plots obtained from INSTRAIN program (A, B, and C), and manually (D) for XY section of coarse- to medium-grained graywacke sample 87-66. A - Five point centre to centre Fry plot; B -Five point centre to centre Normalized Fry plot; C - Centre to centre Fry plot; D- Manually constructed centre to centre Fry plot.

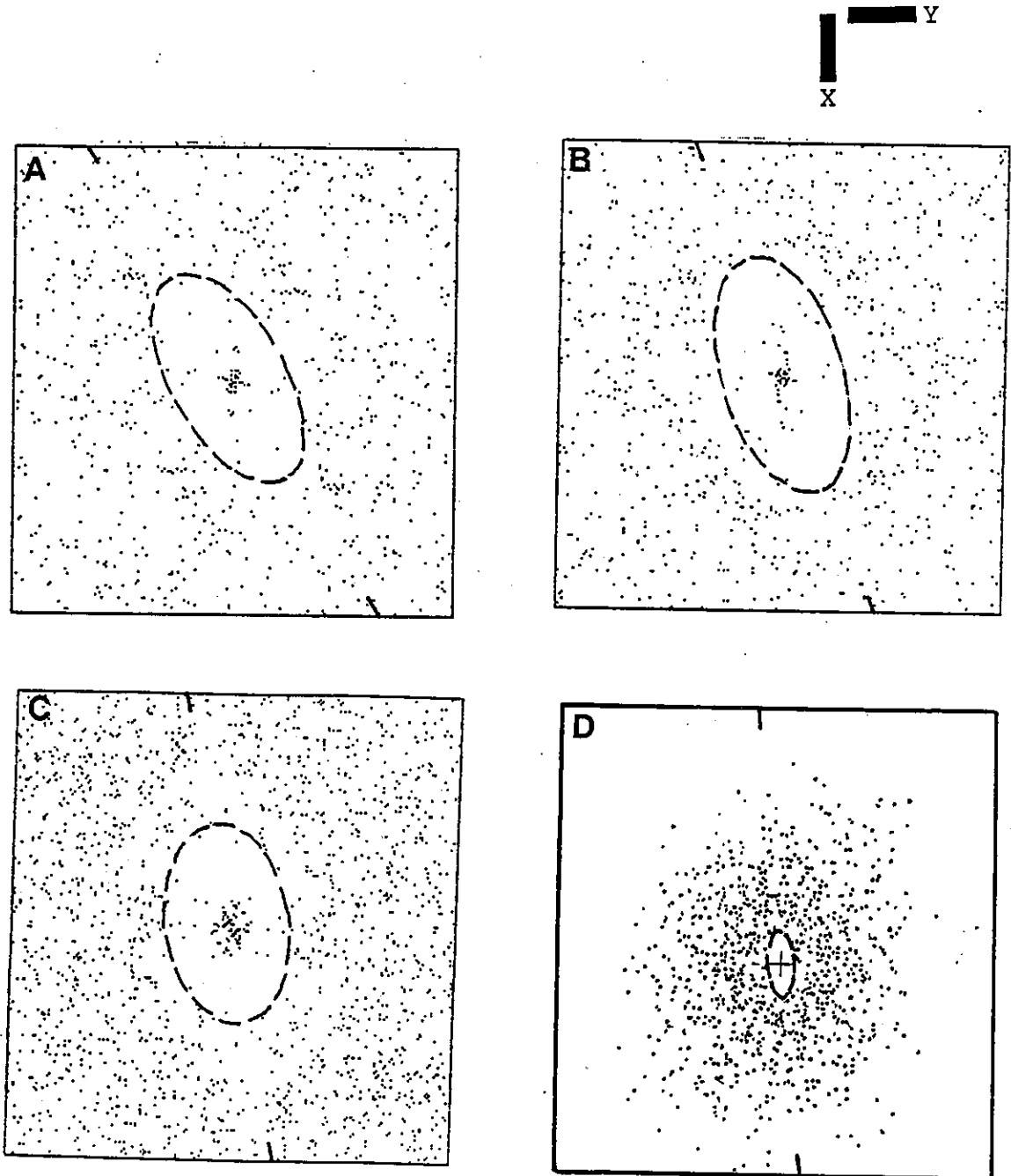


Figure A5.10 Fry plots obtained from INSTRAIN program (A, B, and C), and manually (D) for YZ section of coarse- to medium-grained graywacke sample 87-51. A - Five point centre to centre Fry plot; B -Five point centre to centre Normalized Fry plot; C - Centre to centre Fry plot; D- Manually constructed centre to centre Fry plot.

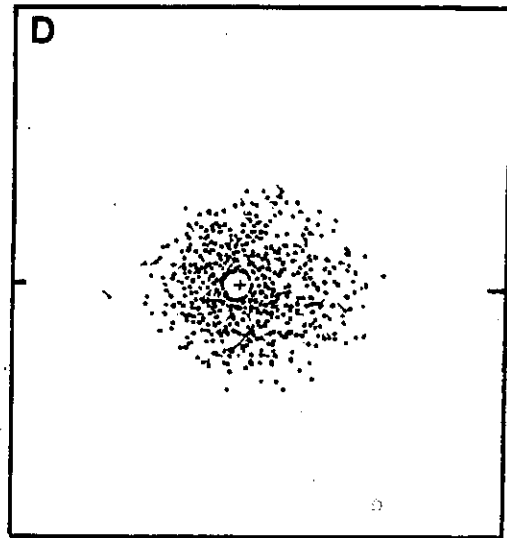
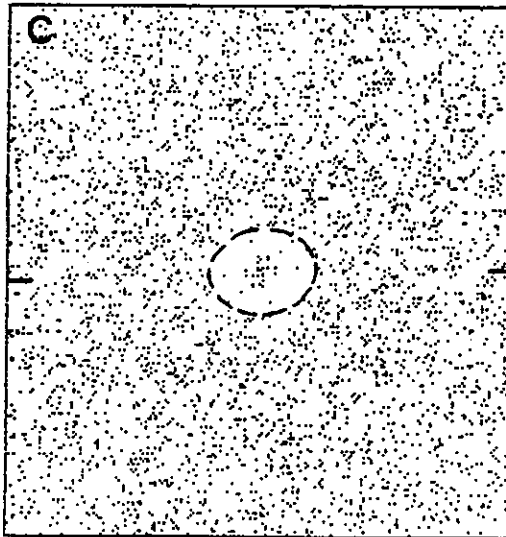
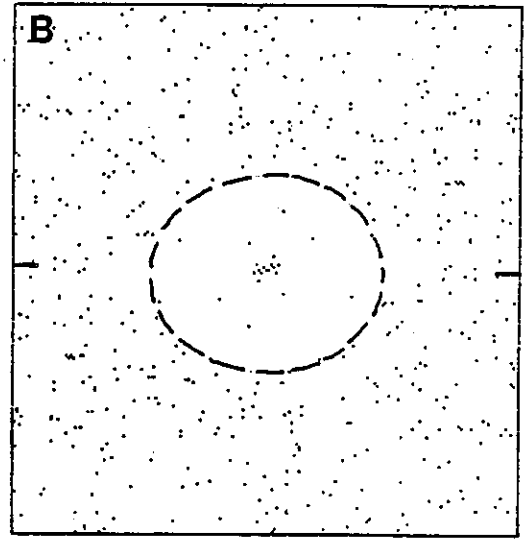
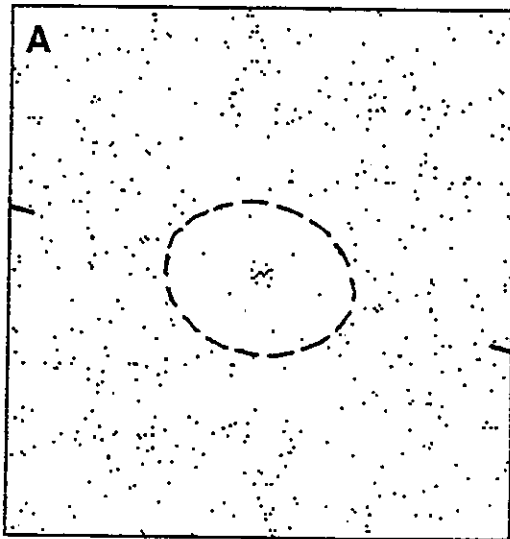


Figure A5.11 Fry plots obtained from INSTRAIN program (A, B, and C), and manually (D) for XZ section of coarse- to medium grained graywacke sample 87-51. A - Five point centre to centre Fry plot; B -Five point centre to centre Normalized Fry plot; C - Centre to centre Fry plot; D- Manually constructed centre to centre Fry plot.

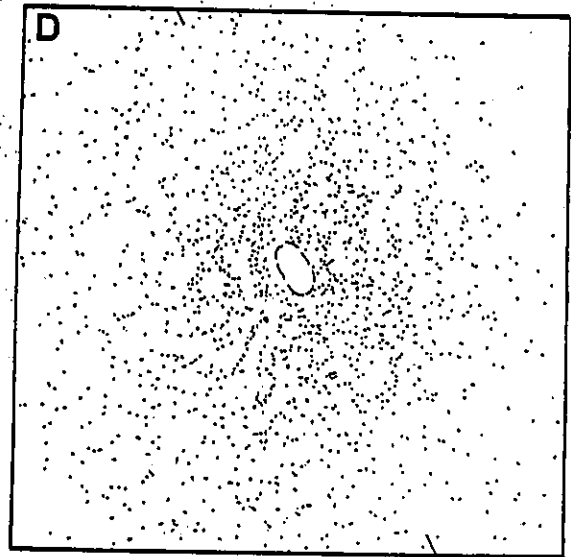
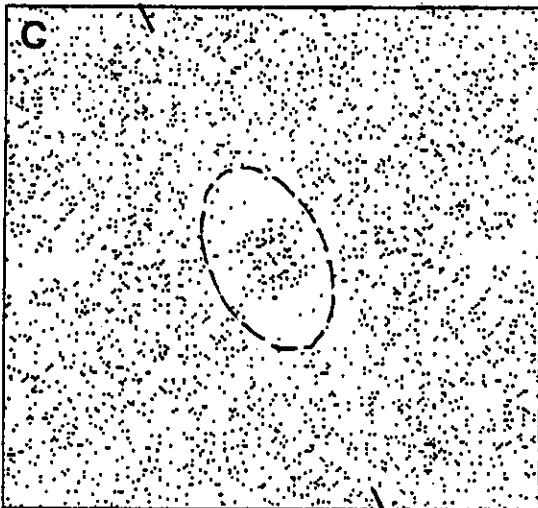
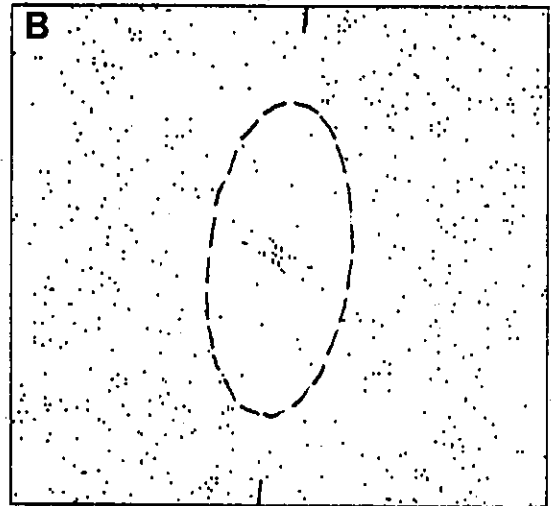
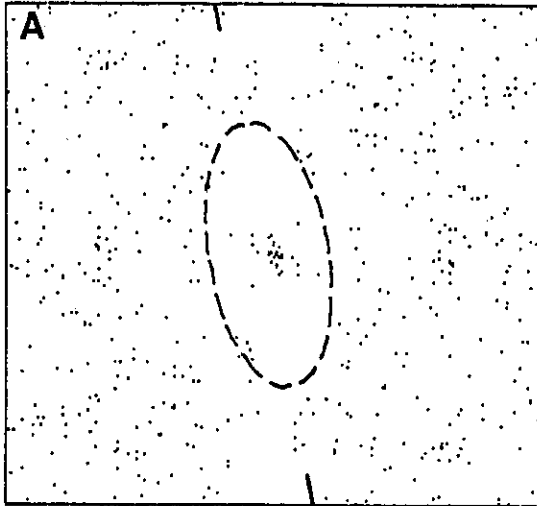


Figure A5.12 Fry plots obtained from INSTRAIN program (A, B, and C), and manually (D) for XY section of coarse- to medium-grained graywacke sample 87-51. A - Five point centre to centre Fry plot; B -Five point centre to centre Normalized Fry plot; C - Centre to centre Fry plot; D- Manually constructed centre to centre Fry plot.

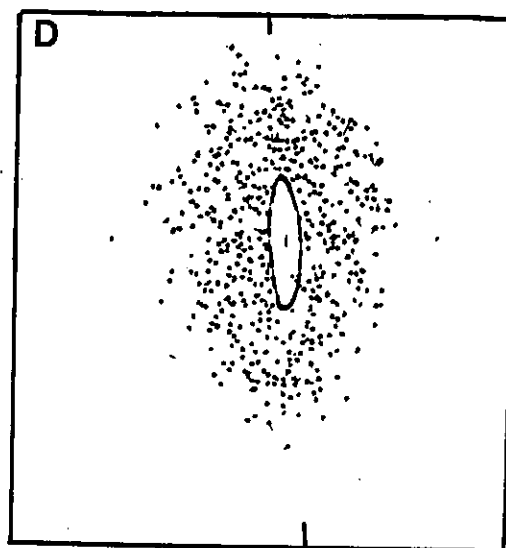
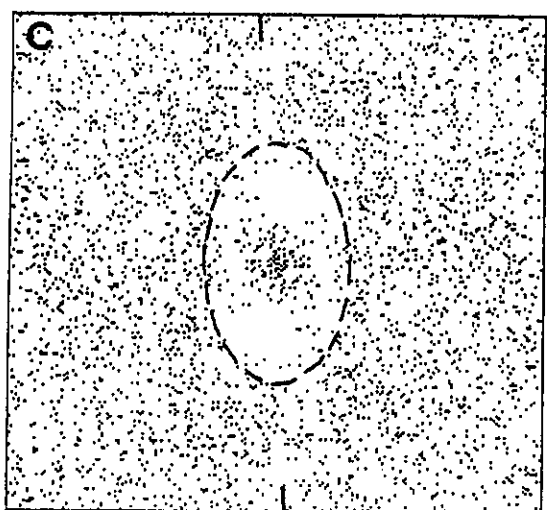
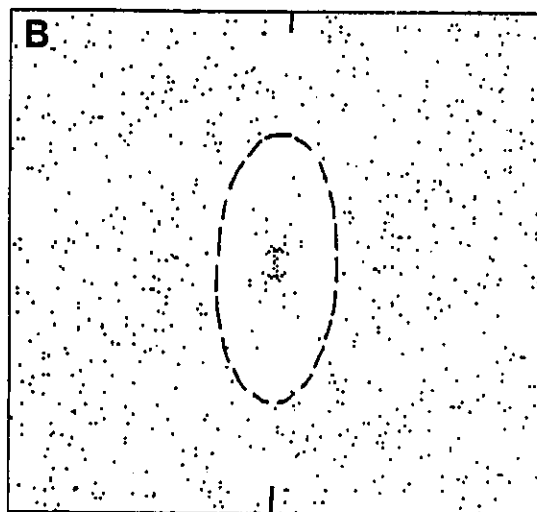
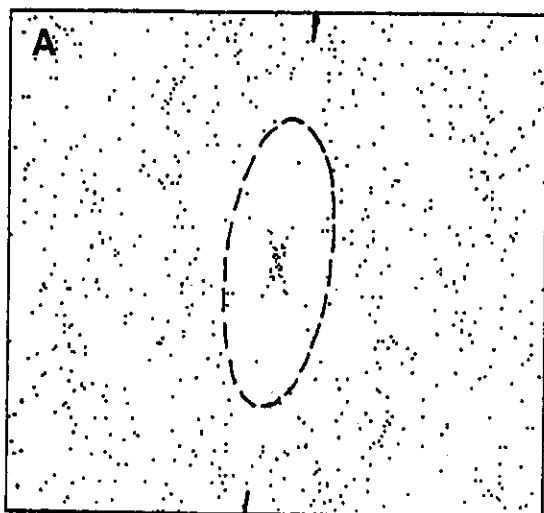


Figure A5.13 Fry plots obtained from INSTRAIN program (A, B, and C), and manually (D) for YZ section of fine-grained graywacke sample 87-34b. A - Five point centre to centre Fry plot; B - Five point centre to centre Normalized Fry plot; C - Centre to centre Fry plot; D - Manually constructed centre to centre Fry plot.

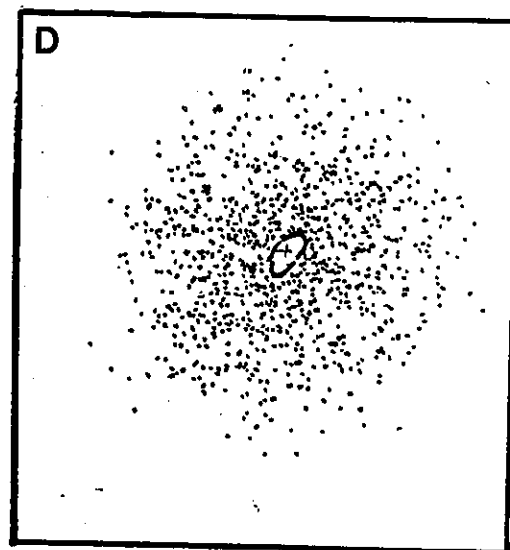
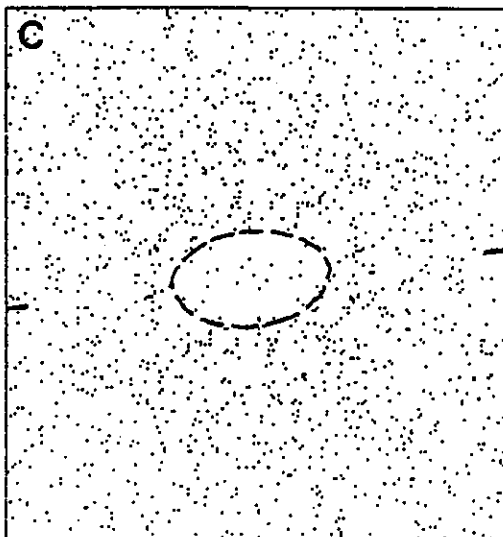
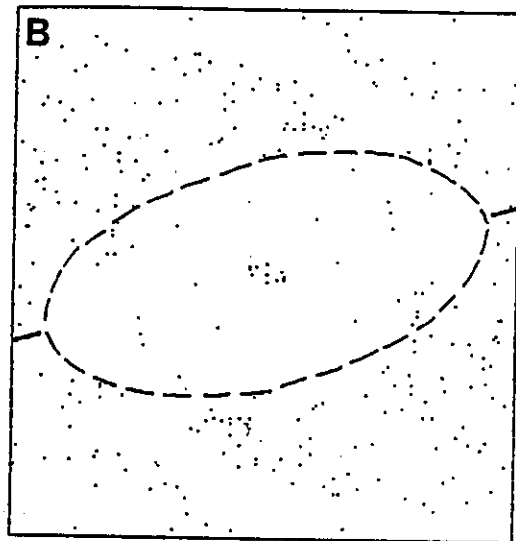
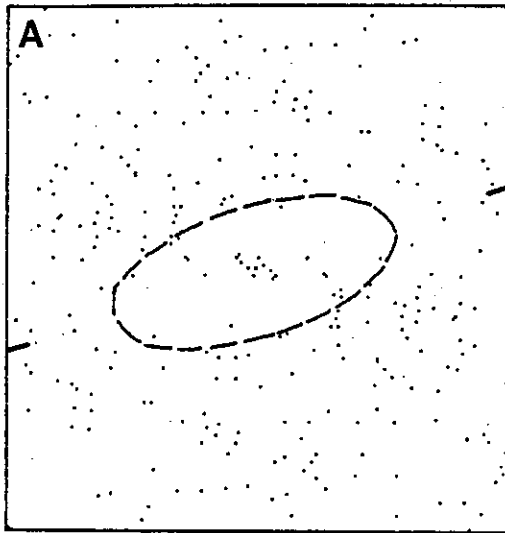


Figure A5.14 Fry plots obtained from INSTRAIN program (A, B, and C), and manually (D) for XZ section of fine-grained graywacke sample 87-34b. A - Five point centre to centre Fry plot; B - Five point centre to centre Normalized Fry plot; C - Centre to centre Fry plot; D - Manually constructed centre to centre Fry plot.

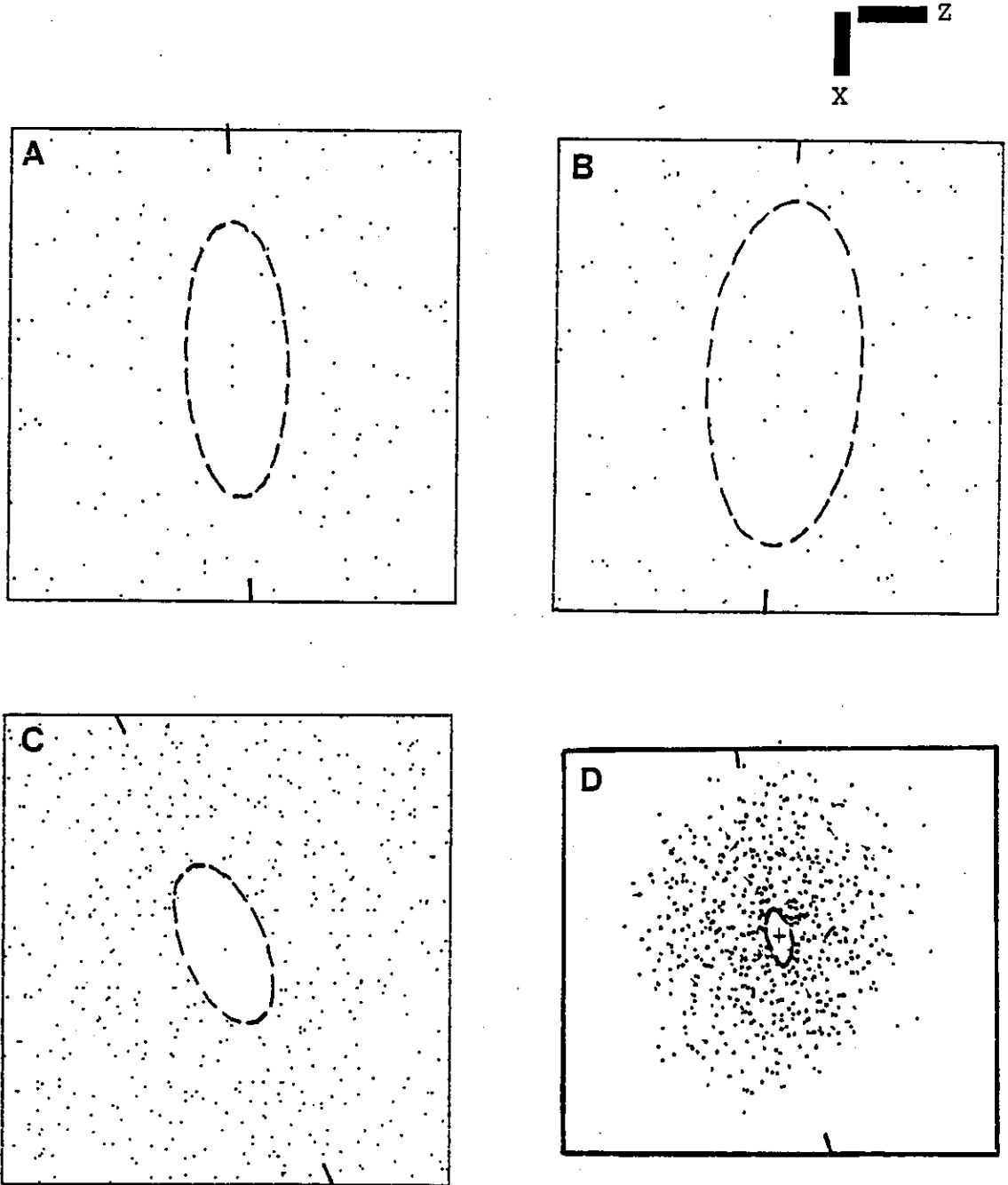




Figure A5.15 Fry plots obtained from INSTRAIN program (A, B, and C), and manually (D) for XY section of fine-grained graywacke sample 87-34b. A - Five point centre to centre Fry plot; B - Five point centre to centre Normalized Fry plot; C - Centre to centre Fry plot; D - Manually constructed centre to centre Fry plot.

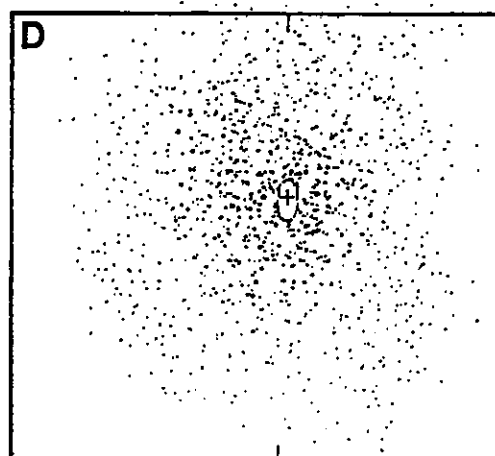
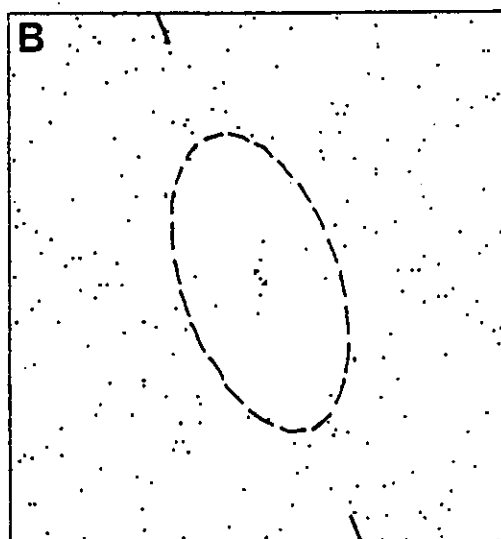
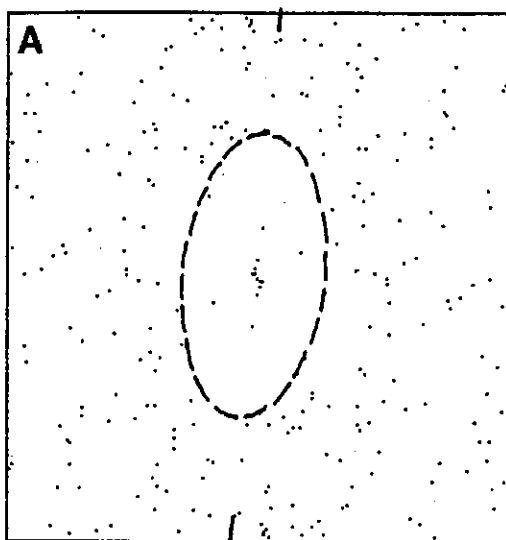


Figure A5.16 Fry plots obtained from INSTRAIN program (A, B, and C), and manually (D) for YZ section of fine-grained siltstone sample 86-78 with metamorphic quartz-biotite-chlorite aggregates. A - Five point centre to centre Fry plot; B - Five point centre to centre Normalized Fry plot; C - Centre to centre Fry plot; D - Manually constructed centre to centre Fry plot.

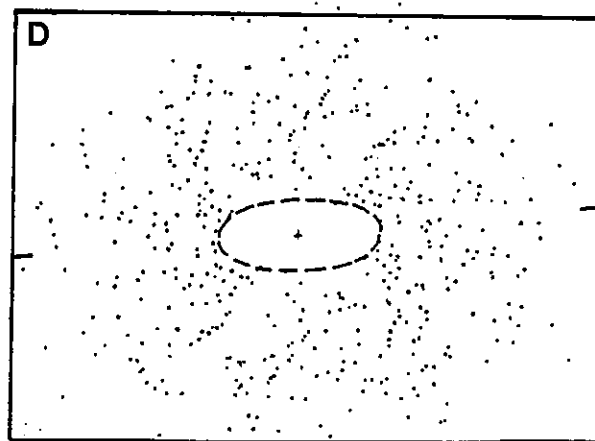
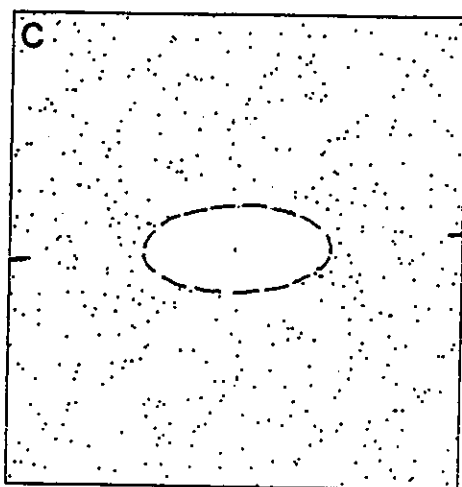
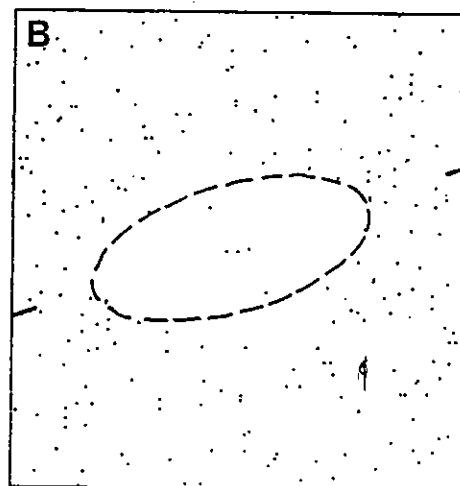
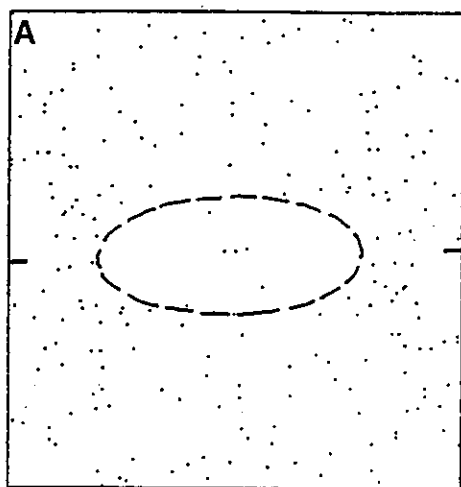


Figure A5.17 Fry plots obtained from INSTRAIN program (A, B, and C), and manually (D) for XZ section of fine-grained siltstone sample 86-78 with metamorphic quartz-biotite-chlorite aggregates. A - Five point centre to centre Fry plot; B - Five point centre to centre Normalized Fry plot; C - Centre to centre Fry plot; D - Manually constructed centre to centre Fry plot.

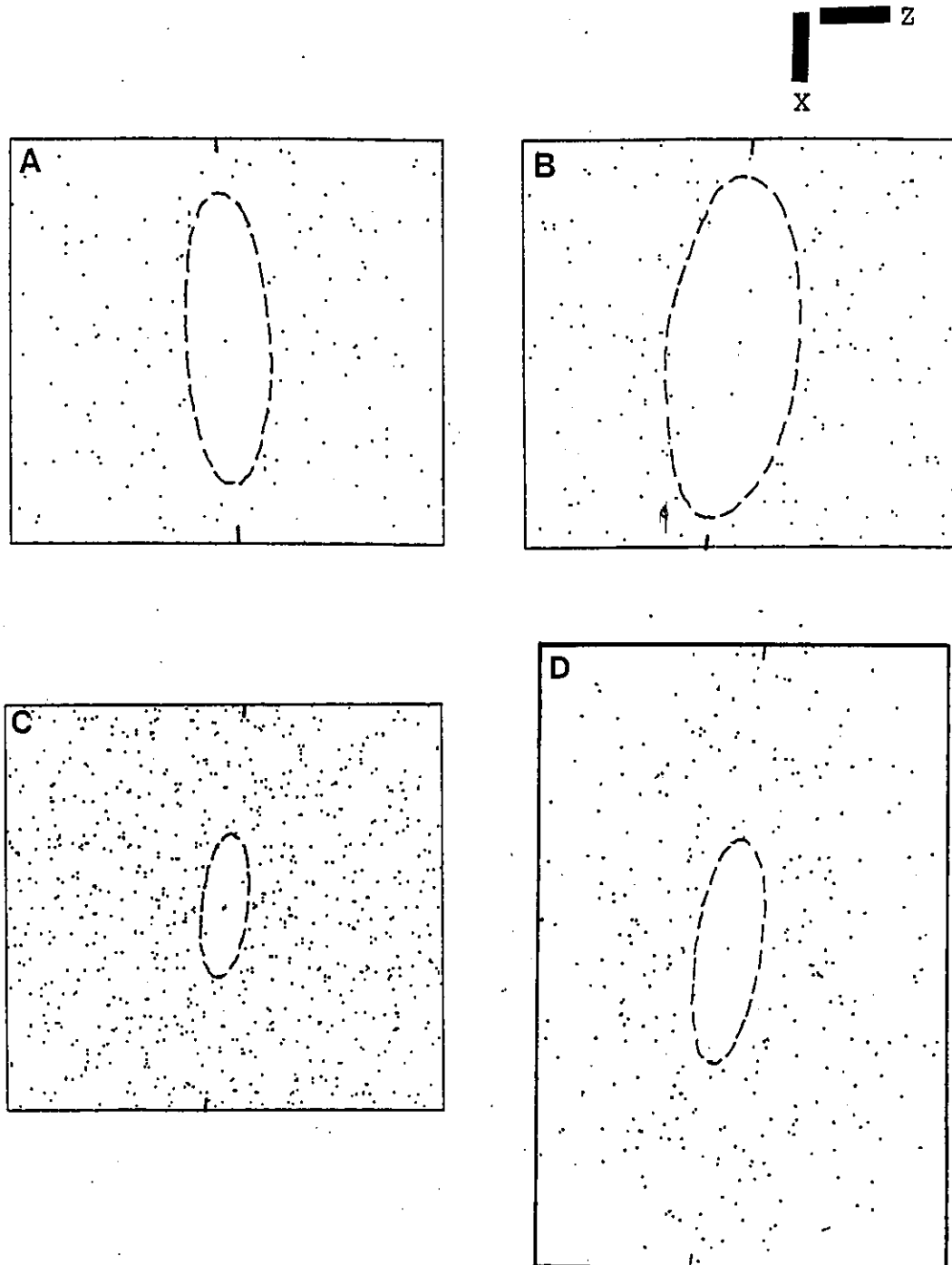


Figure A5.18 Fry plots obtained from INSTRAIN program (A, B, and C), and manually (D) for XY section of fine-grained siltstone sample 86-78 with metamorphic quartz-biotite-chlorite aggregates. A - Five point centre to centre Fry plot; B - Five point centre to centre Normalized Fry plot; C - Centre to centre Fry plot; D - Manually constructed centre to centre Fry plot.

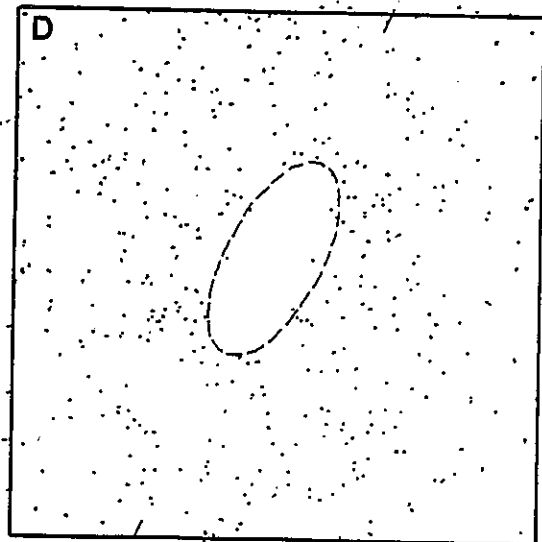
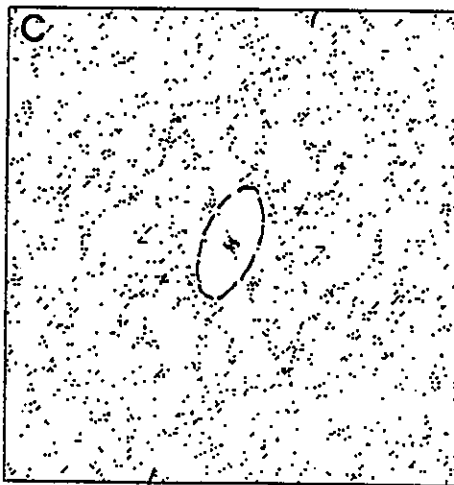
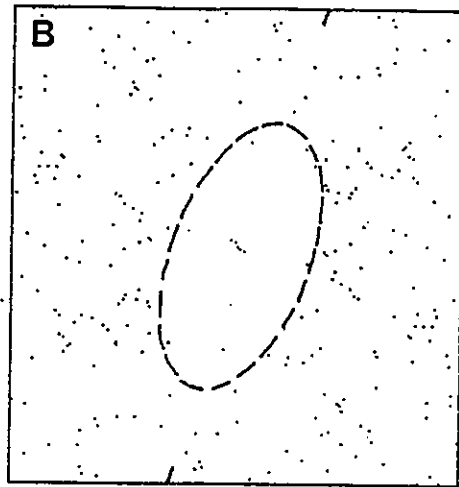
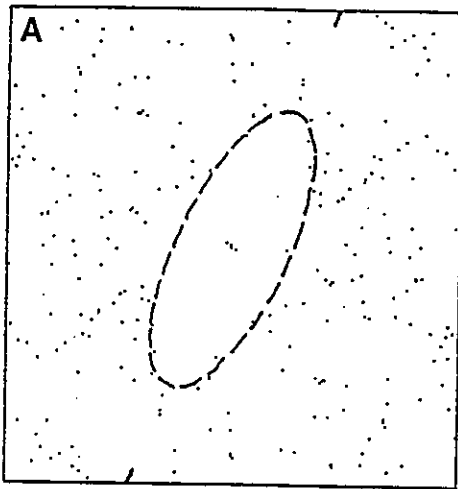


Figure A5.19 Field tracing of D<sub>4</sub> crenulated quartz veins from outcrop at location S6 (Figure A5.23). Note: bedding - wide dashed lines; veins - solid lines; S<sub>3</sub> - single cross hatch; S<sub>4</sub> - double cross hatch; Fs - fine siltstone; Cs - coarse siltstone; G - graywacke; and arrows indicate direction of apparent bedding-parallel slip.

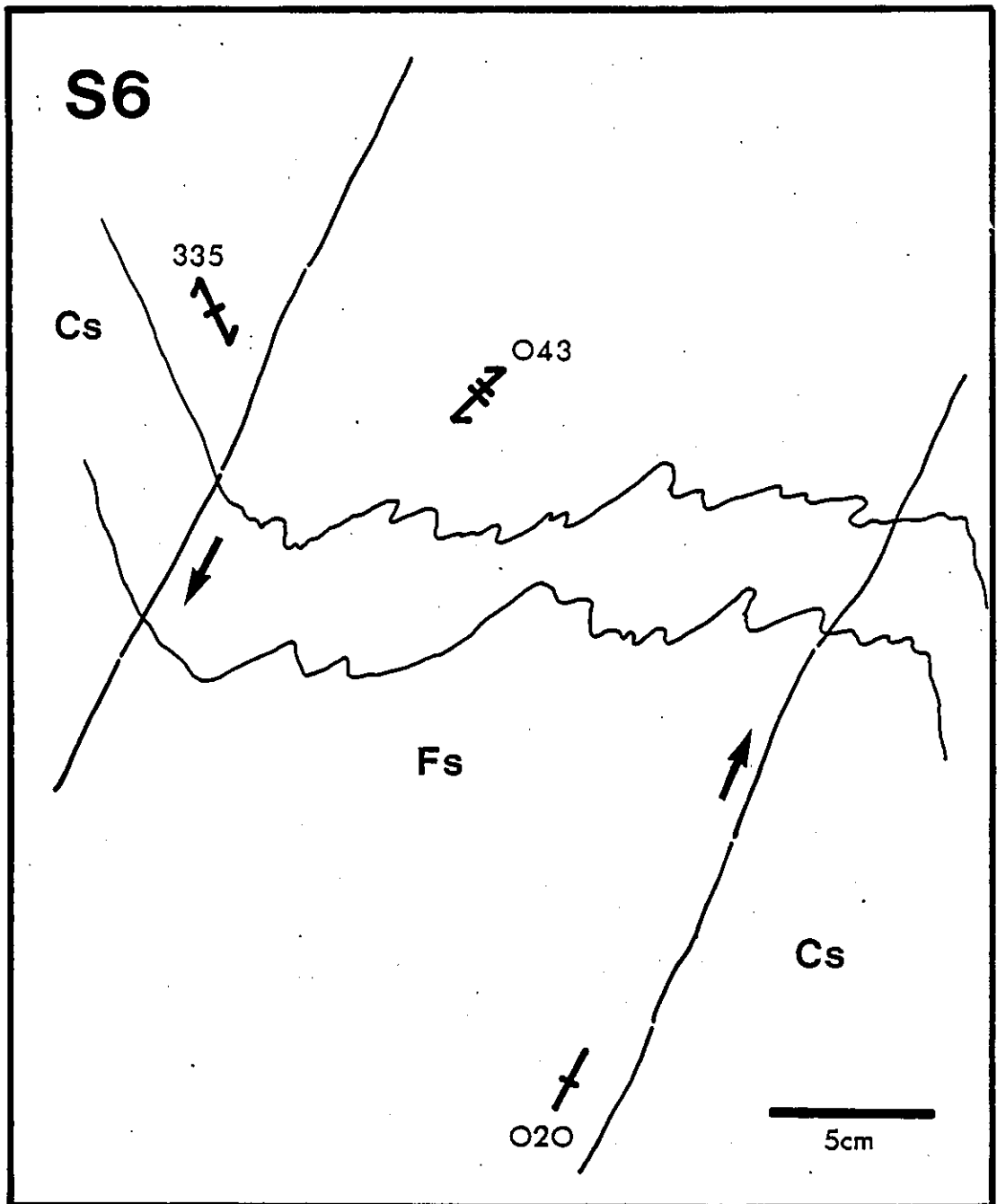


Figure A5.20 Field tracing of D<sub>4</sub> crenulated quartz veins from outcrop at location S3 (Figure A5.23). Note: bedding - wide dashed lines; veins - solid lines; S<sub>3</sub> - single cross hatch; S<sub>4</sub> - double cross hatch; Fs - fine siltstone; Cs - coarse siltstone; G - graywacke; and arrows indicate direction of apparent bedding-parallel slip.

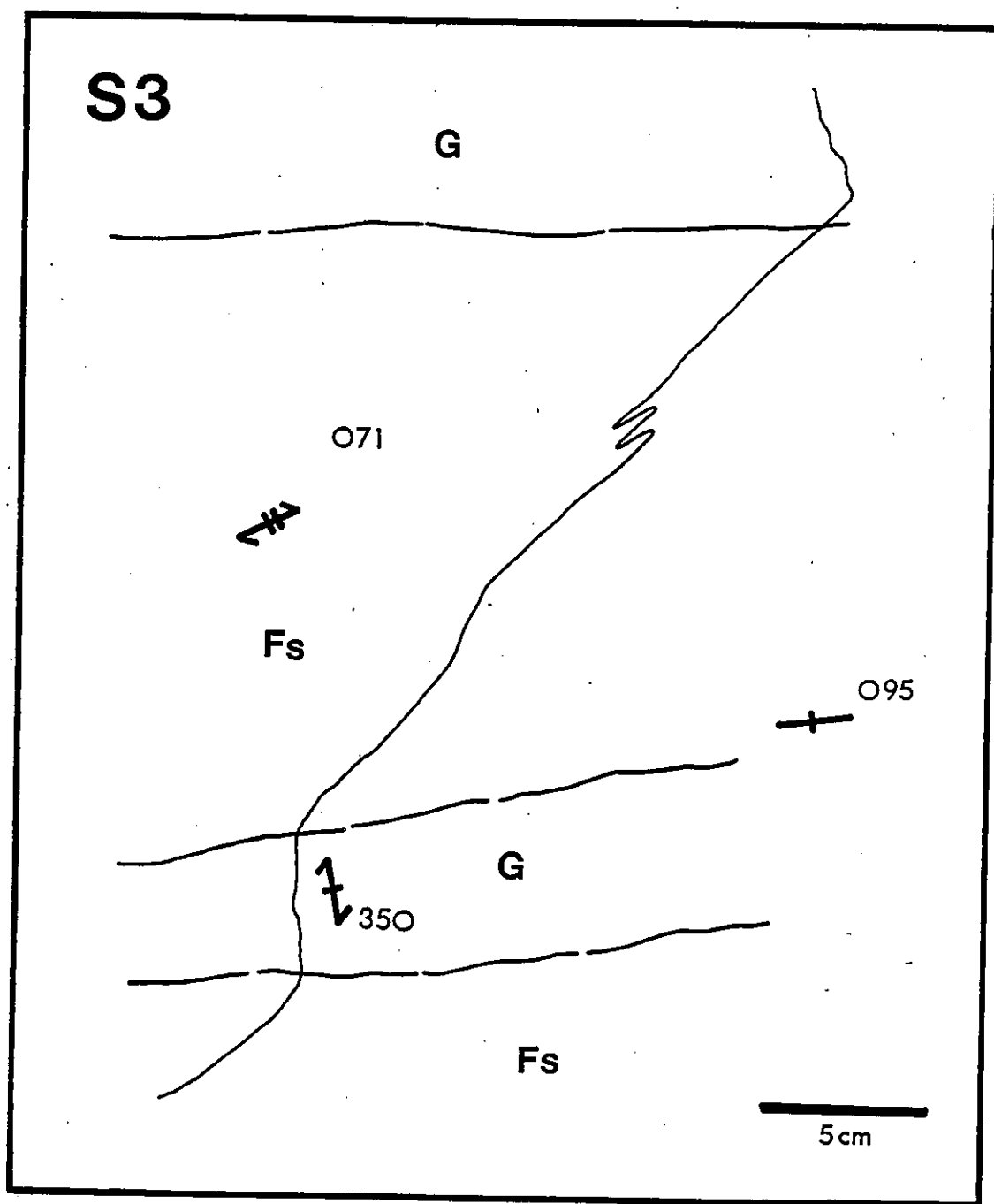


Figure A5.21 Field tracing of D<sub>4</sub> crenulated quartz veins from outcrop at location S2 (Figure A5.23). Note: bedding-wide dashed lines; veins - solid lines; S<sub>3</sub> - single cross hatch; S<sub>4</sub> - double cross hatch; Fs - fine siltstone; Cs - coarse siltstone; G - graywacke; and arrows indicate direction of apparent bedding parallel slip.

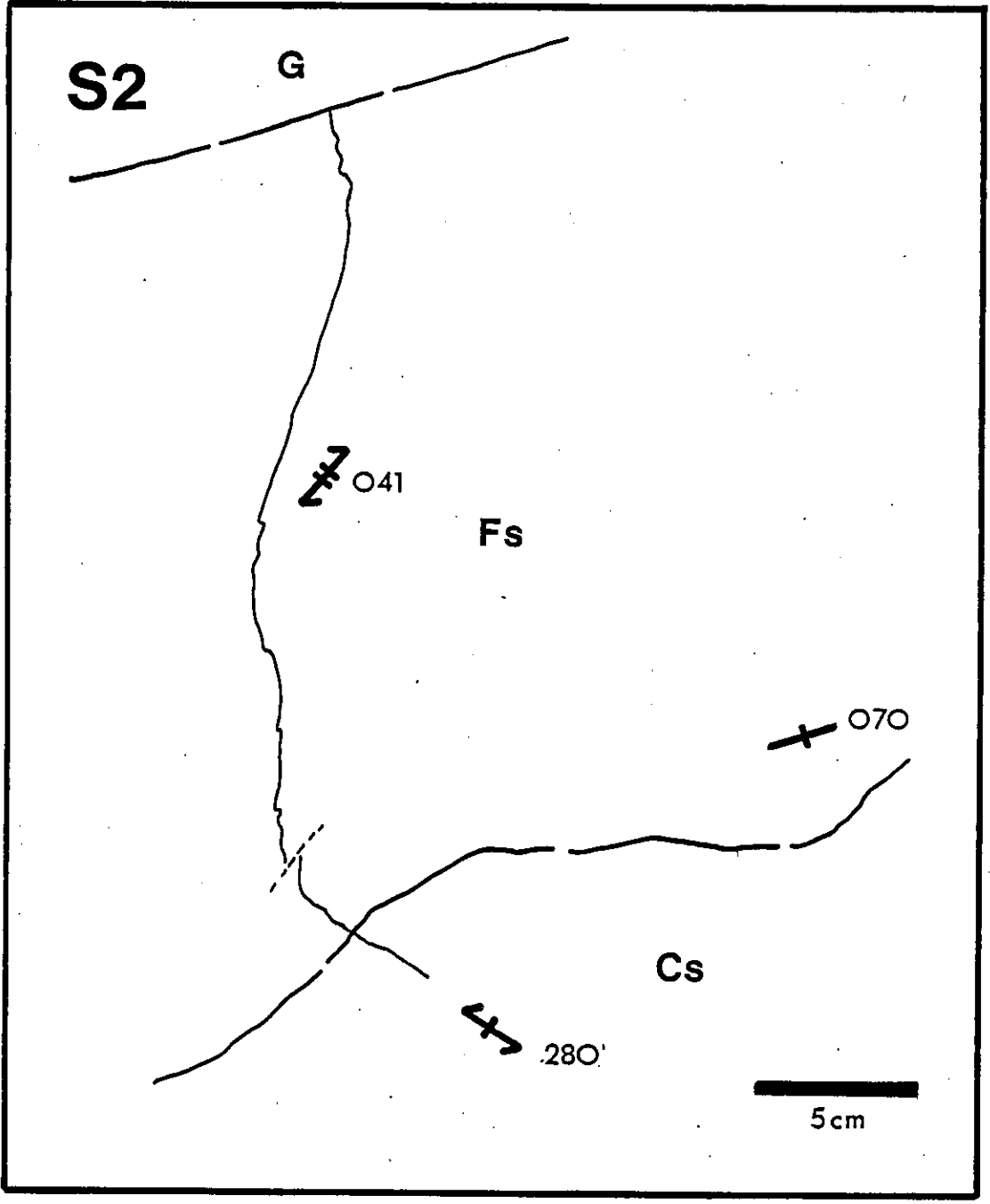


Figure A5.22 Field tracing of D<sub>4</sub> crenulated quartz veins from outcrop at location S5 (Figure A5.23). Note: bedding-wide dashed lines; veins - solid lines; S<sub>3</sub> - single cross hatch; S<sub>4</sub> - double cross hatch; Fs - fine siltstone; Cs - coarse siltstone; G - graywacke; and arrows indicate direction of apparent bedding parallel slip.

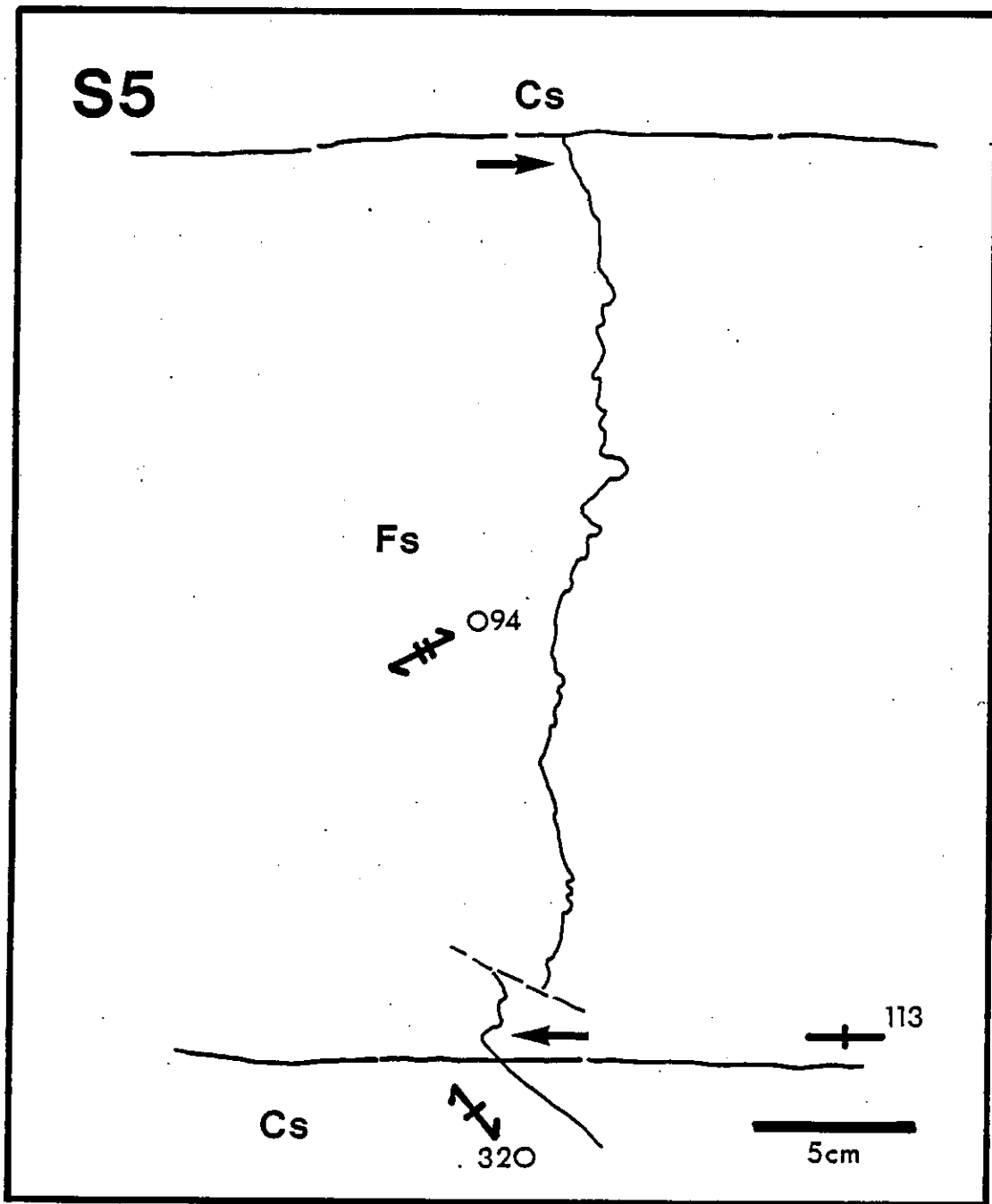
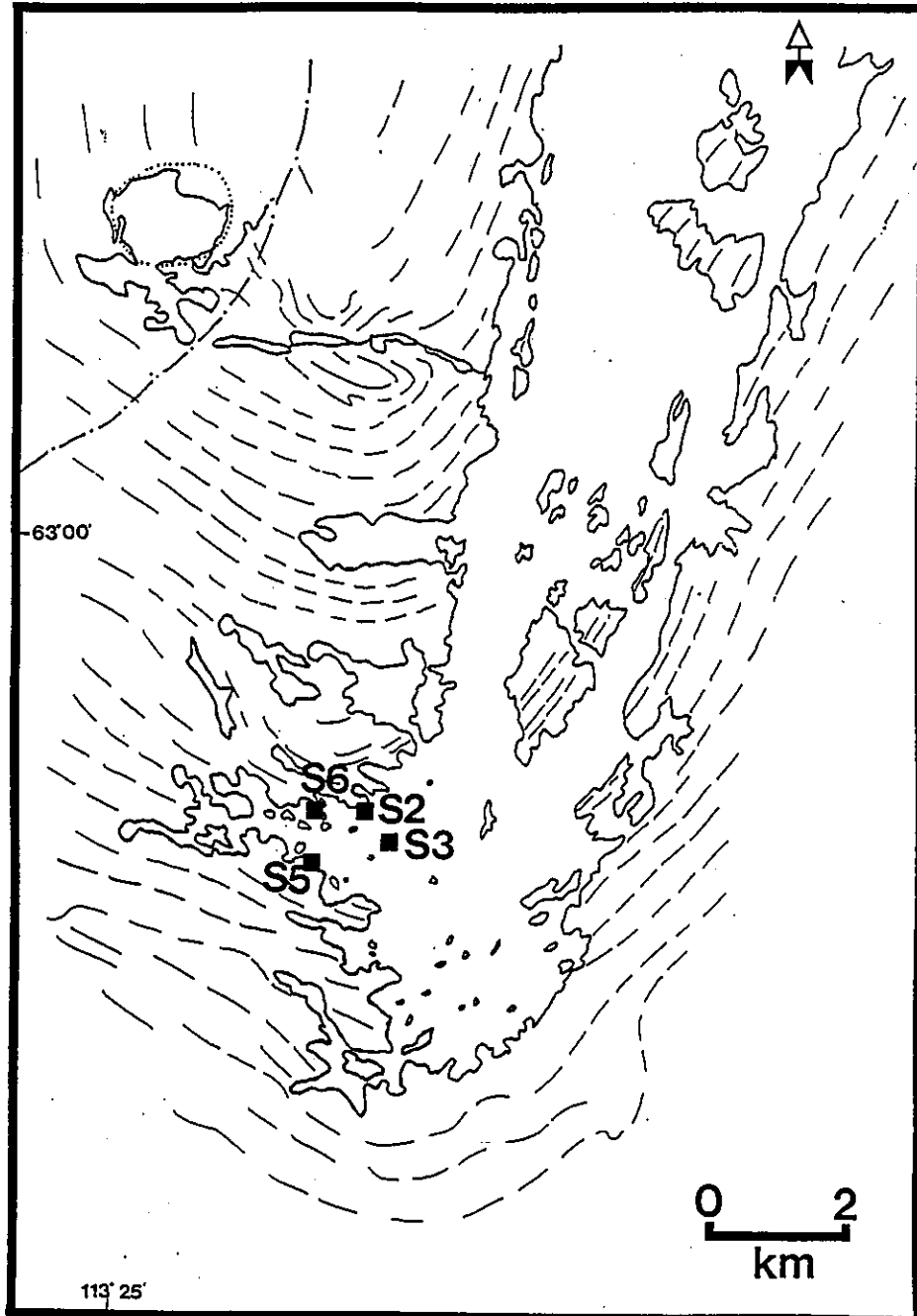




Figure A5.23 Location of  $D_4$  crenulated quartz veins used in estimation of  $D_4$  shear strain.



**Table A5.1 Petrographic and modal analysis of typical graywackes from the West Limb of the Gordon Lake Refold.**

Sample type	Clast size (mm)	Clast/matrix ratio	Clast shape	Sorting	Clast composition	Matrix composition
c/m-GW (86-79)	0.3-0.4	15/85	Sub-rounded	Fair	Qz-95% Pl-5%	CL-15% Qz-55% Ch-10% Bi-17% Op-3%
c/m-GW (86-52)	0.3-0.4	15/85	Sub-rounded	Poor	Qz >95% Pl <5%	CL-15% Mu-40% Qz-20% Bi-15% Ch-5% Op-5%
c/m-GW (22/6/4)	0.2-0.3	25/75	Sub-rounded to sub-angular	Fair	Qz-100%	CL-25% Qz-55% Bi-12% Ch-3% Mu-2% Op-3%
c/m-GW (86-158)	0.2-0.3	20/80	Sub-rounded	Poor	Qz-85% Pl-15%	CL-20% Qz-55% Bi-20% Op-5%
f/m-GW (86-81)	0.2-0.3	25/75	Sub-rounded to rounded	Fair	Qz-90% Pl-10%	CL-25% Qz-45% Mu-10% Ch-10% Bi-5% Op-5%
f-GW (23/6/10)	0.1-0.15	20/80	Sub-angular to sub-rounded	Poor	Qz-95% Pl-5%	CL-20% Qz-52% Mu-10% Ch-10% Op-5% Bi-3%

GW = graywacke; Ss = siltstone

Mineralogy: CL - clasts; Qz - quartz; Mu - muscovite; Ch - chlorite; Bi - biotite; Ca - carbonate; Op - opaque minerals.

Clast Size: c/m - coarse- to medium-grained; m - medium-grained; f/m - fine- to medium- grained; f - fine-grained.

Table A5.2 Petrographic and modal analysis of typical siltstones from the West Limb of the Gordon Lake Refold.

Sample type	Clast size (mm)	Clast/matrix ratio	Clast shape	Sorting	Clast composition	Matrix composition
c-Ss (87-60)	0.04-0.05	55/45	Sub-rounded	Good	Qz-100%	CL-55% Ch-25% Bi-20% Op-5%
c-Ss (86-115)	0.05-0.07	20/80	Sub-angular	Poor	Qz-80% Pl-20%?	CL-20% Ch-30% Qz-25% Mu-10% Bi-10% Op-5%
c-Ss (87-201)	0.05-0.07	25/75	Sub-angular	Fair	Qz-95% Pl-5%	CL-25% Mu-30% Qz-20% Ch-15% Bi-5% Op-5%
c-Ss (21/6/9)	0.05-0.07	40/60	Sub-rounded	Good	Qz-100%	CL-40% Ch-20% Qz-15% Mu-15% Bi-5% Op-5%
f/m-Ss (87-201)	0.005-0.01	30/70	Sub-angular to sub-rounded	Good	Qz-100%	CL-30% Mu-32% Qz-30% Op-5% Bi-3%
f-Ss (86-94)	0.01	40/60	Sub-angular to sub-rounded	Good	Qz-100%	CL-40% Qz-20% Ch-15% Mu-15% Bi-10%

Gw = graywacke; Ss = siltstone

Mineralogy: CL - clasts; Qz - quartz; Mu - muscovite; Ch - chlorite; Bi - biotite; Ca - carbonate; Op - opaque minerals.

Clast Size: c/m - coarse- to medium-grained; m - medium-grained; f/m - fine- to medium- grained; f - fine-grained.

Table A5.3 Petrographic and modal analysis of typical graywackes from the East Limb of the Gordon Lake Refold.

Sample type	Clast size (mm)	Clast/matrix ratio	Clast shape	Sorting	Clast composition	Matrix composition
c/m-GW (87-66)	0.3-0.7	25/75	Sub-rounded to rounded	Fair to Good	Qz-95% Pl-5%	CL-25% Qz-32% Mu-20% Ch-20% Op-3%
c/m-GW (87-51)	0.1-0.5	25/75	Sub-angular to sub-rounded	Fair	Qz-70% Pl-30%	CL-30% Qz-17% Mu-30% Ch-20% Op-3%
m-GW (87-52)	0.1-0.3	25/75	Sub-rounded	Fair	Qz-90% Pl-10%	CL-25% Qz-17% Mu-25% Ch-25% Op-3% Ca?-5%
c/m-GW (87-27)	0.3-0.5	20/80	Sub-rounded	Fair	Qz-80% Pl-20%	CL-20% Qz-35% Mu-20% Ch-20% Op-5%
f-GW (87-34b)	0.1-0.2	15/85	Sub-rounded	Poor	Qz-95% Pl-5%	CL-15% Qz-13% Mu-40% Ch-30% Op-2%
f-GW (87-13)	0.1-0.2	20/80	Sub-rounded to rounded	Fair	Qz-80% Ca-20%	CL-20% Qz-25% Mu-20% Ch-12% Ca-20% Op-3%

GW = graywacke; Ss = siltstone

Mineralogy: CL - clasts; Qz - quartz; Mu - muscovite; Ch - chlorite; Bi - biotite; Ca - carbonate; Op - opaque minerals.

Clast Size: c/m - coarse- to medium-grained; m - medium-grained; f/m - fine- to medium- grained; f - fine-grained.

Table A5.4 Petrographic and modal analysis of typical siltstones from the East Limb of the Gordon Lake Refold.

Sample type	Clast size (mm)	Clast/matrix ratio	Clast shape	Sorting	Clast composition	Matrix composition
c-Ss (87-88)	0.03	50/50	Sub-rounded	Good	Qz-100%	Qz-50% Mu-35% Ch-15% Bi-10%
c-Ss (87-91)	0.01-0.04	15/85	Sub-	Fair	Qz-100%	CL-15% Qz-10% Mu-15% Ch-15% Op-5% Ca-40%
f-Ss (87-147)	<0.01	-	-	-	10% carbonate aggregates	Ca-10% Qz-18% Mu-35% Ch-35% Op-2%
f-Ss (87-65)	<0.01	-	-	-	5% carbonate aggregates	Ca-5% Qz-32% Mu-30% Ch-30% Op-3%
f-Ss (87-84)	<0.01	-	-	-	-	Qz-27% Mu-35% Ch-35% Ca-3%

GW = graywacke; Ss = siltstone

Mineralogy: CL - clasts; Qz - quartz; Mu - muscovite; Ch - chlorite; Bi - biotite; Ca - carbonate; Op - opaque minerals.

Clast Size: c/m - coarse- to medium-grained; m - medium-grained; f/m - fine- to medium- grained; f - fine-grained.

**Table A5.5** D<sub>3</sub> cleavage morphology and microstructure in graywackes from the West Limb of the Gordon Lake Refold.

Sample number & lithology	Clast truncation	Pressure shadows on clasts	Cleavage seams	Clast preferred orientation	Metamorphic minerals and preferred orientation
86-79 YZ (c/m)	10%	5-10%	-	5-10%	Bi - 50%
86-79 XZ (c/m)	80%	40%	Trace (Op)	90%	Bi - 90%
22/6/4 YZ(c/m)	5-10%	-	-	20%	Bi, Ch, Op - 30%
22/6/4 XZ(c/m)	75%	70%	Trace (Op,Bi)	77%	Bi, Ch, Op - 75%
86-52 YZ (m)	70%	15%	Trace (Op)	60%	Bi, Mu - 35%
86-52 XZ (m)	70%	35%	Trace (Op)	70%	Bi, Mu - 65%
86-158 YZ(c/m)	5-10%	5%	-	5-10%	Bi - 35%
86-158 XZ(c/m)	65%	40%	Dis. (Bi,Op)	65%	Bi - 85%
86-81 YZ (f/m)	10%	5-10%	-	15%	Bi, Mu - 30%
86-81 XZ (f/m)	70%	90%	Trace (Op)	85%	Bi, Mu - 75%

Mineralogy: Qz - quartz; Mu - muscovite; Ch - chlorite; Bi - biotite; Ca - Calcium carbonate material; Op - opaque minerals.

Clast Size: c/m - coarse- to medium-grained; m - medium-grained; f/m - fine- to medium- grained; f - fine-grained.

Cleavage Seams: Dis. - discontinuous; Con. - continuous; Ox - iron oxide material.

Orientation of section: YZ - perpendicular to cleavage and lineation; XZ - perpendicular to cleavage and parallel to lineation.

**Table A5.6** D<sub>3</sub> cleavage morphology and microstructure in siltstones from the West Limb of the Gordon Lake Refold.

Sample number & lithology	Clast truncation	Pressure shadows on clasts	Cleavage seams	Clast preferred orientation	Metamorphic minerals and preferred orientation
86-115 YZ (c-Ss) 20%	20%	10-20%	Con. (Ox,Bi) spaced 0.2-0.3 mm	50-60%	Bi, Ch - 55%
86-115 XZ (c-Ss) 85%	85%	80-90%	Con. (Ox,Bi) spaced 0.1 mm	90-95%	Bi, Ch - 85%
87-60 YZ (c-Ss) 5%	5%	-	Trace	5%	Bi, Op - 75%
87-60 XZ (c-Ss) 30%	30%	-	Trace	30-40%	Bi, Op - 90%
87-201 YZ (c-Ss) -	-	-	Con. (Ox,Bi) spaced 0.5 mm	80-90%	Mu, Ch, Bi - 95%
87-201 XZ (c-Ss) -	-	-	Con. (Ox,Bi) spaced 0.5 mm	80-90%	Mu, Ch, Bi - 75%
86-94 YZ (f-Ss) -	-	-	Con. (Ox,Bi) spaced 0.1 mm in zones 1-2 mm apart	-	Bi, Ch, Mu - 90%
86-94 XZ (f-Ss) -	-	-	Con. (Ox,Bi) spaced 0.1 mm in zones 1-2 mm apart	-	Bi, Ch, Mu - 100%
87-201 YZ (f-Ss) -	-	5%	Con. (Ox,Bi) spaced <0.1 mm in zones 0.5-1 mm apart	-	Bi, Ch, Mu - 70%
87-201 XZ (f-Ss) -	-	-	Con. (Ox,Bi) spaced 0.15 mm in zones 0.5-0.7 mm apart	70%	Mu, Ch, Bi - 65%

Mineralogy: Qz - quartz; Mu - muscovite; Ch - chlorite; Bi - biotite; Ca - carbonate; Op - opaque minerals.

Clast Size: c/m - coarse- to medium-grained; m - medium-grained; f/m - fine- to medium- grained; f - fine-grained.

Cleavage Seams: Dis. - discontinuous; Con. - continuous; Ox - iron oxide material.

Orientation of section: YZ - perpendicular to cleavage and lineation; XZ - perpendicular to cleavage and parallel to lineation.

Table A5.7 D<sub>3</sub> cleavage morphology and microstructure in graywackes from the East Limb of the Gordon Lake Refold.

Sample number & lithology	Clast truncation	Pressure shadows on clasts	Cleavage seams	Clast preferred orientation	Metamorphic minerals and preferred orientation
87-66 YZ (c/m)	<5%	<5%	-	5-10%	Mu, Ch - 10-20%
87-66 XZ (c/m)	>90%	>90%	Dis. (Mu, Ch)	>90%	Mu, Ch - >95%
87-51 YZ (m)	25%	25%	Dis. (Ox)	40%	Mu, Ch - 50%
87-51 XZ (m)	>90%	>90%	Con. (Mu, Ch)	>90%	Mu, Ch - >90%
87-34b YZ (f)	30%	30%	Dis. (Ox)	40-50%	Mu, Ch - 60%
87-34b XZ (f)	>90%	>90%	Con. (Mu, Ch)	>90%	Mu, Ch - >90%
87-52 YZ (m)	15%	10%?	Trace	30%	Mu, Ch - 40%
87-52 XZ (m)	>90%	>90%	Con. (Mu, Ch)	>90%	Mu, Ch - >90%
87-27 YZ (c/m)	15%	15%	-	10%	Mu, Ch - 10%
87-27 XZ (c/m)	35%	30%	-	30-40%	Mu, Ch - 20-30%

Mineralogy: Qz - quartz; Mu - muscovite; Ch - chlorite; Bi - biotite; Ca - carbonate; Op - opaque minerals.

Clast Size: c/m - coarse- to medium-grained; m - medium-grained; f/m - fine- to medium- grained; f - fine-grained.

Cleavage Seams: Dis. - discontinuous; Con. - continuous; Ox - iron oxide material.

Orientation of section: YZ - perpendicular to cleavage and lineation; XZ - perpendicular to cleavage and parallel to lineation.



Table A5.8 D<sub>3</sub> cleavage morphology and microstructure in siltstones from the East Limb of the Gordon Lake Refold.

Sample number & lithology	Clast truncation	Pressure shadows on clasts	Cleavage seams	Clast preferred orientation	Metamorphic minerals and preferred orientation
86-115 YZ (c-Ss)	20%	10-20%	Con. (Ox, Bi) spaced 0.2-0.3 mm	50-60%	Bi, Ch - 55%
87-88 YZ (c)	15%?	10-20%?	-	30-40%	Mu, Ch - 50%
87-88 XZ (c)	>90%	>90%	-	>90%	Mu, Ch - >90%
87-91 YZ (c/m)	15%?	10-20%?	Dis. 0.5 mm spacing	30%?	Mu, Ch - 30-40%
87-91 XZ (c/m)	>90%	>90%	Con. (Mu, Ch, Ca)	>90%	Mu, Ch, Ca - >90%
87-147 YZ (f)	-	-	Dis. (Op) 0.15 mm spacing	-	Mu, Ch, Qz - 60%
87-147 XZ (f)	-	-	Con. (Op, Ch, Mu) 0.05-0.1 mm spacing	-	Mu, Ch, Qz - >95%
87-65 YZ (f)	-	-	-	-	Ch, Qz, Mu - 70%
87-65 XZ (f)	-	-	-	-	Ch, Qz, Mu - >95%
87-84 YZ (f)	-	-	-	-	Ch, Qz, Mu - 70%
87-84 XZ (f)			Not Available		

Mineralogy: Qz - quartz; Mu - muscovite; Ch - chlorite; Bi - biotite; Ca - carbonate; Op - opaque minerals.

Clast Size: c/m - coarse- to medium-grained; m - medium-grained; f/m - fine- to medium- grained; f - fine-grained.

Cleavage Seams: Dis. - discontinuous; Con. - continuous; Ox - iron oxide material.

Orientation of section: YZ - perpendicular to cleavage and lineation; XZ - perpendicular to cleavage and parallel to lineation.

Table A5.9 Crenulation cleavage ( $S_4$ ) microstructure from the West Limb of the Gordon Lake Refold.

Sample number	Zonal/Discrete ratio*	Spacing (mm)	Composition	Comments
86-84	95/5	0.05	Mu-80% Ch-10% Qz-10%	ILA - 100° no well developed $S_4$ cleavage seams
86-99	85/15	0.02- 0.05	Mu-30% Ch-30% Qz-10 Bi-20%	$S_4$ cleavage seams with oriented biotite
86-250	20/80	0.02- 0.05	Mu-60% Ch-10% Qz-30%	ILA - 60° $S_4$ cleavage seams with oriented biotite
6/6/3	Microfolds to discrete	0.3- 1.0	Mu-60% Ch-10% Qz-30%	Asymmetric microfolds.
87-127	80/20	0.05- 0.1	Mu-40% Ch-30% Qz-20% Bi-10%	ILA - 85° $S_4$ cleavage seams along limbs of microfolds
87-57	90/10	0.05- 0.1	Mu-70% Ch-10% Qz-20%	Poorly developed cleavage seams
21/6/1	90/10	0.01- 0.05	Mu-85% Qz-10% Bi-10%	Biotite on limbs of microfolds
21/6/3	80/10	0.03- 0.05	Mu-75% Qz-10% Ch-10% Bi-5%	Biotite on limbs of microfolds
86-186	Microfolds to discrete	0.03- 0.05	Mu-80% Ch-10% Qz-10%	Microfolds 0.1-0.15 mm half-wavelength

Mu - muscovite; Qz - quartz; Ch - chlorite; Bi - biotite

ILA - inter-limb angle of crenulation microfolds.

\* - Proportion of crenulation cleavage type from zonal to discrete (Gray, 1977)

Table A5.10 Crenulation cleavage ( $S_{4E}$ ) microstructure from the Centre and East Limb of the Gordon Lake Refold.

Sample Number	Zonal/Discrete Ratio*	Spacing (mm)	Composition (%)	Comments
87-18 <sup>1</sup>	10/90	0.02-0.1	Mu-80% Ch-10% Qz-7% Op-3%	Discrete crenulation forming $S_{3Es}$ and itself re-crenulated at approximately 90°
17/6/3 <sup>1</sup>	50/50	0.05-0.1	Mu-70% Qz-20% Ch-10%	Microfolds (0.1-0.5 mm) with discrete cleavage seams
17/6/2 <sup>1</sup>	Zonal	1.0	Mu-70% Qz-20% Ch-5% Op-5%	Broad zonal crenulations
87-147 <sup>2</sup>	Zonal (dextral) (0.05 mm wide)	0.1-0.2	Mu >90%	Poor zonal crenulations ( $S_{4E}$ ) sub-perpendicular to $S_{3Es}$ cleavage
87-148 <sup>2</sup>	Zonal (dextral) (0.05 mm wide)	0.1-0.2	Mu >90%	Poor zonal crenulations ( $S_{4E}$ ) sub-perpendicular to $S_{3Es}$ cleavage
87-65 <sup>2</sup>	Zonal? (0.01-0.02 mm wide)	0.1-0.2	Mu >90%	Extremely fine zonal crenulation ( $S_{4E}$ ) sub-perpendicular to $S_{3Es}$ cleavage
87-13 <sup>2</sup>	Fractures? (0.01-0.02 mm wide)	0.1	Mu >80% Ch-10%	Extensional(?) fractures found in boudinaged vein 'necks'

Mineralogy: Mu - muscovite; Qz - quartz; Ch - chlorite; Bi - biotite; Op - opaque minerals; Ox - iron oxides.

\* - Proportion of crenulation cleavage type from zonal to discrete (Gray, 1977)

<sup>1</sup>Central region of refold

<sup>2</sup>East Limb of Refold

Table A5.11 Petrographic of metamorphic aggregates from siltstones of the South Gordon Lake region.

Sample number	Proportion (%) <sup>1</sup>	Size (mm)	Composition of aggregate						Op %	Cleavage <sup>2</sup> association	Comments
			Qz %	Bi %	Ch %	Mu %	Ca %	Op %			
87-147	20	0.1-0.3	-	-	2	-	90	8	// S <sub>3s</sub>	Op oriented	
87-5	20	0.2-0.7	50	-	30	10	-	30	// S <sub>3s</sub>	Mu rims	
87-57	15	0.1-0.4	75	10	10	-	-	5	// S <sub>3Es</sub>	Bi rims	
87-127	10	0.1-0.3	35	10	35	-	-	20	// S <sub>3s</sub>		
86-187	25	0.3-1.0	5	-	90	-	-	5	// S <sub>3s</sub>		
86-112	30	0.3-0.8	-	-	95	-	-	5	// S <sub>3s</sub>		
86-7	20	0.1-0.3	10	20	55	-	-	15	// S <sub>3s</sub>	Bi centres	
D48-3.5	25	0.1-0.4	-	-	97	-	-	3	// S <sub>3s</sub>		
BC11-11.5	25	0.2-0.7	50	30	10	-	-	10	// S <sub>3s</sub>		
87-156	10	0.1-0.3	50	-	35	-	-	15	// S <sub>3Es</sub>		
87-95	20	0.2-0.5	35	-	35	20	-	10	// S <sub>3Es</sub>	Mu rims	
87-183	10	0.2-0.4	80	-	15	-	-	5	// S <sub>3s</sub>		
86-78	30	0.5-1.5	20	30	40	-	-	10	// S <sub>3s</sub>	D4 deformed	
21/6/2	5	0.1-0.2	20	-	50	-	-	30	// S <sub>3s</sub>		
87-87	10	0.1-0.2	-	-	-	-	98	2	// S <sub>3Es</sub>		
87-172	10	0.2-0.8	65	5	20	-	-	10	// S <sub>3Es</sub>		
86-64	20	0.1-0.3	75	10	10	-	-	5	// S <sub>3s</sub>	Bi rims	
86-34	15	0.1-0.3	25	50	5	-	-	20	// S <sub>3s</sub>	Bi rims	
E31-13.5	30	0.2-0.5	-	-	90	-	-	10	// S <sub>3s</sub>		
87-148	20	0.1-0.2	10	-	-	-	80	10	// S <sub>3Es</sub>	Op oriented	
86-21	20	0.2-0.5	10	-	65	20	-	5	// S <sub>3s</sub>	Mu rims	
87-65	3	0.1-0.3	5	-	-	-	90	5	// S <sub>3Es</sub>		
87-28	15	0.1-0.5	-	-	-	-	95	5	N/O		
86-152	10	0.1-0.3	45	30	20	-	-	5	// S <sub>3s</sub>		

Mineralogy: Qz - quartz; Mu - muscovite; Ch - chlorite; Bi - biotite; Ca - carbonate; Op - opaque minerals.

<sup>1</sup> Percentage of aggregates in siltstone

<sup>2</sup> Association between orientation of aggregate and cleavage: // - parallel to S<sub>3s</sub>/S<sub>3Es</sub>; N/O - not oriented.

Table A5.12 Petrography of quartz inclusions within biotite porphyroblasts from the West Limb and Centre of the Gordon Lake Refold.

SAMPLE NUMBER	BIOTITE SIZE (mm)	BIOTITE PROPORTION (%)	ORIENTATIONS(°)				COMMENTS
			S <sub>3s</sub>	S <sub>3E</sub> S	S <sub>4</sub>	QIT	
86-94	0.2-0.4	15	286	-	-	// S <sub>3s</sub>	Minor S <sub>4</sub> , up to 30° of inclusion trail curvature, pressure shadows greater around 001 than 010 planes
87-201	0.1-0.2	15	336	-	-	// S <sub>3s</sub>	Minor pressure shadows
86-93	0.2-0.6	20	320	-	-	// S <sub>3s</sub>	Pressure shadows around 001 planes, up to 30° of inclusion trail curvature (340-350°), no D <sub>4</sub>
86-94	0.1-0.2	7	-	-	060	// S <sub>3s</sub>	D <sub>4</sub> folding of biotites, possible rotation of biotites with pressure shadows during D <sub>4</sub>
7/6/3	0.05-0.1	5	315	-	045	// S <sub>3s</sub>	Minor inclusion trail curvature and pressure shadows
6/6/3	0.1-0.4	10	-	-	100	// S <sub>3s</sub> ?	Intense pressure shadows around biotites, both deformed by broad D <sub>4</sub> folds, inclusion trails rotated from parallelism with S <sub>3s</sub> ?
86-115	0.05-0.1	5	325	-	-	// S <sub>3s</sub>	Coarse siltstone, poorly developed inclusion trails
6/6/2	0.1-0.2	25	315	-	-	// S <sub>3s</sub>	Poorly developed inclusion trails
21/6/5	0.05-0.1	3	300	-	-	// S <sub>3s</sub>	Minor D <sub>4</sub> crenulation and inclusion trail curvature
21/6/6	0.05	2	302	-	-	// S <sub>3s</sub>	Minor D <sub>4</sub> crenulation and inclusion trail curvature
21/6/8	0.05-0.1	3	305	-	-	// S <sub>3s</sub>	Minor D <sub>4</sub> crenulation and inclusion trail curvature
21/6/9	0.05	2	320	-	-	// S <sub>3s</sub>	Minor D <sub>4</sub> crenulation, poor inclusion trails and ragged biotites

QIT - Quartz inclusion trail orientation within biotite porphyroblast

Table A5.13 Petrography of quartz inclusions within biotite porphyroblasts from the East Limb of the Gordon Lake Refold.

Sample number	Biotite size (mm)	Biotite proportion(%)	Orientations(°)				Comments
			S <sub>3s</sub>	S <sub>3E<sub>s</sub></sub>	S <sub>4</sub>	QIT	
29/6/7 (E)	0.05-0.2	5	040	000	-	070	Ragged biotites, with earlier inclusion trails sub// S <sub>3s</sub> , some evidence of biotite rotation
23/6/4 (C)	0.1-0.6	50	-	330?	-	070	Biotites well aligned along S <sub>3E<sub>s</sub></sub> , both 001 and 010 planes, near higher grade contact
11/6/4 (E)	0.2-1.5	35	-	330?	-	050	Large biotites in quartz with fine polygonal texture
17/6/3 (C)	0.05-0.1	1	-	-	040	// S <sub>3s</sub>	Poorly developed inclusion trails
17/6/5 (C)	0.1-0.3	3	-	020	-	?	Random inclusion trails
*87-147 (E)	0.1-0.3	20	-	024	-	084	Opaque mineral inclusions in carbonate porphyroblasts
*87-148 (E)	0.1-0.2	10	-	025	-	085	Opaque mineral inclusions in carbonate porphyroblasts

QIT - Quartz inclusion trail orientation within biotite porphyroblast.

\* - opaque inclusions within carbonate aggregates.

Sample location: E - East limb of refold; C - Centre of refold.

**Table A5.14 Petrography and microstructure of graywackes and siltstones analyzed by Fry Technique.**

Sample number	Lithology type	Clast size (mm)	Clast/matrix ratio	Degree of pressure solution	Clast truncation	Clast undulatory extinction	Associated metamorphic minerals
22/6/4 <sup>1</sup>	c/m-GW	0.2-0.3	25/75	Moderate	Moderate	Minor	Bi, Ch, Mu
87-51 <sup>2</sup>	c/m-GW	0.1-0.5	25/75	Moderate	Moderate	Minor	Mu, Ch
87-66 <sup>2</sup>	c/m-GW	0.3-0.7	25/75	Moderate	Moderate	Minor	Mu, Ch
87-34b <sup>3</sup>	f-GW	0.1-0.2	15/85	Minor - Moderate	Moderate	Minor	Ch, Mu
86-115 <sup>1</sup>	c-Ss	0.05-0.07	15/85	Intense	Moderate	Minor	Bi, Ch, Mu
86-78 <sup>1</sup>	f-Ss	Qu-Bi-Ch aggregates 0.5-1.5 mm	30/75	Intense	-	-	Qz, Bi, Ch

GW = Graywacke; Ss = Siltstone

Clast Size: c/m - coarse- to medium-grained; m - medium grained; f/m - fine- to medium-grained; f - fine-grained

Mineralogy: Bi - biotite; Ch - chlorite; Mu - muscovite.

- <sup>1</sup> Sample from west limb of refold  
<sup>2</sup> Sample from east limb of refold  
<sup>3</sup> Sample from centre of refold

Table A5.15 Measured ellipse ratios from Fry analyses and calculation of k value. (Bracketed numerals indicate the number of data points.)

	Five Point Normalized Fry		Five Point Fry		Centre to Centre		Manual	
	R	Phi	R	Phi	R	Phi	R	Phi
22-6-4 YZ	1.17 (192)	73	1.22 (192)	75	1.41 (500)	87	1.13 (71)	70
22-6-4 XZ	2.25 (193)	84	1.95 (193)	66	2.23 (502)	90	2.1 (82)	82
22-6-4 XY	2.05 (197)	65	1.68 (197)	80	1.53 (366)	90	1.4 (81)	67
k VALUE	6.18		3.09		1.29		3.08	
87-51 YZ	1.13 (173)	-1	1.28 (173)	-15	1.321 (500)	1	1.13 (70)	1
87-51 XZ*	2.22 (191)	-2	2.75 (191)	-7	1.68 (600)	2	4.38 (70)**	-88
87-51 XY	2.22 (196)	-4	2.22 (196)	11	1.7 (600)	26	1.92 (45)	27
k VALUE	9.38		4.36		2.18		7.08	
87-66 YZ	1.28 (174)	-53	1.75 (174)**	69	1.19 (500)	-88	1.23 (60)	62
87-66 XZ*	2.11 (170)	-70	2.06 (170)**	-58	1.69 (543)	-78	2.63 (100)	-86
87-66 XY	1.5 (215)	-36	2.23 (215)**	-24	2.37 (600)**	4	2.08 (40)	7
k VALUE	1.79		1.64		7.21		4.70	
86-78 YZ	2.21 (94)	18	2.23 (94)	1	2.12 (96)	4	2.18 (92)	4
86-78 XZ	2.83 (58)	-7	3.48 (58)	3	3.36 (71)	6	3.68 (62)	-9
86-78 XY	2.08 (59)	73	2.81 (59)	67	2.13 (80)	71	2.23 (60)	66
k VALUE	0.89		1.47		1.01		1.04	

SAMPLE NO: 22-6-4 (Coarse- to medium-grained graywacke from West Limb, near Kidney Pond)

SAMPLE NO: 87-51 (Coarse- to medium-grained graywacke from Zenith Island, East Limb)

SAMPLE NO: 87-66 (Coarse- to medium-grained graywacke form Zenith Island, East Limb)

SAMPLE NO: 86-78 (Fine-grained siltstone with quatrz-biotite-chlorite aggregates from West Limb near Kidney Pond)

\* Note repeats used in Flinn calculation in preference to originals

\*\* Poorly defined ellipse void



Table A5.16 Measured ellipse ratios from Fry analyses and calculation of k value. (Bracketed numerals indicate the number of data points.)

	Five Point Normalized Fry		Five Point Fry		Centre to Centre		Manual	
	R	Phi	R	Phi	R	Phi	R	Phi
86-115 YZ	1.7 (187)	69	2.04 (187)	65	1.621 (500)	90	1.57 (100)	79
86-115 XZ	2.04 (186)**	80	2.81 (186)	84	3 (501)	70	2 (105)	86
86-115 XY	1.54 (183)	84	1.55 (183)	80	1.59 (600)	88	1.62 (40)	30
k VALUE	0.77		0.53		0.95		1.09	
87-34b YZ	1.97 (174)	15	2.23 (174)	18	1.68 (500)	6	2.33 (86)	55
87-34b XZ	2.26 (256)	88	2.77 (256)	-88	2.13 (184)	65	2.57 (80)	78
87-34b XY	2.02 (194)	-70	2 (194)	85	1.57 (600)	59	2.13 (35)	90
k VALUE	1.05		0.81		0.84		0.85	
Repeats for internal check of precision								
87-51 XZ	2.8 (191)	85	3.46 (191)	0	2.72 (191)	0	-	-
87-66 XZ	1.61 (170)	87	1.46 (170)	-78	1.66 (170)	-82	-	-

External accuracy analysis from Babcock (personal communication, 1989), University of Colorado.

22-6-4 YZ	1.52
22-6-4 XZ	2.00
22-6-4 XY	2.00
k VALUE	1.92

SAMPLE NO: 22-6-4 (Coarse- to medium-grained graywacke from West Limb, near Kidney Pond.)

SAMPLE NO: 86-115 (Coarse-grained siltstone from West Limb, near Kidney Pond.)

SAMPLE NO: 87-34b (Fine-grained greywacke from Central-East Limb of refold.)

SAMPLE NO: 87-66 (Coarse- to medium-grained greywacke from Zenith Island, East Limb.)

SAMPLE NO: 87-51 (Coarse- to medium-grained graywacke from Zenith Island, East Limb.)

\* Note repeats used in Flinn calculations in preference to originals

\*\* Poorly defined ellipse void

**Table A5.17 Summary of measured/uncorrected ellipse data and Flinn k values.**

UNCORRECTED ELLIPSE RATIOS

	22-6-4YZ	87-51YZ	87-61YZ	86-78YZ	86-115YZ	87-34bYZ
A	1.17	1.13	1.28	2.21	1.70	1.97
B	1.22	1.28	1.75	2.23	2.04	2.23
C	1.41	1.32	1.19	2.12	1.62	1.68
D	1.13	1.13	1.23	2.18	1.57	2.33

	22-6-4XZ	87-51XZ	87-61XZ	86-78XZ	86-115XZ	87-34bXZ
A	2.25	2.22	2.11	2.83	2.04	2.26
B	1.95	2.75	2.06	3.48	2.81	2.77
C	2.23	1.68	1.69	3.36	3.00	2.13
D	2.10	4.38	2.63	3.68	2.00	2.57

	22-6-4XY	87-51XY	87-66XY	86-78XY	86-115XY	87-34bXY
A	2.05	2.22	1.52	2.08	1.54	2.02
B	1.68	2.22	2.23	2.81	1.55	2.00
C	1.53	1.70	2.37	2.13	1.59	1.57
D	1.40	1.92	2.08	2.23	1.62	2.13

K VALUES

	22-6-4	87-51	87-61	86-78	86-115	87-34b
A	6.18	9.38	1.79	0.89	0.77	1.05
B	3.09	4.36	1.64	1.47	0.53	0.81
C	1.29	2.18	7.21	1.01	0.95	0.84
D	3.08	7.08	4.70	1.04	1.09	0.85

- A - Five Point Normalized Centre to Centre Fry Plot
- B - Five Point Centre to Centre Fry Plot
- C - Centre to Centre Fry Plot
- D - Manually Constructed Fry Plot

- SAMPLE NO: 22/6/4 (Coarse- to medium-grained graywacke from West Limb near Kidney Pond)
- SAMPLE NO: 87-51 (Coarse- to medium-grained graywacke from Zenith Island, East Limb)
- SAMPLE NO: 87-66 (Coarse- to medium-grained graywacke from Zenith Island, East Limb)
- SAMPLE NO: 86-78 (Fine-grained siltstone with quartz-biotite-chlorite aggregates from West Limb near Kidney Pond Zone)
- SAMPLE NO: 86-115 (Coarse-grained siltstone from West Limb, near Kidney Pond Zone)
- SAMPLE NO: 87-34b (Fine-grained graywacke from Central-east Limb of refold)

**Table A5.18** Summary of corrected ellipse data after applying matrix method of Shimamoto and Ikeda (1976) and Flinn k values.

## CORRECTED ELLIPSE RATIOS

	22-6-4YZ	87-51YZ	87-61YZ	86-78YZ	86-115YZ	87-34bYZ
A	1.14	1.08	1.32	1.94	1.58	1.69
B	1.20	1.28	1.43	1.89	1.74	1.96
C	1.43	1.20	1.00	1.95	1.70	1.58
D	1.25	1.48	1.24	2.02	1.46	1.95

	22-6-4XZ	87-51XZ	87-61XZ	86-78XZ	86-115XZ	87-34bXZ
A	2.31	2.34	2.02	3.70	2.11	3.07
B	1.99	2.79	2.81	4.88	3.00	3.60
C	2.20	1.90	2.01	3.97	2.78	2.56
D	1.86	3.14	2.60	4.32	2.24	3.69

	22-6-4XY	87-51XY	87-66XY	86-78XY	86-115XY	87-34bXY
A	2.02	2.17	1.53	1.91	1.33	1.82
B	1.66	2.18	1.97	2.58	1.52	1.84
C	1.54	1.59	2.14	2.04	1.63	1.50
D	1.49	2.13	2.09	2.14	1.54	1.89

## K VALUES

	22-6-4	87-51	87-66	86-78	86-115	87-34b
A	7.29	14.63	1.66	0.97	0.57	0.85
B	3.30	4.21	2.26	1.78	0.70	0.88
C	1.26	2.95	0.9	1.09	0.90	0.86
D	1.96	2.35	4.54	1.12	1.17	0.94

- A - Five Point Normalized Centre to Centre Fry Plot  
 B - Five Point Centre to Centre Fry Plot  
 C - Centre to Centre Fry Plot  
 D - Manually Constructed Fry Plot

SAMPLE NO: 22/6/4 (Coarse- to medium-grained graywacke from West Limb near Kidney Pond)

SAMPLE NO: 87-51 (Coarse- to medium-grained graywacke from Zenith Island, East Limb)

SAMPLE NO: 87-66 (Coarse- to medium-grained graywacke from Zenith Island, East Limb)

SAMPLE NO: 86-78 (Fine-grained siltstone with quartz-biotite-chlorite aggregates from West Limb near Kidney Pond Zone)

SAMPLE NO: 86-115 (Coarse-grained siltstone from West Limb, near Kidney Pond Zone)

SAMPLE NO: 87-34b (Fine-grained graywacke from Centre-East Limb of re-fold)

Table A5.19 Calculation of shear strains from siltstone-hosted,  $S_{3S}$ -parallel veins that were folded and rotated during  $D_4$ ; using shear strain equations from Ramsay (1967) and De Paor (1987) and orthographic net technique from De Paor (1983, 1986).

	$\theta$	$\theta'$	$l$ (cm)	$l'$ (cm)	$e$	$\gamma$	$\gamma_{min}$	$\gamma_{max}$	$d$
S6	52	112	29.5	19.4	-0.34	<u>1.19</u>	<u>1.03</u>	<u>1.32</u>	0.29
S3	92	137	28.4	23.2	-0.18	<u>1.03</u>	<u>1.07</u>	<u>1.07</u>	0.00
S2	51	102	23.8	26.6	-0.11	<u>1.02</u>	<u>1.10</u>	<u>1.53</u>	0.34
S5	50	92	32.8	26.5	-0.19	<u>0.87</u>	<u>1.21</u>	<u>1.77</u>	0.44

$\theta$  = the orientation of the vein before deformation  
 $\theta'$  = the orientation of the vein after deformation  
 $l$  = the length of the vein before deformation  
 $l'$  = the length of the vein after deformation  
 $\gamma = \cot \theta' - \cot \theta$  - shear strain equation from Ramsay (196) and De Paor (1987)  
 $e = (l' - l)/l$  - extension equation (Ramsay, 196)  
 $\gamma_{min}$  - minimum shear strain from orthographic technique  
 $\gamma_{max}$  - maximum shear strain from orthographic technique  
 $d$  = dilation from orthographic technique

Table A5.20 Extensional and shortening data from deformed quartz veins.

Vein Type	Description	Vein orientation	(Strike/Dip)			l (cm)	l' (cm)	e
			S <sub>0</sub>	S <sub>3s</sub>	S <sub>3Es</sub>			
4	East Limb	030/80	037/75	-	030/80	71	116	+0.63
4	East Limb	030/80	037/75	-	030/80	74	124	+0.68
4	East Limb	030/80	037/90	-	030/80	90	130	+0.44
1	S0 parallel	125/90	125/90	326/90	-	92	73	-0.21

l - estimated original length of vein from photograph  
 l' - measured final length of vein from photograph  
 e - calculated extension where  $e = (l' - l)/l$

APPENDIX A6: QUARTZ VEIN MICROSTRUCTURE

**Table A6.1** Quartz microstructure of typical Bedding-parallel (Type 1), D<sub>3</sub>-deformed (Type 2), and Syn-D<sub>3</sub> veins.

Sample number	Vein type	Quartz microstructure	Mineralogy	Fluid inclusion morphology
87-1	Bedding-parallel deformed by D <sub>3</sub>	Grain size: 0.05-0.5 mm, average 0.2 mm even G/D, minor U/E, S-P, No SGB	Qz-80% Ch-5% SL-15%	Minor secondary microfractures with inclusions cross-cutting grain boundaries, Types I and VII
86-23	Bedding-parallel deformed by D <sub>3</sub>	Grain size 0.05-0.3 mm, average 0.1 mm, even G/D, no U/E, S-P, No SGB	Qz-70% Mu-10% Bi-10% Mu-10%	None visible
86-110	Pre-D <sub>3</sub>	Grain size 0.05-0.4 mm, average 0.1 mm, even G/D, no U/D, S-P, No SGB	Qz-90% Ch-5% Bi-5%	Minor to moderate microfractures with inclusions cross-cutting grain boundaries, Types I and VII
86-126	Pre-D <sub>3</sub>	Grain size 0.05-0.3 mm, average 0.15 mm, even G/D, no U/D, S-P, No SGB	Qz-90% Ch-7% Bi-3%	Minor cross-cutting inclusion Types I and VII
86-1	Syn-D <sub>3</sub> lense	Grain size 5-10 mm, 1R minor zones (10%) of fine new grains and sub-grains, SGB, abundant U/E	Qz-100%	Abundant microfractures with inclusions, Types I, VII confined to zones with least

Mineralogy: Qz - quartz; Bi - biotite; Mu - muscovite; Ch - chlorite; Ca - carbonate; Kf - K-rich feldspar; SL - siltstone selvages.

Microstructure: G/D - grain size distribution/variation; S-P - sub-polygonal shape; 1R - irregular; SGB - serrated grain boundaries; U/E undulatory extinction.

Fluid inclusions: Type I - Two phase aqueous; Type II - Three phase H<sub>2</sub>O-CO<sub>2</sub>; Type III - Two phase vapour dominated; Type IV - Three phase aqueous; Type V - CO<sub>2</sub>-rich; Type VI - Liquid-rich; Type VII - Vapour-rich.

**Table A6.2** Quartz microstructure of typical  $S_{3S}$ -parallel (Type 3) and East Limb (Type 4) veins.

Sample number	Vein type	Quartz microstructure	Mineralogy	Fluid inclusion morphology
86-29	$S_{3S}$ -parallel	Grain size 0.1-0.6 mm, average 0.25 mm, moderate U/E, SGB, moderate G/D	Qz-90% Ch-7% Bi-3%	Abundant solid inclusions and microfractures with secondary inclusions, Types I, VI, and VII cross-cutting grain boundaries
86-12	$S_{3S}$ -parallel	Grain size 1.0-2.0 mm, IR aligned zones of fine new grains and sub-grains (5-10% of sample), SGB, abundant U/E	Qz-90% Kf-10%	Abundant microfractures with secondary inclusions mainly Type 1 and IV
87-18	East Limb	Grain size bimodal with ~ 1 mm grains and zones (5-10%) of fine grains and sub-grains, Moderate U/E, SGB	Qz-60% Ch-35% Ca-5%	Minor secondary inclusions along microfractures and isolated groups of Type VII
87-78	East Limb	Grain size bimodal with 0.2-0.3 mm grains and 50% zones 0.02-0.05 mm fine new grains and sub-grains, SGB and U/E in coarse zones	Qz-45% Ca-35% Ch-20%	Isolated arrays of Type VII and VI, no microfractures
87-75	East	Grain size bimodal with 0.2-0.4 mm grains and 35% zones 0.02-0.05 mm fine new grains and sub-grains, SGB and U/E in coarse zones	Qz-80% Ca-20%	Minor secondary microfractures and isolated arrays of Type VII

Mineralogy: Qz - quartz; Bi - biotite; Mu - muscovite; Ch - chlorite; Ca - carbonate; Kf - K-rich feldspar; SL - siltstone selvages.

Microstructure: G/D - grain size distribution/variation; S-P - sub-polygonal shape; IR - irregular; SGB - serrated grain boundaries; U/E undulatory extinction.

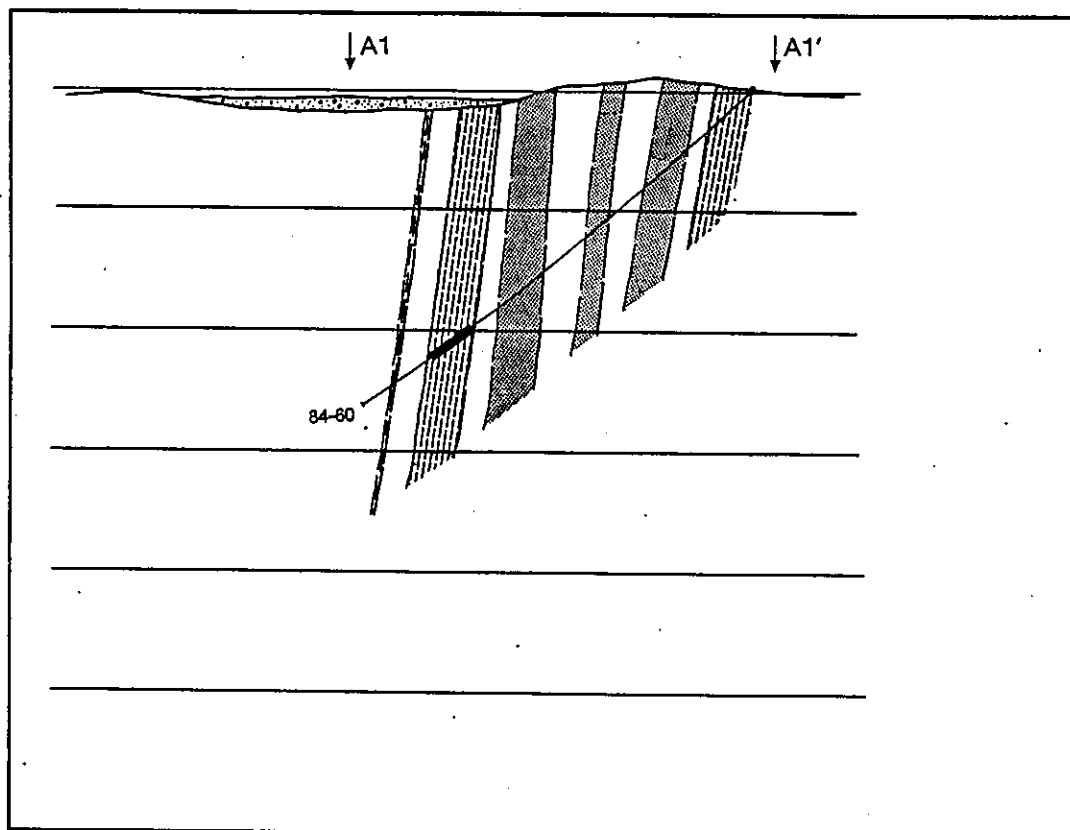
Fluid inclusions: Type I - Two phase aqueous; Type II - Three phase  $H_2O-CO_2$ ; Type III - Two phase vapour-dominated; Type IV - Three phase aqueous; Type V -  $CO_2$ -rich; Type VI - Liquid-rich; Type VII - Vapour-rich.









APPENDIX A7: KIDNEY POND GEOLOGICAL  
CROSS-SECTIONS

ARSENOPYRITE COMPOSITIONAL  
DATA

Figure A7.1 Geological cross-section of the Kidney Pond Quartz-Breccia Zone 1 along A1 - A1' from Figure 7.5.

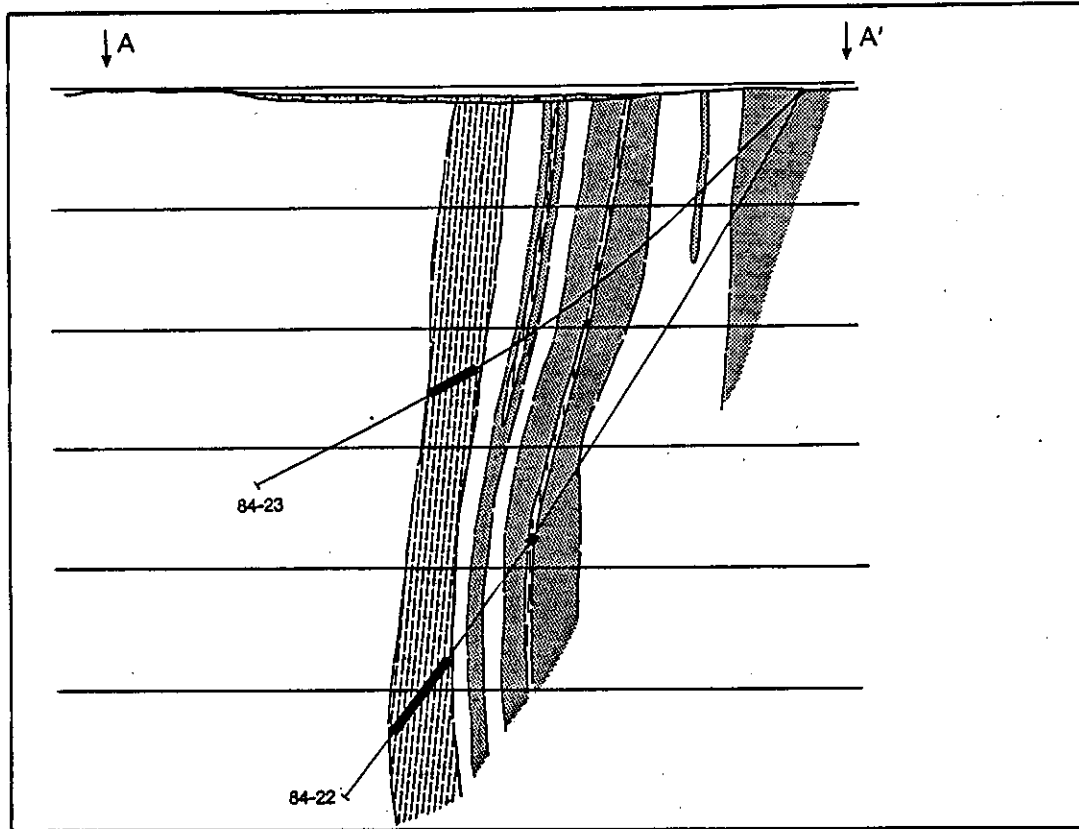


CROSS-SECTION A1 (FACING SOUTH-EAST)







-  Graywacke beds
-  Grey siltstone beds
-  Black siltstone beds
-  F<sub>1</sub> anticline axial trace
-  Diamond drill hole with gold-bearing quartz-breccia intersections (solid black)
-  Location of cross-section on map

0 52.5  
metres  
(Horizontal and Vertical Scale)

Figure A7.2 Geological cross-section of the Kidney Pond Quartz-Breccia Zone 1 along A - A' from Figure 7.5.

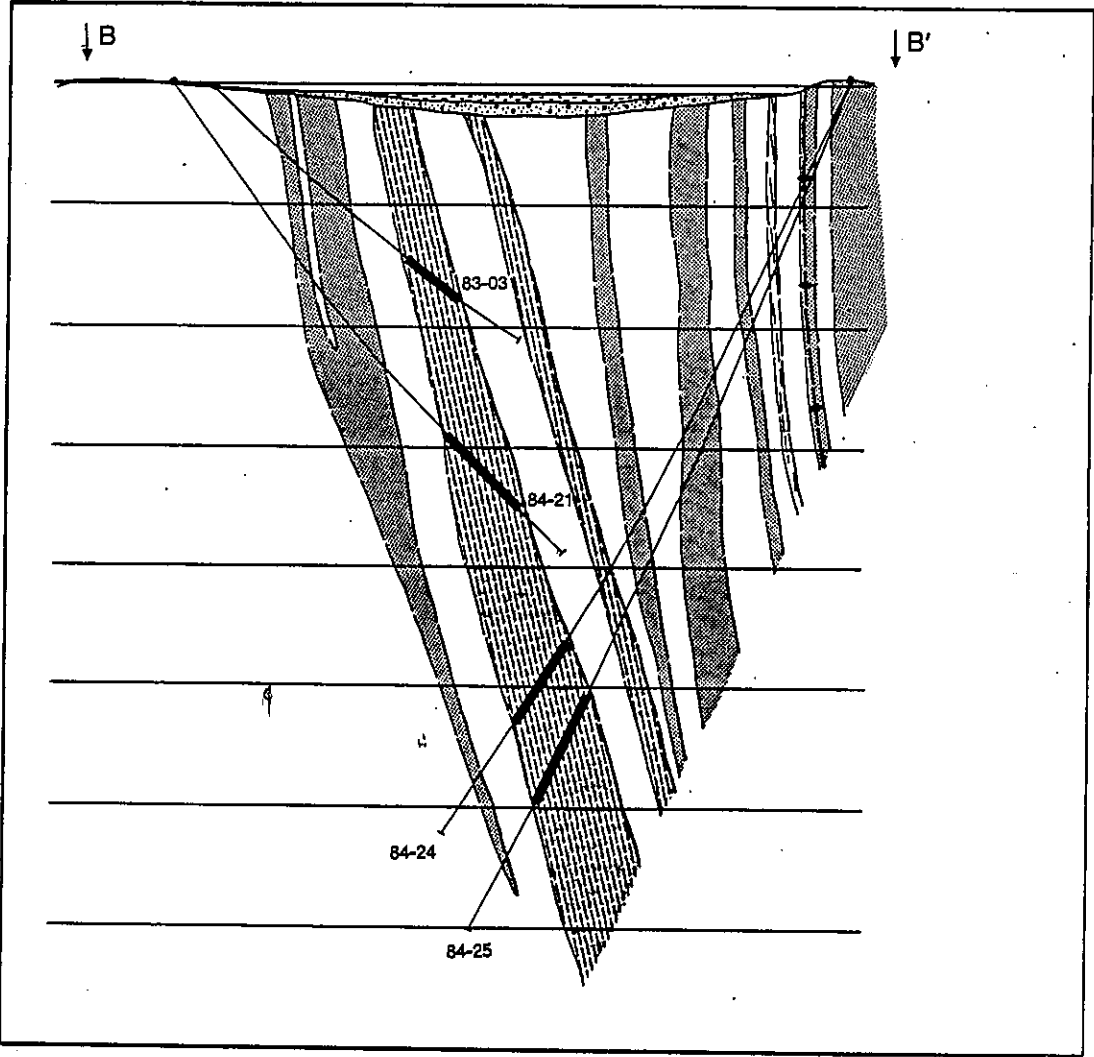


CROSS-SECTION A (FACING SOUTH-EAST)







-  Graywacke beds
-  Grey siltstone beds
-  Black siltstone beds
-  F<sub>1</sub> anticline axial trace
-  Diamond drill hole with gold-bearing quartz-breccia intersections (solid black)
-  Location of cross-section on map

0 ————— 52.5  
metres  
(Horizontal and Vertical Scale)

Figure A7.3 Geological cross-section of the Kidney Pond Quartz-Breccia Zone 1 along B - B' from Figure 7.5.



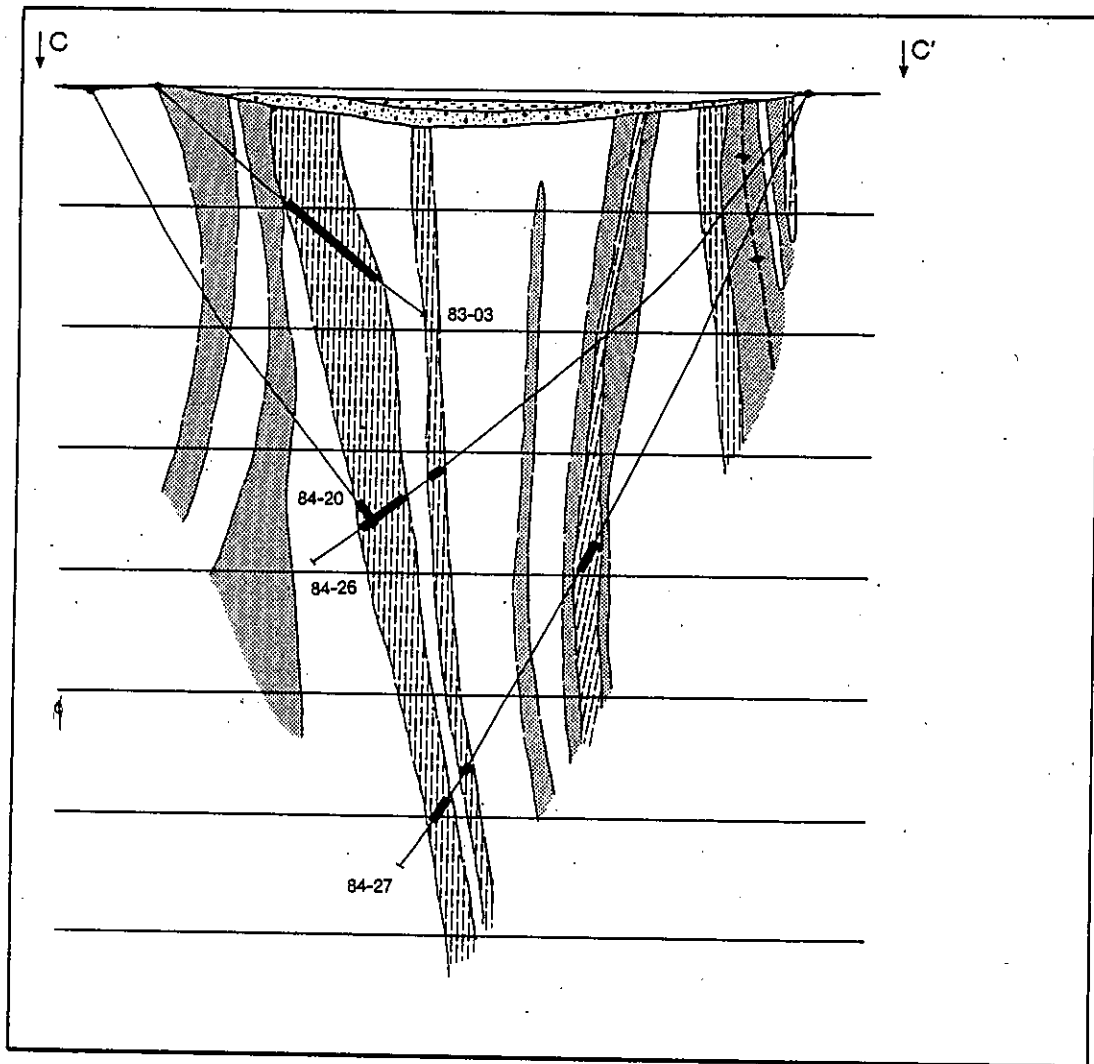
CROSS-SECTION B (FACING SOUTH-EAST)

-  Graywacke beds
-  Grey siltstone beds
-  Black siltstone beds
-  F<sub>1</sub> anticline axial trace
-  Diamond drill hole with gold-bearing quartz-breccia intersections (solid black)
-  Location of cross-section on map







0 ————— 52.5  
metres

(Horizontal and Vertical Scale)

Figure A7.4 Geological cross-section of the Kidney Pond Quartz-Breccia Zone 1 along C - C' from Figure 7.5.

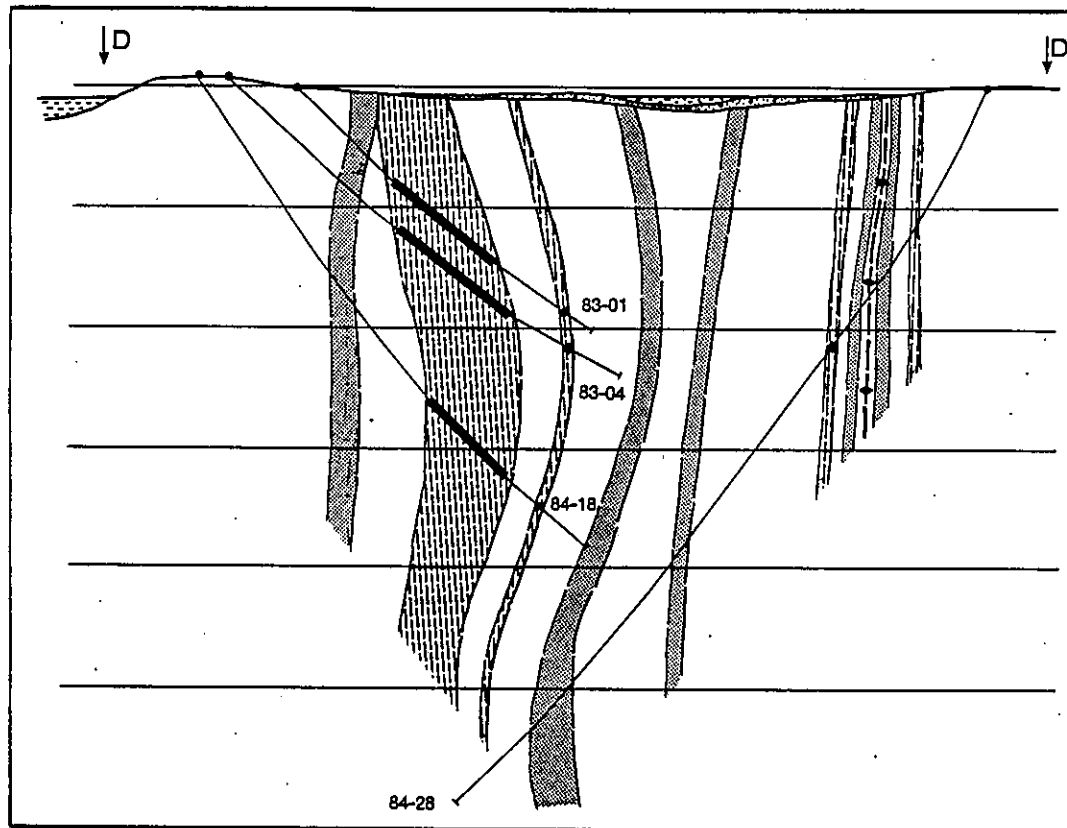


CROSS-SECTION C (FACING SOUTH-EAST)







-  Graywacke beds
-  Grey siltstone beds
-  Black siltstone beds
-  F<sub>1</sub> anticline axial trace
-  Diamond drill hole with gold-bearing quartz-breccia intersections (solid black)
-  Location of cross-section on map

0 ————— 52.5  
metres  
(Horizontal and Vertical Scale)

Figure A7.5 Geological cross-section of the Kidney Pond Quartz-Breccia Zone 1 along D - D' from Figure 7.5.



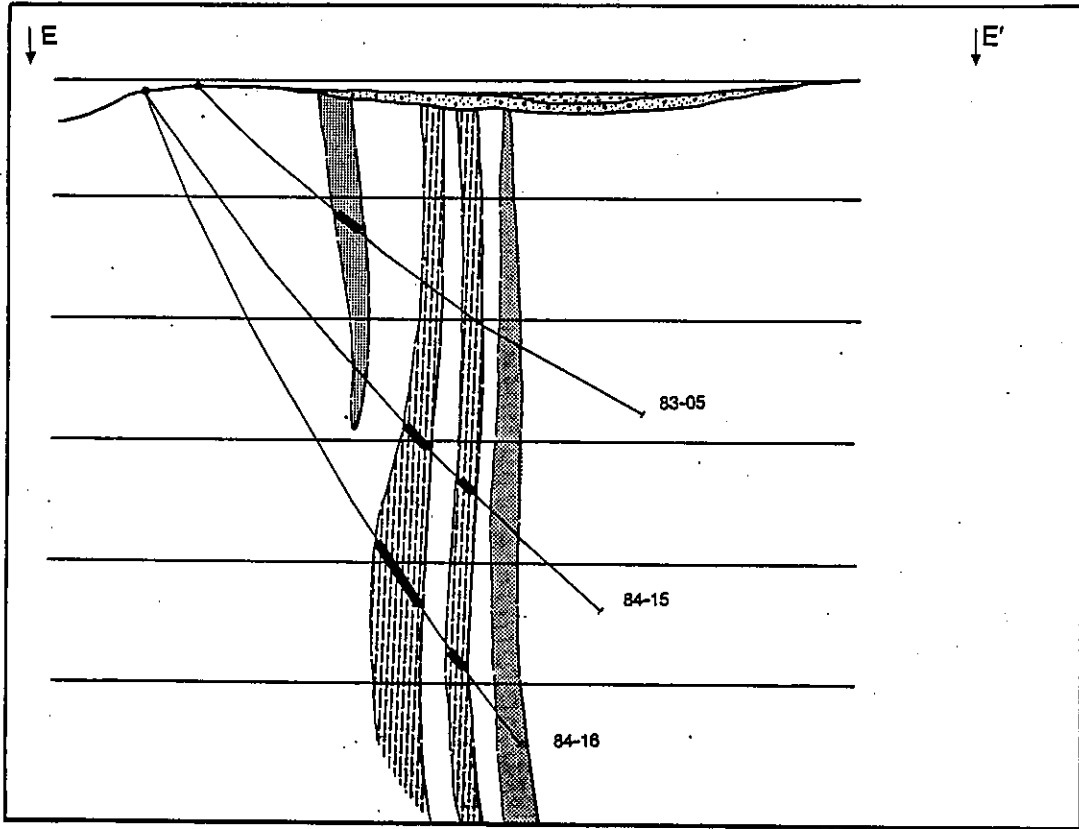
CROSS-SECTION D (FACING SOUTH-EAST)

-  Graywacke beds
-  Grey siltstone beds
-  Black siltstone beds
-  F<sub>1</sub> anticline axial trace
-  Diamond drill hole with gold-bearing quartz-breccia intersections (solid black)
-  Location of cross-section on map







0 52.5  
metres

(Horizontal and Vertical Scale)

Figure A7.6 Geological cross-section of the Kidney Pond Quartz-Breccia Zone 1 along E - E' from Figure 7.5.

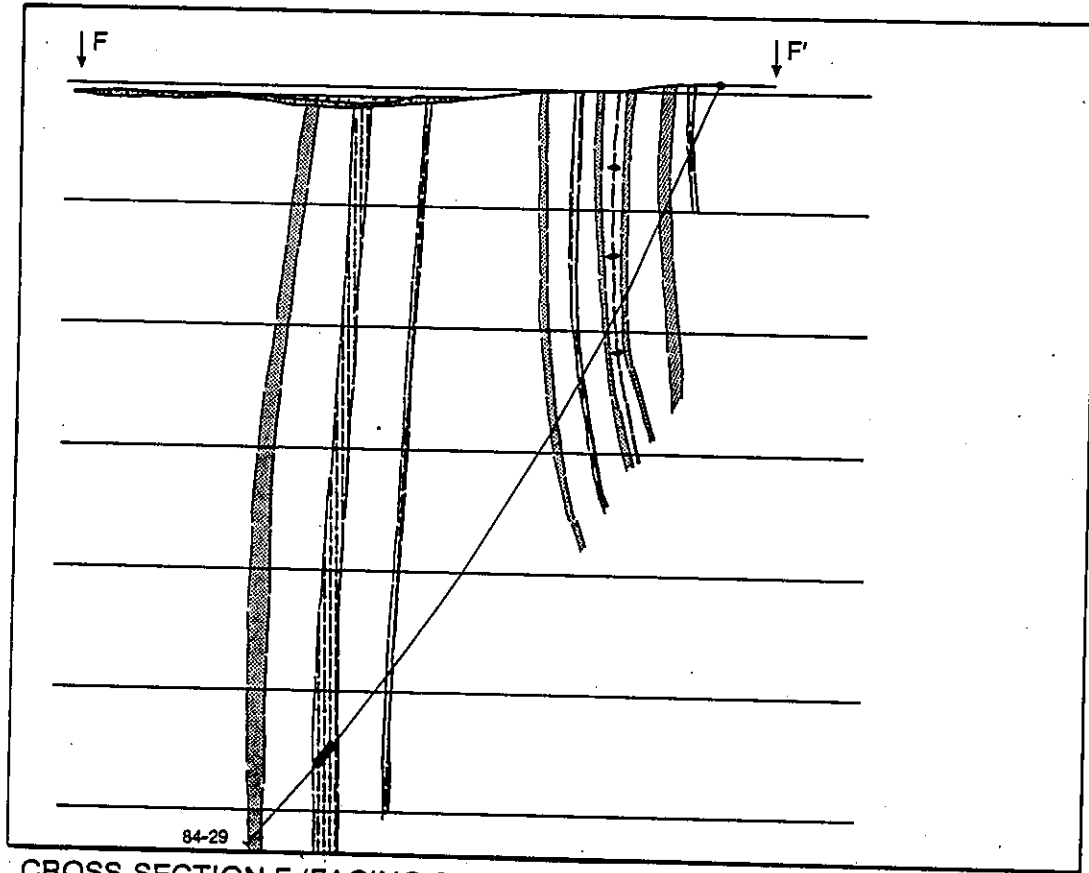


CROSS-SECTION E (FACING SOUTH-EAST)







-  Graywacke beds
-  Grey siltstone beds
-  Black siltstone beds
-  F<sub>1</sub> anticline axial trace
-  Diamond drill hole with gold-bearing quartz-breccia intersections (solid black)
-  Location of cross-section on map

0 52.5  
 metres  
 (Horizontal and Vertical Scale)

Figure A7.7 Geological cross-section of the Kidney Pond Quartz-Breccia Zone 1 along F - F' from Figure 7.5.



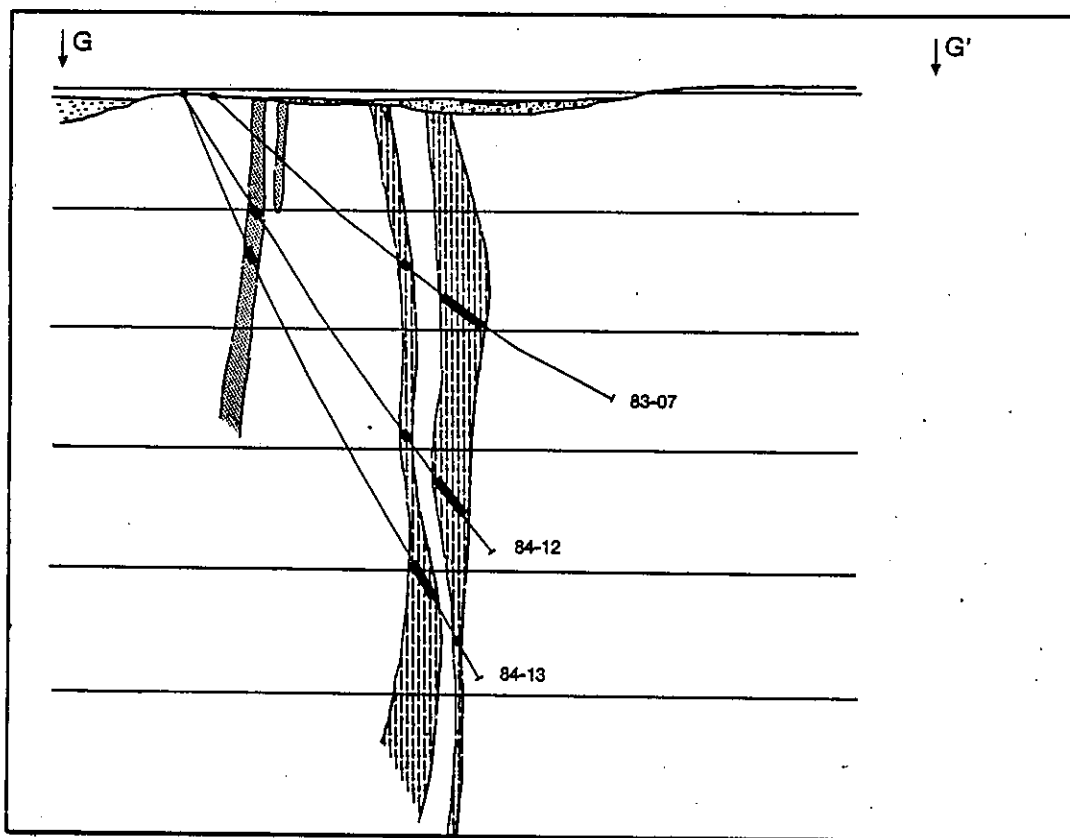
CROSS-SECTION F (FACING SOUTH-EAST)

-  Graywacke beds
-  Grey siltstone beds
-  Black siltstone beds
-  F<sub>1</sub> anticline axial trace
-  Diamond drill hole with gold-bearing quartz-breccia intersections (solid black)
-  Location of cross-section on map







0 ————— 52.5  
metres  
(Horizontal and Vertical Scale)



Figure A7.8 Geological cross-section of the Kidney Pond Quartz-Breccia Zone 1 along G - G' from Figure 7.5.

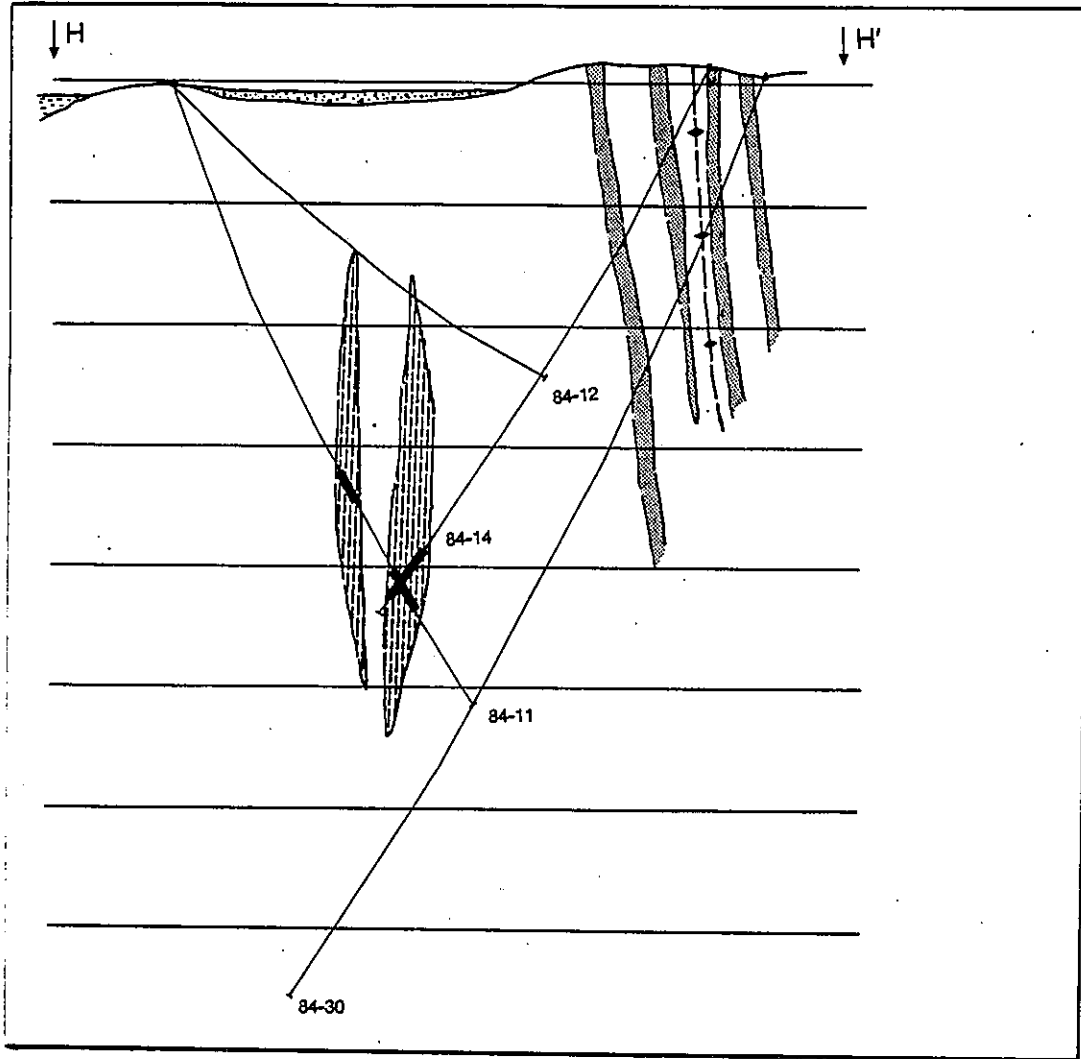


CROSS-SECTION G (FACING SOUTH-EAST)






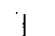
-  Graywacke beds
-  Grey siltstone beds
-  Black siltstone beds
-  F<sub>1</sub> anticline axial trace
-  Diamond drill hole with gold-bearing quartz-breccia intersections (solid black)
-  Location of cross-section on map

0 ————— 52.5  
metres  
(Horizontal and Vertical Scale)

Figure A7.9 Geological cross-section of the Kidney Pond Quartz-Breccia Zone 1 along H - H' from Figure 7.5.

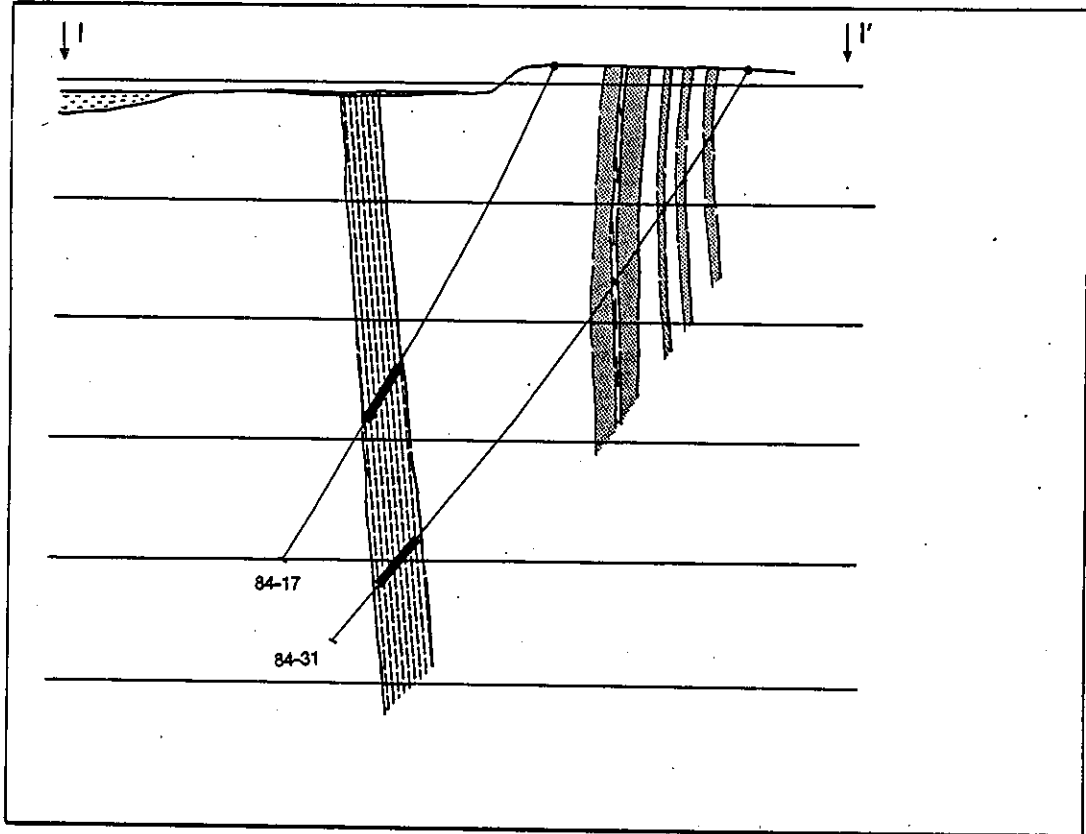


CROSS-SECTION H (FACING SOUTH-EAST)







-  Graywacke beds
-  Grey siltstone beds
-  Black siltstone beds
-  F<sub>1</sub> anticline axial trace
-  Diamond drill hole with gold-bearing quartz-breccia intersections (solid black)
-  Location of cross-section on map

0 52.5  
metres  
(Horizontal and Vertical Scale)

Figure A7.10 Geological cross-section of the Kidney Pond Quartz-Breccia Zone 1 along I - I' from Figure 7.5.



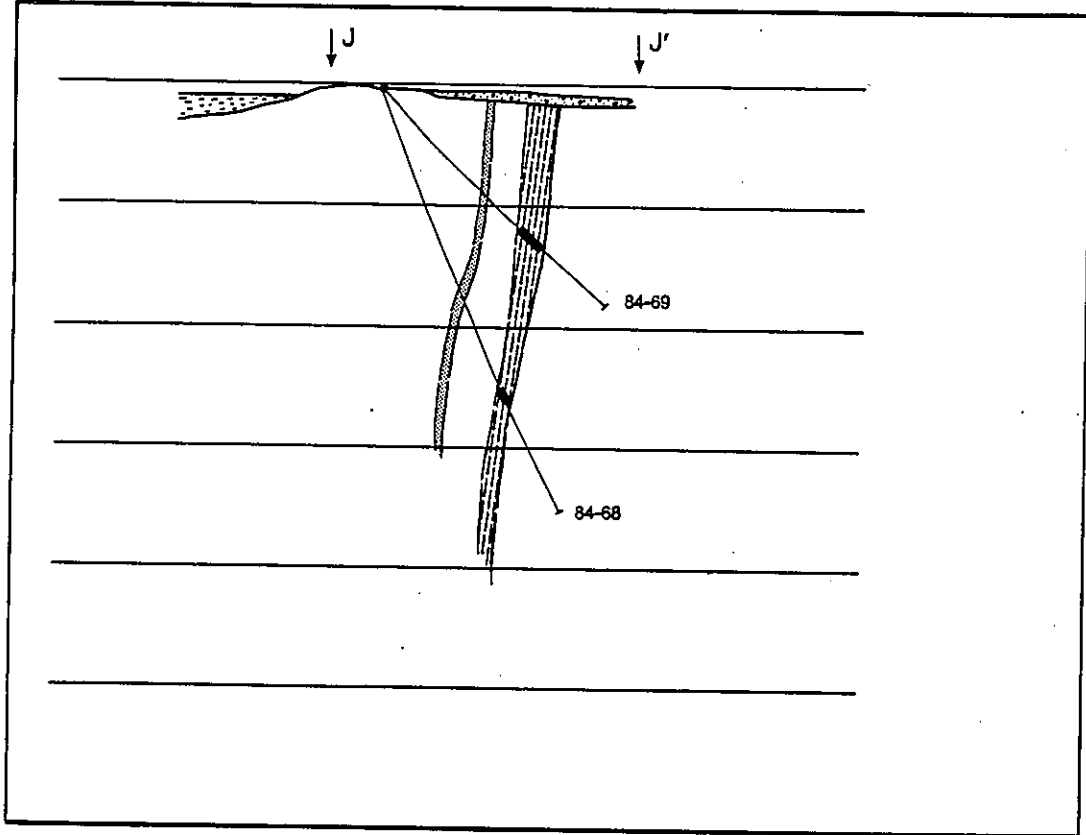
CROSS-SECTION I (FACING SOUTH-EAST)

-  Graywacke beds
-  Grey siltstone beds
-  Black siltstone beds
-  F<sub>1</sub> anticline axial trace
-  Diamond drill hole with gold-bearing quartz-breccia intersections (solid black)
-  Location of cross-section on map







0 52.5  
metres

(Horizontal and Vertical Scale)

Figure A7.11 Geological cross-section of the Kidney Pond Quartz-Breccia Zone 1 along J - J' from Figure 7.5.



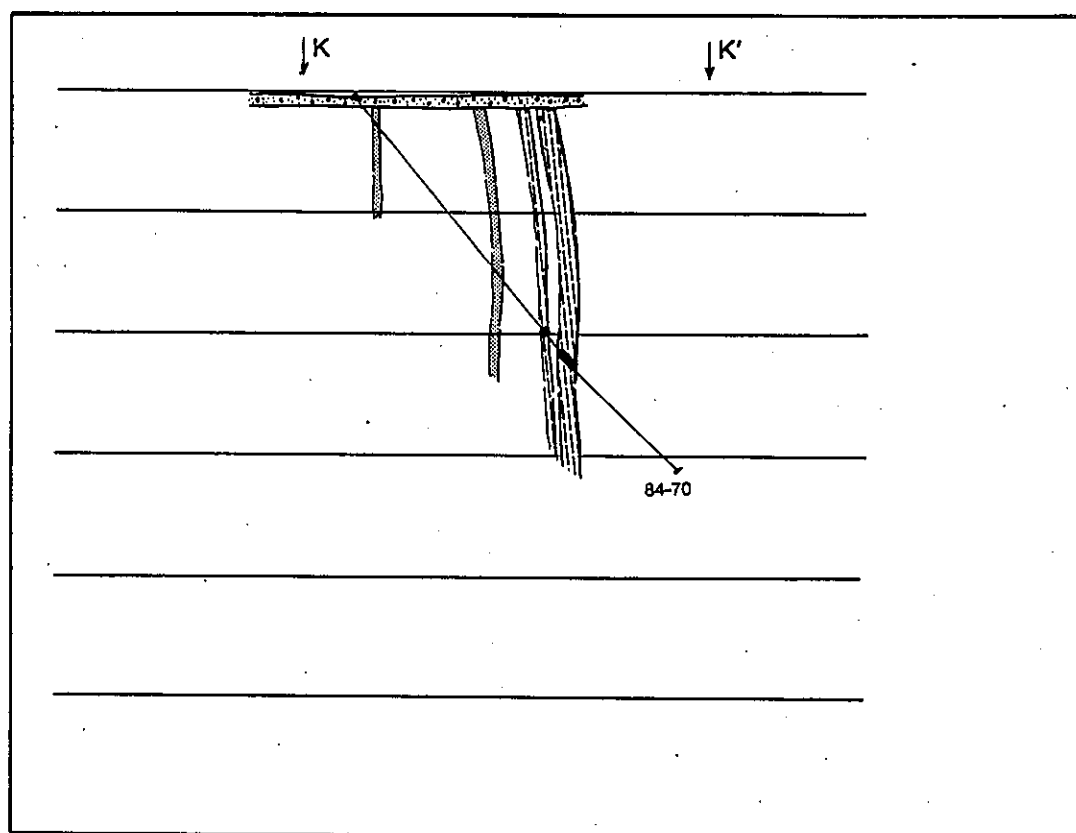
CROSS-SECTION J (FACING SOUTH-EAST)

-  Graywacke beds
-  Grey siltstone beds
-  Black siltstone beds
-  F<sub>1</sub> anticline axial trace
-  Diamond drill hole with gold-bearing quartz-breccia intersections (solid black)
-  Location of cross-section on map







0 ————— 52.5  
metres

(Horizontal and Vertical Scale)

Figure A7.12 Geological cross-section of the Kidney Pond Quartz-Breccia Zone 1 along K - K' from Figure 7.5.



CROSS-SECTION K (FACING SOUTH-EAST)

-  Graywacke beds
-  Grey siltstone beds
-  Black siltstone beds
-  F<sub>1</sub> anticline axial trace
-  Diamond drill hole with gold-bearing quartz-breccia intersections (solid black)
-  Location of cross-section on map

0 52.5  
metres  
(Horizontal and Vertical Scale)

Figure A7.13 Graph of At.% arsenic for the fine needle-shaped arsenopyrite and coarse pyramidal arsenopyrite from the Kidney Pond Zone 1 quartz-breccia.

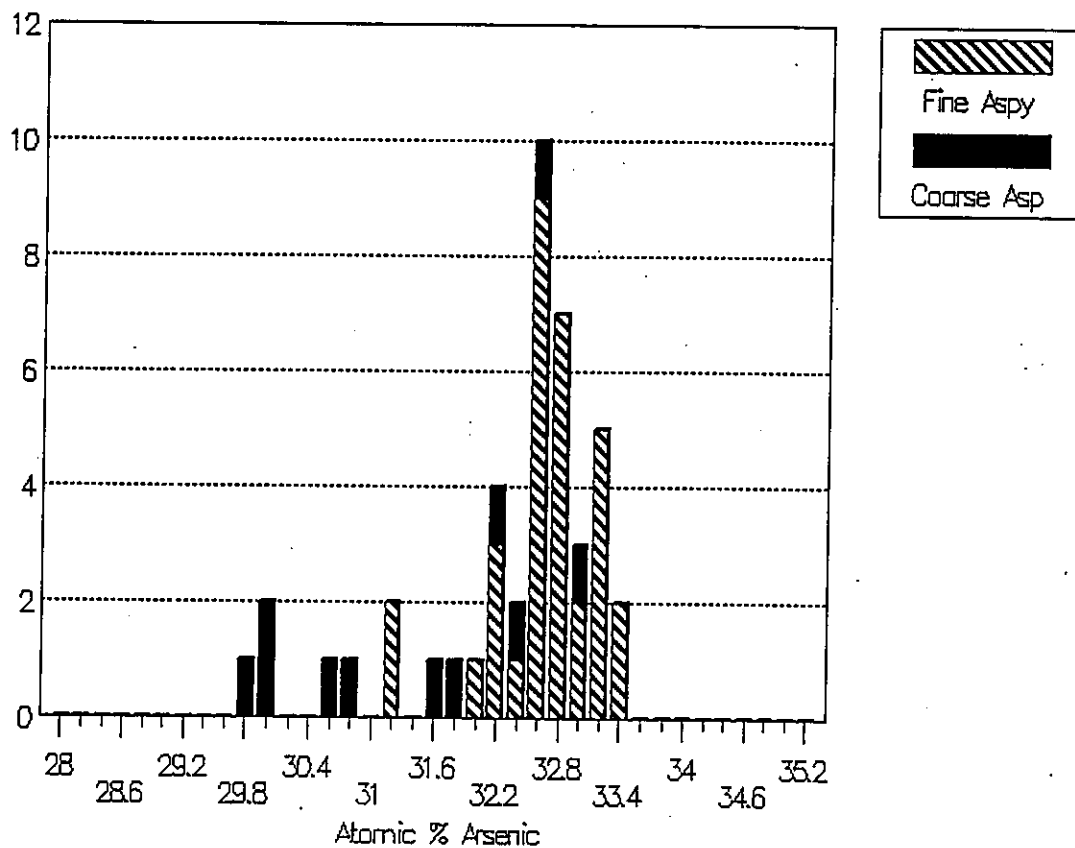


Table A7.1 Gold Occurrences of the Knight Bay Property from Caelles (1984, 1985, 1987a, 1987b) and Burston and Caelles (1986).

Occurrence Name	Strike (m)	Width (m)	Minimum Depth (m)	Host Lithology	Structural Association	Typical Au assays (g/tonne)/m
Kidney Pond:						
- Zone 1	>300	6-30	>120	Black siltstone	Parallel bedding	(Total reserves 173,000 tonnes @ 16g/tonne)
- Zone 2	240	1-5m	>30	Grey-black siltstone	Sub-parallel bedding	16/2.3 & 26/5.8
- Zone 3	75?	0.5-6	>20	Graywacke/siltstone	Sub-parallel S <sub>3</sub> and/or bedding	2/1.8
- Zone 4	90	1-6	>45	Black siltstone	Sub-parallel bedding	3/7.3 & 6/2.2
Bulge	45-60	0.25-6	>30	Grey-black siltstone	Sub-parallel S <sub>3</sub>	29/1.0
VIV-15	>30	1-3	>30	Black siltstone	Sub-parallel bedding	6/2.6
VIV-8	Pod?	5	>12	Black siltstone	Sub-parallel bedding	Traces
T-11/T-2	>100	1-12	>35	Grey-black graywacke	Sub-parallel bedding	13/2.4
T-15/Chane	Series of pods	1-6	>35	Grey-black graywacke	Discordant to bedding	-
Wolverine	>75	3-15	>50	Grey-black graywacke	Discordant to bedding	54/2.4
Salish:						
- Zone 1	>30	1-3	>12	Graywacke/siltstone	Shear zone parallel S <sub>3</sub>	2/2.1
- Zone 2	>30	1-3	>12	Graywacke/siltstone	Shear zone parallel S <sub>3</sub>	-

Table A7.2 Compositions (in atomic %) of fine needle-shaped arsenopyrite from the Kidney Pond Zone 1 quartz-breccia determined by the Jeol Superprobe 733 microprobe system operated at Dalhousie University. The system used an accelerating voltage of 15 kV, a beam current of 10 nano-amps, and a forty second count for each analysis. The arsenopyrite standard sp200 (Kretschmar and Scott, 1976) was used for calibration.

	Fe	As	S	Cu	Zn	Ni	Co	Pb	Au	TOTAL
CD20-21.5/1	33.44	32.25	34.27	0.00	0.04	0.00	0.00	0.00	0.00	99.76
CD20-21.5/2	33.95	32.40	33.61	0.04	0.00	0.00	0.00	0.00	0.00	100.81
CD20-21.5/8	33.04	33.13	33.64	0.03	0.00	0.07	0.08	0.00	0.00	100.59
CD20-21.5/10	32.98	33.40	33.10	0.00	0.00	0.53	0.00	0.00	0.00	100.56
CD20-21.5/11	33.28	32.60	34.08	0.02	0.00	0.02	0.00	0.00	0.00	100.89
CD20-21.5/13	33.21	33.48	33.24	0.00	0.01	0.00	0.06	0.00	0.00	101.01
CD20-21.5/16	33.16	32.85	33.98	0.02	0.00	0.00	0.00	0.00	0.00	100.22
CD20-21.5/17	33.43	31.94	34.62	0.00	0.00	0.00	0.00	0.00	0.00	99.82
CD20-21.5/18	33.54	32.11	34.34	0.00	0.00	0.00	0.00	0.00	0.00	99.75
CD20-21.5/19	33.32	32.85	33.81	0.01	0.00	0.00	0.00	0.00	0.00	100.73
17.665.5/51	32.99	33.13	33.77	0.00	0.02	0.00	0.09	0.00	0.00	100.74
17.665.5/52	32.98	32.61	34.11	0.00	0.00	0.00	0.31	0.00	0.00	100.56
17.665.5/53	32.41	32.73	34.21	0.00	0.00	0.42	0.22	0.00	0.00	100.82
17.665.5/63	32.91	32.72	34.32	0.00	0.05	0.00	0.00	0.00	0.00	101.77
17.665.5/64	32.75	32.55	34.60	0.03	0.02	0.00	0.05	0.00	0.00	101.06
17.665.5/67	33.35	31.87	34.56	0.00	0.06	0.00	0.22	0.00	0.00	101.59
17.665.5/68	33.10	32.75	34.12	0.00	0.04	0.00	0.00	0.00	0.00	101.57





Table A7.4 Compositions (in atomic %) of coarse pyramidal arsenopyrite from the Kidney Pond Zone 1 quartz-breccia determined by the Jeol Superprobe 733 microprobe system operated at Dalhousie University. The system used an accelerating voltage of 15 kV, a beam current of 10 nanoamps, and a forty second count for each analysis. The arsenopyrite standard sp200 (Kretschmar and Scott, 1976) was used for calibration. (Grouped data indicate repeated analyzes from same arsenopyrite crystal.)

	Fe	As	S	Cu	Zn	Ni	Co	Pb	Au	TOTAL
100-P/41	31.13	31.84	35.65	0.00	0.00	0.00	1.38	0.00	0.00	99.41
100-P/42	30.76	33.83	33.70	0.08	0.03	0.00	2.41	0.00	0.00	101.46
100-P/22	33.34	31.21	35.42	0.00	0.02	0.00	0.00	0.00	0.00	101.27
100-P/23	33.39	31.21	35.40	0.00	0.00	0.00	0.00	0.00	0.00	100.85
100-P/24	33.29	30.77	35.94	0.00	0.00	0.00	0.00	0.00	0.00	100.86
100-P/25	32.74	31.05	36.20	0.00	0.00	0.00	0.00	0.00	0.00	100.25
100-P/28	33.14	31.73	35.09	0.00	0.04	0.00	0.00	0.00	0.00	100.50
100-P/29	33.02	28.74	38.24	0.00	0.00	0.00	0.00	0.00	0.00	100.45
100-P/30	33.25	29.70	37.04	0.00	0.00	0.00	0.00	0.00	0.00	101.06
100-P/33	33.33	32.39	34.29	0.00	0.00	0.00	0.00	0.00	0.00	101.86
100-P/34	33.38	29.80	36.83	0.00	0.00	0.00	0.00	0.00	0.00	101.52
100-P/35	33.33	27.82	38.85	0.00	0.00	0.00	0.00	0.00	0.00	100.85
100-P/37	33.16	33.99	32.83	0.02	0.00	0.00	0.00	0.00	0.00	100.60
100-P/38	33.00	31.21	35.78	0.00	0.01	0.00	0.00	0.00	0.00	101.03
17-665.5/48	32.85	32.30	34.66	0.01	0.04	0.00	0.13	0.00	0.00	100.75
17-665.5/49	33.01	32.08	34.70	0.01	0.03	0.00	0.17	0.00	0.00	101.01
17-665.5/50	32.62	32.46	34.81	0.00	0.02	0.00	0.09	0.00	0.00	101.98
17-665.5/54	33.32	31.65	34.98	0.02	0.04	0.00	0.00	0.00	0.00	100.97
17-665.5/55	33.28	31.70	34.92	0.00	0.00	0.00	0.09	0.00	0.00	100.87
17-665.5/56	32.69	31.60	35.55	0.04	0.00	0.00	0.11	0.00	0.00	100.64
17-665.5/57	32.96	31.56	35.17	0.18	0.03	0.00	0.11	0.00	0.00	100.74
17-665.5/59	33.16	32.33	34.48	0.00	0.01	0.00	0.02	0.00	0.00	100.80
17-665.5/60	33.16	31.98	34.86	0.00	0.00	0.00	0.00	0.00	0.00	101.06
17-665.5/61	33.15	32.90	33.93	0.00	0.00	0.00	0.02	0.00	0.00	101.38
86-160/81	33.23	30.67	36.10	0.00	0.00	0.00	0.00	0.00	0.00	100.43
86-160/83	32.87	29.33	37.75	0.00	0.05	0.00	0.00	0.00	0.00	101.71
86-160/84	33.17	29.22	37.61	0.00	0.00	0.00	0.00	0.00	0.00	101.99
86-160/85	33.05	31.09	35.82	0.04	0.00	0.00	0.00	0.00	0.00	101.79
86-160/86	32.98	30.64	36.33	0.05	0.00	0.00	0.00	0.00	0.00	101.67
86-160/91	32.86	29.48	37.63	0.03	0.00	0.00	0.00	0.00	0.00	100.11
86-160/92	32.79	30.52	36.67	0.02	0.01	0.00	0.00	0.00	0.00	101.44

Table A7.5 Summary of arsenopyrite compositional data and sample descriptions. All analysis reported in atomic % arsenic. (Bracketed numerals indicate the number of analyzes per arsenopyrite crystal.)

Fine needle-shaped arsenopyrite

CD20-21.5	86-189	17-665.5	H23-5.5	86-160
32.25	-	33.13	32.86	33.16
32.40	-	32.61	32.54	33.20
32.63 (3)	-	32.73	32.77	32.96
33.13	-	32.72	32.62	33.23
33.40	-	32.55	32.13	
32.68	-	31.87	32.27	
33.48	-	32.75	32.60	
32.85	-	32.59		
31.94	-	32.99		
32.11	-			
32.85	-			

Average Value = 32.71 At.% As

Standard Deviation = 0.39 At.% As

Coarse pyramidal arsenopyrite

CD20-21.5	86-189	17-665.5	H23-5.5	86-160
-	30.64 (8)	32.48 (3)	-	29.74 (3)
-	30.00 (3)	31.65 (4)	-	30.87 (3)
-	32.60 (2)	32.43 (3)	-	30.00 (2)
-	31.84 (1)			
-	33.03 (1)			

Average Value = 31.37 At.% As

Standard Deviation = 1.12 At.% As

Table A7.5 (Continued)

- CD20-21.5 Quartz breccia with black siltstone fragments  
(sulphides include py, pyr, aspy and cpy)
- 86-189 Quartz breccia with black siltstone fragments plus visible gold  
(sulphides include aspy, cpy, py, pyr and sph)
- 17-665.5 Black siltstone with 15% white-grey quartz + minor py/aspy veinlets  
(other sulphides include pyr and cpy)
- H23-5.5 Black siltstone with 5-10% disseminated aspy + veinlets  
(sulphides include py and pyr)
- 86-160 Quartz breccia with dark grey graywacke fragments and disseminated aspy  
(other sulphides include pyr and minor py)

Combined Average = 32.37 At.% As

Combined Standard Deviation = 0.88 At.% As

Sulphide mineralogy: aspy - arsenopyrite; py - pyrite; pyr - pyrrhotite;  
cpy - chalcopyrite.

APPENDIX A8: FLUID INCLUSION MORPHOLOGY,  
THERMOMETRIC DATA, AND  
BULK VOLATILE ANALYSIS

#### A8.1 HEATED CRUSHING STAGE AND GAS CHROMATOGRAPHY TECHNIQUE

All analyzed samples were crushed to 2-5 mm grain size and hand-picked to remove any unwanted material. Approximately 8-10 g was obtained for each sample to allow for duplicate runs (2 g/run) if required. The samples were washed with distilled water six times and put in a water bath for four hours at 50°C. Following this, the samples were again washed six times and placed back in the water bath for a further four hours. Finally the samples were washed six more times and then left to dry at room temperature (E. Spooner, personal communication, 1989). The analytical equipment consisted of a heated crushing unit, a controllable oven containing polymer filled gas-chromatography coils, and a thermal conductivity and photo-ionization detectors (Bray and Spooner, 1989; Thomas et al. 1989). Two crushing runs were completed for each sample, one at an oven temperature of 80°C (to determine N<sub>2</sub>-O<sub>2</sub>-Ar-CO, CH<sub>4</sub>, CO<sub>2</sub>, C<sub>2</sub>H<sub>4</sub>-C<sub>2</sub>H<sub>6</sub>, C<sub>3</sub>H<sub>8</sub>, H<sub>2</sub>O and SO<sub>2</sub> peaks) and one at -70°C (to separate the N<sub>2</sub>-O<sub>2</sub>-Ar-CO and C<sub>2</sub>H<sub>4</sub>-C<sub>2</sub>H<sub>6</sub> peaks). The samples were loaded into a heated stainless steel crusher in which a Helium carrier gas stream was allowed to flow for eight hours prior to crushing; thereby removing any extraneous gases attached to quartz grain surfaces. The samples were then heated to 105°C and simultaneously crushed after building up a high pressure in a hydraulic hand jack. The rapidly released gases were quickly passed into the polymer resin-filled chromatographic coils. The gases were then measured at the two oven settings (80°C and -70°C) by the two detectors. A sample of Brazilian quartz was used as a standard.

The two principal types of errors include those related to sampling and those due to analytical procedure. Analytical errors, including variations in standard measurement, volatile peak measurement and calculations,

and retentivity of polymer resin, are approximately  $\pm 5\%$  (A. Thomas, personal communication, 1989). More important are the sample errors, which include variations in the distribution and types of inclusions within any selected quartz material. It is critical to know what type of inclusions are present in each sample and have some appreciation of their relative abundances; so that a meaningful evaluation of the bulk volatile data might be achieved.

Table A8.1 Fluid inclusion nomenclature used in this study, adapted from Roedder (1984).

Symbol	Description
$T_h$	Temperature of homogenization (usually into the liquid phase, unless stated)
$T_m(\text{ice})$	Final melting temperature of ice
$T_m(\text{hy-ha})$	Final melting temperature of hydrohalite
$T_m(\text{ice/hy-ha})$	Final melting temperature of ice and/or hydrohalite
$T_m(\text{CO}_2)^*$	First melting temperature of $\text{CO}_2$
$T_m(\text{CO}_2)$	Final melting temperature of $\text{CO}_2$
$T_e$	Eutectic temperature
$T_m(\text{halite})$	Temperature of melting/dissolution of halite daughter mineral



**Table A8.2 Quartz microstructure and fluid inclusion morphology of veins from Gordon Lake.**

Sample number	Vein type and description	Microstructure	Inclusion morphology
22/6/10	Granite-hosted vein (white-grey quartz & minor K-feldspar)	Coarse (2-3 mm) grains with 5% recrystallized boundaries made up of fine (20-50 $\mu\text{m}$ ) grains and sub-grains, U/E, SGB	Abundant secondary inclusions along intersecting microfractures
87-13	East limb vein (grey quartz & minor carbonate)	Coarse (0.25-0.5 mm) grains with zones (60%) of recrystallization of, fine (<20 $\mu\text{m}$ ) grains and sub grains, U/E, SGB	Abundant inclusions not aligned along microfractures, but isolated
87-124	S <sub>4</sub> -parallel vein (white-grey quartz)	Coarse (1-3 mm) grains with 30% speckled fine (<20 $\mu\text{m}$ ) grains and sub-grains, U/E, SGB	Minor secondary inclusions along microfractures
87-130	Bedding-parallel vein (white quartz)	Fine (100-200 $\mu\text{m}$ ) sub-polygonal grains, minor to no undulatory extinction, minor U/E, SGB	Moderately abundant secondary inclusions along microfractures
86-88	Pre-D <sub>3</sub> vein (white quartz)	Fine (200-300 $\mu\text{m}$ ) sub-polygonal grains, minor to no undulatory extinction	Moderately abundant secondary inclusions along microfractures
86-124	Pre-D <sub>3</sub> veins (white quartz)	Fine (300-600 $\mu\text{m}$ ) sub-polygonal grains and sub-grains, minor U/E	Minor secondary inclusions along microfractures

Microstructure: U/E - undulatory extinction; SGB - serrated grain boundaries

**Table A8.3** Quartz microstructure and fluid inclusion morphology of Gordon Lake quartz-breccias.

Sample number	Vein type and description	Microstructure	Inclusion morphology
86-59	Black-grey quartz with biotitized and chloritized siltstone fragments	Coarse (0.5-1 mm) elongate grains with 60% fine grain and sub-grain growth, U/E, SGB	Moderately abundant inclusions along microfractures
86-63	Grey-white quartz K-feldspar and biotite	Coarse (1-2 mm) grains 10-20% fine grains and sub-grains along boundaries, U/E, SGB	Abundant inclusions along intersecting microfractures
86-76	Grey-black quartz biotitized and chloritized frag-feldspar	250-500 $\mu$ m grains with 30-40% fine grains and sub-grains along boundaries, U/E, SGB	Moderately abundant inclusions along microfractures
86-77	Grey-black quartz with biotitized siltstone fragments and K-feldspar	Coarse (0.5-1 mm) grains with 30-40% fine grains and sub-grains along boundaries, U/E, SGB	Moderately abundant inclusions along microfractures
86-168	Grey quartz with chlorite, K-feldspar and plagioclase	Fine (50-250 $\mu$ m) grains, and sub-grains, intensely recrystallized, U/E, SGB	Minor inclusions along microfractures
86-189	Black-grey quartz with biotitized fragments fractured along S <sub>3</sub>	Fine (100-300 $\mu$ m) elongate grains and sub-grains, intensely recrystallized, U/E, SGB	Minor inclusions along microfractures

Microstructure: U/E - undulatory extinction; SGB - serrated grain boundaries

**Table A8.4** Fluid inclusion abundance and types in quartz veins from the Gordon Lake region.

Sample number	Fluid inclusion density	Solid inclusion abundance	Type I	Type III to Type VII	Type IV	Type II	Type VI	Type V
22/6/10	High	Minor	XXX 10-15	XXX 10-20	XX 10-15		XXX 10	
87-13	Medium	Minor		XXX 10-20		XX 10-15	XX 10-15	
87-124	Low	Minor	XX 3-5		X 3-5		XX 3-5	
87-130	Medium	Minor	XXX 5-20	XX 5-10			XX 5-15	
86-88	Medium	Minor-Moderate	XX 10-20	XXX 10-20	XX 10-20		XX 10	XX 5-10
86-124	Low	Minor	XX 5-15	XX 5-10			XX 5-15	

Fluid inclusion density: High - inclusions immediately visible at high power x 40; Medium - inclusions require short search at x 40 power; Low - inclusions require extended search at x 40 power.

Solid inclusion density : Abundant - 3-5%; Moderate - 1-3%; Minor - <1% (as % of vein).

Abundance of fluid inclusion type: XXX - common; XX - Not so common; X - rare (with average size in  $\mu$ m).

Type I - two-phase aqueous; Type II - Three-phase  $H_2O-CO_2$ ; Type III - Two-phase vapour-dominated; Type IV - Three-phase aqueous; Type V -  $CO_2$ -rich; Type VI - Liquid-rich; Type VII - Vapour-rich.

**Table A8.5** Fluid inclusion abundance and types in quartz-breccias from the Gordon Lake region.

Sample number	Fluid inclusion density	Solid inclusion abundance	Type I	Type III to Type VII	Type IV	Type II	Type VI	Type V
86-59	Medium	Abundant	XX 5-10	XX 5-10	XX 5-10		XXX 5-10	
86-63	High	Moderate	XXX 5-15		XX 5-15	XXX 5-20	XXX 5-15	
86-76	High	Abundant	X 5-15	X 5-15	XXX 5-20	X? 5-10	XX 5-15	
86-77	Medium	Abundant	XXX 5-15	XX 5-15		X?	XX 5-15	
86-168	Low	Moderate	X 5-10	X 5-10			X 5-10	
86-189	Low	Minor-Moderate	XX 3-10		X 3-10		XX 3-15	

Fluid inclusion density: High - inclusions immediately visible at high power x 40; Medium - inclusions require short search at x 40 power; Low - inclusions require extended search at x 40 power.

Solid inclusion density: Abundant - 3-5%; Moderate - 1-3%; Minor - <1% (as % of vein).

Abundance of fluid inclusion type: XXX - common; XX - Not so common; X - rare (with average size in m).

Type I - two-phase aqueous; Type II - Three-phase H<sub>2</sub>O-CO<sub>2</sub>; Type III - Two-phase vapour-dominated; Type IV - Three-phase aqueous; Type V - CO<sub>2</sub>-rich; Type VI - Liquid-rich; Type VII - Vapour-rich.

**Table A8.6** Fluid inclusion thermometric data for quartz-breccia (86-63).

86-63 Microfracture 1				86-63 Microfracture 2			
Th	Te	Tm(ice)	Tm(halite)	Th	Te	Tm(ice)	Tm(halite)
218.5	-66	-23	-	N/A	-77.1	-20	-
203.7	-64.2	-22.5	-	N/A	-76	-50.4	-
216.9	-69.6	-22.8	-	N/A	-79	-25	-
204.2	-66.1	-22.5	-	244.2	-79	-24	-
207.4	-60.5	-23.4	-	123.7	-60	-22	-
200	-65.5	-23.4	-	158.7	-60	-22.4	-
207.4	-64.2	-24.8	-	145.8	-65	-17.1	-
209.6	-65	-23.1	-				
N/A	-64.2	-22.5	-				
N/A	-66	-23.2	-				

86-63 Microfracture 3				86-63 Microfracture 4			
Th	Te	Tm(ice)	Tm(halite)	Th	Te	Tm(hy/ha)	Tm(halite)
169.7	N/F	N/F	-	145.7	N/F	N/F	-
179.2	N/F	N/F	-	140.5	N/F	N/F	171.8
190.6	N/F	N/F	-	136.8	N/F	N/F	173.1
181.1	N/F	N/F	-	143.5	N/F	N/F	-
178.8	N/F	N/F	-	148.8	N/F	N/F	-
179.2	N/F	N/F	-				
168.2	N/F	N/F	-				
164.5	N/F	N/F	-				
159	N/F	N/F	-				

86-63 Microfracture 5			
Th	Te	Tm(ice)	Tm(halite)
179	N/A	N/A	N/A
208.8	N/A	N/A	N/A
172.6	N/A	N/A	N/A
177.3	N/A	N/A	N/A
160.8	N/A	N/A	N/A
210.9	N/A	N/A	N/A
205.5	N/A	N/A	N/A

86-63 Microfracture 1 Type I, 10-15% vapour, 5-15 microns in size  
 86-63 Microfracture 2 Type I, 10% vapour, 5-15 microns in size  
 86-63 Microfracture 3 Type I, 10-15% vapour, 5-10 microns in size  
 86-63 Microfracture 4 Type IV, 10% vapour, 10% halite, 5-10 microns in size  
 86-63 Microfracture 5 Type I, 10-15% vapour, (+/- halite?), 5-15 microns in size

Th - Temperature of vapour homogenization

Te - Eutectic temperature

Tm(ice) - Final melting temperature of ice

Tm(hy-ha) - Final melting temperature of hydrohalite

Tm(halite) - Melting/dissolution temperature of halite

N/A - data not available, N/F - no freezing

**Table A8.7** Fluid inclusion thermometric data for quartz-breccias (86-76, 86-59, and 86-168).

86-76 Microfracture 1

Th	Te	Tm(hy-ha)	Tm(halite)
152.9	N/F	N/F	176.9
149.1	N/F	N/F	175.5
167.3	N/F	N/F	181.8
163.8	N/F	N/F	176.8
155.8	N/F	N/F	176.8
190.6	N/F	N/F	226.1

86-59 Microfracture 1

Th	Te	Tm(hy-ha)	Tm(halite)
151.5	N/F	N/F	176.5
150.3	N/F	N/F	173.5
N/A	N/F	N/F	150.0?
92.0?	N/F	N/F	N/A
169.8	N/F	N/F	170.0
156.2	N/F	N/F	N/A
158.3	N/F	N/F	N/A
157.5	N/F	N/F	N/A

86-59 Microfracture 2

Th	Te	Tm(ice)	Tm(halite)
194.8	N/F	N/F	-
219.7	N/F	N/F	-
194.0	N/F	N/F	-
212.7	N/F	N/F	-
210.9	N/F	N/F	-
173.4	N/F	N/F	-
158.0?	N/F	N/F	-
152.0?	N/F	N/F	-

86-168 Microfracture 1

Th	Te	Tm(ice)	Tm(halite)
132.8	-78.0	-37.4	-
113.0?	-69.8	-25.8	-
131.9	N/F	N/F	-
80.0?	-63.0	-26.4	-
133.0	-74.0	-26.8	-
128.0	N/F	N/F	-
109.9	-66.7	-27.7	-
N/A	-64.0?	-27.4	-
N/A	-65.0	-26.3	-
128.5	N/A	N/A	-

86-168 Microfracture 2

Th	Te	Tm(hy-ha)	Tm(halite)
132.0	N/F	N/F	181.0
116.0?	N/F	N/F	180.0
133.0	N/F	N/F	178.20

86-76 Microfracture 1	Type IV, 10% vapour, 10% halite, 10-20 microns in size
86-59 Microfracture 1	Type IV, 10% vapour, 10% halite, 5-10 microns in size
86-59 Microfracture 2	Type I, 10% vapour, 5-10 microns in size
86-168 Microfracture 1	Type I, 10% vapour, 5-10 microns in size
86-168 Microfracture 2	Type IV, 10 vapour, 10% halite, 5 microns in size

Th - Temperature of vapour homogenization

Te - Eutectic temperature

Tm(ice) - Final melting temperature of ice

Tm(hy-ha) - Final melting temperature of hydrohalite

Tm(halite) - Melting/dissolution temperature of halite

N/A - data not available, N/F - no freezing

**Table A8.8** Fluid inclusion thermometric data for quartz-breccias (86-189 and 86-77).

86-189 Microfracture 1				86-189 Microfracture 2			
Th	Te	Tm(ice)	Tm(halite)	Th	Te	Tm(ice)	Tm(halite)
268.5	-72.0	-25.2	-	179.5	N/F	N/F	N/A
245.7	-64.0	-25.4	-	185.0	N/F	N/F	N/A
210.0	-75.0	-23.6	-	175.0	N/F	N/F	N/A
217.4	-50.0?	-23.8	-	120.0?	N/F	N/F	N/A
210.0	-69.2	-24.6	-	225.0	N/F	N/F	N/A
216.8	-78.0	-22.6	-	218.5	N/F	N/F	N/A
187.4	-72.0	-23.2	-	206.5	N/F	N/F	N/A
N/A	-72.0	-23.0	-	217.5	N/F	N/F	N/A
N/A	-65.0	-23.0	-				
N/A	-55.0?	-23.0	-				

86-77 Microfracture 1				86-77 Microfracture 2			
Th	Te	Tm(ice)	Tm(halite)	Th	Te	Tm(hy/ha)	Tm(halite)
144.9	-62.2	-13.7	-	162.9	N/F	N/F	-
160.0	-76.0	-29.2	-	160.5	N/F	N/F	-
159.9	-67.5	-16.1	-	124.1	N/F	N/F	-
N/A	-65.0	-14.0	-	164.9	N/F	N/F	-
144.5	N/A	N/A	-	177.7	N/F	N/F	-
170.0	N/A	N/A	-	184.4	N/F	N/F	-
				158.3	N/F	N/F	-
				151.7	N/F	N/F	-
				133.0?	N/F	N/F	-
				159.9	N/F	N/F	-
				178.2	N/F	N/F	-
				159.3	N/F	N/F	-
				141.6	N/F	N/F	-
				162.0	N/F	N/F	-

86-189 Microfracture 1 Type II, 10-20% vapour (+/- CO<sub>2</sub>?), 5-10 microns in size  
 86-189 Microfracture 2 Type IV, 10% vapour, 5-10 microns in size  
 86-77 Microfracture 1 Type 1/II?, 10-25% vapour (+/- CO<sub>2</sub>?), 5-10 microns in size  
 86-77 Microfracture 2 Type I, 5-10% vapour, 5-10 microns in size

Th - Temperature of vapour homogenization  
 Te - Eutectic temperature  
 Tm(ice) - Final melting temperature of ice  
 Tm(hy-ha) - Final melting temperature of hydrohalite  
 Tm(halite) - Melting/dissolution temperature of halite  
 N/A - data not available, N/F - no freezing

Table A8.9 Fluid inclusion thermometric data for quartz vein (22/6/10)

22/6/10 Microfracture 1				22/6/10 Microfracture 2			
Th	Te	Tm(ice)	Tm(halite)	Th	Te	Tm(ice)	Tm(halite)
343.6	-39.9	-16.2	-	237.5	-30.0	-15.6	-
341.5	-38.2	-14.0	-	240.0	-28.0	-15.6	-
241.4	-28.0	-20.5	-	248.0	-30.0	-15.0	-
251.0	-32.2	-17.0	-	220.9	-32.4	-15.3	-
248.4	-28.3	-17.2	-	180.0	-31.5	-15.0	-
277.2	-28.2	-19.2	-	255.7	-29.0	-15.0	-
296.0	-28.2	-20.0	-	244.6	-31.4	-15.4	-
N/A	-24.5	-15.2	-	N/A	-30.0	-17.2	-
291.1	-27.3	-15.6	-				
322.3	-31.5	-11.2	-				
272.2	-28.3	-16.8	-				
265.5	-26.0	-18.0	-				

22/6/10 Microfracture 3				22/6/10 Microfracture 4			
Th	Te	Tm(ice)	Tm(halite)	Th	Te	Tm(ice)	Tm(halite)
N/A	-22.0	-5.0	-	>275.0	-15.1	-5.0	-
>290.0	-13.2	-2.7	-	282.9	-12.0	-4.8	-
N/A	-12.6	N/A	-	256.9	N/A	-4.5	-
265.6	N/A	-3.2	-	296.2	-15.2	-4.5	-
294.3	N/A	N/A	-	281.9	-15.0	-5.1	-
290.8	-19.0	-3.0	-	277.4	-12.0	-4.8	-
>320.0	N/A	N/A	-	>313.3	-15.0	N/A	-
N/A	-16.2	N/A	-	247.5	-16.0	-3.7	-
N/A	-13.6	N/A	-				

22/6/10 Microfracture 1 Type I, 10-20% vapour, 5-20 microns in size  
 22/6/10 Microfracture 2 Type I, 10% vapour (minor halite?), 5-15 microns in size  
 22/6/10 Microfracture 3 Type II, 10-20% vapour (+/-CO<sub>2</sub>), 10-20 microns in size  
 22/6/10 Microfracture 4 Type I, 10% vapour, 5-20 microns in size

Th - Temperature of vapour homogenization  
 Te - Eutectic temperature  
 Tm(ice) - Final melting temperature of ice  
 Tm(hy-ha) - Final melting temperature of hydrohalite  
 Tm(halite) - Melting/dissolution temperature of halite  
 N/A - data not available, N/F - no freezing



**Table A8.10** Fluid inclusion thermometric data for quartz veins (86-88, 87-13, and 87-124).

86-88 Microfracture 1				86-88 Inclusion set 2			
Th	Te	Tm(hy-ha)	Tm(halite)	Th	Te	Tm(ice)	Tm(halite)
154.7	N/A	-18.7	171.7	169.8	N/F	N/F	-
157.2	-54.5	-19.6	176.5	156.5	N/F	N/F	-
175.3	-49.0	-18.6	>235.0				
146.5	-52.0	-19.8	153.6				
N/A	-53.1	-20.1	N/A				
170.1	N/F	N/F	N/A	86-88 Inclusion Set 3			
162.5	N/F	N/F	N/A	Th	Tm(CO2)*	Tm(CO2)	
154.2	N/F	N/F	N/A	17.2	-61.0	-57.3	
178.2	N/F	N/F	N/A	14.4	-62.2	-57.2	
158.3	N/F	N/F	N/A	12.9	-64.4	-58.4	
179.4	N/F	N/F	N/A	5.2	-65.5	-59.0	
165.5	N/F	N/F	172.0?	5.0	-66.5	58.4	
161.1	N/F	N/F	185.0?	12.2	N/A	N/A	
168.0	N/F	N/F	172.5	6.5	N/A	-59.0	
181.2	N/F	N/F	186.0				
87-13 Inclusions				87-124 Microfracture 1			
Th	Te	Tm(ice)	Tm(halite)	Th	Te	Tm(ice)	Tm(halite)
>154.0	-73.4	-33.5	-	151.2	N/F	N/F	-
>240.0	-72.3	?	-	151.5	N/F	N/F	-
262.0?	-41.0?	-14.8	-	159.5	N/F	N/F	-
N/A	-31.0	-10.6	-	189.0	N/F	N/F	-
325.0	-2.2	7.4	-	168.5	N/F	N/F	-
185.0?	-63	-33.1	-				
N/A	N/A	-1.8?	-				
299.9	-2	7.0?	-				
>322.0	N/F	N/F	-				
305.7	N/F	N/F	-				
86-88 Microfracture 1	Type IV, 5-10% vapour, 5-10% halite, (+/-CO2?), 5-15 microns in						
86-88 Inclusion Set 2	Type I, 5-10% vapour, 5-10 microns, along grain boundary.						
86-88 Inclusion Set 3	Type V, 5-10 microns, along grain boundary						
87-13 Inclusions	Type II, 10-30% vapour (+/-CO2), 5-15 microns in size, isolated						
87-124 Microfracture 1	Type 1, 10-15% vapour, 5 microns in size.						

Th - Temperature of vapour homogenization  
 Te - Eutectic temperature  
 Tm(ice) - Final melting temperature of ice  
 Tm(hy-ha) - Final melting temperature of hydrohalite  
 Tm(CO2)\* - First melting of solid CO2  
 Tm(CO2) - Final melting of CO2  
 Tm(halite) - Melting/dissolution temperature of halite  
 N/A - data not available, N/F - no freezing

Table A8.11 Fluid inclusion thermometric data for quartz veins (86-130 and 86-124).

86-130 Microfracture 1				86-124 Microfracture 1			
Th	Te	Tm(ice)	Tm(halite)	Th	Te	Tm(ice)	Tm(halite)
195.3	N/F	N/F	-	140.0?	-66.5	-30.5	-
205.5	N/F	N/F	-	185.5	-73.0	-30.6	-
190.4	-63.5	-34.2	-	N/A	-70.3	-33.5	-
175.6	N/F	N/F	-	169.5	-65.0	-30.2	-
187.1	-66.6	-39?	-	175.0	N/A	N/A	-
233.6	N/F	N/F	-				
175.0?	N/F	N/F	-				
178.7	N/F	N/F	-				
186.7	N/F	N/F	-				
184.2	N/F	N/F	-				
187.6	N/F	N/F	-				
274.9	-57.4	-26.7	-				
252.8	-50.0?	-26.2	-				
247.5	N/F	N/F	-				
234.6	N/F	N/F	-				
234.4	N/F	N/F	-				
281.7	-63.2	-26.6	-				
268.3	-62.8	-24.1	-				
250.4	-65.0	-26.2	-				
182.1	N/F	N/F	-				
263.3	-72.7	-33.8?	-				
257.5	-65.0	-36.6	-				
255.8	-71.6	-35.5	-				
225.6	-70.6	-33.7	-				

86-124 Microfracture 2			
Th	Te	Tm(ice)	Tm(halite)
164.1	N/F	N/F	-
164.0	N/F	N/F	-
166.3	N/F	N/F	-

86-130 Microfracture 1 Type I, 10-15% vapour (minor halite?), 5-20 microns in size  
 86-124 Microfracture 1 Type I, 5-10% vapour, 5-10 microns.  
 86-124 Microfracture 2 Type I, 5-10% vapour, 5-10 microns.

Th - Temperature of vapour homogenization  
 Te - Eutectic temperature  
 Tm(ice) - Final melting temperature of ice  
 Tm(hy-ha) - Final melting temperature of hydrohalite  
 Tm(halite) - Melting/dissolution temperature of halite  
 N/A - data not available, N/F - no freezing

Table A8.12 Temperature of homogenization and salinity data for quartz-breccias.

	Th	Te	Tm(ice/hyha)	Tm(halite)	NaCl(1)	NaCl(2)	CaCl2(1)	NaCl-CaCl2-H2O
86-76	152.9	-	-	176.9	30.6	-	-	-
86-76	149.1	-	-	175.5	30.6	-	-	-
86-76	167.3	-	-	181.8	30.8	-	-	-
86-76	163.8	-	-	176.8	30.6	-	-	-
86-76	155.8	-	-	176.8	30.6	-	-	-
86-76	190.6	-	-	226.1	32.7	-	-	-
86-59	151.5	-	-	176.5	30.6	-	-	-
86-59	150.3	-	-	173.5	30.5	-	-	-
86-59	169.8	-	-	170.0	29.3	-	-	-
86-63	218.5	-66.0	-23.0	-	-	-	22.5	22-25
86-63	203.7	-64.2	-22.5	-	-	-	22.3	22-25
86-63	216.9	-69.6	-22.8	-	-	-	22.5	22-25
86-63	204.2	-66.1	-22.5	-	-	-	22.3	22-25
86-63	207.4	-60.5	-23.4	-	-	-	23.0	22-25
86-63	200.0	-65.5	-24.8	-	-	-	23.0	23-25
86-63	207.4	-64.2	-22.5	-	-	-	24.0	22-25
86-63	209.6	-65.0	-22.5	-	-	-	22.5	22-25
86-63	244.5	-79.0	-24.0	-	-	-	23.5	23-25
86-63	123.7	-60.0	-22.0	-	-	-	22.5	21-23
86-63	158.7	-60.0	-22.4	-	-	-	22.3	22-25
86-63	145.8	-65.0	-17.1	-	-	-	20.0	20-22
86-63	140.5	-	-	171.8	30.4	-	-	-
86-63	136.8	-	-	173.1	30.5	-	-	-
86-168	132.6	-78.0	-37.4	-	-	-	27.0	27-28
86-168	113.0	-69.8	-25.8	-	-	-	24.0	23-25
86-168	133.0	-74.0	-26.8	-	-	-	24.8	24-26
86-168	109.9	-66.7	-27.7	-	-	-	25.0	24-26
86-168	132.0	-	-	181.0	30.9	-	-	-
86-168	116.0	-	-	180.0	30.9	-	-	-
86-168	133.0	-	-	178.2	30.8	-	-	-
86-189	268.5	-72.0	-25.2	-	-	-	24.0	23-25
86-189	245.7	-64.0	-25.4	-	-	-	24.0	-
86-189	210.0	-75.0	-23.6	-	-	-	23.5	22-25
86-189	217.4	-50.0	-23.8	-	-	-	23.5	22-25
86-189	210.0	-69.2	-24.6	-	-	-	24.0	23-25
86-189	216.8	-78.0	-22.6	-	-	-	22.5	21-23
86-189	187.4	-72.0	-23.2	-	-	-	23.0	22-25
86-77	144.9	-62.2	-13.7	-	-	-	17.5	16-19
86-77	160.0	-76.0	-29.2	-	-	-	26.0	25-27
86-77	159.9	-67.5	-16.1	-	-	-	19.5	18-21

NaCl(1) - Equivalent Wt% NaCl calculated from Tm(halite) from Sterner et al. (1988)

NaCl(2) - Equivalent wt% NaCl calculated from Tm(ice) from Roedder (1984)

CaCl2(1) - Equivalent wt% CaCl2 from Tm(ice) in CaCl2-H2O system, Crawford (1981)

NaCl-CaCl2-H2O - Estimated wt% NaCl-CaCl2 from NaCl-CaCl2-H2O system of Vanko et al. (1988)

Table A8.13 Temperature of homogenization and salinity data for quartz veins.

	Th	Te	Tm(ice/hyha)	Tm(halite)	NaCl(1)	NaCl(2)	CaCl2(1)	NaCl-CaCl2-H2O
87-13	154.0	-73.4	-33.5	-	-	-	27.0	26-28
87-13	262.0	-41.0	-14.8	-	-	-	18.0	16-19
87-13	185.0	-31.0	-10.6	-	-	-	14.5	14-16
86-124	140.0	-66.5	-30.5	-	-	-	26.0	25-27
86-124	185.5	-73.0	-30.6	-	-	-	26.0	25-27
86-124	169.5	-65.0	-30.2	-	-	-	27.0	25-27
87-130	190.4	-63.5	-34.2	-	-	-	27.0	27-28
87-130	187.1	-66.6	-39.0	-	-	-	27.5	28-29
87-130	274.9	-57.4	-26.7	-	-	-	24.0	24-26
87-130	252.8	-50.0	-26.2	-	-	-	24.0	24-26
87-130	281.7	-63.2	-26.6	-	-	-	24.0	24-26
87-130	268.3	-62.8	-24.1	-	-	-	22.5	23-25
87-130	250.4	-65.0	-26.2	-	-	-	24.0	24-26
87-130	263.3	-72.7	-33.8	-	-	-	27.0	26-28
87-130	257.5	-65.0	-36.6	-	-	-	27.5	28-29
87-130	255.8	-71.6	-35.5	-	-	-	27.5	27-28
87-130	225.6	-70.6	-33.7	-	-	-	27.0	26-28
86-88	154.7	N/A	-18.7	171.7	30.4	-	20.0	25-30
86-88	157.2	-54.5	-19.6	176.5	30.6	-	21.3	25-30
86-88	175.3	-49.0	-18.6	235.0	33.2	-	20.0	25-30
86-88	146.5	-52.0	-19.8	153.6	29.7	-	21.3	25-30
86-88	165.5	-	-	172.0	30.4	-	-	-
86-88	161.1	-	-	185.0	31.0	-	-	-
86-88	168.0	-	-	172.5	30.4	-	-	-
86-88	181.2	-	-	186.0	31.0	-	-	-
22/6/10	290.0	-13.2	-2.7	-	-	4.5	-	-
22/6/10	290.8	-19.0	-3.0	-	-	4.9	-	-
22/6/10	275.0	-15.1	-5.0	-	-	7.8	-	-
22/6/10	282.9	-12.0	-4.8	-	-	7.6	-	-
22/6/10	296.2	-15.2	-4.5	-	-	7.2	-	-
22/6/10	281.9	-15.0	-5.1	-	-	8.0	-	-
22/6/10	277.4	-12.0	-4.8	-	-	7.6	-	-
22/6/10	247.5	-16.0	-3.7	-	-	6.0	-	-
22/6/10	343.6	-39.9	-16.2	-	-	-	19.0	18-21
22/6/10	341.5	-38.2	-14.0	-	-	-	17.2	17-20
22/6/10	241.4	-28.0	-20.5	-	-	-	21.5	21-24
22/6/10	251.0	-32.2	-17.0	-	-	-	20.3	19-22
22/6/10	248.4	-28.3	-17.2	-	-	-	20.3	19-22
22/6/10	277.2	-28.2	-19.2	-	-	-	21.2	21-23
22/6/10	291.1	-27.3	-15.6	-	-	-	19.2	18-21
22/6/10	322.3	-31.5	-11.2	-	-	-	15.8	15-17
22/6/10	272.2	-28.3	-16.8	-	-	-	20.0	19-22
22/6/10	265.5	-26.0	-18.0	-	-	-	20.5	20-22

NaCl(1) - Equivalent wt% NaCl calculated from Tm(halite) from Sterner et al. (1988)

NaCl(2) - Equivalent wt% NaCl calculated from Tm(ice) from Roedder (1984)

CaCl2(1) - Equivalent wt% CaCl2 from Tm(ice) in CaCl2-H2O system, Crawford (1981)

APPENDIX A9: GEOCHEMICAL DATA  
SAMPLE LOCATIONS  
PRECISION/ACCURACY ANALYSIS  
ISOAGON CALCULATIONS  
SULPHIDE COMPOSITIONAL DATA

Figure A9.1 Sample location map of Gordon Lake for lithology types: graywackes (filled circles); light grey siltstones (open circles); interbedded siltstones (open squares), dark grey to black siltstones (filled triangles), and Spud Lake granites (open triangles).

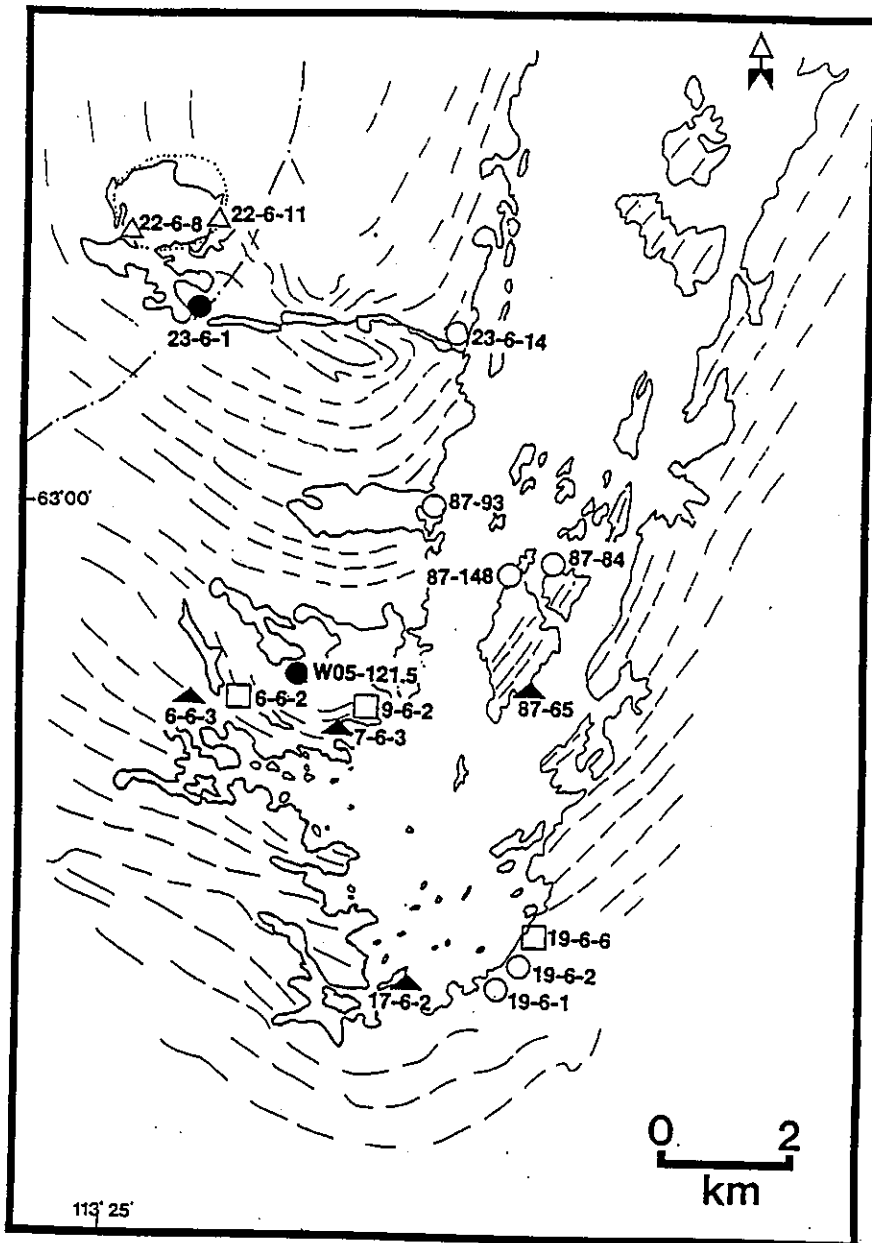


Figure A9.2 Sample location map of Kidney Pond area for lithology types: graywackes (filled circles); interbedded siltstones (open squares), dark grey to black siltstones (filled triangles), and black siltstones with sulphides (filled squares).

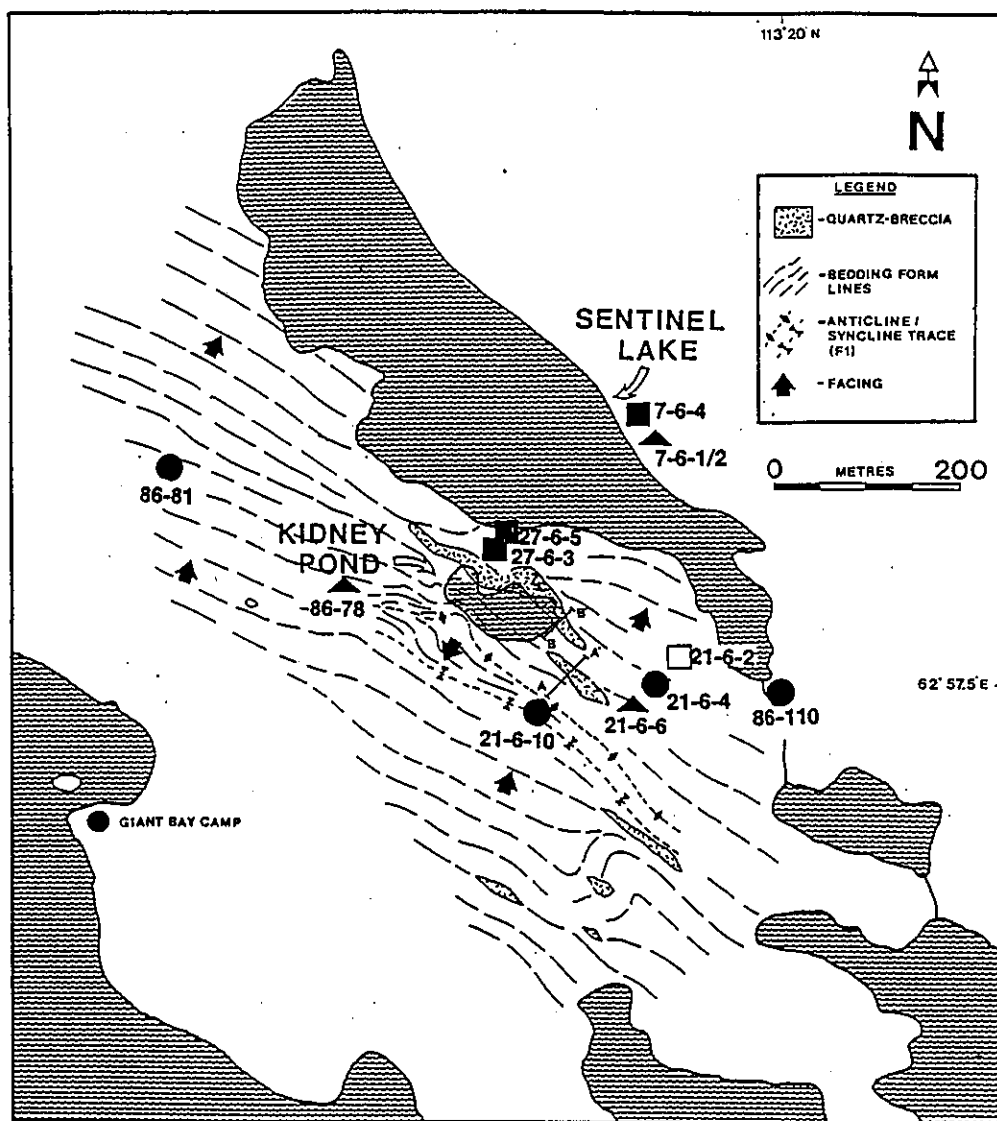


Figure A9.3 Sample location map of underground workings on Kidney Pond Breccia Zone 1 for lithology types: interbedded siltstones (open squares), black siltstones with sulphides (filled squares), and diabase dyke (open triangle).

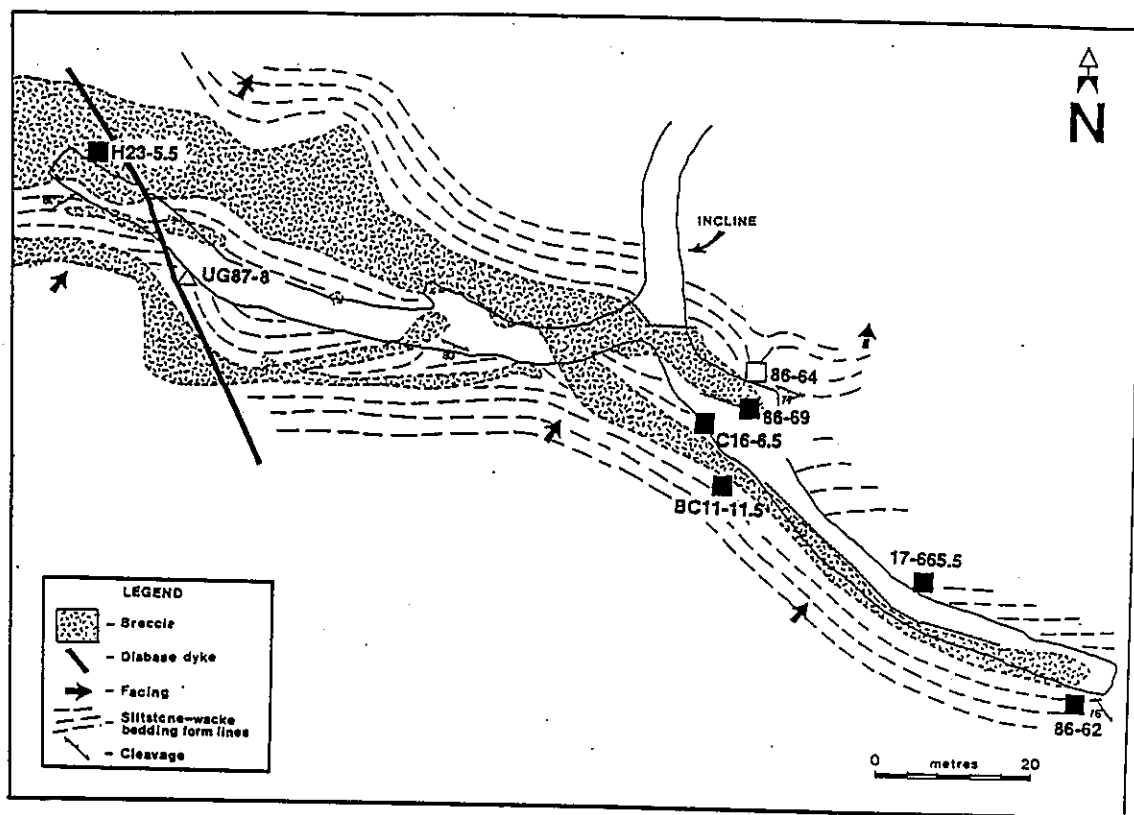




Figure A9.4 Location map of Cameron River Volcanic Belt samples (open triangles) within the Gordon Lake region. (1 - Sleepy Dragon Complex; 2a - Greenschist facies metaturbidites; 2b - Amphibolite facies metaturbidites; 3 - Cameron River Volcanic Belt; 4 - Early and Late Granitoids.

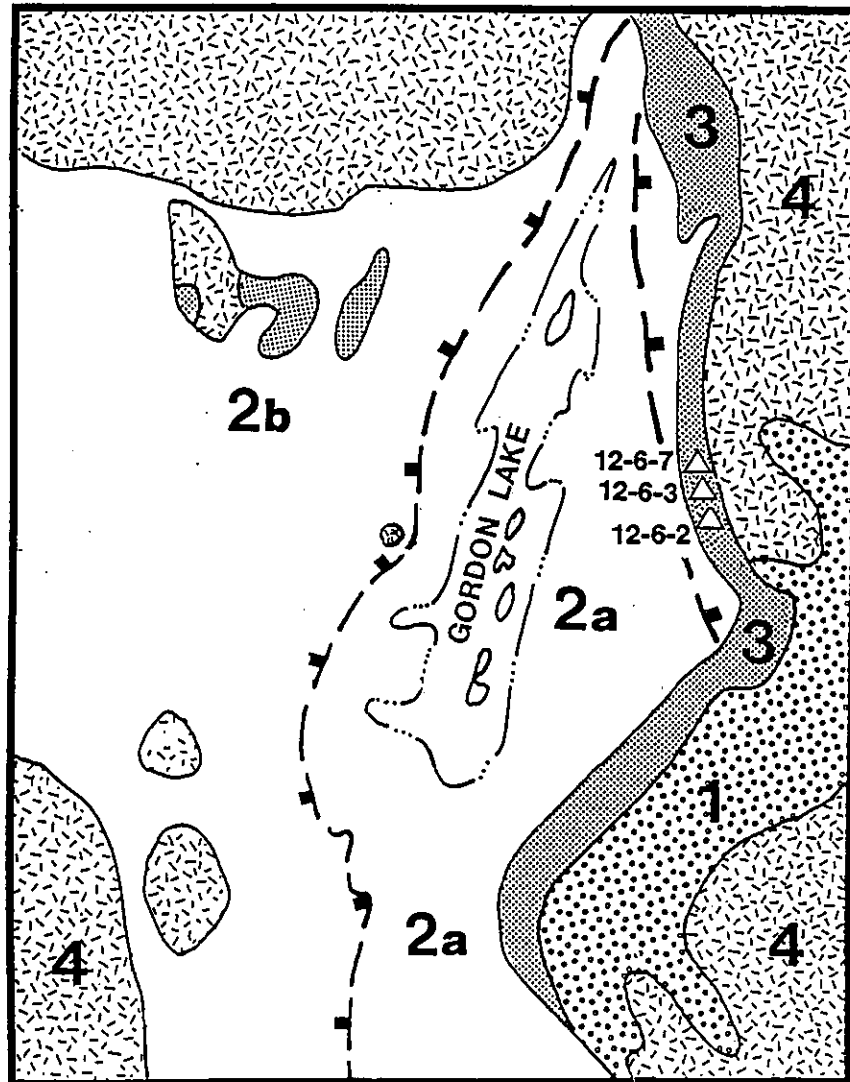


Figure A9.5 Sample location map of Gordon Lake for quartz vein and breccias: quartz veins (diamonds), stratabound type breccias (filled stars) and graywacke hosted breccias (open stars).

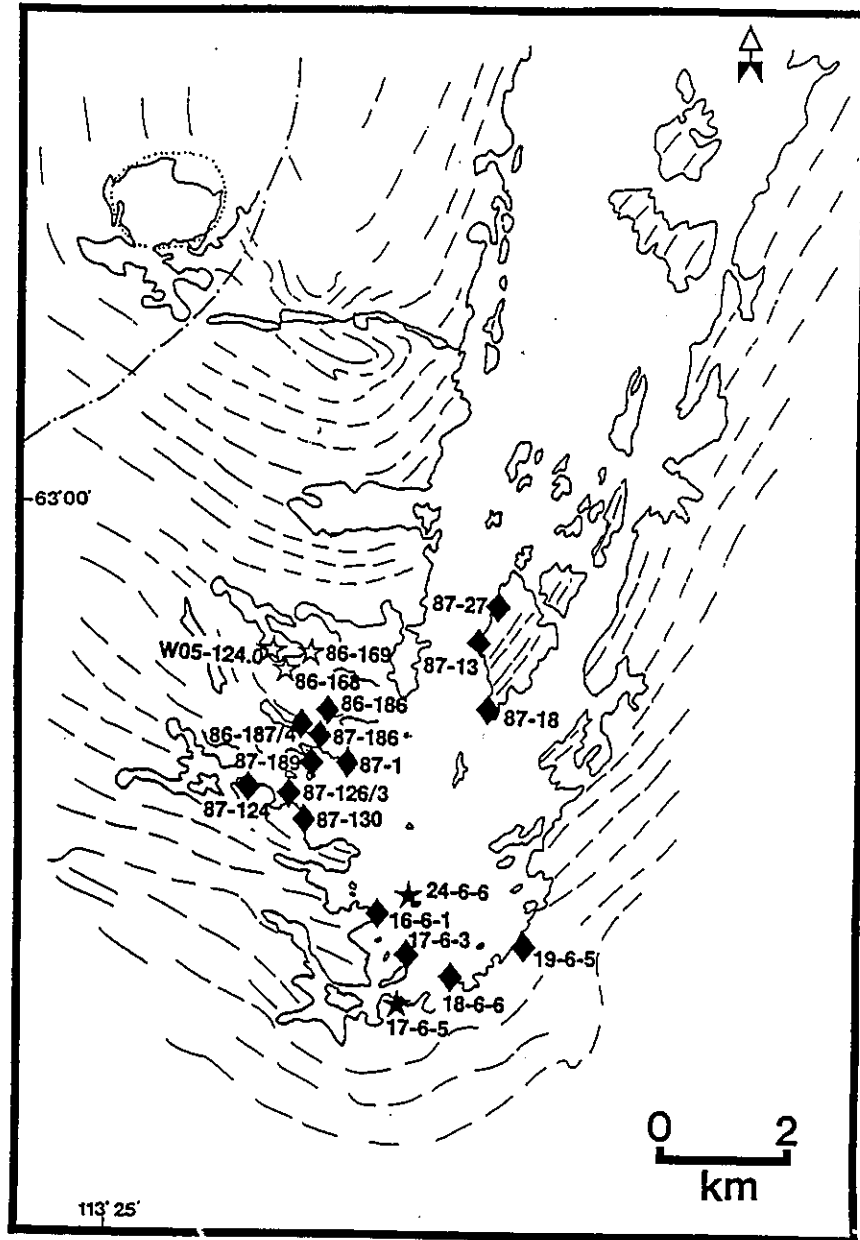


Figure A9.6 Sample location map of Kidney Pond area for quartz veins (diamonds).

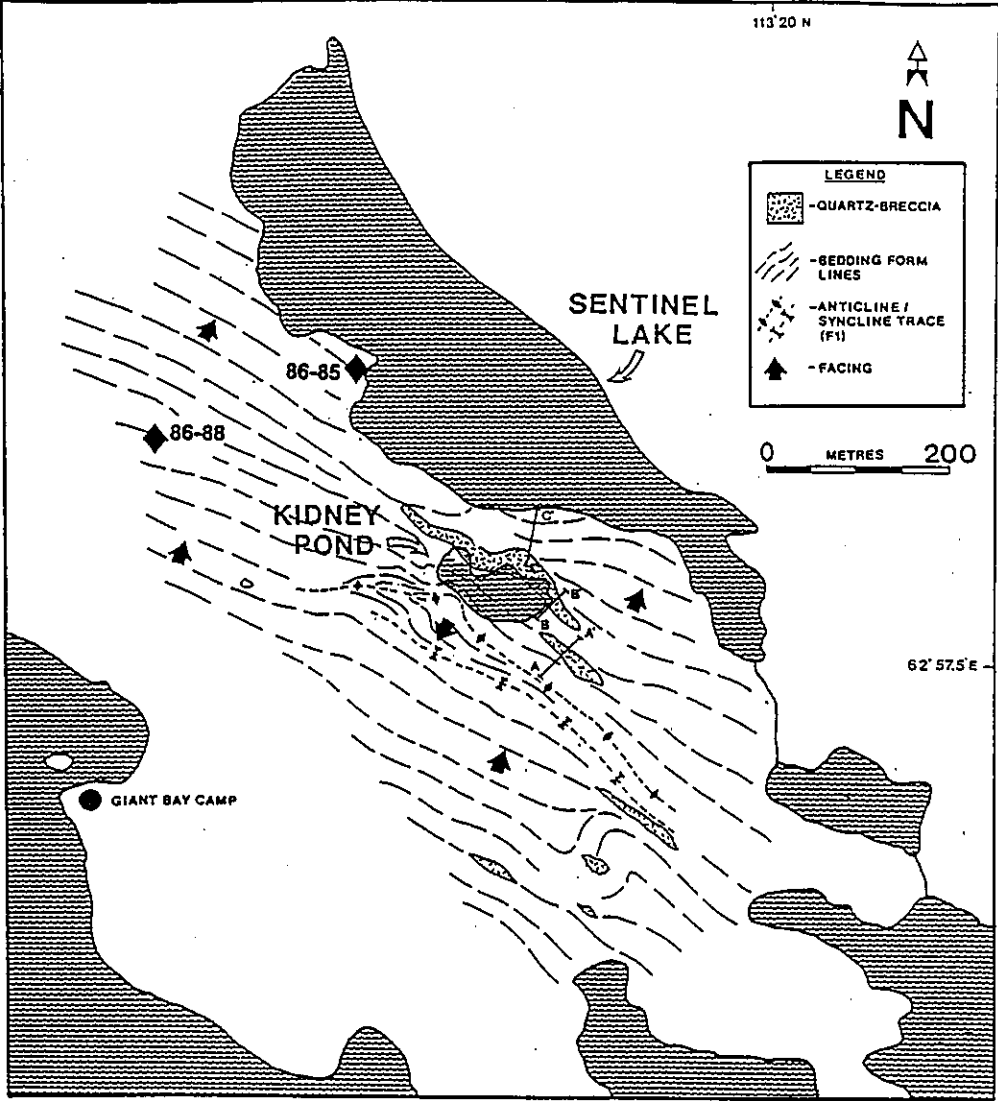


Figure A9.7 Sample location map of underground workings on Kidney Pond Breccia Zone 1 for quartz-breccia (filled stars).

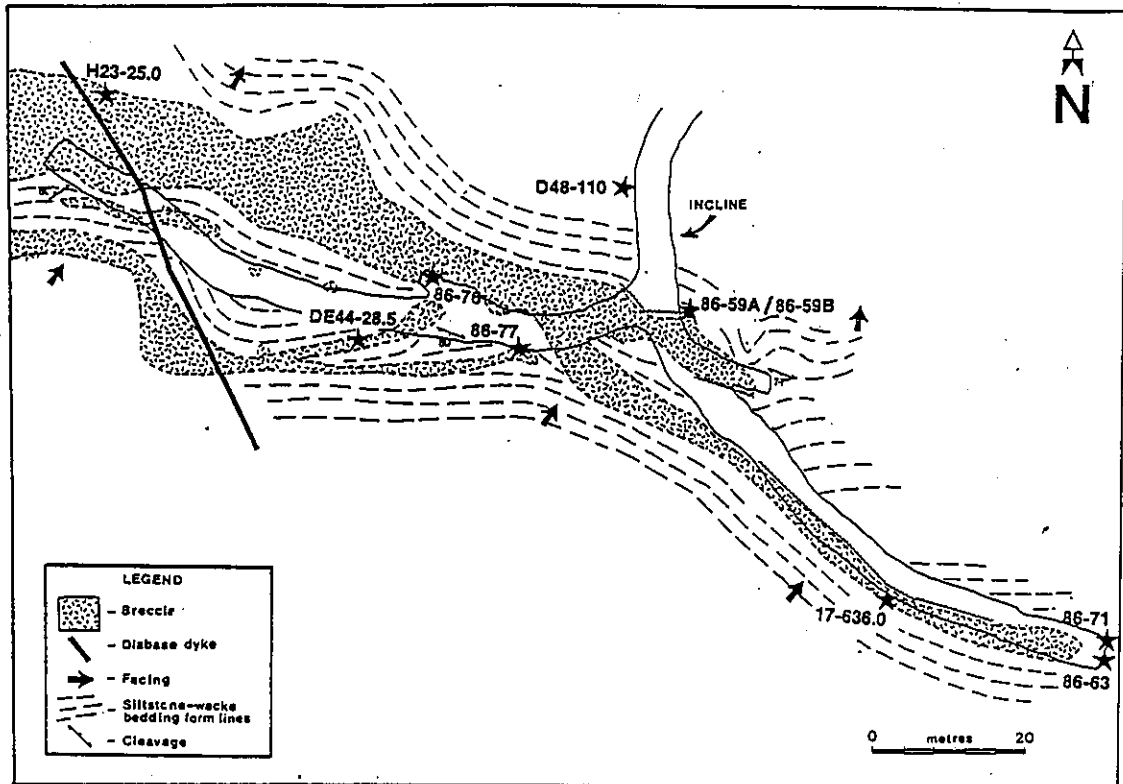


Figure A9.8 Gold precision analysis.

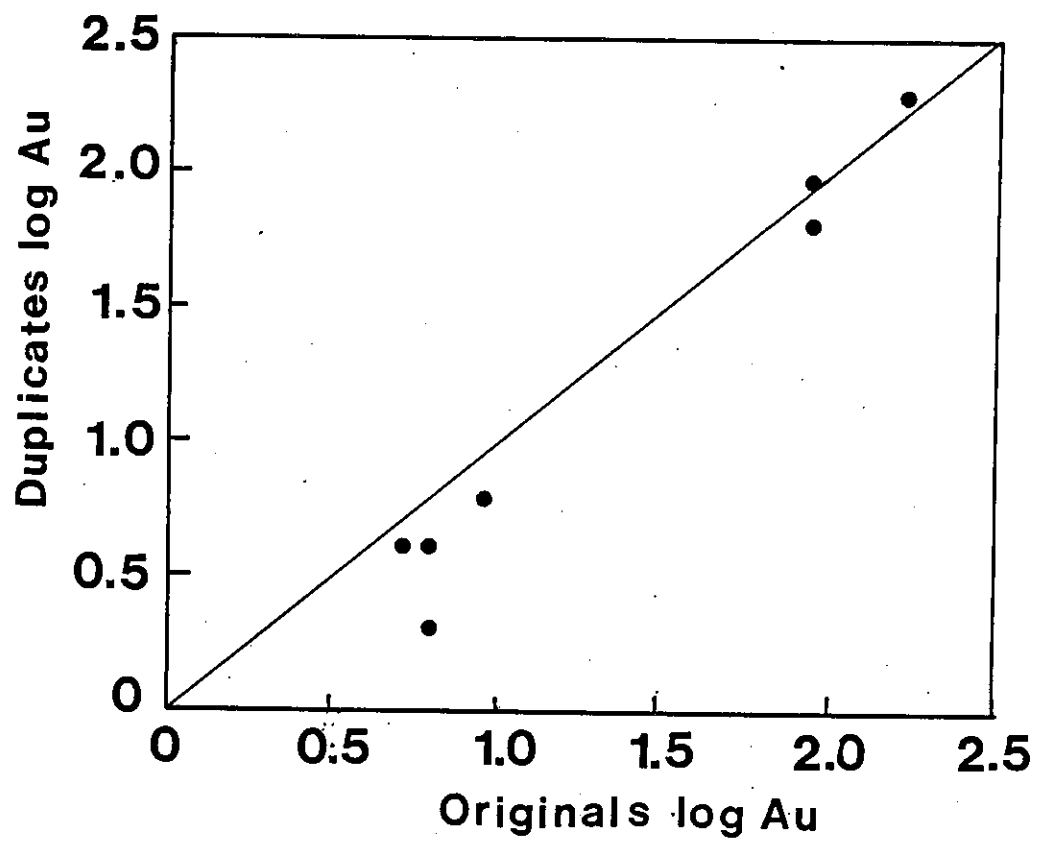


Figure A9.9 Inter-laboratory comparison of some trace elements.

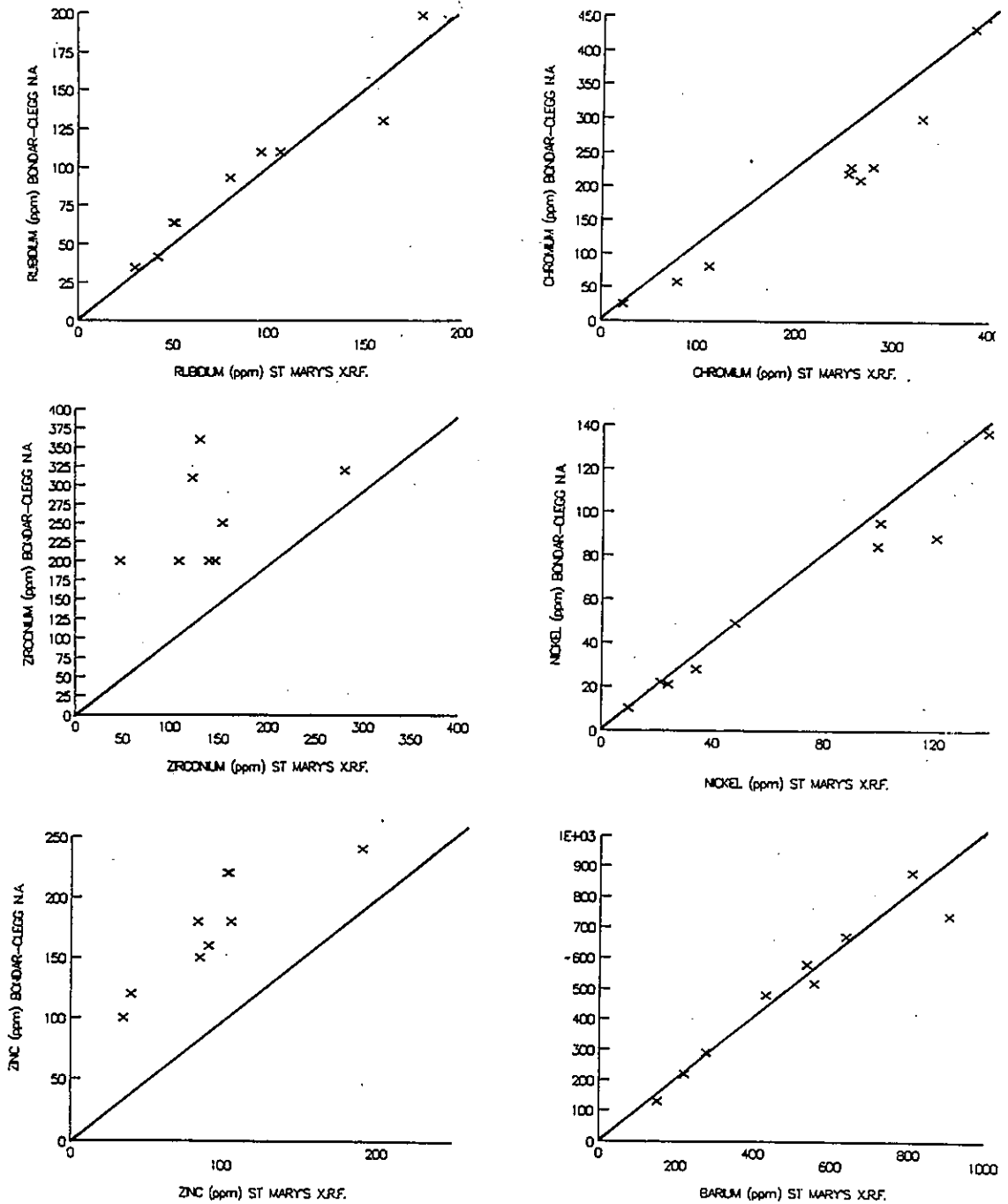


Table A9.1 DUPLICATES: Major\trace element (X.R.F.) data and volatile data. (Major element and volatile data in wt.%, while trace element data in ppm).

	81-81	81-82	81-83	81-84	81-85	81-86	81-87
SiO2	58.67	51.20	58.13	46.63	56.05	64.18	76.13
Al2O3	19.54	20.50	19.14	22.62	17.42	15.64	9.76
Fe2O3	7.45	10.31	8.05	8.85	10.23	6.04	4.19
MgO	3.37	5.02	3.93	4.08	4.69	4.02	3.05
CaO	0.72	0.48	0.44	4.27	2.15	2.34	1.45
Na2O	1.76	2.38	3.14	3.92	3.80	3.33	2.56
K2O	3.99	3.19	2.50	4.13	1.45	1.42	1.24
TiO2	0.81	0.79	0.78	0.92	0.81	0.25	0.28
MnO	0.07	0.09	0.07	0.11	0.11	0.10	0.07
P2O5	0.23	0.17	0.19	0.24	0.22	0.16	0.06
L.O.I.	4.00	6.90	3.50	3.30	2.80	2.40	1.00
TOTAL	100.61	101.03	99.87	99.07	99.73	99.88	99.79
Ba	806.00	555.00	635.00	903.00	277.00	150.00	221.00
Rb	106.00	96.00	80.00	159.00	51.00	50.00	42.00
Sr	181.00	199.00	248.00	637.00	429.00	498.00	281.00
Y	19.00	22.00	20.00	24.00	19.00	11.00	9.00
Zr	140.00	122.00	130.00	280.00	146.00	47.00	47.00
Nb	7.00	7.00	6.00	7.00	5.00	<5	<5
Pb	<10	<10	<10	<10	113.00	<10	<10
Ga	26.00	31.00	26.00	33.00	24.00	18.00	12.00
Zn	84.00	105.00	106.00	91.00	191.00	103.00	35.00
Cu	13.00	27.00	16.00	37.00	118.00	<5	<5
Ni	21.00	49.00	84.00	88.00	95.00	22.00	28.00
TiO2	0.85	0.91	0.85	0.84	0.89	0.30	0.32
V	187.00	239.00	197.00	190.00	223.00	85.00	75.00
Cr	256.00	265.00	253.00	328.00	278.00	111.00	78.00
C%	-	-	0.24	0.2	-	-	-
CO2%	-	-	<0.2	<0.2	-	-	-
S%	-	-	0.102	1.75	-	-	-

- 81-81 - 9-6-2 - Interbedded black and dark grey siltstones.  
 81-82 - 86-187/4 - S4-parallel vein in limonite stained black siltstone.  
 81-83 - 87-84 - Grey siltstone from East limb.  
 81-84 - 27-6-3 - Black (altered?) siltstone adjacent to Kidney Pond Zone 1 with 3-5% coarse arsenopyrite.  
 81-85 - 86-64 - Interbeds of black and dark grey siltstone.  
 81-86 - 86-59B - Zone 1 quartz-breccia, with 50% white feldspar, 25% grey quartz, 25% black siltstone fragments, and <1% pyrite/arsenopyrite.  
 81-87 - 86-169 - T-11 breccia with 20% white feldspar, 60% grey quartz, 8% graywacke fragments and 2-3% biotite/sulphides.

Table A9.2 STANDARDS (from Abbey, 1986): Major\trace element (X.R.F.) data and volatile data. (Major element and volatile data in wt.%, while trace element data in ppm).

	89-41	89-42	89-83	89-84
SiO2	71.38	51.74	71.12	51.54
Al2O3	14.34	14.17	14.33	13.91
Fe2O3	2.04	8.88	2.05	8.87
MgO	1.16	7.86	1.23	7.73
CaO	2.04	9.54	2.05	9.44
Na2O	3.82	2.77	3.58	3.07
K2O	3.89	1.40	3.89	1.37
TiO2	0.24	1.26	0.24	1.24
MnO	0.07	0.14	0.07	0.14
P2O5	0.15	0.30	0.14	0.31
L.O.I.	0.70	1.40	0.80	1.70
TOTAL	99.83	99.46	99.50	99.32
Ba	426.00	548.00	429.00	534.00
Rb	180.00	34.00	179.00	30.00
Sr	178.00	451.00	181.00	448.00
Y	32.00	22.00	33.00	24.00
Zr	117.00	155.00	108.00	154.00
Nb	10.00	29.00	11.00	29.00
Pb	<10	<10	<10	<10
Ga	17.00	18.00	18.00	20.00
Zn	41.00	86.00	40.00	85.00
Cu	<5	39.00	<5	37.00
Ni	10.00	140.00	10.00	136.00
TiO2	0.26	1.29	0.25	1.28
V	19.00	202.00	17.00	191.00
Cr	19.00	380.00	23.00	381.00
C%	-	-	-	-
CO2%	-	-	-	-
S%	-	-	-	-

89-41 - JB-1, Volcanic rock, G.S.C. standard

89-42 - Duplicate of JB-1, Volcanic rock, G.S.C. standard.

89-83 - JG-1, Granitic rock, G.S.C. standard.

89-84 - Duplicate of JG-1, Granitic rock, G.S.C. standard.



Table A9.3 GRAYWACKES: Major\trace element (X.R.F.) data and volatile data. (Major element and volatile data in wt.%, while trace element data in ppm).

	23-6-1	86-81	21-6-4	W05-121.5	86-110	21-6-10
SiO2	57.53	60.89	67.00	44.08	66.09	68.24
Al2O3	18.02	16.55	14.86	23.86	14.30	14.45
Fe2O3	7.77	7.68	4.59	9.70	6.78	4.93
MgO	3.97	3.89	2.40	4.51	3.20	2.69
CaO	1.61	1.53	3.08	2.93	1.19	0.96
Na2O	2.84	3.43	3.96	1.80	2.29	3.32
K2O	4.14	2.17	0.97	6.13	2.68	1.91
TiO2	0.78	0.73	0.61	1.09	0.78	0.59
MnO	0.08	0.08	0.08	0.11	0.06	0.05
P2O5	0.19	0.21	0.11	0.21	0.22	0.11
L.O.I.	1.90	2.50	1.20	4.40	1.90	1.90
TOTAL	98.83	99.66	98.86	98.82	99.49	99.15
Ba	1604	897	173	1993	554	408
Rb	121	63	57	239	99	52
Sr	352	305	316	600	183	206
Y	23	18	15	34	17	15
Zr	172	138	170	212	273	141
Nb	6	<5	6	9	7	<5
Pb	16	<10	17	286	<10	<10
Ga	22	19	15	38	17	15
Zn	93	99	77	125	84	65
Cu	21	36	52	132	46	41
Ni	74	79	57	95	67	56
TiO2	0.81	0.74	0.61	1.08	0.81	0.65
V	171	162	121	307	149	127
Cr	218	237	215	325	344	206
C%	-	0.17	0.09	-	0.13	0.11
CO2%	-	<0.20	<0.20	-	<0.20	<0.20
S%	-	0.124	0.265	-	0.155	0.085

- 23-6-1 Biotite-grade greywacke proximal to Spud Lake granite.  
86-81 Coarse- to medium-grained graywacke, west of Kidney Pond Zone 1.  
21-6-4 Greywacke proximal to Kidney Pond Zone 2.  
W05-121.5 Dark-green altered graywacke from Lynx area, and 3% coarse disseminated arsenopyrite.  
21-6-10 Fine-grained graywacke proximal to Kidney Pond Zone 2.  
86-110 Dark-grey fine-grained graywacke proximal to Kidney Pond Zone 1.

Table A9.4 LIGHT-GREY SILTSTONES: Major\trace element (X.R.F.) data and volatile data. (Major element and volatile data in wt.%, while trace element data in ppm).

	19-6-2	19-6-1	87-93	87-148	23-6-14	87-84
SiO2	58.99	79.48	59.99	59.97	55.67	57.80
Al2O3	18.44	9.22	17.72	16.93	19.75	18.86
Fe2O3	7.20	4.41	7.31	8.14	9.19	8.22
MgO	3.70	2.46	3.67	4.04	3.92	3.93
CaO	1.10	0.23	1.08	1.06	0.31	0.43
Na2O	2.47	0.64	2.29	1.98	1.22	3.09
K2O	3.48	1.60	3.16	2.84	4.05	2.48
TiO2	0.77	0.36	0.75	0.74	0.86	0.78
MnO	0.08	0.04	0.08	0.10	0.09	0.07
P2O5	0.14	0.05	0.19	0.21	0.11	0.21
L.O.I.	3.00	1.80	3.10	4.30	4.20	3.60
TOTAL	99.37	100.29	99.34	100.31	99.37	99.47
Ba	988	391	688	857	930	653
Rb	93	46	100	95	134	84
Sr	278	62	161	159	72	243
Y	20	6	26	22	17	19
Zr	130	53	141	139	112	130
Nb	7	<5	5	6	6	7
Pb	12	<10	<10	<10	<10	<10
Ga	23	12	24	24	24	25
Zn	87	67	106	101	95	106
Cu	34	25	18	27	29	20
Ni	82	49	98	95	47	82
TiO2	0.72	0.44	0.64	0.83	0.89	0.85
V	189	115	161	186	252	199
Cr	226	155	262	249	251	261
C%	0.16	-	0.16	0.43	-	0.23
CO2%	<0.20	-	<0.20	0.50	-	<0.20
S%	0.10	-	0.076	0.052	-	0.09

- 19-6-2 Grey coarse-grained siltstone from south shore of Gordon Lake.  
 19-6-1 Grey to black coarse-grained siltstone from south shore of Gordon Lake.  
 87-93 Grey coarse-grained siltstone from West Bay area.  
 87-148 Grey coarse-grained siltstone from Zenith Island.  
 23-6-14 Grey coarse-grained siltstone with minor black siltstone clasts and veinlets.  
 87-84 Grey coarse-grained siltstone from Zenith Island.

**Table A9.5 DARK GREY/BLACK SILTSTONES: Major\trace element (X.R.F.) data and volatile data. (Major element and volatile data in wt.%, while trace element data in ppm).**

	17-6-2	7-6-4	86-78	21-6-6	7-6-3	7-6-1/2	6-6-3	87-65
SiO2	57.82	43.07	55.76	55.27	56.74	50.37	54.08	56.19
Al2O3	19.38	24.13	20.29	19.82	19.81	19.84	20.87	20.36
Fe2O3	7.61	7.13	7.97	8.54	8.38	10.19	8.48	8.69
MgO	4.13	2.87	4.00	4.25	3.86	4.53	4.13	4.44
CaO	1.05	6.79	0.81	0.79	0.38	1.36	0.91	0.34
Na2O	2.68	2.29	1.52	2.47	1.51	5.62	2.21	2.40
K2O	3.64	4.10	4.03	3.53	3.98	3.99	3.74	3.28
TiO2	0.76	0.97	0.79	0.84	0.82	0.90	0.84	0.80
MnO	0.07	0.09	0.07	0.08	0.06	0.09	0.09	0.08
P2O5	0.13	0.08	0.18	0.14	0.13	0.17	0.14	0.21
L.O.I.	3.00	7.40	3.90	4.00	4.50	2.70	4.00	3.70
TOTAL	100.27	98.92	99.32	99.73	100.17	99.76	99.49	100.49
Ba	805	1100	886	840	994	834	981	835
Rb	88	178	129	101	116	154	102	109
Sr	268	653	188	168	178	457	224	206
Y	19	28	24	20	22	25	19	23
Zr	122	211	126	125	127	153	134	132
Nb	<5	6	7	5	6	6	5	6
Pb	19	37	<10	14	<10	16	11	<10
Ga	23	43	27	25	23	26	27	27
Zn	100	153	96	98	102	105	108	110
Cu	47	53	10	44	27	73	32	23
Ni	73	90	50	82	41	75	68	98
TiO2	0.69	0.93	0.82	0.87	0.80	1.08	0.80	0.97
V	193	239	208	215	221	261	236	215
Cr	224	274	272	266	261	288	278	273
C%	0.14	-	-	0.25	0.34	-	0.16	
CO2%	<0.20	-	-	<0.20	<0.20	-	<0.20	
S%	0.039	-	-	0.055	0.064	-	0.005	

- 17-6-2 Black siltstone with crenulated cleavage and <1% quartz veining.  
 7-6-4 Black 'chert' like siltstone with no cleavage from Buldge zone.  
 86-78 Black siltstone with well developed S3 cleavage and quartz-biotite-chlorite aggregates.  
 21-6-6 Black siltstone with minor limonite staining and sulphide traces.  
 7-6-3 Black siltstone with minor limonite staining.  
 7-6-1/2 Black siltstone from Buldge area with minor limonite staining.  
 6-6-3 Black siltstone with minor limonite staining and sulphide traces.  
 87-65 Black siltstone from Zenith Island.

Table A9.6 SULPHIDE-RICH BLACK SILTSTONES: Major\trace element (X.R.F.) data and volatile data. (Major element and volatile data in wt.%, while trace element data in ppm).

	H23-5.5	17-665.5	86-62	86-69	C16-6.5	27-6-3	BC11-11.5	27-6-5
SiO2	45.96	44.49	41.89	49.02	45.77	45.94	51.49	45.54
Al2O3	27.07	26.80	26.04	21.05	25.63	22.25	22.01	22.19
Fe2O3	6.39	7.43	11.05	9.94	7.78	9.49	7.30	9.08
MgO	1.77	2.48	3.70	5.06	4.74	3.89	3.24	3.32
CaO	2.38	1.31	1.05	2.08	0.66	4.15	2.09	3.59
Na2O	3.03	2.18	1.28	4.79	2.92	4.13	3.76	3.31
K2O	6.11	7.55	6.87	3.19	5.67	4.07	4.72	4.03
TiO2	1.07	1.10	1.26	0.97	1.05	0.93	0.92	0.82
MnO	0.05	0.05	0.06	0.11	0.09	0.11	0.06	0.09
P2O5	0.07	0.17	0.14	0.21	0.16	0.19	0.20	0.17
L.O.I.	5.90	5.70	6.90	3.40	5.00	3.30	3.80	6.50
TOTAL	99.80	99.26	100.24	99.82	99.47	98.45	99.59	98.64
Ba	1585	1768	1586	1091	1539	883	1008	982
Rb	187	215	216	105	175	160	164	172
Sr	443	253	226	469	182	645	432	778
Y	26	31	35	30	30	27	24	26
Zr	230	191	233	186	197	275	184	184
Nb	9	8	13	<5	9	7	9	<5
Pb	<10	14	<10	<10	<10	12	<10	41
Ga	50	38	50	26	41	29	28	30
Zn	80	37	106	50	93	87	51	56
Cu	25	115	96	19	51	65	93	68
Ni	94	101	173	99	81	92	113	91
TiO2	0.91	0.93	1.14	1.06	1.04	0.83	0.92	0.79
V	277	254	272	243	268	188	186	172
Cr	321	324	366	301	299	308	274	240
C%	-	-	0.83	0.47	-	0.21	-	0.43
CO2%	-	-	<0.20	<0.20	-	<0.20	-	<0.20
S%	-	-	2.53	0.928	-	1.64	-	2.42

- H23-5.5 Black siltstone with 5-10% disseminated arsenopyrite and quartz veinlets.  
 17-665.5 Black siltstone with 15% white-grey quartz and minor pyrite/arsenopyrite veinlet  
 86-62 Black siltstone with 5-10% arsenopyrite veinlets and traces of pyrite.  
 86-69 Black siltstone from adjacent to Zone 1 quartz-breccia with 1-2% pyrrhotite and pyrite.  
 C16-6.5 Crenulated black siltstone from Zone 1 breccia with 3% pyrite and quartz veinlet  
 27-6-3 Black siltstone with 3-5% coarse disseminated arsenopyrite.  
 BC11-11.5 Crenulated black siltstone with 5-10% pyrrhotite veinlets.  
 27-6-5 Black siltstone with 5% coarse arsenopyrite and <2% quartz veinlets.

**Table A9.7 INTERBEDDED SILTSTONES: Major\trace element (X.R.F.) data and volatile data. (Major element and volatile data in wt.%, while trace element data in ppm).**

	86-64	6-6-2	21-6-2	9-6-2	19-6-6
SI02	55.43	57.64	58.57	58.53	56.42
AL2O3	17.18	18.32	18.81	19.30	20.14
FE2O3	10.11	8.09	7.39	6.57	7.54
MGO	5.24	3.84	3.90	3.26	4.11
CAO	2.15	1.52	0.61	0.68	0.79
NA2O	4.15	3.43	2.31	1.86	1.40
K2O	1.42	3.28	3.31	3.99	4.27
TIO2	0.80	0.84	0.82	0.80	0.81
MNO	0.11	0.09	0.06	0.07	0.07
P2O5	0.23	0.18	0.15	0.15	0.13
L.O.I.	2.80	2.40	3.80	4.10	3.50
TOTAL	99.62	99.63	99.73	99.31	99.18
Ba	283	950	808	822	1009
Rb	52	92	94	105	121
Sr	422	230	161	183	198
Y	18	20	22	17	21
Zr	148	146	131	135	133
Nb	6	<5	6	5	6
Pb	109	13	<10	12	<10
Ga	26	22	23	25	26
Zn	187	93	86	84	108
Cu	120	45	43	34	41
Ni	99	76	59	24	95
TIO2	0.88	0.82	0.79	0.85	0.80
V	219	193	192	194	209
Cr	271	233	250	244	253
C%	0.26	0.16	0.14	-	0.16
CO2%	<0.20	<0.20	<0.20	-	<0.20
S%	0.436	0.031	0.041	-	0.061

- 86-64 Three x 1 cm wide interbeds of black and dark grey siltstone.
- 6-6-2 Twenty x 5 mm wide interbeds of grey and black fine siltstones with 1-2% quartz veins.
- 21-6-2 Two 2 cm wide black siltstone beds on either side of 3 cm wide black siltstone bed.
- 9-6-2 Interbedded black and dark grey siltstones with 'herring bone' cleavage pattern.
- 19-6-6 Interbedded grey and black siltstones from south shore of Gordon Lake.

**Table A9.8 BEDDING-PARALLEL, PRE-D<sub>3</sub>, AND S<sub>3s</sub>-PARALLEL QUARTZ VEINS: Major\trace element (X.R.F.) data and volatile data. (Major element and volatile data in wt.%, while trace element data in ppm).**

	87-130	87-1	86-85	87-27	86-88	87-189	86-186	87-126-3	17-6-3	87-186
SiO <sub>2</sub>	81.56	82.91	65.12	65.09	90.17	52.99	60.51	66.77	66.09	75.36
Al <sub>2</sub> O <sub>3</sub>	6.67	7.94	12.82	15.70	4.88	21.12	17.91	12.96	15.10	10.38
Fe <sub>2</sub> O <sub>3</sub>	4.79	2.76	7.97	5.67	1.28	8.09	7.39	8.13	6.17	5.38
MgO	2.71	1.41	2.37	2.66	1.02	3.89	3.77	4.40	3.58	3.13
CaO	0.64	1.90	0.14	0.87	0.73	2.54	0.98	1.28	0.81	0.59
Na <sub>2</sub> O	1.14	1.28	2.88	5.74	1.37	4.04	2.10	1.99	2.22	0.98
K <sub>2</sub> O	0.32	0.54	2.97	1.34	0.63	2.87	2.88	0.85	2.61	1.61
TiO <sub>2</sub>	0.22	0.19	0.44	0.70	0.13	0.92	0.74	0.49	0.57	0.40
MnO	0.05	0.05	0.04	0.05	0.02	0.09	0.07	0.07	0.07	0.05
P <sub>2</sub> O <sub>5</sub>	0.09	0.15	0.13	0.28	0.10	0.23	0.18	0.19	0.11	0.21
L.O.I.	1.80	1.00	5.10	2.30	0.20	2.90	3.20	2.70	2.80	2.70
TOTAL	99.99	100.13	99.98	100.40	100.53	99.68	99.73	99.83	100.13	100.79
Ba	52	60	411	545	219	775	694	160	643	373
Rb	6	12	81	69	14	122	82	26	68	46
Sr	108	170	122	340	135	444	239	268	184	115
Y	11	11	22	19	6	25	19	15	18	11
Zr	31	52	117	181	24	197	136	100	92	62
Nb	<5	<5	<5	<5	<5	8	5	5	5	<5
Pb	<10	<10	<10	27	<10	<10	<10	<10	20	<10
Ga	8	15	17	16	7	27	23	14	20	15
Zn	73	34	47	73	18	116	82	121	82	95
Cu	<5	27	93	19	<5	32	<5	<5	37	<5
Ni	39	31	16	40	10	95	55	69	75	47
TiO <sub>2</sub>	0	0	1	1	0	1	1	1	1	0
V	91	46	130	135	24	205	182	135	156	123
Cr	144	56	139	199	52	289	245	171	177	160
C%	.	.	.	.	.	.	.	.	.	.
CO <sub>2</sub> %	.	.	.	.	.	.	.	.	.	.
S%	.	.	.	.	.	.	.	.	.	.

- 87-130 Bedding-parallel vein in grey to black siltstone with 70-90% grey quartz.  
87-1 Bedding-parallel vein in limonite-stained black siltstone with 60-80% white quartz.  
86-85 Bedding-parallel vein in limonite stained black siltstone with 30-50% white quartz.  
87-27 Pre-D<sub>3</sub> vein in graywacke with 10% white quartz and pyrite traces.  
86-88 Pre-D<sub>3</sub> vein in graywacke with 70% white quartz and 10-20% grey quartz.  
87-189 Pre-D<sub>3</sub> veins in graywacke with 20-30% quartz and minor disseminated sulphides.  
86-186 S<sub>3s</sub>-parallel vein in crenulated and limonite stained black siltstone with 20-30% quartz.  
87-126-3 S<sub>3s</sub>-parallel vein in grey-black siltstone with 10-30% quartz.  
17-6-3 S<sub>3s</sub>-parallel vein in crenulated black siltstone with 30% grey quartz.  
87-186 S<sub>3s</sub>-parallel vein in black siltstone with 70-80% grey quartz and arsenopyrite traces.

**Table A9.9 S<sub>4</sub>-PARALLEL, ROTATED 'Z', AND EAST LIMB QUARTZ VEINS: Major\trace element (X.R.F.) data and volatile data. (Major element and volatile data in wt.%, while trace element data in ppm).**

	87-124	86-187/4	16-6-1	19-6-5	87-18	18-6-6	87-13	87-27
SiO <sub>2</sub>	79.06	51.16	86.39	76.79	58.99	53.35	78.16	65.09
Al <sub>2</sub> O <sub>3</sub>	7.67	20.24	5.70	10.07	17.78	17.86	7.16	15.70
Fe <sub>2</sub> O <sub>3</sub>	6.13	10.43	2.23	4.62	7.89	11.33	4.04	5.67
MgO	3.16	5.07	1.55	2.59	3.90	3.50	2.49	2.66
CaO	0.23	0.52	1.51	0.55	1.34	0.49	3.17	0.87
Na <sub>2</sub> O	0.78	2.62	1.42	1.62	2.55	1.08	0.82	5.74
K <sub>2</sub> O	0.66	3.22	0.75	1.56	2.79	4.93	1.03	1.34
TiO <sub>2</sub>	0.20	0.80	0.22	0.42	0.74	0.65	0.26	0.70
MnO	0.06	0.09	0.05	0.04	0.10	0.07	0.06	0.05
P <sub>2</sub> O <sub>5</sub>	0.07	0.17	0.11	0.07	0.20	0.12	0.14	0.28
L.O.I.	1.90	6.70	0.90	1.80	4.20	6.90	3.50	2.30
TOTAL	99.92	101.02	100.83	100.13	100.48	100.28	100.83	100.40
Ba	126	544	157	393	619	1606	239	545
Rb	14	91	16	42	87	170	30	69
Sr	76	197	244	120	227	210	121	340
Y	6	24	12	10	20	21	10	19
Zr	15	119	45	63	122	146	48	181
Nb	<5	7	<5	<5	<5	<5	<5	<5
Pb	<10	<10	<10	<10	<10	<10	<10	27
Ga	13	25	8	14	27	25	10	16
Zn	80	106	28	66	99	50	66	73
Cu	<5	26	24	36	7	97	9	19
Ni	32	46	23	57	88	65	35	40
TiO <sub>2</sub>	0	1	0	1	1	1	0	1
V	84	238	53	127	186	194	71	135
Cr	85	270	83	174	243	174	105	199
C%	-	-	-	-	-	-	-	-
CO <sub>2</sub> %	-	-	-	-	-	-	-	-
S%	-	-	-	-	-	-	-	-

- 87-124 S<sub>4</sub>-parallel vein in foliated black siltstone with 90% grey quartz.  
86-187/4 S<sub>4</sub>-parallel vein in limonite-stained black siltstone with 35% white quartz and sulphide traces.  
16-6-1 Rotated echelon vein in grey siltstone with 90% grey quartz.  
19-6-5 Rotated echelon vein in black-grey siltstone with 85% white quartz.  
87-18 East Limb (Type 4) vein in black siltstone with 30% white-grey quartz and minor carbonate.  
18-6-6 East limb (Type 4) vein in black siltstone with 40-60% grey quartz.  
87-13 East Limb (Type 4) vein in black siltstone with 90% white-grey quartz and minor carbonate plus sulphides.  
87-27 Extensional vein perpendicular to S<sub>3</sub>E<sub>s</sub> cleavage on refold's east limb with 10% quartz and minor pyrite.

Table A9.10 TYPE III AND IV QUARTZ-BRECCIA SAMPLES FROM LYNX INLET AND SOUTH GORDON LAKE: Major\trace element (X.R.F.) data and volatile data. (Major element and volatile data in wt.%, while trace element data in ppm).

	86-168	W05-124	86-169	24-6-6	17-6-5
SiO2	63.07	59.18	75.99	58.09	66.89
AL2O3	12.29	16.73	9.69	14.81	10.23
FE2O3	4.95	6.68	4.17	7.61	8.91
MGO	3.49	3.92	2.97	7.43	5.35
CAO	5.62	3.95	1.44	3.16	0.59
NA2O	5.33	3.88	2.38	1.78	0.85
K2O	0.74	2.72	1.26	1.41	3.78
TiO2	0.27	0.60	0.29	0.80	0.76
MNO	0.09	0.10	0.07	0.13	0.10
P2O5	0.07	0.15	0.07	0.18	0.00
L.O.I.	3.20	1.60	0.90	4.20	1.50
TOTAL	99.12	99.51	99.23	99.60	98.96
Ba	217	515	224	1009	393
Rb	14	102	39	49	183
Sr	322	799	285	337	142
Y	11	20	10	18	10
Zr	74	190	51	161	<5
Nb	<5	6	<5	5	8
Pb	<10	<10	<10	89	<10
Ga	13	21	12	19	17
Zn	35	99	33	86	136
Cu	<5	12	<5	13	10
Ni	40	49	27	207	69
TiO2	0.26	0.62	0.30	0.77	0.86
V	66	121	76	171	249
Cr	98	180	80	512	57
C%	-	-	-	-	-
CO2%	-	-	-	-	-
S%	-	-	-	-	-

- 86-168 Type IV quartz-breccia from Woofarine zone with 60% white feldspar and quartz, 40% altered graywacke, and minor sulphides.
- W05-124 Type IV quartz-breccia from Lynx area with 25% grey quartz, calcic/mica altered graywacke fragments, and 1-3% disseminated arsenopyrite.
- 86-169 Type IV quartz-breccia from T-11 zone with 60% grey quartz, 30% white feldspar, 8 graywacke fragments, and 2% biotite/sulphides.
- 24-6-6 Type III quartz-breccia from middle of Gordon Lake with 90% grey quartz in grey siltstone.
- 17-6-5 Type III quartz-breccia from south shore of Gordon Lake with 90% grey quartz, 7% white feldspar, and 3% biotite.



**Table A9.11 TYPE III QUARTZ-BRECCIA SAMPLES FROM KIDNEY POND ZONE 1: Major\trace element (X.R.F.) data and volatile data. (Major element and volatile data in wt.%, while trace element data in ppm).**

	86-59A	86-598	86-63	86-71	86-76	86-77	DE44-28.5	D48-110	H23-25.0	17-636.0
SiO2	75.33	64.37	60.35	69.95	59.70	86.00	80.83	62.94	61.15	76.40
Al2O3	12.95	15.54	18.51	12.98	13.49	6.59	8.24	21.24	20.64	11.02
Fe2O3	1.95	5.99	4.69	5.63	10.15	1.32	2.38	1.10	2.67	2.69
MgO	1.81	3.85	3.24	2.86	4.65	1.48	2.18	1.10	1.61	2.13
CaO	2.93	2.36	3.07	1.08	2.52	1.11	1.06	4.11	3.71	2.12
Na2O	3.14	3.42	4.94	2.82	2.20	2.24	0.99	6.49	5.20	3.25
K2O	0.67	1.41	2.12	1.80	2.24	0.50	3.38	1.35	2.77	0.46
TiO2	0.09	0.25	0.54	0.49	0.63	0.11	0.31	0.13	0.21	0.12
MnO	0.04	0.10	0.07	0.06	0.11	0.03	0.05	0.04	0.07	0.04
P2O5	0.22	0.15	0.10	0.15	0.17	0.14	0.11	0.06	0.10	0.07
L.O.I.	0.40	2.30	2.00	2.30	3.70	0.80	1.30	1.30	1.90	0.90
TOTAL	99.53	99.74	99.63	100.12	99.56	100.32	100.83	99.86	100.03	99.20
Ba	82	157	227	334	284	58	341	165	491	56
Rb	16	53	85	50	105	14	125	33	94	11
Sr	525	499	764	242	417	296	145	1459	826	418
Y	5	9	23	12	17	7	16	6	10	<5
Zr	27	50	149	91	137	23	64	74	45	37
Nb	<5	<5	<5	<5	<5	<5	<5	<5	<5	<5
Pb	<10	<10	<10	<10	<10	<10	<10	<10	<10	17
Ga	11	19	17	18	27	9	13	16	19	9
Zn	36	103	85	66	93	35	44	28	57	42
Cu	<5	<5	<5	33	72	<5	<5	<5	<5	11
Ni	8	24	46	47	67	8	23	14	13	12
TiO2	0.11	0.30	0.58	0.53	0.66	0.12	0.31	0.11	0.27	0.12
V	35	93	139	116	209	39	64	14	85	32
Cr	51	107	268	178	214	51	107	18	36	59
C%	.	.	.	.	.	.	.	.	.	.
CO2%	.	.	.	.	.	.	.	.	.	.
S%	.	.	.	.	.	.	.	.	.	.

- 86-59A 40% white feldspar, 20% grey quartz, 30% black siltstone fragments, and <1% arsenopyrite/pyrrhotite.
- 86-598 50% white feldspar, 25% grey quartz, 25% black siltstone fragments, and <1% pyrite/arsenopyrite.
- 86-63 50% white feldspar, 15% grey quartz, 33% black siltstone, and 1-3% arsenopyrite/pyrite.
- 86-71 Two quartz veins in black siltstone, 50% grey quartz and <1% pyrrhotite/arsenopyrite.
- 86-76 2% white feldspar, 60% grey quartz, 35% black siltstone fragments, and 3% pyrite/arsenopyrite/pyrrhotite.
- 86-77 15% white feldspar, 70% grey quartz, 15% black siltstone fragments, and <1% pyrrhotite/arsenopyrite.
- DE44-28.5 70% white quartz, 25% green (chloritized?) altered black siltstone fragments, and pink adularia veins.
- D48-110.0 80% white quartz, 10% gray quartz, 10% black siltstone fragments, and minor sulphides.
- H23-25.0 90% white feldspar, 7-8% grey quartz/black siltstone fragments, and 2-3% biotite.
- 17-636.0 50% white feldspar, 50% grey quartz/black siltstone fragments.

**Table A9.12 MAFIC DYKE, CAMERON RIVER VOLCANIC, AND SPUD LAKE GRANITIC ROCKS: Major\trace element (X.R.F.) data and volatile data. (Major element and volatile data in wt.%, while trace element data in ppm).**

	UG87-4	12-6-2	12-6-3	12-6-7	22-6-8	22-6-11
SiO2	48.36	53.51	52.48	76.33	72.51	73.22
Al2O3	14.98	14.77	17.33	11.59	14.89	14.40
Fe2O3	13.21	11.85	13.13	1.97	0.92	0.85
MgO	6.14	3.70	3.47	0.85	0.78	0.68
CaO	8.34	9.44	7.52	1.78	0.45	0.42
Na2O	1.94	1.62	2.03	2.63	4.11	3.96
K2O	2.01	0.68	0.36	2.79	4.91	4.93
TiO2	1.37	1.12	1.35	0.26	0.14	0.13
MnO	0.18	0.31	0.39	0.09	0.02	0.02
P2O5	0.23	0.07	0.12	0.10	0.38	0.35
L.O.I.	2.70	1.80	0.70	1.00	0.50	0.50
TOTAL	99.46	98.87	98.88	99.39	99.61	99.46
Ba	530	209	48	488	307	313
Rb	104	13	<5	96	251	241
Sr	366	217	246	84	72	62
Y	25	22	30	18	17	17
Zr	110	76	82	110	61	57
Nb	<5	<5	<5	7	9	8
Pb	<10	<10	<10	24	16	15
Ga	23	19	21	14	20	20
Zn	119	395	293	122	34	26
Cu	100	93	98	24	8	7
Ni	118	94	135	12	5	<5
TiO2	1.32	1.14	1.41	0.28	0.14	0.14
V	234	339	402	30	<5	<5
Cr	86	225	275	43	25	23
C%	-	-	-	-	-	-
CO2%	-	-	-	-	-	-
S%	-	-	-	-	-	-

- UG87-4 Mafic dyke material from within quartz-breccia at Kidney Pond Zone 1.  
 12-6-2 Dark-green fine-grained mafic volcanic rock from Cameron River Volcanic Belt at Fenton Lake.  
 12-6-3 Light-grey limonite-stained felsic volcanic from Cameron River Volcanic Belt at Fenton Lake.  
 12-6-7 Quartz-feldspar porphyry volcanic rock from Cameron River Volcanic Belt at Fenton Lake.  
 22-6-8 White muscovite-rich granite from Spud Lake Pluton.  
 22-6-11 Pink muscovite-rich granite from Spud Lake Pluton.

Table A9.13 DUPLICATES: Trace element and gold (N.A.) data. All analyses in ppm except Na (wt.%), Fe (wt.%), Ir (ppb), and Au (ppb).

	81-81	81-82	81-83	81-84	81-85	81-86	81-87
Na	1.4	2	2.65	3.07	3.69	3.31	1.8
Sc	24.8	27.8	25.8	24.6	27.5	10	12
Cr	230	210	220	300	230	81	58
Fe	5.4	7.3	6	7.2	7.4	3.3	3
Co	39	48	51	74	63	47	170
Ni	24	48	99	120	100	21	34
Zn	180	220	180	160	240	220	<100
As	19	105	17	9000	125	3610	1340
Se	<5	<5	<5	<5	<5	<5	<5
Br	<2	<2	<2	11	<2	16	4.9
Rb	110	110	93	130	64	64	42
Zr	<200	310	360	320	<200	<200	<200
Mo	3	3	3	<4	3	3	4
Ag	<2	<2	<2	<2	<2	<2	<2
Cd	<5	<5	<5	<21	<5	<5	<5
Sn	<100	<100	<100	<100	<100	<100	<100
Sb	0.2	0.2	1.7	12.8	0.2	1.3	0.6
Te	<10	<10	<10	<33	<10	<32	<24
Cs	5	2.9	4.8	6.5	3.3	2.5	2.7
Ba	880	520	670	740	290	130	220
La	26	17	34	33	40	16	10
Ce	45	36	70	77	78	27	<5
Sm	2.7	2.9	5.6	5.1	6.7	1.9	1.7
Eu	<1	<1	1	1	2	1	<1
Tb	0.5	0.7	0.9	0.8	0.9	<0.5	0.7
Yb	<2	2	2	<2	3	<2	<2
Lu	0.3	0.4	0.4	0.4	0.4	0.3	0.3
Hf	3	3	3	6	4	<1	<1
Ta	1	1.1	0.9	<0.5	0.8	<0.5	2.7
W	175	179	79	77	99	262	1040
Ir	<50	<50	<50	<50	<50	<50	<50
Au	4	<2	4	190	92	63	<6
Th	7.9	7.3	7.8	12	9.2	3.1	2.8
U	2.6	2.1	2.5	3.2	2.6	<0.2	<0.2

81-81 - 9-6-2 - Interbedded black and dark grey siltstones.

81-82 - 86-187/4 - S4-parallel vein in limonite stained black siltstone.

81-83 - 87-84 - Grey siltstone from East limb.

81-84 - 27-6-3 - Black (altered?) siltstone adjacent to Kidney Pond Zone 1 with 3-5% coarse arsenopyrite.

81-85 - 86-64 - Interbeds of black and dark grey siltstone.

81-86 - 86-59B - Zone 1 quartz-breccia, with 50% white feldspar, 25% grey quartz, 25% black siltstone fragments, and <1% pyrite/arsenopyrite.

81-87 - 86-169 - T-11 breccia with 20% white feldspar, 60% grey quartz, 8% graywacke fragments and 2-3% biotite/sulphides.

**Table A9.14 STANDARDS (from Abbey, 1983):** Trace element and gold (N.A.) data. All analyses in ppm except Na (wt.%), Fe (wt.%), Ir (ppb), and Au (ppb).

	89-41	89-42	89-83	89-84
Na	2.74	2.2	2.57	2.04
Sc	6.9	32.4	6.9	29.9
Cr	22	460	25	430
Fe	1.5	6.9	1.4	6.6
Co	7	53	7	54
Ni	<10	150	<10	140
Zn	170	<100	120	150
As	0.8	1.4	<0.5	1.9
Se	<5	<5	<5	<5
Br	<2	<2	<2	<2
Rb	200	40	200	35
Zr	260	<200	<200	250
Mo	<1	1	<1	2
Ag	<2	<2	<2	<2
Cd	<5	<5	<5	<5
Sn	<100	<100	<100	<100
Sb	0.2	0.2	0.1	0.3
Te	<10	<10	<10	<10
Cs	11	0.7	11	1.2
Ba	520	490	480	580
La	27	46	26	44
Ce	54	73	53	72
Sm	4.8	5.7	4.7	5.6
Eu	<1	<1	<1	2
Tb	1.1	0.8	0.9	1
Yb	3	3	4	<2
Lu	0.6	0.4	0.6	0.4
Hf	3	3	3	3
Ta	1.9	1.9	2.1	2
W	17	2	14	<2
Ir	<50	<50	<50	<50
Au	<2	<2	<2	5
Th	14	10	14	10
U	5.8	2	5.8	1.9

89-41 - JB-1, Volcanic rock, G.S.C. standard.

89-42 - Duplicate of JB-1, Volcanic rock, G.S.C. standard.

89-83 - JG-1, Granitic rock, G.S.C. standard.

89-84 - Duplicate of JG-1, Granitic rock, G.S.C. standard.

**Table A9.15 GRAYWACKES: Trace element and gold (N.A.) data. All analyses in ppm except Na (wt.%), Fe (wt.%), Ir (ppb), and Au (ppb).**

	23-6-1	86-81	21-6-4	W05-121.5	21-6-10	86-110
Na	2.1	2.63	3.03	1.5	2.42	1.8
Sc	22	21.4	15	34.7	15	18
Cr	210	200	190	320	170	290
Fe	5.9	5.6	3.6	7.6	3.9	5.1
Co	100	78	140	73	68	110
Ni	90	85	72	120	54	63
Zn	140	210	<100	130	110	160
As	8.6	17	14	9000	20	38
Se	<5	<5	<5	<5	<5	<5
Br	<2	<2	<2	14	<2	<2
Rb	150	75	67	240	63	120
Zr	350	<200	350	440	<200	580
Mo	4	3	5	6	3	4
Ag	<2	<2	<2	<2	<2	<2
Cd	<5	<5	6	<13	<5	<5
Sn	<100	<100	<100	<100	<100	<100
Sb	0.1	0.2	0.2	4.4	0.3	0.2
Te	<10	<10	<10	<24	<10	<10
Cs	6.9	3.2	3.6	6.4	2	6.6
Ba	1600	970	220	2000	470	610
La	50	33	40	44	28	44
Ce	96	67	73	82	54	80
Sm	7.3	5	5.2	7.3	4	5.6
Eu	2	1	1	3	<1	2
Tb	1.1	0.6	0.9	0.5	0.7	1
Yb	2	2	<2	<2	2	<2
Lu	0.3	0.4	0.2	0.5	0.3	<0.2
Hf	3	3	4	5	4	8
Ta	1.9	1	2.3	<0.5	1.2	1.9
W	506	241	688	60	333	511
Ir	<50	<50	<50	<50	<50	<50
Au	<2	7	16	2650	23	21
Th	12	7.4	7.4	10	6.4	13
U	2.9	2.6	2.3	3.4	2.1	3.8

- 23-6-1 Biotite-grade greywacke proximal to Spud Lake granite.  
 86-81 Coarse- to medium-grained graywacke, west of Kidney Pond Zone 1.  
 21-6-4 Greywacke proximal to Kidney Pond Zone 2.  
 W05-121.5 Dark-green altered graywacke from Lynx area, and 3% coarse disseminated arsenopyrite.  
 21-6-10 Fine-grained graywacke proximal to Kidney Pond Zone 2.  
 86-110 Dark-grey fine-grained graywacke proximal to Kidney Pond Zone 1.

Table A9.16 LIGHT-GREY SILTSTONES: Trace element and gold (N.A.) data. All analyses in ppm except Na (wt.%), Fe (wt.%), Ir (ppb), and Au (ppb).

	19-6-2	19-6-1	87-93	87-148	23-6-14	87-84
Na	1.9	0.55	1.8	1.4	0.88	2.67
Sc	25.5	12	19	23.6	34.5	25.9
Cr	210	100	200	230	250	230
Fe	5.7	3.4	5	6	7.4	6.2
Co	82	150	72	53	26	56
Ni	93	52	120	94	45	100
Zn	130	<100	180	170	120	220
As	20	9.2	53.1	43	39	18
Se	<5	<5	<5	<5	<5	<5
Br	<2	<2	<2	<2	<2	<2
Rb	110	52	130	110	150	97
Zr	<200	<200	300	340	<200	<200
Mo	2	4	4	2	2	2
Ag	<2	<2	<2	<2	<2	<2
Cd	<5	<5	<5	<5	<5	<5
Sn	<100	<100	<100	<100	<100	<100
Sb	0.3	0.3	0.1	2.4	0.2	2
Te	<10	<10	<10	<10	<10	<10
Cs	3.5	2.2	4.3	6.2	4.4	4.8
Ba	1100	520	780	950	1000	740
La	33	5	41	47	<2	33
Ce	64	10	88	92	<5	67
Sm	5.6	1.3	8	7.2	0.78	6.1
Eu	<1	<1	2	2	<1	1
Tb	0.9	0.7	1.1	0.7	<0.5	0.8
Yb	2	<2	3	2	3	2
Lu	0.4	0.2	0.4	0.4	0.4	0.4
Hf	3	<1	3	4	3	3
Ta	1.2	2.2	1	0.9	0.8	0.8
W	260	921	180	73	67	86
Ir	<50	<50	<50	<50	<50	<50
Au	<2	<2	6	<2	3	6
Th	7.8	3.6	9.1	9.2	9.2	8.4
U	2.3	1.2	3	2.7	2.9	2.7

19-6-2 Grey coarse-grained siltstone from south shore of Gordon Lake.

19-6-1 Grey to black coarse-grained siltstone from south shore of Gordon Lake.

87-93 Grey coarse-grained siltstone from West Bay area.

87-148 Grey coarse-grained siltstone from Zenith Island.

23-6-14 Grey coarse-grained siltstone with minor black siltstone clasts and veinlets.

87-84 Grey coarse-grained siltstone from Zenith Island.

Table A9.17 DARK GREY/BLACK SILTSTONES: Trace element and gold (N.A.) data. All analyses in ppm except Na (wt.%), Fe (wt.%), Ir (ppb), and Au (ppb).

	17-6-2	86-78	21-6-6	7-6-3	7-6-1/2	6-6-3	87-65
Na	1.8	1.2	1.5	1	4.27	1.7	1.9
Sc	24.7	26.8	28.9	29.2	32.5	30.7	26.8
Cr	210	230	240	250	270	250	240
Fe	5.6	6	6.8	6.9	8.4	6.7	6
Co	33	37	40	22	47	34	54
Ni	84	45	71	43	73	69	100
Zn	140	260	200	220	120	160	260
As	28	59.2	51.1	29	354	32	29
Se	<5	<5	<5	<5	<5	<5	<5
Br	<2	<2	<2	<2	<2	<2	<2
Rb	100	150	120	140	170	110	130
Zr	<200	<200	240	<200	290	<200	<200
Mo	3	3	2	4	4	2	3
Ag	<2	<2	<2	<2	<2	<2	<2
Cd	<5	<5	<5	<5	<5	<5	<5
Sn	<100	<100	<100	<100	<100	<100	<100
Sb	0.2	0.1	0.2	0.3	0.5	0.3	1.7
Te	<10	<10	<10	<10	<10	<10	<10
Cs	3	4.8	3.4	5.3	20	4.8	5.3
Ba	830	930	900	1100	880	1100	920
La	19	14	21	27	33	20	33
Ce	44	39	43	57	66	47	73
Sm	4	3.6	4	4.5	5.3	4.8	6.3
Eu	1	1	1	1	2	<1	1
Tb	0.8	0.7	0.7	0.7	0.6	0.7	0.9
Yb	<2	2	2	2	4	3	2
Lu	0.3	0.4	0.4	0.4	0.4	0.5	0.4
Hf	3	3	4	3	3	4	3
Ta	0.8	0.9	0.7	0.8	0.8	0.9	0.6
W	53	184	42	49	88	77	61
Ir	<50	<50	<50	<50	<50	<50	<50
Au	5	- 7	100	<2	13	12	15
Th	7.1	7.9	7.8	8.5	10	8.3	8.8
U	2.1	2.3	2.4	2.5	2.9	2.3	2.4

- 17-6-2 Black siltstone with crenulated cleavage and <1% quartz veining.  
 7-6-4 Black 'chert' like siltstone with no cleavage from Buldge zone.  
 86-78 Black siltstone with well developed S3 cleavage and quartz-biotite-chlorite aggregates.  
 21-6-6 Black siltstone with minor limonite staining and sulphide traces.  
 7-6-3 Black siltstone with minor limonite staining.  
 7-6-1/2 Black siltstone from Buldge area with minor limonite staining.  
 6-6-3 Black siltstone with minor limonite staining and sulphide traces.  
 87-65 Black siltstone from Zenith Island.

Table A9.18 SULPHIDE-RICH BLACK SILTSTONES: Trace element and gold (N.A.) data. All analyses in ppm except Na (wt.%), Fe (wt.%), Ir (ppb), and Au (ppb).

	H23-5.5	17-665.5	86-62	86-69	C16-6.5	27-6-3	BC11-11.5	27-6-5	7-6-4
Na	<1.4	1.4	<1.5	3.55	2.34	3.38	2.95	2.88	<1.8
Sc	31.3	37	38.4	29.5	29.7	26.7	26.5	22.9	30.9
Cr	300	340	380	270	250	310	260	240	290
Fe	4.7	6.1	7.7	7.2	6.3	7.2	5.7	7.2	6.3
Co	65	67	170	59	130	77	79	58	80
Ni	130	170	220	130	130	120	140	100	110
Zn	130	270	180	150	360	170	170	140	190
As	9000	5250	9000	366	5040	9000	3990	9000	9000
Se	<5	<5	<5	<5	<5	<5	<5	<5	<5
Br	28	10	23	<2	11	19	9	34	32
Rb	190	230	240	120	190	180	150	180	180
Zr	240	<470	430	<200	<490	<200	<450	<200	<200
Mo	5	7	<4	4	<3	4	5	<4	10
Ag	<2	<2	<2	<2	<5	<2	<5	<2	<2
Cd	<18	<5	<18	<5	<5	<17	<5	<20	<18
Sn	<100	<100	<100	<100	<320	<100	<280	<100	<100
Sb	11.4	1.6	8.5	0.3	2	12.5	1.6	24.9	20.7
Te	<33	<29	<31	<10	<54	<28	<48	<37	<33
Cs	6	4.8	6.8	5.4	6.6	7.3	4.7	4	4.5
Ba	1500	1800	1700	1100	1600	850	1000	900	1100
La	58	45	67	52	26	35	53	37	56
Ce	100	79	130	98	39	74	120	74	110
Sm	7.6	7	10	8.2	6.5	5.4	7.8	6	8.7
Eu	2	<1	3	3	3	2	2	2	2
Tb	0.9	0.6	1.3	1.2	0.7	0.9	0.8	<0.5	1.1
Yb	<2	<2	3	3	<2	<2	3	<2	<2
Lu	0.6	0.8	0.7	0.5	0.7	0.6	<0.2	0.6	0.5
Hf	4	<1	5	4	<1	6	3	3	3
Ta	0.7	0.6	1.1	0.7	0.6	1	0.6	0.5	0.7
W	71	80	<37	54	113	70	192	96	43
Ir	<50	<50	<50	<50	<50	<50	<50	<50	<50
Au	940	3970	3210	339	317	170	449	375	3970
Th	11	11	14	11	12	13	9.2	8.7	13
U	3.3	2.8	3.6	3.4	3.4	3.7	2.4	1.5	3.4

- H23-5.5 Black siltstone with 5-10% disseminated arsenopyrite and quartz veinlets.  
 17-665.5 Black siltstone with 15% white-grey quartz and minor pyrite/arsenopyrite veinlet  
 86-62 Black siltstone with 5-10% arsenopyrite veinlets and traces of pyrite.  
 86-69 Black siltstone from adjacent to Zone 1 quartz-breccia with 1-2% pyrrhotite and pyrite.  
 C16-6.5 Crenulated black siltstone from Zone 1 breccia with 3% pyrite and quartz veinlet  
 27-6-3 Black siltstone with 3-5% coarse disseminated arsenopyrite.  
 BC11-11.5 Crenulated black siltstone with 5-10% pyrrhotite veinlets.  
 27-6-5 Black siltstone with 5% coarse arsenopyrite and <2% quartz veinlets.



**Table A9.19 INTERBEDDED SILTSTONES: Trace element and gold (N.A.) data.** All analyses in ppm except Na (wt.%), Fe (wt.%), Ir (ppb), and Au (ppb).

	86-64	6-6-2	21-6-2	9-6-2	19-6-6
Na	3.37	2.53	1.7	1.2	1.3
Sc	25.6	26.6	26.2	22.2	26.4
Cr	220	220	250	200	230
Fe	7	6.3	5.9	5	5.7
Co	58	99	64	36	75
Ni	120	83	52	21	100
Zn	270	140	160	180	210
As	118	32	29	18	25
Se	<5	<5	<5	<5	<5
Br	<2	<2	<2	<2	<2
Rb	56	110	110	120	130
Zr	<200	<200	<200	<200	<200
Mo	3	2	3	3	4
Ag	<2	<2	<2	<2	<2
Cd	<5	<5	<5	<5	<5
Sn	<100	<100	<100	<100	<100
Sb	0.2	0.2	0.5	0.2	0.3
Te	<10	15	<10	11	<10
Cs	3.5	5.4	2.9	4.4	6.1
Ba	270	1000	850	880	1000
La	37	18	22	24	24
Ce	82	33	48	40	53
Sm	6.4	3.9	4.3	2.6	5.2
Eu	2	2	2	1	1
Tb	0.9	0.9	0.8	0.5	0.8
Yb	2	3	2	2	2
Lu	0.4	0.3	0.3	0.2	0.3
Hf	3	3	3	3	3
Ta	0.8	1.3	1.2	1	1
W	98	351	153	167	140
Ir	<50	<50	<50	<50	<50
Au	85	<2	6	5	<2
Th	8.7	9.4	7.7	8.1	8.4
U	2.7	2.8	2.4	2.4	2.6

86-64 Three x 1 cm wide interbeds of black and dark grey siltstone.

6-6-2 Twenty x 5 mm wide interbeds of grey and black fine siltstones with 1-2% quartz veins.

21-6-2 Two 2 cm wide black siltstone beds on either side of 3 cm wide black siltstone bed.

9-6-2 Interbedded black and dark grey siltstones with 'herring bone' cleavage pattern.

19-6-6 Interbedded grey and black siltstones from south shore of Gordon Lake.

**Table A9.20 BEDDING-PARALLEL, PRE-D<sub>3</sub>, AND S<sub>3</sub>S-PARALLEL QUARTZ VEINS: Trace element and gold (N.A.) data. All analyses in ppm except Na (wt.%), Fe (wt.%), Ir (ppb), and Au (ppb).**

	87-130	87-1	86-85	86-88	87-189	86-186	87-126-3	17-6-3	87-186
Na	0.78	1.2	2.43	0.87	3.09	1.8	1.6	1.3	0.72
Sc	7.2	6.2	13	3.3	24.6	23.6	13	19	12
Cr	68	40	89	54	240	230	130	150	110
Fe	3.4	2.1	5.6	1	5.7	5.8	5.7	4.5	3.3
Co	170	180	72	230	60	50	94	130	59
Ni	34	38	24	16	120	49	65	77	43
Zn	<100	<100	130	<100	170	140	190	130	130
As	16	2.7	646	16	25	50.8	87.8	46	56.8
Se	<5	<5	<5	<5	<5	<5	<5	<5	<5
Br	7.1	<2	24	9.3	<2	<2	<2	<2	4.3
Rb	17	26	91	21	140	100	39	72	60
Zr	<200	<200	260	<200	<200	260	290	<200	<200
Mo	4	3	3	5	3	3	3	3	2
Ag	<2	<2	<2	<2	<2	<2	<2	<2	<2
Cd	<5	<5	<5	<5	<5	<5	<5	<5	<5
Sn	<100	<100	<100	<100	<100	<100	<100	<100	<100
Sb	<0.1	0.6	0.9	0.2	0.3	0.1	<0.1	0.3	0.1
Te	<10	<10	<10	<10	<10	<10	<10	<10	<10
Cs	0.8	0.6	1	1.1	12	3.2	1.4	2.6	2.5
Ba	73	<50	400	330	760	780	210	640	410
La	9	17	20	3	61	34	25	24	19
Ce	19	30	36	<5	110	63	48	60	40
Sm	2.1	2.6	2.8	0.6	8.6	5.1	3.8	4.3	2.9
Eu	<1	2	1	<1	3	1	2	<1	<1
Tb	0.8	0.8	0.6	0.9	1.2	1	0.9	1.1	0.6
Yb	<2	<2	<2	<2	2	3	<2	<2	<2
Lu	<0.2	<0.2	0.3	<0.2	0.4	0.4	0.2	<0.2	0.2
Hf	<1	<1	3	<1	4	3	3	2	2
Ta	3	3.1	1.3	4.1	1.1	1.3	1.7	2	1
W	1130	1120	313	1700	142	248	574	692	300
Ir	<50	<50	<50	<50	<50	<50	<50	<50	<50
Au	210	16	8	<5	28	22	58	9	54
Th	1.8	5.1	7.7	1.5	10	8.8	5.1	5.1	3.6
U	0.8	1.8	2.7	<0.2	3.3	2.6	1.6	1.5	1.3

- 87-130 Bedding-parallel vein in grey to black siltstone with 70-90% grey quartz.  
 87-1 Bedding-parallel vein in limonite-stained black siltstone with 60-80% white quartz  
 86-85 Bedding-parallel vein in limonite stained black siltstone with 30-50% white quartz  
 87-27 Pre-D<sub>3</sub> vein in graywacke with 10% white quartz and pyrite traces.  
 86-88 Pre-D<sub>3</sub> vein in graywacke with 70% white quartz and 10-20% grey quartz.  
 87-189 Pre-D<sub>3</sub> veins in graywacke with 20-30% quartz and minor disseminated sulphides.  
 86-186 S<sub>3</sub>s-parallel vein in crenulated and limonite stained black siltstone with 20-30% quartz.  
 87-126-3 S<sub>3</sub>s-parallel vein in grey-black siltstone with 10-30% quartz.  
 17-6-3 S<sub>3</sub>s-parallel vein in crenulated black siltstone with 30% grey quartz.  
 87-186 S<sub>3</sub>s-parallel vein in black siltstone with 70-80% grey quartz and arsenopyrite traces.

**Table A9.21 S<sub>4</sub>-PARALLEL, ROTATED 'Z', AND EAST LIMB QUARTZ VEINS: Trace element and gold (N.A.) data. All analyses in ppm except Na (wt.%), Fe (wt.%), Ir (ppb), and Au (ppb).**

	87-124	86-187/4	16-6-1	19-6-5	87-18	18-6-6	87-13	87-27
Na	0.5	2	0.79	0.95	1.9	1.1	0.27	3.95
Sc	5.5	28	6.5	14	25	28.2	5.9	16
Cr	39	220	54	140	220	140	56	160
Fe	4.4	7.5	1.7	3.6	6.1	8.8	2.4	4.2
Co	130	52	210	72	61	68	66	93
Ni	39	47	24	56	90	76	36	43
Zn	180	150	<100	110	150	140	120	<100
As	<0.5	108	7.6	14	25	45	14	27
Se	<5	<5	<5	<5	<5	<5	<5	<5
Br	8.7	<2	11	<2	<2	<2	<2	<2
Rb	23	110	21	53	120	220	34	51
Zr	<200	<200	<200	<200	<200	<200	<200	280
Mo	2	2	5	4	2	6	2	3
Ag	<2	<2	<2	<2	<2	<2	<2	<2
Cd	<5	<5	<5	<5	<5	<5	<5	<5
Sn	<100	<100	<100	<100	<100	<100	<100	<100
Sb	<0.1	0.2	0.8	0.2	1.8	0.6	0.6	11.1
Te	<10	<10	<10	<10	<10	<10	<10	<10
Cs	1.3	2.7	<0.5	2.2	3.5	6.3	2	2.4
Ba	180	590	180	460	690	1900	240	620
La	<2	17	27	13	30	26	10	48
Ce	<5	38	47	29	61	51	19	93
Sm	0.49	3.1	3.4	2.7	5.9	2.5	1.5	6.7
Eu	<1	1	2	<1	2	1	<1	2
Tb	<0.5	0.7	1.2	0.5	0.9	0.6	<0.5	1
Yb	<2	4	<2	<2	2	<2	<2	<2
Lu	<0.2	0.4	0.3	0.2	0.4	0.3	<0.2	0.4
Hf	<1	3	<1	1	4	3	<1	3
Ta	2.1	1.1	3.4	1.3	0.9	1	1	1.5
W	840	179	1380	469	187	226	345	486
Ir	<50	<50	<50	<50	<50	<50	<50	<50
Au	4	6	7	<2	21	4	<2	45
Th	0.8	7.6	2.2	4.1	7.4	15	1.8	12
U	<0.2	2	0.4	1.2	2.3	3.8	0.7	3.6

87-124 S<sub>4</sub>-parallel vein in foliated black siltstone with 90% grey quartz.

86-187/4 S<sub>4</sub>-parallel vein in limonite-stained black siltstone with 35% white quartz and sulphide traces.

16-6-1 Rotated echelon vein in grey siltstone with 90% grey quartz.

19-6-5 Rotated echelon vein in black-grey siltstone with 85% white quartz.

87-18 East Limb (Type 4) vein in black siltstone with 30% white-grey quartz and minor carbonate.

18-6-6 East limb (Type 4) vein in black siltstone with 40-60% grey quartz.

87-13 East Limb (Type 4) vein in black siltstone with 90% white-grey quartz and minor carbonate plus sulphides.

87-27 Extensional vein perpendicular to S<sub>3</sub>E<sub>s</sub> cleavage on re-fold's east limb with 10% quartz and minor pyrite.

**Table A9.22 TYPE III AND IV QUARTZ-BRECCIA SAMPLES FROM LYNX INLET AND SOUTH GORDON LAKE: Trace element and gold (N.A.) data. All analyses in ppm except Na (wt.%), Fe (wt.%), Ir (ppb), and Au (ppb).**

	86-168	W05-124.0	86-169	24-6-6	17-6-5
Na	4.73	2.87	1.9	1.3	0.6
Sc	16	17	13	20	21.9
Cr	76	160	79	450	38
Fe	3.6	5.1	3	5.6	6.8
Co	59	97	170	160	68
Ni	70	73	49	200	82
Zn	<100	240	110	130	180
As	3430	2880	1450	64.5	11
Se	<5	<5	<5	<5	<5
Br	12	8.3	7.5	2	7.4
Rb	25	130	55	61	230
Zr	<200	<200	<200	350	<200
Mo	3	2	4	2	1
Ag	<2	<2	<2	<2	<2
Cd	<5	<5	<5	<5	<5
Sn	<100	<210	<100	<100	<100
Sb	2	1.5	0.8	0.4	0.3
Te	<30	<35	<26	<10	<10
Cs	0.6	7.8	3	3.3	32
Ba	390	580	320	1000	380
La	23	39	11	19	4
Ce	46	68	19	32	6
Sm	3	5.1	1.8	3.8	0.58
Eu	<1	<1	<1	1	<1
Tb	<0.5	0.8	0.6	0.9	<0.5
Yb	<2	<2	<2	<2	<2
Lu	<0.2	0.5	<0.2	0.3	<0.2
Hf	<1	2	<1	3	<1
Ta	<0.5	1.5	2.9	2.3	1.3
W	240	507	1140	793	392
Ir	<50	<50	<50	<50	<50
Au	542	330	9	<4	<2
Th	5.5	12	3	8.6	0.3
U	1.4	3.2	<0.2	2.9	<0.2

- 86-168 Type IV quartz-breccia from Woofarine zone with 60% white feldspar and quartz, 40% altered graywacke, and minor sulphides.
- W05-124 Type IV quartz-breccia from Lynx area with 25% grey quartz, calcic/mica altered graywacke fragments, and 1-3% disseminated arsenopyrite.
- 86-169 Type IV quartz-breccia from T-11 zone with 60% grey quartz, 30% white feldspar, 8% graywacke fragments, and 2% biotite/sulphides.
- 24-6-6 Type III quartz-breccia from middle of Gordon Lake with 90% grey quartz in grey siltstone.
- 17-6-5 Type III quartz-breccia from south shore of Gordon Lake with 90% grey quartz, 7% white feldspar, and 3% biotite.

**Table A9.23** TYPE III QUARTZ-BRECCIA SAMPLES FROM KIDNEY POND ZONE 1: Trace element and gold (N.A.) data. All analyses in ppm except Na (wt.%), Fe (wt.%), Ir (ppb), and Au (ppb).

	86-59A	86-59B	86-63	86-71	86-76	86-77	DE44-28.5	D48-110	H23-25.0	17-636.0
Na	2.64	3.35	3.49	2.34	1.8	1.5	0.47	4.58	3.77	2.22
Sc	4.6	10	16	14	20.6	3.6	8.7	2.4	9.4	6.2
Cr	<20	66	190	110	130	<20	87	<54	<43	46
Fe	1.6	3.4	3.2	3.8	6.2	1	1.9	1	2	2
Co	110	49	86	83	65	310	140	140	71	220
Ni	15	46	72	82	95	14	30	<10	34	12
Zn	<100	220	150	140	<100	<100	120	240	120	<100
As	1200	3940	3700	1700	9000	383	182	4400	2060	45
Se	<5	<5	<5	<5	<5	<5	<5	<5	<5	<5
Br	15	18	17	14	15	12	3.6	19	11	12
Rb	23	66	95	76	110	23	150	31	110	26
Zr	<200	<200	540	480	<200	<200	<200	<200	<200	<200
Mo	3	5	<2	3	4	4	5	<2	3	6
Ag	<2	<2	<2	<2	<2	<2	<2	<4	4	<2
Cd	<5	<5	10	<5	<14	<5	<5	<5	<5	<5
Sn	<100	<100	<220	<100	<100	<100	<100	<290	<230	<100
Sb	0.4	1.4	1.1	0.7	4.7	0.3	0.3	1.4	0.8	0.1
Te	<22	<34	<37	<28	<24	<10	<10	<48	<37	<10
Cs	2.1	2.8	5.7	2.1	4.7	1.9	1.5	4	5.4	0.7
Ba	100	230	180	500	240	110	420	170	630	60
La	7	18	25	33	31	4	18	4	11	8
Ce	14	31	49	58	56	<5	34	<18	<18	21
Sm	1.5	1.9	4.2	5.4	5.6	0.92	2.8	0.72	2	1.3
Eu	<1	1	<1	2	2	<1	1	<1	2	<1
Tb	<0.5	<0.5	0.8	0.8	0.6	0.7	0.8	0.6	<0.5	0.9
Yb	<2	<2	<2	<2	<2	<2	<2	<2	<2	<2
Lu	<0.2	0.4	0.4	<0.2	0.5	<0.2	0.2	<0.2	<0.2	0.2
Hf	<1	<1	<1	2	3	<1	<1	<1	<1	<1
Ta	1.8	<0.5	1.6	1.4	<0.5	3.3	2.6	1.6	1	3.9
W	782	266	409	498	232	1460	998	834	439	1560
Ir	<50	<50	<50	<50	<50	<50	<50	<50	<50	<50
Au	27	87	222	100	267	7	22	190	16900	8
Th	1.4	3.5	7	6.1	8.2	0.4	2.7	<0.7	1.1	1.2
U	<0.2	0.5	1.7	1.8	1.5	<0.2	1	<0.5	<0.6	<0.2

- 86-59A 40% white feldspar, 20% grey quartz, 30% black siltstone fragments, and <1% arsenopyrite/pyrrhotite.
- 86-59B 50% white feldspar, 25% grey quartz, 25% black siltstone fragments, and <1% pyrite/arsenopyrite.
- 86-63 50% white feldspar, 15% grey quartz, 33% black siltstone, and 1-3% arsenopyrite/pyrite.
- 86-71 Two quartz veins in black siltstone, 50% grey quartz and <1% pyrrhotite/arsenopyrite.
- 86-76 2% white feldspar, 60% grey quartz, 35% black siltstone fragments, and 3% pyrite/arsenopyrite/pyrrhotite.
- 86-77 15% white feldspar, 70% grey quartz, 15% black siltstone fragments, and <1% pyrrhotite/arsenopyrite.
- DE44-28.5 70% white quartz, 25% green (chloritized?) altered black siltstone fragments, and pink adularia veins.
- D48-110.0 80% white quartz, 10% gray quartz, 10% black siltstone fragments, and minor sulphides.
- H23-25.0 90% white feldspar, 7-8% grey quartz/black siltstone fragments, and 2-3% biotite.
- 17-636.0 50% white feldspar, 50% grey quartz/black siltstone fragments.

**Table A9.24 MAFIC DYKE, CAMERON RIVER VOLCANIC, AND SPUD LAKE GRANITIC ROCKS: Trace element and gold (N.A.) data. All analyses in ppm except Na (wt.%), Fe (wt.%), Ir (ppb), and Au (ppb).**

	86UG-8	12-6-2	12-6-3	12-6-7	22-6-8	22-6-11
Na	2	1.2	1.4	2.25	2.77	2.28
Sc	40.8	46.5	60.6	5	2	1.8
Cr	100	190	290	20	<20	<20
Fe	12	10	11	1.7	0.8	0.7
Co	99	130	160	110	130	130
Ni	140	130	150	15	<10	<10
Zn	170	490	410	150	<100	<100
As	9.2	19	14	6.7	<0.5	<0.5
Se	<5	<5	<5	<5	<5	<5
Br	3.2	3	<2	<2	<2	2.2
Rb	120	19	<5	120	280	290
Zr	<200	<200	<200	<200	<200	<200
Mo	<1	2	1	2	2	2
Ag	<2	<2	<2	<2	<2	<2
Cd	<5	<5	<5	<5	<5	<5
Sn	<100	<100	<100	<100	<100	<100
Sb	0.1	0.8	0.2	0.2	<0.1	<0.1
Te	<10	<10	<10	<10	<10	<10
Cs	7.7	1.5	0.6	3.2	24	23
Ba	510	240	83	600	360	400
La	21	6	7	31	14	14
Ce	39	10	16	56	30	32
Sm	4.8	3.4	3.9	3.6	3.3	3.9
Eu	2	<1	2	<1	<1	<1
Tb	1	1	1.3	1.1	0.9	1.1
Yb	4	3	4	2	<2	<2
Lu	0.5	0.6	0.7	0.2	<0.2	<0.2
Hf	2	2	2	3	1	<1
Ta	0.8	1.1	1.1	3.1	4.3	4.7
W	87	371	282	681	956	1030
Ir	<50	<50	<50	<50	<50	<50
Au	<2	<2	<2	<2	<2	<5
Th	2.6	0.8	0.5	23.6	8.7	8
U	0.3	0.4	<0.2	12	12	5.3

- UG87-4 Mafic dyke material from within quartz-breccia at Kidney Pond Zone 1.  
 12-6-2 Dark-green fine-grained mafic volcanic rock from Cameron River Volcanic Belt at Fenton Lake.  
 12-6-3 Light-grey limonite-stained felsic volcanic from Cameron River Volcanic Belt at Fenton Lake.  
 12-6-7 Quartz-feldspar porphyry volcanic rock from Cameron River Volcanic Belt at Fenton Lake.  
 22-6-8 White muscovite-rich granite from Spud Lake Pluton.  
 22-6-11 Pink muscovite-rich granite from Spud Lake Pluton.

Table A9.25 PRECISION ANALYSIS: major/trace element (X.R.F.) data and volatile data. (Major element and volatile data in wt.%, while trace element data in ppm).

	81-81	9-6-2	% Dev.	81-82	86-187/4	% Dev.
SiO <sub>2</sub>	58.67	58.53	0.24	51.20	51.16	0.08
Al <sub>2</sub> O <sub>3</sub>	19.54	19.30	1.24	20.50	20.24	1.28
Fe <sub>2</sub> O <sub>3</sub>	7.45	6.57	13.39	10.31	10.43	1.15
MgO	3.37	3.26	3.37	5.02	5.07	0.99
CaO	0.72	0.68	5.88	0.48	0.52	7.69
Na <sub>2</sub> O	1.76	1.86	5.38	2.38	2.62	9.16
K <sub>2</sub> O	3.99	3.99	0.00	3.19	3.22	0.93
TiO <sub>2</sub>	0.81	0.80	1.25	0.79	0.80	1.25
MnO	0.07	0.07	0.00	0.09	0.09	0.00
P <sub>2</sub> O <sub>5</sub>	0.23	0.15	53.33	0.17	0.17	0.00
L.O.I.	4.00	4.10	2.44	6.90	6.70	2.99
TOTAL	100.61	99.31	1.31	101.03	101.02	0.01
Ba	806	822	1.95	555	544	2.02
Rb	106	105	0.95	96	91	5.49
Sr	181	183	1.09	199	197	1.02
Y	19	17	11.76	22	24	8.33
Zr	140	135	3.70	122	119	2.52
Nb	7	5	40.00	7	7	0.00
Pb	<10	12	16.67	<10	<10	0.00
Ga	26	25	4.00	31	25	24.00
Zn	84	84	0.00	105	106	0.94
Cu	13	34	61.76	27	26	3.85
Ni	21	24	12.50	49	46	6.52
TiO <sub>2</sub>	0.85	0.85	0.00	0.91	0.91	0.00
V	187	194	3.61	239	238	0.42
Cr	256	244	4.92	265	270	1.85
C%	-	-	-	-	-	-
CO <sub>2</sub> %	-	-	-	-	-	-
S%	-	-	-	-	-	-

81-81 duplicate of 9-6-2, interbedded black and dark grey siltstones.

81-82 duplicate of 86-187/4, S<sub>4</sub>-parallel vein in limonite-stained black siltstone.

% Dev. - positive percentage deviation between duplicate and original, expressed as  $((V' - V)/V) \times 100$ , where V' = duplicate analysis and V = original analysis.

Table A9.26 PRECISION ANALYSIS: major/trace element (X.R.F.) data and volatile data. (Major element and volatile data in wt.%, while trace element data in ppm).

	81-83	87-84	% Dev.	81-84	27-6-3	% Dev.
SiO2	58.13	57.80	0.57	46.63	45.94	1.50
Al2O3	19.14	18.86	1.48	22.62	22.25	1.66
Fe2O3	8.05	8.22	2.07	8.85	9.49	6.74
MgO	3.93	3.93	0.00	4.08	3.89	4.88
CaO	0.44	0.43	2.33	4.27	4.15	2.89
Na2O	3.14	3.09	1.62	3.92	4.13	5.08
K2O	2.50	2.48	0.81	4.13	4.07	1.47
TiO2	0.78	0.78	0.00	0.92	0.93	1.08
MnO	0.07	0.07	0.00	0.11	0.11	0.00
P2O5	0.19	0.21	9.52	0.24	0.19	26.32
L.O.I.	3.50	3.60	2.78	3.30	3.30	0.00
TOTAL	99.87	99.47	0.40	99.07	98.45	0.63
Ba	635	653	2.76	903	883	2.27
Rb	80	84	4.76	159	160	0.63
Sr	248	243	2.06	637	645	1.24
Y	20	19	5.26	24	27	11.11
Zr	130	130	0.00	280	275	1.82
Nb	6	7	14.29	7	7	0.00
Pb	<10	<10	0.00	<10	12	20.00
Ga	26	25	4.00	33	29	13.79
Zn	106	106	0.00	91	87	4.60
Cu	16	20	20.00	37	65	43.08
Ni	84	82	2.44	88	92	4.35
TiO2	0.85	0.85	0.00	0.84	0.83	1.20
V	197	199	1.01	190	188	1.06
Cr	253	261	3.07	328	308	6.49
C%	0.24	0.23	4.35	0.2	0.21	4.76
CO2%	<2	<2	0.00	<2	<2	0.00
S%	0.102	0.09	13.33	1.75	1.64	5.49

81-83 duplicate of 87-84, grey siltstone from East limb.

81-84 duplicate of 27-6-3, Sulphide-rich black siltstone from adjacent to Kidney Pond Zone 1 with 3-5% coarse arsenopyrite.

% Dev. - positive percentage deviation between duplicate and original, expressed as  $((V' - V)/V) \times 100$ , where V' = duplicate analysis and V = original analysis.



Table A9.27 PRECISION ANALYSIS: major/trace element (X.R.F.) data and volatile data. (Major element and volatile data in wt.%, while trace element data in ppm).

	81-85	86-64	% Dev.	81-86	86-598	% Dev.
SiO2	56.05	55.43	1.12	64.18	64.37	0.30
Al2O3	17.42	17.18	1.40	15.64	15.54	0.64
Fe2O3	10.23	10.11	1.19	6.04	5.99	0.83
MgO	4.69	5.24	10.50	4.02	3.85	4.42
CaO	2.15	2.15	0.00	2.34	2.36	0.85
Na2O	3.80	4.15	8.43	3.33	3.42	2.63
K2O	1.45	1.42	2.11	1.42	1.41	0.71
TiO2	0.81	0.80	1.25	0.25	0.25	0.00
MnO	0.11	0.11	0.00	0.10	0.10	0.00
P2O5	0.22	0.23	4.35	0.16	0.15	6.67
L.O.I.	2.80	2.80	0.00	2.40	2.30	4.35
TOTAL	99.73	99.62	0.11	99.88	99.74	0.14
Ba	277	283	2.12	150	157	4.46
Rb	51	52	1.92	50	53	5.66
Sr	429	422	1.66	498	499	0.20
Y	19	18	5.56	11	9	22.22
Zr	146	148	1.35	47	50	6.00
Nb	5	6	16.67	<5	<5	0.00
Pb	113	109	3.67	<10	<10	0.00
Ga	24	26	7.69	18	19	5.26
Zn	191	187	2.14	103	103	0.00
Cu	118	120	1.67	<5	<5	0.00
Ni	95	99	4.04	22	24	8.33
TiO2	0.89	0.88	1.14	0.30	0.30	0.00
V	223	219	1.83	85	93	8.60
Cr	278	271	2.58	111	107	3.74
C%	-	-	-	-	-	-
CO2%	-	-	-	-	-	-
S%	-	-	-	-	-	-

81-85 duplicate of 86-64, interbeds of black and dark grey siltstone.

81-86 duplicate of 86-598, Zone 1 breccia, with 50% white feldspar, 25% grey quartz, 25% black siltstone fragments, and <1% pyrite/arsenopyrite.

% Dev. - positive percentage deviation between duplicate and original, expressed as  $((V' - V)/V) \times 100$ , where V' = duplicate analysis and V = original analysis.

**Table A9.28 PRECISION ANALYSIS OF STANDARDS** (from Abbey, 1983): major/trace element (X.R.F.) data and volatile data. (Major element and volatile data in wt.%, while trace element data in ppm).

	89-83	89-41	% Dev.	89-84	89-42	% Dev.
SiO2	71.12	71.38	0.36	51.54	51.74	0.39
Al2O3	14.33	14.34	0.07	13.91	14.17	1.83
Fe2O3	2.05	2.04	0.49	8.87	8.88	0.11
MgO	1.23	1.16	6.03	7.73	7.86	1.65
CaO	2.05	2.04	0.49	9.44	9.54	1.05
Na2O	3.58	3.82	6.28	3.07	2.77	10.83
K2O	3.89	3.89	0.00	1.37	1.40	2.14
TiO2	0.24	0.24	0.00	1.24	1.26	1.59
MnO	0.07	0.07	0.00	0.14	0.14	0.00
P2O5	0.14	0.15	6.67	0.31	0.30	3.33
L.O.I.	0.80	0.70	14.29	1.70	1.40	21.43
TOTAL	99.50	99.83	0.33	99.32	99.46	0.14
Ba	429	426	0.70	534	548	2.55
Rb	179	180	0.56	30	34	11.76
Sr	181	178	1.69	448	451	0.67
Y	33	32	3.13	24	22	9.09
Zr	108	117	7.69	154	155	0.65
Nb	11	10	10.00	29	29	0.00
Pb	<10	<10	0.00	<10	<10	0.00
Ga	18	17	5.88	20	18	11.11
Zn	40	41	2.44	85	86	1.16
Cu	<5	<5	0.00	37	39	5.13
Ni	10	10	0.00	136	140	2.86
TiO2	0.25	0.26	3.85	1.28	1.29	0.78
V	17	19	10.53	191	202	5.45
Cr	23	19	21.05	381	380	0.26
C%	-	-	-	-	-	-
CO2%	-	-	-	-	-	-
S%	-	-	-	-	-	-

89-83 duplicate 89-41, JB-1, Volcanic rock, G.S.C. standard.

89-84 duplicate of 89-42, JG-1, Granitic rock, G.S.C. standard.

% Dev - positive percentage deviation between duplicate and original, expressed as  $((V' - V)/V) \times 100$ , where  $V'$  = duplicate analysis and  $V$  = original analysis.

Table A9.29 PRECISION ANALYSIS: major/trace element (X.R.F.) data and volatile data. (Major element and volatile data in wt.%, while trace element data in ppm).

	81-87	86-169	% Dev.
SI02	76.13	75.99	0.18
AL2O3	9.76	9.69	0.72
FE2O3	4.19	4.17	0.48
MGO	3.05	2.97	2.69
CAO	1.45	1.44	0.69
NA2O	2.56	2.38	7.56
K2O	1.24	1.26	1.59
TIO2	0.28	0.29	3.45
MNO	0.07	0.07	0.00
P2O5	0.06	0.07	14.29
L.O.I.	1.00	0.90	11.11
TOTAL	99.79	99.23	0.56
Ba	221	224	1.34
Rb	42	39	7.69
Sr	281	285	1.40
Y	9	10	10.00
Zr	47	51	7.84
Nb	<5	<5	0.00
Pb	<10	<10	0.00
Ga	12	12	0.00
Zn	35	33	6.06
Cu	<5	<5	0.00
Ni	28	27	3.70
TIO2	0.32	0.30	6.67
V	75	76	1.32
Cr	78	80	2.50
C%	-	-	-
CO2%	-	-	-
S%	-	-	-

81-87 duplicate of 86-169, T-11 breccia with 20% white feldspar, 60% grey quartz, 8% graywacke fragments, and 2-3% biotite/sulphides.

% Dev. - positive percentage deviation between duplicate and original, expressed as  $((V' - V)/V) \times 100$ , where  $V'$  = duplicate analysis and  $V$  = original analysis.

Table A9.30 PRECISION ANALYSIS: trace element and gold (N.A.) data. All analyses in ppm except Na (wt.%), Fe (wt.%), Ir (ppb), and Au (ppb).

	Reported Detection Limit	81-81			81-82 86-187/4		
		81-81	9-6-2	% Dev.	81-82	86-187/4	% Dev.
Na	0.02 %	1.4	1.2	16.67	2	2	0.00
Sc	0.2 ppm	24.8	22.2	11.71	27.8	28	0.71
Cr	20 ppm	230	200	15.00	210	220	4.55
Fe	0.2 %	5.4	5	8.00	7.3	7.5	2.67
Co	5 ppm	39	36	8.33	48	52	7.69
Ni	10 ppm	24	21	14.29	48	47	2.13
Zn	100 ppm	180	180	0.00	220	150	46.67
As	0.5 ppm	19	18	5.56	105	108	2.78
Se	5 ppm	<5	<5	0.00	<5	<5	0.00
Br	0.5 ppm	<2	<2	0.00	<2	<2	0.00
Rb	5 ppm	110	120	8.33	110	110	0.00
Zr	200 ppm	<200	<200	0.00	310	<200	55.00
Mo	1 ppm	3	3	0.00	3	2	50.00
Ag	2 ppm	<2	<2	0.00	<2	<2	0.00
Cd	5 ppm	<5	<5	0.00	<5	<5	0.00
Sn	100 ppm	<100	<100	0.00	<100	<100	0.00
Sb	0.1 ppm	0.2	0.2	0.00	0.2	0.2	0.00
Te	10 ppm	<10	11	9.09	<10	<10	0.00
Cs	0.5 ppm	5	4.4	13.64	2.9	2.7	7.41
Ba	50 ppm	880	880	0.00	520	590	11.86
La	2 ppm	26	24	8.33	17	17	0.00
Ce	5 ppm	45	40	12.50	36	38	5.26
Sm	0.1 ppm	2.7	2.6	3.85	2.9	3.1	6.45
Eu	1 ppm	<1	1	0.00	<1	<1	0.00
Tb	0.5 ppm	0.5	0.5	0.00	0.7	0.7	0.00
Yb	2 ppm	<2	2	0.00	2	4	50.00
Lu	0.2 ppm	0.3	<0.2	50.00	0.4	0.4	0.00
Hf	1 ppm	3	3	0.00	3	3	0.00
Ta	0.5 ppm	1	1	0.00	1.1	1.1	0.00
W	1 ppm	175	167	4.79	179	179	0.00
Ir	50 ppb	<50	<50	0.00	<50	<50	0.00
Au	2 ppb	4	5	20.00	2	6	66.67
Th	0.2 ppm	7.9	8.1	2.47	7.3	7.6	3.95
U	0.2 ppm	2.6	2.4	8.33	2.1	2	5.00

81-81 duplicate of 9-6-2, interbedded black and dark grey siltstones.

81-82 duplicate of 86-187/4, S4-parallel vein in limonite-stained black siltstone.

% Dev.- positive percentage deviation between duplicate and original, expressed as  $((V' - V)/V) \times 100$ , where  $V'$  = duplicate analysis and  $V$  = original analysis.

Table A9.31 PRECISION ANALYSIS: trace element and gold (N.A.) data. All analyses in ppm except Na (wt.%), Fe (wt.%), Ir (ppb), and Au (ppb).

	Reported Detection Limit	81-83	87-84	% Dev.	81-84	27-6-3	% Dev.
Na	0.02 %	2.65	2.67	0.75	3.07	3.38	9.17
Sc	0.2 ppm	25.8	25.9	0.39	24.6	26.7	7.87
Cr	20 ppm	220	230	4.35	300	310	3.23
Fe	0.2 %	6	6.2	3.23	7.2	7.2	0.00
Co	5 ppm	51	56	8.93	74	77	3.90
Ni	10 ppm	99	100	1.00	120	120	0.00
Zn	100 ppm	180	220	18.18	160	170	5.88
As	0.5 ppm	17	18	5.56	>9000	>9000	0.00
Se	5 ppm	<5	<5	0.00	<5	<5	0.00
Br	0.5 ppm	<2	<2	0.00	11	19	42.11
Rb	5 ppm	93	97	4.12	130	180	27.78
Zr	200 ppm	360	<200	80.00	320	<200	60.00
Mo	1 ppm	3	2	50.00	<4	4	0.00
Ag	2 ppm	<2	<2	0.00	<2	<2	0.00
Cd	5 ppm	<5	<5	0.00	<21	<17	23.53
Sn	100 ppm	<100	<100	0.00	<100	<100	0.00
Sb	0.1 ppm	1.7	2	15.00	12.8	12.5	2.40
Te	10 ppm	<10	<10	0.00	<33	<28	17.86
Cs	0.5 ppm	4.8	4.8	0.00	6.5	7.3	10.96
Ba	50 ppm	670	740	9.46	740	850	12.94
La	2 ppm	34	33	3.03	33	35	5.71
Ce	5 ppm	70	67	4.48	77	74	4.05
Sm	0.1 ppm	5.6	6.1	8.20	5.1	5.4	5.56
Eu	1 ppm	<1	1	0.00	1	2	50.00
Tb	0.5 ppm	0.9	0.8	12.50	0.8	0.9	11.11
Yb	2 ppm	2	2	0.00	<2	<2	0.00
Lu	0.2 ppm	0.4	0.4	0.00	0.4	0.6	33.33
Hf	1 ppm	3	3	0.00	6	6	0.00
Ta	0.5 ppm	0.9	0.8	12.50	<0.5	1	50.00
W	1 ppm	79	86	8.14	77	70	10.00
Ir	50 ppb	<50	<50	0.00	<50	<50	0.00
Au	2 ppb	4	6	33.33	190	170	11.76
Th	0.2 ppm	7.8	8.4	7.14	12	13	7.69
U	0.2 ppm	2.5	2.7	7.41	3.2	3.7	13.51

81-83 duplicate of 87-84, grey siltstone from East limb.

81-44 duplicate of 27-6-3, Sulphide-rich black siltstone from adjacent to Kidney Pond Zone 1 with 3-5% coarse arsenopyrite.

% Dev. - positive percentage deviation between duplicate and original, expressed as  $((V'-V)/V) \times 100$ , where  $V'$  = duplicate analysis and  $V$  = original analysis.

Table A9.32 PRECISION ANALYSIS: trace element and gold (N.A.) data. All analyses in ppm except Na (wt.%), Fe (wt.%), Ir (ppb), and Au (ppb).

	Reported Detection Limit	81-85			81-86		
		81-85	86-64	% Dev.	81-86	86-59B	% Dev.
Na	0.02 %	3.69	3.37	9.50	3.31	3.35	1.19
Sc	0.2 ppm	27.5	25.6	7.42	10	10	0.00
Cr	20 ppm	230	220	4.55	81	66	22.73
Fe	0.2 %	7.4	7	5.71	3.3	3.4	2.94
Co	5 ppm	63	58	8.62	47	49	4.08
Ni	10 ppm	100	120	16.67	21	46	54.35
Zn	100 ppm	240	270	11.11	220	220	0.00
As	0.5 ppm	125	118	5.93	3610	3940	8.38
Se	5 ppm	<5	<5	0.00	<5	<5	0.00
Br	0.5 ppm	<2	<2	0.00	16	18	11.11
Rb	5 ppm	64	56	14.29	64	66	3.03
Zr	200 ppm	<200	<200	0.00	<200	<200	0.00
Mo	1 ppm	3	3	0.00	3	5	40.00
Ag	2 ppm	<2	<2	0.00	<2	<2	0.00
Cd	5 ppm	<5	<5	0.00	<5	<5	0.00
Sn	100 ppm	<100	<100	0.00	<100	<100	0.00
Sb	0.1 ppm	0.2	0.2	0.00	1.3	1.4	7.14
Te	10 ppm	<10	<10	0.00	<32	<34	5.88
Cs	0.5 ppm	3.3	3.5	5.71	2.5	2.8	10.71
Ba	50 ppm	290	270	7.41	130	230	43.48
La	2 ppm	40	37	8.11	16	18	11.11
Ce	5 ppm	78	82	4.88	27	31	12.90
Sm	0.1 ppm	6.7	6.4	4.69	1.9	1.9	0.00
Eu	1 ppm	2	2	0.00	1	1	0.00
Tb	0.5 ppm	0.9	0.9	0.00	<0.5	<0.5	0.00
Yb	2 ppm	3	2	50.00	<2	<2	0.00
Lu	0.2 ppm	0.4	0.4	0.00	0.3	0.4	25.00
Hf	1 ppm	4	3	33.33	<1	1	0.00
Ta	0.5 ppm	0.8	0.8	0.00	<0.5	<0.5	0.00
W	1 ppm	99	98	1.02	262	266	1.50
Ir	50 ppb	<50	<50	0.00	<50	<50	0.00
Au	2 ppb	92	85	8.24	63	87	27.59
Th	0.2 ppm	9.2	8.7	5.75	3.1	3.5	11.43
U	0.2 ppm	2.6	2.7	3.70	<0.2	0.5	60.00

81-85 duplicate of 86-64, interbeds of black and dark grey siltstone.

81-86 duplicate of 86-59B, Zone 1 breccia, with 50% white feldspar,  
25% grey quartz, 25% black siltstone fragments, and <1% pyrite/arsenopyrite.

% Dev. - positive percentage deviation between duplicate and original,  
expressed as  $((V' - V)/V) \times 100$ , where  $V'$  = duplicate analysis  
and  $V$  = original analysis.

Table A9.33 PRECISION ANALYSIS OF STANDARDS (from Abbey, 1983): trace element and gold (N.A.) data. All analyses in ppm except Na (wt.%), Fe (wt.%), Ir (ppb), and Au (ppb).

	Reported Detection Limit	89-83	89-41	% Dev.	89-84	89-42	% Dev.
Na	0.02 %	2.57	2.74	6.61	2.04	2.2	7.84
Sc	0.2 ppm	6.9	6.9	0.00	29.9	32.4	8.36
Cr	20 ppm	25	22	12.00	430	460	6.98
Fe	0.2 %	1.4	1.5	7.14	6.6	6.9	4.55
Co	5 ppm	7	7	0.00	54	53	1.85
Ni	10 ppm	<10	<10	0.00	140	150	7.14
Zn	100 ppm	120	170	41.67	150	<100	33.33
As	0.5 ppm	<0.5	0.8	60.00	1.9	1.4	26.32
Se	5 ppm	<5	<5	0.00	<5	<5	0.00
Br	0.5 ppm	<2	<2	0.00	<2	<2	0.00
Rb	5 ppm	200	200	0.00	35	40	14.29
Zr	200 ppm	<200	260	30.00	250	<200	20.00
Mo	1 ppm	<1	<1	0.00	2	1	50.00
Ag	2 ppm	<2	<2	0.00	<2	<2	0.00
Cd	5 ppm	<5	<5	0.00	<5	<5	0.00
Sn	100 ppm	<100	<100	0.00	<100	<100	0.00
Sb	0.1 ppm	0.1	0.2	100.00	0.3	0.2	33.33
Te	10 ppm	<10	<10	0.00	<10	<10	0.00
Cs	0.5 ppm	11	11	0.00	1.2	0.7	41.67
Ba	50 ppm	480	520	8.33	580	490	15.52
La	2 ppm	26	27	3.85	44	46	4.55
Ce	5 ppm	53	54	1.89	72	73	1.39
Sm	0.1 ppm	4.7	4.8	2.13	5.6	5.7	1.79
Eu	1 ppm	<1	<1	0.00	2	1	50.00
Tb	0.5 ppm	0.9	1.1	22.22	1	0.8	20.00
Yb	2 ppm	4	3	25.00	<2	3	50.00
Lu	0.2 ppm	0.6	0.6	0.00	0.4	0.4	0.00
Hf	1 ppm	3	3	0.00	3	3	0.00
Ta	0.5 ppm	2.1	1.9	9.52	2	1.9	5.00
W	1 ppm	14	17	21.43	<2	2	0.00
Ir	50 ppb	<50	<50	0.00	<50	<50	0.00
Au	2 ppb	<2	<2	0.00	5	<2	60.00
Th	0.2 ppm	14	14	0.00	10	10	0.00
U	0.2 ppm	5.8	5.8	0.00	1.9	2	5.26

89-83 duplicate 89-41, JB-1, Volcanic rock, G.S.C. standard.

89-84 duplicate of 89-42, JG-1, Granitic rock, G.S.C. standard.

% Dev - positive percentage deviation between duplicate and original, expressed as  $((V' - V)/V) \times 100$ , where  $V'$  = duplicate analysis and  $V$  = original analysis.

Table A9.34 PRECISION ANALYSIS: trace element and gold (N.A.) data. All analyses in ppm except Na (wt.%), Fe (wt.%), Ir (ppb), and Au (ppb).

	Reported Detection Limit	81-87	86-169	% Dev.
Na	0.02 %	1.8	1.9	5.26
Sc	0.2 ppm	12	13	7.69
Cr	20 ppm	58	79	26.58
Fe	0.2 %	3	3	0.00
Co	5 ppm	170	170	0.00
Ni	10 ppm	34	49	30.61
Zn	100 ppm	<100	110	9.09
As	0.5 ppm	1340	1450	7.59
Se	5 ppm	<5	5	0.00
Br	0.5 ppm	4.9	7.5	34.67
Rb	5 ppm	42	55	23.64
Zr	200 ppm	<200	<200	0.00
Mo	1 ppm	4	4	0.00
Ag	2 ppm	<2	<2	0.00
Cd	5 ppm	<5	<5	0.00
Sn	100 ppm	<100	<100	0.00
Sb	0.1 ppm	0.6	0.8	25.00
Te	10 ppm	<24	<26	7.69
Cs	0.5 ppm	2.7	3	10.00
Ba	50 ppm	220	320	31.25
La	2 ppm	10	11	9.09
Ce	5 ppm	<5	19	73.68
Sm	0.1 ppm	1.7	1.8	5.56
Eu	1 ppm	<1	<1	0.00
Tb	0.5 ppm	0.7	0.6	16.67
Yb	2 ppm	<2	<2	0.00
Lu	0.2 ppm	0.3	<0.2	50.00
Hf	1 ppm	<1	<1	0.00
Ta	0.5 ppm	2.7	2.9	6.90
W	1 ppm	1040	1140	8.77
Ir	50 ppb	<50	<50	0.00
Au	2 ppb	<6	9	33.33
Th	0.2 ppm	2.8	3	6.67
U	0.2 ppm	<0.2	<0.2	0.00

81-87 duplicate of 86-169, T-11 breccia with 20% white feldspar, 60% grey quartz, 8% graywacke fragments, and 2-3% biotite/sulphides.

% Dev.- positive percentage deviation between duplicate and original, expressed as  $((V'-V)/V) \times 100$ , where  $V'$  = duplicate analysis and  $V$  = original analysis.



Table A9.35 ACCURACY ANALYSIS (using standards of Abbey, 1983): major/trace element (X.R.F.) data and volatile data. (Major element and volatile data in wt.%, while trace element data in ppm).

	89-41	JG-1	% Dev.	89-42	JB-1	% Dev.
SiO2	71.38	72.36	1.37	51.74	52.60	1.66
AL2O3	14.34	14.20	0.98	14.17	14.62	3.18
FE2O3	2.04	0.37	81.86	8.88	2.36	73.42
MGO	1.16	0.76	34.48	7.86	7.76	1.27
CAO	2.04	2.17	6.37	9.54	9.35	1.99
NA2O	3.82	3.39	11.26	2.77	2.79	0.72
K2O	3.89	3.96	1.80	1.40	1.42	1.43
TiO2	0.24	0.27	12.50	1.26	1.34	6.35
MNO	0.07	0.06	14.29	0.14	0.15	7.14
P2O5	0.15	0.09	40.00	0.30	0.26	13.33
L.O.I.	0.70	0.82	17.14	1.40	1.62	15.71
TOTAL	99.83	99.31	100.00	99.46	101.02	0.01
Ba	426	460	7.98	548	490	10.58
Rb	180	185	2.78	34	41	20.59
Sr	178	185	3.93	451	440	2.44
Y	32	31	3.13	22	26	18.18
Zr	117	110	5.98	155	155	0.00
Nb	10	-	-	29	-	-
Pb	<10	26	160.00	<10	11.5	15.00
Ga	17	15	11.76	18	17	5.56
Zn	41	40	2.44	86	84	2.33
Cu	>5	4	20.00	39	56	43.59
Ni	10	8.2	18.00	140	135	3.57
TiO2	0.26	0.27	3.85	1.29	1.34	3.88
V	19	24	26.32	202	210	3.96
Cr	19	53	178.95	380	400	5.26
C%	-	-	-	-	-	-
CO2%	-	-	-	-	-	-
S%	-	-	-	-	-	-

89-41 analysis of G.S.C. standard JG-1.

89-42 analysis of G.S.C. standard JB-1.

% Dev. - positive percentage deviation between duplicate and original, expressed as  $((V'-V)/V) \times 100$ , where  $V'$  = duplicate analysis and  $V$  = original analysis.

Table A9.36 ACCURACY ANALYSIS (using standards of Abbey, 1983): trace element and gold (N.A.) data. All analyses in ppm except Na (wt.%), Fe (wt.%), Ir (ppb), and Au (ppb).

	89-41	JG-1	% DEV.	89-42	JB-1	% DEV.
Na	2.74	-	-	2.2	-	-
Sc	6.9	x	-	32.4	x	-
Cr	22	53	140.91	460	400	13.04
Fe	1.5	-	-	6.9	-	-
Co	7	6.4	8.33	53	39	26.42
Ni	<10	8.2	16.00	150	135	10.00
Zn	170	40	76.47	<100	84	16.00
As	0.8	0.3	62.50	1.4	2	42.86
Se	<5	x	-	<5	x	-
Br	<2	x	-	<2	x	-
Rb	<200	185	7.50	40	41	2.50
Zr	260	110	57.69	<200	155	22.50
Mo	1	2	100.00	1	20	1900.00
Ag	<2	0.05	97.50	<2	0.06	97.00
Cd	<5	x	-	<5	x	-
Sn	<100	4	96.00	<100	2	98.00
Sb	0.2	x	-	0.2	x	-
Te	<10	x	-	<10	x	-
Cs	11	10	9.09	0.7	1	42.86
Ba	520	460	11.54	490	490	0.00
La	27	22	18.52	46	36	21.74
Ce	54	43	20.37	73	67	8.22
Sm	4.8	4.6	4.17	5.7	4.8	15.79
Eu	1	0.7	30.00	1	1.5	50.00
Tb	1.1	x	-	0.8	x	-
Yb	3	1.5	50.00	3	2.1	30.00
Lu	0.6	x	-	0.4	0.3	25.00
Hf	3	x	-	3	x	-
Ta	1.9	x	-	1.9	x	-
W	17	x	-	<2	x	-
Ir	<50	x	-	<50	x	-
Au	<2	x	-	<2	x	-
Th	14	13.5	3.57	10	9	10.00
U	5.8	3.3	43.10	2	1.8	10.00

89-41 analysis of G.S.C. standard JG-1.

98-42 analysis of G.S.C. standard JB-1.

% Dev.- positive percentage deviation between duplicate and original, expressed as  $((V' - V)/V) \times 100$ , where  $V'$  = duplicate analysis and  $V$  = original analysis.

x - no data available

**Table A9.37 GOLD DATA FROM HEAVY AND LIGHT SEPARATES.**  
(Heavy and light separates analyzed by a combined fire assay/N.A. technique, while total by N.A. only.)

	Heavy Separates		Light Separates		Total	
	Weight (g)	Au (ppb)	Weight (g)	Au (ppb)	Weight (g)	Au (ppb)
86-59A	0.017	746	10	25	10	27
86-71	0.229	6310	10	161	10	100
86-76	2.985	2770	10	103	10	267
86-168	0.727	>10000	10	333	10	542
87-13	0.133	174	10	<1	10	<2
87-124	0.005	<2000	10	4	10	4
87-130	0.006	>10000	10	48	10	210
87-186	0.078	289	10	15	10	54
17/6/5	3.934	<2	10	1	10	<2
18/6/6	1.295	32	10	2	10	4

Estimated sulphide/gold content (%) of heavy separates from polished grain mounts

	Aspy	Pyr	Py	Cpy	Ga	Sph	Au
86-59A	70	-	30	-	-	-	-
86-71	20	20	60	-	-	-	-
86-76	65	5	45	Tr	-	Tr?	-
86-168	80	20	-	-	-	-	-
87-13	50	10?	40	-	-	-	-
87-124	40	-	60	-	-	-	-
87-130	70	-	30	-	-	-	-
87-186	80	10	10	-	-	-	-
17/6/5	-	-	-	-	-	-	-
18/6/6	5	5	90	-	-	-	-

- 86-59A Type III quartz-breccia from Kidney Pond Zone 1 with 40% white feldspar, black siltstone fragments and <1% arsenopyrite/pyrrhotite.
- 86-71 Two quartz veins in black siltstone with 50% grey quartz and 1% pyrite/arsenopyrite.
- 86-76 Type III quartz-breccia from Kidney Pond Zone 1 with 2% white feldspar, 60% grey, quartz, 35% black siltstone fragments, and 3% pyrite/arsenopyrite/pyrrhotite.
- 86-168 Type IV quartz-breccia from Woofrine zone with 60% white feldspar and quartz, 40% altered graywacke fragments, and minor sulphides.
- 87-13 East limb (Type 4) vein in black siltstone with 90% white-grey quartz and carbonate plus sulphides.
- 87-124 S4-parallel vein in well foliated black siltstone with 90% grey quartz.
- 87-130 Bedding-parallel vein in limonite-stained black siltstone with 60-80% white quartz.
- 87-186 S3s-parallel vein in black siltstone with 70-80% grey quartz and arsenopyrite traces.
- 17/6/5 Type III quartz-breccia from south shore of Gordon Lake with 90% grey quartz, 7% white feldspar, and 3% biotite.
- 18/6/6 East limb (Type 4) vein in black siltstone with 40-60% grey quartz.

Table A9.38 Mean and standard deviation of major/trace element (X.R.F.) data and volatile data for eight sulphide-rich black siltstones (adjacent to quartz-breccia zones) and six dark grey/black siltstones (distal to quartz-breccia zones). Sulphide-rich black siltstones include: H23-5.5, 17-665.5, 86-62, 86-69, C16-6.5, 27-6-3, BC11.11.5, and 27-6-5. Dark grey/black siltstones include: 86-78, 6-6-2, 21-6-2, 9-6-2, 6-6-3, and 7-6-3.

	Sulphide-rich black siltstones			Dark grey/black siltstones		
	Mean (ppm/%)	Standard Deviation	Log Mean (ppm)	Mean (ppm/%)	Standard Deviation	Log Mean (ppm)
SiO <sub>2</sub> %	46.263	2.696	5.665	56.887	1.595	5.755
Al <sub>2</sub> O <sub>3</sub> %	24.130	2.317	5.383	19.567	0.864	5.292
Fe <sub>2</sub> O <sub>3</sub> %	8.558	1.476	4.932	7.813	0.657	4.893
MgO %	3.525	1.018	4.547	3.832	0.274	4.583
CaO %	2.164	1.133	4.335	0.818	0.355	3.913
Na <sub>2</sub> O %	3.175	1.034	4.502	2.140	0.653	4.330
K <sub>2</sub> O %	5.276	1.424	4.722	3.722	0.316	4.571
TiO <sub>2</sub> %	1.015	0.126	4.006	0.818	0.019	3.913
MnO %	0.077	0.024	2.889	0.073	0.012	2.865
P <sub>2</sub> O <sub>5</sub> %	0.164	0.041	3.214	0.155	0.019	3.190
Ba ppm	1305.250	324.597	3.037	906.833	73.440	2.874
Rb ppm	174.250	32.931	2.176	106.333	12.815	1.972
Sr ppm	428.500	194.761	2.623	194.000	24.826	2.190
Y ppm	28.625	3.314	1.406	20.667	2.285	1.255
Zr ppm	210.000	30.846	2.273	133.167	6.619	2.041
Nb ppm	8.125	2.421	0.864	5.667	0.745	0.705
Pb ppm	14.625	10.062	1.168	11.000	1.155	0.955
Ga ppm	36.500	9.138	1.494	24.500	1.979	1.317
Zn ppm	70.000	23.076	1.826	94.833	8.415	1.895
Cu ppm	66.500	31.914	1.787	31.833	11.567	1.419
Ni ppm	105.500	26.926	1.990	53.000	17.243	1.610
V ppm	232.500	40.583	2.302	207.333	16.469	2.238
Cr ppm	304.125	34.603	2.425	256.333	15.670	2.335
C %	0.485	0.222	3.686	0.200	0.081	3.301
CO <sub>2</sub> %	0.200	0.000	3.301	0.200	0.000	3.301
S %	1.879	0.648	4.274	0.035	0.021	2.547

Table A9.39 Mean and standard deviation of gold and trace element (N.A.) data for eight sulphide-rich black siltstones (adjacent to quartz-breccia zones) and six dark grey/black siltstones (distal to quartz-breccia zones). Sulphide-rich black siltstones include: H23-5.5, 17-665.5, 86-62, 86-69, C16-6.5, 27-6-3, BC11.11.5, and 27-6-5. Dark grey/black siltstones include: 86-78, 6-6-2, 21-6-2, 9-6-2, 6-6-3, and 7-6-3

	Sulphide-rich black siltstones			Dark grey/black siltstones		
	Mean (ppm)	Standard Deviation	Log Mean	Mean (ppm)	Standard Deviation	Log Mean
Sc	30.250	4.933	1.481	26.950	2.658	1.431
Cr	293.750	45.260	2.468	233.333	18.856	2.368
Co	88.125	37.751	1.945	48.667	25.792	1.687
Ni	142.500	34.551	2.154	52.167	19.752	1.717
Zn	196.250	73.814	2.293	186.667	41.096	2.271
As	6330.750	3008.135	3.801	33.200	12.551	1.521
Se	5.000	0.000	0.699	5.000	0.000	0.699
Br	17.000	10.149	1.230	2.000	0.000	0.301
Rb	185.000	36.401	2.267	123.333	15.986	2.091
Zr	335.000	126.590	2.525	200.000	0.000	2.301
Mo	4.500	1.118	0.653	2.833	0.687	0.452
Ag	2.750	1.299	0.439	2.000	0.000	0.301
Cd	11.625	6.670	1.065	5.000	0.000	0.699
Sn	150.000	87.178	2.176	100.000	0.000	2.000
Sb	7.850	7.864	0.895	0.267	0.125	-0.574
Te	33.750	12.507	1.528	11.000	1.826	1.041
Cs	5.700	1.087	0.756	4.600	0.831	0.663
Ba	1306.250	359.198	3.116	976.667	98.770	2.990
La	46.625	12.599	1.669	20.833	4.180	1.319
Ce	89.250	27.142	1.951	44.000	7.703	1.643
Sm	7.312	1.345	0.864	3.950	0.718	0.597
Eu	2.250	0.661	0.352	1.333	0.471	0.125
Tb	0.863	0.260	-0.064	0.717	0.121	-0.145
Yb	2.375	0.484	0.376	2.333	0.471	0.368
Lu	0.587	0.169	-0.231	0.350	0.096	-0.456
Hf	3.375	1.654	0.528	3.167	0.373	0.501
Ta	0.725	0.198	-0.140	1.017	0.177	0.007
W	89.125	44.622	1.950	163.500	96.860	2.214
Ir	0.050	0.000	-1.301	0.050	0.000	-1.301
Au	1.221	1396.582	0.087	0.006	3.399	-2.247
Th	11.238	1.661	1.051	8.317	0.549	0.920
U	3.012	0.699	0.479	2.450	0.171	0.389

**Table A9.40** Compositions (in atomic %) of pyrrhoite, pyrite, chalcopyrite, and sphalerite from the Kidney Pond Zone 1 quartz-breccia. Analyzed by a Jeol Superprobe 733 microprobe system of Dalhousie University, Halifax, Nova Scotia. The system used an accelerating voltage of 15 kV, a beam current of 10 nano-amps, and a forty second count for each analysis.

	Fe	As	S	Cu	Zn	Ni	Co	Pb	Au	TOTAL	
CD20-21.5/4	25.25	0.00	50.07	24.68	0.00	0.00	0.00	0.00	0.00	96.40	cpy
CD20-21.5/14	24.84	0.00	50.14	25.02	0.00	0.00	0.00	0.00	0.00	97.85	cpy
CD20-21.5/15	46.01	0.00	53.99	0.00	0.00	0.00	0.00	0.00	0.00	96.74	pyr
86-189/22	45.73	0.00	54.27	0.00	0.00	0.00	0.00	0.00	0.00	97.42	pyr
86-189/26	6.11	0.00	50.66	0.00	43.23	0.00	0.00	0.00	0.00	100.48	sph
86-189/27	45.49	0.00	54.51	0.00	0.00	0.00	0.00	0.00	0.00	96.48	pyr
86-189/39	46.52	0.00	53.48	0.00	0.00	0.00	0.00	0.00	0.00	96.29	pyr
86-189/40	24.40	0.00	50.77	24.83	0.00	0.00	0.00	0.00	0.00	97.44	cpy
86-189/43	32.79	0.00	67.03	0.00	0.00	0.00	0.00	0.00	0.00	99.33	py
86-189/44	33.30	0.00	66.70	0.00	0.00	0.00	0.00	0.00	0.00	99.35	py
86-189/45	45.78	0.00	54.22	0.00	0.00	0.00	0.00	0.00	0.00	96.96	pyr
17-665.5/58	24.68	0.00	50.74	33.93	0.00	0.00	0.00	0.00	0.00	98.77	cpy
17-665.5/62	33.47	0.15	66.37	0.00	0.00	0.00	0.00	0.00	0.00	98.82	py
17-665.5/66	33.13	0.12	66.75	0.00	0.00	0.00	0.00	0.00	0.00	98.12	py
17-665.5/71	25.29	0.00	51.59	23.12	0.00	0.00	0.00	0.00	0.00	98.32	cpy
86-160/82	45.28	0.00	54.72	0.00	0.00	0.00	0.00	0.00	0.00	97.34	pyr

CD20-21.5 Quartz breccia with black siltstone fragments

(sulphides include py, pyr, aspy and cpy)

86-189 Quartz breccia with black siltstone fragments plus visible gold

(sulphides include aspy, cpy, py, pyr and sph)

17-665.5 Black siltstone with 15% white-grey quartz + minor py/aspy veinlets

(other sulphides include pyr and cpy)

86-160 Quartz breccia with dark grey graywacke fragments and disseminated aspy

(other sulphides include pyr and minor py)

Sulphide mineralogy: aspy - arsenopyrite; py - pyrite; pyr - pyrrhotite;  
cpy - chalcopyrite.

APPENDIX A10:  $^{40}\text{Ar}/^{39}\text{Ar}$  STEP HEATING DATA

BIOTITE AND HORNBLENDE COM-  
POSITIONAL DATA

### A10.1 INTRODUCTION TO $^{40}\text{Ar}/^{39}\text{Ar}$ DATING TECHNIQUES

The  $^{40}\text{Ar}/^{39}\text{Ar}$  dating technique, an adaptation of the K-Ar dating system, was developed by Merrihue and Turner (1966). This technique, described in detail by Fitch et al. (1969), Dallmeyer (1979), Faure (1986), and McDougall and Harrison (1988), is summarized below. In conventional K-Ar dating,  $^{40}\text{Ar}$  is measured by a mass spectrometer and  $^{40}\text{K}$  determined from direct chemical analysis of potassium. However, in  $^{40}\text{Ar}/^{39}\text{Ar}$  dating  $^{39}\text{Ar}$  is produced by irradiation and the resulting isotopic ratios of  $^{40}\text{Ar}$  and  $^{39}\text{Ar}$  are both measured by a mass spectrometer.  $^{40}\text{Ar}$  occurs in many minerals and is a direct result of the  $^{40}\text{K}$  decay system over time, whereby  $^{40}\text{K} \rightarrow ^{40}\text{Ca}$  (88%) +  $^{40}\text{Ar}$  (12% with a half-life of  $1.885 \times 10^9$  years), whereas  $^{39}\text{Ar}$  (with a shorter half-life of 265 years) is produced by the irradiation of  $^{39}\text{K}$  in a nuclear reactor.

The derivation of an age from the measured isotopes of  $^{39}\text{Ar}$  and  $^{40}\text{Ar}$  (Merrihue and Turner, 1966) is based on the decay system of  $^{40}\text{K}$  where:

$$^{40}\text{Ar} + ^{40}\text{Ca} = ^{40}\text{K} (e^{\lambda t} - 1) \quad (1)$$

(whereby  $\lambda$  is the decay constant of  $^{40}\text{K}$ ,  $^{40}\text{Ar}$  and  $^{40}\text{Ca}$  are the present day atomic abundances). Therefore, the amount of  $^{40}\text{Ar}$  naturally produced during a time  $t$  is:

$$^{40}\text{Ar} = \frac{\lambda_e}{\lambda} ^{40}\text{K} (e^{\lambda t} - 1) \quad (2)$$

(where  $\lambda_e$  = partial decay constant of the  $^{40}\text{Ar}$  branch from  $^{40}\text{K}$ ). The amount of  $^{39}\text{Ar}$  produced during nuclear irradiation is expressed by:

$$^{39}\text{Ar} = ^{39}\text{K} T \int \phi_\epsilon \sigma_\epsilon \delta\epsilon \quad (3)$$

(where  $T$  = irradiation time,  $\phi_\epsilon$  = neutron flux density at energy  $\epsilon$ , and  $\sigma_\epsilon$  = capture area for neutrons at energy  $\epsilon$ , all integrated over a range of available energies). By



comparing equations 2 and 3, a ratio for  $^{40}\text{Ar}/^{39}\text{Ar}$  is obtained:

$$\frac{^{40}\text{Ar}}{^{39}\text{Ar}} = \frac{\lambda e^{40\text{K}} (e^{\lambda t} - 1)}{\lambda^{39\text{K}} T \int \phi_{\epsilon} \sigma_{\epsilon} d\epsilon} \quad (4)$$

This equation is simplified by the introduction of a J factor:

$$J = \frac{\lambda e^{40\text{K}} T}{\lambda^{39\text{K}}} \int \phi_{\epsilon} \sigma_{\epsilon} d\epsilon \quad (5)$$

(where J, the flux monitor, is calculated from standard sample of known age which is irradiated simultaneously with unknown samples). Equation 5 is substituted into equation 4 and gives:

$$\frac{^{40}\text{Ar}}{^{39}\text{Ar}} = \frac{e^{\lambda t} - 1}{J} \quad (6)$$

$$\text{where } J = \frac{e^{\lambda t} - 1}{(^{40}\text{Ar}/^{39}\text{Ar})} \quad (7)$$

Equation 6 can be simplified and rearranged in terms of t:

$$t = \frac{1}{\lambda} \ln \left[ \frac{^{40}\text{Ar}}{^{39}\text{Ar}} J + 1 \right] \quad (8)$$

Rather than measuring the total outgassing of  $^{40}\text{Ar}$ , the  $^{40}\text{Ar}/^{39}\text{Ar}$  technique has the added advantage of measuring the ratio of  $^{40}\text{Ar}$  to  $^{39}\text{Ar}$  at progressive temperatures and calculating step ages. These step ages are then plotted against cumulative  $^{39}\text{Ar}$  released, producing an age spectrum. This spectrum provides information concerning the thermal history of the sample, in addition to its time of formation and final outgassing. The thermal history of a mineral is controlled by its ability to hold argon within its lattice at a certain temperatures; known as the blocking or closure temperature (Dodson, 1973). Typical blocking temperatures of hornblende, muscovite, and biotite are  $500 \pm 50^{\circ}\text{C}$ ,  $350 \pm 50^{\circ}\text{C}$ , and  $300 \pm 50^{\circ}\text{C}$ , respectively (Jäger, 1979)

The two fundamental types of errors that occur in  $^{40}\text{Ar}/^{39}\text{Ar}$  dating are related to the sample (grain size, quality, and purity) and the analytical equipment. The analytical errors include: i) uncertainty in the measurement of the  $^{39}\text{Ar}$  and  $^{40}\text{Ar}$  peak overlap (in the case of Archean ages the amount of  $^{40}\text{Ar}$  gas outgassed is at least one and possibly two orders of magnitude greater than the  $^{39}\text{Ar}$  outgassed); ii) the accuracy of the J-value; iii) the uncertainty in mass spectrometer discrimination; and iv) uncertainties due to the presence of interfering isotopes and atmospheric argon within system during sample measurement.

## 10.2 CALCULATION OF AVERAGE PLATEAU AGES AND ERRORS

An average plateau age (APA) is "that part of an age spectrum diagram composed of contiguous gas fractions that together represent more than 50% of the total  $^{39}\text{Ar}$  released from the sample and for which no difference in age can be detected between any two gas fractions at the 95% level of confidence" (Fleck et al. 1976). The 95% confidence level is evaluated by the Critical-Value Test of McIntyre (1963). This test states that the differences between all possible pairs of apparent ages must be less than the Critical-Value (C.V.) which is expressed as:

$$\text{C.V.} = 1.96 \left[ \frac{\sigma_1^2}{n_1} + \frac{\sigma_2^2}{n_2} \right]^{1/2} \quad (9)$$

(where  $\sigma_1$  and  $\sigma_2$  are the standard deviation of the apparent ages and  $n_1$  and  $n_2$  are the number of determinations of the parameter; which in this case is one). Once an acceptable plateau is obtained from a spectrum, the APA is calculated by weighing the  $^{40}\text{Ar}/^{39}\text{Ar}$  apparent step ages against the amount of  $^{39}\text{Ar}$  released as follows:

$$\text{APA} = \frac{[(^{39}\text{Ar}_1 \times \text{AA}_1) + (^{39}\text{Ar}_2 \times \text{AA}_2) + \dots + (^{39}\text{Ar}_i \times \text{AA}_i)]}{^{39}\text{Ar}_T} \quad (10)$$

(where  $^{39}\text{Ar}_1$  to  $^{39}\text{Ar}_i$  are the abundance of  $^{39}\text{Ar}$  out-gassed, in mV, from steps 1 to  $i$ ;  $\text{AA}_1$  to  $\text{AA}_i$  are the apparent step ages from 1 to  $i$ ; and  $^{39}\text{Ar}_T$  = total  $^{39}\text{Ar}$  outgassed from sample).

The error in the average plateau age is derived from a root mean square analysis incorporating the  $J$  value and errors limit on the apparent step age below (P. Reynolds, 1989, personal communication), and are expressed as:

$$|dt|^2 = \left| \frac{dt}{dJ} \right|^2 dJ^2 + \left| \frac{dt}{dR} \right|^2 dR^2 \quad (11)$$

$$\text{where } t = \frac{1}{\lambda} \log (1 + JR), \quad (12)$$

$$|dt^2| = \left| \frac{R}{(1+JR)} \right|^2 dJ^2 + \left| \frac{J}{(1+JR)} \right|^2 dR^2 \quad (13)$$

and  $R$  is the average  $^{40}\text{Ar}/^{39}\text{Ar}$  ratio for each step ( $R_1, R_2, R_3 \dots R_i$ ) and  $dR$  = error in each  $R$  ( $dR_1, dR_2, dR_3 \dots dR_i$ ). Therefore:

$$R = \frac{[(^{39}\text{Ar}_1 \times R_1) + (^{39}\text{Ar}_2 \times R_2) + \dots + (^{39}\text{Ar}_i \times R_i)]}{^{39}\text{Ar}_T} \quad (14)$$

and

$$|dR|^2 = \left| \frac{dR}{dR_1} \right|^2 dR_1^2 + \left| \frac{dR}{dR_2} \right|^2 dR_2^2 + \dots + \left| \frac{dR}{dR_i} \right|^2 dR_i^2 \quad (15)$$

Since  $J$ ,  $dJ$ , and are known, and  $R$  and  $dR$  are obtained from equations (14) and (15),  $dt$  can be calculated from equation (13).

**Table A10.1** Summary of step-heating data and calculation of average plateau age and error for hornblende (TS12-6-4) from the Cameron River Volcanic Belt.

Temperature step (C)	<sup>39</sup> Ar (mv)	<sup>39</sup> Ar (%)	Atm.Ar (%)	<sup>40</sup> Ar/ <sup>36</sup> Ar	<sup>39</sup> Ar/ <sup>36</sup> Ar	<sup>40</sup> Ar/ <sup>39</sup> Ar	dR	Step Age (Ma)
200-750	4.00	8.00	76.00	12.30	387.00	0.10	1.00	1467 +/- 94
750-800	3.00	5.00	67.00	8.40	441.00	0.30	1.00	1302 +/- 66
800-850	3.00	6.00	56.00	10.80	527.00	0.40	1.00	1567 +/- 56
850-900	4.00	8.00	53.00	10.10	562.00	0.50	1.00	1502 +/- 34
900-950	5.00	11.00	34.00	10.00	869.00	0.90	1.00	1646 +/- 34
950-925	2.00	5.00	30.00	11.50	991.00	0.90	1.00	1799 +/- 23
925-950	8.00	17.00	16.00	19.20	1894.00	1.60	1.00	2216 +/- 36
950-975	5.00	10.00	10.00	17.00	2849.00	2.20	1.00	2426 +/- 25
975-1000	3.00	7.00	20.00	22.80	1459.00	1.00	2.00	2368 +/- 30
1000-1050	2.00	4.00	27.00	21.90	1093.00	0.70	2.00	2402 +/- 47
1050-1100	5.00	11.00	12.00	22.70	2371.00	1.60	2.00	2571 +/- 57
1100-1140	4.00	9.00	22.00	24.50	1369.00	0.80	2.00	2620 +/- 48

Total Gas Age = 2092 Ma

J = 0.00245            No interfering isotope correction

Spectrum fails average plateau criteria of Fleck et al. (1976) and Critical-Value test. No plateau defined.

**Table A10.2** Summary of step-heating data and calculation of average plateau age and error for muscovite (TS22-6-8) from the Spud Lake granite.

Temperature step (C)	<sup>39</sup> Ar (mv)	<sup>39</sup> Ar (%)	Atm.Ar (%)	<sup>40</sup> Ar/ <sup>36</sup> Ar	<sup>39</sup> Ar/ <sup>36</sup> Ar	<sup>40</sup> Ar/ <sup>39</sup> Ar	dR	Step Age (Ma)
200-600	8.00	3.00	9.00	3449.00	3.10	1014.93	15.48	2253 +/- 19
600-650	<1.00	<1.00	44.00	669.00	0.60	573.81	48.03	1585 +/- 84
650-700	8.00	3.00	4.00	8208.00	6.40	1220.15	31.48	2496 +/- 34
700-750	14.00	5.00	3.00	9475.00	7.50	1208.71	27.20	2483 +/- 29
750-780	41.00	14.00	2.00	16606.00	12.50	1298.42	21.42	2581 +/- 22
780-810	105.00	34.00	2.00	16525.00	12.40	1301.73	19.92	2584 +/- 20
810-840	54.00	18.00	3.00	9665.00	7.40	1265.33	24.04	2545 +/- 24
840-870	22.00	7.00	4.00	7341.00	5.30	1315.29	7.00	2599 +/- 17
870-900	19.00	6.00	6.00	4847.00	3.80	1176.88	32.95	2447 +/- 36
900-950	14.00	5.00	6.00	4582.00	3.30	1251.82	23.53	2542 +/- 25
950-1000	11.00	4.00	12.00	2560.00	1.80	1206.40	29.03	2494 +/- 31
1000-1050	7.00	2.00	22.00	1331.00	0.80	1225.36	46.69	2502 +/- 50

Total Gas Age = 2546 Ma

J = 0.00245            No interfering isotope correction

Error estimates at one sigma standard deviation

(Using equations 7 to 13 from Section A10.2 and heating steps 750-780 to 840-870 inclusive)

Average plateau age = 2575 Ma

Average <sup>40</sup>Ar/<sup>39</sup>Ar (R) value= 1294

dR = 11.893            dJ = 0.000005

Plateau age error dt = +/- 12.91 Ma

**Table A10.3** Summary of step-heating data and calculation of average plateau age and error for quartz-breccia biotite (TS83-04) from the Kidney Pond Zone 1.

Temperature step (C)	<sup>39</sup> Ar (mv)	<sup>39</sup> Ar (%)	Atm.Ar (%)	<sup>40</sup> Ar/ <sup>36</sup> Ar	<sup>39</sup> Ar/ <sup>36</sup> Ar	<sup>40</sup> Ar/ <sup>39</sup> Ar	dR	Step Age (Ma)
200-500	3.00	<1.00	40.00	747.00	0.60	684.02	23.33	1773 +/- 37
500-550	6.00	1.00	10.00	2829.00	2.80	899.13	14.66	2098 +/- 19
550-600	32.00	7.00	3.00	11119.00	8.50	1272.06	34.35	2550 +/- 36
600-650	60.00	13.00	2.00	18835.00	14.70	1261.93	25.11	2540 +/- 26
650-700	88.00	19.00	23.00	10558.00	8.30	1234.46	23.21	2510 +/- 25
700-750	59.00	12.00	2.00	15902.00	11.90	1302.75	19.15	2584 +/- 20
750-800	20.00	4.00	2.00	11910.00	9.10	1268.89	22.33	2548 +/- 23
800-850	26.00	5.00	3.00	10981.00	8.30	1277.36	16.86	2557 +/- 18
850-900	29.00	6.00	3.00	11061.00	8.40	1276.84	18.64	2556 +/- 19
900-950	52.00	11.00	2.00	12494.00	9.30	1305.68	18.41	2587 +/- 19
950-1000	65.00	14.00	3.00	11815.00	8.90	1287.36	20.08	2568 +/- 21
1000-1050	30.00	6.00	4.00	8428.00	6.20	1304.19	20.08	2585 +/- 21

Total Gas Age = 2546 Ma

J = 0.00245                      No interfering isotope correction

Error estimates at one sigma standard deviation

(Using equations 7 to 13 from Section A10.2 and heating steps 700-750 to 1000-1050 inclusive)

Average plateau age = 2573 Ma

Average <sup>40</sup>Ar/<sup>39</sup>Ar (R) value= 1292

dR = 7.912                      dJ = 0.000005

Plateau age error dt = +/- 8.85 Ma

**Table A10.4** Summary of step-heating data and calculation of average plateau age and error for metamorphic biotite (TS86-94) from an uncrenulated siltstone bed of the Burwash Formation.

Temperature step (C)	<sup>39</sup> Ar (mv)	<sup>39</sup> Ar (%)	Atm.Ar (%)	<sup>40</sup> Ar/ <sup>36</sup> Ar	<sup>39</sup> Ar/ <sup>36</sup> Ar	<sup>40</sup> Ar/ <sup>39</sup> Ar	dR	Step Age (Ma)
200-500	14.00	2.00	3.00	9357.00	9.50	946.92	7.95	2162 +/- 11
500-550	24.00	4.00	1.00	22360.00	19.80	1113.60	6.57	2372 +/- 08
550-600	62.00	11.00	<1.00	54210.00	44.20	1220.60	6.47	2494 +/- 07
600-650	81.00	15.00	<1.00	94614.00	77.30	1221.77	8.70	2496 +/- 10
650-700	45.00	8.00	<1.00	107988.00	87.80	1227.90	6.26	2502 +/- 07
700-750	53.00	10.00	<1.00	78188.00	64.10	1215.10	7.78	2488 +/- 09
750-800	23.00	4.00	<1.00	40188.00	32.30	1233.69	5.80	2509 +/- 06
800-850	16.00	3.00	<1.00	34745.00	28.40	1214.49	6.07	2487 +/- 07
850-900	76.00	14.00	<1.00	41051.00	33.00	1236.23	6.43	2511 +/- 07
900-950	83.00	15.00	<1.00	34100.00	27.10	1246.91	7.48	2523 +/- 08
950-1000	41.00	7.00	1.00	27838.00	22.20	1237.30	8.78	2513 +/- 10
1000-1050	25.00	5.00	3.00	11042.00	8.70	1224.52	9.06	2498 +/- 10
1050-1140	12.00	2.00	6.00	4591.00	3.50	1222.61	11.74	2496 +/- 13

Total Gas Age = 2490 Ma

J = 0.00245

No interfering isotope correction

Spectrum fails average plateau criteria of Fleck et al. (1976) and Critical-Value test. No plateau defined.

**Table A10.5** Summary of step-heating data and calculation of average plateau age and error for metamorphic biotite (TS86-84) from an crenulated siltstone bed of the Burwash Formation.

Temperature step (C)	<sup>39</sup> Ar (mv)	<sup>39</sup> Ar (%)	Atm.Ar (%)	<sup>40</sup> Ar/ <sup>36</sup> Ar	<sup>39</sup> Ar/ <sup>36</sup> Ar	<sup>40</sup> Ar/ <sup>39</sup> Ar	dR	Step Age (Ma)
200-500	8.00	9.00	8.00	3485.00	3.70	860.00	4.90	2042 +/- 07
500-550	4.00	5.00	2.00	17059.00	17.90	932.90	6.81	2144 +/- 09
550-600	7.00	8.00	1.00	28340.00	26.10	1071.15	13.92	2323 +/- 17
600-650	14.00	15.00	<1.00	47001.00	42.00	1111.61	6.00	2369 +/- 07
650-700	18.00	19.00	<1.00	37546.00	32.50	1144.76	5.72	2408 +/- 07
700-750	9.00	10.00	<1.00	37317.00	32.00	1155.94	4.39	2421 +/- 05
750-800	11.00	12.00	2.00	16975.00	14.60	1138.49	9.34	2401 +/- 11
800-850	7.00	7.00	2.00	13390.00	11.40	1145.97	8.48	2409 +/- 10
850-900	7.00	7.00	3.00	8950.00	7.50	1163.03	10.70	2417 +/- 12
900-950	3.00	3.00	7.00	4280.00	3.40	1149.33	18.73	2413 +/- 22
950-1000	2.00	2.00	13.00	2269.00	1.70	1152.42	25.58	2416 +/- 30
1000-1050	2.00	2.00	29.00	1015.00	0.60	1139.92	46.51	2400 +/- 54
1050-1140	2.00	2.00	47.00	634.00	0.30	1089.77	44.68	2337 +/- 54

Total Gas Age = 2355 Ma

J = 0.00245      No interfering isotope correction

Error estimates at one sigma standard deviation

(Using equations 7 to 13 from Section A10.2 and heating steps 650-700 to 1050-1140 inclusive)

Average plateau age = 2408 Ma

Average <sup>40</sup>Ar/<sup>39</sup>Ar (R) value = 1146

dR = 3.842      dJ = 0.000005

Plateau age error dt = +/- 5.22 Ma



Table A10.6 Microprobe major oxide data for hornblende (12-6-4) from the Cameron River Volcanic Belt using a Joel Superprobe 733 microprobe system operated at Dalhousie University and conventional geological standards for calibration. The microprobe has an accelerating voltage of 15 kV with a beam current of 10 nano-amps and does a forty second count for each analysis.

	12-6-4/40	12-6-4/41	12-6-4/42	12-6-4/44	12-6-4/45	12-6-4/49	12-6-4/50	12-6-4/51
SiO2	51.40	51.41	49.75	47.82	47.47	45.24	45.83	46.23
TiO2	0.14	0.14	0.29	0.00	0.42	0.49	0.42	0.32
Al2O3	4.01	4.03	7.16	32.82	9.22	12.71	11.77	12.23
Cr2O3	0.03	0.03	0.05	0.03	0.00	0.04	0.07	0.20
FeO	20.36	20.36	16.35	2.61	20.07	20.47	19.63	20.29
MnO	0.40	0.40	0.41	0.01	0.40	0.53	0.57	0.58
MgO	9.89	9.88	11.12	0.98	8.24	6.30	6.90	6.28
CaO	11.63	11.63	11.96	13.19	11.54	11.89	11.58	11.83
Na2O	0.32	0.32	0.61	1.03	0.81	0.81	0.64	0.64
K2O	0.00	0.00	0.00	0.45	0.00	0.00	0.00	0.00
TOTAL	98.18	98.2	97.7	98.94	98.17	98.48	97.41	98.6

	12-6-4/52	12-6-4/56	12-6-4/57	12-4-6/58*12-4-6/59*
SiO2	47.57	44.31	44.18	45.29 45.47
TiO2	0.37	0.50	0.44	0.53 0.44
Al2O3	10.04	13.37	13.97	11.29 12.70
Cr2O3	0.09	0.06	0.09	0.02 0.09
FeO	21.22	19.79	19.74	21.73 19.24
MnO	0.50	0.53	0.53	0.41 0.53
MgO	7.00	6.74	6.00	6.35 6.73
CaO	11.32	11.77	11.61	11.70 11.60
Na2O	0.75	0.89	0.92	0.84 0.82
K2O	0.00	0.00	0.01	0.00 0.00
TOTAL	98.86	97.96	97.49	98.16 97.62

(Data taken from separate grains, except for \* where two analysis from one grain were taken)

Table A10.7 Microprobe major oxide data for quartz-breccia biotite (83-04) using the Joel Superprobe 733 microprobe system operated at Dalhousie University and conventional geological standards for calibration. The microprobe has an accelerating voltage of 15 kV with a beam current of 10 nano-amps and does a forty second count for each analysis.

	83-04/1	83-04/2	83-04/3	83-04/4	83-04/5	83-04/6	83-04/7	83-04/8
SI02	38.57	38.06	37.30	38.85	37.01	37.47	37.67	38.09
TI02	1.18	1.14	1.18	1.22	1.27	1.30	1.50	1.08
Al2O3	18.42	18.49	17.54	18.38	17.52	17.80	18.19	18.35
CR2O3	0.00	0.00	0.03	0.00	0.03	0.00	0.00	0.00
FE0	14.88	14.77	14.15	14.42	14.58	14.53	14.63	14.36
MNO	0.42	0.43	0.41	0.46	0.40	0.50	0.43	0.38
MGO	13.54	13.74	13.43	14.00	13.57	13.24	13.33	13.67
CAO	0.00	0.00	0.05	0.00	0.07	0.00	0.00	0.00
NA2O	0.07	0.02	0.07	0.04	0.13	0.00	0.02	0.03
K2O	9.66	9.18	8.98	8.46	9.26	9.68	9.71	9.15
CL	0.00	0.00	0.01	0.00	0.00	0.01	0.00	0.00
F	0.15	0.31	0.35	0.48	0.00	0.28	0.27	0.23
TOTAL	96.89	96.14	93.50	96.31	93.84	94.81	95.75	95.34
	83-04/9	83-04/10						
SI02	37.15	38.05						
TI02	1.42	1.22						
Al2O3	17.95	17.31						
CR2O3	0.00	0.00						
FE0	14.54	14.49						
MNO	0.46	0.48						
MGO	13.22	13.62						
CAO	0.00	0.05						
NA2O	0.00	0.07						
K2O	9.52	9.53						
CL	0.01	0.00						
F	0.25	0.41						
TOTAL	94.52	95.23						

Table A10.8 Microprobe major oxide data for uncrenulated metamorphic biotite (TS86-94) and crenulated metamorphic biotite (TS86-84), using the Joel Superprobe 733 microprobe system operated at Dalhousie University and conventional geological standards for calibration. The microprobe has an accelerating voltage of 15 kV with a beam current of 10 nano-amps and does a forty second count for each analysis.

	86-94/13	86-94/14	86-94/16	86-94/17	86-94/18*	86-94/19*	86-94/20	86-94/21
SiO2	36.81	36.68	36.17	35.83	36.62	35.64	35.85	35.77
TiO2	1.74	1.74	1.69	1.67	1.73	1.66	1.64	1.72
Al2O3	18.60	18.82	18.73	18.51	18.29	18.53	18.92	18.72
CR2O3	0.03	0.04	0.00	0.04	0.07	0.00	0.04	0.05
FeO	18.57	19.07	18.77	18.40	18.90	18.62	18.55	18.23
MnO	0.17	0.14	0.16	0.17	0.18	0.19	0.13	0.17
MgO	10.38	10.15	10.01	10.01	10.40	10.11	10.29	10.19
CaO	0.00	0.00	0.00	0.00	0.00	0.00	0.01	0.00
Na2O	0.05	0.04	0.02	0.04	0.01	0.06	0.03	0.06
K2O	10.07	9.10	9.08	8.94	9.46	9.76	9.52	9.67
Cl	0.00	0.00	0.01	0.00	0.00	0.01	0.01	0.00
F	0.33	0.34	0.38	0.30	0.42	0.30	0.40	0.30
TOTAL	96.75	96.12	95.02	93.91	96.08	94.88	95.39	94.88
	86-94/22	86-94/23	86-84/26	86-84/27	86-84/33	86-84/34	86-84/35	
SiO2	34.72	35.85	36.01	35.26	35.78	35.09	36.23	
TiO2	1.63	1.75	1.78	1.78	1.68	1.65	1.75	
Al2O3	17.97	18.94	18.41	18.24	18.74	18.28	18.46	
CR2O3	0.00	0.02	0.00	0.03	0.05	0.06	0.04	
FeO	18.20	18.39	18.45	18.72	17.60	18.84	18.53	
MnO	0.18	0.15	0.14	0.12	0.10	0.12	0.11	
MgO	9.90	10.16	10.42	9.96	10.36	10.42	10.62	
CaO	0.01	0.00	0.01	0.00	0.00	0.01	0.00	
Na2O	0.09	0.06	0.00	0.01	0.01	0.00	0.01	
K2O	9.08	9.62	9.64	9.97	9.32	9.53	9.33	
Cl	0.00	0.00	0.01	0.00	0.00	0.01	0.00	
F	0.42	0.34	0.46	0.24	0.38	0.41	0.36	
TOTAL	92.20	95.28	95.33	94.33	94.02	94.42	95.44	

(Data taken from separate grains, except for \* where two analysis from one grain were taken)

## RESUME

Name: Timothy R. Stokes

Birthdate: 13th August 1958

### Education:

PhD Geology; May 1986 - May 1991; Dalhousie University, Halifax, Nova Scotia, Canada.

MSc (Applied) in Mineral Exploration; September 1980 - December 1983; McGill University, Montreal, Quebec, Canada.

BSc Mining Engineering, September 1976 - June 1979, Camborne School of Mines, Redruth, Cornwall, England.

### Experience:

Sept. - Nov. 1990; Consultant geologist for a structural mapping project in the Cobequid Highlands, Nova Scotia.

July - Oct. 1989; Consultant geologist for structural mapping project of the Montague Gold Mines, Dartmouth, Nova Scotia.

May - Sept. 1988; Consultant geologist to Atomic Energy Control Board of Canada, examining the Cobequid Fault of NE Nova Scotia for neotectonic activity and paleoseismicity.

May - July 1987; Consultant geologist involved in underground structural mapping of the Beaver Dam Gold Mine, Nova Scotia.

June - Sept. 1986; Consultant Geologist involved in structural analysis of drill core of the Eastville Pb-Zn property, Colchester Co., Nova Scotia.

July - Aug. 1985; Exploration geologist for Newmont Holdings Ltd. on gold properties in the Kalgoorlie Gold District of Western Australia.

June - Oct. 1983; Consultant geologist involved in gold-silver exploration in Selkirk Mountains of SE British Columbia.

June - Aug. 1982; Geologist for Canadian Refractories Ltd. involved in exploration for graphite in SE

Quebec.

May - Sept. 1981; Senior geologist for Archer Cathro and Associates involved in gold and uranium exploration in the Wernecke Mts. of the Central Yukon, Canada.

March - Sept. 1980; Junior geologist for Archer Cathro and Associates involved in uranium and copper exploration in the Wernecke Mts. of the Central Yukon, Canada.

July - Sept. 1979; Student worker for English China Clays, England, involved with openpit mining and geological mapping.

July - Sept. 1978; Student worker for Outokumpu Mines Limited, Finland, within underground copper, lead, and cobalt mine.

Specialties:

Structural and economic geology of ore deposits and gold-quartz vein systems. Archean geology. Paleo-seismicity and environmental geology.

Publications:

Stokes, T.R., Zentilli, M. and Culshaw, N. 1990. Structural and lithologic controls of gold bearing quartz-breccia zones in Archean metaturbidites, Gordon Lake, Northwest Territories, Canada. *Canadian Journal of Earth Sciences*, 27: 1577-1589.

Stokes, T.R., Zentilli, M, and Culshaw, N. 1990.  $^{40}\text{Ar}/^{39}\text{Ar}$  dating and geochemical constraints on a proposed structural focusing model for the formation of gold-bearing breccias zones at Gordon Lake, N.W.T. Open File Report, 1989-90 Northwest Territories Mineral Development Agreement, N.W.T. Geology Division, Yellowknife, N.W.T. 85 p.

Stokes, T.R., Zentilli, M. and Culshaw, N. 1989. A structural and lithologic model for the formation of gold-bearing quartz-breccias at Gordon Lake, N.W.T. Open File Report, 1988-89 Northwest Territories Mineral Development Agreement, N.W.T. Geology Division, Yellowknife, N.W.T. 35 p.

Stokes, T.R., Culshaw, N. and Zentilli, M. 1988. Structural mapping of the Gordon Lake 'Refold', N.W.T.: a model for the focussing of late-stage, gold-bearing quartz-breccia vein systems. Open File

Report, 1987-88 Northwest Territories Mineral Development Agreement, N.W.T. Geology Division, Yellowknife, N.W.T. 19 p.

Stokes, T.R. 1988. A documentation of structures in unconsolidated sediments along the north shore of the Minas Basin, Nova Scotia: A reconnaissance neotectonic survey. Open File Report submitted as part of a 1988 contract with Atomic Energy Control Board, (in association with the MAGNEC Group). 95 p.

Doig, R., Murphy, J.B., Nance, R.D., and Stokes, T.R. 1990. Review of the geochronology of the Cobequid Highlands, Avalon Composite Terrane, Nova Scotia. Geological Survey of Canada Current Research (in press)

Extended Abstracts:

Stokes, T.R., Zentilli, M., and Culshaw, N. 1991. Structural control of gold-bearing quartz-breccia zones in Archean metaturbidites of the Gordon Lake region, Slave Province, Northwest Territories, Canada. (Submitted to Gold'91, Belo Horizonte, Brazil.)

Stokes, T.R., Zentilli, M., and Culshaw, N. 1990. Carbon-rich metasedimentary rocks as controls for gold mineralization in the Gordon Lake region, N.W.T. In: Exploration Overview 1990, Northwest Territories. Edited by S. Goff, N.W.T. Geology Division, Yellowknife, N.W.T.

Stokes, T.R., Zentilli, M., Culshaw, N. and Reynolds, P. 1989. Structural, geochemical and  $^{40}\text{Ar}/^{39}\text{Ar}$  dating constraints on the formation of gold-bearing, metaturbidite-hosted quartz breccia/vein systems of the Gordon Lake region, N.W.T. In: Exploration Overview 1989, Northwest Territories. Edited by W.A. Padgham, N.W.T. Geology Division, Yellowknife, N.W.T. p. 52-54.

Stokes, T.R., Zentilli, M. and Culshaw, N. 1988. Structure and lithologic controls of gold-bearing quartz-breccia bodies in metaturbidites, Gordon Lake, N.W.T. In: Exploration Overview 1988, Northwest Territories. Edited by W.A. Padgham, N.W.T. Geology Division, Yellowknife, N.W.T. p. 53-56.

## Abstracts:

Stokes, T.R., and Murphy, J.B. 1991. Structural features and tectonic implications of a sub-horizontal cleavage in metavolcanics and metasediments of the Jeffers Group, Cobequid Highlands, Nova Scotia. Program with Abstracts, 1991 Atlantic Geoscience Symposium, Amherst, Nova Scotia.

Stokes, T.R., Zentilli, M., Culshaw, N. and Reynolds, P. 1990.  $^{40}\text{Ar}/^{39}\text{Ar}$  dating constraints on gold-quartz, breccia mineralization of the south Gordon Lake region, N.W.T. Program with Abstracts, 1990 Atlantic Geoscience Symposium, Wolfville, Nova Scotia.

Stokes, T.R., Zentilli, M. and Culshaw, N. 1989. Gold bearing quartz-breccia type deposits in metaturbidites of the Archean Slave Province, Gordon Lake, N.W.T., Canada: structural control, metamorphic fluid focussing and the possible role of carbonaceous strata. "1989, Gold in Europe Conference", Toulouse, France. p. 37.

Stokes, T.R., Zentilli, M. and Culshaw, N. 1989. Controls of the formation of gold-bearing quartz-breccia zones hosted in Archean metaturbidites and exploration criteria for their recognition. Program with Abstracts, 1989 G.A.C.- M.A.C. Meeting, Montreal, Quebec. p. A-46.

Stokes, T.R. and Keppie, D. 1989. Neotectonic and Paleoseismic phenomena along the north shore of the Minas Basin, Nova Scotia. Program with Abstracts, 1989 G.A.C.- M.A.C. Meeting, Montreal, Quebec. p. A105-A106.

Stokes, T.R. 1989. Mechanisms for dilational breccia formation in metaturbidites and their relationship to gold mineralizing processes at Gordon Lake, N.W.T. Program with Abstracts, 1989 Atlantic Geoscience Symposium, Amhearst, Nova Scotia.

Stokes, T.R., Culshaw, N. and Zentilli, M. 1988. Syn-late metamorphic fluid focussing in the formation of turbidite hosted gold-quartz veins in the Archean Yellowknife Basin, N.W.T.; A Meguma Analogue? Program with Abstracts, 1988 Atlantic Geoscience Symposium, Amhearst, Nova Scotia.

Stokes, T.R., Zentilli, M., and Patterson, J. 1987. Fracture controlled Pb-Zn mineralization near Eastville, Colchester Co., Nova Scotia. Program with

Abstracts, 1987 Atlantic Geoscience Symposium, Fredericton, Nova Scotia.

Stokes, T.R., Culshaw, N. and Zentilli, M. 1987. Structural controls on the location of turbidite hosted gold-quartz veins, Yellowknife Supergroup, N.W.T. Program with Abstracts, 1987 G.A.C.- M.A.C. Annual Meeting, Saskatoon, Saskatchewan.

Stokes, T.R., Culshaw, N. and Zentilli, M. 1987. Classification of metaturbidite hosted gold-quartz veins within the Yellowknife Supergroup, Gordon Lake, N.W.T. Program with Abstracts, 1987 G.A.C.- M.A.C. Summer Field Meeting, Yellowknife, N.W.T.

Stokes, T.R., Culshaw, N. and Zentilli, M. 1987. Refolding and uplift fluid focussing, mechanisms controlling the emplacement of turbidite hosted gold-quartz veins in the South Gordon Lake region, N.W.T. In: Exploration Overview 1987, Northwest Territories. Edited by C.E. Ellis, N.W.T. Geology Division, Yellowknife, N.W.T.

Doig, R., Murphy, J.B., Nance, R.D. and Stokes, T.R. 1990. Geochronology of the Cobequid Highlands: A review and new U-Pb age dates. In: Program and Summaries, Nova Scotia Department of Mines and Energy Report 90-3, p.38.



## REFERENCES

- ABBEY, S. 1983. Studies in "standard samples" of silicate rocks and minerals 1969-1982. Geological Survey of Canada, Paper 83-15.
- ABRAHAM, A.P. AND SPOONER, E.T.C. 1988. Tonalite hosted gold-quartz vein/shear zone mineralization, Arcadia Bay, Coronation Gulf, N.W.T. In Exploration Overview of the Northwest Territories 1988. Edited by W.A. Padgham. Northwest Territories Geology Division, D.I.A.N.D., Yellowknife, N.W.T., Extended Abstract, pp. 21-25.
- AGAR, S.M. 1988. Shearing of partially consolidated sediments in a lower trench slope setting, Shimanto Belt, SW Japan. Journal of Structural Geology, 10: 21-32.
- ALEXANDER, E.C., JR., MICKELSON, G.M., AND LANPHERE, M.A. 1978. MMhb-1: A new  $^{40}\text{Ar}/^{39}\text{Ar}$  dating standard. U.S. Geological Survey, Open-File Report 701, pp. 6-8.
- ANNELS, A.E. AND ROBERTS, D.E. 1989. Turbidite-hosted gold mineralization at the Dolaucothi Gold Mines, Dyfed, Wales, United Kingdom. Economic Geology, 84: 1293-1314.
- ATKINSON, D.J. 1987. Report on preliminary mapping and geochemistry of the Western Plutonic Complex. 15th Annual Geoscience Forum, Yellowknife, N.W.T., Geological Investigations and Abstracts of Papers, pp. 19-20.
- ATKINSON, D.J. 1989. Geology of the Western Plutonic Complex, southwestern Slave Province. In Exploration Overview of the Northwest Territories 1989. Edited by W.A. Padgham. Northwest Territories Geology Division, D.I.A.N.D., Yellowknife, N.W.T., Abstract, p. 25.
- AYERS, L.D. AND CERNY, P. 1982. Metallogeny of granitoid rocks in the Canadian Shield. Canadian Mineralogist, 20: 436-439.
- BARAGAR, W.R.A. AND MCGLYNN, J.C. 1976. Early Archean basement in the Canadian Shield: A review of the evidence. Geological Survey of Canada, Paper 76-14, 20 p.
- BAUER, R.L. 1986. Multiple folding and pluton emplacement in Archean migmatites of the southern Vermillion granite complex, northeastern Minnesota. Canadian Journal of Earth Sciences, 23: 1753-1764.
- BEACH, A. 1975. The geometry of en-echelon vein arrays. Tectonophysics, 28: 245-263.

- BEACH, A. 1977. Vein arrays, hydraulic fracturing and pressure solution structures in a deformed flysch sequence, S.W. England. *Tectonophysics*, 40: 210-225.
- BELL, H. 1986. Geology of the Haile gold mine, Lancaster County, South Carolina. Geological Society of America, Southeastern Section. Centennial Field Guide, Volume 6, p. 247-250.
- BHATIA, M.R. 1983. Plate tectonics and geochemical composition of sandstones. *Journal of Geology*, 91: 611-627.
- BHATIA, M.R. AND CROOK, K.A.W. 1986. Trace element characteristics of graywackes and tectonic setting discrimination of sedimentary basins. *Contributions to Mineralogy and Petrology*, 92: 181-193.
- BODNAR, R.J., REYNOLDS, T.J., AND KUEHN, R.H. 1985. Fluid inclusion systematics in epithermal systems. In *Geology and geochemistry of epithermal deposits*. Edited by B.R. Gerger and P.M. Bethke. *Reviews in Economic Geology*, Volume 2, p. 73-97.
- BORRADAILE, G., SARVAS, R.D., DUTKA, R., STEWART, R. AND STUBLEY, M. 1988. Transpression in slates along the margin of an Archean gneiss belt, northern Ontario - magnetic fabrics and petrofabrics. *Canadian Journal of Earth Sciences*, 25: 1069-1077.
- BOSTOCK, H.H. 1980. Geology of the Itchen area, District of MacKenzie, N.W.T. Geological Survey of Canada, Memoir 391, 101 p.
- BOTTRELL, S.H., SHEPHERD, T.J., YARDLEY, B.W.D. AND DUBESSY, J. 1988. A fluid inclusion model for the genesis of the ores of the Dolgellau Gold Belt, North Wales. *Journal of the Geological Society, London*, 145: 139-145.
- BOULTER, C.A., FOTIOS, M.G., AND PHILLIPS, G.N. 1987. The Golden Mile, Kalgoorlie: A giant gold deposit localized in ductile shear zones by structurally induced infiltration of an auriferous metamorphic fluid. *Economic Geology*, 82: 1661-1678.
- BOUMA, A.H. 1962. Sedimentology of some flysch deposits. Elsevier, Amsterdam, 168 p.
- BOWERS, T.S., AND HELGESON, H.C. 1983a. Calculation of the thermodynamic and geochemical consequences of non ideal mixing in the system H<sub>2</sub>O-CO<sub>2</sub>-NaCl on phase relations in geologic systems: Equation of state for H<sub>2</sub>O-CO<sub>2</sub>-NaCl fluids

at higher pressures and temperatures. *Geochimica et Cosmochimica Acta*, 47: 1247-1275.

BOWRING, S.A., WILLIAMS, I.S., COMPSTON, W., AND PODOSEK, F.A. 1989. Remnants of earth's oldest known continental crust, Slave Province, N.W.T. In *Exploration Overview of the Northwest Territories 1989*. Edited by W.A. Padgham. Northwest Territories Geology Division, D.I.A.N.D., Yellowknife, N.W.T., Abstract, p. 27.

BOYLE, R.W. 1953. On the colour of black and grey quartz from Yellowknife, Northwest Territories, Canada. *American Mineralogist*, 38: 528-535.

BOYLE, R.W. 1954. A decrepitation study of quartz from the Cambell and Negus-Rycon shear zone systems, Yellowknife, Northwest Territories. Geological Survey of Canada Bulletin 30, 19 p.

BOYLE, R.W. 1961. The geology, geochemistry, and origin of the gold deposits of the Yellowknife District. Geological Survey of Canada, Memoir 310, 190 p.

BOYLE, R.W. 1979. The geochemistry of gold and its deposits. Geological Survey of Canada, Bulletin 280, 584 p.

BOYLE, R.W. 1986. Gold deposits in turbidite sequences: Their geology, geochemistry, and history of the theories of their origin. In *Turbidite Hosted Gold Deposits*. Edited by D.J. Keppie, R.W. Boyle and S.J. Haynes, Geological Association of Canada Special Paper 32, pp. 1-13.

BOYLE, R.W. 1987. Gold history and genesis of deposits. Van Nostrand Reinhold Co. New York. 676 p.

BRAY, C.J. AND SPOONER, E.T.C. 1989. Fluid inclusion volatile analysis using heated crushing (105°C) / gas chromatography with in-series photoionization/thermal conductivity and digital peak processing. In *Program and Abstracts of Second Biennial Pan-American Conference on Fluid Inclusions, PACROFI II, Volume 2, Blacksburg, Virginia*, pp. 12-13.

BROPHY, J.A. 1986. Structural setting, age, and wall rock gold geochemistry of auriferous quartz veins in turbidites of the Yellowknife Supracrustal Basin. In *Exploration Overview of the Northwest Territories 1986*. Edited by J.C.E. Crux and C.D. Gault. Northwest Territories Geology Division, D.I.A.N.D., Yellowknife, N.W.T., Abstract, p. 18.

BROPHY, J.A. 1987a. Geology, geochemistry of select

auriferous quartz-vein deposits in the Burwash Formation. 1987 Geological Association of Canada Summer Field Meeting, Program with Abstracts, p. 19.

BROPHY, J.A. 1987b. Tom and Ptarmigan Mines. In: A guide to the geology of the Yellowknife Volcanic Belt and its bordering rocks. Edited by W.A. Padgham. Geological Association of Canada, Mineral Deposits Division, pp. 195-198.

BRUN, J.P., GAPAIS, D., AND THEOFF, B. LE. 1981. The mantled gneiss domes of Kupio (Finland) interfering diapirs. *Tectonophysics*, 74: 284-304.

BUBAR, D.S. AND HESLOP, J.B. 1985. Geology of the Gondor massive sulphide deposit, Slave Province, N.W.T. *Canadian Institute of Mining and Metallurgy Bulletin*, 78: 52-60.

BURK, R., HODGSON, C.J., AND QUATERMAIN, R.A. 1986. The geological setting of the Teck-Corona Au-Mo-Ba deposit, Hemlo, Ontario, Canada. In *Gold'86 Proceedings*, Toronto. Edited by A.J. MacDonald. p. 311-326.

BURROWS, D.R., WOOD, P.C., AND SPOONER, E.T.C. 1986. Carbon isotope evidence for a magmatic origin for Archean gold-quartz vein ore deposits. *Nature*, 321: 851-854.

BURRUSS, R.C. 1981. Mixing of H<sub>2</sub>O-CO<sub>2</sub> in fluid inclusions; geobarometry and Archean gold deposits. *Geochimica and Cosmochimica Acta*, 50: 847-852.

BURSTON, M.J. AND CAELLES, J.C. 1986. 1986 Underground program and ore reserves for the No.1 Zone of the Gordon Lake gold deposit, MacKenzie Mining District (N.W.T.), Canada. Unpublished report, Giant Bay Resources Ltd., Burnaby, British Columbia. 21 p.

CABRI, L.J., CHRYSOULIS, S.J., DE VILLIERS, J.P.R., LAFLAMME, J.H.G., AND BUSECK, P.R. 1989. The nature of "invisible" gold in arsenopyrite. *Canadian Mineralogist*, 27: 353-362.

CAELLES, J. 1984. Geological report on the 1984 drill exploration program on the Giant Bay Resources Mahe, Ad, Pol, Ar, Bear and Lynx Claim Group, MacKenzie Mining District, N.W.T., Canada. Unpublished report, Giant Bay Resources Ltd., Burnaby, British Columbia. 15 p.

CAELLES, J. 1985. 1985 Mineral reserve calculation for the No.1 Zone of the Gordon Lake gold property, MacKenzie Mining District, N.W.T., Canada. Unpublished report, Giant Bay Resources Ltd., Burnaby, British Columbia, 16 p.

CAELLES, J.C. 1987a. Report on the 1987 surface diamond drilling and underground exploration program in the No. 1 or Main Zone on the Giant Bay Resources Ltd. Gordon Lake Property, McKenzie Mining District, N.W.T., Canada. Unpublished Report. Unpublished report, Giant Bay Resources Ltd., Burnaby, British Columbia, 8 p.

CAELLES, J.C. 1987b. Report on the 1987 surface drilling and program (outside the Main or No. 1 Zone on the Giant Bay Resources Ltd. Gordon Lake Property, McKenzie Mining District, N.W.T., Canada. Unpublished Report, Giant Bay Resources Ltd., Burnaby, British Columbia, 13 p.

CAMERON, E. 1988. Archean gold: Relation to granulite formation and redox zoning in the crust. *Geology*, 16: 109-112.

CATHELINEAU, M., BOIRON, M.C., HOLLINGER, P., MARION, P., AND DENIS, M. 1989. Gold in arsenopyrites: Crystal chemistry, location, state, physical and chemical conditions of deposition genesis. *In Economic Geology Monograph 6. Edited by R.R. Keays, R.H. Ramsay, and D.I. Groves.* pp. 328-341.

CHARY, N.K. 1971. An isotopic and geochemical study of gold-quartz veins in the Con-Rycon mine, Yellowknife, N.W.T. Unpublished MSc Thesis, University of Alberta, Edmonton. 90 p.

CLEE, T.E., BARR, K.G., AND BERRY, M.J. 1974. Fine structure of the crust near Yellowknife. *Canadian Journal of Earth Sciences*, 11: 1534-1549.

CLIFFORD, P.M., CROCKET, J. AND FEUTEN, F. 1983. Distribution and localization of gold in Meguma Group rocks, Nova Scotia. Part 1: Structural effects and pressure solution - preliminary results. *In Current Research, Part B, Geological Survey of Canada, Paper 83-1B, pp. 279-283.*

COLEMAN, L.C. 1957. Mineralogy of the Giant Yellowknife gold mine, Yellowknife, N.W.T. *Economic Geology*, 52: 400-425.

COLLINS, P.L.F. 1979. Gas hydrates in CO<sub>2</sub>-bearing fluid inclusions and the uses of freezing data for estimation of salinity. *Economic Geology*, 74: 1435-1444.

COLVINE, A.C., ANDREWS, A.J., CHERRY, M.E., DUROCHER, M.E., FYON, A.J., LAVIGNE, JR., M.J., MACDONALD, A.J., MARMONT, S., POULSEN, K.H., SPRINGER, J.S., AND TROOP, D.G. 1984. An integrated model for the origin of Archean lode gold

deposits. Ontario Geological Survey, Open File Report 5524. 84 p.

CONDIE, K.C. 1981. Archean Greenstone Belts. (Development in PreCambrian Geology, Volume 3. Elsevier, New York.

COOK, N.J. AND CHRYSOULIS, S.L. 1990. Concentrations of "invisible gold" in the common sulphides. Canadian Mineralogist, 28: 1-16.

CRAW, D. 1990. Fluid evolution during uplift of the Annapurna Himalayas, central Nepal. Lithos, 24: 137-150.

CRAWFORD, M.L. 1981. Phase equilibria in aqueous fluid inclusions. In Short course in fluid inclusions: Applications to petrology. Edited by L.S. Hollister and M.L. Crawford, Mineralogical Association of Canada Short Course Handbook, Volume 6, pp. 75-100.

CRAWFORD, M.L. AND HOLLISTER, L.S. 1986. Metamorphic fluids: The evidence from fluid inclusions. In Fluid-rock interactions during metamorphism. Edited by J.V. Walther and Wood, B.J., Advances in Physical Geochemistry, Volume 5, pp. 1-35.

CRAWFORD, M.L., FILER, J., AND WOOD, C. 1979. Saline fluid inclusions associated with retrograde metamorphism. Bulletin Minéralogique, 102: 562-568.

CROCKET, J.H., CLIFFORD, P.M., FEUTEN, F., AND KABIR, A. 1983. Distribution of gold in Meguma Group rocks, Nova Scotia. Part 2: Implications of background geochemistry and cleavage development - a preliminary report. In Current Research, Part B, Geological Survey of Canada, Paper 83-1B, pp. 285-290.

CROCKET, J.H., FEUTEN, F., CLIFFORD, P.M., AND KABIR, A. 1986. Distribution of gold and arsenic in turbidites at Harrington Cove, Nova Scotia: Implications on gold mineralization. In Turbidite hosted gold deposits. Edited by J.D. Keppie, R.W. Boyle, and S.J. Haynes, Geological Association of Canada, Special Paper 32, pp. 149-159.

DALLMEYER, R.D. 1979.  $^{40}\text{Ar}/^{39}\text{Ar}$  dating: principles, techniques, and applications in orogenic terranes. In Lectures in Isotope Geology. Edited by E. Jaeger and J.C. Hunziker. Springer-Verlag, Berlin, pp.77-104.

DAVIDSON, A. 1967. Metamorphism and intrusion in the Benjamin Lake map-area. Northwest Territories. Unpublished PhD thesis, University of British Columbia, Vancouver. 204 p.

DAVIDSON, A. 1972. Granite studies in the Slave Province (Parts of 85I). In Report of Activities, Part A, Geological Survey of Canada, Paper 72-1A, p. 109-115.

DE PAOR, D.G. 1983. Orthographic analysis of geological structures - I: Deformation theory. *Journal of Structural Geology*, 5: 255-277.

DE PAOR, D.G. 1986. Orthographic analysis of geological structures - II: Practical Applications. *Journal of Structural Geology*, 8: 87-100.

DE PAOR, D.G. 1987. Stretch in shear zones: Implications for section balancing. *Journal of Structural Geology*, 9: 893-895.

DEVANEY, J.R. AND WILLIAMS, H.R. 1989. Evolution of an Archean subprovince boundary: A sedimentological and structural study of part of the Wabigoon-Quetico boundary in northern Ontario. *Canadian Journal of Earth Sciences*, 26: 1013-1026.

DEWY, J.F. 1980. Episodicity, sequence and style at convergent plate boundaries. In The continental crust and its mineral deposits. Edited by D.W. Strangway. pp. 553-574.

DIXON, J.M. AND SUMMERS, J.M. 1983. Patterns of total and incremental strain in subsiding troughs: Experimental centrifuged models of inter-diapir synclines. *Canadian Journal of Earth Sciences*, 20: 1843-1861.

DODSON, M.H. 1973. Closure temperature in cooling geochronological and petrological systems. *Contributions to Mineralogy and Petrology*, 40: 259-274.

DRURY, S.A. 1977. Structures induced by granite diapirs in the Archean greenstone belt at Yellowknife, Canada: Implications for Archean geotectonics. *Journal of Geology*, 85: 345-358.

DURNEY, D.W. 1972. Solution transfer, an important geological deformation mechanism. *Nature*, 235: 315-317.

EASTON, R.M. 1984. Compilation of geochronologic data for the Yellowknife Greenstone Belt (85J/B, 85J/9) and vicinity, District of MacKenzie, N.W.T. In Contributions to the Geology of the Northwest Territories Volume 1. Edited by J.A. Brophy. pp 1-20.

EASTON, R.M. 1985. The nature and significance of Pre-

- Yellowknife Supergroup rocks in the Point Lake area, Slave Structural Province, Canada. In Evolution of Archean supracrustal sequences. Edited by L.D. Ayres, P.C. Thurston, K.D. Card, and W. Weber, Geological Association of Canada Special Paper 28, pp. 153-178.
- ELLIS, C. 1988. Operating mines. In Exploration Overview of the Northwest Territories 1988. Edited by W.A. Padgham Northwest Territories Geology Division, D.I.A.N.D., Yellowknife, Northwest Territories, pp. 7-9.
- ENGLISH, P.J. 1981. Gold-quartz veins in metasediments of the Yellowknife Supergroup, N.W.T: A fluid inclusion study. Unpublished MSc Thesis, University of Alberta. 109 pp.
- ERSLEV, E.A. 1988. Normalized centre-to-centre strain analysis of packed aggregates. Journal of Structural Geology, 2: 201-209.
- ETHERIDGE, M.A., WALL, V.J., AND VERNON, R.H. 1983. The role of the fluid phase in regional metamorphism and deformation. Journal of Metamorphic Geology, 1: 205-226.
- FAURE, G. 1986. Principles of isotope geology. 2nd edition. Wiley, New York.
- FITCH, F.J., MILLER, J.A., AND MITCHELL, J.G. 1969. A new approach to radio-isotopic dating in orogenic belts. In Time and place in orogeny. Edited by P.E. Kent, G.E. Satterthwaite, and A.M. Spencer. Geological Society of London Special Publication 3, pp. 157-195.
- FITCHES, W.R., CAVE, R., CRAIG, J., AND MALTMAN, A.J. 1986. Early veins as evidence of detachment in the Lower Palaeozoic rocks of the Welsh Basin. Journal of Structural Geology, 8: 607-620.
- FLECK, R.J., SUTTER, J.F., ELLIOT, D.H. 1977. Interpretation of discordant  $^{40}\text{Ar}/^{39}\text{Ar}$  age-spectra of Mesozoic tholeiites from Antarctica. Geochimica and Cosmochimica Acta, 41: 15-32.
- FLINN, D. 1962. On folding during three dimensional progressive deformation. Quarterly Journal of the Geological Society of London, 118: 385-428.
- FOLINSBEE, R.E. 1942. Zone facies metamorphism in relation to ore deposits of the Yellowknife-Beaulieu region, Northwest Territories. Unpublished PhD thesis, University of Minnesota, Minneapolis. 180 p.
- FOLINSBEE, R.E., BAADSGAARD, H., CUMMING, G.L., AND GREEN,



D.C. 1968. A very ancient island arc. American Geophysical Union, Geophysical Monograph 12, pp. 441-448.

FORTIER, Y.O. 1946. Yellowknife-Beaulieu region, Northwest Territories. Geological Survey of Canada, Paper 46-23. 1 map.

FORTIER, Y.O. 1947. Ross Lake, Northwest Territories. Geological Survey of Canada, Paper 47-16, 4 p. and map.

FOSTER, R.P. AND WILSON J.F. 1984. Geological setting of Archean gold deposits in Zimbabwe. In Gold'82: The geology, geochemistry and genesis of gold deposits. Edited by R.P. Foster, Geological Society of Zimbabwe, Special Publication No.1, pp. 521-551.

FOSTER, R.P., FURBER, F.M.W., GILLIGAN, J.M., AND GREEN, D. 1986. Shamva Gold Mine, Zimbabwe; A product of calc-alkaline-linked exhalative, volcanoclastic, and epiclastic sedimentation in the Late Archean. In Turbidite hosted gold deposits. Edited by J.D. Keppie, R.W. Boyle and S.J. Haynes. Geological Association of Canada Special Paper 32, p. 41-66.

FRIPP, R.E.P. 1976. Stratabound gold deposits in Archean banded iron formation, Rhodesia. Economic Geology, 71: 58-75.

FRY, N. 1979b. Random point distributions and strain measurements in rocks. Tectonophysics, 60: 89-105.

FYFE, W.S., AND KERRICH, R. 1982. Gold: natural concentration processes: In Gold '82 - The geology, geochemistry and genesis of gold deposits. Edited by R.P. Foster. Geological Society of Zimbabwe, Special Publication No. 1., pp. 99-127.

FYFE, W.S., PRICE, N.J., AND THOMPSON, A.B. 1978. Fluids in the earth's crust. Elsevier, Amsterdam, 383p.

FYSON, W.K. 1975. Fabrics and deformation of Archean meta-sedimentary rocks, Ross Lake - Gordon Lake area, Slave Province, Northwest Territories. Canadian Journal of Earth Sciences, 12: 765-776.

FYSON, W.K. 1977. Structures induced by granite diapirs in the Archean greenstone belt at Yellowknife, Canada, Implications for Archean geotectonics: A discussion. Journal of Geology, 86: 767-769.

FYSON, W.K. 1980. Fold fabrics and emplacement of an Archean granitoid pluton, Cleft Lake, Northwest

Territories. Canadian Journal of Earth Sciences, 17: 325-332.

FYSON, W.K. 1981. Divergent fold overturning and regional tectonics, southern Slave Province, NWT. Precambrian Research, 14: 878-893.

FYSON, W.K. 1982. Complex evolution of folds and cleavages in Archean rocks, Yellowknife, N.W.T. Canadian Journal of Earth Sciences, 19: 878-893.

FYSON, W.K. 1984a. Basement controlled structural fronts forming an apparent re-fold pattern in the Yellowknife domain, Slave Province. Canadian Journal of Earth Sciences, 21: 822-828.

FYSON, W.K. 1984b. Fold and cleavage patterns in Archean metasediments of the Yellowknife Domain, Slave Province. In Precambrian tectonics illustrated. Edited by A. Kroner. Elsevier, Amsterdam, pp. 281-293.

FYSON, W.K. 1987a. A succession of quartz veins in Archean metaturbidites, Yellowknife Bay, Slave Province. Canadian Journal of Earth Sciences, 24: 698-710.

FYSON, W.K. 1987b. Guide to structures in metasedimentary rocks around Yellowknife. In A guide to the geology of the Yellowknife Volcanic belt and its bordering rocks. Edited by W.A. Padgham. Geological Association of Canada, Mineral Deposits Division, pp. 89-103.

FYSON, W.K. 1990. Structural development of angular volcanic belts in the Archean Slave Province. Canadian Journal of Earth Sciences, 27: 403-413.

FYSON, W.K., AND HELMSTAEDT, H. 1988. Structural patterns and tectonic evolution of supracrustal domains in the Archean Slave Province, Canada. Canadian Journal of Earth Sciences, 25: 301-315.

GAIR, J.E. 1962. Geology and ore deposits of the Nova Lima and Rio Acima quadrangles, Minas Gerais, Brazil. United States Geological Survey, Professional Paper 341-A.

GIBB, R.A. AND THOMAS, M.D. 1980. Correlation of gravity anomalies with Yellowknife Supergroup rocks, North Arm, Great Slave Lake. Canadian Journal of Earth Sciences, 17: 1506-1516.

GIBBINS, W.A. 1981. Gold and Precambrian iron-formation in the N.W.T. In Gold workshop volume. Edited by R.D. Morton; Yellowknife Gold Workshop Committee, Yellowknife,

p. 258-287.

GLASSON, M.J. AND KEAYS, R.R. 1978. Gold mobilization during cleavage development in sedimentary rocks from the auriferous slate belt of Central Victoria, Australia: Some important boundary conditions. *Economic Geology*, 73: 496-511.

GOLDFARB, R.J., LEACH, D.L., MILLER, M.L., AND PICKTHORN, W.J. 1986. Geology, metamorphic setting, and genetic constraints of epigenetic lode-gold mineralization within the Cretaceous Valdez Group, south-central Alaska. In *Turbidite Hosted Gold Deposits*. Edited by D.J. Keppie, R.W. Boyle and S.J. Haynes. Geological Association of Canada Special Paper 32, pp. 87-105.

GOLDFARB, R.J., LEACH, D.L., ROSE, S.C., AND LANDIS, G.P. 1989. Fluid inclusion geochemistry of gold-bearing quartz veins of the Juneau Gold Belt, southeastern Alaska: Implications for ore genesis. In *Economic Geology Monograph 6*. Edited by R.R. Keays, R.H. Ramsay, and D.I. Groves. pp. 363-375.

GRAVES, M.C. 1988. Lithogeochemical evidence for the provenance of the Meguma Group, Southern Nova Scotia. (Abstract) *Maritime Sediments and Atlantic Geology*, 24(2): 196.

GRAVES, M.C. AND ZENTILLI, M. 1982. A review of the geology of gold in Nova Scotia. In *Geology of Canadian Gold Deposits*. Edited by R.W. Hodder and W. Petruk. Canadian Institute of Mining and Metallurgy, Special Volume 24., pp. 233-242.

GRAY, D.R. 1977. Morphologic classification of crenulation cleavage. *Journal of Geology*, 85: 229-235.

GRAY, D.R. 1978. Cleavages in deformed psammitic rocks from southeastern Australia: Their nature and origin. *Geological Society of America*, 89: 577-590.

GRAY, D.R. 1979. Microstructure of crenulation cleavages: An indicator of cleavage origin. *American Journal of Science*, 279: 97-128.

GREEN, D.C. AND BAADSGAARD, H. 1971. Temporal evolution and petrogenesis of an Archean crustal segment at Yellowknife, N.W.T., Canada. *Journal of Petrology*, 12: 177-217.

GREEN, D.C., BAADSGAARD, H., AND CUMMING, G.L. 1968. Geochronology of the Yellowknife area, Northwest

Territories, Canada. Canadian Journal of Earth Sciences, 5: 725-735.

GREENER, P.E. 1981. Pore pressure: fundamentals, general ramifications, and implications for structural geology (revised 2nd edition). American Association of Petroleum Geologists, Education Course Note Series, no. 4, 131p.

GRIGORYEVA, T.A. AND SUKNEVA, L.S. 1981. Effects of sulphur and of antimony and arsenic sulphides on the solubility of gold. Geokhimiya: 10, 1534-1540.

GROVES, D.I., PHILLIPS, N., HO, S.E., HOUSTON, S.M., AND STANDING, C.A. 1987. Cratonic-scale distribution of Archean greenstone gold deposits: predictive capacity of the metamorphic model. Economic Geology, 82: 2045-2058.

GROVES, D.I., PHILLIPS, N.G., FALCONER, L.J., HOUSTON, S.M., HO, S.E., BROWNING, P., DAHL, N., AND MCNAUGHTON, N.J. 1988. Evidence for an epigenetic origin for BIF-hosted gold deposits in greenstone belts of the Yilgarn Block, Western Australia. In Recent advances in understanding Precambrian gold deposits. Edited by S.E. Ho and D.I. Groves. University of Western Australia, Geology Department and University Extension Publication No. 11, pp. 167-179.

GUHA, J. AND KANWAR, R. 1987. Vug brines-fluid inclusions: A key to the understanding of secondary gold enrichment processes and the evolution of deep brines in the Canadian Shield. In Saline water and gases in crystalline rocks. Edited by P. Fritz and S.K. Frape, Geological Association of Canada Special Paper 33, pp. 95-101.

GUHA, J., ARCHAMBAULT, G, AND LEROY, J. 1983. A correlation between the evolution of mineralizing fluids and the geomechanical development of a shear zone as illustrated by the Henderson 2 Mine, Quebec. Economic Geology, 78: 1605-1618.

HARDY, L.S. 1989. Hydrothermal potassium feldspar at the Haile gold mine, South Carolina. Economic Geology, 84: 2307-2310.

HARRISON, T.M., DUNCAN, I., AND MCDOUGALL, I. 1985. Diffusion of  $^{40}\text{Ar}$  in biotite: Temperature, pressure and compositional effects. Geochimica et Cosmochimica Acta, 49: 2461-2468.

HAYNES, S.J. 1986. Geology and chemistry of turbidite-hosted gold deposits, greenschist facies, eastern Nova Scotia, Canada. In Turbidite Hosted Gold Deposits. Edited

by D.J. Keppie, R.W. Boyle and S.J. Haynes. Geological Association of Canada Special Paper 32, pp. 161-177.

HELMSTAEDT, H., GOODWIN, J.A., PATTERSON, J.G., AND KING, J. 1979. Preliminary geological map, southern end of Yellowknife greenstone belt. INAC, NAP, Geology Division, Yellowknife, N.W.T. EGS 1979.

HELMSTAEDT, H., KING, J., AND BOODLE, R. 1980. Preliminary geology map of Banting and Walsh Lakes area. INAC, NAP Geology Division, Yellowknife, NWT, EGS 1980-5.

HELMSTAEDT, H., KING, J., GOODWIN, J.A., AND PATTERSON, J.G. 1981. Geology of the southwest end of the Yellowknife Greenstone Belt. In Proceedings of the gold workshop, Yellowknife, NWT. Edited by R.D. Morton. pp. 232-249.

HELMSTAEDT, H. AND PADGHAM, W.A. 1986a. A new look at the stratigraphy of the Yellowknife Supergroup at Yellowknife, N.W.T. - implications for the age of gold-bearing shear zones and Archean basin evolution. Canadian Journal of Earth Sciences, 23: 454-475.

HELMSTAEDT, H. AND PADGHAM, W.A. 1986b. Stratigraphic and structural setting of the gold-bearing shear zones in the Yellowknife greenstone belt. In Gold in the Western Shield. Edited by L.A. Clark. Canadian Institute of Mining and Metallurgy Special Publication 38, pp. 322-345.

HELMSTAEDT, H., PADGHAM, W.A., AND BROPHY, J.A. 1986. Multiple dikes in Lower Kam Group, Yellowknife greenstone belt: Evidence for Archean sea-floor spreading? Geology: 14, 562-566.

HENDERSON, J.B. 1970. Stratigraphy of the Yellowknife Supergroup, Yellowknife Bay - Prosperous Lake area, District of MacKenzie. Geological Survey of Canada, Paper 70-26, 12 p.

HENDERSON, J.B. 1972. Sedimentology of Archean turbidites at Yellowknife, Northwest Territories. Canadian Journal of Earth Sciences, 9: 882-902.

HENDERSON, J.B. 1975. Sedimentology of the Archean Yellowknife Supergroup at Yellowknife, District of MacKenzie. Geological Survey of Canada, Bulletin 246.

HENDERSON, J.B. 1981. Archean basin evolution in the Slave Structural Province. In Precambrian plate tectonics. Edited by A. Kroner. Elsevier, Amsterdam, pp. 213-235.

HENDERSON, J.B. 1985. Geology of the Yellowknife-Hearne

Lake area, District of Mackenzie: A segment across an Archean basin. Geological Survey of Canada Memoir 414.

HENDERSON, J.B. 1987. The Burwash Formation at Yellowknife, Northwest Territories. In A guide to the geology of the Yellowknife Volcanic belt and its bordering rocks. Edited by W.A. Padgham. Geological Association of Canada, Mineral Deposits Division, pp. 21-32.

HENDERSON, J.B. AND EASTON, R.M. 1977. Archean supracrustal-basement rock relationships in the Keskarrah Bay map-area, Slave Structural Province, District of MacKenzie. In Report of Activities, Part A, Geological Survey of Canada, Paper 77-1A, pp. 217-221.

HENDERSON, J.B., VAN BREEMEN, O., AND LOVERIDGE, W.D. 1987. Some U-Pb zircon dates from Archean basement, supracrustal and intrusive rocks, Yellowknife-Hearne Lake area, District of MacKenzie. In Radiogenic Age and Isotopic Studies: Report I. Geological Survey of Canada, Paper 87-2, pp. 111-121.

HENDERSON, J.F. 1941a. Gordon Lake, District of MacKenzie, Northwest Territories. Geological Survey of Canada, Map 644A.

HENDERSON, J.F. 1941b. Gordon Lake South, District of MacKenzie, Northwest Territories. Geological Survey of Canada, Map 645A.

HENDERSON, J.F. 1943. Structure and metamorphism of early Precambrian rocks between Gordon Lake and the Great Slave Lake, N.W.T. American Journal of Science: 241, 440-446.

HENDERSON, J.F. AND BROWN, I.C. 1966. Geology and structure of the Yellowknife greenstone belt, District of MacKenzie. Geological Survey of Canada, Bulletin 141.

HENDERSON, J.F. AND JOLLIFFE, A.W. 1939. Relation of gold deposits to structure, Yellowknife and Gordon Lake areas, Northwest Territories. Canadian Institute of Mining and Metallurgy, Transactions, 42: 314-336.

HENDERSON, J.R. 1983. Analysis of structure as a factor controlling gold mineralization in Nova Scotia. Geological Survey of Canada, Current Research, Part B, Paper 83-1B, pp. 13-21.

HENLEY, R.W. 1973. Solubility of gold in hydrothermal chloride solutions. Chemical Geology, 11: 73-87.

HENLEY, R.W., NORRIS, R.J., AND PATERSON, C.J. 1976.

Multistage ore genesis of post-metamorphic lode emplacement. *Mineralium Deposita*, 11: 180-196.

HEYEN, G., RAMBOZ, C. AND DUBESSY, A. 1982. Simulation des equilibres de phases dans le systeme  $\text{CO}_2\text{-H}_2\text{O}$  en dessous de  $50^\circ\text{C}$  et de 100 bar. Application aux inclusions fluides. *C.R. Academy of Science, Paris*, 294: 203-206.

HIBBARB, J. AND KARIG, D.E. 1987. Sheath-like folds and progressive fold deformation in Tertiary sedimentary rocks of the Shimanto accretionary complex, Japan. *Journal of Structural Geology*, 9: 845-857.

HO, S.E. 1987. Fluid inclusions: their potential as an exploration tool for Archean gold deposits. In Recent advances in understanding Precambrian gold deposits. Edited by S.E. Ho and D.I. Groves. University of Western Australia, Geology Department and University Extension Publication No. 11, pp. 239-264.

HODGSON, C.J. AND HAMILTON, J.V. 1989. Gold mineralization in the Abitibi Greenstone Belt: End-stage result of Archean collisional tectonics? In Economic Geology Monograph 6. Edited by R.R. Keays, R.H. Ramsay, and D.I. Groves. pp. 86-100.

HODGSON, C.J. AND MACGEEHAN, P.J. 1982. A review of the geological characteristics of 'gold-only' deposits in the Superior Province of the Canadian Shield. In Geology of Canadian Gold Deposits. Edited by R.W. Hodder and W. Petruk. Canadian Institute of Mining and Metallurgy, Special Volume 24. pp. 211-229.

HODGSON, C.J. AND TROOP, D.G. 1988. A new computer-aided methodology for area selection in gold exploration: A case study from the Abitibi greenstone belt. *Economic Geology*, 83: 952-977.

HOFFMAN, P.F. 1980. Wopmay Orogen: A Wilson cycle of early Proterozoic age in the northwest of the Canadian Shield. In The continental crust and its mineral deposits. Edited by D.W. Strangway. Geological Association of Canada, Special Paper 20, pp. 522-549.

HOFFMAN, P.F. 1986. Crustal accretion in a 2.7-2.5 Ga "granite-greenstone" terrane, the Slave Province, N.W.T: A prograding trench-arc system? In Workshop on tectonic evolution of greenstone belts. Edited by M.J. de Wit and L.D. Ashwal. Lunar and Planetary Institute, Houston, Texas, Technical Report 86-10, p. 120.

HOLLISTER, L.S. AND CRAWFORD, M.L. 1981. Short course in

fluid inclusions: Applications to petrology. Mineralogical Association of Canada Short Course Handbook, Volume 6. 304 p.

HUDLESTON, P.J. 1976. Early deformational history of Archean rocks in the Vermillion district, northeastern Minnesota. Canadian Journal of Earth Sciences, 13: 579-592.

HUDLESTON, P.J., SCHULTZ-ELA, D., AND SOUTHWICK, D.L. 1988. Transpression in an Archean greenstone belt, northern Minnesota. Canadian Journal of Earth Sciences, 25: 1060-1068.

HUTCHINSON, R.W. AND BURLINGTON, J.L. 1984. Some broad characteristics of greenstone belt lodes. In Gold'82: The geology, geochemistry and genesis of gold deposits. Edited by R.P. Foster, Geological Society of Zimbabwe, Special Publication No.1, pp. 339-372.

ISACHSEN, C.E. AND BOWRING, S.A. 1989. Yellowknife Volcanic Belt, N.W.T.: Constraints on timing and duration of greenstone belt magmatism and deformation. In Exploration Overview of the Northwest Territories 1988. Edited by W.A. Padgham Northwest Territories Geology Division, D.I.A.N.D., Yellowknife, Northwest Territories, p. 37.

JAEGER, E. 1979. Introduction to geochronology. In Lectures in isotope geology. Edited by E. Jäger and J.C. Hunziker. Springer-Verlag, Berlin. pp. 1-12.

JAMES, D.T. 1989. Basement-cover relations between the Archean Yellowknife Supergroup and the Sleepy Dragon Complex north of Fenton Lake, District of Mackenzie, Northwest Territories. In Current Research, Part C, Geological Survey of Canada, Paper 89-1C, pp. 29-36.

JAMES, D.T. 1990. Basement-cover relations between the Archean Yellowknife Supergroup and the Sleepy Dragon Complex in the Brown Lake area, Slave Province, Northwest Territories. In Current Research, Part C, Geological Survey of Canada, Paper 89-1C, pp. 189-195.

JENNER, G.A., FRYER, B.J., AND MCLENNAN, S.M. 1981. Geochemistry of the Archean Yellowknife Supergroup. Geochimica et Cosmochimica Acta, 45: 1111-1124.

JOLLIFFE, A.W. 1942. Yellowknife Bay, Northwest Territories. Geological Survey of Canada, Map 709A.

JOLLIFFE, A.W. 1946. Prosperous Lake, District of



MacKenzie, Northwest Territories. Geological Survey of Canada Map 868A.

KAMINENI, D.C. 1973. Petrology and geochemistry of some Archean metamorphic rocks near Yellowknife, District of MacKenzie. Unpublished PhD thesis, University of Ottawa, 228 p.

KAMINENI, D.C., DIVI, S.R., AND TELLA, S. 1979. Time relations of metamorphism and deformation in Archean metasedimentary rocks near Yellowknife, Canada. *Neus Jahrbuch fur Mineralogie Monatshefte, Jahrgang 1979*, p. 34-48.

KEYS, R.R. 1984. Archean gold deposits and their source rocks: The upper mantle connection. *In* Gold'82: The geology, geochemistry and genesis of gold deposits. Edited by R.P. Foster, Geological Society of Zimbabwe, Special Publication No.1, pp. 17-52.

KEYS, R.R. AND SCOTT, R.B. 1976. Precious metals in ocean-ridge basalts: Implications for basalts as source rocks for gold mineralization. *Economic Geology*, 71: 705-720.

KEHLENBECK, M.M. 1985. Folds and folding in the Beardmore-Geraldton fold belt. *Canadian Journal of Earth Sciences*, 23: 158-171.

KENNEDY, G.C. 1950. A portion of the system silica-water. *Economic Geology*, 45: 629-653.

KERRICH, R. 1976. Some effects of tectonic recrystallization on fluid inclusions in vein quartz. *Contributions to Mineralogy and Petrology*, 59: 195-202.

KERRICH, R. 1979. Lode gold deposits in greenstone belts-chemical and hydrodynamic constraints. *In* Gold: exploration and outlook. Edited by T. Anderson, P. Chamois, and D. Desoyers, Proceedings of Adams Club Annual Special Symposium 1979, pp. 13-33.

KERRICH, R. 1981. A synthesis of data on metal distribution, rare earth elements, and stable isotopes, with special reference to Yellowknife. *In* Proceedings of the Gold Workshop. Edited by R.D. Morton; Yellowknife, N.W.T. pp. 95-173.

KERRICH, R. 1989. Geodynamic setting and Hydraulic regimes: Shear zones hosted mesothermal gold deposits. *In* Mineralization and shear zones. Edited by J.T. Bursnall. Geological Association of Canada, Short Course Notes,

Volume 6, pp. 89-197.

KERRICH, R. AND ALLISON, I. 1978. Vein geometry and hydrostatics during Yellowknife mineralization. *Canadian Journal of Earth Science*, 15: 1653-1660.

KERRICH, R. AND FYFE, W.S. 1987. The formation of gold deposits with particular reference to Archean rocks and Yellowknife: A synthesis of geochemical data. In A guide to the geology of the Yellowknife Volcanic belt and its bordering rocks. Edited by W.A. Padgham. Geological Association of Canada, Mineral Deposits Division, pp. 155-173.

KERRICH, R., AND FYFE, W.S. 1988. The formation of gold deposits with particular reference to Archean greenstone belts and Yellowknife. In Contributions to the Geology of the Northwest Territories Volume 3. Edited by W.A. Padgham. pp. 37-96.

KERRICH, R.W., FYFE, W.S., AND ALLISON, I. 1977. Iron reduction around gold-quartz veins, Yellowknife District, Canada. *Economic Geology*, 72: 657-663.

KERRICH, R. AND WATSON, G.P. 1984. The Macassa Mine Archean lode gold deposit, Kirkland lake, Ontario: Geology, patterns of alteration, and hydrothermal regimes. *Economic Geology*, 79: 1104-1130.

KERSWILL, J.A. 1984. The Lupin gold deposit, Contwoyto Lake area, N.W.T.; styles of gold distribution and possible genetic models. Geological Association of Canada, Program with Abstracts, 9: 78.

KERSWILL, J.A. 1986. Gold deposits hosted by iron formation in the Contwoyto Lake area, Northwest Territories. In Gold'86 Poster Papers and Abstracts. Edited by A.M. Chater. Geological Association of Canada, Mineral Deposits Division, pp. 82-85.

KERSWILL, J.A., WOOLLETT, G.N., STRACHAN, D.M., AND GARDINER, J. 1983. Geological setting and gold distribution at the Lupin gold deposit, Contwoyto Lake area, N.W.T. Program with Abstracts, District 5, C.I.M. Conference, Calgary.

KING, J.E., DAVIS, W.J., RELF, C., AND AVERY, R.W. 1988. Deformation and plutonism in the western Contwoyto Lake map area, Central Slave Province, District of MacKenzie, N.W.T. Geological Survey of Canada, Current Research, Part C, Paper 88-1C, pp. 161-176.

- KING, J.E., DAVIS, W.J. AND RELF, C. 1989. Discussion of "Accretion of the Archean Slave Province. *Geology*, 17: 962-963.
- KLIGFIELD, R., HUNZIKER, J, AND DALLMEYER. 1986. Dating of deformation phases using  $^{40}\text{Ar}/^{39}\text{Ar}$  techniques: Results from the Northern Apennines. *Journal of Structural Geology*, 8: 781-798.
- KNIPE, R.J. AND NEEDHAM, D.T. 1986. Deformation processes in accretionary wedges - examples from the SW margin of the Southern Uplands, Scotland. In *Collision tectonics*. Edited by M.P. Coward and A.C. Reis. Blackwell Scientific, Oxford. pp. 51-65.
- KNUTSEN, W.G. 1984a. Report on the Giant Bay Resources Ltd. MAHE, AD, POL, AR, BEAR and LYNX claim group, Gordon Lake area, MacKenzie Mining District, Canada. Unpublished report, Giant Bay Resources Ltd., Burnaby, British Columbia.
- KNUTSEN, W.G. 1984b. Summary report and ore reserve studies Giant Bay Resources Ltd. gold property, Gordon Lake, N.W.T. Unpublished report, Giant Bay Resources Ltd., Burnaby, British Columbia.
- KONTAK, D.J. AND SMITH, P.K. 1987. Alteration haloes and their implications for gold mineralization in the Meguma Group of Nova Scotia. In Nova Scotia Department of Mines and Energy, Report 87-1, pp. 65-74.
- KONTAK, D.J. AND SMITH, P.K. 1989. Fluid inclusion studies of quartz vein polytypes from the Beaver Dam and caribou gold deposits, Meguma Zone, Nova Scotia: Evidence for a single vein-forming event. Atlantic Geoscience Society Colloquium '89, Amherst, Nova Scotia, Abstract with Programs.
- KONTAK, D.J., MACDONALD, D. AND SMITH, P.K. 1988. Fluid inclusion study of the Beaver Dam Gold Deposit, Meguma Terrane, Nova Scotia. In Mines and Minerals Branch, Report of Activities 1988, Part A. Edited by D.R. Macdonald and Y. Brown. Nova Scotia Department of Mines and Energy, Report 88-3, pp. 63-69.
- KONTAK, D.J., SMITH, P.K, KERRICH, R., AND WILLIAMS, P.F. 1990. Integrated model for Meguma Group lode gold deposits, Nova Scotia, Canada. *Geology*, 18: 238-242.
- KRETSCHMAR, U. AND SCOTT, S.D. 1976. Phase relations involving arsenopyrite in the system Fe-As-S and their application. *Canadian Mineralogist*, 14: 364-386.

- KRETSCHMAR, U. 1973. Phase relations involving arsenopyrite in the system Fe-As-S and their applications. Unpublished Phd Thesis, University of Toronto, Toronto, Ontario. 146 p.
- KREULEN, R. 1980. CO<sub>2</sub>-rich fluids during regional metamorphism on Naxos (Greece): carbon isotopes and fluid inclusions. *American Journal of Science*, 280: 745-771.
- KROUGH, T.E. AND GIBBINS, W. 1978. U-Pb isotopic ages of basement and supracrustal rocks in the Point Lake area of the Slave Structural Province, Canada. In Geological Association of Canada - Mineralogical Association of Canada, Program with Abstracts, 3: 438.
- KUBILIUS, W.P. AND FERRY, J.M. 1989. Oxidation and arsenic loss during regional metamorphism of the Meguma Group, Nova Scotia: Implications for gold mineralization. In Geological Association of Canada, Program with Abstracts, 14: A2.
- KUHNS, R.J., KENNEDY, P., BROWN, P., MACKIE, B, KUSINS, R., AND FRIESEN, R. 1986. Geology and mineralization associated with the Golden Giant deposit, Ontario, Canada. In Gold'86 Proceedings, Toronto. Edited by A.J. MacDonald. pp. 327-354.
- KUSKY, T.M. 1986. Are greenstone belts in the Slave Province, N.W.T. allochthonous? In Workshop on tectonic evolution of greenstone belts. Edited by M.J. de Wit and L.D. Ashwal. Lunar and Planetary Institute, Houston, Texas, technical Report 86-10, pp. 135-139.
- KUSKY, T.M. 1988. Thrusting between the Cameron River greenstone belt and the Sleepy Dragon Complex, Slave Province, District of MacKenzie. In Contributions to the geology of the Northwest Territories, Volume 3. Edited by W.A. Padgham. pp. 97-102.
- KUSKY, T.M. 1989. Accretion of the Archean Slave Province. *Geology*, 17: 63-67.
- KUSKY, T.M. 1990. Evidence for Archean ocean opening and closing in the southern Slave Province. *Tectonics*, 9: 1533-1563.
- LAMBERT, M.B. 1978. The Back River volcanic complex - A cauldron subsidence structure of Archean age. In Current Research, Part A, Geological Survey of Canada, Paper 82-1A, pp.153-167.

- LHOTKA, P.G. AND NESBITT, B.E. 1989. Geology of unmineralized and gold-bearing iron formation, Contwoyto Lake, Point Lake region, Northwest Territories, Canada. Canadian Journal of Earth Sciences, 26: 46-64.
- LINDGREN, W. 1933. Mineral deposits. 4th Edition. McGraw-Hill, New York, 930 p.
- LORD, C.S. 1951. Mineral Industry of District of MacKenzie, Northwest Territories. Geological Survey of Canada, Memoir 261, 336 p.
- MAWER, C.K. 1985. Origin of bedding-concordant auriferous quartz veins, Meguma Terrane, Nova Scotia. Maritime Sediments and Atlantic Geology, 21: 1-9.
- MAWER, C.K. 1987. Mechanics of formation of gold-bearing quartz veins, Nova Scotia, Canada. Tectonophysics, 135: 99-119.
- MCCONNEL, G.W. 1964. Yellowknife gold-quartz deposits. Economic Geology, 59: 328-330
- MCDUGALL, I. AND HARRISON, T.M. Geochronology and Thermochronology by the  $^{40}\text{Ar}/^{39}\text{Ar}$  method. Oxford Monographs on Geology and Geophysics No.9, Oxford.
- MCGLYNN, J.C. AND HENDERSON, J.B. 1970. Archean volcanism and sedimentation in the Slave Structural Province. In Symposium on basins and geosynclines of the Canadian Shield. Edited by A. Baer. Geological Survey of Canada, Paper 70-40, pp. 31-44.
- MCGRATH, P.H., HENDERSON, J.B., AND LINDIA, F.M. 1983. Interpretation of a gravity profile over a contact zone between an Archean granodiorite and the Yellowknife Supergroup using an interactive computer program with partial automatic optimization. In Current Research, Part B, Geological Survey of Canada, Paper 83-1B, pp. 189-194.
- MCINTYRE, D.B. 1963. Precision, and resolution in geochronometry. In: The Fabric of geology. Edited by C.C. Albritton. Addison-Wesley, New York, pp. 112-134.
- MCKEAG, S.A. AND CRAW, D. 1989. Contrasting fluids in gold-bearing quartz vein systems formed progressively in a rising metamorphic belt: Otago Schist, New Zealand. Economic Geology, 84: 22-33.
- MCKEAG, S.A., CRAW, D., AND NORRIS, R.J. 1989. Origin and deposition of a graphitic schist-hosted metamorphogenic Au-W deposit, Macraes, East Otago, New Zealand. Mineralium

Deposita, 24: 124-131.

MEINTZER, R.E. AND WISE, M.A. 1987. Granitoids and pegmatites of the Yellowknife area, N.W.T. In A guide to the geology of the Yellowknife Volcanic belt and its bordering rocks. Edited by W.A. Padgham. Geological Association of Canada, Mineral Deposits Division, pp. 123-136.

MELLING, D.R., BLACKBURN, C.E., WATKINSON, D.H., AND PARKER, J.R. 1988. Geological setting of gold, western Wabigoon Subprovince, Canadian Shield: Exploration targets in mixed volcanic successions. Canadian Journal of Earth Sciences, 25: 2075-2088.

MELLING, D.R., WATKINSON, D.H., POULSEN, K.H., CHORLTON, L.B. AND HUNTER, A.D. 1986. The Cameron Lake gold deposit, Northwest Ontario, Canada: Geological setting, structure and alteration. In Proceedings of Gold'86 Symposium, Toronto. Edited by A.J. MacDonald. pp. 149-169.

MERRIHUE, C. AND TURNER, G. 1966. Potassium-argon dating by activation with fast neutrons. Journal of Geophysical Research, 71: 2852-2857.

MITCHELL, A.H.G. AND GARSON, M.S. 1981. Mineral deposits and global tectonic settings. Academic Press Inc., New York.

MUEKE, G.K, ELLIAS, P, AND REYNOLDS, P.H. 1988. Hercynian/Alleghanian overprinting of an Acadian terrane:  $^{40}\text{Ar}/^{39}\text{Ar}$  studies in the Meguma Zone, Nova Scotia, Canada. Chemical Geology: 73, 153-167.

NEWHOUSE, W.H. 1936. A zonal gold mineralization, Nova Scotia. Economic Geology, 31: 805-831.

NEWTON, R.C., SMITH, J.V, AND WINDLEY, B.F. 1980. Carbonic metamorphism, granulites and crustal growth. Nature, 288; 45-50.

NIKIC, Z., BAADSGAARD, H., FOLINSBEE, R.E., KRUPICKA, J., LEECH, A.P., AND SASAKI, A. 1980. Boulders from the basement, the trace of an ancient crust. In Selected studies of Archean gneisses and Lower Proterozoic rocks, Southern Canadian Shield. Edited by G.B. Morey and G.N. Hanson; Geological Society of America, Special Paper 182, pp. 169-175.

NISBET, E.G. 1987. The young earth: An introduction to Archean geology. Allen and Unwin, Boston.

- NORRIS, R.J. AND HENLEY, R.W. 1976. Dewatering of a metamorphic pile. *Geology*, 4: 333-336.
- OHLE, E.L. AND BATES, R.L. 1981. *Geology, geologists and mineral exploration. Economic Geology 75th Anniversary Volume*, pp. 766-774.
- OLIVER, J. 1986. Fluids expelled tectonically from orogenic belts: Their role in hydrocarbon migration and other geologic phenomena. *Geology*, 14: 99-102
- ONASCH, C.M. 1986. Ability of the Fry method to characterise pressure solution. *Tectonophysics*, 122: 187-193.
- PADGHAM, W.A. 1984. Gold deposits of the N.W.T: Classes, styles, genesis, exploration methods and success probabilities. In *Contributions to the Geology of the Northwest Territories, Volume 1. Edited by J.A. Brophy. INAC-NAP, Geology Division, Yellowknife, NWT*, pp. 121-129.
- PADGHAM, W.A. 1985. Observations and speculations on supracrustal successions in the Slave Structural Province. In *Evolution of Archean supracrustal sequences. Edited by L.D. Ayres, P.C. Thurston, K.D. Card, and W. Weber, Geological Association of Canada Special Paper 28*. pp. 133-151.
- PADGHAM, W.A. 1986. Turbidite hosted gold-quartz veins in the Slave Structural Province, N.W.T. In *Turbidite hosted gold deposits. Edited by J.D. Keppie, R.W. Boyle, and S.J. Haynes, Geological Association of Canada, Special Paper 32*. pp. 119-134.
- PADGHAM, W.A. 1987. The Yellowknife Volcanic Belt: Setting and stratigraphy. In *A guide to the geology of the Yellowknife Volcanic belt and its bordering rocks. Edited by W.A. Padgham. Geological Association of Canada, Mineral Deposits Division*, pp. 11-20.
- PADGHAM, W.A. AND BROPHY, J.A. 1984. Gold deposits of the Northwest Territories. In *Gold in the Western Shield. Edited by L.A. Clark. Canadian Institute of Mining and Metallurgy Special Publication 38*, pp. 3-23.
- PASTERIS, J.D., WOPENKA, B., AND SEITZ, J.C. 1988. Practical aspects of quantitative laser Raman microprobe spectroscopy for the study of fluid inclusions. *Geochimica et Cosmochimica Acta*, 52: 979-988.
- PATERSON, C.J. 1986. Controls on gold mineralization in metamorphic-hydrothermal systems, Otago, New Zealand. In

- Turbidite Hosted Gold Deposits. Edited by D.J. Keppie, R.W. Boyle and S.J. Haynes. Geological Association of Canada Special Paper 32. pp. 25-39.
- PATERSON, C.J. AND RANKIN, P.C. 1979. Trace element distribution in the schist surrounding a quartz-scheelite lode, Glenorchy, New Zealand. New Zealand Journal of Geology and Geophysics, 22: 329-338.
- PATTERSON, G.C. 1984. Field trip guidebook to the Hemlo area. Ontario Geological Survey Miscellaneous Paper 118. 33 p.
- PERCIVAL, J.A. AND WILLIAMS, H.R. 1989. Late Archean Quetico accretionary complex, Superior Province, Canada. Geology, 17: 23-25.
- PETTIJOHN, F.J. 1975. Sedimentary rocks. 2nd edition. Harper & Brothers, New York.
- PHILLIPS, G.N. AND GROVES, D.I. 1987. Source requirements for the Golden Mile, Kalgoorlie: Significance to the metamorphic replacement model for Archean gold deposits. Canadian Journal of Earth Sciences, 24: 1643-1651.
- PHILLIPS, W.J. 1972. Hydraulic fracturing and mineralization. Journal of the Geological Society of London, 128: 337-359.
- PHILLIPS, W.J. 1986. Hydraulic fracturing effects in the formation of mineral deposits. Institution of Mining and Metallurgy Transactions, Section B, 95: 17-24.
- PICHAVANT, M., RAMBOZ, C., AND WEISBROD, A. 1982. Fluid immiscibility in natural processes: Use and misuse of fluid inclusion data. Chemical Geology, 37: 1-27.
- PICKERING, K., STOW, D., WATSON, M., AND HISCOTT, R. 1987. Deep water facies, processes and models: A review and classification schemes for modern and ancient sediments. Earth Sciences Reviews, 23: 75-174.
- PIFFNER, O.A. AND RAMSAY, J.G. 1982. Constraints on geological strain rates, arguments from finite strain states of naturally deformed rocks. Journal of Geophysical Research, 87: 311-321.
- POWELL, C., MCA. 1974. Timing of slaty cleavage during folding of Precambrian rocks, Northwest Tasmania. Geological Society of America, 85: 1043-1060.
- RAMA, S.N.I., HART, S.R., AND ROEDDER, E. 1965. Excess



radiogenic argon in fluid inclusions. Journal of Geophysical Research, 70: 509-511.

RAMSAY, C.R. 1973. Metamorphism and gold mineralization of Archean metasediments near Yellowknife, N.W.T., Canada. Unpublished PhD thesis, University of Alberta.

RAMSAY, C.R. AND KAMINENI, D.C. 1977. Petrology and evolution of an Archean metamorphic aureole in the Slave Craton, Canada. Journal of Petrology, 18: 460-486.

RAMSAY, J.G. 1967. Folding and fracturing of rocks. McGraw-Hill Book Company, London, England. 568 p.

RAMSAY, J.G. 1974. Development of chevron folds. Geological Society of America Bulletin, 85: 1741-1754.

RAMSAY, J.G. 1980. The crack-seal mechanism of rock deformation. Nature, 284: 135-139.

RAMSAY, J.G. AND HUBER, M. 1983. Techniques of modern structural geology. Volume 1: Strain analysis. Academic Press, London. p. 308.

RAMSAY, J.G. AND HUBER, M. 1987. Techniques of modern structural geology. Volume 2: Folds and fracturing. Academic Press, London. pp. 308-700.

RANSOM, A.H. AND ROBB, M.E. 1986. The Salmita gold deposit, Courageous Lake, Northwest Territories. In Gold in the Western Shield. Edited by L.A. Clark, pp. 285-305.

READ, J.J. AND MEINERT, L.D. 1986. Gold-bearing quartz vein mineralization at the Big Hurrah Mine, Seward Peninsula, Alaska. Economic Geology, 81: 1760-1774.

RELF, C. 1987. A study of alteration along shear zones, West Mirage Islands, N.W.T. Unpublished MSc thesis, Memorial University, St Johns, Newfoundland.

RELF, C. 1989. Archean deformation of the Contwoyto formation metasediments, western Contwoyto Lake area, Northwest Territories. In Current research, Part C, Geological Survey of Canada, Paper 89-1C, pp. 95-105.

REYNOLDS, P.H., ELIAS, P., MUECKE, G.K. AND GRIST, A.M. 1987. Thermal history of the southwestern Meguma Zone, Nova Scotia, from a  $^{40}\text{Ar}/^{39}\text{Ar}$  - fission track dating study of intrusive rocks. Canadian Journal of Earth Sciences, 18: 386-394.

ROBERT, F. AND KELLY, W.C. 1987. Ore-forming fluids in

Archean gold-bearing quartz veins in the Sigma Mine, Abitibi Greenstone Belt, Quebec, Canada. *Economic Geology*, 82: 1464-1482.

ROBERT, F., CREVIER, M., AND DUMOULIN, M. 1989. The Sigma Gold Deposit. In Archean gold deposits in the Rouyn-Noranda, Val d'Or and Chibougamau areas. Edited by A. Simard and F. Chartrand. Geological Association of Canada - Mineralogical Association of Canada, Field Excursion Guide A7.

ROBERTS, R.G. 1986. Ore deposit models #11. Archean lode gold deposits. *Geoscience Canada*, 14: 37-52.

ROEDDER, E. 1982. Fluid-inclusion evidence bearing on the environments of gold deposition. In Gold'82: The geology, geochemistry and genesis of gold deposits. Edited by R.P. Foster, Geological Society of Zimbabwe, Special Publication No.1, pp. 129-163.

ROEDDER, E. 1984. Fluid inclusions. *Reviews in Mineralogy*, Volume 12, Mineralogical Society of America, 644 p.

ROEDDER, E. AND BODNAR, R.J. 1980. Geologic pressure determinations from fluid inclusion studies. *Annual Review of Earth and Planetary Science*, 8: 263-301.

ROERING, C. AND SMIT, C.A. 1987. Bedding-parallel shear and quartz vein formation in Witwatersrand quartzites. *Journal of Structural Geology*, 9: 419-427.

ROMBERGER, S.E. 1984. Geochemistry of hydrothermal precious metal deposits. 1984 Exploration for Gold Short Course, Department of Geology, McGill University, Montreal.

ROMBERGER, S.E. 1986. The solution chemistry of gold applied to the origin of hydrothermal deposits. In Gold in the Western Shield. Edited by L.A. Clark, C.I.M. Special Volume 38, pp. 167-186.

RUBEY, W.W. AND HUBBERT, M.K. 1959. Role of fluid overpressures in mechanics of overthrusting II. *Geological Society of America Bulletin*, 70: 167-206.

SANDIFORD, M. AND KEAYS, R.R. 1986. Structural and tectonic constraints on the origin of gold deposits in the Ballarat Slate Belt, Victoria. In Turbidite Hosted Gold Deposits. Edited by D.J. Keppie, R.W. Boyle and S.J. Haynes. Geological Association of Canada Special Paper 32. pp. 15-24.

SAWKINS, F.J. AND RYE, D.M. 1974. Relationship of

Homestake-type gold deposits to iron rich Precambrian sedimentary rock. Institution of Mining and Metallurgy Transactions, Section B, 93: 56-59.

SAWYER, E.W. 1986. The influence of source rock type, chemical weathering, and sorting on the clastic sediments from the Quetico metasedimentary belts, Superior Province, Canada. Chemical Geology, 55: 77-95.

SCHARER, U. AND ALLEGRE, C.J. 1982. Investigation of the Archean crust by single grain dating of detrital zircon: A graywacke of the Slave Province, Canada. Canadian Journal of Earth Science, 19: 1910-1918.

SEWARD, T.M. 1973. Thiocomplexes of gold and transport of gold in hydrothermal ore solutions. Geochimica et Cosmochimica Acta, 37: 379-399.

SEWARD, T.M. 1982. The transport and deposition of gold in hydrothermal systems. In The geology, geochemistry and genesis of gold deposits. Edited by R.P. Foster. Geological Society of Zimbabwe, Special Publication No. 1. pp. 165-189.

SEWARD, T.M. 1984. The transport and deposition of gold in hydrothermal systems. In Gold'82: The geology, geochemistry and genesis of gold deposits. Edited by R.P. Foster, Geological Society of Zimbabwe, Special Publication No.1, pp. 165-182.

SHEPHERD, T.J., RANKIN, A.H. AND ALDERTON, D.H.M. 1985. A practical guide to fluid inclusion studies. Blackie & Son Limited, Glasgow, Scotland.

SHIMAMOTO, T. AND IKEDA, Y. 1976. A simple algebraic method for strain estimations from deformed ellipsoidal objects. 1. Basic theory. Tectonophysics, 36: 315-337.

SIBSON, R.H. 1986. Brecciation processes in fault zones: inferences from earthquake rupturing. In Internal structure of fault zones. Edited by C. Wang. Pure and Applied Geophysics, Volume 124, pp. 159-176.

SIBSON, R.H., 1987. Earthquake rupturing as a mineralizing agent in hydrothermal systems. Geology, 15: 701-704.

SIBSON, R.H. 1990. Faulting and fluid flow. In Fluids in tectonically active regimes of the continental crust. Edited by B.E. Nesbitt. Mineralogical Association of Canada, Short Course Handbook, Volume 18, pp. 93-132.

- SIBSON, R.H., MOORE, J. MCM., AND RANKIN, A.H. 1975. Seismic pumping - a hydrothermal fluid transport mechanism. *Journal of Geological Society of London*, 131: 653-659.
- SIBSON, R.H., ROBERT, F., AND POULSEN, K.H. 1988. High-angle reverse faults, fluid-pressure cycling, and mesothermal gold-quartz deposits. *Geology*, 16: 551-555.
- SISSON, V.B. AND HOLLISTER, L.S. 1988. Low-pressure facies series in an accretionary prism, southern Alaska. *Geology*, 16: 358-361.
- SMITH, P.K. 1984. Geology and lithogeochemistry of the Cochrane Hill gold deposit - an indication of metalliferous source beds. In Nova Scotia Department of Mines and Energy, Report 84-1, pp. 203-230.
- SMITH, P.K., HAYNES, S.J., AND REILLY, B.A. 1985. Turbidite-hosted gold deposits, Meguma Domain, eastern Nova Scotia. Geological Association of Canada, Excursion Guidebook 11, Fredericton, New Brunswick. 67 p.
- SMITH, T.J., CLOKE, P.L., AND KESLER, S.E. 1984. Geochemistry of fluid inclusions from the McIntyre-Hollinger gold deposit, Timmins, Ontario, Canada. *Economic Geology*, 79: 1265-1285.
- SPENCER, E.W. 1969. Introduction to the structure of the earth. McGraw-Hill, Inc., New York. 597 p.
- SPRINGER, J. 1983. Invisible gold. In The geology of gold in Ontario. Edited by A.C. Colvine. Ontario Geological Survey Miscellaneous Paper 110. pp. 240-250.
- SPOONER, E.T.C., BRAY, C.J., WOOD, P.C., BURROWS, D.R., AND CALLAN, N.J. 1987. Au-quartz vein and Cu-Au-Ag-Mo-anhydrite mineralization, Hollinger-McIntyre Mines, Timmins, Ontario:  $\delta^{13}\text{C}$  values (McIntyre) fluid inclusion gas chemistry, pressure (depth) estimates, and  $\text{H}_2\text{O}-\text{CO}_2$  phase separation as a precipitation and dilation mechanism. Ontario Geological Survey Miscellaneous Paper, 136: 35-56.
- STEED, G.M. AND MORRIS, J.H. 1986. Gold mineralization in Ordovician graywackes at Clonibret, Ireland. In Turbidite Hosted Gold Deposits. Edited by D.J. Keppie, R.W. Boyle and S.J. Haynes. Geological Association of Canada Special Paper 32. pp. 67-86.
- STERNER, S.M., HALL, D.L., AND BODNAR, R.J. 1988. Synthetic fluid inclusions V: Solubility relations in the system  $\text{NaCl}-\text{KCl}-\text{H}_2\text{O}$  under vapour saturated conditions. *Geochimica et Cosmochimica Acta*, 52: 989-1005.

SWATTON, S.P. Structure, mineralogy, and stable isotopes: Bullmoose Lake gold deposit, N.W.T. Unpublished MSc thesis, University of Alberta.

TALBOT, C.J. 1970. The minimum strain ellipsoid using deformed quartz veins. *Tectonophysics*, 9: 47-76.

TARNEY, J., DALZIEL, I.W.D. AND DE WIT, M. 1976. Marginal basin 'Rocas Verdes' complex from Chile: A model for Archean greenstone belt formation. In *The early history of the earth*. Edited by B.F. Windley, Wiley, pp. 131-146.

TAYLOR, M., KESLER, S.E., CLOKE, P.L. AND KELLY, W. 1983. Fluid inclusion evidence for fluid mixing, Mascot-Jefferson City zinc district, Tennessee. *Economic Geology*, 78: 1425-1439.

THOMAS, A.V., PASTERIS, J.D., BRAY, C.J., AND SPOONER, E.T.C. 1989. H<sub>2</sub>O-CH<sub>4</sub>-NaCl-CO<sub>2</sub> inclusions from the Tanco granitic pegmatite: Estimates of internal pressure and composition from microthermometry, laser raman spectroscopy and gas chromatography. In *Program and Abstracts of Second Biennial Pan-American Conference on Fluid Inclusions, PACROFI II, Volume 2, Blacksburg, Virginia*, p. 65.

THOMPSON, P.H. 1978. Archean regional metamorphism in the Slave Structural Province - a new perspective of some old rocks. In *Metamorphism of the Canadian Shield*. Edited by J.A. Frazer and W.W. Heywood. Geological Survey of Canada, Paper 78-10, pp. 84-102.

THOMPSON, P.H. 1989a. Moderate overthickening of thinned sialic crust and the origin of granitic magmatism and regional metamorphism in low-P-high-T terranes. *Geology*, 17: 520-523.

THOMPSON, P.H. 1989b. An empirical model for metamorphic evolution of the Archean Slave Province and adjacent Thelon Tectonic Zone, north-western Canadian Shield. In *Evolution of Metamorphic Belts*. Edited by J.S. Daley, R.A. Cliff and B.W. Yardley. Geological Society Special Publication: 43, pp. 245-263.

THOMPSON, P.H. AND HENDERSON, J.B. 1983. Polymetamorphism in the Healy Lake map area: Implications for the Thelon Tectonic Zone. In *Current Activities Forum, 1983, Program with abstracts*, Geological Survey of Canada Paper, 83-8, p. 2.

THORPE, R.I. 1971. Comments on rock ages in the Yellowknife area, District of MacKenzie. Report of

- Activities, Part B, Geological Survey of Canada, Paper 71-1B, pp. 76-79.
- TREMBLAY, L.P. 1952. Giauque Lake, District of MacKenzie, N.W.T. Geological Survey of Canada, Map 1017A.
- VAN BREEMEN, O. 1989. Geochronology of granitoid rocks in the Slave Province and Thelon Tectonic Zone. In Exploration Overview of the Northwest Territories 1989. Edited by W.A. Padgham. Northwest Territories Geology Division, D.I.A.N.D., Yellowknife, N.W.T., Abstract p. 56.
- VAN BREEMEN, O., HENDERSON, J.B., SULLIVAN, R.W. AND THOMPSON P.H. 1987. U-Pb, zircon and monazite ages from the Eastern Slave Province, Healy Lake area, N.W.T; In Radiogenic Age and Isotopic Studies: Report I, Geological Survey of Canada, Paper 87-2, pp. 101-110.
- VANKO, D.A., BODNAR, R.J., AND STERNER, S.M. 1988. Synthetic fluid inclusions: VIII. Vapour-saturated halite solubility in part of the system NaCl-CaCl<sub>2</sub>-H<sub>2</sub>O with applications to fluid inclusions from oceanic hydrothermal systems. *Geochimica et Cosmochimica Acta*, 52: 2451-2456.
- WALSH, J.F., KESLER, S.E., DUFF, D, AND CLOKE, P.L. 1988. Fluid inclusion geochemistry of high-grade, vein-hosted gold ore at the Pamour Mine, Porcupine Belt, Ontario. *Economic Geology*, 83: 1347-1367.
- WALTHER, J.V. AND ORVILLE, P.M. 1982. Volatile production and transport in regional metamorphism. *Contributions to Mineralogy and Petrology*, 79: 252-25.
- WEBB, D.R. AND KERRICH, R. 1986. Recent age-dating on the gold-bearing quartz-veins at the Con Mine, Yellowknife, Northwest Territories. In Exploration Overview of the Northwest Territories 1986. Edited by J.C.E. Crux and C.D. Gault. Northwest Territories Geology Division, D.I.A.N.D., Yellowknife, N.W.T., Abstract, p. 37.
- WHETTON, J.T. AND HAWKINS, J.W. 1970. Diagenetic origin of graywacke matrix minerals. *Sedimentology*, 15: 347-361.
- WILKINS, R.W.T. AND BARKAS, J.P. 1978. Fluid inclusions, deformation and recrystallization in granite tectonites. *Contributions to Mineralogy and Petrology*, 65: 293-299.
- WILLIAMS, G. AND CHAPMAN, T. 1983. Strains developed in the hanging wall of thrusts due to their slip/propagation rate: A dislocation model. *Journal of Structural Geology*, 5: 563-571.

- WILLIAMS-JONES, A.E. AND SAMSON, I.M. 1990. Theoretical estimation of halite solubility in the system NaCl-CaCl<sub>2</sub>-H<sub>2</sub>O: Applications to fluid inclusions. *Canadian Mineralogist*, 28: 299-304.
- WILLIAMS-JONES, A.E., SAMSON, I.M., AND LINNEN, R. 1989. Fluid evolution and its role in the genesis of the granite-related Madeleine copper deposit, Gaspé, Quebec. *Economic Geology*, 84: 1515-1524.
- WILSON, G.C. AND RUCKLIDGE, J.C. 1987. Geology, geochemistry and economic significance of carbonaceous host rocks in gold deposits of the Timmins area. Ontario Geological Survey, Miscellaneous Paper 136, pp.66-76.
- WILSON, J.W.J., KESLER, S.E., CLOKE, P.L., AND KELLY, W.C. 1980. Fluid inclusion geochemistry of the Granisle and Bell porphyry copper deposits, British Columbia. *Economic Geology*, 75: 45-61.
- WINKLER, H.G.F. 1974. Petrogenesis of metamorphic rocks. Springer-Verlag, New York.
- WIWCHAR, G.M. 1957. Consolidated Discovery Yellowknife Mine. In Structural geology of Canadian ore deposits, Volume 2. Canadian Institute of Mining and Metallurgy, pp. 201-209.
- WOOD, B.J. AND WALTHER, J.V. 1986. Fluid flow during metamorphism and its implications for fluid-rock ratios. In Fluid-rock interactions during metamorphism. Edited by J.V. Walther and B.J. Wood. Springer-Verlag, New York. pp. 89-108.
- WOOD, P.C., BURROWS, D.R., THOMAS, A.V. AND SPOONER, E.T.C. 1986. The Hollinger-McIntyre Au-quartz vein system, Timmins, Ontario, Canada: geologic characteristics, fluid properties and light stable isotope geochemistry. In Gold'86. Edited by A.J. MacDonald. pp. 56-80.
- WU, X., DELBOVE, F., AND TOURAY, J.C. 1990. Conditions of formation of gold-bearing arsenopyrite: A comparison of synthetic crystals with samples from the Le Châlet gold deposit, Creuse, France. *Mineralium Deposita*, 25: S8-S12.
- YARDLEY, B.W. 1983. Quartz veins and devolatilization during metamorphism. Geological Society of London, *Journal*, 140: 657-663.
- YARDLEY, B.W. 1986. Fluid migration and veining in Connemara Schists, Ireland. In Fluid-rock interactions during metamorphism. Edited by J.V. Walther and B.J. Wood.

Advances in Physical Geochemistry Volume 5, pp. 89-131.

YARDLEY, B.W., 1989. An introduction to metamorphic petrology. Longman Scientific and Technical, Harlow, England. 248 p.



